Medical Radiology
Diagnostic Imaging

M.F. Reiser
H. Hricak
M. Knauth

U. Joseph Schoepf
Fabian Bamberg
Gorka Bastarrika
Balazs Ruzsics
Rozemarijn Vliegenthart
Editors

CT Imaging of Myocardial Perfusion and Viability

Beyond Structure and Function

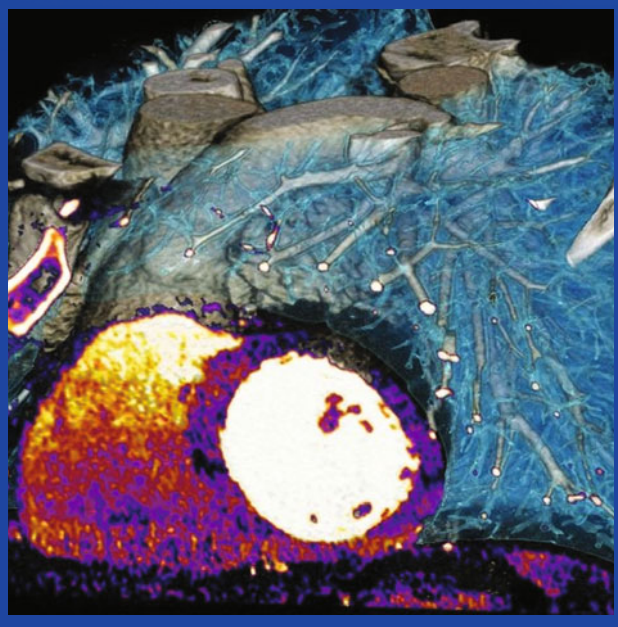

Springer

Medical Radiology

Diagnostic Imaging

For further volumes:
http://www.springer.com/series/4354

U. Joseph Schoepf • Fabian Bamberg
Gorka Bastarrika • Balazs Ruzsics
Rozemarijn Vliegenthart
Editors

CT Imaging of Myocardial Perfusion and Viability

Beyond Structure and Function

Springer

Editors
U. Joseph Schoepf
Department of Radiology and Radiological Sciences
Medical University of South Carolina
Charleston, SC
USA

Fabian Bamberg
Ludwig-Maximilians-University
Munich, Bayern
Germany

Gorka Bastarrika
Cardiothoracic Imaging Division, Department of Medical Imaging
Sunnybrook Health Sciences Centre
Toronto, ON
Canada

Balazs Ruzsics
Department of Cardiology
Royal Liverpool and Broadgreen University
Liverpool
UK

Rozemarijn Vliegenthart
Center for Medical Imaging
University Medical Center Groningen
Groningen
The Netherlands

ISSN 0942-5373 ISSN 2197-4187 (electronic)
ISBN 978-3-642-33878-6 ISBN 978-3-642-33879-3 (eBook)
DOI 10.1007/978-3-642-33879-3
Springer Heidelberg New York Dordrecht London

Library of Congress Control Number: 2013953604

Preface

"...τὴν δὲ δὴ καρδίαν ἅμμα τῶν φλεβῶν καὶ πηγὴν τοῦ περιφερομένου κατὰ πάντα τὰ μέλι
σφοδρῶς αἵματος..."

Plato, Timaios, 360 BC

We are embarking on yet another exciting journey in our exploration of the determinants of the human body. Much has happened in the last decade that has decisively enhanced our abilities to noninvasively assess health and disease of the heart. Innovation in medicine ordinarily is a slow process; many years pass before a new test or procedure matures to the stage of universal acceptance and integration into clinical algorithms and guidelines. This process is welcome and necessary, as it ensures sufficient vetting of new techniques before they are applied on a large, universal scale and prevents unsuitable, unduly hyped fancies of the moment to enter the greater field of medicine. Because of its disruptive nature as the only noninvasive modality that enables interrogation of the coronary arteries, the use of cardiac CT has evolved at a breathtaking speed and has found entrance in general clinical practice, widespread acceptance, and inclusion into guidelines much faster than we could have dreamt of 15 years ago, when we embarked on applying modern era CT systems to cardiac imaging.

Now that general cardiac CT applications are firmly and irrevocably ensconced in the wider consciousness of medicine, it is time to explore new frontiers and further expand our boundaries. We are no longer content with mere morphe, it is the combination and interdependence of structure and function that tweaks our curiosity and ambition. In recent years, exciting new techniques have emerged that aim at the combined CT assessment of coronary artery disease and its consequences on the function of the heart muscle. These novel approaches have been enabled by constantly evolving technical innovation and by the ingenuity of clinicians and researchers who explore ever new avenues for applying our technical prowess to improving the human condition. The concomitant application of CT techniques for detecting coronary artery stenosis and their relationship to myocardial function, ischemia, infarction, and viability is of particular attractiveness. One single, rapid modality can comprehensively and noninvasively provide all information, whereas in past decades a barrage of multiple tests was required to obtain similar insights for the purpose of guiding beneficial and appropriate patient management. As such, CT imaging of myocardial ischemia, infarction, and viability is a true paradigm for the synergies that we need to create to face our challenges in the healthcare of the future.

We are proud to present to you the first tome on these exciting new developments in imaging and we hope that you will share our excitement. We are exceedingly grateful to our many expert contributors from around the globe who made time in their busy schedules to bring to you their cutting edge experiences in the application of a broad spectrum of approaches to tackle this fascinating feat. Our gratitude goes out to our dear friend Max Reiser for setting us on this path and to the editorial team at Springer who again so expertly steered the realization of this ambitious project.

Charleston, Munich, Toronto, Liverpool, Groningen, October 2013 The Editors

Contents

Contributors

Suhny Abbara Cardiac MRCT Program, Massachusetts General Hospital, Boston, MA, USA

Rishi Agrawal Cardiac MRCT Program, Massachusetts General Hospital, Boston, MA, USA

Amr M. Ajlan Department of Radiology, King Abdulaziz University Hospital, Jeddah, Saudi Arabia

Donya A. Al-Hassan Department of Radiology, St Paul's Hospital, Vancouver, BC, Canada

Fabian Bamberg Department of Clinical Radiology, Ludwig-Maximilians University, Marchioninistrasse, Munich, Germany

Gorka Bastarrika Cardiothoracic Imaging, Department of Medical Imaging, Sunnybrook Health Sciences Centre, Toronto, ON, Canada

Christoph Becker Department of Clinical Radiology, Ludwig-Maximilians University, Munich, Germany

Bernhard Bischoff Department of Clinical Radiology, Ludwig-Maximilians University, Munich, Germany

Daniel T. Boll Department of Radiology, Duke University Medical Center, Durham, NC, USA

Young Jun Cho Department of Radiology, Konyang University College of Medicine, Daejeon, Korea

Yeon Hyeon Choe Department of Radiology and Cardiovascular Imaging Center, Samsung Medical Center, Sungkyunkwan University School of Medicine, Seoul, Korea

Ullrich Ebersberger Department of Cardiology and Intensive Care Medicine, Heart Center Munich-Bogenhausen, Munich, Germany

Lucas L. Geyer Department of Clinical Radiology, University Hospitals, Ludwig-Maximilians University, Munich, Germany

Tobias J. Heye Department of Radiology, Duke University Medical Center, Durham, NC, USA

J. Matthias Kerl Department of Diagnostic and Interventional Radiology, Goethe-University Frankfurt am Main, Frankfurt, Germany

Teruhito Kido Department of Radiology, Ehime University School of Medicine, Shitsukawa Toon Ehime, Japan

Sung Min Ko Department of Radiology, Konkuk University Hospital, Konkuk University School of Medicine, Gwangjin-gu, Seoul, Korea

Akira Kurata Department of Radiology, Ehime University School of Medicine, Shitsukawa Toon Ehime, Japan

Jonathon Leipsic Department of Radiology, St Paul's Hospital, Vancouver, BC, Canada; The Division of Nuclear Medicine, Department of Radiology, Providence Health Care, University of British, Vancouver, BC, Canada

Daniel Lubbers Center for Medical Imaging—North East Netherlands, University of Groningen, University Medical Center Groningen, Groningen, The Netherlands; Department of Radiology, Nij Smellinghe Hospital, Drachten, The Netherlands

Andreas H. Mahnken Department of Radiology, Marburg University Hospital, Philipps University, Marburg, Germany

Daniele Marin Department of Radiology, Duke University Medical Center, Durham, NC, USA

Felix G. Meinel Division of Cardiovascular Imaging, Department of Radiology and Radiological Sciences, Medical University of South Carolina, Charleston, SC, USA

Teruhito Mochizuki Department of Radiology, Ehime University School of Medicine, Shitsukawa Toon Ehime, Japan

John W. Nance Jr. Russell H. Morgan Department of Radiology and Radiological Science, Johns Hopkins Hospital, Baltimore, MD, USA

Konstantin Nikolaou Department of Clinical Radiology, Ludwig-Maximilians University, Munich, Germany

Narinder S. Paul Joint Department of Medical Imaging and the Peter Munk Cardiac Centre, Toronto General Hospital, University of Toronto, Toronto, ON, Canada

Balazs Ruzsics Royal Liverpool and Broadgreen University Hospital, Liverpool, UK

U. Joseph Schoepf Department of Radiology and Radiological Science, Medical University of South Carolina, Charleston, SC, USA; Division of Cardiology, Department of Medicine, Medical University of South Carolina, Charleston, SC, USA

Justin R. Silverman Department of Radiology and Radiological Science, Medical University of South Carolina, Charleston, SC, USA

Rozemarijn Vliegenthart Center for Medical Imaging—North East Netherlands, University of Groningen, University Medical Center Groningen, Groningen, The Netherlands; Department of Radiology, University of Groningen, University Medical Center Groningen, Groningen, The Netherlands

Abbreviations

ABG	Coronary artery bypass grafting
ACS	Acute coronary syndrome
ACS	Acute coronary syndrome
AP	Angina pectoris
ATP	Adenosine triphosphate
CABG	Coronary artery bypass graft
CABG	Coronary artery bypass grafting
CAD	Coronary artery disease
CAD	Coronary artery disease
CAD	Coronary artery disease
CAD	Coronary artery disease
CAD	Coronary artery disease
CCA	Conventional coronary angiography
CCTA	Coronary computed tomography angiography
cCTA	Coronary computed tomography angiography
CCTA	Coronary CT angiography
cCTA	Coronary CT angiography
CHF	Congestive heart failure
CMR	Cardiac magnetic resonance
CT	Computed tomography
CT	Computed tomography
CTP	CT stress myocardial perfusion
CTP	Myocardial perfusion computed tomography
DECT	Dual-energy computed tomography
DECT	Dual-energy computer tomography
DSCT	Dual-source computed tomography
DSE	Dobutamine stress echocardiography
ECG	Electrocardiography
ED	End diastolic
ED	End-systole
EF	Ejection fraction
ES	End systolic
ES	End-systole
FDG	Fluorine-18-labeled deoxyglucose
FFR	Coronary fractional flow reserve
FFR	Fractional flow reserve
FFR	Fractional flow reserve
HU	Hounsfield Unit
ICA	Invasive coronary angiography
ICA	Invasive coronary angiography
ICA	Invasive coronary angiography
IVUS	Intravascular ultrasound
LA	Left atrium

LDA	Low-density area
LGE	Late Gadolinium enhancement
LV	Left ventricle
LV	Left ventricular
LV	Left ventricular
LVEF	Left ventricular ejection fraction
MBF	Myocardial blood flow
MBF	Myocardial blood flow
MBF	Myocardial blood flow
MDCT	Multi-detector computed tomography
MDCT	Multidetector computed tomography
MDCT	Multidetector CT
MDCT	Multidetector CT
MDCT	Multidetector-row CT
MI	Myocardial infarction
MI	Myocardial infarction
MI	Myocardial infarction
MPI	Myocardial perfusion imaging
MPS	Myocardial perfusion scintigraphy
MPS	Myocardial perfusion scintigraphy or SPECT
MR	Magnetic resonance
MRI	Magnetic resonance imaging
MRP	MRI stress myocardial perfusion
MRPI	Magnetic resonance myocardial perfusion imaging
MVO	Microvascular obstruction
NPV	Negative predictive value
NPV	Negative predictive value
NPV	Negative predictive value
PCI	Percutaneous coronary intervention
PCI	Percutaneous coronary intervention
PCI	Percutaneous coronary intervention
PET	Positron emission tomography
PET	Positron emission tomography
PPV	Positive predictive value
PPV	Positive predictive value
PPV	Positive predictive value
PTP	Pretest probability
RA	Right atrium
RV	Right ventricle
RVEF	Right ventricular ejection fraction
RVOT	Right ventricular outflow tract
SPECT	Single photon emission computed tomography
SPECT	Single photon emission computed tomography
SPECT	Single-photon emission computed tomography
Tc	Technetium
TCFA	Thin-cap fibroatheroma

Part I
Structure

Coronary CT Angiography: State of the Art

John W. Nance Jr.

Contents

Abstract

Technical advancements in computed tomography have provided the basis for safe, rapid, noninvasive detection of coronary artery disease with high diagnostic accuracy. While there are well-established limitations in the pure anatomic assessment of coronary atherosclerosis, there is a growing body of data demonstrating that coronary computed tomography angiography provides valuable prognostic information and may have outcome and cost benefits over traditional diagnostic testing in selected clinical scenarios. Appropriate utilization necessitates proper technique and patient selection. The exact clinical role of computed tomography-based anatomic assessment of coronary artery disease is still evolving, and emerging techniques are encouraging for improved performance and expanded applications in the future.

Abbreviations

ACS	Acute coronary syndrome
AP	Angina pectoris
CABG	Coronary artery bypass graft
CAD	Coronary artery disease
cCTA	Coronary computed tomography angiography
IVUS	Intravascular ultrasound
ICA	Invasive coronary angiography
MI	Myocardial infarction
NPV	Negative predictive value
PCI	Percutaneous coronary intervention
PPV	Positive predictive value
PTP	Pretest probability
TCFA	Thin-cap fibroatheroma

J. W. Nance Jr. (✉)
House Officer, Russell H. Morgan Department of Radiology and Radiological Science, Johns Hopkins Hospital, Baltimore, MD, USA
e-mail: jnance5@jhmi.edu

U. J. Schoepf et al. (eds.), *CT Imaging of Myocardial Perfusion and Viability*, Medical Radiology. Diagnostic Imaging,
DOI: 10.1007/174_2012_767, © Springer-Verlag Berlin Heidelberg 2012
Published Online: 16 November 2012

1 Introduction

Anatomic assessment of the coronary arteries began in earnest in 1958 with Dr. F. Mason Sones's inadvertent injection of contrast material into the right coronary artery of a patient undergoing a diagnostic aortogram (Bruschke et al. 2009). Since then, invasive coronary angiography (ICA) has had a profound effect on the understanding and management of coronary artery disease (CAD). ICA remained the dominant option for the anatomic evaluation of the coronary arteries for nearly 40 years, when rapid advances in computed tomography technology began to produce the temporal and spatial resolution necessary for reliable imaging of the heart and its vessels. The introduction of 64-detector computed tomography systems in 2004 moved coronary computed tomography angiography (cCTA) beyond feasibility testing into clinical practice. Predictably, the abilities and clinical role of cCTA are still evolving. While the high negative predictive value (NPV) of cCTA has provided the basis for endorsement by the major cardiovascular and radiological societies for certain indications, much more high-quality data will be necessary before we can expect a true paradigm shift in the approach to CAD diagnosis and management.

1.1 Basis for Anatomic Imaging of the Coronary Arteries

As this book emphasizes, comprehensive evaluation of the myocardium necessitates much more information than simply identifying and characterizing atherosclerotic disease. Yet assessment of coronary artery morphology plays a major role in establishing a diagnosis, risk-stratification, and therapeutic management in patients with suspected CAD. The current clinical reliance on coronary anatomy is a factor of both pathophysiological and historical factors.

The clinical manifestations of myocardial ischemia can be broadly classified into two categories on the basis of chronicity and underlying pathophysiology—ischemic equivalent chest pain syndrome (angina pectoris or angina equivalent; AP) and acute coronary syndrome (ACS). In both situations, coronary atherosclerosis is the underlying cause in the vast majority of patients. Myocardial ischemia is a result of an imbalance between myocardial oxygen demand and myocardial oxygen delivery. Oxygen demand is a function of heart rate, myocardial contractility, and left ventricular wall stress, which are increased in periods of physical exertion or mental stress. Since myocardial oxygen extraction is nearly maximal at rest, the normal physiological response to increased demand is coronary artery vasodilatation resulting in increased myocardial blood flow. The ability to increase coronary flow over that at rest is termed coronary flow reserve. Atherosclerotic narrowing of the coronary arteries causes a fall in pressure across the stenosis as predicted by the Hagen–Poiseuille equation, with the drop in perfusion across the stenosis inversely proportional to the fourth power of the minimal luminal diameter. Mild stenosis has a negligible hemodynamic effect; however, luminal diameter narrowing above ≈ 50 % causes recruitment of flow reserve at rest (Hendel 2009) resulting in decreased exercise capacity and possibly causing exertional ischemia, clinically manifested as stable AP. At ≈ 80 % luminal diameter narrowing, the coronary reserve is totally recruited at rest, and symptoms of unstable AP may result. This relationship between atherosclerotic coronary artery narrowing and decreased myocardial oxygen delivery forms the basis for anatomic imaging in patients with suspected CAD.

In contrast to stable chest pain syndromes, myocardial ischemia in ACS is usually secondary to sudden rupture of a preexisting atherosclerotic coronary artery lesion, again leading to a mismatch in myocardial oxygen supply and demand. The severity of blood flow reduction will affect the clinical manifestation, ranging from ischemia (unstable AP) to varying levels of myocardial necrosis (myocardial infarction; MI). The likelihood of plaque rupture is more closely related to plaque morphology than stenosis severity (Virmani et al. 2002); however, significant luminal narrowing is detected in nearly all patients with MI at subsequent ICA (Roe et al. 2000), forming the basis for anatomic imaging in cases of acute chest pain/suspected ACS.

Our understanding of the pathogenesis of CAD continues to evolve. While early clinicians worked on the assumption that there was a fairly simple relationship between coronary atherosclerosis and disease manifestation, there is now abundant data showing that the clinical relevance of CAD is related to a host of other factors. Furthermore, correlation between diameter stenosis and functional relevance (likelihood of producing clinically significant ischemia) is suboptimal (see below). The widespread use of ICA over the past half-century, however, has led to abundant data supporting its value. CAD assessment using a simple 1-, 2-, or 3-vessel obstructive disease grading scheme is one of the most important prognostic factors in patients with coronary artery disease, and coronary morphology has been firmly incorporated into clinical guidelines of CAD management, particularly when revascularization is considered (Patel et al. 2012a, b; Smith et al. 2011).

1.2 Limitations

1.2.1 Limitations of Anatomic Imaging

With the advent of new diagnostic tests, such as myocardial perfusion imaging and direct measurements of coronary artery perfusion pressure, we have learned that anatomic imaging results correlate poorly with the functional relevance of disease. It is especially difficult to predict the relevance of intermediate severity lesions (50–70 % stenosis). Many factors outside the coronary arteries have been identified that play a role in myocardial blood flow, including ventricular hypertrophy, microvascular disease, the metabolic state of the myocardium itself, and collateral vessel formation. In addition, the common 1-, 2-, and 3-vessel obstructive disease ranking employed by anatomic imaging tests does not include information on the length of stenoses, plaque morphology, or entrance and exit angles, all of which have been shown to affect pressure gradients (Mark et al. 2010). Anatomic imaging in patients with acute chest pain is also problematic, as ACS is often caused by rupture of a mild/moderate stenosis, with culprit lesions displaying less than 70 % stenosis in up to 80 % of patients with ACS (Roe et al. 2000).

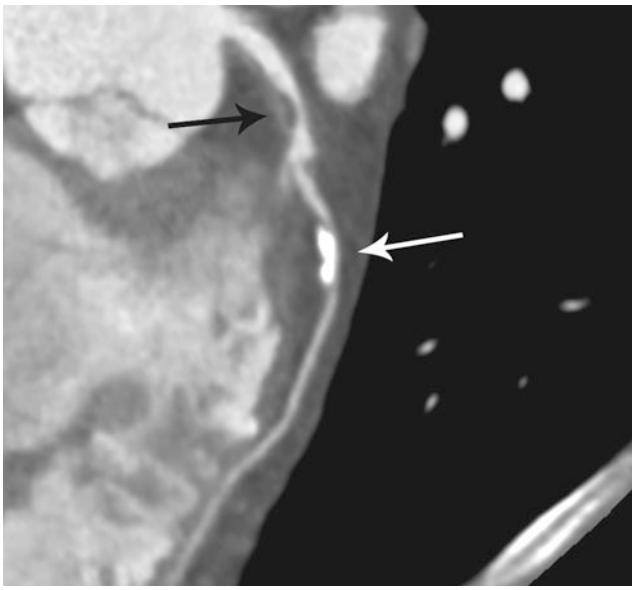

Fig. 1 The degree of stenosis from a distal left anterior descending coronary artery calcified plaque (*white arrow*) is difficult to determine due to blooming artifacts. Compare to the more proximal noncalcified plaque, more easily characterized as causing a 60 % stenosis (Image courtesy of Dr. Stefan Zimmerman, Johns Hopkins Hospital, Baltimore, Maryland, USA)

1.2.2 Technical Limitations of cCTA

Despite advances in cCTA technology, attaining diagnostic-quality studies remains problematic in patients with extremely fast or irregular heart rates (cardiac motion, stair-step artifacts), obese patients (quantum mottle, poor signal to noise ratio), and those who are unable to perform an adequate breath-hold (respiratory motion). While ICA is able to provide temporal resolution of approximately 33 ms, cCTA is currently limited to 75–175 ms. Considering that the translational motion of the coronary arteries ranges from 30 to 90 mm/s at higher heart rates (Lu et al. 2001), some authors have proposed that temporal resolution of 30–50 ms will be necessary for "motion-free" imaging (Lu et al. 2001; Otero et al. 2009). In addition, quantitative imaging of CAD using cCTA remains limited by spatial resolution, with cubic voxels in current scanners ranging from 0.35 to 0.5 mm per edge (Otero et al. 2009) compared with approximately 0.15 mm^3 in ICA. This results in a typical coronary artery (3 mm) being represented by approximately half as many voxels in cCTA compared to ICA (9 vs. 18 voxels, respectively) and precluding the establishment of cCTA as a clinically reliable method for atherosclerosis quantification. Further advances in temporal and spatial resolution should continue to mitigate these limitations.

cCTA evaluation of individuals with high levels of coronary artery calcium has also traditionally been considered problematic. Blooming artifacts can limit assessment of the coronary lumen and result in overestimation of stenosis severity (Fig. 1). A recent meta-analysis, however, found that newer scanners (64-detector and higher) provided high sensitivities and specificities in patients with severe coronary calcifications (den Dekker et al. 2012); in addition, newer acquisition and reconstruction techniques may continue to decrease the impact of coronary artery calcium on the diagnostic accuracy of cCTA (Renker et al. 2011; Schwarz et al. 2012).

1.2.3 Limitations in the Currently Available Evidence for cCTA

There are increasing calls throughout medicine for high-quality evidence establishing the value of diagnostic tests, including cCTA. While the exact methodology for diagnostic imaging validation is not yet established, the evidence required to establish a test as valuable, both on an individual and societal level, generally follows a certain pattern. First, of course, the safety of the test must be established, followed by validation of diagnostic accuracy against a reference standard. The value of prognostic data are increasingly emphasized, as is the ultimate effect on clinical management and outcomes. Finally, the growing economic impact of healthcare throughout the developed world has led to greater emphasis on cost-effectiveness analyses. The quality of the evidence, of course, is also important, with greater weight given to data from large-scale, multicenter randomized trials.

Table 1 Limitations in the currently available evidence for cCTA, stratified by generalized data parameters

Diagnostic accuracy
Most reports consist of single-center studies conducted at academic centers with considerable experience in cCTA, limiting the applicability to mainstream clinical practice
There are limited data for newer techniques utilizing dose-saving techniques; the high diagnostic accuracy seen in most studies is therefore accompanied by relatively high radiation exposure
High variability in treatment of small, highly calcified, or otherwise uninterpretable coronary artery segments; i.e., some studies utilize intent-to-treat designs, others exclude these segments
Technical advancements continue to occur at a rate that quickly renders results obsolete
Anatomic endpoints may be inferior to functional endpoints in guiding patient care
Most studies define "obstructive disease" as stenosis $\geq$ 50 %, and this endpoint is compared to ICA; however, management often relies on the identification of $\geq$ 70 % stenosis
Outcome variables are heterogeneous and may not be clinically validated
Most studies use populations referred for ICA, resulting in inherent referral bias
Asymptomatic patients, acutely symptomatic patients, and/or those with known CAD are variably included and/or combined in analyses, limiting the applicability of data to established clinical indications
Prognosis
Limited large-scale trials currently available
Significant inter- and intra-study heterogeneity in patient populations limits the applicability of data to established clinical indications
CAD classification and reporting are variable and are not limited to standard/recommended clinical practice. In addition, the diagnostic accuracy of more advanced CAD reporting is not well established
Most studies include coronary revascularization as an endpoint, which may not have been warranted or may have been performed as a result of cCTA findings, leading to verification bias
There is low incidence of adverse cardiac outcomes, especially when revascularization is excluded or when all-cause mortality is used as the primary endpoint. Therefore, large cohorts with specific inclusion criteria and long follow-up is required
There are variable risk and prevalence in certain subpopulations (e.g., younger patients (Min et al. 2011), female patients (Shaw et al. 2010), African Americans (Nance et al. 2011), and diabetics (Van Werkhoven et al. 2010))
Economic impacts and effects on clinical management and outcomes
Limited large-scale randomized trials, with data primarily coming from small single-center observational cohorts, larger cohorts utilizing insurance claims data, or simulation models based on prior data
Significant disagreement on the value of different endpoints (for example, cost/quality-adjusted life year, cost/correct diagnosis, incremental cost-effectiveness ratio, etc.)
High variability in patient populations between studies (especially pretest probability) has led to significantly different conclusions
The influence of cCTA utilization on the non-surgical management of CAD is particularly inconclusive from the available data
The effects and optimal management of incidentally detected findings are not well established

Compared to other cardiac imaging techniques, cCTA is relatively young, and this is reflected in the quantity of available evidence. There are limited large-scale trials, especially regarding prognosis, outcomes, and cost-effectiveness. In addition, the data that are available are often subjected to heterogeneous patient populations (which do not clearly reflect the indications set forth in current clinical guidelines), referral bias, and marked variability in experimental design. More detailed limitations in the evidence are provided in Table 1. As such, the clinical role of cCTA is evolving rapidly as new data become available. Fortunately, several large-scale, well-designed trials are underway that should provide considerable value in optimizing cCTA utilization.

1.3 Current Use of Anatomic Data from cCTA

The high NPV of cCTA for the detection of obstructive CAD ($\geq$ 50 % stenosis) forms the basis for currently accepted clinical utilization (Fig. 2). Of note, more advanced characterization of CAD (e.g. quantification, plaque morphological analysis, etc.) is considered experimental at this time. Broadly speaking, cCTA is considered acceptable to detect atherosclerosis in patients with suspected CAD, to rule out significant disease in patients presenting with acute chest pain, to rule out an ischemic etiology in patients without known CAD and new-onset heart failure, for the detection of CAD prior to noncoronary cardiac surgery, and for risk assessment in patients with

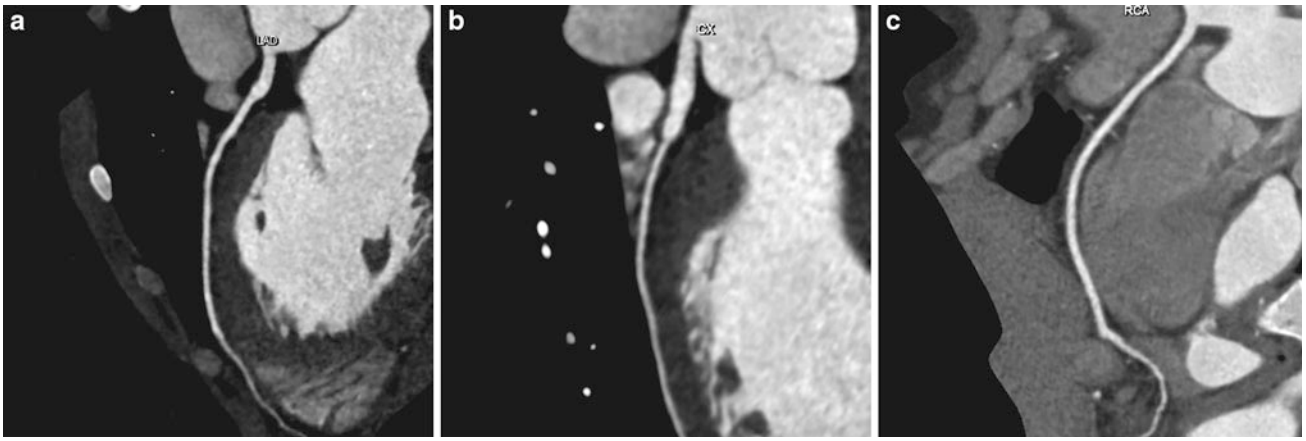

Fig. 2 Normal cCTA shows left anterior descending (**a**), left circumflex (**b**), and right (**c**) coronary arteries without evidence of atherosclerosis (Images courtesy of Dr. Stefan Zimmerman, Johns Hopkins Hospital, Baltimore, Maryland, USA)

prior percutaneous coronary intervention (PCI) or coronary artery bypass graft (CABG) (Taylor et al. 2010). Optimal integration of cCTA into clinical practice requires the ordering physician to consider all diagnostic and prognostic data available before the test is performed and integrate that information with cCTA results. In addition, the abilities (i.e., high sensitivity) and limitations (i.e., limited positive predictive value) of cCTA must be considered within the clinical situation. Finally, the relative value of alternative diagnostic strategies should be considered in each individual scenario.

The preceding considerations are reflected in the current guidelines for acceptable use of cCTA. The pretest probability (PTP) of disease is an integral component of diagnostic decision-making (Taylor et al. 2010). For example, a patient presenting to the emergency department with acute chest pain and high PTP of significant CAD will likely receive ICA regardless of cCTA results, resulting in increased costs with minimal effect on outcomes or management. Consider, however, a similar patient with low-to-intermediate PTP. The high NPV of cCTA results in the test being well suited to rule out significant CAD in a large proportion of this population, allowing fast, safe discharge (Bamberg et al. 2012). Similar Bayesian techniques should be used on an individual basis for other indications.

2 Technique

There are two basic goals in the acquisition, reconstruction, and interpretation of cCTA examinations: provide maximum diagnostic value while minimizing radiation dose. Newer technologies have increased the quality of anatomic imaging while decreasing ionizing radiation burden; however, proper patient selection, preparation, and post-processing are still vital for optimal performance. This section will highlight the most important considerations and advances in cCTA techniques.

2.1 Patient Selection and Preparation

As noted above, there are multiple patient-specific factors that have a dramatic effect on image quality. Obese patients will require increased tube output for adequate images, and very obese patients should not undergo cCTA. The patients must be able to hold their breath for the duration of the scan, which will be variable depending on the hardware and specific acquisition protocol employed. Patients with very high heart rates or irregular heart rhythms should be carefully assessed and possibly excluded. Preprocedural beta-blocker administration may be used in some cases to reduce heart rate. In addition, some institutions routinely administer nitroglycerin to promote coronary artery vasodilatation and improve image quality. Finally, optimal cCTA acquisition necessitates adequate opacification of the coronary artery lumen; therefore, vascular access must be adequate for high flow rate (4–6 mL/s) administration of intravenous contrast material. Appropriate contrast bolus timing is vital, and both test-bolus and automated bolus tracking techniques can be used.

2.2 Dataset Acquisition

The characteristics of the raw dataset are a major determinate of ultimate image quality. The major parameters influencing the quality of subsequently reconstructed axial 2D images will be spatial and temporal resolution. In addition, detector coverage and acquisition time play a role

in the quality of the examination along the z-axis, affecting subsequent multiplanar and 3D reconstructions. It is important to note that while technical advances are often presented as a solution for a specific imaging parameter (e.g., increased volumetric coverage to improve quality along the z-axis), they usually affect other parameters as well, not always positively.

2.2.1 Temporal Resolution

Temporal resolution is largely a function of the time necessary to acquire a full 360° dataset. As noted above, some authors have proposed that temporal resolution of 30–50 ms will be necessary for true "motion-free" imaging (Lu et al. 2001; Otero et al. 2009). The most obvious method of improving temporal resolution is via faster gantry rotation times, which are now as low as 280–400 ms. However, further improvements will be limited by the mechanical properties of current components, as massive centrifugal forces are generated with such rotational speeds, especially with the increasing mass of wide-detector arrays. Additional techniques to improve temporal resolution include the utilization of half-scan reconstructions (since 360° of data may be acquired with one half gantry rotation). The advent of "dual-source" scanners, containing two sets of X-ray sources and detectors offset at 90°, has allowed further improvement via quarter-scan reconstructions. There are tradeoffs, as both half-scan and quarter-scan reconstruction is subject to misregistration artifacts, and dual-source CT techniques increase X-ray cross-scatter. Multisegment reconstruction, using combined data from adjacent slices, is also available, but has the disadvantage of necessitating decreased pitch, increasing dose, and overall acquisition time. Different commercial products provide specific combinations of these features, and temporal resolution varies accordingly, with the most popular current systems providing resolution of 75–175 ms.

2.2.2 Spatial Resolution

Both intrinsic limitations and reconstruction techniques contribute to the ultimate spatial resolution of cCTA. While spatial resolution is scientifically measured as the minimal allowable distance between 2 structures before they cannot be recognized as separate, voxel size is often used as an indirect surrogate for spatial resolution in cCTA. The x–y lengths are a function of intrinsic CT limitations (e.g., focal spot size and sampling density) and reconstruction techniques, while the z-axis length is largely a function of detector width. As explained above, current voxel dimensions of approximately 0.5 mm^3 are considered adequate for qualitative assessment of the major coronary artery segments but are considered inadequate for quantitative imaging or evaluation of extremely small coronary vessels.

The signal-to-noise ratio, which is related to spatial resolution, is an important consideration as detector widths continue to decrease. Either increased dose, improved reconstruction techniques, or increased detector efficiency will be necessary to maintain adequate photon collection. Technical advances will also be required to compensate for photon loss with improvements in gantry rotation and scan acquisition times.

2.2.3 Volumetric Coverage

The advent of multidetector CT systems, providing increased volumetric (z-axis) coverage with each gantry rotation, was arguably the initial technical advancement that led to the growth of cCTA. While improvements in spatial and temporal resolution have led to improved diagnostic accuracy, the initial feasibility of coronary imaging necessitated full cardiac volume acquisitions in a single breathhold. With increased detectors, fewer rotations of the gantry are necessary to provide complete coverage and total acquisition time is decreased. Continued advancements have led to decreased stair-step artifacts, respiratory motion artifacts, and misregistration artifacts. Faster acquisition times also reduce the significance of heart rhythm abnormalities. Currently, 256- and 320-channel systems have been developed, providing coverage up to 160 mm with a single gantry rotation. These wide-detector systems have made single heartbeat acquisitions a reality. However, while isophasic datasets may intuitively seem attractive, they may not be necessary for anatomic imaging, and the most recent advances in volumetric coverage are driven as much by the prospect of myocardial perfusion imaging as a desire for improved anatomic assessments. Indeed, the wide-cone X-ray beams used for extended z-axis coverage in some systems may come at the expense of decreased spatial resolution from cone-beam artifact, scatter, or roof-top effect. At this time, most of these systems have not been validated as thoroughly as more traditional 64-slice scanners.

Another technique has been introduced to decrease scan acquisition times by using a high-pitch (3.4) spiral acquisition rather than complete cardiac volumetric coverage. This acquisition protocol, which is available in patients with low (< 60 beats/minute) and stable heart rates, can acquire a complete dataset in 250 ms, within one cardiac cycle. The technique also results in very low-radiation dose (Fink et al. 2011).

2.3 Image Reconstruction and Interpretation

Multiple phases of the cardiac cycle will be available following a retrospectively ECG-gated cCTA acquisition. Either automated or manual means should be used to

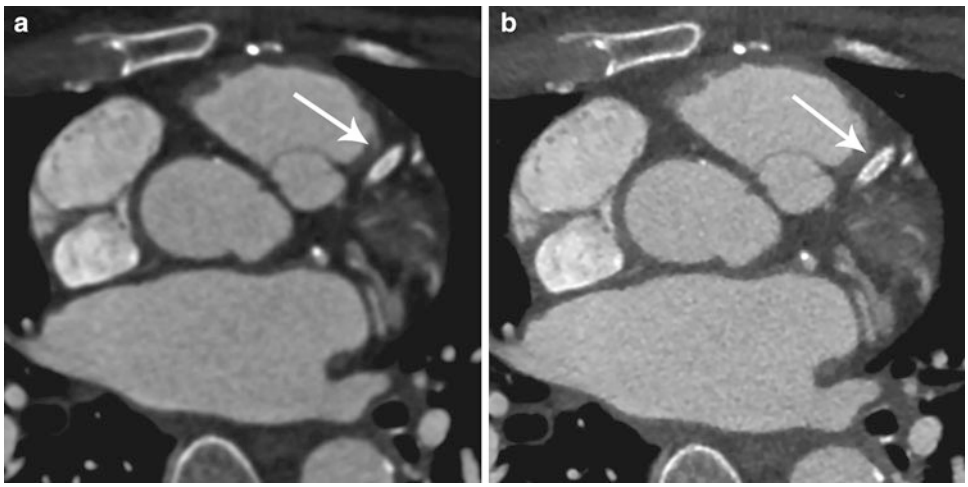

Fig. 3 Filtered back projection reconstruction (**a**) provides inferior spatial resolution compared to iterative reconstruction (**b**) in the assessment of a left anterior descending coronary artery stent (*arrow*) (Images courtesy of Dr. Stefan Zimmerman, Johns Hopkins Hospital, Baltimore, Maryland, USA)

determine the optimal phase for coronary analysis. The appropriate cardiac phase may vary between the left and right coronary circulation. Traditional cCTA dataset reconstruction utilizes filtered back projection techniques; however, there is an increasing interest in iterative reconstruction, which has become more practical with increased computing power. Preliminary data suggest that the greatest role for iterative reconstruction may be in radiation dose reduction, as image quality is maintained at decreased tube currents (Leipsic et al. 2010). Iterative reconstruction may also result in improved image quality (Fig. 3), particularly in the assessment of heavily calcified vessels and stents (Renker et al. 2011).

Most authors advocate the use of several different reconstructions for cCTA anatomical interpretation. Axial images are traditionally used for primary analysis; furthermore, abnormalities seen on additional reformations should be confirmed with axial source images. Multiplanar imaging is available, allowing visualization of the coronary arteries in short- or long-axis, and curved multiplanar reformations allow single-image display of the entire coronary artery length and rotation of the artery along its long axis. Thick-slab maximum intensity projections provide a vascular map, while volume-rendered 3D images allow an overview of coronary anatomy, especially in cases of CABG, but are inadequate for assessment of the coronary artery lumen (Fig. 4).

Computer-aided detection and automated atherosclerosis characterization and quantification programs are becoming increasingly available, and some have shown promising preliminary results (Arnoldi et al. 2009; Blackmon et al. 2009); however, manual assessment remains the mainstay of interpretation at this time. While the current evidence for cCTA is based on relatively simple reporting schemes (similar to ICA), several groups have published studies suggesting the value of more complicated reporting and scoring systems (Chow et al. 2011b ; Kazmi et al. 2011; Min et al. 2007). The Society of Cardiovascular Computed Tomography published a consensus document on cCTA interpretation and reporting in 2009 (Raff et al. 2009a), and we anticipate more guidance and standardization as techniques and data evolve.

3 cCTA in Stable Patients with Suspected CAD

The initial diagnostic evaluation of patients without known CAD presenting with stable chest pain or angina equivalent is complex. Optimizing diagnosis and management of these patients, however, is a major priority considering the scope of the disease and its current and future economic impact. Several strategies are available for initial diagnostic workup, including direct ICA, exercise ECG, exercise and pharmacologically stressed scintigraphy, exercise and pharmacologically stressed echocardiography, and stress magnetic resonance imaging. Anatomic imaging with cCTA has been proposed as a fast, reliable, and possibly cost-effective modality for the initial approach to suspected CAD; in addition, cCTA may have a role as a "gatekeeper" to ICA in certain patients with nondiagnostic or equivocal functional test results.

Currently available evidence on diagnostic accuracy, prognostic value, and effects on outcomes and costs highlight both the advantages and limitations of the technique. Repeatedly, the data show the importance of proper patient selection in order for cCTA to provide cost-effective

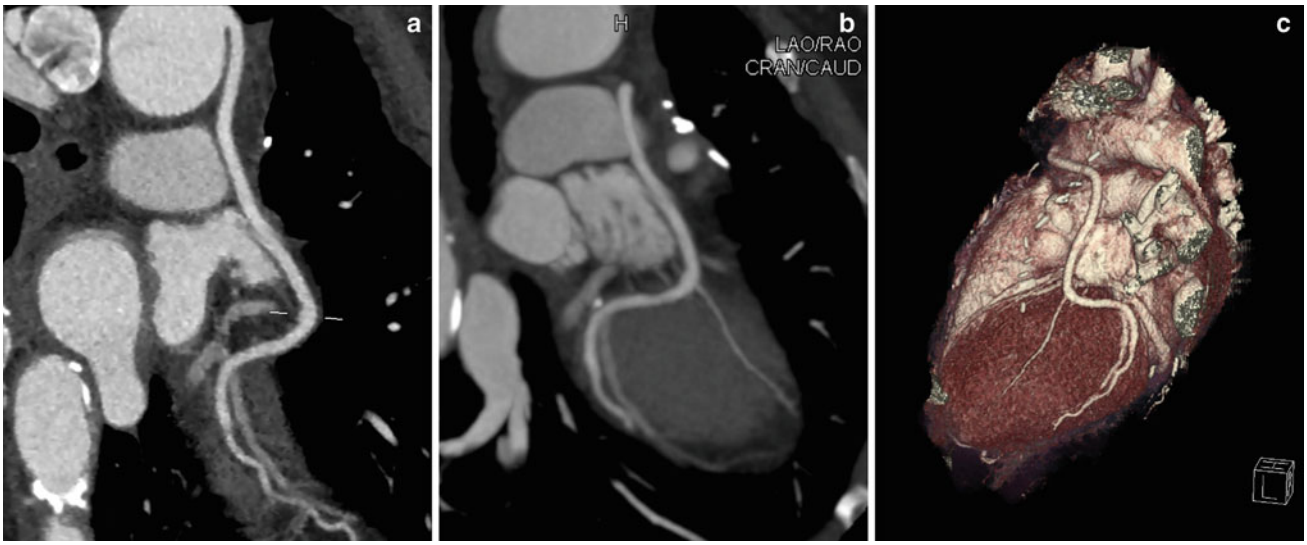

Fig. 4 Curved multiplanar reformation (**a**), thick-slab maximum intensity projection (**b**), and 3D volume rendering (**c**) reconstructions play a role in the assessment of a saphenous vein coronary artery bypass graft to the left circumflex territory (Images courtesy of Dr. Stefan Zimmerman, Johns Hopkins Hospital, Baltimore, Maryland, USA)

therapeutic value. Patient populations with low to intermediate prevalence of disease are most likely to benefit from evaluation with cCTA, while high CAD prevalence increases costs and radiation burden without a positive effect on outcomes.

3.1 Diagnostic Accuracy

Hundreds of studies on various aspects of cCTA diagnostic accuracy have been published over the past decade. As highlighted in Table 1, there are multiple limitations in the available evidence; however, the available data are promising. cCTA consistently shows high diagnostic accuracy to detect obstructive CAD with ICA as the reference standard (Fig. 5). The reported sensitivity and NPV of cCTA are particularly notable, often approaching 100 % in meta-analyses (Mowatt et al. 2008; Sun and Ng 2012). Larger prospective multicenter studies are limited, with only 4 such studies using exclusively 64-slice scanners or higher currently available. Two of the studies include patients with known CAD (Miller et al. 2008) or unstable patients (Meijboom et al. 2008); predictably, the prevalence of CAD was high in these cohorts (56 and 68 %, respectively). Prevalence of 68 % might be expected to negatively impact NPV; however, the authors demonstrated an impressive NPV of 97 %. The other two studies are more applicable in our population. ACCURACY, which included only stable patients being referred to ICA for stable chest pain syndrome and/or abnormal stress test results, had the lowest prevalence of disease, 25 %. Predictable, NPV was excellent in this cohort (99 %) (Budoff et al. 2008).

The positive predictive value (PPV) of cCTA is more limited (ranging from 64–97 % in the 4 prospective studies mentioned above), especially in higher prevalence populations. This could lead to unnecessary, costly, and possibly dangerous subsequent workup, and highlights the need for clinicians to perform robust pretest assessments and order the examination only when appropriate. Further study of cCTA diagnostic accuracy should also increase the evidence comparing cCTA to other noninvasive modalities, such as myocardial perfusion scintigraphy.

3.2 Prognostic Value

The highest-level evidence on the prognostic value of cCTA in stable symptomatic patients uniformly demonstrate the value of cCTA as a rule out test, with a normal scan associated with annualized major adverse cardiac event rates ranging from 0.17 to 0.4 % (Bamberg et al. 2011; Hulten et al. 2011) and all-cause mortality rates ranging from 0.28 to 0.36 % (Chow et al. 2011b; Min et al. 2011). These data support the evidence showing the high NPV of cCTA and compare favorably with other diagnostic strategies, including ICA, myocardial perfusion scintigraphy, and stress echocardiography (Lichtlen et al. 1995; Metz et al. 2007; Shaw and Iskandrian 2004). While the length of protection afforded by a normal cCTA examination is not well-established, one analysis of 1,816 patients with at least 4-year follow-up showed annualized death rates of only 0.22 % (Min et al. 2011), suggesting that 4 years may be a reasonable post-test interval. Current evidence also suggests that there is prognostic value in the detection of obstructive

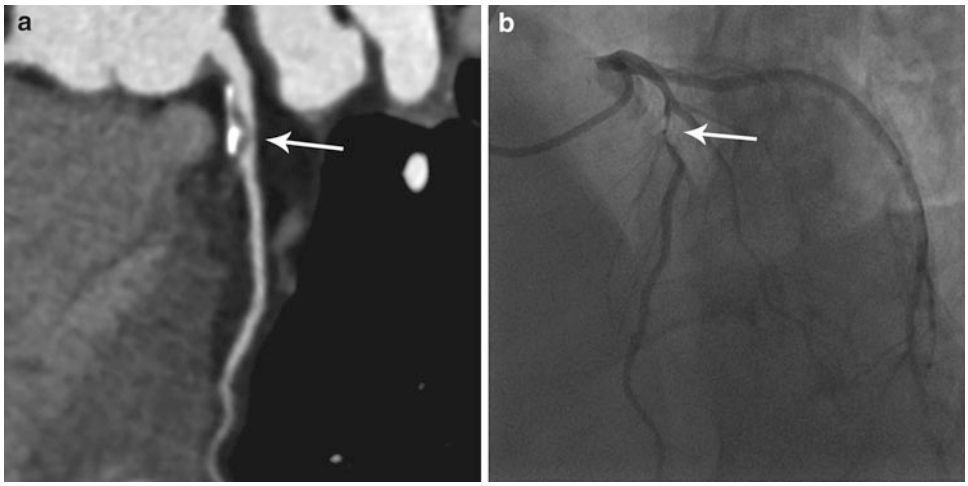

Fig. 5 An obstructive plaque (*arrows*) was detected in the proximal left anterior descending artery on cCTA (**a**), determined to represent an 80–90 % stenosis on subsequent ICA (**b**) (Images courtesy of Dr. Stefan Zimmerman, Johns Hopkins Hospital, Baltimore, Maryland, USA)

disease, with significantly increased rates of major adverse cardiac events (annualized rates up to 11.9 % in one meta-analysis (Bamberg et al. 2011)) and all-cause mortality (up to 2.9 % (Chow et al. 2011b)) in patients with obstructive disease. The prognostic value of more advanced analyses, such as plaque morphology and segmental stenosis scoring, is also being examined and is discussed below in Emerging Applications.

An ongoing goal is to establish the incremental prognostic value of cCTA beyond more established tests. Early data are favorable, with several studies showing increased prognostic value over coronary artery calcium scoring (Bamberg et al. 2011; Hadamitzky et al. 2011) and myocardial perfusion scintigraphy (Shaw et al. 2008; van Werkhoven et al. 2009). In addition, researchers are seeking to refine the population-specific prognostic value of cCTA, e.g., in younger patients, females, or diabetics.

3.3 Outcomes and Costs

There are substantial methodological weaknesses in all of the currently available data on outcomes and costs of cCTA in stable symptomatic patients; however, two large-scale randomized clinical trials are currently underway. The RESCUE trial will compare cCTA to myocardial perfusion scintigraphy in 4,300 patients with stable angina or angina equivalent and the PROMISE trial will compare cCTA to traditional stress testing (ECG, echocardiography, or scintigraphy) in 10,000 symptomatic patients with low to intermediate PTP of CAD. Both studies will follow patients to compare outcomes and costs.

Until then, we must rely on the available observational cohorts and simulation models, which currently suggest that cCTA provides incremental cost-benefit (cost/correct diagnosis) and cost-effectiveness (cost/quality adjusted life year) compared with alternative strategies in populations below a certain prevalence of disease. These data are variably driven by improved outcomes using cCTA-based strategies (Ladapo et al. 2009), decreased costs (Dorenkamp et al. 2011; Genders et al. 2009; Min et al. 2008a), or some combination. Importantly, no current data have shown adverse outcomes when cCTA is used. cCTA has not been shown to be cost-effective in populations with PTP greater than 37–55 % (Dorenkamp et al. 2011; Genders et al. 2009) or disease prevalence greater than 30–50 % (Min et al. 2010; Shreibati et al. 2011) due to high downstream resource utilization (particularly subsequent ICA) (Min et al. 2008a; Shreibati et al. 2011). Of note, real-world observational studies have shown decreased downstream resource utilization following clinical cCTA implementation, possibly due to more appropriate patient selection and clinical management (Karlsberg et al. 2010).

4 cCTA in Patients with Acute Chest Pain

The workup and triage of patients presenting to the emergency department with acute chest pain represents a common and difficult diagnostic dilemma across the developed world. While ECG, clinical decision rules, and sensitive cardiac biomarkers are available and can lead to rapid triage to ICA in a minority of cases, greater than 80 % of patients have a nondiagnostic initial workup and require either serial clinical and laboratory monitoring or additional testing (Anderson et al. 2007). Furthermore, approximately 80 % of those patients will eventually receive a diagnosis of non-cardiac chest pain (Roger et al. 2012), and a small but concerning percentage of discharged patients actually have ACS. The process is not only expensive but also results in a significant diversion of resources as patients are monitored or prepared for time-consuming tests such as cardiac

scintigraphy. The speed and excellent NPV of cCTA form the basis for its utilization in these situations, with the primary goal of providing safe, rapid discharge for the large percentage of patients without ACS.

4.1 Diagnostic Accuracy and Prognostic Value

Many studies have been published on the diagnostic accuracy of cCTA; however, studies encompassing only patients presenting to the emergency department with acute chest pain and low to intermediate PTP of ACS are more limited. Nevertheless, early data again suggested that cCTA is very reliable in excluding CAD. Recently, more robust data have emerged that again displays the excellent NPV of cCTA for the detection of patients with ACS. Importantly, and in contrast to diagnostic studies in which other imaging is used as the reference standard, these investigations have used index hospitalization and follow-up data to determine positive findings (i.e., ACS) and calculate diagnostic accuracy and prognostic value.

One of the first large prospective observational studies evaluating cCTA in the setting of acute chest pain was the ROMICAT trial, which enrolled 368 patients with low to intermediate risk. The NPV of cCTA in the detection of any CAD (50 % of the subjects) was 100 %, while the NPV was 98 % when cCTA detected CAD but no significant stenoses (Hoffmann et al. 2006). Three multicenter randomized controlled trials have been performed that displayed similar data, all enrolling patients with low to intermediate PTP presenting to the emergency department with acute chest pain. The CT-STAT trial randomized 699 patients to either cCTA or myocardial perfusion scintigraphy and found no difference in adverse events after 6 months (Goldstein et al. 2011). The ROMICAT II trial randomized 1,000 patients to either cCTA or standard evaluation and demonstrated a 100 % NPV for cCTA in the exclusion of ACS. In addition, there was no difference in major adverse cardiac events between the two strategies after 28 days (Hoffmann et al. 2012). A 2012 study randomizing 1,370 patients to cCTA or standard care also showed the value of negative cCTA examinations, with zero deaths or MIs after 30 days in the 640 patients with a negative study (Litt et al. 2012).

As before, the PPV of cCTA in these situations is much more limited, hence the evolution of the test into a largely "rule-out" role. In addition, the ability of cCTA to detect functional stenoses in these patients is also limited; however, this fact per se does not undermine cCTA's value as a rapid triage test.

4.2 Outcomes and Costs

The importance of proper patient selection is again emphasized in cost-effectiveness data for cCTA utilization in the emergency department. Several of the large observational studies presented in Sect. 3.3 included patients with acute chest pain, and some of the conclusions can justifiably be extrapolated to this population. Namely, patients with a high risk of ACS or CAD should not undergo cCTA, as downstream ICA utilization will be high and drive up costs without outcome benefits. Model-based analyses specific to the acute chest pain setting have shown cCTA-based strategies can be more cost-effective than stress ECG, stress echocardiography, and myocardial perfusion scintigraphy under certain conditions, including disease prevalence <70 % (Khare et al. 2008; Ladapo et al. 2008).

Fortunately, the randomized controlled trials mentioned above have also provided fairly robust data on the potential value of cCTA. While the CT-STAT trial demonstrated a 38 % cost savings per patient in the cCTA arm, ROMICAT II found no differences in cumulative per-patient costs between cCTA and traditional care. Importantly, however, there is strong data pointing to several other benefits of a cCTA-based approach. CT-STAT demonstrated a 54 % reduction in the time to diagnosis when cCTA was used, while ROMICAT II and the study by Litt et al. showed significant decreases in total length of stay compared to traditional care (median 8.6 vs. 26.7 and 18.0 vs. 24.8 h, respectively). In both of the latter studies, nearly half of patients undergoing cCTA were discharged directly from the emergency department, compared to 12–23 % of those patients in the standard care arms. Litt et al. also showed that while there was no difference in rates of subsequent ICA, patients who had undergone cCTA were more likely to have positive ICA findings, suggesting that cCTA may lead to more appropriate clinical decision-making.

5 Other Indications

5.1 Evaluation of Patients with New Heart Failure

The differentiation of ischemic cardiomyopathy from non-ischemic dilated cardiomyopathy, the two major causes of heart failure in the developed world, has important prognostic and management implications. Perhaps most importantly, patients with systolic dysfunction secondary to CAD may be amenable to revascularization. As such, ICA is employed in the diagnostic workup of certain patients with

new-onset or newly diagnosed heart failure. cCTA may represent a noninvasive alternative to ICA in some patients, especially considering its high NPV, and current guidelines consider cCTA use acceptable in patients without known CAD with low or intermediate PTP (Taylor et al. 2010). The justification for this is largely based on broader studies, with only limited population-specific evidence. However, the little data that are available are generally favorable, with sensitivities and specificities ≥ 90 % for the detection of CAD or ischemic heart disease. Furthermore, one small prospective study found that all patients with a negative cCTA examination could avoid ICA, suggesting some cost benefits (Ghostine et al. 2008; Hamilton-Craig et al. 2012). Further evaluation on prognosis, outcomes, and costs will be necessary to refine the role of cCTA in this situation.

5.2 Patients Prior to Noncoronary Cardiac Surgery

ICA is widely utilized prior to noncoronary cardiac surgery, especially valvular surgery, and is considered acceptable in this situation by current practice guidelines (Patel et al. 2012a). Again, cCTA may offer an attractive alternative in this situation, but population-specific data are limited. Several studies have shown high diagnostic accuracy in preoperative coronary evaluation (Mark et al. 2010); furthermore, two studies examining outcomes have shown that cCTA is safe, with one study finding no MACE in the perioperative period or at 3 month follow-up in patients with a negative cCTA (Buffa et al. 2010) and another study finding no difference in operative mortality or postoperative MI between patients who had received cCTA compared to those who had received ICA (Nardi et al. 2011). Again, the value of cCTA may lie in its ability to prevent unnecessary catheterization in a large number of patients. Of the two studies mentioned above, 81–85 % of patients undergoing cCTA had negative examinations and were able to safely avoid ICA.

5.3 Patients with Coronary Artery Stents

In-stent restenosis remains a considerable problem in modern cardiology practice. Unfortunately, there are several limitations associated with cCTA stent evaluation, and current guidelines consider cCTA acceptable only in the evaluation of left main coronary artery stents ≥ 3 mm in asymptomatic patients (Taylor et al. 2010). The main problem involves poor image quality rendering a significant proportion of stents unevaluable. High-density stent material is subject to beam-hardening and blooming artifacts, and partial volume averaging can result in artificial luminal narrowing of up to 60 %. The percentage of unevaluable stents varies widely between reports; however, even with specialized reconstruction techniques, at least 8 % of stents cannot be reliably assessed with current scanners (Mahnken 2012). Various parameters have been associated with stent evaluability, including strut thickness, stent location, and stent material; however, the strongest evidence points to stent diameter as the most important parameter, with accessability rates varying from 100 % in stents ≥ 3.5 mm to 33 % when diameter is <3 mm (Sheth et al. 2007).

Of note, meta-analyses have shown that the diagnostic accuracy of cCTA is quite good when only assessable segments are considered, with pooled sensitivities and specificities of 86–90 % and 91–93 %, respectively. However, including nonassessable segments decreased both parameters to around 80 % (Carrabba et al. 2010; Sun and Almutairi 2010). Interestingly, one study has compared stent assessment with ICA and cCTA using intravascular ultrasound (IVUS) as the reference standard and demonstrated a higher diagnostic accuracy with the use of cCTA (Hang et al. 2011). This raises questions regarding the reliability of prior diagnostic data comparing cCTA with ICA as the reference standard.

5.4 Patients with Prior CABG

Currently available evidence has been deemed adequate to justify the use of cCTA in the assessment of symptomatic patients who have had prior CABG (Taylor et al. 2010). Symptoms may result from flow-limiting lesions in ungrafted native arteries, native arteries distal to graft insertion, the proximal and distal anastomoses, or the grafts themselves. cCTA has shown good diagnostic accuracy in the assessment of grafts, with overall sensitivity and specificity ≥ 97 % to detect graft occlusion or significant stenosis (Hamon et al. 2008; Stein et al. 2008). Predictably, accuracy is higher in the detection of occlusion compared to stenosis and when assessing venous versus arterial grafts (secondary to the smaller size and increased adjacent surgical clips associated with arterial grafts). However, cCTA is somewhat limited in the assessment of distal anastomosis sites and, perhaps more importantly, the native coronary arteries (Fig. 6). Studies have shown that as many as 9 % of native arteries (both ungrafted and distal to graft insertion) are unevaluable, largely due to small size and high burden of dense calcifications. Furthermore, diagnostic accuracy is reduced when assessing native coronary arteries of prior CABG patients compared to those who have not undergone CABG, even among exclusively evaluable segments (Ropers et al. 2006). Despite these limitations, cCTA appears to be a viable alternative to ICA. Recent studies evaluating prognostic value have strengthened the evidence

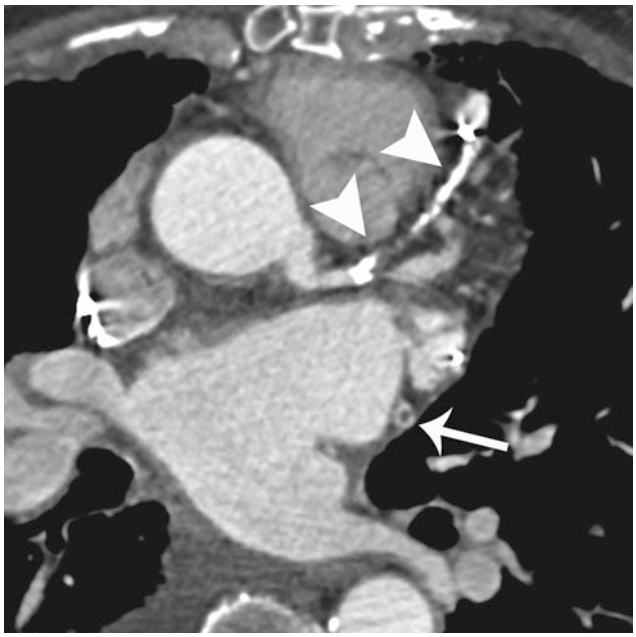

Fig. 6 An occluded saphenous vein graft (*arrow*) is easily detected on axial source images in a patient with prior CABG. Also note the heavily calcified native left anterior descending coronary artery (*arrowheads*), which can limit the diagnostic accuracy of cCTA in these vessels

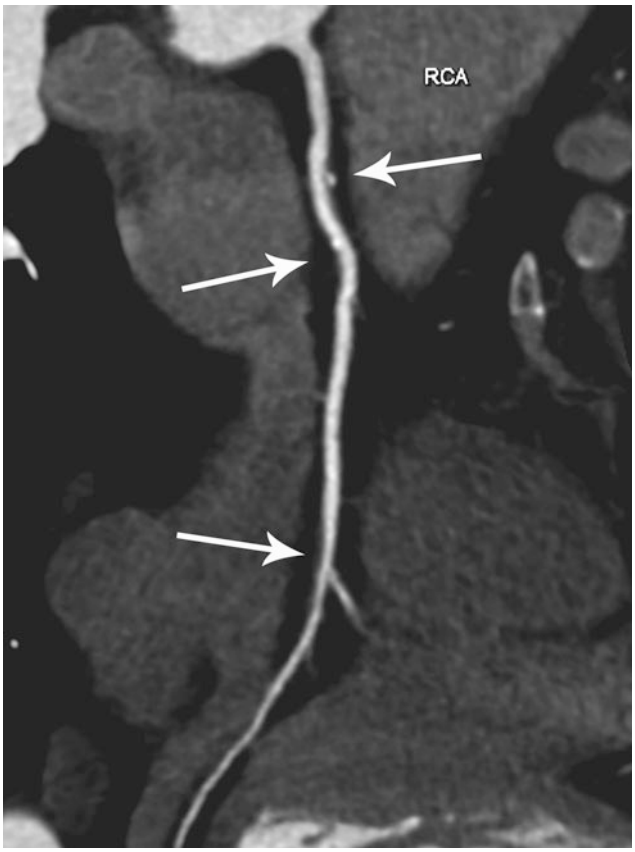

Fig. 7 Several nonobstructive plaques are detected throughout the right coronary artery (*arrows*); none of these lesions were detected at subsequent ICA (Image courtesy of Dr. Stefan Zimmerman, Johns Hopkins Hospital, Baltimore, Maryland, USA)

for cCTA, showing significant efficacy for the prediction of adverse events and death, including incremental prognostic value over clinical assessment alone (Chow et al. 2011a; Small et al. 2011).

6 Emerging Applications

6.1 Detailed Plaque Analysis

The traditional strengths of cCTA lie in its high diagnostic accuracy in the detection or exclusion of CAD, particularly obstructive disease. However, there is much more information available on a standard cCTA acquisition beyond presence and degree of stenosis. Compared to ICA, cCTA is able to visualize complete atheroma burden, rather than simply the portion of disease resulting in intraluminal filling defects (Fig. 7). In addition, morphological characteristics beyond size can be identified, such as plaque composition and contrast material enhancement. Considering the known limitations of traditional anatomic imaging, further characterization may improve the prognostic value of cCTA. Furthermore, volumetric plaque quantification may provide an expanded clinical role for cCTA by allowing serial disease monitoring to detect progression, regression, or treatment response.

6.1.1 Basis for Atherosclerotic Characterization and Quantification

A large body of evidence has emerged over the past several decades suggesting that the relative danger of a given atheroma is less dependent on percent luminal narrowing than lesion histology. In fact, nearly 70 % of culprit lesions in ACS do not display significant luminal stenosis. Plaque rupture, which is the cause of ACS in approximately 60 % of cases, is most likely to occur in lesions with a thin fibrous cap (less than 65 μm thick), a lipid-rich necrotic core, macrophage infiltration of the cap, vaso vasorum within the plaque, and positive remodeling of the arterial wall. Such "vulnerable plaques" have been termed thin-cap fibroatheromas (TCFA).

Several imaging modalities have been used for vulnerable plaque detection, including intravascular ultrasound with radiofrequency backscatter analysis ("virtual histology" [IVUS-VH]) and optical coherence tomography. cCTA is unable to visualize the fibrous cap of TCFA; however, as the technical abilities of cCTA have improved, multiple findings have been found to correlate with culprit

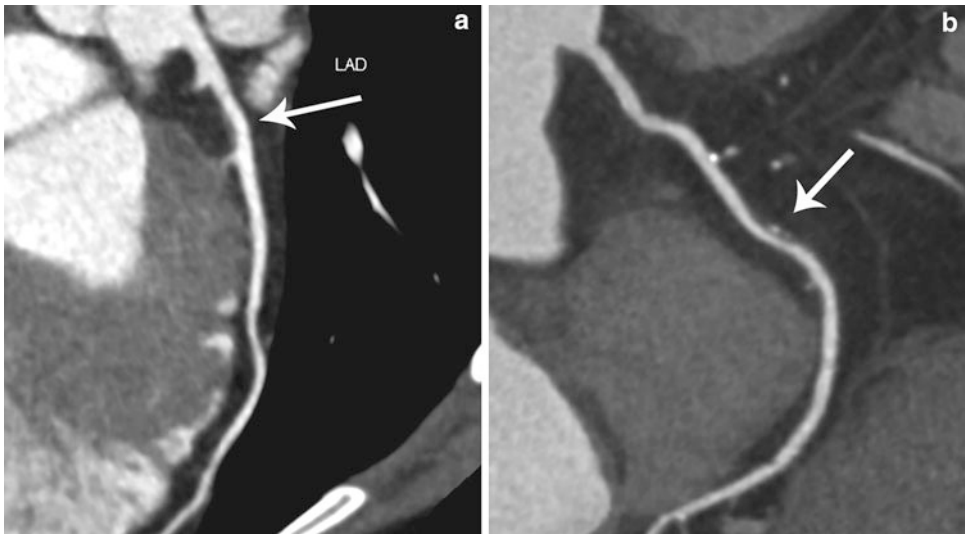

Fig. 8 Positive remodeling (*arrow* in **a**) and spotty calcifications (*arrow* in **b**) are two cCTA findings that have been associated with "vulnerable" plaque (Images courtesy of Dr. Stefan Zimmerman, Johns Hopkins Hospital, Baltimore, Maryland, USA)

lesions in ACS or TCFA detected with IVUS-VH or optical coherence tomography, including the presence and extent of positive remodeling, the presence of spotty calcifications (calcifications with maximum size <3 mm; Fig. 8), a ring-like enhancement pattern surrounding the atheroma, greater plaque volume, lower attenuation values, and less overall calcium (Cheezum et al. 2012). More simplified classification and reporting of lesions as calcified, noncalcified, and mixed is already standard practice at most institutions and may also have diagnostic efficacy in identifying the relative risk of specific atheromas.

While qualitative identification of certain imaging features will likely provide some prognostic benefit to cCTA analysis, accurate and precise quantification of overall disease burden and specific plaque components will be necessary to maximize the value of routine cCTA examinations. In addition, cCTA quantification of atherosclerotic burden has been proposed as a means of monitoring disease over time, allowing objective assessment of the effects of medical interventions and potentially prompting data-driven changes in clinical management.

6.1.2 Plaque Characterization and Quantification with cCTA

There is strong evidence showing high diagnostic accuracy for cCTA in the detection of plaque compared to IVUS (Voros et al. 2011a). In addition, cCTA is able to reliably differentiate calcified, noncalcified, and mixed lesions (Pohle et al. 2007). The ability of cCTA to further characterize primarily noncalcified plaques into lipid-rich versus fibrous, however, has proven more difficult to establish. Initial efforts attempted to stratify lesions based on CT number; however, there is significant overlap in attenuation values between lipid-rich and fibrous plaques secondary to variability in luminal contrast material concentration, degree of stenosis, tube settings, and reconstruction techniques. Several groups have shown that there is correlation between CT numbers and IVUS-VH echogenicity (Voros et al. 2011b), but data are not currently sufficient to support widespread clinical use. Preliminary studies have suggested that histogram analysis may allow the identification of lipid-rich plaques, and direct visualization of lipid cores have been reported in some patients with the use of high-resolution CT (Seifarth et al. 2012). In addition, dedicated plaque analysis software has become available that attempts to characterize tissue as either lipid rich, fibrous, or calcified on the basis of three-dimension continuity, position, and shape in addition to CT numbers. Importantly, more established classification schemes have been shown to have value in identifying vulnerable plaque, as mixed atheromas have been shown to represent TCFA and culprit lesions more often than calcified or purely noncalcified plaques. In addition, the CT findings mentioned above, including positive remodeling and ring-like plaque enhancement, correlate with culprit lesions in patients with ACS and TCFA detected at IVUS-VH and optical coherence tomography.

Data on the diagnostic accuracy of plaque and plaque component quantification are also mixed. In general, most studies have found good correlation between cCTA and IVUS-VH in quantifying plaque volume, luminal diameter, and luminal area. Mean differences in cCTA and IVUS-VH values are small; however, wide limits of agreement are consistently reported, limiting the applicability of the technique to individual patients. The most important limitations arise in the assessment of calcified plaque volume and percentage stenosis, which is routinely overestimated due to blooming artifact (with greater than 100 % overestimation of calcified plaque volume reported). In contrast, noncalcified and mixed plaque assessment is much better,

especially in higher volume lesions and larger proximal coronary arteries (Voros et al. 2011a). Future improvements in quantitative atherosclerotic imaging will necessitate increased spatial resolution and decreased artifacts from high-density contrast material or calcium.

A major obstacle in the widespread adoption of detailed plaque analysis is a lack of outcomes data, both on the value of imaging findings and the subsequent effect on patient management. The majority of outcomes studies currently available have analyzed calcified, noncalcified, and mixed plaque. This characterization scheme does appear to have prognostic value, with the presence and extent of mixed and noncalcified plaques shown to be associated with increased mortality and adverse cardiac events (Nance et al. 2012). One large prospective study demonstrated increases in mortality rates from 1.4 % in patients with calcified plaque to 3.3 and 9.6 % in those with mixed and noncalcified plaques, respectively (Ahmadi et al. 2011). In addition, mixed plaque has been shown to predict abnormalities on myocardial perfusion scintigraphy examinations (whereas the presence of obstructive disease did not) (Lin et al. 2008). The value of more specific plaque features and quantitative data are less clear, with few studies available. One large study (1,059 patients) demonstrated a 23-fold increased risk of ACS occurrence over 27 months in patients with both positive remodeling and low attenuation plaque. The authors also found prognostic value in increased plaque remodeling index, total plaque volume, and low attenuating plaque volume (Motoyama et al. 2009). Semi-quantitative plaque grading schemes have also shown prognostic value; for example, calculating risk scores based on total segment involvement, total segment involvement plus degree of stenosis, or plaque location and extent (Min et al. 2007).

Data on the value of cCTA in serial imaging are likewise limited. Several studies have been performed that suggest disease monitoring is feasible; however, these have examined limited patient populations with very specific CAD profiles, and generalizability is uncertain. In addition, several studies have demonstrated problems with reproducibility (Mark et al. 2010).

6.2 Asymptomatic Patients

Morbidity and mortality from CAD in asymptomatic patients is significant, as up to half of men and greater than 60 % of women who experience sudden cardiac death from CAD were previously asymptomatic. Clinical risk assessments and coronary artery calcium scoring have been shown to help predict events; however, risk may be underestimated in certain patient subpopulations (such as diabetics, smokers, patients with chronic kidney disease, young females, and individuals with family history of premature CAD). cCTA, while currently not indicated in the assessment of asymptomatic patients, has been proposed as a way to improve risk stratification.

In order to justify the costs and radiation exposure associated with cCTA, data will need to establish prognostic value over clinical risk assessments and coronary artery scoring alone. Presently, these data are not available. One of the largest studies to date showed an effect on statins and aspirin use 90 days following cCTA; however, there were no differences in subsequent hard events during the follow-up period, and there were significantly higher rates of subsequent testing in the cCTA population. Of note, the patient population had both low clinical risk and low prevalence of disease (22 %), and results may not be generalizable to a potential high-risk population (Choi et al. 2008). A more encouraging study found that cCTA was superior to coronary artery calcium scoring in reclassifying patient risk (as initially determined with clinical risk models), and a combined cCTA and clinical risk assessment was significantly better at predicting cardiac events compared with clinical risk assessment alone. Unsurprisingly, the study population demonstrated a higher prevalence of disease (54 %) (Hadamitzky et al. 2010).

7 Incidental Findings

There are questions and concerns regarding the clinical and economic impacts of incidentally detected extracardiac findings on cCTA. Examinations necessarily acquire imaging data for multiple structures that surround the heart, including the lungs, bones, mediastinum, pericardium, great vessels, and upper abdomen. The incidence of cases with extracardiac findings has been reported to range from 15 to 67 %. Of these, 4–25 % can be considered "potentially significant," possibly requiring follow-up or additional investigation, and 5–11 % can be considered "critical," requiring immediate evaluation or intervention (Mark et al. 2010). Unfortunately, data on the long-term implications of incidental findings are limited. As a result, there is disagreement on whether to reconstruct the full anatomic dataset for review (including the entire thoracic cross-sectional area) or to limit the field of view to only what is necessary for coronary analysis. Limited data from the prospective ROMICAT study does suggest that extracardiac findings can impact patient management in a small number of patients (Lehman et al. 2009); however, sophisticated analyses comparing the benefits of incidental finding detection against the costs and anxiety of potential further workup are limited. There is evidence that suggests the real-world impact of incidental findings may be marginal, despite their relative frequency: one study found 43 % of

patients receiving cCTA had an extracardiac finding, yet only 4 % of those patients underwent follow-up imaging or intervention at an average cost of $17.42 per patient that underwent cCTA (Lee et al. 2010). In addition, real-world data have shown decreased total health expenditures in patients receiving cCTA (Min et al. 2008b), arguing against a large economic impact due to incidental findings, and simulation models have shown that follow-up accounts for only a small amount of overall costs (Ladapo et al. 2009).

8 Radiation Dose

There is a considerable attention given to the ionizing radiation burden associated with cCTA. Despite considerable problems in measuring radiation dose and quantifying the potential harm associated with it, every effort should be made to minimize exposure. 2007 data acquired for the multicenter PROTECTION I trial showed median effective dose of 12.1 mSv across 50 sites performing cCTA, with high variability between sites (median effective dose ranging from 5 to 30 mSv) (Hausleiter et al. 2009). In comparison, myocardial perfusion scintigraphy dose averages range from 9 to 21 mSv and ICA is associated with doses of 5–7 mSv (Budoff et al. 2005; Coles et al. 2006; Einstein et al. 2007).

Established and ongoing advances in radiation dose reduction should help to alleviate concerns. ECG-dependent tube current modulation, in which the tube current is decreased during portions of the cardiac cycle unlikely to be used for primary coronary analysis, has been available for several years and lowers dose by approximately 25 % without negatively affecting image quality (Hausleiter et al. 2009). Decreasing tube current and voltage settings according to patient body habitus was reported to reduce dose by 31 % in the randomized, prospective PROTECTION II trial (Hausleiter et al. 2010). The most dramatic decreases to date have resulted from the use of prospective ECG-triggered axial CT acquisitions, which decreased dose by 69 % with no adverse effect on image quality or downstream testing in the recent PROTECTION III trial (Hausleiter et al. 2012). A combined approach utilizing these techniques along with a high-pitch acquisition protocol has allowed effective doses approaching 1 mSv in non-obese patients with low, regular heart rates. These ultra-low dose examinations are not associated with decreased image quality in preliminary analyses (Fink et al. 2011). Advanced post-processing techniques such as iterative reconstruction should allow further dose reductions while maintaining diagnostic accuracy (Leipsic et al. 2010). While these controlled studies are promising, perhaps more encouraging is real-world data showing that dose reduction programs are effective, with one multicenter study involving nearly 5,000 patients demonstrating a reduction in median effective dose from 21 to 10 mSv one year following the implementation of a collaborative dose reduction program (Raff et al. 2009b). It will remain the responsibility of providers to maintain awareness of new dose lowering techniques and implement them when available.

9 Conclusion

The diagnostic capability of cCTA in the anatomic assessment of CAD is well established, and continuing technical advances are further improving image quality while decreasing radiation dose. Current evidence on the ultimate clinical value of cCTA is limited and mixed but overall favorable for the currently accepted indications. Of course, the application of data from highly controlled trials will only be applicable in a real-world setting if providers are disciplined in patient selection and post-test management decisions. Ongoing work is expanding the evidence on prognosis, outcomes, and cost-effectiveness in order to establish the optimal role for cCTA in clinical practice. However, data on both ICA and cCTA suggest that the value of pure anatomic imaging of the heart and coronary arteries is inherently limited. The remainder of this book will describe the capabilities of cCTA beyond anatomic assessment.

References

Ahmadi N, Nabavi V, Hajsadeghi F, Flores F, French WJ, Mao SS, Shavelle D, Ebrahimi R, Budoff M (2011) Mortality incidence of patients with non-obstructive coronary artery disease diagnosed by computed tomography angiography. Am J Cardiol 107(1):10–16

Anderson JL, Adams CD, Antman EM, Bridges CR, Califf RM, Casey DE Jr, Chavey WE 2nd, Fesmire FM, Hochman JS, Levin TN, Lincoff AM, Peterson ED, Theroux P, Wenger NK, Wright RS, Smith SC Jr, Jacobs AK, Halperin JL, Hunt SA, Krumholz HM, Kushner FG, Lytle BW, Nishimura R, Ornato JP, Page RL, Riegel B (2007) ACC/AHA 2007 guidelines for the management of patients with unstable angina/non ST-elevation myocardial infarction: a report of the American College of Cardiology/American Heart Association Task Force on Practice Guidelines (Writing Committee to Revise the 2002 Guidelines for the Management of Patients With Unstable Angina/Non ST-Elevation Myocardial Infarction): developed in collaboration with the American College of Emergency Physicians, the Society for Cardiovascular Angiography and Interventions, and the Society of Thoracic Surgeons: endorsed by the American Association of Cardiovascular and Pulmonary Rehabilitation and the Society for Academic Emergency Medicine. Circulation 116(7):e148-304

Arnoldi E, Gebregziabher M, Schoepf UJ, Goldenberg R, Ramos-Duran L, Zwerner PL, Nikolaou K, Reiser MF, Costello P, Thilo C (2009) Automated computer-aided stenosis detection at coronary CT angiography: initial experience. Eur Radiol 20(5):1160–1167

Bamberg F, Sommer WH, Hoffmann V, Achenbach S, Nikolaou K, Conen D, Reiser MF, Hoffmann U, Becker CR (2011) Meta-analysis and systematic review of the long-term predictive value of

assessment of coronary atherosclerosis by contrast-enhanced coronary computed tomography angiography. J Am Coll Cardiol 57(24):2426–2436

Bamberg F, Marcus RP, Schlett CL, Schoepf UJ, Johnson TR, Nance JW Jr, Hoffmann U, Reiser MF, Nikolaou K (2012) Imaging evaluation of acute chest pain: systematic review of evidence base and cost-effectiveness. J Thorac Imaging 27(5):289–295

Blackmon KN, Streck J, Thilo C, Bastarrika G, Costello P, Joseph Schoepf U (2009) Reproducibility of automated noncalcified coronary artery plaque burden assessment at coronary CT angiography. J Thorac Imaging 24(2):96–102

Bruschke AV, Sheldon WC, Shirey EK, Proudfit WL (2009) A half century of selective coronary arteriography. J Am Coll Cardiol 54(23):2139–2144

Budoff MJ, Cohen MC, Garcia MJ, Hodgson JM, Hundley WG, Lima JA, Manning WJ, Pohost GM, Raggi PM, Rodgers GP, Rumberger JA, Taylor AJ, Creager MA, Hirshfeld JW Jr, Lorell BH, Merli G, Rodgers GP, Tracy CM, Weitz HH (2005) ACCF/AHA clinical competence statement on cardiac imaging with computed tomography and magnetic resonance. Circulation 112(4):598–617

Budoff MJ, Dowe D, Jollis JG, Gitter M, Sutherland J, Halamert E, Scherer M, Bellinger R, Martin A, Benton R, Delago A, Min JK (2008) Diagnostic performance of 64-multidetector row coronary computed tomographic angiography for evaluation of coronary artery stenosis in individuals without known coronary artery disease: results from the prospective multicenter ACCURACY (Assessment by Coronary Computed Tomographic Angiography of Individuals Undergoing Invasive Coronary Angiography) trial. J Am Coll Cardiol 52(21):1724–1732

Buffa V, De Cecco CN, Cossu L, Fedeli S, Vallone A, Ruopoli R, Luzietti M, Angelica G, David V, Musumeci F (2010) Preoperative coronary risk assessment with dual-source CT in patients undergoing noncoronary cardiac surgery. Radiol Med 115(7):1028–1037

Carrabba N, Schuijf JD, de Graaf FR, Parodi G, Maffei E, Valenti R, Palumbo A, Weustink AC, Mollet NR, Accetta G, Cademartiri F, Antoniucci D, Bax JJ (2010) Diagnostic accuracy of 64-slice computed tomography coronary angiography for the detection of in-stent restenosis: a meta-analysis. J Nucl Cardiol 17(3):470–478

Cheezum MK, Hulten EA, Fischer C, Smith RM, Slim AM, Villines TC (2012) Prognostic value of coronary CT angiography. Cardiol Clin 30(1):77–91

Choi EK, Choi SI, Rivera JJ, Nasir K, Chang SA, Chun EJ, Kim HK, Choi DJ, Blumenthal RS, Chang HJ (2008) Coronary computed tomography angiography as a screening tool for the detection of occult coronary artery disease in asymptomatic individuals. J Am Coll Cardiol 52(5):357–365

Chow BJ, Ahmed O, Small G, Alghamdi AA, Yam Y, Chen L, Wells GA (2011a) Prognostic value of CT angiography in coronary bypass patients. JACC Cardiovasc Imaging 4(5):496–502

Chow BJ, Small G, Yam Y, Chen L, Achenbach S, Al-Mallah M, Berman DS, Budoff MJ, Cademartiri F, Callister TQ, Chang HJ, Cheng V, Chinnaiyan KM, Delago A, Dunning A, Hadamitzky M, Hausleiter J, Kaufmann P, Lin F, Maffei E, Raff GL, Shaw LJ, Villines TC, Min JK (2011b) Incremental prognostic value of cardiac computed tomography in coronary artery disease using CONFIRM: COroNary computed tomography angiography evaluation for clinical outcomes: an InteRnational Multicenter registry. Circ Cardiovasc Imaging 4(5):463–472

Coles DR, Smail MA, Negus IS, Wilde P, Oberhoff M, Karsch KR, Baumbach A (2006) Comparison of radiation doses from multislice computed tomography coronary angiography and conventional diagnostic angiography. J Am Coll Cardiol 47(9):1840–1845

den Dekker MA, de Smet K, de Bock GH, Tio RA, Oudkerk M, Vliegenthart R (2012) Diagnostic performance of coronary CT angiography for stenosis detection according to calcium score: systematic review and meta-analysis. Eur Radiol 22(12):2688–2698

Dorenkamp M, Bonaventura K, Sohns C, Becker CR, Leber AW (2011) Direct costs and cost-effectiveness of dual-source computed tomography and invasive coronary angiography in patients with an intermediate pretest likelihood for coronary artery disease. Heart 98:460–467

Einstein AJ, Henzlova MJ, Rajagopalan S (2007) Estimating risk of cancer associated with radiation exposure from 64-slice computed tomography coronary angiography. JAMA 298(3): 317–323

Fink C, Krissak R, Henzler T, Lechel U, Brix G, Takx RA, Nance JW, Abro JA, Schoenberg SO, Schoepf UJ (2011) Radiation dose at coronary CT angiography: second-generation dual-source CT versus single-source 64-MDCT and first-generation dual-source CT. AJR Am J Roentgenol 196(5):W550–W557

Genders TS, Meijboom WB, Meijs MF, Schuijf JD, Mollet NR, Weustink AC, Pugliese F, Bax JJ, Cramer MJ, Krestin GP, de Feyter PJ, Hunink MG (2009) CT coronary angiography in patients suspected of having coronary artery disease: decision making from various perspectives in the face of uncertainty. Radiology 253(3):734–744

Ghostine S, Caussin C, Habis M, Habib Y, Clement C, Sigal-Cinqualbre A, Angel CY, Lancelin B, Capderou A, Paul JF (2008) Non-invasive diagnosis of ischaemic heart failure using 64-slice computed tomography. Eur Heart J 29(17):2133–2140

Goldstein JA, Chinnaiyan KM, Abidov A, Achenbach S, Berman DS, Hayes SW, Hoffmann U, Lesser JR, Mikati IA, O'Neil BJ, Shaw LJ, Shen MY, Valeti US, Raff GL (2011) The CT-STAT (Coronary computed tomographic angiography for systematic triage of acute chest pain patients to treatment) trial. J Am Coll Cardiol 58(14):1414–1422

Hadamitzky M, Meyer T, Hein F, Bischoff B, Martinoff S, Schomig A, Hausleiter J (2010) Prognostic value of coronary computed tomographic angiography in asymptomatic patients. Am J Cardiol 105(12):1746–1751

Hadamitzky M, Distler R, Meyer T, Hein F, Kastrati A, Martinoff S, Schomig A, Hausleiter J (2011) Prognostic value of coronary computed tomographic angiography in comparison with calcium scoring and clinical risk scores. Circ Cardiovasc Imaging 4(1):16–23

Hamilton-Craig C, Strugnell WE, Raffel OC, Porto I, Walters DL, Slaughter RE (2012) CT angiography with cardiac MRI: non-invasive functional and anatomical assessment for the etiology in newly diagnosed heart failure. Int J Cardiovasc Imaging 28(5):1111–1122

Hamon M, Lepage O, Malagutti P, Riddell JW, Morello R, Agostini D, Hamon M (2008) Diagnostic performance of 16- and 64-section spiral CT for coronary artery bypass graft assessment: meta-analysis. Radiology 247(3):679–686

Hang CL, Lee YW, Guo GB, Youssef AA, Yip HK, Liu CF, Chua S, Chang HW, Cheng YF, Chen SM (2011) Evaluation of coronary artery stent patency by using 64-slice multi-detector computed tomography and conventional coronary angiography: A comparison with intravascular ultrasonography. Int J Cardiol [Epub ahead of print]

Hausleiter J, Meyer T, Hermann F, Hadamitzky M, Krebs M, Gerber TC, McCollough C, Martinoff S, Kastrati A, Schomig A, Achenbach S (2009) Estimated radiation dose associated with cardiac CT angiography. JAMA 301(5):500–507

Hausleiter J, Martinoff S, Hadamitzky M, Martuscelli E, Pschierer I, Feuchtner GM, Catalan-Sanz P, Czermak B, Meyer TS, Hein F, Bischoff B, Kuse M, Schomig A, Achenbach S (2010) Image quality and radiation exposure with a low tube voltage protocol for coronary CT angiography results of the PROTECTION II Trial. JACC Cardiovasc Imaging 3(11):1113–1123

Hausleiter J, Meyer TS, Martuscelli E, Spagnolo P, Yamamoto H, Carrascosa P, Anger T, Lehmkuhl L, Alkadhi H, Martinoff S, Hadamitzky M, Hein F, Bischoff B, Kuse M, Schomig A, Achenbach S (2012) Image quality and radiation exposure with prospectively ECG-triggered axial scanning for coronary CT angiography: the multicenter, multivendor, randomized PROTECTION-III study. JACC Cardiovasc Imaging 5(5):484–493

Hendel RC (2009) Is computed tomography coronary angiography the most accurate and effective noninvasive imaging tool to evaluate patients with acute chest pain in the emergency department? CT coronary angiography is the most accurate and effective noninvasive imaging tool for evaluating patients presenting with chest pain to the emergency department: antagonist viewpoint. Circ Cardiovasc Imaging 2(3):264–275; discussion 275

Hoffmann U, Nagurney JT, Moselewski F, Pena A, Ferencik M, Chae CU, Cury RC, Butler J, Abbara S, Brown DF, Manini A, Nichols JH, Achenbach S, Brady TJ (2006) Coronary multidetector computed tomography in the assessment of patients with acute chest pain. Circulation 114(21):2251–2260

Hoffmann U, Truong QA, Schoenfeld DA, Chou ET, Woodard PK, Nagurney JT, Pope JH, Hauser TH, White CS, Weiner SG, Kalanjian S, Mullins ME, Mikati I, Peacock WF, Zakroysky P, Hayden D, Goehler A, Lee H, Gazelle GS, Wiviott SD, Fleg JL, Udelson JE (2012) Coronary CT angiography versus standard evaluation in acute chest pain. N Engl J Med 367(4):299–308

Hulten EA, Carbonaro S, Petrillo SP, Mitchell JD, Villines TC (2011) Prognostic value of cardiac computed tomography angiography: a systematic review and meta-analysis. J Am Coll Cardiol 57(10):1237–1247

Karlsberg RP, Budoff MJ, Thomson LE, Friedman JD, Berman DS (2010) Reduction in downstream test utilization following introduction of coronary computed tomography in a cardiology practice. Int J Cardiovasc Imaging 26(3):359–366

Kazmi MH, Small G, Sleiman L, Chow BJ (2011) Determining patient prognosis using computed tomography coronary angiography. Expert Rev Med Devices 8(5):647–657

Khare RK, Courtney DM, Powell ES, Venkatesh AK, Lee TA (2008) Sixty-four-slice computed tomography of the coronary arteries: cost-effectiveness analysis of patients presenting to the emergency department with low-risk chest pain. Acad Emerg Med 15(7):623–632

Ladapo JA, Hoffmann U, Bamberg F, Nagurney JT, Cutler DM, Weinstein MC, Gazelle GS (2008) Cost-effectiveness of coronary MDCT in the triage of patients with acute chest pain. Am J Roentgenol 191(2):455–463

Ladapo JA, Jaffer FA, Hoffmann U, Thomson CC, Bamberg F, Dec W, Cutler DM, Weinstein MC, Gazelle GS (2009) Clinical outcomes and cost-effectiveness of coronary computed tomography angiography in the evaluation of patients with chest pain. J Am Coll Cardiol 54(25):2409–2422

Lee CI, Tsai EB, Sigal BM, Plevritis SK, Garber AM, Rubin GD (2010) Incidental extracardiac findings at coronary CT: clinical and economic impact. Am J Roentgenol 194(6):1531–1538

Lehman SJ, Abbara S, Cury RC, Nagurney JT, Hsu J, Goela A, Schlett CL, Dodd JD, Brady TJ, Bamberg F, Hoffmann U (2009) Significance of cardiac computed tomography incidental findings in acute chest pain. Am J Med 122(6):543–549

Leipsic J, Labounty TM, Heilbron B, Min JK, Mancini GB, Lin FY, Taylor C, Dunning A, Earls JP (2010) Estimated radiation dose reduction using adaptive statistical iterative reconstruction in coronary CT angiography: the ERASIR study. Am J Roentgenol 195(3):655–660

Lichtlen PR, Bargheer K, Wenzlaff P (1995) Long-term prognosis of patients with anginalike chest pain and normal coronary angiographic findings. J Am Coll Cardiol 25(5):1013–1018

Lin F, Shaw LJ, Berman DS, Callister TQ, Weinsaft JW, Wong FJ, Szulc M, Tandon V, Okin PM, Devereux RB, Min JK (2008) Multidetector computed tomography coronary artery plaque predictors of stress-induced myocardial ischemia by SPECT. Atherosclerosis 197(2):700–709

Litt HI, Gatsonis C, Snyder B, Singh H, Miller CD, Entrikin DW, Leaming JM, Gavin LJ, Pacella CB, Hollander JE (2012) CT angiography for safe discharge of patients with possible acute coronary syndromes. N Engl J Med 366(15):1393–1403

Lu B, Mao SS, Zhuang N, Bakhsheshi H, Yamamoto H, Takasu J, Liu SC, Budoff MJ (2001) Coronary artery motion during the cardiac cycle and optimal ECG triggering for coronary artery imaging. Invest Radiol 36(5):250–256

Mahnken AH (2012) CT imaging of coronary stents: past, present, and future. ISRN Cardiol 2012:139823

Mark DB, Berman DS, Budoff MJ, Carr JJ, Gerber TC, Hecht HS, Hlatky MA, Hodgson JM, Lauer MS, Miller JM, Morin RL, Mukherjee D, Poon M, Rubin GD, Schwartz RS (2010) ACCF/ACR/AHA/NASCI/SAIP/SCAI/SCCT 2010 expert consensus document on coronary computed tomographic angiography: a report of the American College of Cardiology Foundation Task Force on Expert Consensus Documents. J Am Coll Cardiol 55(23): 2663–2699

Meijboom WB, Meijs MF, Schuijf JD, Cramer MJ, Mollet NR, van Mieghem CA, Nieman K, van Werkhoven JM, Pundziute G, Weustink AC, de Vos AM, Pugliese F, Rensing B, Jukema JW, Bax JJ, Prokop M, Doevendans PA, Hunink MG, Krestin GP, de Feyter PJ (2008) Diagnostic accuracy of 64-slice computed tomography coronary angiography: a prospective, multicenter, multivendor study. J Am Coll Cardiol 52(25):2135–2144

Metz LD, Beattie M, Hom R, Redberg RF, Grady D, Fleischmann KE (2007) The prognostic value of normal exercise myocardial perfusion imaging and exercise echocardiography: a meta-analysis. J Am Coll Cardiol 49(2):227–237

Miller JM, Rochitte CE, Dewey M, Arbab-Zadeh A, Niinuma H, Gottlieb I, Paul N, Clouse ME, Shapiro EP, Hoe J, Lardo AC, Bush DE, de Roos A, Cox C, Brinker J, Lima JA (2008) Diagnostic performance of coronary angiography by 64-row CT. N Engl J Med 359(22):2324–2336

Min JK, Shaw LJ, Devereux RB, Okin PM, Weinsaft JW, Russo DJ, Lippolis NJ, Berman DS, Callister TQ (2007) Prognostic value of multidetector coronary computed tomographic angiography for prediction of all-cause mortality. J Am Coll Cardiol 50(12): 1161–1170

Min JK, Kang N, Shaw LJ, Devereux RB, Robinson M, Lin F, Legorreta AP, Gilmore A (2008a) Costs and clinical outcomes after coronary multidetector CT angiography in patients without known coronary artery disease: comparison to myocardial perfusion SPECT. Radiology 249(1):62–70

Min JK, Shaw LJ, Berman DS, Gilmore A, Kang N (2008b) Costs and clinical outcomes in individuals without known coronary artery disease undergoing coronary computed tomographic angiography from an analysis of Medicare category III transaction codes. Am J Cardiol 102(6):672–678

Min JK, Gilmore A, Budoff MJ, Berman DS, O'Day K (2010) Cost-effectiveness of coronary CT angiography versus myocardial perfusion SPECT for evaluation of patients with chest pain and no known coronary artery disease. Radiology 254(3):801–808

Min JK, Dunning A, Lin FY, Achenbach S, Al-Mallah M, Budoff MJ, Cademartiri F, Callister TQ, Chang HJ, Cheng V, Chinnaiyan K, Chow BJ, Delago A, Hadamitzky M, Hausleiter J, Kaufmann P, Maffei E, Raff G, Shaw LJ, Villines T, Berman DS (2011) Age- and Sex-Related Differences in All-Cause Mortality Risk Based on Coronary Computed Tomography Angiography Findings Results From the International Multicenter CONFIRM (Coronary CT

Angiography Evaluation for Clinical Outcomes: An International Multicenter Registry) of 23,854 Patients Without Known Coronary Artery Disease. J Am Coll Cardiol 58(8):849–860

Motoyama S, Sarai M, Harigaya H, Anno H, Inoue K, Hara T, Naruse H, Ishii J, Hishida H, Wong ND, Virmani R, Kondo T, Ozaki Y, Narula J (2009) Computed tomographic angiography characteristics of atherosclerotic plaques subsequently resulting in acute coronary syndrome. J Am Coll Cardiol 54(1):49–57

Mowatt G, Cook JA, Hillis GS, Walker S, Fraser C, Jia X, Waugh N (2008) 64-Slice computed tomography angiography in the diagnosis and assessment of coronary artery disease: systematic review and meta-analysis. Heart 94(11):1386–1393

Nance JW Jr, Bamberg F, Schoepf UJ, Kang DK, Barraza JM Jr, Abro JA, Bastarrika G, Headden GF, Costello P, Thilo C (2011) Coronary atherosclerosis in African American and white patients with acute chest pain: characterization with coronary CT angiography. Radiology 260(2):373–380

Nance JW Jr, Schlett CL, Schoepf UJ, Oberoi S, Leisy HB, Barraza JM Jr, Headden GF, Nikolaou K, Bamberg F (2012) Incremental prognostic value of different components of coronary atherosclerotic plaque at cardiac CT angiography beyond coronary calcification in patients with acute chest pain. Radiology 264(3):679–690

Nardi P, Pellegrino A, Romagnoli A, Mve Mvondo C, De Propris S, Sperandio M, Versaci F, Simonetti G, Chiariello L (2011) Multidetector computed tomographic coronary angiography as an alternative to conventional coronary angiography in non-coronary surgical patients. J Cardiovasc Surg (Torino) 52(3):429–435

Otero HJ, Steigner ML, Rybicki FJ (2009) The "post-64" era of coronary CT angiography: understanding new technology from physical principles. Radiol Clin North Am 47(1):79–90

Patel MR, Bailey SR, Bonow RO, Chambers CE, Chan PS, Dehmer GJ, Kirtane AJ, Samuel Wann L, Parker Ward R, Douglas PS, Patel MR, Bailey SR, Altus P, Barnard DD, Blankenship JC, Casey DE Jr, Dean LS, Fazel R, Gilchrist IC, Kavinsky CJ, Lakoski SG, Le DE, Lesser JR, Levine GN, Mehran R, Russo AM, Sorrentino MJ, Williams MR, Wong JB, Wolk MJ, Bailey SR, Douglas PS, Hendel RC, Kramer CM, Min JK, Patel MR, Shaw L, Stainback RF, Allen JM (2012a) ACCF/SCAI/AATS/AHA/ASE/ASNC/HFSA/HRS/SCCM/SCCT/SCMR/STS 2012 appropriate use criteria for diagnostic catheterization: A report of the American College of Cardiology Foundation Appropriate Use Criteria Task Force, Society for Cardiovascular Angiography and Interventions, American Association for Thoracic Surgery, American Heart Association, American Society of Echocardiography, American Society of Nuclear Cardiology, Heart Failure Society of America, Heart Rhythm Society, Society of Critical Care Medicine, Society of Cardiovascular Computed Tomography, Society for Cardiovascular Magnetic Resonance, Society of Thoracic Surgeons. J Thorac Cardiovasc Surg 144(1):39–71

Patel MR, Dehmer GJ, Hirshfeld JW, Smith PK, Spertus JA, Masoudi FA, Dehmer GJ, Patel MR, Smith PK, Chambers CE, Ferguson TB Jr, Garcia MJ, Grover FL, Holmes DR Jr, Klein LW, Limacher MC, Mack MJ, Malenka DJ, Park MH, Ragosta M 3rd, Ritchie JL, Rose GA, Rosenberg AB, Russo AM, Shemin RJ, Weintraub WS, Wolk MJ, Bailey SR, Douglas PS, Hendel RC, Kramer CM, Min JK, Patel MR, Shaw L, Stainback RF, Allen JM (2012b) ACCF/SCAI/STS/AATS/AHA/ASNC/HFSA/SCCT 2012 appropriate use criteria for coronary revascularization focused update: a report of the American College of Cardiology Foundation Appropriate Use Criteria Task Force, Society for Cardiovascular Angiography and Interventions, Society of Thoracic Surgeons, American Association for Thoracic Surgery, American Heart Association, American Society of Nuclear Cardiology, and the Society of Cardiovascular Computed Tomography. J Thorac Cardiovasc Surg 143(4):780–803

Pohle K, Achenbach S, Macneill B, Ropers D, Ferencik M, Moselewski F, Hoffmann U, Brady TJ, Jang IK, Daniel WG (2007) Characterization of non-calcified coronary atherosclerotic plaque by multi-detector row CT: comparison to IVUS. Atherosclerosis 190(1):174–180

Raff GL, Abidov A, Achenbach S, Berman DS, Boxt LM, Budoff MJ, Cheng V, DeFrance T, Hellinger JC, Karlsberg RP (2009a) SCCT guidelines for the interpretation and reporting of coronary computed tomographic angiography. J Cardiovasc Comput Tomogr 3(2):122–136

Raff GL, Chinnaiyan KM, Share DA, Goraya TY, Kazerooni EA, Moscucci M, Gentry RE, Abidov A (2009b) Radiation dose from cardiac computed tomography before and after implementation of radiation dose-reduction techniques. JAMA 301(22):2340–2348

Renker M, Nance JW Jr, Schoepf UJ, O'Brien TX, Zwerner PL, Meyer M, Kerl JM, Bauer RW, Fink C, Vogl TJ, Henzler T (2011) Evaluation of heavily calcified vessels with coronary CT angiography: comparison of iterative and filtered back projection image reconstruction. Radiology 260(2):390–399

Roe MT, Harrington RA, Prosper DM, Pieper KS, Bhatt DL, Lincoff AM, Simoons ML, Akkerhuis M, Ohman EM, Kitt MM, Vahanian A, Ruzyllo W, Karsch K, Califf RM, Topol EJ (2000) Clinical and therapeutic profile of patients presenting with acute coronary syndromes who do not have significant coronary artery disease.The Platelet Glycoprotein IIb/IIIa in Unstable Angina: Receptor Suppression Using Integrilin Therapy (PURSUIT) Trial Investigators. Circulation 102(10):1101–1106

Roger VL, Go AS, Lloyd-Jones DM, Benjamin EJ, Berry JD, Borden WB, Bravata DM, Dai S, Ford ES, Fox CS, Fullerton HJ, Gillespie C, Hailpern SM, Heit JA, Howard VJ, Kissela BM, Kittner SJ, Lackland DT, Lichtman JH, Lisabeth LD, Makuc DM, Marcus GM, Marelli A, Matchar DB, Moy CS, Mozaffarian D, Mussolino ME, Nichol G, Paynter NP, Soliman EZ, Sorlie PD, Sotoodehnia N, Turan TN, Virani SS, Wong ND, Woo D, Turner MB (2012) Heart disease and stroke statistics–2012 update: a report from the American Heart Association. Circulation 125(1):e2–e220

Ropers D, Pohle FK, Kuettner A, Pflederer T, Anders K, Daniel W G, Bautz W, Baum U, Achenbach S (2006) Diagnostic accuracy of noninvasive coronary angiography in patients after bypass surgery using 64-slice spiral computed tomography with 330-ms gantry rotation. Circulation 114(22):2334–2341; quiz 2334

Schwarz F, Nance JW Jr, Ruzsics B, Bastarrika G, Sterzik A, Schoepf UJ (2012) Quantification of coronary artery calcium on the basis of dual-energy coronary CT angiography. Radiology 264(3):700–707

Seifarth H, Schlett CL, Truong QA, Hoffmann U (2012) Cardiac CT in the emergency department. Cardiol Clin 30(1):117–133

Shaw LJ, Iskandrian AE (2004) Prognostic value of gated myocardial perfusion SPECT. J Nucl Cardiol 11(2):171–185

Shaw LJ, Berman DS, Hendel RC, Borges Neto S, Min JK, Callister TQ (2008) Prognosis by coronary computed tomographic angiography: matched comparison with myocardial perfusion single-photon emission computed tomography. J Cardiovasc Comput Tomogr 2(2):93–101

Shaw LJ, Min JK, Narula J, Lin F, Bairey-Merz CN, Callister TQ, Berman DS (2010) Sex differences in mortality associated with computed tomographic angiographic measurements of obstructive and nonobstructive coronary artery disease: an exploratory analysis. Circ Cardiovasc Imaging 3(4):473–481

Sheth T, Dodd JD, Hoffmann U, Abbara S, Finn A, Gold HK, Brady TJ, Cury RC (2007) Coronary stent assessability by 64 slice

multi-detector computed tomography. Catheter Cardiovasc Interv 69(7):933–938

Shreibati JB, Baker LC, Hlatky MA (2011) Association of coronary CT angiography or stress testing with subsequent utilization and spending among Medicare beneficiaries. JAMA 306(19):2128–2136

Small GR, Yam Y, Chen L, Ahmed O, Al-Mallah M, Berman DS, Cheng VY, Chinnaiyan K, Raff G, Villines TC, Achenbach S, Budoff MJ, Cademartiri F, Callister TQ, Chang HJ, Delago A, Dunning A, Hadamitzky M, Hausleiter J, Kaufmann P, Lin F, Maffei E, Min JK, Shaw LJ, Chow BJ (2011) Prognostic assessment of coronary artery bypass patients with 64-slice computed tomography angiography: anatomical information is incremental to clinical risk prediction. J Am Coll Cardiol 58(23):2389–2395

Smith SC Jr, Benjamin EJ, Bonow RO, Braun LT, Creager MA, Franklin BA, Gibbons RJ, Grundy SM, Hiratzka LF, Jones DW, Lloyd-Jones DM, Minissian M, Mosca L, Peterson ED, Sacco RL, Spertus J, Stein JH, Taubert KA (2011) AHA/ACCF secondary prevention and risk reduction therapy for patients with coronary and other atherosclerotic vascular disease: 2011 update: a guideline from the American Heart Association and American College of Cardiology Foundation endorsed by the World Heart Federation and the Preventive Cardiovascular Nurses Association. J Am Coll Cardiol 58(23):2432–2446

Stein PD, Yaekoub AY, Matta F, Sostman HD (2008) 64-slice CT for diagnosis of coronary artery disease: a systematic review. Am J Med 121(8):715–725

Sun Z, Almutairi AM (2010) Diagnostic accuracy of 64 multislice CT angiography in the assessment of coronary in-stent restenosis: a meta-analysis. Eur J Radiol 73(2):266–273

Sun Z, Ng KH (2012) Diagnostic value of coronary CT angiography with prospective ECG-gating in the diagnosis of coronary artery disease: a systematic review and meta-analysis. Int J Cardiovasc Imaging 28(8):2109–2119

Taylor AJ, Cerqueira M, Hodgson JM, Mark D, Min J, O'Gara P, Rubin GD, Kramer CM, Berman D, Brown A, Chaudhry FA, Cury RC, Desai MY, Einstein AJ, Gomes AS, Harrington R, Hoffmann U, Khare R, Lesser J, McGann C, Rosenberg A, Schwartz R, Shelton M, Smetana GW, Smith SC Jr (2010) ACCF/SCCT/ACR/AHA/ASE/ASNC/NASCI/SCAI/SCMR 2010 appropriate use criteria for cardiac computed tomography. A report of the American College of Cardiology Foundation Appropriate Use Criteria Task Force, the Society of Cardiovascular Computed Tomography, the American College of Radiology, the American Heart Association, the American Society of Echocardiography, the American Society of Nuclear Cardiology, the North American Society for Cardiovascular Imaging, the Society for Cardiovascular Angiography and Interventions, and the Society for Cardiovascular Magnetic Resonance. J Am Coll Cardiol 56(22):1864–1894

van Werkhoven JM, Schuijf JD, Gaemperli O, Jukema JW, Boersma E, Wijns W, Stolzmann P, Alkadhi H, Valenta I, Stokkel MP, Kroft LJ, de Roos A, Pundziute G, Scholte A, van der Wall EE, Kaufmann PA, Bax JJ (2009) Prognostic value of multislice computed tomography and gated single-photon emission computed tomography in patients with suspected coronary artery disease. J Am Coll Cardiol 53(7):623–632

Van Werkhoven JM, Cademartiri F, Seitun S, Maffei E, Palumbo A, Martini C, Tarantini G, Kroft LJ, de Roos A, Weustink AC, Jukema JW, Ardissino D, Mollet NR, Schuijf JD, Bax JJ (2010) Diabetes: prognostic value of CT coronary angiography–comparison with a nondiabetic population. Radiology 256(1):83–92

Virmani R, Burke AP, Farb A, Kolodgie FD (2002) Pathology of the unstable plaque. Prog Cardiovasc Dis 44(5):349–356

Voros S, Rinehart S, Qian Z, Joshi P, Vazquez G, Fischer C, Belur P, Hulten E, Villines TC (2011a) Coronary atherosclerosis imaging by coronary CT angiography: current status, correlation with intravascular interrogation and meta-analysis. JACC Cardiovasc Imaging 4(5):537–548

Voros S, Rinehart S, Qian Z, Vazquez G, Anderson H, Murrieta L, Wilmer C, Carlson H, Taylor K, Ballard W, Karmpaliotis D, Kalynych A, Brown C 3rd (2011b) Prospective validation of standardized, 3-dimensional, quantitative coronary computed tomographic plaque measurements using radiofrequency backscatter intravascular ultrasound as reference standard in intermediate coronary arterial lesions: results from the ATLANTA (assessment of tissue characteristics, lesion morphology, and hemodynamics by angiography with fractional flow reserve, intravascular ultrasound and virtual histology, and noninvasive computed tomography in atherosclerotic plaques) I study. JACC Cardiovasc Interv 4(2):198–208

Part II
Function

CT Assessment of Global and Regional Cardiac Function: State of the Art

Rishi Agrawal and Suhny Abbara

Contents

Abstract

Reliable assessment of cardiac function is an important tool for diagnosis and prognosis of multiple cardiac and extracardiac diseases. Echocardiography and MRI are the most commonly used methods to evaluate cardiac function, but can be limited or contraindicated in certain patients. Functional evaluation with CT may play an important role in these patients and in those patients being evaluated for coronary artery disease. Functional imaging requires a retrospectively gated acquisition and special attention must be paid to the contrast injection technique for appropriate analysis. Left and right ventricular analysis is evaluated both quantitatively and qualitatively. Quantitative measurements with CT have shown close correlation with values obtained with CMR. Acute and chronic infarcts and non-ischemic cardiomyopathies can have a characteristic appearance on imaging. Functional and volumetric measurements of the left atrium can be carried out with similar technique for evaluation of patients with mitral disease or atrial fibrillation.

Abbreviations

CMR	Cardiac magnetic resonance
DSCT	Dual-source computed tomography
ED	End diastolic
EF	Ejection fraction
ES	End systolic
LA	Left atrium
LV	Left ventricle
LVEF	Left ventricular ejection fraction
MDCT	Multi-detector computed tomography
PET	Positron emission tomography
RA	Right atrium
RV	Right ventricle
RVEF	Right ventricular ejection fraction
RVOT	Right ventricular outflow tract

R. Agrawal · S. Abbara (✉)
Cardiac MRCT Program, Massachusetts General Hospital, Boston, MA, USA
e-mail: SAbbara@Partners.org

U. J. Schoepf et al. (eds.), *CT Imaging of Myocardial Perfusion and Viability*, Medical Radiology. Diagnostic Imaging,
DOI: 10.1007/174_2012_790, © Springer-Verlag Berlin Heidelberg 2013
Published Online: 30 March 2013

1 Introduction

1.1 Value of Functional Information of RV and LV

Reliable assessment of cardiac function is important for diagnosis and prognosis in multiple disease states of both cardiac and non-cardiac origin. For example, left ventricular (LV) ejection fraction is an independent predictor of survival in patients after myocardial infarction (Hammermeister et al. 1979). Additionally, in patients studied after coronary artery surgery, LV ejection fraction was shown to be a more important predictor of survival than the number of coronary arteries bypassed (Mock et al. 1982). Independent examination of LV function is important because the degree of coronary stenosis and LV function is nonlinear; once a certain threshold stenosis is reached, LV function begins to decline precipitously. Conversely, LV dysfunction, even in a regional distribution, does not always predict an underlying coronary lesion. (Juergens and Fischbach 2006) CTA provides the unique ability to evaluate both structure and function with a single test, offering convenience for both patients and clinicians.

Right ventricular (RV) function also carries important prognostic implications in numerous diseases such as acute pulmonary embolism, liver failure, arrhythmogenic right ventricular dysplasia, and congenital heart disease. Reliable and accurate assessment of the RV by CTA can be particularly helpful due to the difficulties in imaging the RV with other modalities. Function and volume measurements of the left atrium also carry prognostic significance. In particular, they are important predictors of recurrence of atrial fibrillation after pulmonary vein isolation or left atrial ablation.

In comparison to coronary artery imaging alone, functional imaging of the heart involves measurement of chamber volumes including both end-systolic volume (ESV) and end-diastolic volume (EDV). Using this information, stroke volume (SV), ejection fraction (EF), and cardiac output (CO) can be calculated. Function is also assessed qualitatively by examining the movement and wall thickening of the myocardium.

1.2 Existing Noninvasive Methods to Quantify Function

There are many noninvasive methods to quantify cardiac function including echocardiography, radionuclide ventriculography (RVG), gated single photon emission computed tomography (SPECT), gated positron emission tomography (PET), and cardiac magnetic resonance imaging (CMR). With improvements in CT technology such as multi detector-row computed tomography (MDCT) and dual source computed tomography (DSCT), CT has played an increasing role in determining cardiac function.

1.2.1 Echocardiography

Transthoracic echocardiography continues to be the most commonly used technique to evaluate cardiac function due to its widespread availability, portability, and cost. Echocardiography has the ability to measure chamber sizes and volumes, to calculate ejection fraction, and to analyze valvular function. Doppler imaging improves quantification by allowing measurement of velocities and pressure gradients through valve planes and orifices. Newer techniques like 3D ultrasound and newer software allow more reliable quantification of ventricular function.

Echocardiography, however, is limited in large patients owing to reduced ultrasound beam penetration. Additionally, evaluation of the right ventricle is limited due to suboptimal acoustic windows. Trans-esophageal echocardiography improves on these limitations but introduces additional risks associated with anesthesia and esophageal injury. Because formulas used to calculate atrial and ventricular volumes use geometric assumptions of cardiac shape, measurements in patients with remodeled cardiac chambers can be inaccurate.

1.2.2 Radionuclide Imaging

Nuclear medicine techniques to quantify cardiac function include RVG, SPECT, and PET. Whereas the purpose of RVG is to quantify left ventricular function, SPECT and PET are performed for evaluation of cardiac perfusion and metabolism. RVG utilizes ^{99m}Tc-labeled erythrocytes to directly image the blood pool and, as such, does not rely on geometric assumptions to quantify ventricular function (de Geus-Oei et al. 2011). A gated image is obtained by combining counts over multiple heartbeats, though first-pass imaging can also be performed. Both SPECT and PET rely on ventricular contour analysis to measure function. The advantage of both SPECT and PET is the additional information that each of these modalities affords. Compared to SPECT, PET offers greater spatial resolution, which may more accurately measure left ventricular function, particularly in patients with a small left ventricular volume (Slart et al. 2004). Functional data obtained with both SPECT (Bavelaar-Croon et al. 2000) and PET (Slart et al. 2004) correlates closely with functional data obtained with CMR.

There are certain limitations associated with each of these modalities. Because RVG image data is combined over multiple heartbeats, its utility can be limited in patients with an irregular rhythm. Gated SPECT is limited by low spatial resolution. Additionally, in patients with prior myocardial infarct, SPECT may show very little or no radiotracer uptake in the corresponding region of the

myocardium, preventing accurate delineation of the endocardial border (Stollfuss et al. 1998). PET suffers from lower temporal resolution than MRI, which may contribute to underestimation of cardiac function. Also, because papillary muscle signal is merged with the myocardial wall in PET, cavity volume is reduced compared to MRI which includes papillary muscle in the ventricular cavity (Slart et al. 2004). All three methods have the disadvantage of using ionizing radiation to generate images.

1.2.3 MRI

Cardiac MRI is now considered the gold standard for the assessment of cardiac function offering both high temporal resolution, allowing accurate imaging of end-systole and end-diastole, and moderately high spatial resolution, permitting accurate delineation of cardiac contours. Many studies have shown CMR to be highly accurate and reproducible (Setser et al. 2000). Imaging can be performed in any imaging plane, though quantitative assessment is usually accomplished in the short-axis plane using Simpson's method. Two-chamber, three-chamber, and four-chamber views can be obtained easily to evaluate regional wall motion abnormalities and valvular function. Detection of delayed myocardial enhancement and the development of a multitude of cardiac-gated pulse sequences have expanded the role of cardiac MRI quite extensively.

Cardiac MRI may be contraindicated in patients with pacemakers and many other metallic implanted devices. Additionally, due to the length of the study and the need to include the chest within the bore of the magnet, cardiac MRI is limited in patients with claustrophobia. The discovery of nephrogenic systemic fibrosis (NSF) in patients with renal failure receiving certain gadolinium-based contrast agents has decreased the use of IV gadolinium-based contrast in patients with renal failure. However, for strictly functional measurements, IV contrast is not needed.

1.3 Indications/Contraindications

Most cardiac CT performed today is done for the purpose of evaluating the coronary arteries rather than for the explicit purpose of measuring right or left ventricular function. Some circumstances call for the use of cardiac CT as the primary tool for determining cardiac function, usually in situations when other imaging modalities such as echocardiography or CMR are limited. For example, it is useful in patients with contraindications to MRI such as claustrophobia or implanted metallic devices. It is also useful in patients whose echocardiography study may be limited due to large body habitus. Additionally, cardiac CT is less operator-dependent compared to echocardiography and can be performed relatively quickly, making it useful in patients who cannot hold their breath or lay still for prolonged periods of time. Current ACR appropriateness criteria calls for the use of cardiac CT for the evaluation of cardiac function in patients post-myocardial infarction or in patients with heart failure if other methods of noninvasive imaging are inadequate. It is also an accepted modality for evaluation of right ventricular function and for evaluation of the pulmonary veins and left atrium prior to invasive pulmonary vein isolation. There are few contraindications to cardiac CT, the major reason being severe allergy to iodinated contrast. Even patients with mild allergy to iodinated contrast can be pre-treated with steroids and diphenhydramine to reduce the risk of allergic reaction. Patients with renal failure have an increased risk of contrast-induced nephropathy, though this is not an absolute contraindication.

1.4 Drawbacks

1.4.1 Temporal Resolution

One of the main challenges of imaging the heart is to reduce blurring artifact created with cardiac motion. The most important hardware parameter that deals with this challenge is the temporal resolution which is a function of the gantry rotation speed. For the purposes of generating an image, only a half-gantry (i.e. 180°) rotation is needed on traditional single source scanners. Scanners with faster gantry rotation have improved ability to freeze cardiac motion. Because the position of the ventricular wall at end-diastole and end-systole is averaged over the rotation interval, scanners with slower gantry rotation times (i.e. longer rotation interval) have greater potential for overestimation of ESV and underestimation of EDV (Fig. 1). Early attempts at functional cardiac imaging using 4-slice MDCT suffered from poor temporal resolution. To compensate, multi-segment reconstruction algorithms were utilized. Using this method, data from 2 (or more) different heartbeats acquired at the same phase of the cardiac cycle are combined to make an image. Two-segment reconstruction maximally decreases the temporal resolution to one half (e.g. from 210 to 105 ms), however, the degree of reduction is highly dependent on the heart rate and at some heart rates there is no improvement in temporal resolution. This technique is also susceptible to image artifacts if the heart is not in the exact same position during the second heartbeat or if there is significant beat-to-beat variability in heart rate.

Modern-day single source CT scanners have much improved gantry rotation times (down to 270 ms), largely eliminating the need for multi-segment reconstruction. Dual source CT improves on this temporal resolution by adding a second X-ray source and detector, positioned 95° from each other, approximately halving the temporal resolution of a single source system. Currently, the fastest available DSCT

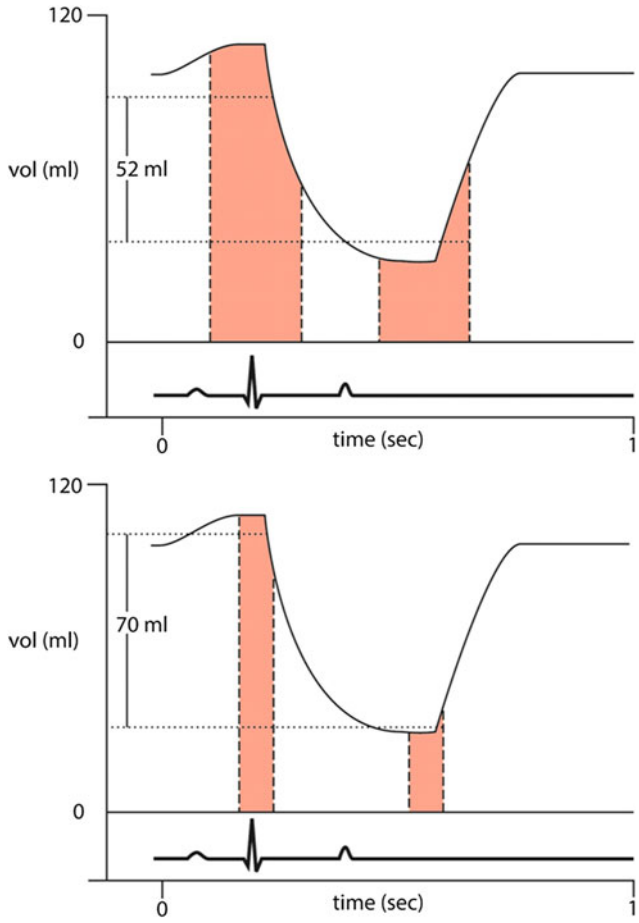

Fig. 1 Effect of temporal resolution on volume measurement. Identical time-volume curves are shown in a patient with a heart rate of 60 bpm. *Red bars* indicate sampling by the scanner. The *top* image represents a scanner with a half-gantry rotation time of 200 ms. The image data is averaged through both end-systole and end-diastole causing over-estimation of the volumes in end-systole and under-estimation of end-diastole. The *bottom* image represents a scanner with a half-gantry rotation time of 100 ms. Because the image is generated over a shorter time frame, end-systole and end-diastole more closely reflect the true values, yielding a higher ejection fraction

can cover a 180° arc of projections in ~75 ms. In comparison, MRI has a temporal resolution of approximately 30 ms. Despite these limitations, numerous studies have demonstrated close correlation between both single and dual source CT with CMR for the measurement of ventricular volumes and calculation of cardiac function.

1.4.2 Radiation Dose

Another consideration of functional cardiac CT is the additional radiation dose it requires compared to prospectively triggered axial or high-pitch spiral ("FLASH") mode coronary CTA. Conventional retrospective technique uses full, non-ECG-modulated current delivered throughout the cardiac cycle (Fig. 2). In comparison to a prospectively triggered acquisition, the radiation dose is higher; however, functional data cannot be extracted using prospective triggering. To limit the dose of radiation delivered to the patient, ECG-modulation can be employed. This is discussed in greater detail in the next section.

2 Technique

2.1 Retrospective Acquisition

In order to extract functional data from a cardiac CT exam, the heart must be imaged in both end-systole and end-diastole. To ensure that the appropriate cardiac phases are imaged, retrospective gating is usually performed. With this technique, a sustained current is generated by the X-ray tube to image throughout the cardiac cycle, during which time the table moves continuously, resulting in a helical acquisition. A low pitch is used in order to image each part of the heart throughout the R–R interval. A simultaneous ECG tracing is obtained corresponding with the image data. This differs from the prospective-triggered axial acquisition in which the tube current is only on during a pre-specified portion of the cardiac cycle, and the table moves in a step-and-shoot fashion. In addition to evaluating cardiac function, retrospective gating is helpful in evaluating patients who have arrhythmias or who are prone to premature or dropped beats because it allows reconstruction of any phase of the cardiac cycle.

ECG-modulation during a retrospectively gated acquisition may be used to reduce the radiation dose. ECG-modulation allows the user to use full current during a certain pre-defined phase of the cardiac cycle, for example between 45–70 % of the R–R interval. During the remaining phases, the tube current is reduced to a pre-specified level (usually 20 % of the maximum, but the level is customizable on some scanner models) (Fig. 3). ECG-modulation with MinDose (Somatom Definition, Siemens Medical Solutions, Germany) reduces this baseline current further to just 4 % (Fig. 4). The reduction in radiation dose depends on the width of the pulse window chosen to deliver the maximum radiation and on the amount of current delivered at baseline. Approximately 40–60 % reduction in radiation dose can be realized using these techniques (Hausleiter et al. 2006, 2007).

2.2 Implication of Scanner Type

Using modern 64-slice MDCT with retrospective gating, a continuous helical scan is obtained over multiple heartbeats with coverage of the entire heart. Due to the retrospective technique, a low pitch is used, creating regions of oversampling. Newer scanners with expanded z-axis coverage, such as 320-slice MDCT (Aquilion One Dynamic Volume

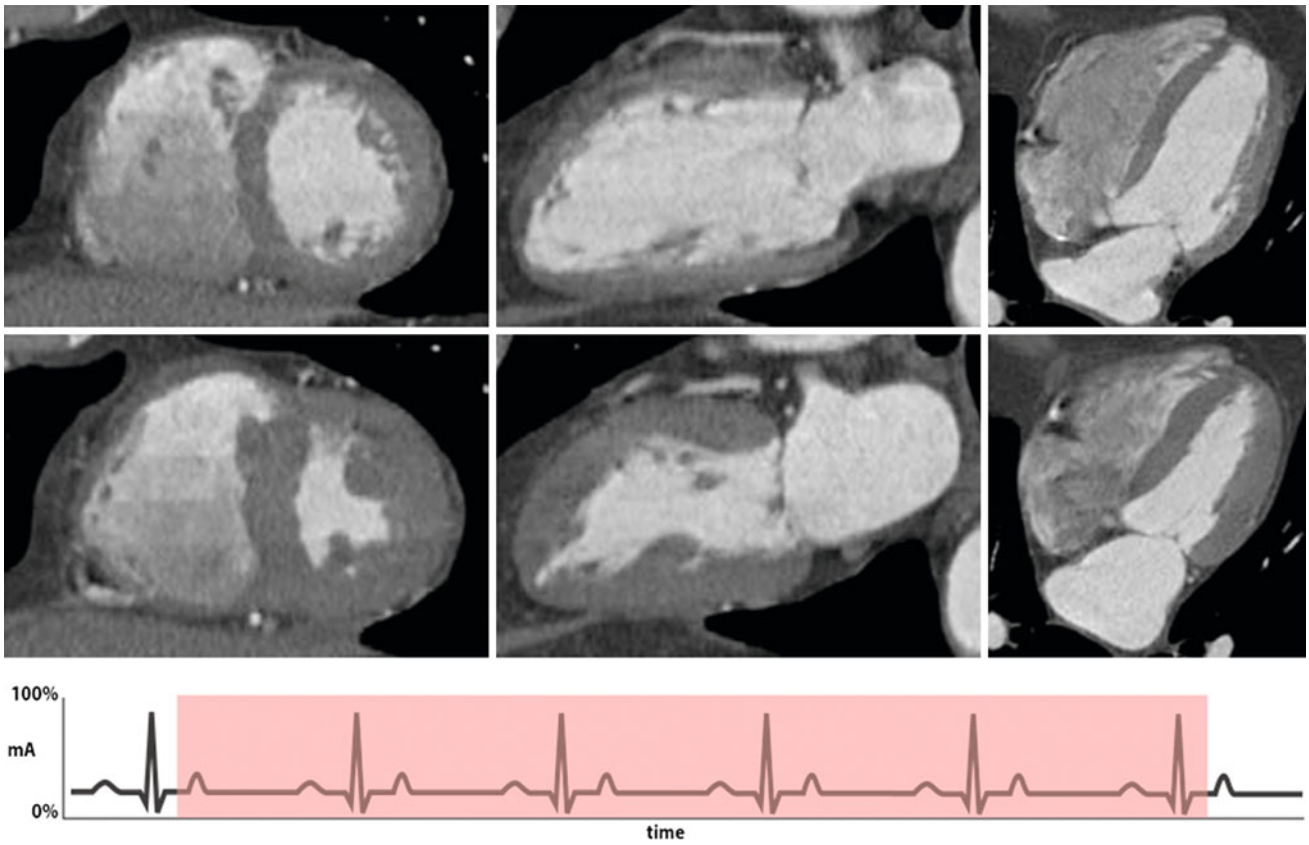

Fig. 2 Example of retrospective gating without tube current modulation. Short-axis (*left*), two-chamber (*middle*), and four-chamber (*right*) views of the heart at end-diastole (*top row*) and end-systole (*bottom row*). With full current delivered at both time points, there is no difference in image quality between the two sets of images. This technique results in a higher radiation dose. An example ECG tracing without tube current modulation is shown demonstrating a sustained acquisition over multiple heartbeats

CT, Toshiba Medical System, Tochigi-ken, Japan), have a detector width of 16 cm allowing a single-heartbeat acquisition. Dual-flash imaging with DSCT during end-systole and end-diastole has been offered as a potential method to obtain functional data without using retrospective gating, with significant reduction in radiation dose. This technique, however, is rarely used in clinical practice and is still under investigation.

2.3 Beta Blockers

Most studies performed for evaluation of the coronary arteries employ the use of beta-blockers to reduce the heart rate for improved image quality. A target heart rate in the high 50 to low 60 s is required for most scanners. While beta-blockade has been shown to improve the diagnostic image quality of the coronary arteries, there is evidence to suggest there are concurrent effects on left ventricular function. A study by Port using echocardiography demonstrated a reduction in ejection fraction in healthy adults after administration of propranolol (Port et al. 1980; Mo et al. 2011). The proposed mechanism is that through negative inotropic action on the heart, ESV increases, thus decreasing the EF. Other studies in healthy patients using cardiac CT for measurement of left ventricular function show similar results, although differences in ESV and EF were modest (Mo et al. 2011).

Studies in patients with heart disease have shown that beta-blockade can produce decreases in measured function, again resulting from increases in ESV (Dell'Italia and Walsh 1989; Jensen et al. 2010). Because most cardiac CTAs performed today are for evaluation for coronary artery disease, the use of beta-blockers for improving image quality usually takes precedence over potential fluctuations in measured LVEF. Scanners with improved temporal resolution (up to 73 ms) have precluded the need for beta-blockade in many patients, particularly when retrospective gating is utilized.

2.4 Contrast Injection

Depending on the cardiac chambers of interest, the injection parameters may require modification from a traditional

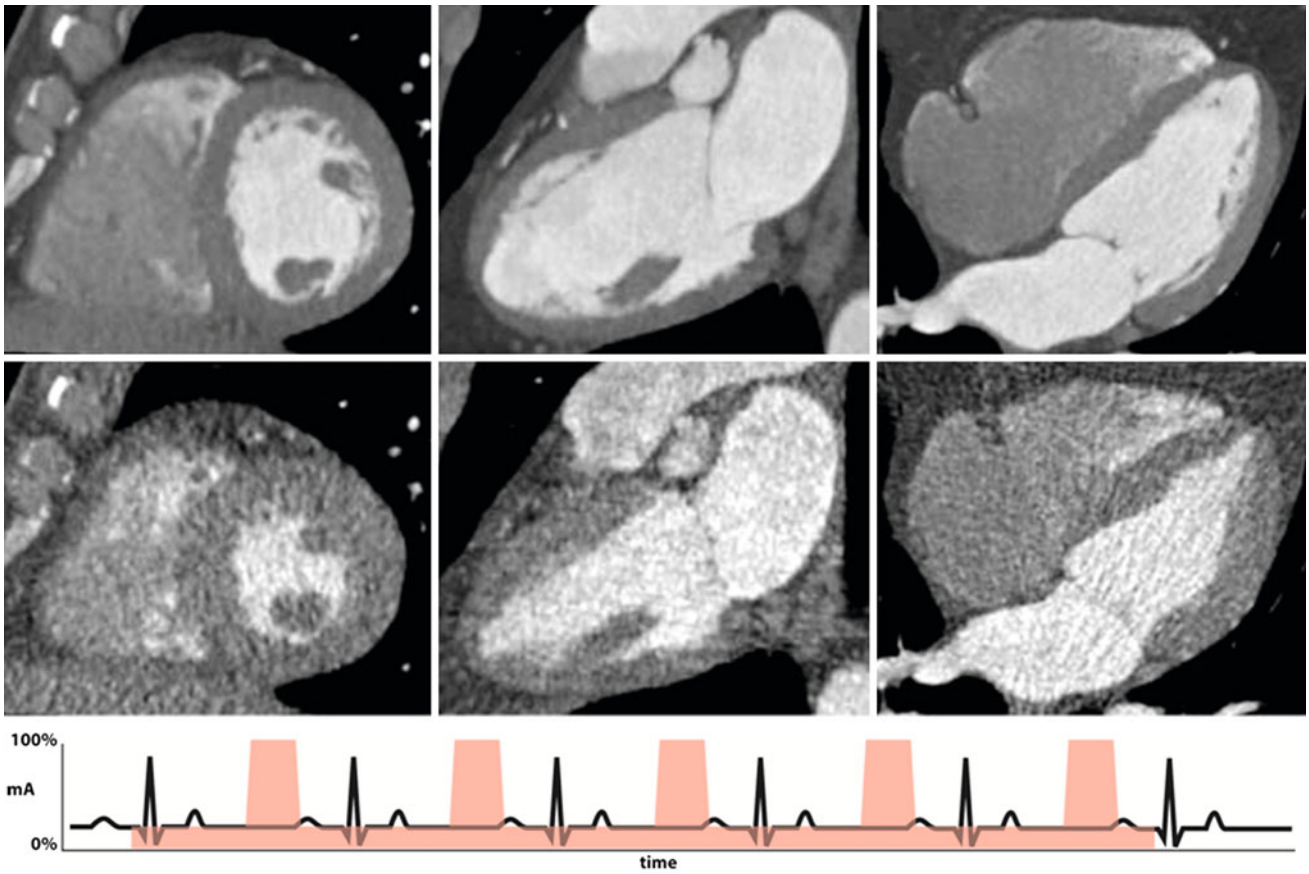

Fig. 3 Example of retrospective gating with tube current modulation. Short-axis (*left*), two-chamber (*middle*), and four-chamber (*right*) views of the heart at end-diastole (*top row*) and end-systole (*bottom row*). Notice the difference in image noise at end-diastole, obtained at full tube current, and end-systole, obtained at 20 % of maximum tube current. Despite the increased image noise at end-systole, images are adequate for delineation of endocardial contours for functional measurement. An example ECG tracing with tube current modulation at 20 % is shown

coronary CTA. Typical coronary CTA employs either bolus tracking or test bolus technique to measure the transit time of the contrast from the site of injection to the ascending aorta. Many institutions utilize a saline chaser after injection of contrast medium. This results in a tighter contrast bolus and reduces streak artifact in the central veins of the thoracic inlet. This technique provides high contrast opacification of the coronary arteries and adequate delineation of the LV endocardium.

In order to achieve adequate, reliable, contrast opacification of both the RV and LV, a multiphasic injection is needed. This involves contrast injection at a normal flow rate (4–7 cc/sec) to opacify the left heart followed by a slower rate (2–4 cc/sec) to opacify the right heart. This is then followed by a saline chaser. An alternative technique is to first inject contrast and follow with a mixture of contrast and saline in a 60:40 or 50:50 ratio. A typical injection may consist of 50 ml of contrast at 6 cc/sec followed by an additional 50 ml of the contrast/saline mixture at 6 cc/sec. Using a multiphasic technique allows contrast opacification of both the left and the right ventricles and reduces the chance of generating streak artifact from highly concentrated contrast in the SVC, right atrium, or right ventricle (Gao et al. 2012). Lee et al. (2012) analyzed the accuracy of CT in measuring RV function using automated processing software and compared the results to CMR. Low attenuation of the RV blood pool correlated with greater discrepancy with CMR; whereas, when the RV blood pool was greater than 176 HU, measurements were closer to those of CMR, underscoring the importance of proper contrast injection technique.

2.5 Reconstruction Phases

After retrospective scanning, the user has the ability to select the number of phases available for reconstruction. A phase is an interval of the cardiac cycle, usually expressed as a percentage of the RR interval. For example, for reconstruction of cine images, reconstruction of equally spaced phases over the RR interval are obtained, generally in 5 or 10 % increments (yielding 20 or 10 phases,

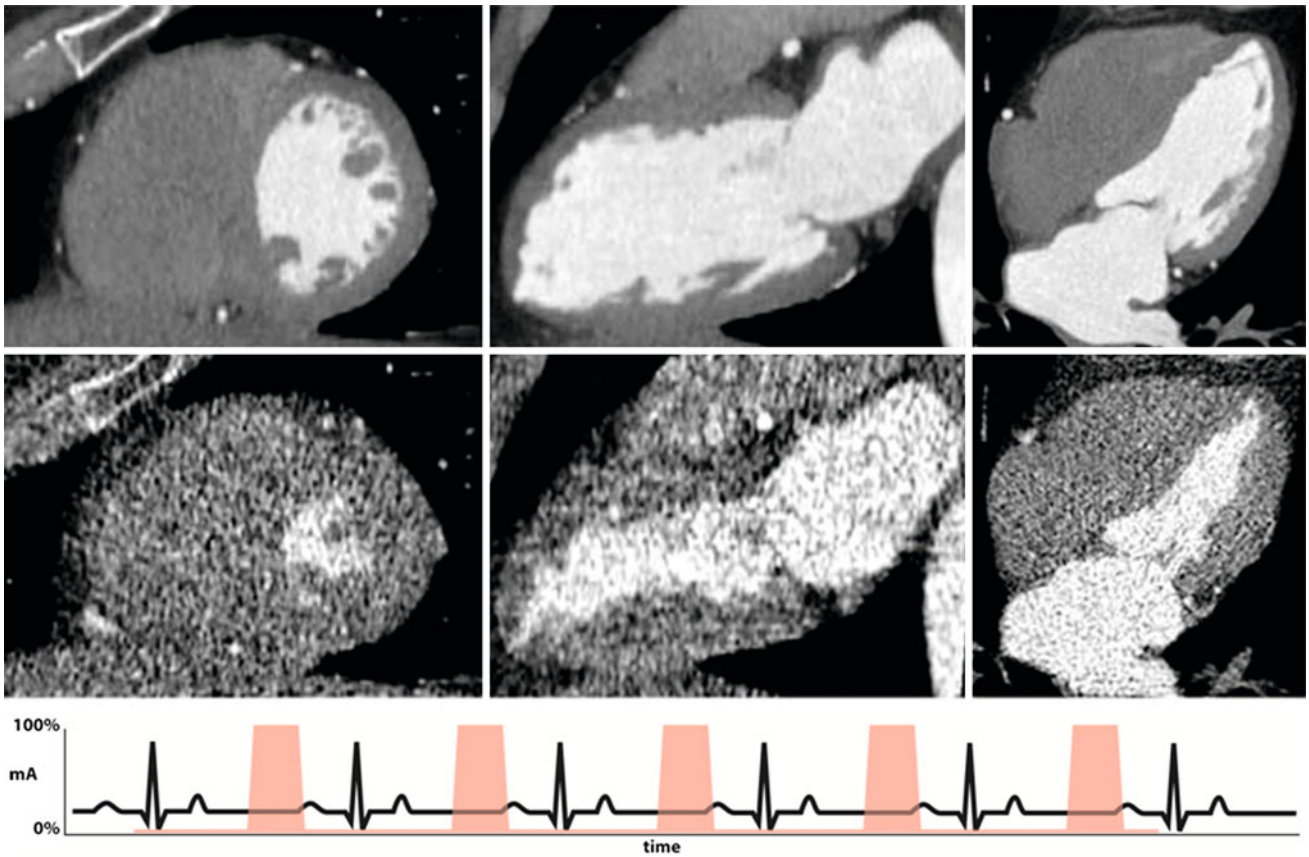

Fig. 4 Example of retrospective gating with tube current modulation down to 4 % of the maximum current. Short-axis (*left*), two-chamber (*middle*), and four-chamber (*right*) views of the heart at end-diastole (*top row*) and end-systole (*bottom row*). There is significant difference in image noise at end-diastole at full tube current and end-systole, obtained at 4 % of maximum tube current. Despite the increased image noise at end-systole images are quite adequate for delineation of endocardial contours for functional measurement in this relatively thin patient. An example ECG tracing with tube current modulation at 4 % is shown

respectively). Increasing the number of phases reconstructed from 10 to 20 doubles the number of images generated for review. A study by Ko et al. (2011) compared 10 and 20 phase reconstruction with respect to cardiac function using a 64-slice scanner. No significant difference in LV volume or EF was observed between the two methods. The increase in the number of phases reconstructed does not change the inherent temporal resolution of the scanner, which is a function of the gantry rotation.

Newer scanners with faster gantry rotation times may be able to take better advantage of more reconstruction intervals. First and second generation dual source CT (DSCT) has the advantage of significantly improved temporal resolution compared to conventional single source CT. Puesken et al. (2008) compared 10 and 20 phase reconstruction using a first generation DSCT. Though use of 20 phases changed the selection of the ES and ED phase in about half of patients, this change resulted in an average 1.9 % change in EF, suggesting that 10 phase reconstruction may be adequate in DSCT as well.

2.6 Post-Processing

One of the major advantages of CT over other modalities is that images are readily acquired as a volumetric dataset. This allows reconstruction of the image in any plane. Modern software packages allow reconstruction of cine images on-the-fly allowing instantaneous visualization of an abnormality in an orthogonal plane. Short axis, 4-chamber, 3-chamber, and 2-chamber views are used to evaluate global function and to evaluate regional wall motion abnormalities. 3-D images of the ventricular blood pool can be obtained with the myocardium subtracted, simulating conventional catheter ventriculography.

2.7 Semi-automatic Versus Automatic Versus Manual

There are multiple methods available to quantify right and left ventricular volumes ranging from time-intensive

manual techniques to fully automated software packages. All techniques rely on measurements in end-diastole and end-systole.

The area-length method is a technique borrowed from echocardiography and can be used in calculating left ventricular volume with CT. As the name implies, this technique relies on the measurement of the area and length of the left ventricle. The area is calculated in either the vertical or horizontal long axis plane. The length is measured as the distance from the mitral valve plane to the apex. Using the following formula, left ventricular volume is then calculated.

$$\text{Volume} = \frac{8}{3} \times \frac{A^2}{\pi \times L}$$

This formula uses geometric assumptions about the left ventricle, specifically assuming an ellipsoid shape. A variation of the area-length method is the *biplane* area-length method which uses both the vertical and horizontal long axes to calculate the volume.

Simpson's method is commonly used in calculating ventricular volume in CMR and can be used to calculate both left and right ventricular volume. In contrast to the area-length method, Simpson's method does not rely on assumptions about ventricular shape. Using this technique, contours are drawn around the endocardial border in end-systole and end-diastole in the short-axis plane. Each contour represents a volume determined by the slice thickness and gap or overlap. The contours are summed using the following formula where A is the cross-sectional area and S is the slice thickness plus gap, or slice thickness minus overlap.

$$\text{Volume} = \sum A_N \times S$$

Studies comparing area-length method and Simpson's method have shown close agreement between the two, even in patients with regional wall motion abnormalities, although there is slight overestimation of EDV, ESV, and SV using the area-length method (Lessick et al. 2008).

Semi-automated and fully automated software packages are available from multiple vendors. These use a threshold-based segmentation that detects the difference in attenuation between the ventricular chamber and the myocardium; thus, adequate opacification of the blood pool is required. The main advantage of these techniques is the significant time savings over manual processing. A byproduct of semi-automated and fully automated segmentation is that once the mitral valve plane is defined, all available phases can be segmented, allowing time-volume curves to be drawn. Studies comparing manual, semi-automated, and fully automated software have shown close correlation of ventricular volumes using these methods with significant reduction in processing time and good interobserver variability (Greupner et al. 2011; Juergens et al. 2008; Plumhans et al. 2009).

A caveat of the threshold-based methods is that papillary muscles are excluded from the blood pool. This results in systematic underestimation of EDV and ESV as well as overestimation of EF compared to CMR. However, when the same software tools and measurement methods are used for analysis of both the CT and MR, close agreement between the two modalities is observed (de Jonge et al. 2011).

The threshold method is also susceptible to errors from high-attenuation material. For example, streak artifact from dense contrast in the central veins or right heart can lead to errors in contour detection. Pacemaker leads can cause the software to include the right atrial or ventricular chambers in the LV blood pool. Ventricular septal defects can cause similar errors owing to a continuous, unbroken column of contrast (Juergens et al. 2008; van Ooijen et al. 2012).

2.8 Calculation of Values

Once EDV and ESV are acquired, simple subtraction of the values yields the stroke volume (SV); that is, the amount of blood ejected from the ventricle with each beat. Importantly, the SV calculated using this method includes blood flow in any direction, not exclusively flow through the ventricular outflow tract. Regurgitant flow through the mitral or tricuspid valve and ventricular septal defects will be included in this value. As an internal check, and in the absence of valvular regurgitation or shunting, the stroke volume in the RV and LV should be the same.

$$\text{SV(ml)} = \text{EDV} - \text{ESV}$$

Cardiac output can then be obtained by multiplying the SV by the heart rate.

$$\text{CO(ml/min)} = \text{SV} \times \text{HR}$$

The ejection fraction is calculated by determining the percentage of blood exiting the ventricle using the EDV as the baseline.

$$\text{EF}(\%) = \frac{\text{SV}}{\text{EDV}} \times 100$$

Normalization of these values to the body surface area (BSA) is helpful to stratify results.

3 Left Ventricle

3.1 Normal Values

Numerous studies have defined the normal values of left ventricular volume using CMR and echocardiography. Because of differences in temporal resolution, image quality, and measurement technique, values obtained with other modalities should not be translated to CT (Lin et al. 2008). Values normalized to BSA are given below.

Normal values for the left ventricle using MDCT				
Parameter	Men		Women	
	Mean	SD	Mean	SD
ESV (ml)	48.56	16.13	29.58	11.1
EDV (ml)	143.58	28.11	102.14	12.61
ESVI (ml/m^2)	24.48	8.51	17.63	6.66
EDVI (ml/m^2)	72.35	15.09	60.86	13.31
EF (%)	66.9	7.3	71.6	7.9

ESV end-systolic volume, *EDV* end-diastolic volume, *ESVI* end-systolic volume index, *EDVI* end-diastolic volume index, *EF* ejection fraction (Nevsky et al. 2011)

3.2 Comparison with Echo, MR

The combination of excellent temporal resolution and good spatial resolution make CMR the current gold standard for the evaluation of left ventricular function. Numerous studies have evaluated measurements of left ventricular function using CCT compared with CMR. A meta-analysis of 8–16 slice MDCT compared to CMR demonstrated close correlation of ESV, EDV, and LVEF. The use of multi-segmental reconstruction algorithms showed improvement in correlation, likely owing to increased temporal resolution allowed by these techniques (van der Vleuten et al. 2006).

Current scanner technologies, including 64-, 128-, 256-, 320-slice single source CT, and dual source CT (64 and 128 slice), have also shown excellent correlation with CMR even without the use of multi-segmental reconstruction algorithms due to improvement in temporal resolution.

3.3 Wall Motion Abnormalities

3.3.1 Introduction

Abnormal wall motion can be divided into regional abnormalities affecting parts of the myocardium and global abnormalities affecting an entire chamber. Regional wall motion abnormalities at rest are usually attributed to rest ischemia or myocardial infarction and can be mapped to a coronary territory; global abnormalities are usually due to either severe multivessel disease or non-ischemic cardiomyopathy.

3.3.2 Segmental Assessment

CT data are acquired in an axial plane in relation to the body axis. Volumetric data is then reconstructed in planes analogous to those used in echocardiography and nuclear medicine, i.e., long and short axes with respect to the ventricular long axis. For diagnostic consistency among imaging modalities and to allow correlation between coronary anatomy and wall segments, the traditional AHA 17-segment model is used in CT when describing regional wall motion abnormalities. Using this model, the basal and mid-ventricular LV levels are divided into six segments, the apical level is divided into four segments, and the apex constitutes a final segment.

Regional wall motion abnormalities are usually assessed qualitatively based on cine images. Wall motion abnormalities can be described as *akinetic* in the absence of systolic thickening, *hypokinetic* when wall motion is subnormal, or *dyskinetic* when there is paradoxical motion compared to other regions (i.e., outward bulging during systole, lack of coordination). Quantitative measurements can also be made based on the amount of wall thickening compared to adjacent normal myocardium. There is significant regional variation within the same patient, and more so between patients, but estimates for normal myocardial thickness are 6–8 mm at end-diastole and 10–14 mm at end-systole for normal systolic thickening of approximately 5 mm (Juergens and Fischbach 2006).

3.3.3 Global Assessment

Global function or dysfunction refers to both the qualitative assessment of myocardial movement and wall thickening as well as the quantitative measurement of volume and

CT versus MRI	n	CT scanner	EDV			ESV			EF		
			r	Bias (ml)	SD (ml)	r	Bias (ml)	SD (ml)	r	Bias (%)	SD (%)
Dual source CT											
Takx et al. (2012)	20	DSCT[a]	0.89	−5.1	21.6	0.95	−5.7	14.7	0.87	5.1	7.6
Bastarrika et al. (2008)	12	DSCT	0.70	16.6	18.6	0.39	4.9	6.9	0.64	−0.3	3.2
Brodoefel et al. (2007)	20	DSCT	0.98	−2.2		0.99	−1.4		0.95	0.7	

(continued)

(continued)

CT versus MRI	n	CT scanner	EDV			ESV			EF		
			r	Bias (ml)	SD (ml)	r	Bias (ml)	SD (ml)	r	Bias (%)	SD (%)
Busch et al. (2008)	15	DSCT	0.81	3.7	25.4	0.79	−2.6	17.3	0.64	3.8	9.4
Jensen et al. (2010)	32	DSCT	0.87	−1.3	17.7	0.92	1.0	8.3	0.83	−1.0	4.5
Lunders	30	DSCT	0.96	−0.3	18.2	0.98	1.1	7.8	0.97	−1.1	7.8
van der Vleuten et al. (2009)	34	DSCT	0.96	11.0	54.8	0.97	3.5	31.9	0.90	0.4	4.5
64 SLICE CT											
Akram et al. (2009)	20	64	0.80	0.6	21.4	0.86	−2.3	8.5	0.92	1.6	3.4
Annuar et al. (2008)	32	64	0.98	−8.8	12.5	0.98	−6.3	9.8	0.92	−2.3	6.7
Guo et al. (2009)	51	64	0.93	5.7	27.8	0.92	0.8	17.5	0.89	1.3	5.7
Maffei et al. (2012)	79	64	0.59	3.3	25.8	0.76	2.6	35.1	0.73	0.6	21.1
Sarwar et al. (2009)	21	64	0.91			0.94			0.90		
Schlosser et al. (2007)	21	64		−19.9	20.3		−13.4	10.3		3.9	7.5
Wu et al. (2008a)	41	64	0.96			0.98			0.95		
Wu et al. (2008b)	63	64	0.98	−0.6	15.2	0.99	1.1	10.6	0.97	−0.2	−4.2
4-16 SLICE CT											
Belge et al. (2006)	40	16	0.92			0.95			0.95		
Dewey et al. (2006)	88	16	0.87	−6.2	20.7	0.92	−5.2	12.9	0.91	2.1	5.2
Fischbach et al. (2007)	30	16	0.96	−16.8	19.4	0.94	6.9	10.2	0.83	−2.5	4.2
Grude et al. (2003)	30	4	0.80	14.2	17.3	0.89	17.8	10.3	0.85	−8.5	4.7
Halliburton	15	4	0.26	−35.2		0.62	−22.4		0.30	−1.6	
Heuschmid et al. (2005)	31	16	0.86	13.2	21.9	0.91	8.7	15.9	0.87	1.4	5.2
Juergens et al. (2004)	30	4	0.93	0.4	11.8	0.94	0.2	7.2	0.89	0.3	0.5
Koch et al. (2004) SAX	19	16	0.98	−3.2		0.98	−7.3		0.95	3.0	
Koch et al. (2004) 3D TH			0.96	−4.8		0.98	−4.6		0.91	0.3	
Mahnken et al. (2005)	21	16	0.99	−1.0	1.9	0.99	−0.4	1.6	0.99	−0.1	1.0
Mahnken et al. (2003) (std)	15	4		−7.5	3.4		−1.7	4.4		0.8	3.3
Mahnken et al. (2003) (mult)				−0.3	1.0		−0.3	1.0		0.5	2.1
Matthias	37	4	0.80	14.1	17.3	0.89	17.8	10.3	0.85	−0.9	4.7
Raman et al. (2006)	26	16	0.97	−2.7	7.8	0.97	−1.0	7.4	0.97	0.3	3.6
Salm et al. (2006)	25	16							0.86	−1.5	8.6
Schlosser et al. (2007) (std)	18	16		−17.2	13.1		−9.1	10.9		2.6	7.3
Schlosser et al. (2007) (auto)				−20.3	15.7		−9.2	13.9		1.0	9.0
Sugeng et al. (2006)	31	16	0.98	26.0	21.4	0.97	19.0	25.5	0.92	−2.8	6.6
Yamamuro et al. (2005)	50	8	0.97	−0.4	15.2	0.99	1.1	8.6	0.96	−1.2	4.6

EDV end-diastolic volume, *ESV* end-systolic volume, *EF* ejection fraction, *SD* standard deviation

[a] Indicates second generation DSCT

function. Qualitatively, normal myocardium should demonstrate brisk systolic contraction and wall thickening. Hypofunctioning myocardium can be uniform or it can demonstrate regional variation with some segments demonstrating worse function compared to others. Global function can also be described as hyperdynamic, commonly seen in patients with hypertrophic cardiomyopathy. Assessment of global LV function carries important prognostic implications. Data from the Coronary Artery Surgery Study (CASS) registry showed that in patients with cardiac ischemia, the ejection fraction was more closely associated with adverse outcomes than the number of diseased coronary vessels; as the EF decreased below 45 %, the risk of death increased in a linear fashion. (Mock et al. 1982).

3.4 Disease Entities of the LV

3.4.1 Chronic Ischemia

Segments of myocardium that are chronically ischemic but still metabolically active may demonstrate reduced function in the form of segmental hypokinesis. This is referred to as hibernating myocardium. Hibernating myocardium is clinically important to differentiate from nonviable myocardium because revascularization by angioplasty, stenting, or grafting may restore function to these segments. PET and CMR are now the most commonly used tools to evaluate for viable, hibernating myocardium although CT is beginning to play a larger role in this realm. This topic is discussed in further detail in subsequent chapters.

3.4.2 Acute Infarcts

Within a few minutes after an acute myocardial infarct, there is development of a regional wall motion abnormality in the distribution of a coronary territory, usually demonstrated by an akinetic segment. Depending on the transmurality of the infarct and remaining functioning myocardium, regional wall motion abnormalities may improve over time as stunned but still viable myocardium regains function (Mahias-Narvarte 1987). Sarwar et al. (2009) examined 64-slice CT compared to CMR for evaluating global and regional left ventricular function specifically in patients recently reperfused after acute myocardial infarction. Quantification of LV volumes and EF by CT was shown to correlate well with values obtained by CMR. CCT demonstrated 89 % sensitivity and 92 % specificity in detecting abnormal segments (on a per-segment basis) using CMR as the standard.

In the setting of acute chest pain, functional evaluation of the left ventricle with CT has been shown to add incremental value to the assessment of the coronary arteries by CTA. In the Rule Out Myocardial Infarction Using Computer Assisted Tomography (ROMICAT) trials, patients with chest pain, initial negative troponin, non-ischemic EKG, but clinical suspicion for acute coronary syndrome (ACS) were arranged to have a coronary CTA with retrospective gating. The diagnostic accuracy of CTA for the detection of ACS was 77 % with coronary evaluation alone; the addition of a resting regional LV function increased the diagnostic accuracy to 87 %. LV wall motion abnormalities can also help to direct attention to lesions that are too small to resolve by CTA such as side branches or small vessels (Seneviratne et al. 2010).

3.4.3 Chronic Infarcts

The appearance of a chronic infarct can be variable by CT depending on the territory and severity of the infarct. Transmural infarcts will demonstrate focal wall thinning in a coronary distribution with regional akinesis or dyskinesis. (Figure 5) Fatty metaplasia or calcification can be seen in place of normal myocardium.

In cases of transmural infarction, a left ventricular aneurysm may form. In the strict definition, an aneurysm is a focal contour deformity with wall thinning that moves paradoxically (i.e. dyskinetic) in relation to the rest of the myocardium. Most aneurysms involve the apical anterior wall resulting from a transmural LAD infarct. Inferior basal wall infarcts are second most common location. In cases of non-transmural infarction, residual functioning or hibernating myocardium prevents aneurysm formation but may result in focal akinesis or hypokinesis (Glower and Ei 2003).

3.4.4 Non-ischemic Cardiomyopathies

Non-ischemic cardiomyopathies are intrinsic diseases of the heart muscle and can be divided into primary and secondary diseases. Some secondary causes include alcohol, chemotherapy, sarcoid, and genetic diseases. The World Health Organization and the International Society and Federation of Cardiology Task Force divides primary cardiomyopathies into 5 categories: dilated cardiomyopathy, hypertrophic cardiomyopathy, restrictive cardiomyopathy, arrhythmogenic right ventricular dysplasia, and unclassified disease. These diseases are characterized primarily by either normal function or global hypokinesis, although regional variation may be evident in some cases.

Functional imaging in patients with dilated cardiomyopathy typically shows an enlarged left ventricle with global LV hypokinesis. The right ventricle can be involved in some cases. Not infrequently, the apex is completely akinetic. (Figure 6) Hypertrophic cardiomyopathy is characterized by poor base-to-apex shortening and obliteration of the cavity at the LV apex. The calculated ejection fraction is usually supranormal. In patients with restrictive cardiomyopathy, LV contraction is preserved but relaxation in diastole is impaired. Common causes of restrictive disease

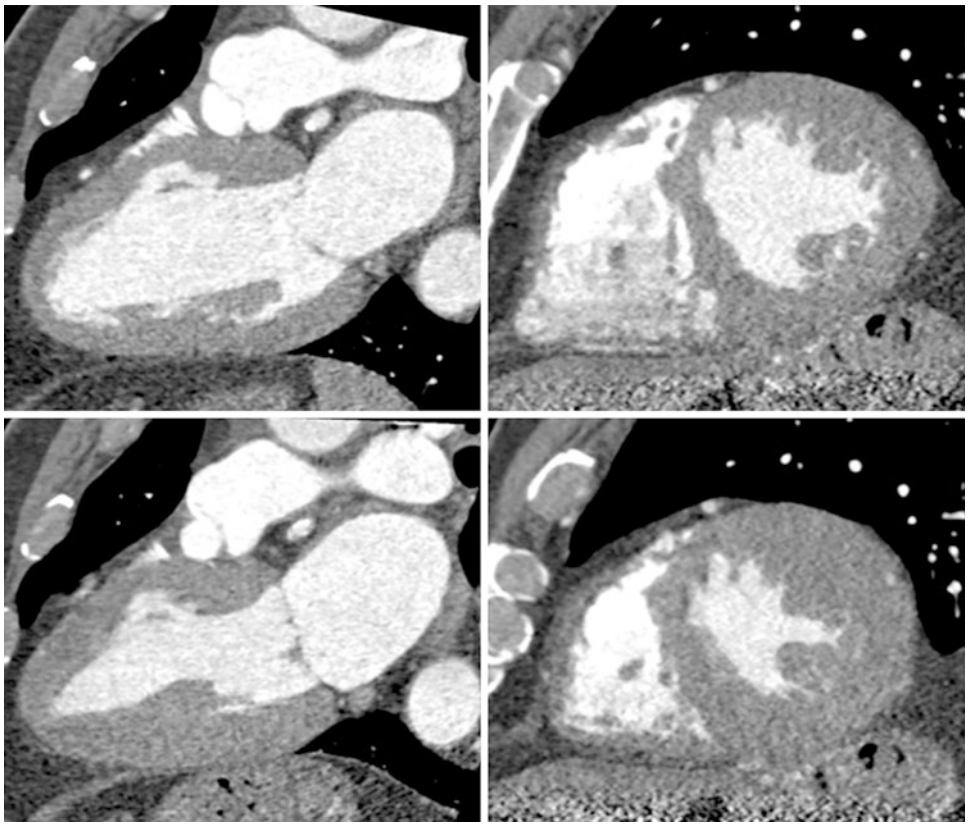

Fig. 5 Two-chamber (*left*) and short-axis (*right*) views of the *left* ventricle in end-diastole (*top row*) and end-systole (*bottom row*). This patient had a remote history of LAD infarct. Note the focal anterior wall thinning with only minimal increase in wall thickness on systolic images, consistent with nontransmural remote infarct

include amyloid, sarcoid, hemochromatosis, and glycogen storage diseases.

Tako-tsubo cardiomyopathy is an uncommon entity that can mimic an acute coronary syndrome. Patients usually describe a recent emotional stressor; thus, the alternative term of "broken-heart syndrome" has also been used. Functional imaging demonstrates dyskinesis of the mid and apical segments causing a ballooning of the LV in systole. Basilar function is usually preserved. Function returns to normal within a few days.

3.4.5 Heart Transplant

Patients with heart transplant typically present a unique problem for cardiac CT owing to a high resting heart rate and body mass index, as well as altered cardiac anatomy (Ferencik et al. 2007). Improvements in immunosuppressive therapies have increased survival to approximately 50 % at 10 years and 30 % at 15 years (Taylor et al. 2008). Longer survival has uncovered new challenges, such as cardiac allograph vasculopathy. CCTA can offer a one-stop-shop solution for follow up of these patients by evaluating both the coronary vessels and cardiac function. Studies using both MDCT and DSCT have shown accurate assessment of left ventricular function compared to CMR (Mastrobuoni et al. 2011; Bastarrika et al. 2008). The use of DSCT with improved temporal resolution is especially helpful in these patients due to the high resting heart rate.

4 Right Ventricle

4.1 Normal Values

Normal values for the right ventricle using MDCT	
ESD (mm)	29.6 ± 5.3
EDD (mm)	37.0 ± 5.7
EDV (ml)	174.9 ± 48.0
ESV (ml)	82.1 ± 29.2
EF (%)	57.9 ± 8.0

(Lin et al. 2008)

4.2 Indications

Imaging of the RV poses special challenges because of its unique shape and the presence of irregular trabeculations. Echocardiography is particularly problematic because the RV is mostly retrosternal in position and acoustic windows are limited. Thus, cross-sectional imaging plays an important role in patients with right heart disease. Assessment of right ventricular function carries important prognostic information in patients with acute diseases, such as acute respiratory distress syndrome and pulmonary embolism

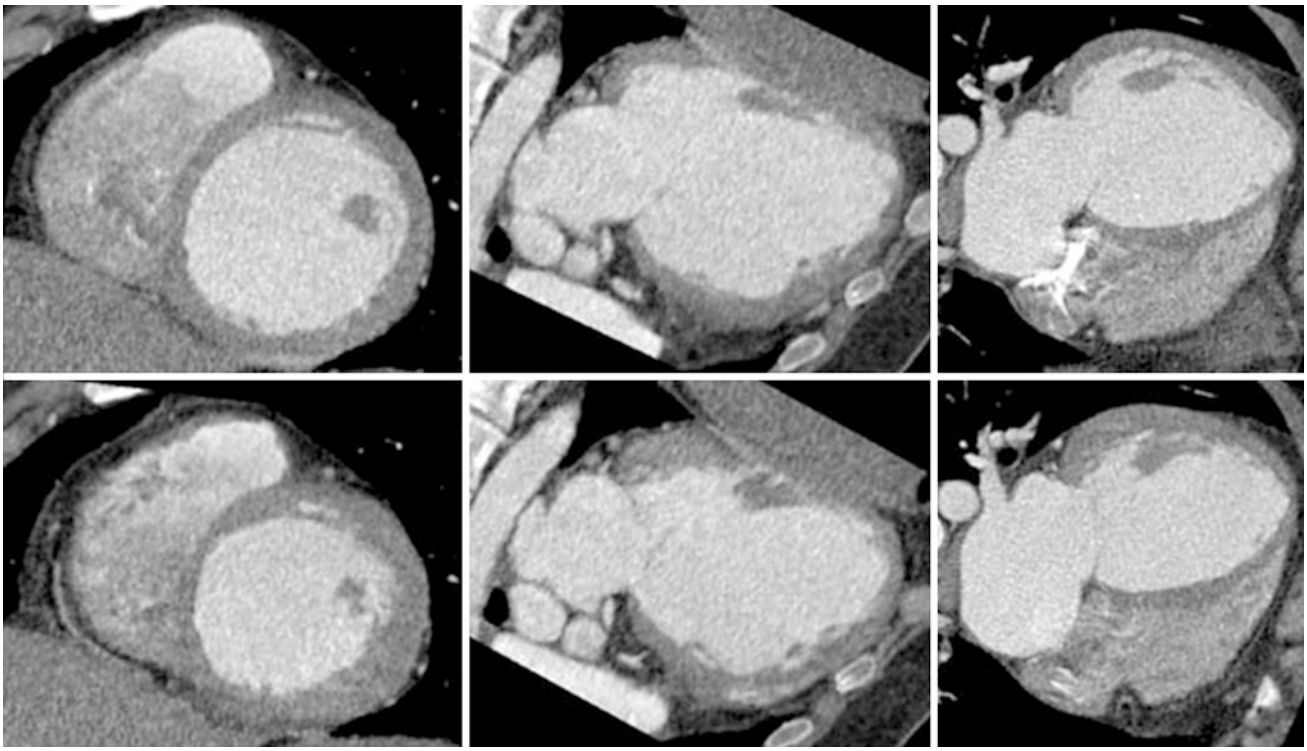

Fig. 6 Short-axis (*left*), two-chamber (*middle*), and four-chamber (*right*) views of the *left* ventricle in end-diastole (*top row*) and end-systole (*bottom row*) in a patient with dilated cardiomyopathy. The *left* ventricle is markedly enlarged. Note the lack of significant movement or wall thickening on systolic images (*bottom*) indicating globally reduced systolic function. The EF in this patient was 15 %

(PE). For example, in patients with acute PE, right ventricular dysfunction is associated with higher rates of intubation, ICU admission, and death. Rapid selection of patients with right ventricular dysfunction can help assess those patients who need catheter-directed thrombolysis or surgical embolectomy (Kang et al. 2011).

Measurement of RV volume and function also carries important prognostic significance in chronic lung diseases resulting in cor pulmonale. In patients with COPD, increased RV end-diastolic volume and decreased RV function are strongly associated with decreased survival (Burgess et al. 2002). A multitude of diffuse lung diseases are associated with cor pulmonale including interstitial lung disease, vascular disorders causing pulmonary hypertension, and sleep-related breathing disorders.

Liver disease is an established cause of increased right heart volumes. This can occur through portopulmonary hypertension, hepatopulmonary syndrome, or as a result of TIPS therapy (Dupont et al. 2011). Finally, many congenital heart diseases, such as tetralogy of Fallot, transposition of the great vessels, arrhythmogenic right ventricular dysplasia/cardiomyopathy, and double outlet right ventricle, affect the RV (Savino et al. 2007). In these patients, serial measurement of RV function can be an important part of surveillance.

4.3 Pulmonary Embolism

4.3.1 RV:LV Ratio

Small, subsegmental pulmonary emboli do not usually induce RV dysfunction because of the compensatory mechanisms of the pulmonary arterial system. However, as the clot burden in the pulmonary arteries increases, signs of RV strain can begin to show; a 30–40 % obstruction of the pulmonary arterial tree can result in modest increases in right ventricular pressure. With continued increase in pulmonary arterial obstruction, right ventricular failure can develop causing increases in right and left atrial volume (Fishman et al. 2008). Many of these functional changes in the right ventricle can be gleaned without retrospective imaging or even cardiac gating.

The relative volume of the RV can be estimated by comparing the short-axis dimension with the LV. This measurement should be obtained perpendicular to the long axis of the heart, ideally using a 4-chamber reconstruction, measuring from the right ventricular free wall to the septum. An RV:LV ratio greater than 1 is a sign of increased right ventricular volume (Fig. 7).

This sign can be quickly assessed in patients being evaluated for pulmonary embolism as an indicator of right ventricular volume overload and right heart strain. Often, a

Fig. 7 Four-chamber view of the heart demonstrates bowing of the interventricular septum with convexity into the *left* ventricle. The maximal dimension of the RV (*solid line*) was much greater than the LV (*dotted line*). The RV:LV ratio in this patient was 1.6. Notice segmental pulmonary emboli in the *right* and *left* lower lobe pulmonary arteries (*arrows*)

crude measurement can be made on axial images, roughly approximating a 4-chamber view. However, measurement in the 4-chamber view is more sensitive for the stratification of patients with severe disease. A study by Quiroz et al. demonstrated that measurement of the RV:LV ratio in the 4-chamber view increased the receiver operating curve for the prediction of adverse events including the need for resuscitation, mechanical ventilation, pressors, thrombolysis, or surgical embolectomy (Quiroz et al. 2004).

4.3.2 Septal Bowing

Static images of the heart may show straightening or concave bowing of the interventricular septum into the left ventricular cavity. This can be a sign of increased right ventricular volume, pressure, or both. Gated images can help to distinguish between these two entities. Increased right ventricular pressure will demonstrate bowing of the septum throughout the cardiac cycle; whereas, in volume overload, the septal bowing often normalizes during systole. The presence of increased right ventricular wall thickness suggests chronic pressure overload.

4.3.3 Systemic Vein Diameter

As right ventricular failure progresses, excess volume is translated to the right atrium and systemic veins. Measurements of the SVC, azygous vein, and coronary sinus are usable surrogates for right ventricular dysfunction in patients with PE. These measurements can be done relatively quickly in the axial plane and have been shown to correlate with elevated PA pressures measured by echocardiography. For example, coronary sinus dimension of 16 mm or greater was shown to correlate with peak systolic PA pressures of greater than 30 mmHg compared to a median diameter of 10 mm in patients with pressures less than 30 mmHg. A reasonable cutoff for the SVC is 25 mm in diameter and 10 mm in diameter for the azygos vein (Staskiewicz et al. 2010).

4.4 ARVD/C

Arrhythmogenic right ventricular dysplasia is a cardiomyopathy in which there is replacement of myocardium in the RV by fibrofatty tissue. Patients may be asymptomatic, but may also present with arrhythmias and sudden cardiac death; biventricular heart failure can be seen in late stages of the disease. Partially in an attempt to detect earlier disease, revisions to the original 1994 International Task Force criteria have been proposed, increasing the emphasis on imaging, specifically with echocardiography, CMR, and angiography (Marcus et al. 2010). Major criteria by angiography include RV akinesia, dyskinesia, or aneurysm. Evaluation of suspected ARVD has been included as an appropriate indication for functional CCT in the 2010 ACCF appropriateness criteria (Taylor et al. 2010).

4.5 Congenital Heart Disease

Serial measurement of RV volume and function may be important in following patients with some congenital heart disease. Common congenital anomalies like atrial or ventricular septal defects and partial anomalous pulmonary venous return represent an over-circulation phenomenon with chronic left-to-right shunts. Depending on the severity of shunting, these patients may demonstrate RV dilatation as well as pulmonary artery enlargement. Patients with repaired tetralogy of Fallot often have incompetent pulmonic valves and a dilated right ventricle. In these patients, serial quantification of RV function is important because it affects the timing of pulmonic valve replacement.

5 Left Atrium

5.1 Indication

Left atrial volume and functional measurement is recognized as a marker for the evaluation of patients with atrial

fibrillation, left heart failure with normal ejection fraction, mitral valve disease, and stroke. An enlarged left atrium is a risk factor for recurrent atrial fibrillation after pulmonary vein isolation (Abecasis et al. 2009; Helms et al. 2009). Cross-sectional imaging of the left atrium with MDCT or CMR can be used for treatment planning for left atrial ablation or pulmonary vein isolation. Measurement of the left atrial volume is more accurate and correlates more closely with the clinical course (Tsang et al. 2006).

5.2 Normal Values

Normal values for left atrium using MDCT in women and men		
Indexed measurement	Women	Men
EDV/BSA (ml/m^2)	40 ± 9 (37–43)	41 ± 10 (38–44)
ESV/BSA (ml/m^2)	18 ± 6 (16–20)	22 ± 6 (20–24)
SV/BSA (ml/m^2)	22 ± 4 (21–23)	19 ± 6 (17–21)
EF (%)	55 ± 8 (52–57)	46 ± 8 (43–48)
Diameter/BSA (mm/m^2)	18 ± 4 (17–19)	17 ± 2 (16–18)

EDV end-diastolic volume, *ESV* end-systolic volume, *SV* stroke volume, *BSA* body surface area
Normal values in units indicated ± SD (95 % CI)
(Stojanovska et al. 2011)

5.3 Comparison with Other Techniques

Two-dimensional echocardiography is the most commonly used method to assess left atrial size due to availability and portability. In some cases, measurement of the left atrium by echocardiography can be limited. As is the case in imaging of the left ventricle, image quality is degraded in patients with a large body habitus. Because of the posterior position of the left atrium, lateral resolution can be reduced, limiting accurate delineation of the endocardial contour (Avelar et al. 2010). Additionally, foreshortening of the maximal left atrial plane can cause underestimation of the volume. These variables may be responsible for the increased interobserver variability of echocardiography in assessing left atrial volume compared to CT or MRI (Avelar et al. 2010). Though there is good correlation with CT and MR, many studies have demonstrated systematic underestimation of left atrial volume by echocardiography (Rodevan et al. 1999; Avelar et al. 2010; Christiaens et al. 2009; Kircher et al. 1991). In contrast, volumetric and functional measurements made by CT show close correlation with MRI, although studies have shown a slight trend for overestimating LA volumes and underestimating LA ejection fraction (Wen et al. 2010).

5.4 Technique

Assessment of left atrial volume and function can usually be done using the same data set used to acquire the left ventricle. Retrospective technique with EKG-gated tube current modulation permits adequate delineation of the LA contour while allowing significant reduction in radiation dose.

Volumetric analysis can be obtained manually using Simpson's method. Both semi-automated and fully automated software packages are available as well.

Diastole can be divided into the isovolumetric relaxation phase and the filling phase. The main component of the filling phase is rapid filling, which accounts for 70–80 % of LV blood volume. A short diastases period follows, contributing another 5 % of blood volume. Finally, atrial systole contributes the remaining 15–25 % of LV blood volume before the start of ventricular systole (Braunwald 2008).

5.5 Heart Failure with Preserved Ejection Fraction

Impaired relaxation of the LV results in characteristic changes in LA volume and function. Compared to patients of hypertension and left ventricular hypertrophy, patients with HFpEF have increased LA volume and reduced LA ejection fraction, and these markers have been shown to be a reliable method to differentiate the two conditions (Melenovsky et al. 2007).

6 Summary

Improvements in CT technology have advanced significantly such that accurate and reliable determination of global and regional cardiac function can be made with little additional cost. Advanced post-processing software has significantly reduced the time in generating data. At the same time, hardware improvements have substantially reduced radiation dose. Functional and volume measurement of the LV, RV, and LA have shown excellent correlation with the gold standard CMR.

References

Abecasis J, Dourado R, Ferreira A, Saraiva C (2009) Left atrial volume calculated by multi-detector computed tomography may predict successful pulmonary vein isolation in catheter ablation of atrial fibrillation. Eurospace 11:1289–1294

Akram K, Anderson HD, Voros S (2009) Quantification of left ventricular parameters obtained by automated software for 64-slice multidetector computed tomography and comparison with magnetic resonance imaging. Cardiovasc Intervent Radiol 32(6):1154–1160

Annuar BR, Liew CK, Chin SP, Ong TK, Seyfarth MT, Chan WL, Fong YY, Ang CK, Lin N, Liew HB, Sim KH (2008) Assessment of global and regional left ventricular function using 64-slice multislice computed tomography and 2D echocardiography: a comparison with cardiac magnetic resonance. Eur J Radiol 65(1):112–119

Avelar E et al (2010) Comparison of the accuracy of multidetector computed tomography versus two-dimensional echocardiography to measure left atrial volume. Am J Cardiol 106(1):104–109

Bastarrika G, Arraiza M, De Cecco CN, Mastrobuoni S, Ubilla M, Rabago G (2008) Quantification of left ventricular function and mass in heart transplant recipients using dual-source CT and MRI: initial clinical experience. Eur Radiol 18(9):1784–1790

Bavelaar-Croon CD et al (2000) Left ventricular function: correlation of quantitative gated SPECT and MR imaging over a wide range of values. Radiology 217(2):572–575

Belge B, Coche E, Pasquet A, Vanoverschelde JL, Gerber BL (2006) Accurate estimation of global and regional cardiac function by retrospectively gated multidetector row computed tomography: comparison with cine magnetic resonance imaging. Eur Radiol 16(7):1424–1433

Braunwald E (2008) Braunwald's heart disease: a textbook of cardiovascular medicine. In: Peter L, Robert B, Douglas M Douglas Z. Saunders (eds) Elsevier, Philadelphia

Brodoefel H, Kramer U, Reimann A, Burgstahler C, Schroeder S, Kopp A, Heuschmid M (2007) Dual-source CT with improved temporal resolution in assessment of left ventricular function: a pilot study. Am J Roentgenol 189(5):1064–1070

Burgess MI, Mogulkoc N, Bright-Thomas RJ, Bishop P, Egan JJ, Ray SG (2002) Comparison of echocardiographic markers of right ventricular function in determining prognosis in chronic pulmonary disease. J Am Soc Echocardiogr 15:633–639

Busch S, Johnson TR, Wintersperger BJ, Minaifar N, Bhargava A, Rist C, Reiser MF, Becker C, Nikolaou K (2008) Quantitative assessment of left ventricular function with dual-source CT in comparison to cardiac magnetic resonance imaging: initial findings. Eur Radiol 18(3):570–575

Christiaens L et al (2009) A new method for measurement of LA volumes using 64-slice spiral CT: comparison with 2DE techniques. Int J Cardiol 131:217–224

de Geus-Oei LF et al (2011) Scintigraphic techniques for early detection of cancer treatment-induced cardiotoxicity. J Nucl Med 52(4):560–571

de Jonge GJ et al (2011) Semi-automatic measurement of left ventricular function on dual source computed tomography using five different software tools in comparison with magnetic resonance imaging. Eur J Radiol 80(3):755–766

Dell'Italia LJ, Walsh RA (1989) Effect of intravenous metoprolol on left ventricular performance in Q-wave acute myocardial infarction. Am J Cardiol 63(3):166–171

Dewey M, Müller M, Teige F, Schnapauff D, Schink T, Hamm B, Lembcke A (2006) Multisegment and halfscan reconstruction of 16-slice computed tomography for assessment of regional and global left ventricular myocardial function. Invest Radiol 41(4):400–409

Dupont MVM, Dragean CA, Coche EE (2011) Right ventricle function assessment by MDCT. Am J Roentgenol 196(1):77–86

Ferencik M et al (2007) Analysis of cardiac dimensions, mass and function in heart transplant recipients using 64-slice multi-detector computed tomography. J Heart Lung Transplant 26(5):478–484

Fischbach R, Juergens KU, Ozgun M, Maintz D, Grude M, Seifarth H, Heindel W, Wichter T (2007) Assessment of regional left ventricular function with multidetector-row computed tomography versus magnetic resonance imaging. Eur Radiol 17(4):1009–1017

Fishman AP, Elias JA, Fishman JA, Grippi MA, Senior RM, Pack AI (2008) Fishman's pulmonary diseases and disorders, 4th edn. McGraw Hill Medical, New York

Gao Y, Du X, Liang L, Cao L, Yang Q, Li K (2012) Evaluation of right ventricular function by 64-row CT in patients with chronic obstructive pulmonary disease and cor pulmonale. Eur J Radiol 81(2):345–353

Glower D Di, Lowe J Ei (2003) Left ventricular aneurysm. In: Cohn LH, Edmunds LH Jr (ed) Cardiac surgery in the adult. McGraw-Hill, New York, pp 771–788

Greupner J, Zimmermann E, Hamm B, Dewey M (2011) Automatic versus semi-automatic global cardiac function assessment using 64-row computed tomography. Br J Radiol 34(5):367–374

Grude M, Juergens KU, Wichter T, Paul M, Fallenberg EM, Muller JG, Heindel W, Breithardt G, Fischbach R (2003) Evaluation of global left ventricular myocardial function with electrocardiogram-gated multidetector computed tomography: comparison with magnetic resonance imaging. Invest Radiol 38(10):653–661

Guo YK, Yang ZG, Ning G, Rao L, Dong L, Pen Y, Zhang TM, Wu Y, Zhang XC, Wang QL (2009) Sixty-four-slice multidetector computed tomography for preoperative evaluation of left ventricular function and mass in patients with mitral regurgitation: comparison with magnetic resonance imaging and echocardiography. Eur Radiol 19(9):2107–2116

Hammermeister KE, DeRouen TA, Dodge HT (1979) Variables predictive of survival in patients with coronary disease. Selection by univariate and multivariate analyses from the clinical, electrocardiographic, exercise, arteriographic, and quantitative angiographic evaluations. Circulation 59(3):421–430

Hausleiter J et al (2006) Radiation dose estimates from cardiac multislice computed tomography in daily practice. Circulation 113:1305–1310

Hausleiter J et al (2007) A new algorithm for ECG-based tube current modulation (MinDose) reduces radiation dose estimates in cardiac dual source CT angiography. Circulation 116:II_575

Helms AS et al (2009) Relation of left atrial volume from three-dimensional computed tomography to atrial fibrillation recurrence following ablation. Am J Cardiol 103:989–993

Jensen CJ, Jochims M, Hunold P, Forsting M, Barkhausen J, Sabin GV, Bruder O, Schlosser T (2010) Assessment of left ventricular function and mass in dual-source computed tomography coronary angiography: Influence of beta-blockers on left ventricular function: comparison to magnetic resonance imaging. Eur J Radiol 74(3):484–491

Juergens KU, Grude M, Maintz D, Fallenberg EM, Wichter T, Heindel W, Fischbach R (2004) Multi-detector row CT of left ventricular function with dedicated analysis software versus MR imaging: initial experience. Radiology 230(2):403–410

Juergens KU, Roman F (2006) Left ventricular function studied with MDCT. Eur Radiol 16:342–357

Juergens KU et al (2008) Automated threshold-based 3D segmentation versus short-axis planimetry for assessment of global left ventricular function with dual-source MDCT. Am J Roentgenology 190(2):308–314

Kang DK et al (2011) CT Signs of right ventricular dysfunction. JACC: Cardiovasc Imaging 4(8):841–849

Kircher B et al (1991) Left atrial volume determination by biplane two-dimensional echocardiography: validation by cine CT. Am Heart J 121:864–871

Ko YJ, Kim SS, Park WJ, Jeong JO, Ko SM (2011) Comparison of global left ventricular function using 20 phases with 10-phase reconstructions in multidetector-row computed tomography. Int J Cardiovasc Imaging 28(3):603–611

Koch K, Oellig F, Kunz P, Bender P, Oberholzer K, Mildenberger P, Hake U, Kreitner KF, Thelen M (2004) Assessment of global and regional left ventricular function with a 16-slice spiral-CT using two different software tools for quantitative functional analysis and qualitative evaluation of wall motion changes in comparison with magnetic resonance imaging. Rofo 176(12):1786–1793

Lee H, Kim SY, Gebregziabher M, Hanna EL, Schoepf J (2012) Impact of ventricular contrast medium attenuation on the accuracy of left and right ventricular function analysis at cardiac multi detector-row CT compared with cardiac MRI. Acad Radiol 19:(4):395–405

Lessick J, Ghersin E, Abadi S, Yalonetsky S (2008) Accuracy of the long-axis area-length method for the measurement of left ventricular volumes and ejection fraction using multidetector computed tomograph. Can J Cardiol 24(9):685–689

Lin FY et al (2008) Cardiac chamber volumes, function, and mass as determined by 64-multidetector row computed tomography: mean values among healthy adults free of hypertension and obesity. JACC Cardiovasc Imaging 1(6):782–786

Helena M-N, Adams KF, Willis PW (1987) Evolution of regional left ventricular wall motion abnormalities in acute Q and non-Q wave myocardial infarction. Am Heart J 113(6):1369–1375

Heuschmid M, Rothfuss J, Schröder S, Küttner A, Fenchel M, Stauder N, Mahnken AH, Burgstahler C, Miller S, Claussen CD, Kopp AF (2005) Left ventricular functional parameters: comparison of 16-slice spiral CT with MRI. Rofo 177(1):60–66

Maffei E, Messalli G, Martini C, Nieman K, Catalano O, Rossi A, Seitun S, Guaricci AI, Tedeschi C, Mollet NR, Cademartiri F (2012) Left and right ventricle assessment with Cardiac CT: validation study vs. Cardiac MR. Eur Radiol 22(5):1041–1049

Mahnken AH, Spuentrup E, Niethammer M, Buecker A, Boese J, Wildberger JE, Flohr T, Sinha AM, Krombach GA, Günther RW (2003) Quantitative and qualitative assessment of left ventricular volume with ECG-gated multislice spiral CT: value of different image reconstruction algorithms in comparison to MRI. Acta Radiol 44(6):604–611

Mahnken AH, Koos R, Katoh M, Spuentrup E, Busch P, Wildberger JE, Kühl HP, Günther RW (2005) Sixteen-slice spiral CT versus MR imaging for the assessment of left ventricular function in acute myocardial infarction. Eur Radiol 15(4):714–720

Marcus FI et al (2010) Diagnosis of arrhythmogenic right ventricular cardiomyopathy/dysplasia - proposed modification of the task force criteria. Circulation 121:1533–1541

Mastrobuoni S et al (2011) Allograft morphology and function in heart transplant recipients surviving more than 15 years by magnetic resonance imaging and dual-source computed tomography. Eur J Cardiothorac Surg 40(1):e62–e66

Melenovsky V, Borlaug B, Rosen B et al (2007) Cardiovascular features of heart failure with preserved ejection fraction versus non-failing hypertensive left ventricular hypertrophy in the urban Baltimore community. J Am Coll Cardiol 49:198–207

Mo YH, Jaw FS, Wang YC, Jeng CM, Peng SF (2011) Effects of propranolol on the left ventricular volume of normal subjects during CT coronary angiography. Korean J Radiol 12(3):319

Mock MB et al (1982) Survival of medically treated patients in the coronary artery surgery study (CASS) registry. Circulation 66:562–568

Nevsky G, Jacobs JE, Lim RP, Donnino R, Babb JS, Srichai MB (2011) Sex-specific normalized reference values of heart and great vessel dimensions in cardiac CT angiograph. Am J Roentgenol 196:788–794

Plumhans C et al (2009) Comparison of manual, semi- and fully automated heart segmentation for assessing global left ventricular function in multidetector computed tomography. Invest Radiol 44(8):476–482

Port S, Cobb FR, Jones RH (1980) Effects of propranolol on left ventricular function in normal men. Circulation 61(2):358–366

Puesken M et al (2008) Global left-ventricular function assessment using dual-source multidetector CT: effect of improved temporal resolution on ventricular volume measurement. Eur Radiol 18(10):2087–2094

Quiroz R et al (2004) Right ventricular enlargement on chest computed tomography: prognostic role in acute pulmonary embolism. Circulation 109(20):2401–2404

Raman SV, Shah M, McCarthy B, Garcia A, Ferketich AK (2006) Multi-detector row cardiac computed tomography accurately quantifies right and left ventricular size and function compared with cardiac magnetic resonance. Am Heart J 151(3):736–744

Rodevan O, Bjornerheim R, Ljosland M, Maehle J, Smith HJ, Ihlen H (1999) Left atrial volumes assessed by three- and two-dimensional echocardiography compared to MRI estimates. Int J Card Imaging 15:397–410

Salm LP, Schuijf JD, de Roos A, Lamb HJ, Vliegen HW, Jukema JW, Joemai R, van der Wall EE, Bax JJ (2006) Global and regional left ventricular function assessment with 16-detector row CT: comparison with echocardiography and cardiovascular magnetic resonance. Eur J Echocardiogr 7(4):308–314

Sarwar A et al (2009) Evaluating global and regional left ventricular function in patients with reperfused acute myocardial infarction by 64-slice multidetector CT: a comparison to magnetic resonance imaging. J Cardiovasc Comput Tomogr 3(3):170–177

Savino G et al (2007) CT of cardiac function. J Thoracic Imaging 22(1):86–100

Schlosser T, Mohrs OK, Magedanz A, Voigtlander T, Schmermund A, Barkhausen J (2007) Assessment of left ventricular function and mass in patients undergoing computed tomography (CT) coronary angiography using 64-detector-row CT: comparison to magnetic resonance imaging. Acta Radiologica 48:30–35

Seneviratne SK et al (2010) Incremental diagnostic value of regional left ventricular function over coronary assessment by cardiac computed tomography for the detection of acute coronary syndrome in patients with acute chest pain: from the ROMICAT trial. Circ Cardiovasc Imaging 3(4):375–383

Setser RM, Fischer SE, Lorenz CH (2000) Quantification of left ventricular function with magnetic resonance images acquired in real time. J Magn Reson Imaging 12:430–438

Slart R et al (2004) Comparison of gated PET with MRI for evaluation of left ventricular function in patients with coronary artery disease. J Nucl Med 45(2):176–182

Staskiewicz G et al (2010) Widening of coronary sinus in CT pulmonary angiography indicates right ventricular dysfunction in patients with acute pulmonary embolism. Eur Radiol 20:1615–1620

Stojanovska J et al (2011) Reference normal absolute and indexed values from ECG-gated MDCT: left atrial volume, function, and diameter. Am J Roentgenology 197(3):631–637

Stollfuss JC et al (1998) Regional myocardial wall thickening and global ejection fraction in patients with low angiographic left ventricular ejection fraction assessed by visual and quantitative resting ECG-gated 99mTc-tetrofosmin single-photon emission tomography and magnetic resonance imaging. Eur J Nucl Med 25(5):522–530

Sugeng L, Mor-Avi V, Weinert L, Niel J, Ebner C, Steringer-Mascherbauer R, Schmidt F, Galuschky C, Schummers G, Lang RM, Nesser HJ (2006) Quantitative assessment of left ventricular size and function: side-by-side comparison of real-time three-dimensional echocardiography and computed tomography with magnetic resonance reference. Circulation 114(7):654–661

Takx RA, Moscariello A, Schoepf UJ, Barraza JM Jr, Nance JW Jr, Bastarrika G, Das M, Meyer M, Wildberger JE, Schoenberg SO,

Fink C, Henzler T (2012) Quantification of left and right ventricular function and myocardial mass: comparison of low-radiation dose 2nd generation dual-source CT and cardiac MRI. Eur J Radiol 81(4):e598–e604

Taylor DO et al (2008) Registry of the International Society for Heart and Lung Transplantation: twenty-fifth official adult heart transplant report—2008. J Heart Lung Transplant 27(9):943–956

Taylor AJ et al (2010) ACCF/SCCT/ACR/AHA/ASE/ASNC/SCAI/SCMR 2010 appropriate use criteria for cardiac computed tomography. J Am Coll Cardiol 56(22):1864–1894

Tsang TS et al (2006) Prediction of cardiovascular outcomes with left atrial size: is volume superior to area or diameter? J Am Coll Cardiol 47:1018–1023

van der Vleuten PA et al (2006) Quantification of global left ventricular function: comparison of multidetector computed tomography and magnetic resonance imaging. a meta-analysis and review of the current literature. Acta Radiol 47(10):1049–1057

van der Vleuten PA, de Jonge GJ, Lubbers DD, Tio RA, Willems TP, Oudkerk M, Zijlstra F (2009) Evaluation of global left ventricular function assessment by dual-source computed tomography compared with MRI. Eur Radiol 19(2):271-277

van Ooijen PM, de Jonge GJ, Oudkerk M (2012) Informatics in radiology: postprocessing pitfalls in using CT for automatic and semiautomatic determination of global left ventricular function. Radiographics 32(2):589–599

Wen Z, Zhang Z, Yu W, Fan Z, Du J, Lv B (2010) Assessing the left atrial phasic volume and function with dual-source CT: comparison with 3T MRI. Int J Cardiovasc Imaging 26:88–92

Wu YW, Tadamura E, Kanao S, Yamamuro M, Okayama S, Ozasa N, Toma M, Kimura T, Kita T, Marui A, Komeda M, Togashi K (2008a) Left ventricular functional analysis using 64-slice multidetector row computed tomography: comparison with left ventriculography and cardiovascular magnetic resonance. Cardiology 109(2):135–142

Wu YW, Tadamura E, Yamamuro M, Kanao S, Okayama S, Ozasa N, Toma M, Kimura T, Komeda M, Togashi K (2008b) Estimation of global and regional cardiac function using 64-slice computed tomography: a comparison study with echocardiography, gated-SPECT and cardiovascular magnetic resonance. Int J Cardiol 128(1):69–76

Yamamuro M, Tadamura E, Kubo S, Toyoda H, Nishina T, Ohba M, Hosokawa R, Kimura T, Tamaki N, Komeda M, Kita T, Konishi J (2005) Cardiac functional analysis with multi-detector row CT and segmental reconstruction algorithm: comparison with echocardiography, SPECT, and MR imaging.Radiology 234(2):381–390

Part III
Perfusion

Why Are We Interested in Myocardial Perfusion?

Fabian Bamberg

Contents

Abstract

Cardiac CTA is increasingly asserting its position as an established tool for the detection and characterization of coronary plaque and stenosis, its morphological evaluation capability, however, falling short of hemodynamic assessment. This fact is of high relevance in the process of therapeutic decision making, which explains the dominance of functional imaging techniques, such as nuclear myocardial perfusion imaging, magnetic resonance imaging, or stress echocardiography. There are four major targets of functional imaging that are particularly critical to the selection of a revascularization procedure over medical treatment strategies: (1) Assessment of myocardial perfusion defects to identify treatable coronary artery disease (CAD); (2) Identification of myocardial perfusion status as an important prognostic factor for the occurrence of future cardiovascular events; (3) Assessment of myocardial viability to guide therapy; and (4) Evaluation of the hemodynamic relevance of detected coronary artery stenosis by flow measurements. This chapter reviews the current limitations of morphological assessment of coronary stenosis by cardiac CTA, describes available techniques for functional imaging, and enumerates its major targets, which have been well implemented in current management strategies for patients with suspected or known CAD.

1 Role of Imaging in the Management of Patients with Coronary Artery Disease

Contemporary imaging techniques have achieved a remarkable reliability for evaluating patients with suspected or known coronary artery disease (CAD). This is well in line with the predicted burden of CAD, which has increased substantially over the past few decades (Roger et al. 2011) and will continue to rise, requiring improved management

F. Bamberg (✉)
Department of Clinical Radiology,
Ludwig-Maximilians University,
Marchioninistrasse, Munich, Germany
e-mail: fabian.bamberg@med.uni-muenchen.de

U. J. Schoepf et al. (eds.), *CT Imaging of Myocardial Perfusion and Viability*, Medical Radiology. Diagnostic Imaging,
DOI: 10.1007/174_2012_765, © Springer-Verlag Berlin Heidelberg 2012
Published Online: 23 November 2012

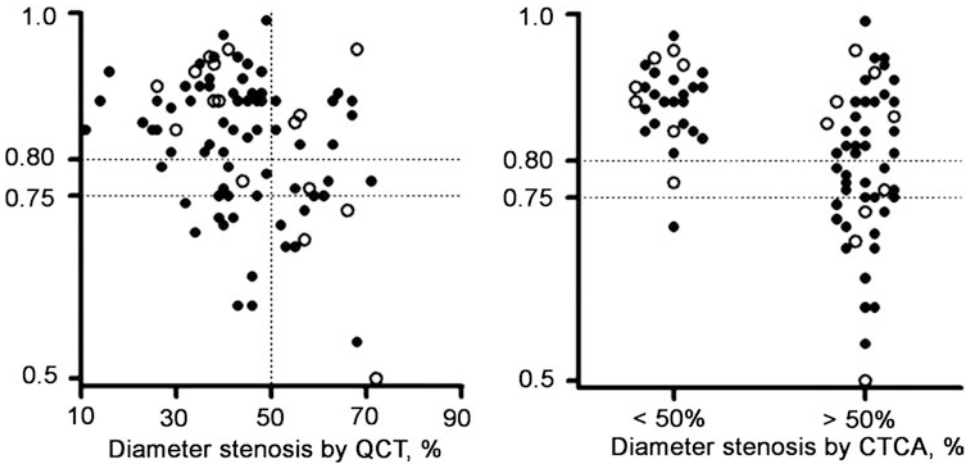

Fig. 1 Scatterplots demonstrating the correlation between quantitative cardiac CTA (QCT) and fractional flow measurements (y-axis) indicating a weak correlation ($r = -0.32$, *right*), especially in coronary stenosis >50 % (*right*). Coronary arteries smaller than 3.5 mm are depicted as *solid circles*, coronary arteries larger than 3.5 mm as *open circles*. From Meijboom et al. (2008)

strategies, especially enhanced diagnostic work-up strategies (Kruip et al. 2003).

The diagnostic work-up relies on several invasive and noninvasive imaging modalities. The current gold standard for the detection and evaluation of coronary stenosis is invasive angiography, a procedure which also enables direct therapeutic intervention; however, this procedure is associated with certain additional risks, such as arrhythmia, intima dissection, local bleeding, and discomfort. As result, only subjects with a high pre-test probability of CAD are referred for invasive angiography, whereas subjects with low- to intermediate pre-test probability of CAD are usually referred for non-invasive testing. Traditionally, myocardial perfusion imaging by single-photon emission computed tomography (SPECT) is the preferred noninvasive option. There is growing evidence that cardiac magnetic resonance imaging (CMR) or stress echocardiography can also serve well as gatekeepers for invasive angiography (Schuijf et al. 2005). SPECT, CMR, and echocardiography all have in common the fact that they identify ischemia by perfusion or wall motion abnormalities. Thus, traditionally, the presence and extent of myocardial ischemia have served as a reference for therapeutic decision making and referral for invasive angiography (Schuijf et al. 2007).

This paradigm has been challenged by the introduction and development of cardiac CT angiography (CTA), an imaging modality that primarily relies on the morphologic assessment of CAD. Cardiac CTA, with continuous technological development, is increasingly diffusing into clinical practice. As detailed by Dr. Nance in *Chapter 1*, current state-of-the-art protocols, though fast and comfortable for patients, involve a reasonable amount of radiation (2–3 mSv or less) and up to 100 ml of iodinated contrast agent. The true value of cardiac CTA lies in its ability to exclude a significant stenosis with high sensitivity and high negative predictive value; on the other hand, not all subjects with a positive finding turn out to have a significant coronary stenosis on subsequent invasive coronary angiography.

2 Limitations of Morphological Imaging by Cardiac CTA

Despite the encouraging capabilities of cardiac CTA, as with other morphologic imaging modalities, cardiac CTA is unable to determine whether or not a detected lesion is hemodynamically significant. Hemodynamic significance is what determines whether either revascularization or medical therapy will be beneficial. In fact, there is a large body of evidence indicating that there is a high discrepancy ratio between the findings on cardiac CTA and subsequent functional tests.

Hacker et al. studied 38 patients (74 % male) with both 64-slice MSCT coronary angiography and SPECT imaging (Hacker et al. 2007). While 102 of 109 (94 %) patients without coronary artery stenosis also had normal SPECT studies, only 23 of 43 (53 %) with significant coronary stenosis had impaired myocardial perfusion based on the SPECT study, indicating that despite detection of a morphological stenosis, perfusion impairment may vary. Recently, Meijboom et al. compared CTA measured degree of stenosis with measurement of fractional flow reserve (FFR) (Meijboom et al. 2008). FFR is considered to be the gold standard for functional assessment of coronary stenosis, by positioning a catheter tipped flow wire proximal and distal to the lesion. Their results indicate that there is no agreement between CTA findings and FFR measured flow ($r = -0.32$, Fig. 1) and that morphologic assessment by

CTA was not able to identify a hemodynamically relevant coronary stenosis.

Overall, these observations are not surprising but emphasize the fact that there are two different imaging approaches to CAD, each of which provides fundamentally different information:

(1) Morphological modalities: Cardiac CTA and invasive coronary angiography, both are well established methods to visualize coronary stenosis and plaque as the anatomic correlate of CAD.
(2) Functional modalities: nuclear myocardial perfusion imaging (i.e. SPECT), echocardiography, MRI, and invasive measurement of fractional flow reserve are equally reliable in providing information pertaining to CAD.

For the decision of whether invasive or medical treatment is indicated, evidence of functionally relevant ischemia is of critical importance. Thus, in subjects in whom a significant stenosis is detected on CT, in the absence of hemodynamic information, the potential benefits of either revascularization or medical therapy remain undetermined. In order to design evaluation algorithms that allow optimal integration of cardiac CTA, investigations comparing MSCT with other noninvasive *functional* modalities are mandatory (Schuijf and Bax 2008). This can also be observed in larger randomized trials using cardiac CTA for patients with acute chest pain. For instance, there is interesting data from the ROMICAT II study, a large randomized trial in 1,000 subjects with initially inconclusive evaluation in the emergency department (Hoffmann et al. 2012). While there was an overall benefit from using cardiac CTA in patients with acute chest pain, the benefit was primarily attributed to patients in whom the presence of a significant coronary stenosis was ruled out. In support, subjects who were found to have CAD by CTA were predominantly referred for subsequent functional testing.

From a CT perspective, this need of functional information has resulted in a new field research, which extends the CT-based technology from morphological to functional assessment.

3 Rationale for Functional Imaging

Functional imaging relies on the detection of the hemodynamic consequences of CAD—known as ischemia—rather than pathological changes in the coronary arteries. In the presence of ischemia, defined as the mismatch of oxygen demand and supply, a sequence of events is initiated, referred to as "the ischaemic cascade" (Nesto and Kowalchuk 1987). Perfusion abnormalities start as diastolic and progress toward a systolic dysfunction; only at the very end of the cascade do ECG changes and angina occur

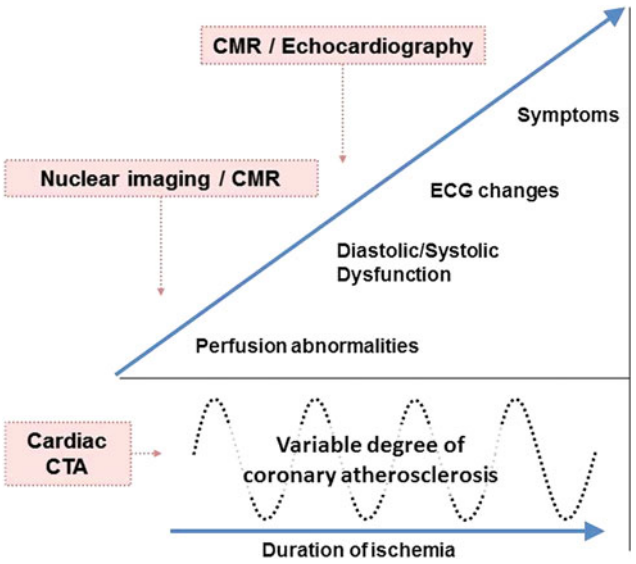

Fig. 2 The ischemic cascade represents the sequence of pathophysiological events following ischemia, with perfusion abnormalities occurring in the beginning, which can be identified by nuclear imaging techniques or CMR. The amount of the underlying degree of coronary atherosclerosis can vary and is detected and characterized by cardiac computed tomography angiography (CTA). Modified from Schuijf et al. (2005) *CMR* cardiac magnetic resonance imaging

(Fig. 2). Accordingly, the occurrence of perfusion abnormalities during stress may be more sensitive for the detection of CAD than the induction of systolic dysfunction (wall motion abnormalities) (Leong-Poi et al. 2002).

As coronary atherosclerosis often occurs without any hemodynamic consequences, the likelihood that a coronary stenosis may be flow limiting is related to the degree of stenosis and vice versa; severe perfusion defects are highly predictive of a critical (>90 %) coronary stenosis (Shaw and Berman 2009). Notably, a perfusion deficit may also be associated with vascular dysfunction in the setting of non-obstructive CAD, as collateral flow in a patient with obstructive CAD may result in normal flow to that region (Aarnoudse et al. 2003).

It is obvious that CAD is not necessarily a prerequisite or an immediate cause of myocardial ischemia, as there are concordant and discordant findings between functional and morphological imaging modalities. Overall, these observations explain the level of discrepancy observed in CTA studies as detailed above.

4 Established Techniques for Functional Imaging

There are three major functional imaging modalities: myocardial perfusion assessment by SPECT, wall motion abnormalities detection by echocardiography, or both of

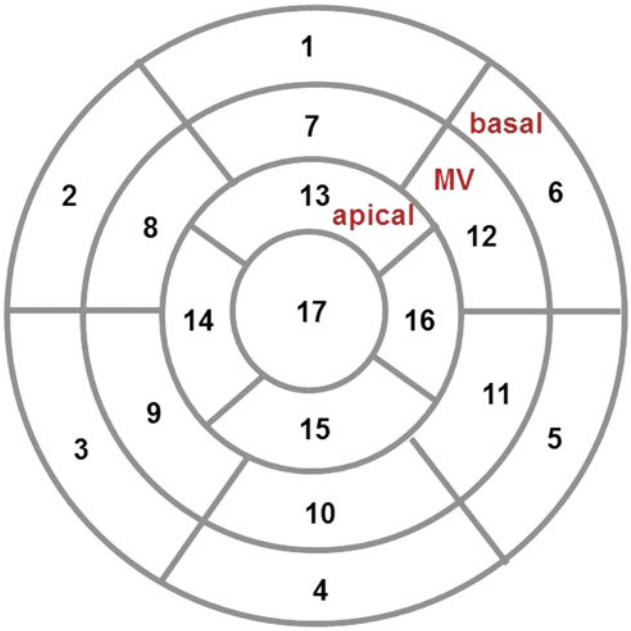

Fig. 3 Seventeen segment model developed for assessment of myocardial perfusion abnormalities, which is used to report findings for all functional imaging modalities. Modified from Cerqueira et al. (2002)

these through CMR (Marcus et al. 2011). Over time, these techniques have become complementary rather than competitive, since they provide different information. Generally, images are interpreted visually by adhering to a 17 myocardium-segment model, developed for SPECT but usually applied to all functional cardiac imaging modalities (Fig. 3) (Cerqueira et al. 2002).

It is important to note that although these functional imaging modalities primarily focus on the detection of perfusion defects as part of the ischemic cascade, usually their diagnostic accuracy is studied and reported for the detection of significant coronary stenosis. This, however, is not the appropriate comparator (as detailed above), given the discrepancy between function and morphologic information.

4.1 Nuclear Myocardial Perfusion Imaging

SPECT, using technetium-, thallium-, or tetrofosmin-based radionuclide tracers, has become the most widely used modality for the assessment of myocardial perfusion. By comparing the uptake and distribution of radionuclide by myocytes under rest and stress conditions, it allows a three-dimensional assessment of the myocardial perfusion and viability. Reversible defects (perfusion abnormalities detected at stress but absent at rest) are indicative of ischemia; persistent defects present both in rest and stress condition represent infarcted myocardium. Examples of a reversible and persistent defect are provided in Figs. 4 and 5, respectively.

The diagnostic accuracy of SPECT in detecting morphologically significant coronary stenosis is relatively high (specificity: 87–94 % and sensitivity: 85–90 %) (Rochmis and Blackburn 1971; Mertes et al. 1993; Kapur et al. 2002; Taillefer et al. 1997; Mark et al. 2003; Merhige et al. 2007). Disadvantages of SPECT include its tracer-dependent radiation dose (9–25 mSv) and a total examination time of ~4–5 h (imaging time 10–20 min per session, with 3–4 h separation time between stress and rest acquisitions). Associated costs are moderately high (approximately $600–$1,000) (Merhige et al. 2007). However, there is evidence that recently improved technology, i.e. ultrafast cameras/multiple scanning detectors (D-SPECT), may reduce radiation dose, shorten study time, and improve sensitivity (Garcia et al. 2011).

4.2 Cardiac Magnetic Resonance Imaging

In contrast to SPECT, MRI is a non-ionizing radiation modality that is increasingly used for the assessment of cardiac function and myocardial perfusion (Cheong 2010). Contrast material (gadolinium chelate) has a fairly linear relationship between its concentration and signal intensity on T1-weighted sequences (Croisille et al. 2006; Donahue et al. 1997). Besides its merit in the evaluation of non-ischemic cardiomyopathies, MRI permits the differentiation between persistent defects (fixed defects, present both in rest and stress conditions, consistent with infarction) and reversible defects (present on stress acquisitions only, consistent with ischemia). Late gadolinium enhancement (pathological myocardial enhancement 10 min after contrast administration) is the hallmark of infarction; an example is provided in Fig. 6.

In contrast to SPECT, MRI allows the visual differentiation between subendocardial and transmural infarction, a very relevant finding for guiding therapeutic intervention. Its diagnostic accuracy for the detection of morphologically significant coronary artery stenosis is high (sensitivity and specificity of 89 and 87 %, respectively) (Christiansen et al. 2010; Klem et al. 2006). There is recent data suggesting that MRI can accurately detect hemodynamically relevant CAD similar or slightly superior to SPECT (Schwitter et al. 2008).

Disadvantages of MRI include the required staff expertise, limited availability in community hospitals, relatively long

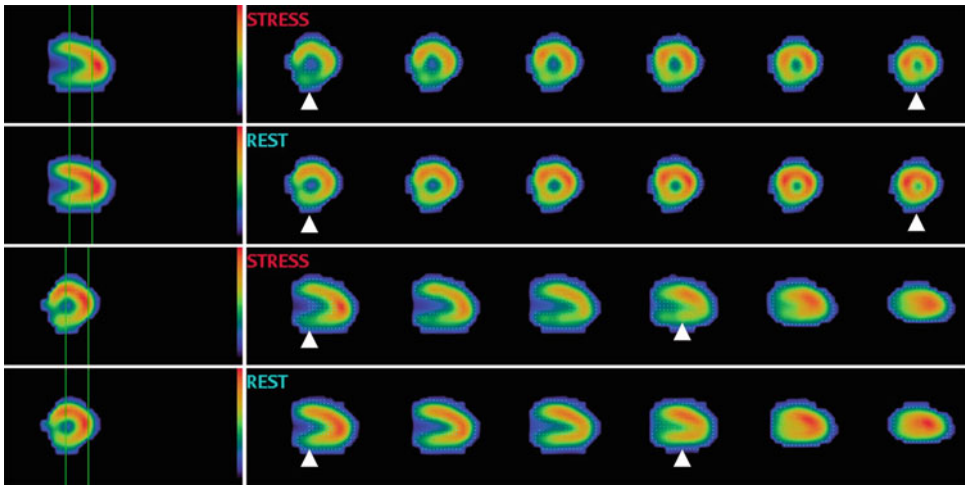

Fig. 4 Myocardial perfusion imaging (tetrofosmin) SPECT study of a 78 year old male with a reversible defect in the posterior wall consistent with ischemia (*arrowheads*). Courtesy of Dr. S. Lehner, Munich, Germany

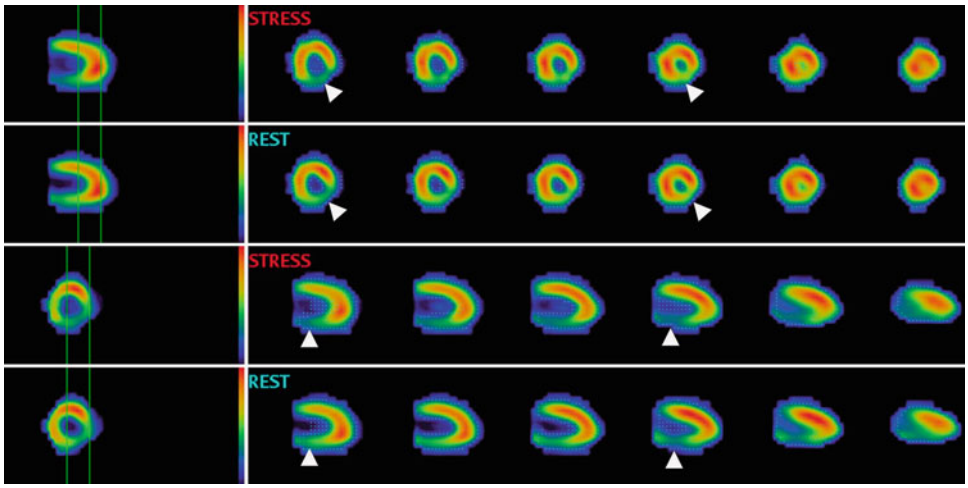

Fig. 5 Myocardial perfusion imaging (tetrofosmin) SPECT study of a 58 year old female with a persistent defect in the posterior wall consistent with infarction (*arrowheads*). Courtesy of Dr. S. Lehner, Munich, Germany

acquisition times (30–45 min), high cost, and contraindication in patients with pacemakers or implanted defibrillators.

4.3 Echocardiography

Echocardiography, the least expensive technique, is well-suited for the assessment of cardiac function, specifically global and regional dysfunction. Strain rate, which is the systolic shortening of the longitudinal and circumferential axes (negative strain) by a thickening or lengthening in the radial direction (positive strain) can be quantified by either Doppler or 2D ultrasound technique (Marwick 2006). Also, in the diastolic phase, left ventricular impairment (diastolic stunning) is a very sensitive marker of myocardial ischemia (Bonow et al. 1985; Wijns et al. 1986; Ehring and Heusch 1990). The ratio of strain changes before and after exercise has a high sensitivity of 97 % and a specificity of 93 % in detecting a significant coronary stenosis (Ishii et al. 2009; Achenbach et al. 2010), which may be improved by administration of contrast media (microbubbles) (Hundley et al. 1998).

Its main limitations include a very high observer dependency associated with a high interobserver variability.

5 Relevance of Functional Imaging for Patient Management

The clinical value of functional imaging for patients with suspected or known CAD is complex but can be simplified and categorized into a number of scenarios in which obtained functional information have shown to be beneficial for patient management.

5.1 Identification of Treatable Ischemia

Most data demonstrate that perfusion imaging is able to effectively identify subjects for subsequent angiography,

Fig. 6 Cardiac magnetic resonance imaging study (1.5 T) of a 61 year old male with an adenosine-stress induced perfusion defect in the inferior and infero-septal wall (*arrowheads*)

with SPECT currently being the most frequently used test in the United States (Min and Berman 2009). Early studies indicate that myocardial perfusion is significantly impaired in the presence of a ≥70 % coronary stenosis (Gould and Lipscomb 1974). SPECT has the ability to identify disease in individual coronary arteries, since perfusion abnormalities correlate closely with coronary artery perfusion territories (Elhendy et al. 2000).

The largest body of evidence of the value of perfusion imaging stems from a cohort of 10,000 subjects without prior CAD, who underwent stress SPECT prior to intervention or medical therapy (Hachamovitch et al. 2003). Despite a non-randomized, retrospective approach, the results indicate that after 2 years of follow-up, subjects with moderate to severe perfusion defects who underwent revascularization had a significantly improved mortality as compared to subjects with no or mild perfusion defects who were revascularized. The value of the assessment of myocardial perfusion imaging has recently been confirmed by the Clinical Outcomes Utilizing Revascularization and Aggressive Drug Evaluation (COURAGE) trial, the largest randomized trial of patients with chronic CAD (Boden et al. 2007). In the main study, in 2,287 patients, a strategy of optimal medical therapy plus revascularization was not associated with an improved outcome compared with optimal medical therapy alone. The nuclear substudy subsequently published by Shaw et al. confirmed the importance of the quantitative noninvasive assessment of perfusion on serial stress SPECT imaging in a subset of 314 patients (Shaw et al. 2008). Patients having significant improvement in ischemia, which was achieved more often in the interventional group, had fewer subsequent cardiovascular events (Fig. 7).

Similarly, stress CMR can be used to accurately detect significant coronary stenosis as shown in a recent meta-analysis pooling results of 1,516 patients with an intermediate likelihood of disease (prevalence 57.4 %) (Nandalur et al. 2007). The results by Nadalur et al. indicate a relatively high sensitivity and specificity of 0.91 and 81 %, respectively.

5.2 Relevance of Myocardial Viability

Assessment of myocardial viability is critical for the management of patients with ischemic cardiomyopathy, as only viable myocardium will benefit from revascularization. From an array of imaging modalities, including PET and contrast echocardiography, CMR and SPECT are the predominant

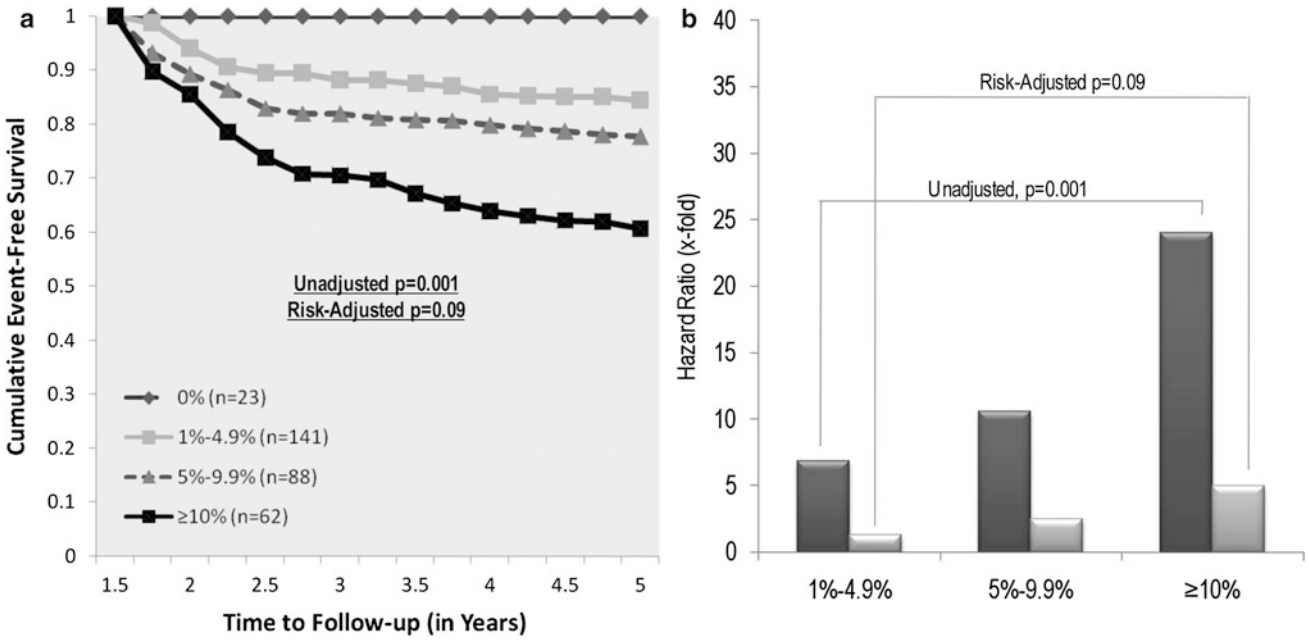

Fig. 7 Kaplan-Maier-survival curves **a** and hazard ratios associated with residual perfusion defects after treatment **b** in the COURAGE trial. From Shaw et al. (2008)

methods used for the assessment of myocardial viability, based on perfusion and scan quantification (Schinkel et al. 2007). On CMR, late gadolinium enhancement represents non-viable myocardium or fibrosis (rarely myocarditis), whereas non-enhancing areas represent viable tissue. In SPECT, fixed and reversible defects (between rest and stress acquisitions) differentiate viable from non-viable myocardium, respectively.

If assessed early after MI, there is evidence that the extension of non-viable, infarcted area may predict recovery of left ventricular function. In a small initial study of 40 patients, Choi et al. demonstrated that the extent of dysfunctional myocardium that was not infarcted or had necrosis comprising less than 25 % of the wall thickness, as determined by CMR, was the best predictor of global improvement in the left ventricular function (Choi et al. 2001).

The transmural extension of non-viable, infarcted myocardium predicts the recovery of left ventricular function after revascularization (Kim et al. 2000). Selvanayagam et al. studied 50 patients with known coronary artery disease and left ventricular dysfunction prior to surgical revascularization (CABG) using CMR (Selvanayagam et al. 2004). Following revascularization, subjects were assessed for improvement of left ventricular function. They found that the likelihood of recovery from left ventricular dysfunction decreased with increase of the transmural extent of late gadolinium enhancement (LGE) on CMR. Specifically, they found that 78 % of myocardial segments without necrosis improved, whereas only 17 % of segments with LGE greater than 75 % transmurality improved at follow-up (Fig. 8).

While improvement of left ventricular function may be a less relevant outcome, there is also evidence from Allman et al. who demonstrated in a meta-analysis of 24 prognostic studies, including 3,088 patients, that the amount of viable myocardium has strong prognostic implications (Allman et al. 2002). Their results show a low annual death rate in patients who had viable myocardium and were revascularized, whereas the death rate in patients with viable myocardium who were treated medically was substantially higher (3.2 vs. 16 % annual death rate, respectively).

5.3 Risk Stratification and Prognosis

Assessment of patient's prognosis plays a central role in the primary and secondary prevention setting and many imaging modalities have been used for risk stratification.

There is strong evidence supporting the prognostic value of SPECT MPI and its ability to risk-stratify patients with suspected or documented CAD in a variety of clinical settings. Primarily, in patients with stable coronary artery disease, the number of ischemic myocardial segments has been shown to be a strong predictor for cardiac events (Brown et al. 1983; Ladenheim et al. 1986). Hachamovitch et al. studied 5,183 consecutive patients who underwent stress/rest SPECT and were followed up for the occurrence of cardiac death or myocardial infarction over a mean period of almost 2 years (Hachamovitch et al. 1998). The presence of mildly abnormal, moderately abnormal, or severely abnormal perfusion defects was associated with an

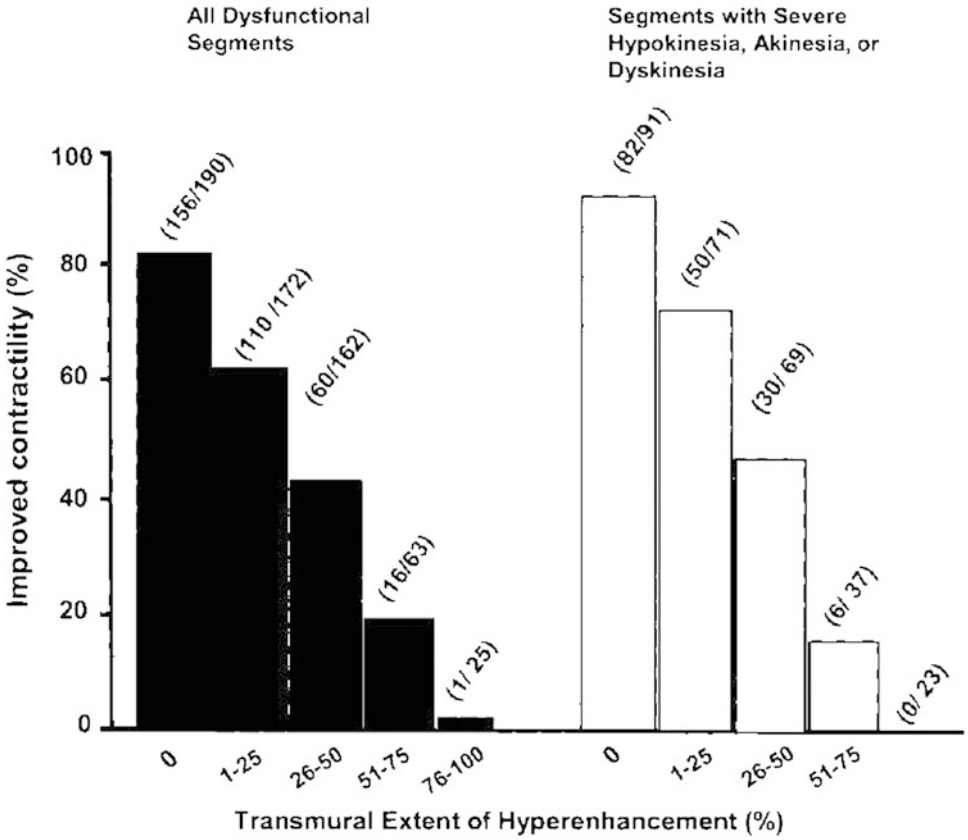

Fig. 8 Relationship between transmural extent of LGE on CMR before surgery and likelihood of increased regional function after surgery in all dysfunctional segments (*left*) and in all segments with severe hypokinesia, akinesia, or dyskinesia. From Selvanayagam et al. (2004)

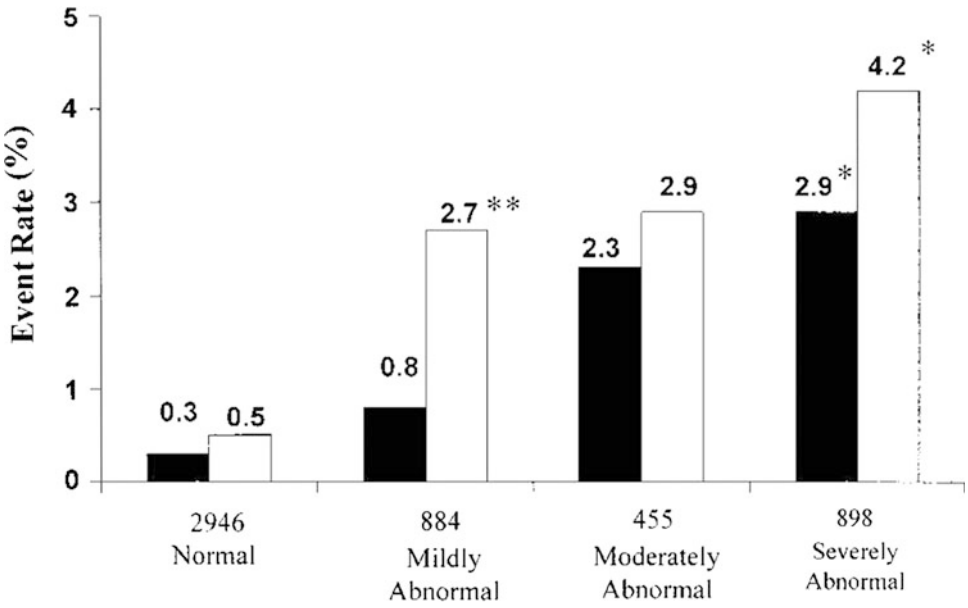

Fig. 9 Annualized event rates associated with findings on SPECT myocardial perfusion imaging. From Hachamovitch et al. (1998)

annualized event rate of 2.7, 2.9, or 4.2 %, respectively (see Fig. 9). There is more recent data from another large-scale study of 2,225 women, who were followed for almost 4 years (Cerci et al. 2011). Similar to the earlier results, the presence of any perfusion abnormality was associated with a significantly higher event rate of 14 %.

Conversely to the risk associated with perfusion abnormalities, there is even stronger evidence that normal myocardial perfusion presents a very low risk for cardiovascular events, approximately 1 % the annual cardiac event rate (Berman et al. 2006). In the study by Hachamovic et al., subjects with a normal MPI study had an annualized event

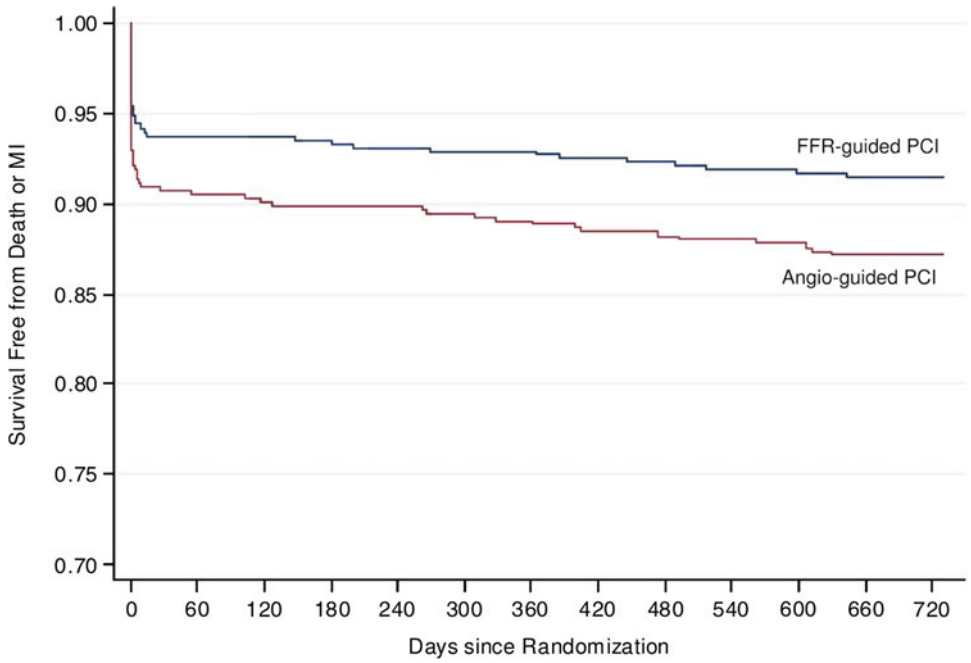

Fig. 10 Kaplan-Meier survival curves demonstrating differences between the FFR-guided and the standard angiography-guided strategy for the occurrence of death and myocardial infarction. From Pijls et al. (2010)

rate for cardiac death and myocardial infarction of less than 0.5 and 0.3 %, respectively (Hachamovitch et al. 1998). A more recent meta-analysis by Shaw et al., pooling 19 studies with more than 39,000 patients with a mean follow-up of 2.3 years, demonstrated an event rate of 0.6 % in association with a negative SPECT perfusion study (Shaw and Iskandrian 2004). In a number of subgroups, such as patients scheduled for non-cardiac surgery, the presence of reversible ischemia has been found to be a significant predictor of perioperative cardiac events (Leppo 1995).

Similar to SPECT, CMR-detected myocardial perfusion defects are predictive of events; however, CMR is the younger of the two technologies and there is less prognostic data available at the time of this writing. In 420 patients with known or suspected CAD, Bodi et al. found that the presence of a perfusion defect on CMR was associated with a 17 % event rate (Bodi et al. 2007). In contrast, subjects without any perfusion deficit on CMR had a significantly lower event rate (5 %). In subjects with acute chest pain (n = 135), none of the subjects with a normal CMR experienced a cardiac event during a 1 year follow-up (Ingkanisorn et al. 2006).

Therefore, there is strong evidence that the identification of myocardial perfusion deficits and more importantly the absence of any defects have overwhelming prognostic value.

5.4 Hemodynamic Relevance of Coronary Artery Stenosis by FFR

Catheter-based invasive flow measurement for FFR has established itself as a complement to invasive angiography. FFR can be performed once a morphological coronary stenosis has been detected and may provide important functional information regarding the indication for an interventional procedure.

In a landmark trial, the Fractional Flow Reserve versus Angiography for Multivessel Evaluation (FAME), 1,005 subjects scheduled for stent revascularization were randomized to either a standard or interventional approach, dependent on whether the FFR measurement indicated ischemia (Tonino et al. 2009; Pijls et al. 2010). The 1-year event rate for major adverse cardiovascular events was 18.3 % in the angiography group and 13.2 % in the FFR group, while the recurrence of angina was similar between the two groups; this demonstrates the clear benefit of using an FFR-guided policy (Tonino et al. 2009). Also, as shown in Fig. 10, after a 2-year follow-up, there was a significant difference in rate of mortality or myocardial infarction, with a rate of 8.4 % for the FFR-based strategy versus 12.9 % in the angiography alone group ($p = 0.02$) (Pijls et al. 2010).

6 Conclusions and Consequences for Cardiac CTA

It is well recognized that functional information with regard to ischemia or flow impairment are key features determining the indication for revascularization procedures in patients with CAD. The large body of evidence accumulated over the last few years demonstrates without doubt that the benefit associated with stent placement or CABG is directly related to information provided by functional

imaging modalities, such as SPECT, CMR, stress echocardiography, or FFR measurement, provided the expected outcome improvement outweighs the risk associated with an intervention. This appears to only be the case if the degree of ischemia is sufficiently high enough to be measurable by functional imaging modalities.

The established paradigm has been challenged by the rapid development and advancement of cardiac CTA, which is increasingly reaching clinical practice. However, the value of cardiac CTA rests in the morphological assessment of coronary artery disease and per se does not provide any functional information. Although there is an overlap of morphological changes and their functional relevance, i.e., with high degree lesions being more likely to cause perfusion defects, clinicians should be aware of the discordance between a morphological attest and a functional test.

There has been an increasing effort to extend the ability of cardiac CTA toward a functional imaging procedure, which would provide a highly attractive combined imaging modality. Substantial advances have been made in the field of CT perfusion and viability imaging through different techniques and approaches, and there is no doubt that cardiac CTA can be used to assess left and right ventricular function as well. This new development and field of research is critical as the wide applicability for various patient populations will depend on the ability to combine functional and morphologic information in a single relevant examination. Only such a noninvasive test may enable us to accommodate the predicted rise in the prevalence of CAD over the coming decades.

References

Aarnoudse WH, Botman KJ, Pijls NH (2003) False-negative myocardial scintigraphy in balanced three-vessel disease, revealed by coronary pressure measurement. Int J Cardiovasc Intervent 5(2):67–71

Achenbach S et al (2010) The year in coronary artery disease. JACC Cardiovasc Imaging 3(10):1065–1077

Allman KC et al (2002) Myocardial viability testing and impact of revascularization on prognosis in patients with coronary artery disease and left ventricular dysfunction: a meta-analysis. J Am Coll Cardiol 39(7):1151–1158

Berman DS et al (2006) Roles of nuclear cardiology, cardiac computed tomography, and cardiac magnetic resonance: assessment of patients with suspected coronary artery disease. J Nucl Med 47(1):74–82

Boden WE et al (2007) Optimal medical therapy with or without PCI for stable coronary disease. N Engl J Med 356(15):1503–1516

Bodi V et al (2007) Prognostic value of dipyridamole stress cardiovascular magnetic resonance imaging in patients with known or suspected coronary artery disease. J Am Coll Cardiol 50(12):1174–1179

Bonow RO et al (1985) Asynchronous left ventricular regional function and impaired global diastolic filling in patients with coronary artery disease: reversal after coronary angioplasty. Circulation 71(2):297–307

Brown KA et al (1983) Prognostic value of exercise thallium-201 imaging in patients presenting for evaluation of chest pain. J Am Coll Cardiol 1(4):994–1001

Cerci MS et al (2011) Myocardial perfusion imaging is a strong predictor of death in women. JACC Cardiovasc Imaging 4(8):880–888

Cerqueira MD et al (2002) Standardized myocardial segmentation and nomenclature for tomographic imaging of the heart: a statement for healthcare professionals from the Cardiac Imaging Committee of the Council on Clinical Cardiology of the American Heart Association. Circulation 105(4):539–542

Cheong BY (2010) Cardiovascular magnetic resonance imaging and computed tomography. Tex Heart Inst J 37(3):316–318

Choi KM et al (2001) Transmural extent of acute myocardial infarction predicts long-term improvement in contractile function. Circulation 104(10):1101–1107

Christiansen JP et al (2010) Stress perfusion imaging using cardiovascular magnetic resonance: a review. Heart Lung Circ 19(12):697–705

Croisille P, Revel D, Saeed M (2006) Contrast agents and cardiac MR imaging of myocardial ischemia: from bench to bedside. Eur Radiol 16(9):1951–1963

Donahue KM, Weisskoff RM, Burstein D (1997) Water diffusion and exchange as they influence contrast enhancement. J Magn Reson Imaging 7(1):102–110

Ehring T, Heusch G (1990) Left ventricular asynchrony: an indicator of regional myocardial dysfunction. Am Heart J 120(5):1047–1057

Elhendy A et al (2000) Accuracy of exercise stress technetium 99 m sestamibi SPECT imaging in the evaluation of the extent and location of coronary artery disease in patients with an earlier myocardial infarction. J Nucl Cardiol 7(5):432–438

Garcia EV, Faber TL, Esteves FP (2011) Cardiac dedicated ultrafast SPECT cameras: new designs and clinical implications. J Nucl Med 52(2):210–217

Gould KL, Lipscomb K (1974) Effects of coronary stenoses on coronary flow reserve and resistance. Am J Cardiol 34(1):48–55

Hachamovitch R et al (1998) Incremental prognostic value of myocardial perfusion single photon emission computed tomography for the prediction of cardiac death: differential stratification for risk of cardiac death and myocardial infarction. Circulation 97(6):535–543

Hachamovitch R et al (2003) Comparison of the short-term survival benefit associated with revascularization compared with medical therapy in patients with no prior coronary artery disease undergoing stress myocardial perfusion single photon emission computed tomography. Circulation 107(23):2900–2907

Hacker M et al (2007) Sixty-four slice spiral CT angiography does not predict the functional relevance of coronary artery stenoses in patients with stable angina. Eur J Nucl Med Mol Imaging 34(1):4–10

Hoffmann U, Truong QA, Schoenfeld DA, Chou ET, Woodard PK, Nagurney JT, Pope JH, Hauser TH, White CS, Weiner SG, Kalanjian S, Mullins ME, Mikati I, Peacock WF, Zakroysky P, Hayden D, Goehler A, Lee H, Gazelle GS, Wiviott SD, Fleg JL, Udelson JE (2012) ROMICAT-II Investigators. N Engl J Med 367(4):299–308. doi:10.1056/NEJMoa1201161

Hundley WG et al (1998) Administration of an intravenous perfluorocarbon contrast agent improves echocardiographic determination of left ventricular volumes and ejection fraction: comparison with cine magnetic resonance imaging. J Am Coll Cardiol 32(5):1426–1432

Ingkanisorn WP et al (2006) Prognosis of negative adenosine stress magnetic resonance in patients presenting to an emergency department with chest pain. J Am Coll Cardiol 47(7):1427–1432

Ishii K et al (2009) Exercise-induced post-ischemic left ventricular delayed relaxation or diastolic stunning: is it a reliable marker in detecting coronary artery disease? J Am Coll Cardiol 53(8):698–705
Kapur A et al (2002) A comparison of three radionuclide myocardial perfusion tracers in clinical practice: the ROBUST study. Eur J Nucl Med Mol Imaging 29(12):1608–1616
Kim RJ et al (2000) The use of contrast-enhanced magnetic resonance imaging to identify reversible myocardial dysfunction. N Engl J Med 343(20):1445–1453
Klem I et al (2006) Improved detection of coronary artery disease by stress perfusion cardiovascular magnetic resonance with the use of delayed enhancement infarction imaging. J Am Coll Cardiol 47(8):1630–1638
Kruip MJHA et al (2003) Diagnostic strategies for excluding pulmonary embolism in clinical outcome studies—a systematic review. Ann Intern Med 138(12):941–951
Ladenheim ML et al (1986) Extent and severity of myocardial hypoperfusion as predictors of prognosis in patients with suspected coronary artery disease. J Am Coll Cardiol 7(3):464–471
Leong-Poi H et al (2002) Perfusion versus function: the ischemic cascade in demand ischemia: implications of single-vessel versus multivessel stenosis. Circulation 105(8):987–992
Leppo JA (1995) Preoperative cardiac risk assessment for noncardiac surgery. Am J Cardiol 75(11):42D–51D
Marcus RP et al (2011) Myocardial perfusion imaging by computed tomography: today and tomorrow. Int J Clin Pract Suppl 173:14–22
Mark DB et al (2003) 34th Bethesda conference: task force #5–is atherosclerosis imaging cost effective? J Am Coll Cardiol 41(11):1906–1917
Marwick TH (2006) Measurement of strain and strain rate by echocardiography: ready for prime time? J Am Coll Cardiol 47(7):1313–1327
Meijboom WB et al (2008) Comprehensive assessment of coronary artery stenoses: computed tomography coronary angiography versus conventional coronary angiography and correlation with fractional flow reserve in patients with stable angina. J Am Coll Cardiol 52(8):636–643
Merhige ME et al (2007) Impact of myocardial perfusion imaging with PET and (82)Rb on downstream invasive procedure utilization, costs, and outcomes in coronary disease management. J Nucl Med 48(7):1069–1076
Mertes H et al (1993) Symptoms, adverse effects, and complications associated with dobutamine stress echocardiography. Experience in 1118 patients. Circulation 88(1):15–19
Min JK, Berman D (2009) Anatomic and functional assessment of coronary artery disease: convergence of 2 aims in a single setting. Circ Cardiovasc Imaging 2(3):163–165
Nandalur KR et al (2007) Diagnostic performance of stress cardiac magnetic resonance imaging in the detection of coronary artery disease: a meta-analysis. J Am Coll Cardiol 50(14):1343–1353
Nesto RW, Kowalchuk GJ (1987) The ischemic cascade: temporal sequence of hemodynamic, electrocardiographic and symptomatic expressions of ischemia. Am J Cardiol 59(7):23C–30C
Pijls NH et al (2010) Fractional flow reserve versus angiography for guiding percutaneous coronary intervention in patients with multivessel coronary artery disease: 2-year follow-up of the FAME (fractional flow reserve versus angiography for multivessel evaluation) study. J Am Coll Cardiol 56(3):177–184
Rochmis P, Blackburn H (1971) Exercise tests. a survey of procedures, safety, and litigation experience in approximately 170,000 tests. JAMA 217(8):1061–1066
Roger VL et al (2011) Heart disease and stroke statistics–2011 update: a report from the American Heart Association. Circulation 123(4): e18–e209
Schinkel AF et al (2007) Assessment of myocardial viability in patients with heart failure. J Nucl Med 48(7):1135–1146
Schuijf JD, Bax JJ (2008) Defining noninvasive imaging strategies in coronary artery disease: Which patients require further evaluation after coronary angiography with multislice computed tomography? J Nucl Cardiol 15(3):301–304
Schuijf JD et al (2005) Cardiac imaging in coronary artery disease: differing modalities. Heart 91(8):1110–1117
Schuijf JD, Bax JJ, van der Wall EE (2007) Anatomical and functional imaging techniques: basically similar or fundamentally different? Neth Heart J 15(2):43–44
Schwitter J et al (2008) MR-IMPACT: comparison of perfusion-cardiac magnetic resonance with single-photon emission computed tomography for the detection of coronary artery disease in a multicentre, multivendor, randomized trial. Eur Heart J 29(4):480–489
Selvanayagam JB et al (2004) Value of delayed-enhancement cardiovascular magnetic resonance imaging in predicting myocardial viability after surgical revascularization. Circulation 110(12): 1535–1541
Shaw LJ, Berman DS (2009) Functional versus anatomic imaging in patients with suspected coronary artery disease. Cardiol Clin 27(4):597–604
Shaw LJ, Iskandrian AE (2004) Prognostic value of gated myocardial perfusion SPECT. J Nucl Cardiol 11(2):171–185
Shaw LJ et al (2008) Optimal medical therapy with or without percutaneous coronary intervention to reduce ischemic burden: results from the Clinical Outcomes Utilizing Revascularization and Aggressive Drug Evaluation (COURAGE) trial nuclear substudy. Circulation 117(10):1283–1291
Taillefer R et al (1997) Comparative diagnostic accuracy of Tl-201 and Tc-99 m sestamibi SPECT imaging (perfusion and ECG-gated SPECT) in detecting coronary artery disease in women. J Am Coll Cardiol 29(1):69–77
Tonino PA et al (2009) Fractional flow reserve versus angiography for guiding percutaneous coronary intervention. N Engl J Med 360(3):213–224
Wijns W et al (1986) Effect of coronary occlusion during percutaneous transluminal angioplasty in humans on left ventricular chamber stiffness and regional diastolic pressure-radius relations. J Am Coll Cardiol 7(3):455–463

CT Evaluation of the Myocardial Blood Supply: Technical Options

Daniele Marin, Tobias J. Heye, and Daniel T. Boll

Contents

Abstract

The purpose of this book chapter is to provide an overview of novel technical advances and persistent challenges of coronary CT imaging targeting the evaluation of myocardial perfusion.

1 Introduction

A large body of the literature has demonstrated the ability of coronary computed tomographic (CT) imaging to diagnose substantial coronary artery stenosis, suggesting the use of this test as a noninvasive alternative to conventional cardiac angiography in the work-up of patients suspected of having coronary artery disease (CAD) (Hoffmann et al. 2012; Litt et al. 2012). With use of the latest CT technology, it is now possible to image the entire heart during a single heartbeat, with substantial reduction of patient radiation exposure and motion artifacts. High-quality coronary CT studies yield a high level of diagnostic accuracy for the detection of CAD. In addition, recent evidence suggests that compared to a standard stress test evaluation, coronary CT may accelerate the diagnostic work-up of patients with acute chest pain in the emergency department.

In addition to the anatomic assessment of the coronary artery lumen, another intriguing clinical application of coronary CT is the possibility of quantitative assessment of myocardial perfusion, allowing for a global anatomic and functional assessment of the heart in patients with CAD. Analysis of myocardial perfusion has important clinical implications for stratification of patients with acute CAD into different risk and management categories. For example, in patients with acute myocardial infarction the presence of areas of microvascular obstruction (i.e., areas of hypodensity relative to the surrounding myocardium during the early perfusion phase) and the extent of infarct size (defined by areas of delayed enhancement) correlate with an increased risk of complications, including the development of adverse

D. Marin · T. J. Heye · D. T. Boll (✉)
Department of Radiology, Duke University Medical Center, Durham, NC, USA
e-mail: daniel.boll@duke.edu

U. J. Schoepf et al. (eds.), *CT Imaging of Myocardial Perfusion and Viability*, Medical Radiology. Diagnostic Imaging,
DOI: 10.1007/174_2012_758, © Springer-Verlag Berlin Heidelberg 2012
Published Online: 31 October 2012

left ventricular remodeling. When combined with the assessment of regional function, analysis of the early and late contrast-enhancement patterns also provides valuable information on tissue viability, and hence the likelihood of functional recovery after revascularization. Finally, myocardial perfusion assessment may provide the only valuable indicator for the identification of flow-limiting coronary artery stenoses in patients with limited quality coronary CTA due to motion artifacts and/or coronary calcifications.

In this chapter, we will briefly review important technical advances and persistent challenges for the application of coronary CT in the assessment of myocardial perfusion. The following chapters of this book will elucidate additional details of the individual strategies of different vendors for the assessment myocardial perfusion.

2 Improvements in Temporal Resolution

Coronary artery motion, which becomes particularly detrimental at increased heart rates (above 75 beats per minute), is a leading cause of suboptimal or clinically nondiagnostic coronary CT exams. To minimize the risk of cardiac motion, coronary CT should be performed using the best possible temporal resolution allowed by the CT scanner. Several strategies are available to reach this goal (Primak et al. 2006). One of the most effective strategies to decrease CT acquisition time is to minimize the number of projections used to reconstruct the image, including only those projections gathered in the shortest possible time window for image reconstruction. The minimum amount of data required to reconstruct a CT image is 180° plus the angle (in degrees) of the X-ray beam in the plane of the image (known as the fan angle). The effective data acquisition time—to acquire the necessary data to reconstruct an image of a single section—is therefore directly proportional to the rotation time of the gantry. However, faster gantry rotation requires a slower pitch in cardiac acquisition mode to avoid discontinuities in the anatomic coverage of the heart between images reconstructed from consecutive cardiac cycles. In addition, significant development efforts are needed to account for the substantial increase in mechanical forces ($\sim$17 G for 0.42 s rotation time, $\sim$28 G for 0.33 s rotation time) and increased data transmission rates using faster gantry rotation times. For example, rotation times of less than 0.2 s (mechanical forces >75 G), which are required to provide a temporal resolution of less than 100 ms independent of the heart rate, appear to be beyond today's mechanical limits.

One option to partially overcome the technical limitations for CT image reconstruction, while improving temporal resolution for coronary CTA, is the development of a scanner design with multiple X-ray sources and detectors. The dual-source CT systems (SOMATOM Definition and SOMATOM Definition Flash, Siemens Healthcare, Forchheim, Germany) are the first and second generation of these new concept designs. Equipped with two X-ray tubes and two corresponding detectors mounted onto the rotating gantry with an angular offset of approximately 90°, dual-source CT systems can combine the data from the two separate X-ray sources and detectors, virtually eliminating the need for multisegment reconstruction techniques for coronary CT (Petersilka et al. 2008; Flohr et al. 2006). With dual-source CT technology, the half-scan sinogram using a standard parallel geometry of a conventional single-source CT system can be split up into two quarter-scan sinograms, which are simultaneously acquired by the two acquisition systems in the same relative phase of the patient's cardiac cycle and at the same anatomical level due to the $\sim$90° angle between both detectors. The two quarter-scan segments are appended by means of a smooth transition function to avoid streaking or other artifacts from potential discontinuities at the respective start and end projections (transition angle 30°). With this approach, constant temporal resolution equivalent to a quarter of the gantry rotation time is achieved in a centered region of the scan field of view. Data from one cardiac cycle only are used to reconstruct an image, thus minimizing the risk of motion artifacts between consecutive heartbeats. This approach is radically different from that of other conventional single-source CT systems, which can theoretically provide similar temporal resolution by means of multisegment reconstruction approaches. With these approaches, temporal resolution strongly depends on the heart rate; a stable and predictable heart rate and complete periodicity of the heart motion are required for adequate performance.

Dual-source CT systems are also compatible with multisegment reconstruction techniques, which may result in interesting applications in particular clinical settings. Using a two-segment reconstruction, the quarter-scan segments acquired by each of the two detectors are independently divided into smaller sub-segments acquired in subsequent cardiac cycles—similar to two-segment reconstruction in conventional single source CT. The temporal resolution of multisegment reconstruction techniques is directly affected by the patient's heart rate, with an average temporal resolution of 60 ms using a 0.33-s gantry rotation time (minimum temporal resolution 42 ms). While multisegment reconstruction techniques using a dual-source CT are generally not recommended for coronary CTA examinations, this approach may be beneficial for advanced functional analysis, such as the assessment of myocardial wall perfusion, wall motion abnormalities, or the determination of cardiac function indices, such as cardiac chambers volumetric analysis and ejection fraction evaluation.

The recent introduction of second generation of dual-source CT systems with the use of two 128-section detector rows have further improved temporal resolution for coronary CTA, introducing new strategies for faster acquisition times. Using previously unexplored high pitch settings (beam pitch up to 3.4, corresponding to a table speed of 458 mm/s), this new system allows ultrafast CT acquisition, allowing prospective ECG-triggered scanning of the heart within a single heartbeat with continuous movement of the table during scanning (Flohr et al. 2009; Achenbach et al. 2009). The high pitch acquisition technique also yields substantial reduction of patient radiation dose, due to virtual elimination of partial overlap during spiral CT acquisition (Achenbach et al. 2010). While very promising, the high pitch technique may not be adequate for larger patient populations or highly attenuating anatomical areas, such as the abdomen and pelvis. This is based on the technical limitations in the maximum tube current output of the currently available X-ray tubes using high pitch settings, which in turn may result in increased image noise and clinically unacceptable image quality.

Recently, a novel vendor-specific motion-correction algorithm (SnapShot Freeze; GE Healthcare, Waukesha, Wis) has been developed that uses information from adjacent cardiac phases within a single cardiac cycle to characterize and correct for cardiac motion. By using information obtained from adjacent pixels, this approach may correct for the complex and elastic motion deformations in the heart and coronaries during the cardiac cycle. This effect may result in potentially motion-free, high quality coronary CT images. Preliminary phantom studies suggest that blurring secondary to cardiac motion can be decreased by a factor of six with this new motion correction algorithm, which would correspond to an effective gantry rotation speed of 0.058 s (58 ms) (Scott Schubert 2012). Additionally, early clinical experience demonstrates that this motion correction algorithm significantly improves image quality, interpretability, and diagnostic accuracy of coronary CTA studies without the use of rate control medications (Leipsic et al. 2012).

3 Dual-Energy CT Applications

For decades, dual-energy imaging has been used for tissue differentiation with several X-ray-based imaging modalities, exploiting the fact that the tissues in the human body show different absorption characteristics when penetrated with different X-ray energy spectra at different kV settings of the X-ray tube (Coursey et al. 2010). The ability to separate different materials using dual-energy may substantially improve the interpretation of myocardial perfusion CT studies by providing enhanced information on iodine distribution within the myocardium with the additional help of color-coded iodine distribution maps. These techniques may result in improved diagnostic accuracy for the detection of areas of decreased or absent perfusion caused by flow-limiting coronary stenosis (Ruzsics et al. 2008, 2009).

Although early work in the 1970 and 1980s demonstrated that dual-energy CT technology improved tissue characterization, its utility was limited because of noise in the low-kilovoltage images and the amount of time required for data acquisition, which led to misregistration. Newer CT technologies allow for more rapid data acquisition and have sparked renewed interest in dual-energy applications. Manufacturers continue to improve dual-energy CT scanners, and those that are currently available differ in terms of the number of X-ray tubes, the number and arrangement of detector arrays, the energy of fan beams, and the rotation of X-ray tubes and detector arrays. Current dual-energy CT scanners also offer improved temporal resolution, which is helpful for coronary CT applications, and increased photon flux, which is critical for imaging diagnostically challenging larger patient populations.

The dual-source CT scanners (SOMATOM Definition and SOMATOM Definition Flash, Siemens Healthcare, Forchheim, Germany) allow operation of both X-ray tubes at different kV and mA settings, with the possibility of acquiring closely co-registered dual-energy data. Another major advantage of using a dual-source approach for dual-energy acquisition is the possibility of using different filtration for independent shaping of the two X-ray spectra (Primak et al. 2009). The X-ray spectra generated at low (80 kV) and high (140 kV) peak tube potentials have a high degree of spectral overlap, resulting in a separation between the average energies of the two spectra much less than the 60 keV difference in peak potential. The ability of DECT to discriminate between two materials relies primarily on the difference between the energy ratio of the materials, which is determined by the separation between the high- and low-energy spectra and the difference between the effective atomic numbers of the evaluated materials. The smaller the spectral separation, the harder it is to discriminate between two materials, especially for materials with close atomic numbers (e.g., calcium and iron).

Using additional filtration for one or both tube potentials (kV) can increase spectral separation, resulting in increased dual-energy contrast between different materials (Leschka et al. 2010; Primak et al. 2010). This effect can significantly enhance the performance of dual-energy material decomposition algorithms designed to discriminate between different materials, such as calcium (e.g., bone or calcified plaque) and iodinated contrast material. This effect may result in improved sensitivity of a dual-source dual-energy CT technique for detecting areas of different myocardial perfusion due to ischemia. In addition, improvements in

material decomposition using dual-energy may also result in better discrimination between calcium and iron, which are indistinguishable using conventional magnetic resonance imaging (MRI) and single-energy CT techniques. Detection of iron deposition within a coronary plaque has important clinical implications as intraplaque hemorrhage has been advocated as an early indicator of plaque vulnerability, possibly allowing lesion early intervention before acute plaque complications and myocardial infarction.

Finally, another important clinical benefit of differential filtration of the X-ray spectra using a dual-source dual-energy technique is the possibility of greater customization of the peak tube voltage settings for the lower energy tube. This capability may substantially reduce the number of nondiagnostic dual-energy CT scans in large patients due to unacceptable noise in the 80 kV images. In these patients, the tube voltage of the lower energy X-ray tube could be increased from 80 to 100 kV, resulting in a much larger photon flux. At the same time, the energy separation between the two X-ray spectra can be increased by appropriate selection of the filtration. This approach cannot be used with single-source dual-energy techniques because the separation between the 100 and 140 kV spectra is too small to produce sufficient dual-energy contrast using fixed filtration settings.

Another innovative vendor's approach to dual-energy CT using a single-source CT scanner involves the use of a fast kilovoltage switching technology—also known as dynamic switching. This technique exploits recently developed detectors with a new scintillator material with a chemically replicated garnet crystal structure (Gemstone Detector, GE Healthcare, Waukesha, Wis). The light emission speed of the scintillator is markedly faster than that of gadolinium oxysulfide, which is the standard scintillator material used in conventional CT systems. The afterglow is also reduced with the garnet crystal scintillator. The fast light emission and low afterglow of the scintillator enable faster data sampling. These technological advances result in minimal delay between paired 80- and 140-kVp projections (less than 0.25 ms apart in time), without limitations in the scanned field-of-view. In addition, the fast kilovoltage switching technology allows more efficient beam-hardening correction from the projection data using information collected from two different kilovoltage peaks with the same projection angle. This approach increases accuracy of calculated material density images and mass attenuation coefficients. In addition, due to the nearly perfect spatial co-registration of the two X-ray energy datasets, synthesized virtual monochromatic spectral images can be generated across a broad range of energy values (from 40 to 140 keV). These images have the potential to virtually eliminate beam-hardening artifacts, which occur secondary to preferential absorption of low-energy photons as the polychromatic X-ray beam penetrates an object. Beam hardening artifacts are responsible for substantial CT number inaccuracies in diagnostic CT, representing a well-known source of error during assessment of myocardial perfusion. The latter effect is caused by substantial hardening of the X-ray beam as it penetrates the high iodine concentrations of contrast material in the ventricular chambers and large vessels of the mediastinum, yielding regional areas of artificially low attenuation within the myocardium. While conventional beam-hardening correction algorithms used in abdominal CT imaging for the past several decades have been specifically optimized to correct for beam-hardening artifacts resulting from bone, these algorithms have not been implemented for correction of beam-hardening effects from iodinated contrast material in the cardiovascular system. It is conceivable that virtual monochromatic spectral imaging with or without the additional help of recently developed reconstruction algorithm specifically developed for cardiac applications will substantially mitigate the detrimental effect of beam hardening, resulting in more accurate and reproducible quantitative assessment of myocardial perfusion using CT.

Another important advantage of virtual monochromatic spectral images is the potential for decreased noise, with simultaneous increase in contrast-to-noise ratio in the cardiovascular system (Matsumoto et al. 2011). This beneficial effect has been demonstrated using a relatively narrow range of synthesized monochromatic energy values. Radiologists should be aware of a progressive increase in noise with the use of monochromatic energies away from the optimal spectrum. This increase in image noise is inversely proportional to the energy separation of the low and high kVp incident spectra, thus emphasizing the importance of having well-separated energy spectra for optimal dual-energy imaging (Matsumoto et al. 2011).

The third innovative approach for dual-energy CT is the use of a double-layer detector technology to simultaneously and equi-directionally collect information regarding individual photon energy values during single-source CT acquisition at standard radiation dose. Information regarding the different energy photons within the X-ray spectrum may increase the quantitative potential of CT. CT numbers do not accurately reflect the linear attenuation coefficient of tissue owing to imprecise assumptions regarding photon energies. Furthermore, CT numbers cannot always help differentiate between different types of tissue. For example, a tissue composed of higher atomic number elements may have the same CT number as a tissue composed of lower atomic number elements if the former tissue is not very dense and the latter tissue is sufficiently dense. The inability of energy-integrating detectors to differentiate between photons of different energies still presents major limitations. First, the differences in soft-tissue X-ray attenuation are

smaller at higher energies than at lower energies. However, higher energy photons dominate the measured signal, resulting in relatively poor soft-tissue contrast. Second, to visualize these subtle differences in soft-tissue contrast, image noise must be kept low, requiring larger X-ray exposures.

4 Radiation Dose-Reduction Strategies

One of the most important limitations for the widespread use of coronary CT in the evaluation of the coronary arteries and myocardial perfusion is the potential hazard to the patient from ionizing radiation exposure. Scientific evidence has suggested that the risk of radiation-induced cancers in individual patients is small (although real) at the doses relevant to CT (3.5–25 mSv for a standard CT examination (Sodickson et al. 2009; Brenner and Hall 2007).

In response to concerns over mounting radiation exposure, the radiological community (i.e., radiologists, technologists, medical physicists, and CT manufacturers) has been striving during the past decade to develop imaging strategies that deliver the lowest dose necessary to obtain the desired information with CT. Besides the obvious importance of avoiding medically unnecessary imaging tests, many technological and operator-dependent advances have been implemented, leading to a substantial decrease in the radiation dose from a given CT examination. This includes the use of: (a) solid-state scintillating detectors with high absorption efficiency, (b) more powerful X-ray tubes and generators that enable more efficient filtration of low-energy photons, (c) beam-shaping filters (also known as bow-tie filters) that vary the X-ray intensity depending on the patient cross-section, and (d) automated adjustment of scanner output according to the patient size. Other dose-reduction techniques that are gaining widespread use include: (a) the use of in-plane bismuth breast shields to decrease breast dose in female patients, (b) the reduction of scan range along with the use of adaptive section collimation that minimizes unnecessary exposure owing to overscanning, (c) the implementation of CT protocols that limits the number of acquisition phases in multiphasic studies without penalizing diagnostic information, and (d) the appropriate selection of dose-efficient tube potential settings. More recently, iterative reconstruction techniques and algorithms for reconstruction of virtual nonenhanced images from contrast material-enhanced dual-energy CT datasets are emerging as promising strategies for additional control of CT radiation dose.

Additional effective strategies are also available to decrease patient radiation dose in cardiac CT examinations. These strategies include modulation of the X-ray current with respect to the cardiac phase (i.e., the so-called ECG pulsing), adaptation of the pitch factor to the patient's heart rate, and sequential cardiac CT data acquisition (prospective triggering). The latter approach, although very effective for minimizing radiation dose, entails a non negligible risk of misregistration between successive acquisitions due to breathing or other motion. Finally, the use of high pitch acquisition techniques using a dual-source CT system has been recently introduced as a new and effective way to decrease patient's radiation exposure, as detailed above (Achenbach et al. 2010).

5 Optimization of Tube Voltage Selection

Selection of the optimal tube potential and filtration is currently an active area of research. Studies have shown that the most dose-efficient tube potential depends not only on the diagnostic task but also the patient size (Guimarães et al. 2010). The use of lower tube voltages significantly decreases radiation dose due to the approximately quadratic relationship between kV and radiation dose. To cite an example, using a constant tube current–time product, a drop in tube voltage from 140 to 80 kV yields a reduction in radiation dose by 68 % $[1 - (80/140)^2 = 0.68]$. Another advantage of selecting lower tube voltage settings is the possibility of improving image quality, if kVp changes are accompanied by appropriate increase in tube current–time product parameters. This scanning method—often referred to as a low-tube voltage, high-tube current CT technique—improves the magnitude of iodine contrast enhancement (by a factor of two, for example, when tube voltage is decreased from 140 to 80 kVp) due to the greater likelihood of photoelectric interactions at lower tube voltages. In most patients, this improvement comes with only a small to moderate increase in noise (which is inversely related to image quality on CT) due to a compensatory increase in tube output settings. Several studies focussing on reduced 100 or 80 kVp with higher tube current–time product settings for CT angiography have reported significantly lower radiation dose and similar image quality compared to a standard 120 kVp technique. This may be explained by the increased attenuation of vividly enhancing arterial structures compared to poorly enhancing adjacent tissues, resulting in a greater contrast-to-noise ratio at lower tube voltages (Szucs-Farkas et al. 2009; Leschka et al. 2008; Wintersperger et al. 2005). Another benefit of the low-tube voltage technique for CT angiography is the potential for reducing the volume of iodinated contrast material. A contrast medium volume of 45 mL (370 mgI/mL) may be sufficient for thoracoabdominal CT angiography at 80 kVp in intermediate-size patients. Although the use of low-tube voltage CT settings is appealing, it remains to be determined which clinical applications and patient group would benefit the most from this technique. At our institution, we believe this CT technique should be preferred for everyone,

assuming at least equivalent image quality to be consistent with the As Low As Reasonably Achievable (ALARA) paradigm. Automatic kV selection tools will soon be available to assist radiologists in the selection of optimal tube voltage settings, with consideration of the patient's body size and diagnostic task (Guimarães et al. 2010; Yu et al. 2010). In addition, improvements in X-ray tubes and generators will continue to increase generator power levels to allow higher tube current values for use with lower tube potentials.

6 Filtration

Optimization of the composition, shape, and thickness of the X-ray filter will allow delivery of X-ray intensities that are matched to the patient attenuation profile and will narrow the spectrum of energy photons within the X-ray beam. In addition, the use of high power levels also allows for more aggressive beam filtration, which reduces the number of low-energy photons in the beam and results in a decrease in patient dose.

7 Adaptive Noise Reduction Filters and Iterative Reconstruction Algorithms

Filtered back-projection (FBP) algorithms are currently the standard reconstruction technique in CT. Although fast and robust, filtered back-projection techniques may accentuate image noise and result in streak artifacts. In an attempt to foster the use of low-radiation dose CT protocols, CT manufacturers have been investigating new strategies to decrease noise on CT images. One promising approach is the use of adaptive noise reduction filters (Szucs-Farkas et al. 2011; Kalra et al. 2004). By applying a post-processing two-dimensional smoothing technique in all three dimensions of space, along with an edge detection algorithm, these filters allow significant reduction of noise while preserving the spatial resolution and contrast information of digital imaging and communications in medicine (DICOM) data. Preliminary experience has indicated a potential for substantial reduction in radiation dose, using a prototype noise reduction filter.

Another promising strategy for decreasing noise and artifacts on CT images comes from the recent implementation of new iterative reconstruction techniques (Silva et al. 2010). Based on their level of sophistication and image reconstruction velocity, these techniques can be categorized as: (a) iterative reconstructions performed from the image data alone (Iterative Reconstruction in Image Space, Siemens Medical Solutions, Inc.), (b) iterative reconstructions performed from both the projection and image data (Adaptive Statistical Iterative Reconstruction [ASiR], GE Healthcare, Inc.; Sinogram Affirmed Iterative Reconstruction [Safire], Siemens Healthcare Solutions, Inc.; iDose, Philips Healthcare, Inc., AIDR 3D, Toshiba Medical Systems), and (c) iterative reconstruction performed from projection data alone (MBiR or Veo, GE Healthcare, Inc.). Iterative reconstruction algorithms may be used to either reduce the amount of image noise (and thus improve image quality) in large patients, or maintain diagnostically adequate noise while decreasing radiation dose in nonobese patients. Accumulating evidence in the literature again suggests a substantial potential for reduction in radiation dose while preserving diagnostic image quality using ASiR with a standard CT technique (120 kVp) (Leipsic et al. 2010a, b).

In the management of CT radiation dose, the role and combination of different strategies for radiation dose reduction cannot be overemphasized. The radiation dose for a routine single-phase CT scan of the abdomen and pelvis could decrease from the average value of 10 mSv to less than 1 mSv (submillisievert levels), with the appropriate use of multiple DOSE-reduction strategies. This would result in a radiation dose exposure to the patient that is only one-third of the average annual dose from background radiation sources such as radon and cosmic rays.

8 Conclusions

In conclusion, rapid advances in technology have greatly enhanced the effectiveness of coronary CT as a noninvasive imaging modality for obtaining combined anatomic and functional information in patients with CAD. Most recent and clinically relevant technologic advances include the remarkable improvements in temporal resolution and development of new motion correction algorithm for better modeling of cardiac motion and potential correction of motion-related artifacts. In addition, the widespread use of dual-energy CT techniques has increased the diagnostic sensitivity, accuracy, and precision of the myocardial perfusion assessment, further consolidating the role of CT in cardiac imaging. Although radiation dose remains the major barrier for the widespread acceptance of cardiac CT in daily clinical practice, the combined use of different strategies for radiation dose reduction has the potential to synergistically decrease the radiation burden of coronary CT, with the ultimate goal of achieving submillisievert effective dose levels.

References

Achenbach S et al (2009) High-pitch spiral acquisition: a new scan mode for coronary CT angiography. J Cardiovasc Comput Tomogr 3:117

Achenbach S et al (2010) Coronary computed tomography angiography with a consistent dose below 1 mSv using prospectively electrocardiogram-triggered high-pitch spiral acquisition. Eur Heart J 31:340

Brenner DJ, Hall EJ (2007) Computed tomography—an increasing source of radiation exposure. N Engl J Med 357:2277

Coursey CA et al (2010) Dual-energy multidetector CT: how does it work, what can it tell us, and when can we use it in abdominopelvic imaging? 1. Radiographics 30:1037

Flohr TG et al (2006) First performance evaluation of a dual-source CT (DSCT) system. Eur Radiol 16:256

Flohr TG et al (2009) Dual-source spiral CT with pitch up to 3.2 and 75 ms temporal resolution: image reconstruction and assessment of image quality. Med Phys 36:5641

Guimarães LS et al (2010) Appropriate patient selection at abdominal dual-energy CT using 80 kV: relationship between patient size, image noise, and image quality. Radiology 257:732

Hoffmann U et al (2012) Coronary CT angiography versus standard evaluation in acute chest pain. N Engl J Med 367:299

Kalra MK et al (2004) Detection and characterization of lesions on low-radiation-dose abdominal ct images postprocessed with noise reduction filters1. Radiology 232:791

Leipsic J et al (2010a) Estimated radiation dose reduction using adaptive statistical iterative reconstruction in coronary CT angiography: the ERASIR study. Am J Roentgenol 195:655

Leipsic J et al (2010b) Adaptive statistical iterative reconstruction: assessment of image noise and image quality in coronary CT angiography. Am J Roentgenol 195:649

Leipsic J et al (2012) Effect of a novel vendor-specific motion-correction algorithm on image quality and diagnostic accuracy in persons undergoing coronary CT angiography without rate-control medications. J Cardiovasc Comput Tomogr 6:164

Leschka S et al (2008) Low kilovoltage cardiac dual-source CT: attenuation, noise, and radiation dose. Eur Radiol 18:1809

Leschka S et al (2010) Performance of dual-energy CT with tin filter technology for the discrimination of renal cysts and enhancing masses. Acad Radiol 17:526

Litt HI et al (2012) CT angiography for safe discharge of patients with possible acute coronary syndromes. N Engl J Med 366:1393

Matsumoto K et al (2011) Virtual monochromatic spectral imaging with fast kilovoltage switching: improved image quality as compared with that obtained with conventional 120-kVp CT. Radiology 259:257

Petersilka M, Bruder H, Krauss B, Stierstorfer K, Flohr TG (2008) Technical principles of dual source CT. Eur J Radiol 68:362

Primak AN, McCollough CH, Bruesewitz MR, Zhang J, Fletcher JG (2006) Relationship between noise, dose, and pitch in cardiac multi–detector row CT1. Radiographics 26:1785

Primak A, Giraldo JCR, Liu X, Yu L, McCollough C (2009) Improved dual-energy material discrimination for dual-source CT by means of additional spectral filtration. Med Phys 36:1359

Primak AN et al (2010) Dual-source dual-energy CT with additional tin filtration: dose and image quality evaluation in phantoms and in vivo. Am J Roentgenol 195:1164

Ruzsics B et al (2008) Dual-energy CT of the heart for diagnosing coronary artery stenosis and myocardial ischemia-initial experience. Eur Radiol 18:2414

Ruzsics B et al (2009) Comparison of dual-energy computed tomography of the heart with single photon emission computed tomography for assessment of coronary artery stenosis and of the myocardial blood supply. The Am J Cardiol 104:318

Silva AC, Lawder HJ, Hara A, Kujak J, Pavlicek W (2010) Innovations in CT dose reduction strategy: application of the adaptive statistical iterative reconstruction algorithm. Am J Roentgenol 194:191

Sodickson A et al (2009) Recurrent CT, cumulative radiation exposure, and associated radiation-induced cancer risks from CT of adults1. Radiology 251:175

Szucs-Farkas Z et al (2009) Endoleak detection with CT angiography in an abdominal aortic aneurysm phantom: effect of tube energy, simulated patient size, and physical properties of endoleaks1. Radiology 251:590

Szucs-Farkas Z et al (2011) Nonlinear three-dimensional noise filter with low-dose CT angiography: effect on the detection of small high-contrast objects in a phantom model. Radiology 258:261

Wintersperger B et al (2005) Aorto-iliac multidetector-row CT angiography with low kV settings: improved vessel enhancement and simultaneous reduction of radiation dose. Eur Radiol 15:334

Scott Schubert G P. C. T. P (2012) Marketing, GE Healthcare, Introducing the discovery CT750 HD FREEdom Edition

Yu L, Li H, Fletcher JG, McCollough CH (2010) Automatic selection of tube potential for radiation dose reduction in CT: a general strategy. Med Phys 37:234

CT Evaluation of the Myocardial Blood Supply: Single-Source, Single-Energy CT

Konstantin Nikolaou

Contents

Abstract

Cardiac CT has evolved into a useful clinical tool assessing the morphology of the coronary arteries non-invasively. However, the diagnostic accuracy can still be limited. Especially in stenoses with unclear hemodynamic significance, morphological assessment of the CT coronary angiography tends to overestimate disease, leading to false-positive results. Recent technical developments offer the opportunity to assess myocardial perfusion, combining morphological with functional information. In this chapter, single-source CT techniques providing perfusion information on the myocardium, i.e., both single-shot and dynamic multiphasic acquisition techniques, will be explained and discussed.

1 Introduction

Assessment of myocardial viability and myocardial perfusion plays a critical role in the evaluation of patients suffering from coronary artery disease (CAD), as patterns of myocardial perfusion are associated with short- and long-term prognosis and the hemodynamic relevance of a coronary artery stenosis (Hendel et al. 2009). Cardiac CT, which has evolved as a useful tool for the assessment of obstructive and nonobstructive CAD, has mainly been limited to the morphological assessment of CAD, i.e., CT coronary angiography (Budoff et al. 2006). However, imaging of myocardial viability and quantification of myocardial perfusion would greatly complement noninvasive coronary CT angiography. Within recent years, a number of studies have focused on the demonstration of myocardial "perfusion" deficits using multidetector (MD-)CT. However, most of the studies used either a single volume data acquisition during the angiographic phase or double exposure with the acquisition of an additional delayed phase dataset. However, this approach is based on static imaging rather than on dynamic imaging. Therefore, these kinds of datasets represent a more kind of blood volume

K. Nikolaou (✉)
Department of Clinical Radiology,
University Hospitals Munich - Grosshadern Campus,
Munich, Germany
e-mail: konstantin.nikolaou@med.lmu.de

U. J. Schoepf et al. (eds.), *CT Imaging of Myocardial Perfusion and Viability*, Medical Radiology. Diagnostic Imaging,
DOI: 10.1007/174_2012_759, © Springer-Verlag Berlin Heidelberg 2012
Published Online: 6 November 2012

distribution (early phase) and a delayed contrast agent distribution, i.e., an approach similar to delayed imaging in magnetic resonance imaging (MRI) reflecting myocardial viability (Koyama et al. 2004). However, real dynamic myocardial perfusion imaging (MPI) with CT techniques would be based on the dynamic visualization of a contrast agent during its first pass through the cardiac chambers, coronary arteries, and myocardium. Such CT techniques would offer the benefit of providing linearity of contrast concentration and density and would potentially allow the quantitative calculation of myocardial perfusion for a reliable assessment of hemodynamically significant vessel changes. Given the great promise of a combined cardiac CT examination to assess morphology and function, much research has been recently focused on the development of CT-based MPI techniques. In this chapter, recent developments in cardiac CT with respect to MPI will be reviewed, with a special focus on single-source, single-energy dynamic perfusion CT.

2 Technical Aspects, Acquisition Protocol, and Radiation Dose

Time resolved whole-brain perfusion CT is a well-established quantitative technique in assessing various perfusion parameters, such as cerebral blood flow, cerebral blood volume, mean time transit, and time to peak, with an acceptable mean X-ray exposure of typically 5–7 mSv (Orrison et al. 2011). Translation to the myocardium, however, is challenging due to its inherent rapid motion, and represents a novel approach that is currently under investigation. A dynamic approach is based on sequential CT acquisitions of the myocardium, to determine the myocardial enhancement over a defined period of time. Derived time-tissue-attenuation curves can be used to estimate myocardial blood flow (MBF), similar to ischemic brain imaging.

Up to now, the technical challenges of time-resolved CT MPI have been substantial. A long acquisition time, i.e., a long temporal coverage of the myocardial contrast passage, has to be ensured, resulting in a mandatory imaging time of approximately 30–40 s. High temporal resolution is required for (semi-)quantification of perfusion data, and therefore the interval between imaging at identical positions should not exceed one or two heartbeats. While with earlier CT generations (e.g., 64-slice CT), the anatomical coverage was limited to the detector width of a given CT system (typically around 4 cm coverage for 64-slice CT), and thus only parts of the myocardium could be covered in a dynamic fashion (Kido et al. 2008), recent technical developments have changed this paradigm.

Today, there are two technical options to cover the whole myocardium for dynamic perfusion imaging. First, CT with wide detectors, e.g., 256- or 320-slice CT, cover up to 16 cm without table movement (Gramer et al. 2012; Hsiao et al. 2010). And second, the latest generation of dual-source CT systems, enabling a so-called "shuttle mode", composes two adjacent slabs of myocardium of 4 cm each, resulting in nearly 8 cm of myocardial coverage in a dynamic fashion (see Table 1, Fig. 1) (Bamberg et al. 2010).

Overall, a perfusion sequence on MDCT is comparable to an ECG-triggered test bolus technique. To obtain a reasonable signal-time curve with a modest amount of contrast agent, high speed injections with a saline flush technique are preferable to acquire good quality signal-time curves (e.g., ~40–50 ml of contrast agent injected at a flow rate of about 5–8 ml/s). While all previous efforts in CT MPI were typically region-of-interest (ROI) based, i.e., measuring the time-density curves in a small portion of the myocardium defined by a ROI, recent studies have extended these principles into quantitative three-dimensional (3D) imaging techniques. It was shown that regional MBF can be derived in patients in combination with CT-based morphological assessment of CAD, i.e., CTCA (Bamberg et al. 2010, 2011; Wang et al. 2012).

There are many technical aspects that need further optimization in cardiac CT perfusion imaging. Even if modern techniques for reduction of radiation exposure are applied, typical study protocols employed for dynamic 3D imaging of the myocardium will still result in a comparably high total radiation exposure of an approximately 10–13 mSv-equivalent radiation dose (including the perfusion imaging and a prospective CTCA). On the other hand, this radiation exposure is similar to that of established retrospective CTCA examinations on 64-slice CT (with a reported median of 12 mSv in a large multicenter study) (Hausleiter et al. 2009) and comparable to or lower than nuclear perfusion imaging, the clinical standard for the assessment of myocardial perfusion (radiation exposure for stress-only 99 m technetium [Tc] sestamibi is approximately 10.0 mSv, but that for 2-day 99 mTc sestamibi or 201Tl is 20.0 mSv or higher) (Einstein et al. 2007).

Further technical research will be necessary in CT MPI, to develop strategies to reduce radiation exposure and determine the impact of heart rate and different injection protocols on image quality, diagnostic accuracy, and radiation exposure. Independent of the technical acquisition protocol used (single-source dynamic, single-source static, and dual-source/dual-energy static), the protocol includes the administration of adenosine as a stressing agent to better depict myocardial perfusion defects due to the induced "steal-effect" caused by the vasodilatation. Adenosine is a short-lasting vasodilator, and continuous ECG monitoring is mandatory. Contraindications for administration of adenosine include Wolff-Parkinson-White (WPW) syndrome, atrio-ventricular (AV) block, and sick-sinus syndrome as well as asthma. Finally, besides the development of dose-reduction algorithms and optimized contrast agent injection protocols for dynamic MPI

Table 1 Example for a dynamic CT perfusion acquisition protocol using a second-generation dual-source CT scanner

Scanner	2nd gen. DSCT
Myocardial coverage	7.3 cm
Scan type	Shuttle mode
Scan duration	30 s
Contrast timing	Test bolus −4 s
Tube current and tube voltage	200 mAs, 100 kV
Contrast application	50 cc, 370–400 mg Iodine, 5 ml/s
Stressing agent	Adenosine, 140 µg/kg BW
Temporal resolution	<63 bpm: every heartbeat >63 bmp: every second heart beat e.g., in a HR of 100 bpm: 12 acq. In 30 s, temporal resolution = 2.5 s
Radiation dose	~10 mSv

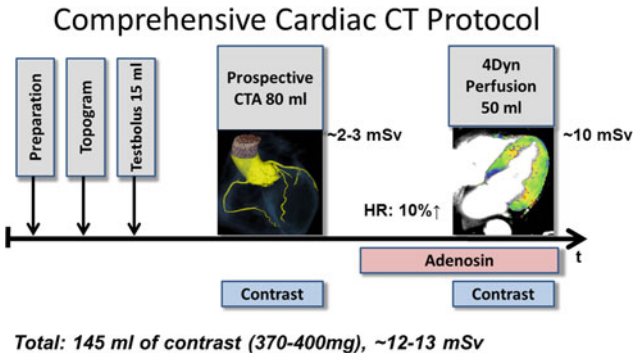

Fig. 1 A comprehensive cardiac CT protocol in patients with suspected coronary artery disease (CAD) could comprise a morphologic CT angiography of the coronary arteries and a dynamic perfusion scan of the myocardium. According to published data, the combination of CTA plus CT perfusion could increase the diagnostic accuracy in the detection of hemodynamically significant coronary artery stenosis, namely reducing the number of false-positive findings by CTA. Today, the typical total amount of contrast volume and radiation dose for such a protocol amounts to ~145 ml of contrast agent and 12–13 mSv-equivalent dose, respectively. In the future, technical improvements of the acquisition techniques will help to further reduce these values

by CT, work on dedicated reconstruction algorithms such as iterative reconstruction techniques that optimize the contrast-to-noise ratio (CNR) might help further reduce radiation exposure (Gramer et al. 2012).

2.1 Static or Dynamic Imaging for Cardiac CT Perfusion?

As compared to the rather challenging dynamic CT perfusion protocol, a single acquisition after contrast administration and adenosine stress may represent a promising alternative option to define myocardial contrast distribution at a predefined point in time at a relatively low level of radiation exposure. Given the high image quality of the latest high-pitch acquisitions, potentially resulting in radiation exposure of less than 1 mSv, it can be assumed that multiple scans, performed at different timing, may extend the small diagnostic window for delayed contrast distribution using such single-shot techniques. However, static imaging at one given time point—be it by single-source/single-energy or by dual-source/dual-energy techniques—will only allow for depiction of iodine distribution in the myocardium at a given time. Hence, the analysis of myocardial attenuation acquired at a single phase of arterial contrast enhancement without continuous time-resolved image acquisition enables detection of myocardial blood pool deficits but does not allow quantification of perfusion (George et al. 2006, 2007; Ko et al. 2012a, b; Blankstein et al. 2009).

As a perspective for these kinds of acquisition protocols, using the specific spectral characteristics of iodine and myocardium when exposed to different X-ray energy levels, Dual-energy acquisitions have been suggested as an alternative to quantify myocardial iodine concentration (Ruzsics et al. 2009a, b). It remains unclear at which point in time the acquisition should be triggered, as the inflow of contrast is clearly dependent on many factors. Using the data derived from dynamic, time-resolved CT perfusion datasets, Bischoff and colleagues have specifically defined the most valid acquisition time for the detection of ischemia, comparing opacification of ischemic versus nonischemic myocardium over time (Bischoff et al. 2012). Under pharmacological stress using adenosine, a maximum mean HU difference between ischemic and nonischemic myocardium (ranging from 17.7 to 22.5 HU) was observed 24–32 s after injection of contrast medium. Still, the optimal time point for a single-shot acquisition will certainly still be dependent on contrast injection, cardiac output, and scan parameters.

2.2 Do We Need a Quantitative Myocardial Perfusion Analysis?

The main advantage of time-resolved dynamic CT imaging of the myocardial perfusion yields the promise of absolute perfusion quantification. As outlined above, first-pass acquisitions are limited either to the pure visual assessment of hypo-enhanced myocardial areas and/or density/iodine uptake measurements, and do not allow an exact quantification of myocardial perfusion. The typical quantitative parameters that can be calculated from a dynamic time-density curve as acquired by a dynamic perfusion protocol are the MBF and the myocardial blood volume (MBV) (see Fig. 2). The MBF scale units are ml/min/g, and the MBV

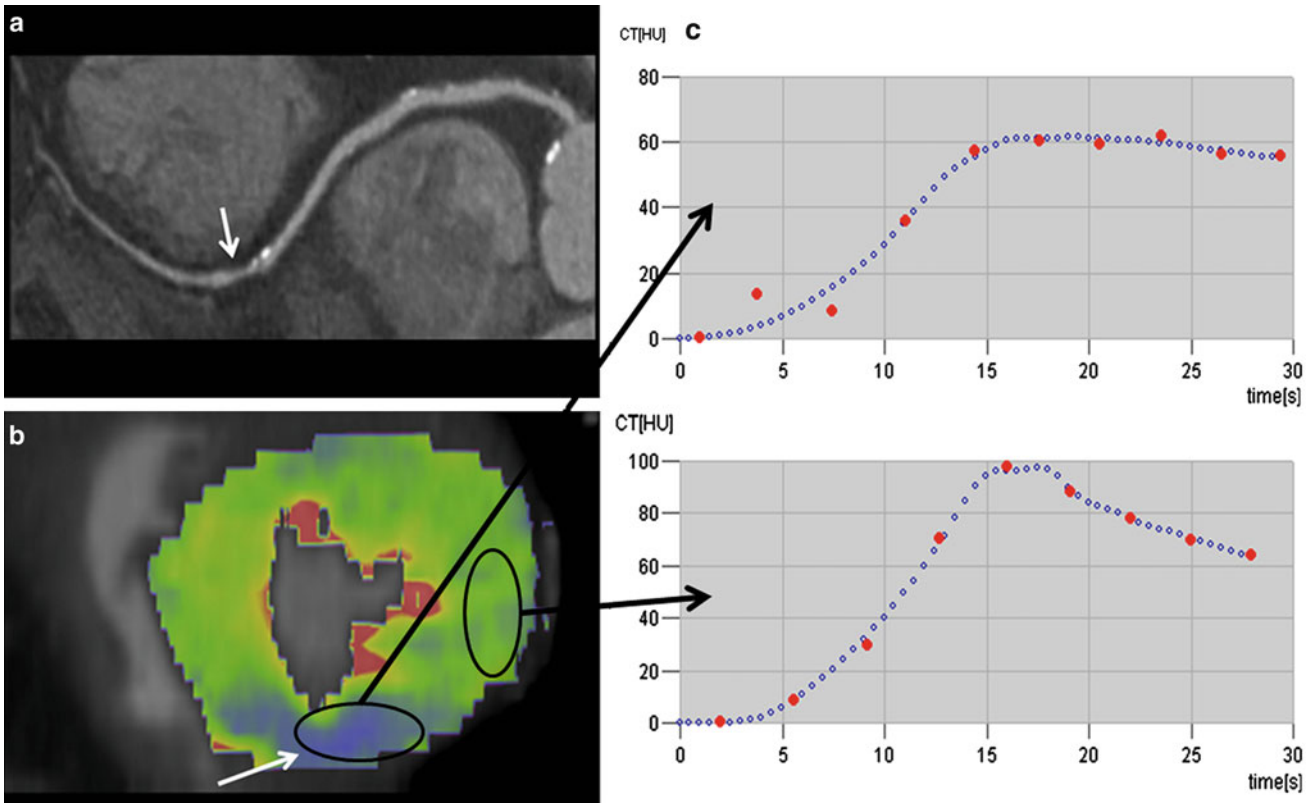

Fig. 2 The multiplanar reformat of a patient with suspected coronary artery disease (CAD) of the right coronary artery (RCA) shows a potentially hemodynamically significant stenosis in the middle segment (**a**, *arrow*). A dynamic perfusion scan (color-coded parameter map) of the same patient depicts a perfusion defect under Adenosine stress in the RCA territory (**b**, *arrow*). From these data, time-density curves can be derived for under perfused (**c**, *upper curve*) and normal myocardium (**c**, *lower curve*), and quantitative perfusion values, such as the myocardia blood flow (MBF), can be calculated

scale units are ml/g. As 3D dynamic acquisition of the heart has recently become possible, the question must be raised, is absolute quantification of myocardial perfusion by CT needed at all, given the fact that these protocols are technically more challenging and less radiation dose effective as compared to single-phase protocols? Ultimately, the goal for cardiac perfusion imaging is to improve diagnostic accuracy for identifying flow-obstructing stenosis compared with CTA and CT perfusion alone and to provide information on the hemodynamic functional relevance of detected lesions.

In a clinical setting, the hemodynamic significance of a given coronary artery stenosis should be defined with invasive fractional flow reserve (FFR) measurements using a flow wire, representing the currently accepted standard for assessing the hemodynamic significance of coronary artery stenotic lesions (Tonino et al. 2009; Serruys et al. 1997). While CT provides a useful noninvasive technique to evaluate coronary artery anatomy, the functional significance of many coronary artery CT findings is often unclear and may lead to increased downstream test utilization (e.g., radionuclide perfusion imaging, stress MR imaging, or FFR) to help guide treatment decisions (Tonino et al. 2009; Shaw et al. 1999; Blankstein et al. 2010). Specifically, Meijboom et al. (2008) showed on the one hand that the diagnostic accuracy of a quantitative assessment of coronary artery stenosis with CT was highly correlated with angiographic findings. However, for the detection of hemodynamically significant coronary artery stenosis, as assessed with FFR, CT angiography only had a sensitivity of approximately 50 %. Thus, the combination of morphologic imaging with perfusion CT could ameliorate this diagnostic insufficiency of morphologic CT imaging alone (Bamberg et al. 2011).

Still, until dynamic myocardial CT perfusion imaging can be introduced to clinical routine, a number of questions need to be answered; such as, can a single perfusion scan under stress conditions differentiate between nonviable myocardium and reversible ischemia? Recent publications on dynamic cardiac CT perfusion imaging have acquired data at stress only and have not included additional dynamic perfusion imaging at rest, as protocols are designed to minimize the total radiation exposure. Acquiring two dynamic acquisitions, radiation dose would often exceed

20 mSv equivalent dose per patient. A solution to this missing rest perfusion dataset could be to use the dedicated coronary CT angiographic acquisition under resting conditions to assess first-pass myocardial perfusion. In this acquisition, a perfusion deficit would typically reflect nonviable myocardium or a high-grade stenosis inducing perfusion defects even at resting conditions. The second stress perfusion dynamic dataset would allow for identification of perfusion defects induced by significant stenosis not leading to myocardial iodine filling defects under resting conditions. Further, focused research will be necessary to determine which optimized combination of CT protocols will allow for differentiation between infarcted and ischemic myocardium by using either first-pass "static," dynamic rest perfusion imaging, or delayed enhancement acquisitions (Vliegenthart et al. 2012).

Another question to be solved is which cut-off value of a quantitative parameter, such as MBF, should be used to optimize the differentiation of normal myocardium from myocardium with reduced perfusion. In a recent publication by Bamberg et al., an MBF of 75 mL/100 mL/min was determined as an ideal cut point, on the basis of maximization of the area under the curve (ROC analysis, detection of significant coronary artery disease as defined by FFR) as a criterion (Bamberg et al. 2011). However, this factor may need further validation across different patient populations. For instance, in subjects with an average MBF higher than this threshold level, findings could be incorrectly categorized as having a nonhemodynamically significant stenosis, even if the stenosis might be significant, i.e., leading to false-negative results. This fact could potentially lead to a decreased negative predictive value (NPV) for dynamic stress perfusion imaging. Thus, the optimal MBF threshold might be depending on the individual overall myocardial perfusion and should be adapted individually.

The inherent advantages of dynamic CT perfusion imaging over static imaging or established imaging modalities, such as scintigraphic techniques, are obvious. On the one hand, dynamic CT perfusion imaging might still be helpful in patients suffering from a multi-vessel CAD, as quantitative parameter maps comprising the whole myocardium in a 3D dataset should help to correctly identify disease by low MBF values in several vessel territories. Here, static single-shot techniques displaying only the relative iodine distribution in the myocardium might result in false-negative findings, as iodine contents in several areas of the myocardium could be homogeneously decreased in a multi-vessel CAD. Furthermore, smaller perfusion defects due to small vessel disease have been reported to be visible on dynamic CT perfusion datasets but cannot be seen scintigraphically or in imaging of the large vessels (with either catheter angiography or CTA) (Schuijf et al. 2006; De Bruyne et al. 2001). This high spatial resolution of CT perfusion is an inherent advantage, however, in a scientific setting comparing CT perfusion to other established imaging techniques, this fact may cause a real CT perfusion defect to appear as a false-positive result. E.g., although SPECT imaging is well established for the evaluation of myocardial perfusion, it may not detect subendocardial, nontransmural perfusion abnormalities because of the limited spatial resolution of approximately 10 mm, and some of the apparent "false-positive" CT perfusion studies may show perfusion abnormalities that may be below the resolution of nuclear MPI (Kido et al. 2008).

In conclusion, investigators who perform further research will need to determine the added value of "dynamic" imaging with MBF quantification to "static" imaging (i.e., a single set of images obtained during early myocardial perfusion) and to determine whether the added radiation exposure associated with dynamic imaging can be offset by improved detection of ischemia, e.g., in patients suffering from multi-vessel CAD.

3 Available Study Data on Dynamic Cardiac CT Perfusion Imaging

Several publications have reported on the diagnostic value and technical optimization of dynamic cardiac perfusion CT (see Table 2). In the first animal work involving five pigs with an induced 80 % LAD stenosis and using a dual-source CT with shuttle mode for dynamic perfusion imaging, Mahnken et al. showed the possibility of quantifying perfusion values and found significant differences between ischemic (related to an 80 % coronary area stenosis) and nonischemic myocardium (74.0 ± 21.9 versus 117.4 ± 18 mL/100 mL/min, $p < 0.002$) (Mahnken et al. 2010). If a scan situation in patients is to be simulated using an animal model, given their biological characteristics, the porcine model is known to be most similar to humans (Swindle et al. 1988). The weight of a pig's heart is in a similar range, and injection of contrast material can be performed at a comparable rate to that used in humans, resulting in a similar opacification pattern of the left ventricle and myocardium. Accordingly, Bamberg et al. performed another in vivo animal study including seven pigs (Bamberg et al. 2012). Using different degrees of flow wire–adjusted induced coronary stenosis and different fluorescent colors, Bamberg et al. were able to simulate different perfusion conditions, both under rest and stress, demonstrating that a dynamic acquisition and derivation of MBF can depict differences in the tributary coronary artery territory similar to the distribution of microspheres in the corresponding histopathological correlation (i.e., 72 vs. 53 % for 75 % stenosis, rest versus stress) (see Fig. 3). The derived quantitative perfusion values were in line with early research on cardiac MRI (Patel et al. 2010).

Table 2 Available clinical study data on dynamic cardiac CT perfusion

	Author	Total (*n*)	Scanner and technique	Predictor of interest	Gold standard	Diagnostic accuracy	Quantitative myocardial blood flow (MBF) values (ml/100 g/min)	Radiation dose (perfusion scan)
Animal studies								
	Mahnken et al. (2010)	5 (pigs)	60 s dyn. perfusion 2nd gen. DSCT rest and stress	Induced 80 % stenosis	Microspheres	n.a.	Non-ischemic area rest 98 ± 19 Non-ischemic area stress: 134 ± 40 Ischemic area rest: 99 ± 14 Ischemic are stress: 74 ± 22	17.7 ± 3 mSv.
	Bamberg et al. (2012)	7 (pigs)	30 s dyn. perfusion 2nd gen. DSCT rest and stress	Variable induced stenosis (50–75 %)	Microspheres and pressure wire (FFR)	n.a.	Non-ischemic area rest: 80 ± 28 Non-ischemic area stress: 110 ± 25 Ischemic area rest: 71 ± 24 Ischemic are stress: 53 ± 19	11.3 ± 2
Patient studies								
	Bamberg et al. (2011)	33	30 s dyn. perfusion 2nd gen. DSCT stress scans only	Hemodyn. sign. stenosis (FFR < 0.075)	Catheter angiography plus pressure wire (FFR)	CTA plus MBF per segment: sens. 91 spec. 98 PPV 78 NPV 99	Non-ischemic area stress: 105 ± 34 Ischemic are stress: 73 ± 26	10.0 ± 2
	Bastarrika et al. (2010)	10	30 s dyn. perfusion 2nd gen. DSCT stress scans only	Perfusion defects under adenosine stress	Cardiac MRI (rest perfusion, stress perfusion, delayed enhancement)	CT perf. versus MR perf: per segment sens. 86 spec. 98 PPV 94 NPV 96	Non-ischemic area stress: 122 ± 49 Ischemic are stress: 96 ± 27	10.3 ± 2
	Wang et al. (2012)	21	30 s dyn. perfusion 2nd gen. DSCT stress scans only	Perfusion defects under adenosine stress	SPECT MPI	CTA plus MBF per vessel: sens. 90 spec. 81 PPV 58 NPV 97	Non-ischemic area stress: 143 ± 31 Ischemic are stress: 90 ± 23	9.5 ± 1.3

In two subsequent patient studies involving an adapted dynamic scan protocol with shuttle mode on a second-generation dual-source CT, Bamberg et al. were able to combine sufficient anatomical coverage, i.e., the whole myocardium, with a sufficiently high temporal resolution and stability of HU values, testing for stress-induced hypoperfusion in patients with known CAD (Bamberg et al. 2010, 2011). Including 33 subjects in the final analysis, an MBF cut point of 75 mL/100 mL/min provided the highest discriminatory power (C statistic, 0.707; $p < 0.001$). While the diagnostic accuracy of CT for the detection of anatomically significant coronary artery stenosis (>50 %) was high, it was low for the detection of hemodynamically significant stenosis as compared to invasive FFR (positive predictive value, PPV, and per coronary segment = 49 %). With use of estimated MBF to reclassify lesions depicted with CT angiography, 30 of 70 (43 %) coronary lesions were correctly re-graded as not hemodynamically significant, which significantly increased PPV to 78 % (see Fig. 4). The presence of a coronary artery stenosis with a corresponding MBF less than 75 mL/100 mL/min had a high risk for hemodynamic significance (odds ratio, 86.9). In another patient study on dynamic whole heart cardiac CT perfusion, Bastarrika et al. scanned 10 patients with known

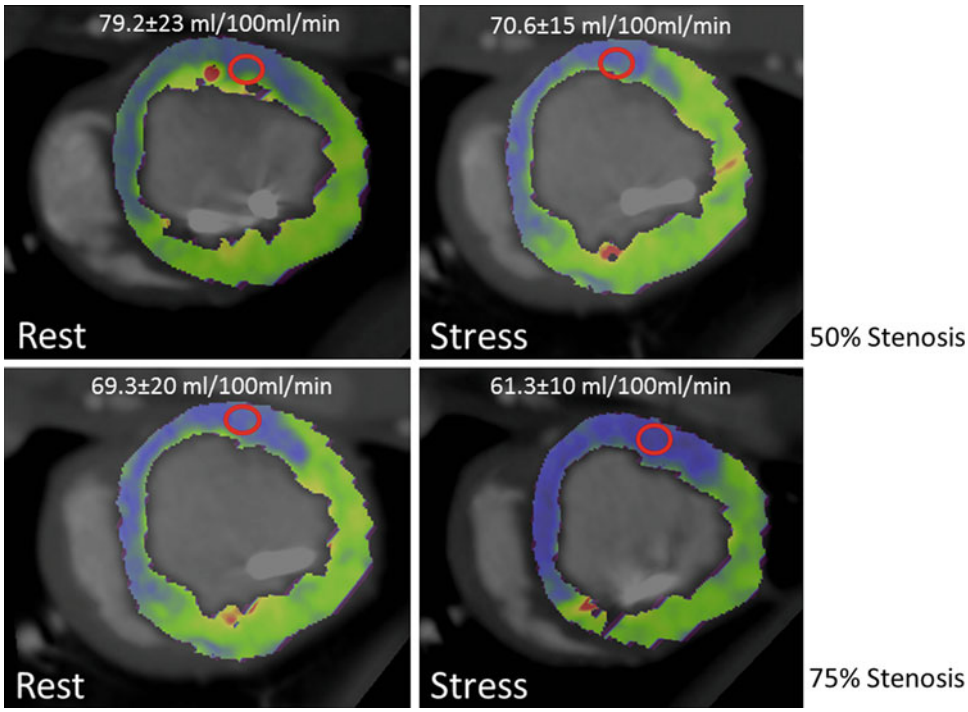

Fig. 3 In an animal model under controlled conditions, inducing various degrees of LAD (*left* anterior descending coronary artery) stenosis by a stent, a balloon, or a pressure wire, dynamic CT perfusion is able to depict, quantify, and differentiate various degrees of stenosis under resting and stress conditions (modified from (Bamberg et al. 2012))

or suspected CAD (Bastarrika et al. 2010). All patients underwent both stress/rest perfusion and delayed-enhancement MRI, as well as a cardiac CT protocol comprising prospective electrocardiogram-triggered coronary CT angiography, dynamic adenosine-stress myocardial perfusion imaging using a shuttle mode on a DSCT system, and delayed enhancement acquisitions. For semi-quantitative evaluation, CT- and MRI-derived myocardial to-left ventricular upslope indices were compared. Additionally, absolute MBF was quantified based on dynamic perfusion CT and correlated with semi-quantitative CT measurements. Sensitivity, specificity, and positive and negative predictive values for detection of myocardial perfusion defects using CT compared with MRI were 86.1, 98.2, 93.9, and 95.7 %, respectively. Semiquantitative analysis of CT data showed significant differences between ischemic and nonischemic myocardium with a signal-intensity upslope that was comparable with MRI-derived values. Moderate correlation was observed between absolute CT quantification of MBF and semiquantitative CT measurements. Recently, Wang et al. performed a prospective study including 21 patients, comparing the diagnostic accuracy of a combined stress CT perfusion and CTA examination versus nuclear MPI, for the detection of hemodynamically significant stenosis (Wang et al. 2012). Again, a second-generation dual-source CT scanner with shuttle mode was applied. There was a significant difference in MBF values between normal (142.9 ± 30.6 mL/100 mL/min) and hypoperfused (90.0 ± 22.8 mL/100 mL/min) segments ($p < 0.001$). With nuclear MPI results as a comparison, the sensitivity, specificity, positive predictive value, and negative predictive value of CT perfusion for identifying segments with perfusion defects were 0.85, 0.92, 0.55, and 0.98, respectively. On a per-vessel basis, sensitivity, specificity, positive predictive value, and negative predictive value for detecting flow-obstructing stenosis were, respectively, 1.00, 0.757, 0.541, and 1.00 for CT perfusion; 0.90, 0.514, 0.346, and 0.947 for CTA; and 0.90, 0.814, 0.581, and 0.966 for CT perfusion combined with CTA. Thus, it could again be shown that CT perfusion combined with CTA improves the diagnostic accuracy for identifying flow-obstructing stenosis compared with CTA alone.

Despite the fact that these initial data on a dynamic basis are promising, further validation of the technique is strongly warranted. To date, it remains unclear whether the CT estimates are a true measure of MBF; this needs to be addressed in greater detail in experimental animal studies using appropriate gold standards, such as fluorescent microspheres or invasive measurement of FFR. While there is early evidence that CT may allow the assessment of transmural perfusion defects (George et al. 2009), further, more systematic research is necessary to establish a reliable CT-based quantification of MBF and to increase the precision of the modeling algorithm. Finally, further validation studies in larger patient cohorts need to be carried out with standardized procedures for CT myocardial perfusion imaging to prove the robustness and reproducibility of the technique. Comparisons using adequate gold standards

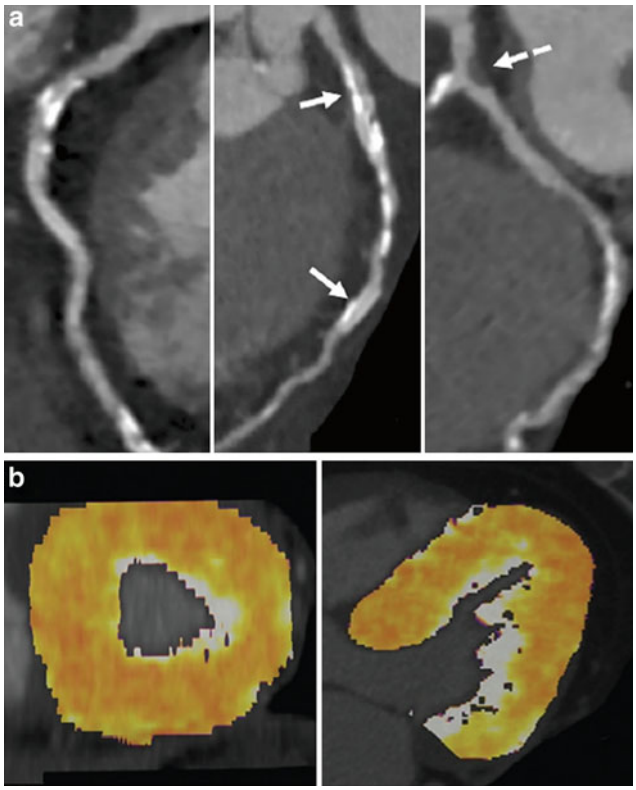

Fig. 4 In this patient with suspected coronary artery disease (CAD), multiplanar reformats of the coronary CT angiography datasets show several stenoses with unclear hemodynamic significance in both the *left* and *right* coronary arteries (**a**, *arrows*). Such patients would typically have to undergo further functional testing (e.g., scintigraphic myocardial perfusion imaging, MPI, or stress-perfusion magnetic resonance imaging, MRI). Adding information from a dynamic CT perfusion dataset (**b**), showing a normal and homogenous myocardial perfusion, the significance of these questionable stenoses could be excluded. Invasive catheter-based angiography confirmed these findings with no significant stenosis to be found. (modified from (Bamberg et al. 2011))

(fractional flow reserve, MRI, or SPECT) are warranted to fully determine the diagnostic accuracy of cardiac CT for the quantification of myocardial perfusion defects in a blinded fashion. If confirmed, larger randomized diagnostic trials will be necessary to determine whether myocardial perfusion imaging by CT will be beneficial compared with established options using appropriate, clinically relevant endpoints. Also, to prove the usefulness of a combined CT approach implementing CTCA with CT myocardial perfusion imaging, information on myocardial viability is of major importance to differentiate between hypoperfused-but-viable from hypoperfused-but-necrotic myocardium. Hence, a third CT acquisition for CT late enhancement might be mandatory in such a comprehensive CT approach.

4 Conclusions

Given the great promise of a combined assessment of morphology and function with a single imaging modality, recent cardiac CT research has focused on several technical approaches to assess myocardial perfusion and viability. A single acquisition after contrast administration and adenosine-stress—performed as a single-energy or dual-energy approach—represents a promising option to define myocardial contrast distribution at a predefined point in time with relatively low radiation exposure. As a second promising acquisition strategy, dynamic multiphasic protocols may enable absolute quantification of myocardial perfusion values. Initial data suggest that MBF estimation by dedicated dynamic CT-based stress perfusion imaging permits accurate identification of hemodynamically significant coronary artery stenosis. Furthermore, even the detection of perfusion differences with respect to varying degrees of coronary stenosis may be possible. Systematic research is necessary to reliably and reproducibly established CT-based quantification of perfusion parameters. Other technical limitations that will need further attention include the reduction of the total acquisition time, correction of breathing motion artifacts, increased coverage, and adequate radiation dose-saving strategies. Ultimately, clinical trials including prospective cohort studies and eventually randomized diagnostic trials are warranted to determine the cost-effectiveness as well as the incremental value of CT-based perfusion imaging in terms of patient outcome and prognosis.

References

Bamberg F, Klotz E, Flohr T, Becker A, Becker CR, Schmidt B, Wintersperger BJ, Reiser MF, Nikolaou K (2010) Dynamic myocardial stress perfusion imaging using fast dual-source CT with alternating table positions: initial experience. Eur Radiol 20(5):1168–1173

Bamberg F, Becker A, Schwarz F, Marcus RP, Greif M, von Ziegler F, Blankstein R, Hoffmann U, Sommer WH, Hoffmann VS, Johnson TR, Becker HC, Wintersperger BJ, Reiser MF (2011) Nikolaou K Detection of hemodynamically significant coronary artery stenosis: incremental diagnostic value of dynamic CT-based myocardial perfusion imaging. Radiology 260(3):689–698

Bamberg F, Hinkel R, Schwarz F, Sandner TA, Baloch E, Marcus R, Becker A, Kupatt C, Wintersperger BJ, Johnson TR, Theisen D, Klotz E, Reiser MF, Nikolaou K (2012) Accuracy of dynamic computed tomography adenosine stress myocardial perfusion imaging in estimating myocardial blood flow at various degrees of coronary artery stenosis using a porcine animal model. Invest Radiol 47(1):71–77

Bastarrika G, Ramos-Duran L, Rosenblum MA, Kang DK, Rowe GW, Schoepf UJ (2010) Adenosine-stress dynamic myocardial CT perfusion imaging: initial clinical experience. Invest Radiol 45(6):306–313

Bischoff B, Bamberg F, Marcus R, Schwarz F, Becker HC, Becker A, Reiser M, Nikolaou K (2012) Optimal timing for first-pass stress CT myocardial perfusion imaging. Int J Cardiovasc Imaging. [Epub ahead of print]

Blankstein R, Di Carli MF (2010) Integration of coronary anatomy and myocardial perfusion imaging. Nat Rev Cardiol 7(4):226–236

Blankstein R, Shturman LD, Rogers IS, Rocha-Filho JA, Okada DR, Sarwar A, Soni AV, Bezerra H, Ghoshhajra BB, Petranovic M, Loureiro R, Feuchtner G, Gewirtz H, Hoffmann U, Mamuya WS, Brady TJ, Cury RC (2009) Adenosine-induced stress myocardial perfusion imaging using dual-source cardiac computed tomography. J Am Coll Cardiol 54(12):1072–1084

Budoff MJ, Achenbach S, Blumenthal RS, Carr JJ, Goldin JG, Greenland P, Guerci AD, Lima JA, Rader DJ, Rubin GD, Shaw LJ, Wiegers SE (2006) Assessment of coronary artery disease by cardiac computed tomography: a scientific statement from the American Heart Association Committee on cardiovascular imaging and intervention, council on cardiovascular radiology and intervention, and committee on cardiac imaging council on clinical cardiology. Circulation 114(16):1761–1791

De Bruyne B, Hersbach F, Pijls NH, Bartunek J, Bech JW, Heyndrickx GR, Gould KL, Wijns W (2001) Abnormal epicardial coronary resistance in patients with diffuse atherosclerosis but "Normal" coronary angiography. Circulation 104(20):2401–2406

Einstein AJ, Moser KW, Thompson RC, Cerqueira MD, Henzlova MJ (2007) Radiation dose to patients from cardiac diagnostic imaging. Circulation 116(11):1290–1305

George RT, Silva C, Cordeiro MA, DiPaula A, Thompson DR, McCarthy WF, Ichihara T, Lima JA, Lardo AC (2006) Multidetector computed tomography myocardial perfusion imaging during adenosine stress. J Am Coll Cardiol 48(1):153–160

George RT, Jerosch-Herold M, Silva C, Kitagawa K, Bluemke DA, Lima JA, Lardo AC (2007) Quantification of myocardial perfusion using dynamic 64-detector computed tomography. Invest Radiol 42(12):815–822

George RT, Arbab-Zadeh A, Miller JM, Kitagawa K, Chang HJ, Bluemke DA, Becker L, Yousuf O, Texter J, Lardo AC, Lima JA (2009) Adenosine stress 64- and 256-row detector computed tomography angiography and perfusion imaging: a pilot study evaluating the transmural extent of perfusion abnormalities to predict atherosclerosis causing myocardial ischemia. Circ Cardiovasc Imaging 2(3):174–182

Gramer BM, Muenzel D, Leber V, von Thaden AK, Feussner H, Schneider A, Vembar M, Soni N, Rummeny EJ, Huber AM (2012) Impact of iterative reconstruction on CNR and SNR in dynamic myocardial perfusion imaging in an animal model. Eur Radiol. [Epub ahead of print]

Hausleiter J, Meyer T, Hermann F, Hadamitzky M, Krebs M, Gerber TC, McCollough C, Martinoff S, Kastrati A, Schomig A, Achenbach S (2009) Estimated radiation dose associated with cardiac CT angiography. JAMA 301(5):500–507

Hendel RC, Budoff MJ, Cardella JF, Chambers CE, Dent JM, Fitzgerald DM, Hodgson JM, Klodas E, Kramer CM, Stillman AE, Tilkemeier PL, Ward RP, Weigold WG, White RD, Woodard PK (2009) ACC/AHA/ACR/ASE/ASNC/HRS/NASCI/RSNA/SAIP/SCAI/SCCT/SCMR/SIR 2008 key data elements and definitions for cardiac imaging: a report of the American college of cardiology/American heart association task force on clinical data standards (writing committee to develop clinical data standards for cardiac imaging). Circulation 119(1):154–186

Hsiao EM, Rybicki FJ, Steigner M (2010) CT coronary angiography: 256-slice and 320-detector row scanners. Curr Cardiol Rep 12(1):68–75

Kido T, Kurata A, Higashino H, Inoue Y, Kanza RE, Okayama H, Higaki J, Murase K, Mochizuki T (2008) Quantification of regional myocardial blood flow using first-pass multidetector-row computed tomography and adenosine triphosphate in coronary artery disease. Circ J 72(7):1086–1091

Ko BS, Cameron JD, Meredith IT, Leung M, Antonis PR, Nasis A, Crossett M, Hope SA, Lehman SJ, Troupis J, DeFrance T, Seneviratne SK (2012a) Computed tomography stress myocardial perfusion imaging in patients considered for revascularization: a comparison with fractional flow reserve. Eur Heart J 33(1):67–77

Ko SM, Choi JW, Hwang HK, Song MG, Shin JK, Chee HK (2012b) Diagnostic performance of combined noninvasive anatomic and functional assessment with dual-source CT and adenosine-induced stress dual-energy CT for detection of significant coronary stenosis. AJR Am J Roentgenol 198(3):512–520

Koyama Y, Mochizuki T, Higaki J (2004) Computed tomography assessment of myocardial perfusion, viability, and function. J Magn Reson Imaging 19(6):800–815

Mahnken AH, Klotz E, Pietsch H, Schmidt B, Allmendinger T, Haberland U, Kalender WA, Flohr T (2010) Quantitative whole heart stress perfusion CT imaging as noninvasive assessment of hemodynamics in coronary artery stenosis: preliminary animal experience. Invest Radiol 45(6):298–305

Meijboom WB, Van Mieghem CA, van Pelt N, Weustink A, Pugliese F, Mollet NR, Boersma E, Regar E, van Geuns RJ, de Jaegere PJ, Serruys PW, Krestin GP, de Feyter PJ (2008) Comprehensive assessment of coronary artery stenoses: computed tomography coronary angiography versus conventional coronary angiography and correlation with fractional flow reserve in patients with stable angina. J Am Coll Cardiol 52(8):636–643

Orrison WW Jr, Snyder KV, Hopkins LN, Roach CJ, Ringdahl EN, Nazir R, Hanson EH (2011) Whole-brain dynamic CT angiography and perfusion imaging. Clin Radiol 66(6):566–574

Patel AR, Antkowiak PF, Nandalur KR, West AM, Salerno M, Arora V, Christopher J, Epstein FH, Kramer CM (2010) Assessment of advanced coronary artery disease: advantages of quantitative cardiac magnetic resonance perfusion analysis. J Am Coll Cardiol 56(7):561–569

Ruzsics B, Chiaramida SA, Schoepf UJ (2009a) Images in cardiology: dual-energy computed tomography imaging of myocardial infarction. Heart 95(3):180

Ruzsics B, Schwarz F, Schoepf UJ, Lee YS, Bastarrika G, Chiaramida SA, Costello P, Zwerner PL (2009b) Comparison of dual-energy computed tomography of the heart with single photon emission computed tomography for assessment of coronary artery stenosis and of the myocardial blood supply. Am J Cardiol 104(3):318–326

Schuijf JD, Wijns W, Jukema JW, Atsma DE, de Roos A, Lamb HJ, Stokkel MP, Dibbets-Schneider P, Decramer I, De Bondt P, van der Wall EE, Vanhoenacker PK, Bax JJ (2006) Relationship between noninvasive coronary angiography with multi-slice computed tomography and myocardial perfusion imaging. J Am Coll Cardiol 48(12):2508–2514

Serruys PW, di Mario C, Piek J, Schroeder E, Vrints C, Probst P, de Bruyne B, Hanet C, Fleck E, Haude M, Verna E, Voudris V, Geschwind H, Emanuelsson H, Muhlberger V, Danzi G, Peels HO, Ford AJ Jr, Boersma E (1997) Prognostic value of intracoronary flow velocity and diameter stenosis in assessing the short- and long-term outcomes of coronary balloon angioplasty: the DEBATE study (Doppler Endpoints Balloon Angioplasty Trial Europe). Circulation 96(10):3369–3377

Shaw LJ, Hachamovitch R, Berman DS, Marwick TH, Lauer MS, Heller GV, Iskandrian AE, Kesler KL, Travin MI, Lewin HC,

Hendel RC, Borges-Neto S, Miller DD (1999) The economic consequences of available diagnostic and prognostic strategies for the evaluation of stable angina patients: an observational assessment of the value of precatheterization ischemia. Economics of noninvasive diagnosis (END) multicenter study group. J Am Coll Cardiol 33(3):661–669

Swindle MM, Smith AC, Hepburn BJ (1988) Swine as models in experimental surgery. J Invest Surg 1(1):65–79

Tonino PA, De Bruyne B, Pijls NH, Siebert U, Ikeno F, Van't Veer M, Klauss V, Manoharan G, Engstrom T, Oldroyd KG, Ver Lee PN, MacCarthy PA, Fearon WF (2009) Fractional flow reserve versus angiography for guiding percutaneous coronary intervention. N Engl J Med 360(3):213–224

Vliegenthart R, Henzler T, Moscariello A, Ruzsics B, Bastarrika G, Oudkerk M, Schoepf UJ (2012) CT of coronary heart disease: Part 1, CT of myocardial infarction, ischemia, and viability. AJR Am J Roentgenol 198(3):531–547

Wang Y, Qin L, Shi X, Zeng Y, Jing H, Schoepf UJ, Jin Z (2012) Adenosine-stress dynamic myocardial perfusion imaging with second-generation dual-source CT: comparison with conventional catheter coronary angiography and SPECT nuclear myocardial perfusion imaging. AJR Am J Roentgenol 198(3):521–529

CT Evaluation of the Myocardial Blood Supply: Ultra-Low Radiation Dose CT Techniques

Beyond Structure and Function: CT Imaging of Myocardial Perfusion and Viability

Christoph Becker and Bernhard Bischoff

Contents

Abstract

An ECG triggered high pitch (3.2) spiral CT scan acquired 8-16 seconds after the administration of contrast media and achievement of 100 HU in the ascending aorta best displays the difference in enhancement between ischemic /infarcted and remote myocardium. If this CT scan is been performed under pharmacological stress and repeated at rest, reversible ischemia may be distinguished agains infarcted myocardium. In our experience, regadenoson is superior to adenosine to provoce stress induced ischemia. The rest scan with beta blockage may be performed before the stress scan to avoid image distorsion by motion artifacts when diagnosing the coronary arteries. This scan protocol is associated with much less radiation compared to dynamic CTA. The total amount of radiation for a stress and rest scan is in the range of 2 mSv and may be sufficient to diagnose clinically relevant ischemia myocardial ischemia. However, this approach does not allow for quantitate assessment of myocardial blood flow and is therefore not suited to follow for changes in myocardial perfusion under treatment.

Cardiac CT primarily reveals coronary atherosclerosis. However, the degree to which coronary atherosclerosis impairs myocardial blood flow is uncertain (Rocha-Filho et al. 2010). For instance, in patients with bypass grafts or stents in the coronary arteries, coronary CT lacks the ability to predict sufficient blood flow to the myocardium particularly if the patient is under exercise.

Recently, CT has begun to offer the ability to determine myocardial blood flow at rest and exercise through perfusion imaging (Blankstein et al. 2009). Quantitative assessment of the myocardial blood flow requires repetitive scanning of the myocardium while the contrast media passes through it. This technique, described in the prior chapter, however, has three major drawbacks. First, even under optimal conditions the radiation exposure is high, compared to a regular coronary

C. Becker (✉) · B. Bischoff
Department of Clinical Radiology, Ludwig-Maximilians University, Marchioninistrasse, Munich, Germany
e-mail: christoph.becker@med.lmu.de

U. J. Schoepf et al. (eds.), *CT Imaging of Myocardial Perfusion and Viability*, Medical Radiology. Diagnostic Imaging,
DOI: 10.1007/174_2012_760, © Springer-Verlag Berlin Heidelberg 2012
Published Online: 20 November 2012

CT examination. Second, this dynamic image acquisition requires breath holding for 30–40 s. For many patients holding their breath for such a long period of time is quite challenging. Third, the scan range depends on the detector width. At least 7–8 cm is needed to cover the entire myocardium in the z-direction. Alternatively, with a smaller detector width, the table needs to alternate between two positions every-other or every-second heartbeat to increase z-coverage (Bamberg et al. 2010). However, this approach results in a reduced temporal resolution and is susceptible to extrasystole and arrhythmia.

The maximum enhancement difference between ischemic and normal myocardium may be seen only during a short period of time while the contrast medium is passing through the myocardium; therefore, the myocardium is acquired only during this particular time frame. This results in significantly reduced radiation exposure when compared with conventional CT perfusion imaging. Although the difference in enhancement between ischemic and normal myocardium may be measured in Hounsfield units, single time-point acquisition does not allow for quantitative assessment of the myocardial blood flow (Blankstein et al. 2009). The information revealed from a single acquisition scan of the myocardium is comparable to the myocardial blood volume imaging derived for a perfusion study.

Reviewing CT perfusion time-density curves reveals that maximum differences in contrast enhancement between ischemic and nonischemic myocardium during stress may be expected about 8–16 s after contrast enhancement of the ascending aorta exceeds 100 HU. This time point may of course depend on a variety of physiological parameters, particularly cardiac output. Optimization and visualization of ischemic versus normal myocardium require provocation by a stress agent, such as adenosine. Adenosine, a vasodilator, improves blood flow in remote myocardium supplied by unaffected coronary vessels. However, in diseased coronary arteries, adenosine will cause a steal phenomenon, detouring the blood and contrast. As a result, blood and contrast flow may be further reduced in myocardial territories that are supplied by coronary arteries with significantly impaired blood flow caused by high-grade stenoses (Blankstein et al. 2009). Adenosine is administered intravenously at an amount of 140 mcg/kg/min for 3 min until the investigation is initiated. A second intravenous line is then required for the administration of the contrast media. The vasodilative effect is terminated immediately upon discontinuation of adenosine injection. Regadenoson is a selective A2A receptor agonist and acts as an alternative for adenosine. The selective receptor binding properties of Regadenoson seem to improve the visualization of ischemic versus remote myocardium. The safety profile of Regadenoson allows administration even in patients with chronic obstructive pulmonary disease. Patel et al. reported that

Fig. 1 Seventy-three-year-old female patient with coronary artery disease treated with several bypass grafts. CT scan revealed an occluded graft to the right coronary artery (*arrowhead*), a patent graft to the left anterior descending coronary artery (*arrow*) but an inconsistent course of the peripheral original vessel (*star*)

prospectively triggered stress CT perfusion with Regadenoson may allow detection of myocardial perfusion deficits even if radiation exposure is substantially reduced (Patel et al. 2011). As of this writing, the use of Regadenoson has not been reported in the scientific literature for the single scan acquisition of myocardium perfusion imaging as it is described here.

Initial attempts to image the myocardial blood volume were performed with retrospective ECG gating technique. Comparing the detection of coronary artery stenoses greater than 50 % by CT blood volume imaging to cardiac catheter, Blankstein et al. reported a sensitivity and specificity of 67 and 83 %, respectively (Blankstein et al. 2009). Moreover, Rocha-Filho et al. reported additional incremental sensitivity (83–91 %) and specificity (71–91 %) for CT blood volume imaging over CT angiography of the coronary arteries for the detection of significant stenoses (Rocha-Filho et al. 2010). However, the radiation exposure with the technique used as reported in these two papers was in the range of 10 mSv.

Prospective ECG triggered scan acquisition is far more radiation dose efficient when compared with retrospective ECG gating technique. Depending on the detector width, this technique allows covering the myocardium within 2–3 heartbeats. However, when using CT systems with a detector width not covering the entire heart, different areas of the myocardium are scanned at different time points

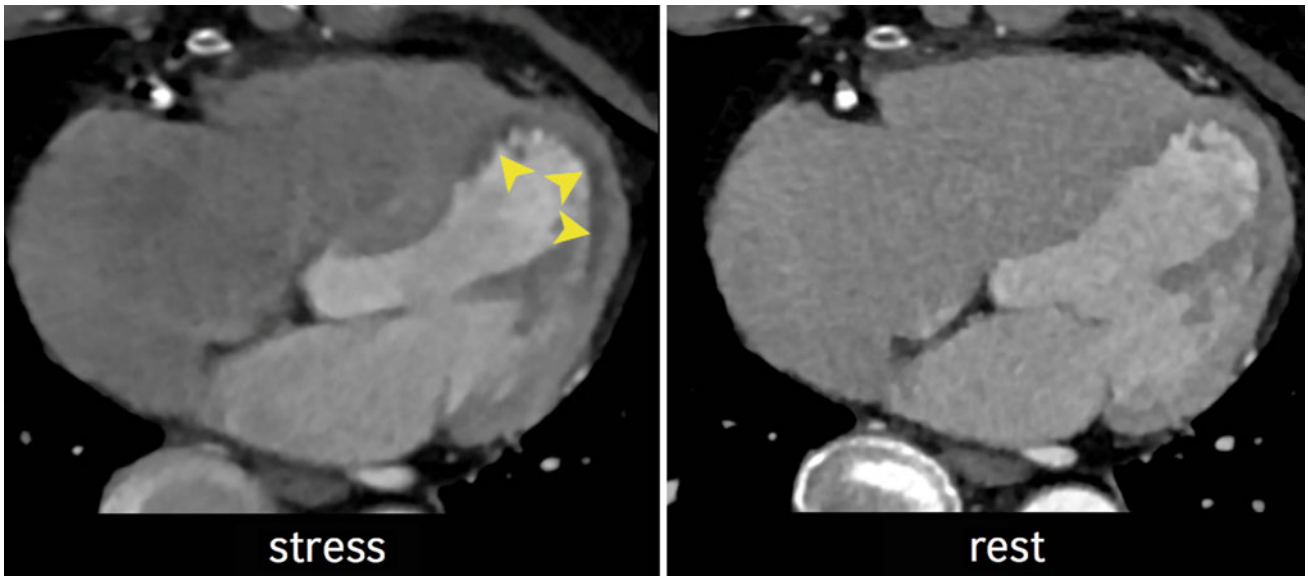

Fig. 2 The CT scan at stress with Regadenoson reveals an area of hypo-attenuation in the sub-endocardial region of the apex (*arrowheads*) that is substantially less pronounced in the scan performed at rest

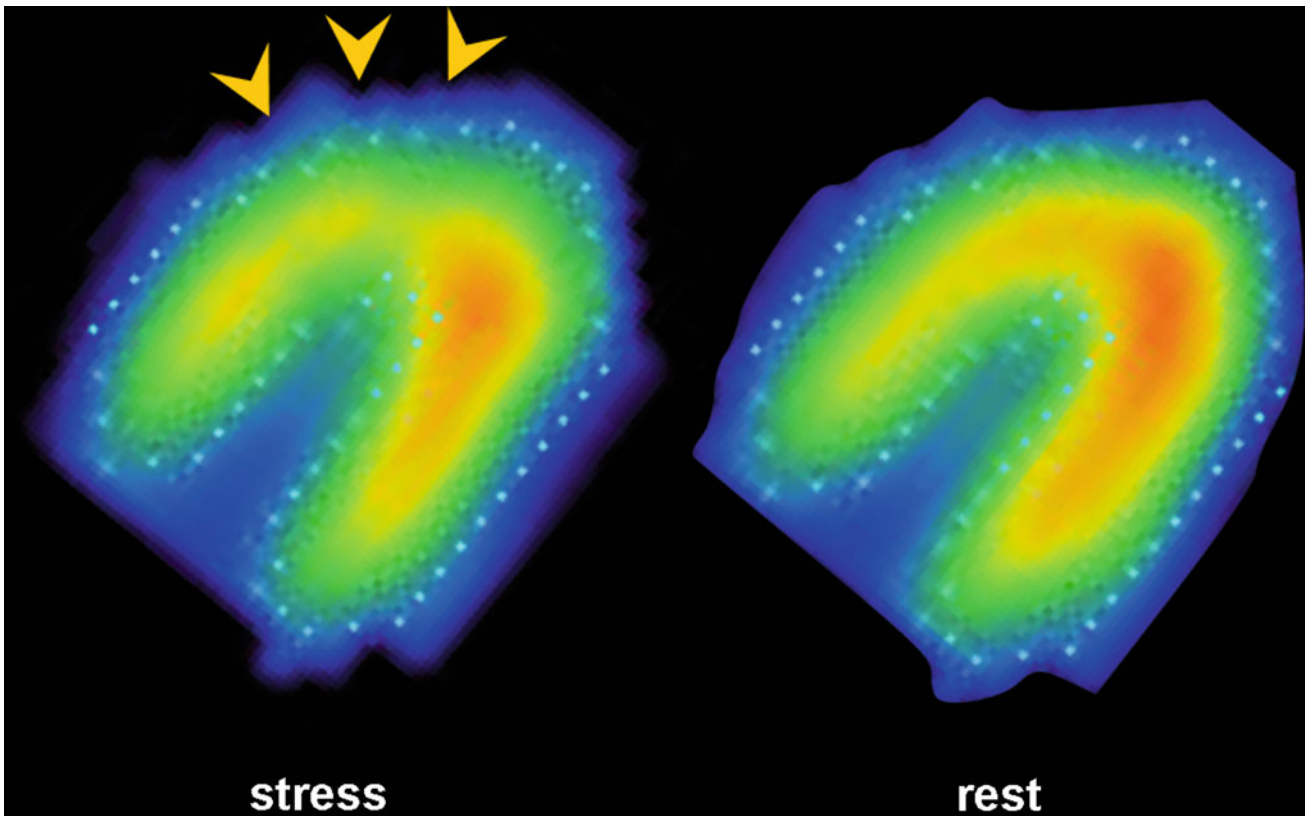

Fig. 3 Corresponding to CTP, SPECT reveals a stress-induced myocardial hypoperfusion in the left ventricular apex (*arrowheads*)

during the passage of contrast medium resulting in differences in myocardial contrast enhancement that may possibly mimic areas of myocardial hypoperfusion. The most effective way to image the myocardium with low radiation exposure is the use of a prospectively ECG triggered high pitch spiral mode with second-generation dual-source CT.

In the high pitch spiral mode, the effective table feed is approximately 48 cm/s. With the typical scan range for the myocardium being 8–10 cm, this range may be acquired within a single heartbeat in roughly 200 ms. The radiation exposure for this protocol may be in the range of 1 mSv. As of this writing, only one paper is available on the use of this technique for myocardial blood volume imaging. Feuchtner et al. reported incremental additional overall accuracy (84–95 %) for the detection of high-grade stenosis with high pitch perfusion imaging over coronary CT angiography (Feuchtner et al. 2011).

If single scan acquisition for the assessment of ischemic myocardium is to be used, it is mandatory to compare the scan at stress with the scan at rest. Ischemic myocardium may be identified by reduced enhancement compared to remote myocardium at stress and equalized enhancement at rest. Alternatively, myocardial infarction may not enhance under any condition. Preferably, the scan at stress is performed during the contraction of the myocardium in the systole, while the scan at rest is performed in the diastolic phase to allow visualization of the coronary arteries within the same acquisition. A contrast volume of 60 ml is injected with a flow of at least 5 ml/s to achieve sufficient enhancement of the myocardium (Feuchtner et al. 2011).

The order in which these two scans, rest and stress, should be performed is unclear. Option one is to perform the stress scan first and then proceed with the rest scan. Here, the advantage is that ischemic myocardium may not be pre-enhanced by a prior contrast application. Discontinuation of adenosine may allow for immediate continuation with the rest scan. Regadenoson has several advantages over adenosine. It is more efficient and selective and may also be used in patients with COPD (Thomas et al. 2008). However, the vasodilative effect of Regadenoson persists for 15–20 min. Therefore, when using Regadenoson instead of adenosine, either the time interval between the stress and rest scans should be at least 15 min or intravenous administration of theophylline should be used to terminate the effect of Regadenoson.

The rest scan may alternatively be performed prior to the stress scan. It is logical to begin with the rest scan, because such an acquisition permits assessment of the coronary arteries. In case coronary artery disease of indeterminate value is discovered, the stress investigation with Regadenoson may be performed right after. As one important consideration, animal studies have shown that beta blocker, typically given to reduce the patient's heart rate during the rest scan in order to improve visualization of the coronary arteries, can interfere, to a minor degree, with Regadenoson if it is given immediately afterward (Zhao et al. 2012). The effect of myocardial pre-enhancement by the rest scan would appear to be insignificant due to the small amount of contrast media given, especially if there is a period of several minutes between rest and stress imaging.

Myocardial ischemia, which typically occurs in the subendocardium, may be detected by comparing the images acquired at rest and stress. If the perfusion deficit is exclusively detected during the acquisition performed at stress or a major difference is observed between the scans at rest and stress, the area of the myocardium is likely been affected by reversible ischemia (Figs. 1–3). Conversely, if the hypo-attenuated myocardium is seen in both phases, stress and rest, it likely corresponds to a myocardial infarction scar. As of this writing, the clinical value of CT low dose blood volume image acquisition has yet to be established.

References

Bamberg F, Klotz E, Flohr T et al (2010) Dynamic myocardial stress perfusion imaging using fast dual-source CT with alternating table positions: initial experience. Eur Radiol 20:1168–1173

Blankstein R, Shturman LD, Rogers IS et al (2009) Adenosine-induced stress myocardial perfusion imaging using dual-source cardiac computed tomography. J Am Coll Cardiol 54:1072–1084

Feuchtner G, Goetti R, Plass A et al (2011) Adenosine stress high-pitch 128-slice dual-source myocardial computed tomography perfusion for imaging of reversible myocardial ischemia: comparison with magnetic resonance imaging. Circ Cardiovasc Imaging 4:540–549

Patel AR, Lodato JA, Chandra S et al (2011) Detection of myocardial perfusion abnormalities using ultra-low radiation dose regadenoson stress multidetector computed tomography. J Cardiovasc Comput Tomogr 5:247–254

Rocha-Filho JA, Blankstein R, Shturman LD et al (2010) Incremental value of adenosine-induced stress myocardial perfusion imaging with dual-source CT at cardiac CT angiography. Radiol 254:410–419

Thomas GS, Tammelin BR, Schiffman GL et al (2008) Safety of regadenoson, a selective adenosine A2A agonist, in patients with chronic obstructive pulmonary disease: a randomized, double-blind, placebo-controlled trial (RegCOPD trial). J Nucl Cardiol Off Publ Am Soc Nucl Cardiol 15:319–328

Zhao G, Zhang S, Shryock JC et al (2012) Selective action of metoprolol to attenuate regadenoson-induced tachycardia in conscious dogs. J Nucl Cardiol Off Publ Am Soc Nucl Cardiol 19:109–117

CT Evaluation of the Myocardial Blood Supply: Dual-Source Dual-Energy CT

Sung Min Ko

Contents

Abstract

With dual-source CT in dual-energy mode, two X-ray tubes are operated independently at different voltages, acquiring two data sets showing different attenuation levels. An "iodine distribution map" is used for the assessment of myocardial blood pool status by analyzing iodine distribution within the myocardium based on the specific absorption characteristics of iodine for high and low X-ray energy spectra. Contrast-enhanced dual-energy computed tomography (DECT) perfusion with the patient at rest enables the evaluation of changes in the status of the myocardial blood supply. Rest DECT iodine distribution maps make hypoperfused myocardium more conspicuous and assist in the identification of areas exhibiting reversible myocardial ischemia. Rest DECT has thus expanded the clinical application of multidetector CT, as a "one stop shop" imaging modality to identify both coronary artery disease and myocardial blood pool deficits in a single examination. Stress DECT perfusion has the potential to become a robust clinical tool for the detection of myocardial ischemia. The combined approach of coronary CT angiography and stress DECT perfusion allows identification of hemodynamically significant coronary lesions in high-risk patients with a large calcified plaque burden or stents. This chapter provides a protocol setup and the characteristic features of dual-source DECT, and derives its benefits and limitations for DECT myocardial perfusion.

Abbreviations

CAD	Coronary artery disease
CCA	Conventional coronary angiography
CCTA	Coronary computed tomography angiography
CT	Computed tomography
DECT	Dual-energy computed tomography
ECG	Electrocardiography
FFR	Fractional flow reserve

S. M. Ko (✉)
Department of Radiology,
Konkuk University Hospital,
Konkuk University School of Medicine,
Gwangjin-gu, Seoul, Korea
e-mail: ksm9723@yahoo.co.kr

U. J. Schoepf et al. (eds.), *CT Imaging of Myocardial Perfusion and Viability*, Medical Radiology. Diagnostic Imaging,
DOI: 10.1007/174_2012_766, © Springer-Verlag Berlin Heidelberg 2012
Published Online: 15 November 2012

HU	Hounsfield Unit
LV	Left ventricular
MDCT	Multidetector computed tomography
MPI	Myocardial perfusion imaging
MR	Magnetic resonance
SPECT	Single-photon emission computed tomography

1 Introduction

Dual-energy computed tomography (DECT) was initially introduced for the purpose of spectral differentiation of material through the utilization of two X-ray spectra; however, technical limitations have prevented the clinical application of this concept for more than two decades (Chiro et al. 1979; Millner et al. 1979). The advent of dual-source CT, with two acquisition systems (two X-ray tubes and two detector arrays) mounted in the same gantry and operated independently with respect to voltage and current settings, has allowed for the analysis of energy-dependent changes in the attenuation of different materials (Flohr et al. 2006; Johnson et al. 2007; Petersilka et al. 2008). The differentiation of iodine in tissue can be of clinical diagnostic value. In addition to the Hounsfield unit (HU) attenuation values, DECT perfusion provides further information based on the specific absorption characteristics of iodine for high- and low-energy X-rays, facilitating specific tissue characterization and mapping of the iodine distribution. This "iodine distribution map" depicts myocardial blood volume, or perfusion status. With this depiction, one can easily visualize blood pool deficits and detect hemodynamically significant coronary artery stenoses. Recently, several single-center studies applying DECT have reported a strong correlation with single-photon emission computed tomography (SPECT) studies for the detection of decreases in the myocardial blood supply. Through the utilization of multiple postprocessing techniques, a single DECT acquisition may potentially detect obstructive coronary artery disease (CAD) and simultaneously provide information concerning the hemodynamic consequences of the detected lesions on myocardial perfusion (Ruzsics et al. 2008, 2009; Wang et al. 2011). DECT examination can also be performed during adenosine stress, improving the diagnostic accuracy for the detection of myocardial ischemia; this also adds incremental value to a coronary computed tomography angiography (CCTA) in the detection of hemodynamically significant coronary stenoses (Ko et al. 2011, 2012a). In recent practice, dual-source DECT of the heart has emerged as an attractive imaging modality for the evaluation of myocardial perfusion, with or without adenosine administration. This chapter provides a protocol setup and the characteristic features of dual-source DECT, and derives its benefits and limitations for DECT myocardial perfusion.

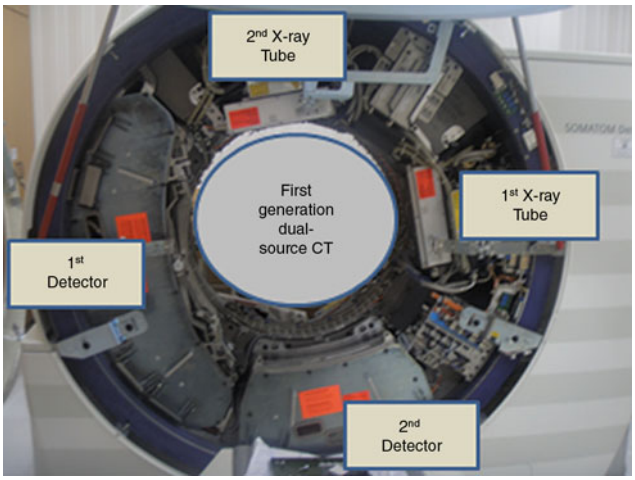

Fig. 1 Diagram of a dual-source DECT scanner. Dual-source CT with two X-ray tubes and two corresponding detector arrays mounted in the same gantry operates independently at different voltage settings (140 kV and 80/100 kV) and simultaneously acquires two data sets showing different attenuation levels

2 Principles of Material Decomposition in Dual-Energy CT

With dual-source CT in dual-energy mode, two X-ray tubes are operated independently at different voltages (80 or 100 kV and 140 kV), simultaneously acquiring two image datasets in the same anatomic location with two different X-ray spectra (Fig. 1). How does dual-source DECT obtain additional information regarding the elementary chemical composition of a scanned material? Material differentiation in CT is based on X-ray attenuation, as quantified in HUs. At low photon energies, X-ray attenuation is dominated by photoelectric absorption; at high photon energies, Compton scattering prevails. Low atomic number materials, such as fat and muscle, are affected by Compton scattering and show a small degree of reduction in the HU value when photon energy increases. On the contrary, higher atomic number materials, such as bone and iodine, are affected by the photoelectric absorption and show rapid decrease of HU value when photon energy increases (Fig. 2).

Iodine is a commonly used CT contrast agent; clinical observation has shown that iodine contrast agents have stronger enhancement at lower tube voltage settings. In dual-source DECT, we observe a greater photoelectric absorption by iodine at 80 kV than at 140 kV. This phenomenon occurs because the mean photon energy of the 80 kV beam (53 keV) is closer to the K-edge of iodine

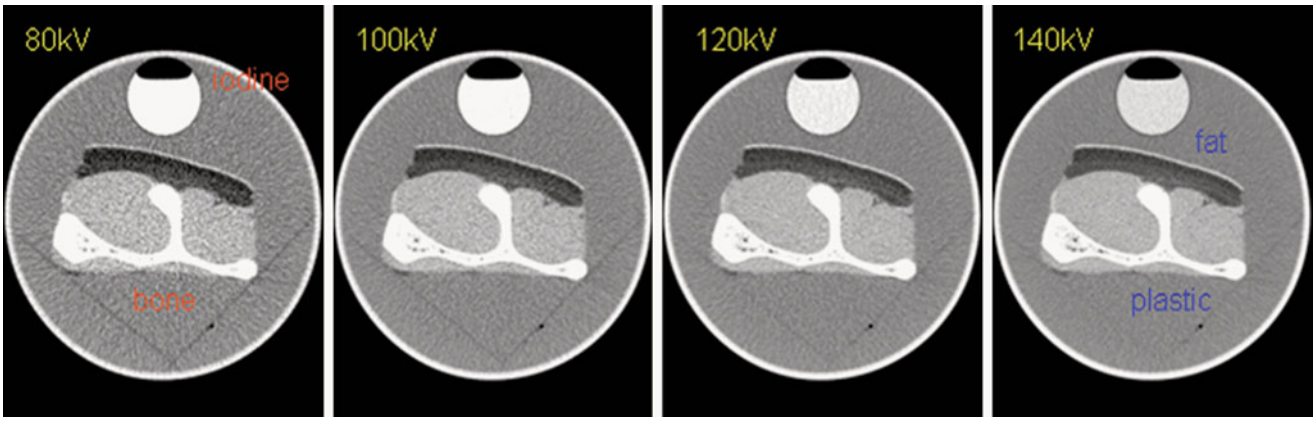

Fig. 2 Basic concept of DECT for material differentiation. Iodine has its maximum attenuation at 80 kV but its CT attenuation markedly decreases with increased voltage. The CT attenuation of bone changes much less when it is scanned with low kV as compared to high kV examination. The CT attenuation of fat increases as the kV setting is increased. Accordingly, changing the X-ray tube's kV setting results in a material-specific change of attenuation (Reproduced with kind permission from Siemens Healthcare)

(33 keV) than that of the 140 kV beam (71 keV). Accordingly, iodine-containing structures are more attenuating at 80 kV than at 140 kV. Dual-source DECT can allow material differentiation on the basis of such energy-dependent attenuation characteristics (Johnson et al. 2007).

Material-specific imaging in dual-source DECT is based on a mathematical algorithm termed "3-material decomposition." This method is capable of measuring the relative concentrations of three pure constituent materials in scanned tissue by evaluating the attenuation properties of each voxel and by comparing these values with the attenuation coefficients of the three pure constituent materials at low and high kV. In the heart, the 3 materials usually analyzed are soft tissue, fat, and iodine. In addition, an iodine distribution image, or iodine distribution map, is produced via material decomposition along with virtual non-contrast images in which the iodine content has been subtracted from the contrast-enhanced images (Johnson et al. 2007; Vlahos et al. 2010).

3 Configuration of Dual-Source Dual-Energy CT

3.1 First Generation Dual-Source Dual-Energy CT (Siemens Definition)

Dual source CT is equipped with two orthogonally mounted X-ray tubes and two corresponding detector systems. The field of view of the B tube array is smaller (26 cm in diameter), compared with the A tube (50 cm in diameter), due to space limitations on the gantry of the dual-source CT scanner (Fig. 3a). Each detector comprises 40 detector rows, the 32 central rows having a 0.6-mm collimation slice width and the 4 outer rows on either side having a 1.2-mm collimated slice width. Using the z-flying focal spot technique, each detector acquires 64 overlapping 0.6-mm slices per rotation. The shortest gantry rotation time is 330 ms. There is an 8 ms interval between the image acquisitions of the 2 tubes in the same plane. The two X-ray tubes are operated independently with respect to their voltage and current settings, allowing simultaneous acquisition of high and low X-ray energy spectra within a single scan, e.g., one tube (B tube) is operated at 100 kV while the other (A tube) is operated at 140 kV. The tube current can be adjusted separately for each kV level (e.g., 100 mAs/rotation at 140 kV and 165 mAs/rotation at 100 kV), permitting noise level matching the two datasets (Flohr et al. 2006; Petersilka et al. 2008; Kang et al. 2010).

3.2 Second Generation Dual-Source Dual-Energy CT (Siemens Definition Flash)

The latest dual-source CT has several major technical improvements, including faster gantry rotation of 280 ms, increasing the scan field of the detector (increased detector z-coverage), increasing the field of view for detector B from 26 to 33 cm, high-pitch modes for rapid helical acquisition, and pre-patient filtration (Fig. 3b). Of these, pre-patient filtration is arguably the most important. This technical advance improves the discrimination of materials by minimizing the overlap of the two energy spectra. With pre-patient filtration, the lower-energy photons in the 140 kV beam are removed by a tin filter placed at the X-ray tube (Sn140 kV), resulting in a higher mean beam energy. This filtration increases the energy separation by minimizing the overlap of high and low kV spectra and, therefore, improves both the material differentiation and decomposition. In addition, radiation dose is reduced as the low-energy

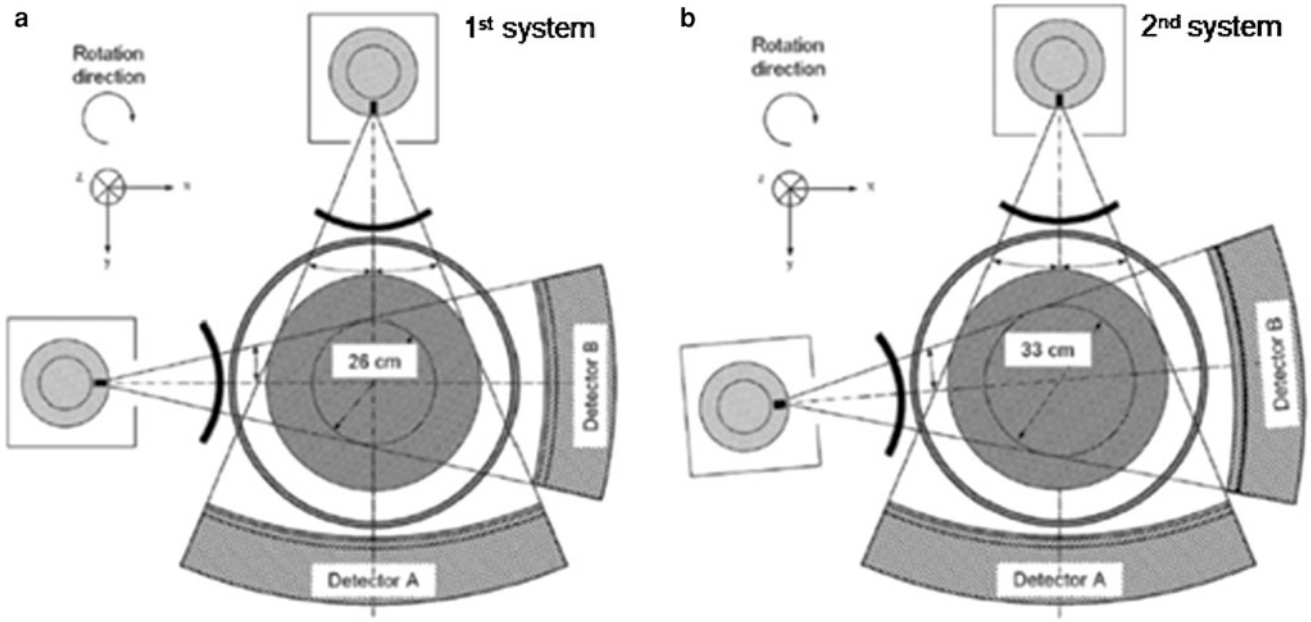

Fig. 3 Schematic illustration of first (Siemens SOMATOM Definition) and second (Siemens SOMATOM Definition Flash)- generation dual-source DECT systems. The first-generation dual-source CT system (**a**) has the A tube, which is associated with a 50 cm field of view for detector A and is operated at 140 kV, and the B tube, which is associated with a 26 cm field of view for detector B and is operated at 80/100 kV. The second-generation dual-source CT system (**b**) has a larger 33 cm field of view for detector B, achieved by increasing the angle between the X-ray tubes and detectors from 90° to 94° (Reproduced with kind permission from Siemens Healthcare)

photons are removed from the high-energy X-ray tube spectrum. Pre-patient filtration facilitates the use of a 100 kV low-energy beam, which enables greater tissue penetration and less image noise, compared with 80 kV (Kang et al. 2010).

4 Methodology for Dual-Energy CT Image Acquisition

4.1 Image Acquisition of Rest Dual-Energy CT

DECT acquisition can be performed using the following parameters: 330-ms gantry rotation time, heart rate adaptive pitch of 0.2–0.43, 32 × 2 × 0.6-mm collimation with z-flying focal spot technique, and 165-ms temporal resolution. One tube of the dual-source CT system is operated with 82–114 mAs/rotation at 140 kV, the second tube with 165 mAs/rotation at 80 kV for slim (≤140 lbs) individuals, and 165 mAs/rotation at 100 kV for average-sized (≤200 lbs) and larger patients (Ruzsics et al. 2008). With the scout image, the anatomic range extends from 2 cm below the level of the tracheal bifurcation to the diaphragm in a craniocaudal direction. Oral β-blocker administration is given if the resting heart rate is higher than 70 beats per minute. The retrospectively gated scan uses electrocardiography (ECG)-based tube current modulation with the Mindose protocol. Wider full-dose pulsing window (i.e., 35–75 %) is applied for faster and irregular heart rates, and narrow full dose windows (i.e., 60–80 %) for slower and more regular heart rates. Tube current reduction to 4 % was applied outside the adjusted pulsing windows.

DECT examinations are contrast enhanced, using the routine clinical contrast agent injection protocol, which is controlled by either the test-bolus or bolus-tracking technique. With the test-bolus technique, the time delay between the start of contrast injection and the start of data acquisition is determined by an injection of 20 ml of a nonionic contrast agent at 6 ml/s through an 18-gauge intravenous antecubital catheter, followed by 30 ml of saline, using a dual-head power injector. The peak time of the test bolus enhancement, as measured by a repetitive scanning at the level of the aortic root, is used as the delay time. Actual contrast agent enhancement is achieved by injecting an initial bolus of undiluted contrast agent, which is then followed by a constant 50 ml volume of a 70 %/30 % saline/contrast agent mixture, and finally 30 ml of pure saline, all injected at 6 ml/s. The initial iodine bolus volume is computed per CT examination using the following formula: volume (milliliters) = duration of CT data acquisition (seconds) × 6. If the duration of CT data acquisition is less than 10 s, a minimum of 60 ml of contrast medium is required (Ruzsics et al. 2008). There is no established optimal scan protocol (amount and speed of contrast

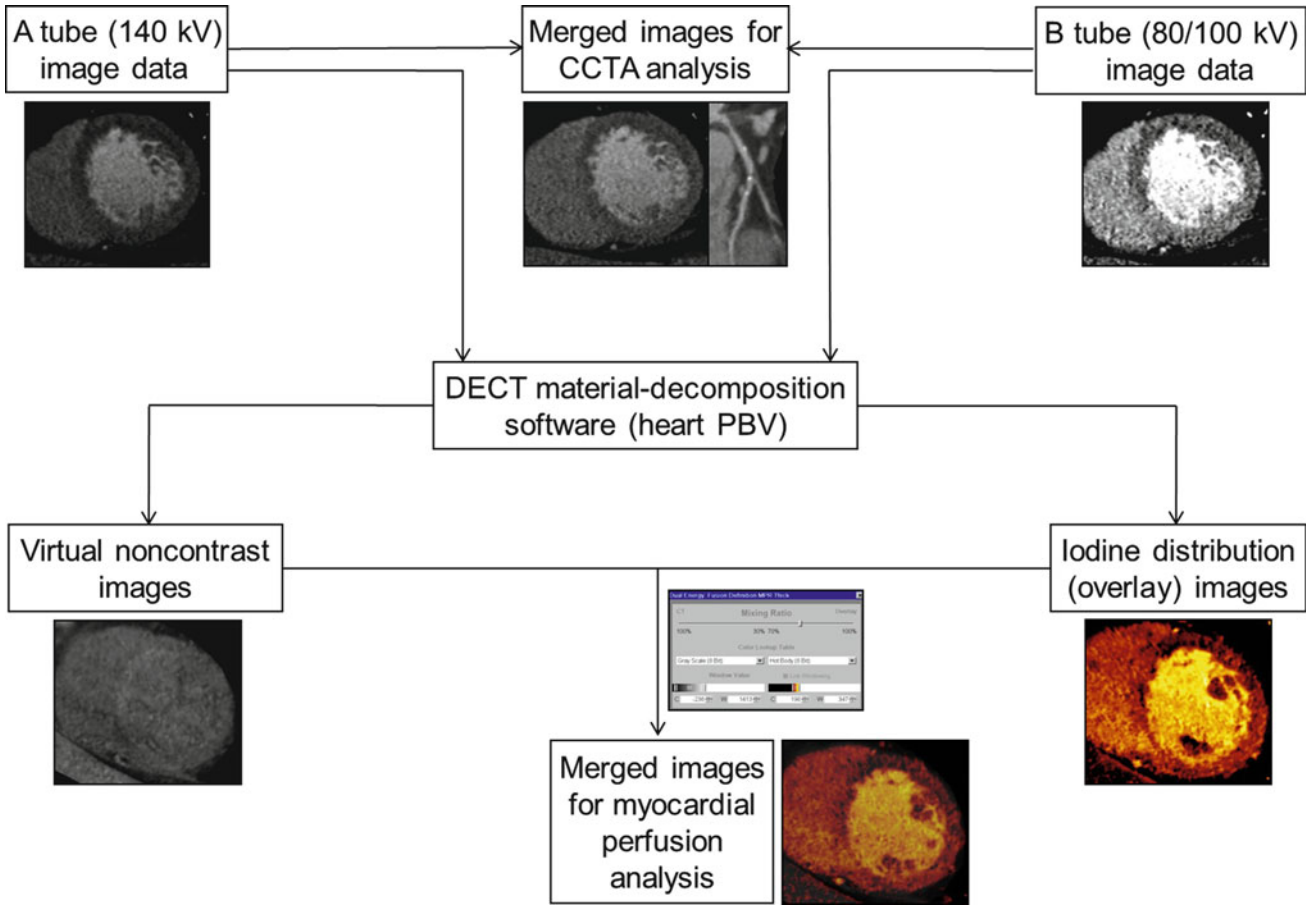

Fig. 4 Diagram of image postprocessing of DECT for analysis of myocardial perfusion. Merged images, which are produced by mixing 140 kV and 80/100 kV datasets at a ratio of 7:3, respectively, are equivalent to coronary CT angiography images obtained at approximately 120 kV. Using dual-energy material decomposition software, the iodine component is separated from the images obtained from high (A tube) and low (B tube)-energy X-ray spectra and is displayed in color-coded iodine distribution (overlay) images. Grayscale virtual non-contrast images are generated by removing iodine from the source images. Final images are obtained by mixing iodine distribution images and virtual non-contrast images, typically at a ratio 7:3, for assessment of the myocardial blood pool

administration, scan delay time, etc.) with a bolus-tracking technique. In our center, with the bolus tracking technique, the region of interest is placed into the aortic root, and image acquisition is started seven seconds after the signal density level reaches the predefined threshold of 120 HU. For DECT examinations, a dual-head power injector is used to administer a 3-phase bolus at a rate of 4.5 ml/s. According to scan time and patient's body mass index, 60–80 ml of undiluted contrast agent is injected, followed by 45 ml of 70 %/30 % contrast agent/saline mixture, and finally 45 ml of saline (Ko et al. 2011).

4.2 Image Acquisition of Stress Dual-Energy CT

Patients undergoing stress DECT perfusion are instructed not to drink coffee or tea, and not to have oral β-blockers for at least 24 h prior to the examination. Two intravenous lines are inserted (18-gauge for contrast medium delivery; 20-gauge for adenosine infusion). Before the examination, the heart rate of each patient is measured. Beta-blockers and nitroglycerine are avoided because of their impact on myocardial perfusion. Stress DECT perfusion is performed using the same imaging parameters as the rest DECT. Blood pressure, standard ECG, and clinical symptoms are carefully monitored during the adenosine infusion and after imaging. Any adverse side effect (e.g., severe tachycardia, tachyarrhythmia, allergic reaction) is grounds for termination of the examination. Adenosine infusion is started at a constant rate of 140 μg/kg/min over six minutes. Retrospectively gated imaging with ECG-based tube current modulation (Mindose protocol) and pitch adaptation is obtained four minutes after the initiation of the adenosine infusion. In our center, contrast agent administration with the bolus tracking technique is the same as that in rest DECT, except that image acquisition starts nine seconds after the signal density level reaches the predefined

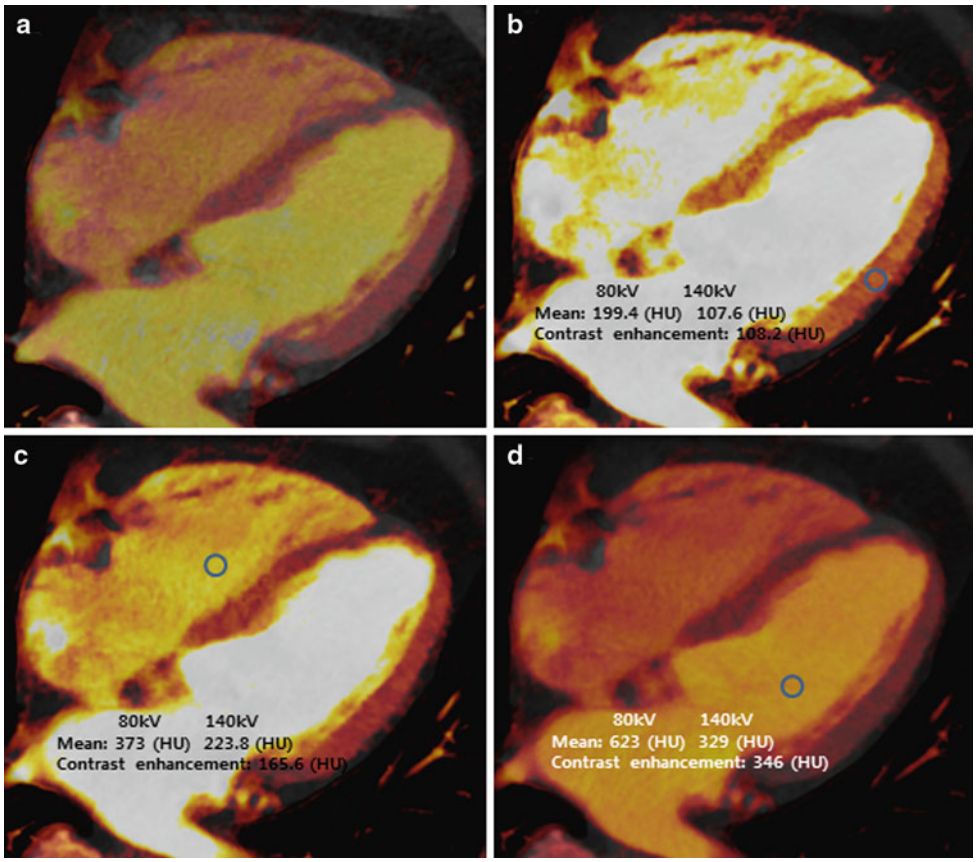

Fig. 5 Normalization of iodine distribution map. **a** Color-coded "iodine distribution map," which is superimposed on grayscale "virtual non-contrast image" multiplanar reformat of the myocardium. Because of a broad range of iodine concentration within the myocardium, the map must be normalized to an area of normal myocardial perfusion **b**, the right ventricle **c**, or the left ventricle **d**. Usually, areas of highest iodine content in the myocardium are recommended for normalization of the iodine distribution map

threshold of 120 HU at the aortic root for increasing differences in contrast enhancement between ischemic and non-ischemic myocardium (Ko et al. 2011).

4.3 Image Reconstruction of Dual-Energy CT

The data sets for the assessment of coronary artery and myocardial perfusion are reconstructed during the phase that depicts the fewest motion artifacts within the full-dose window, usually in the mid-diastolic phase, with reconstruction windows set at 60–75 % of the R–R interval. The recently implemented automatic phase finding algorithm (BestPhase^{TM}) is useful for identifying optimal reconstruction phases during systole and diastole without user interaction.

Standard DECT cardiac scan protocol includes a series of different image reconstructions from the same contrast enhanced DECT scan. The first set of transverse gray-scale images is reconstructed using a B26f kernel with a temporal resolution of 165 ms, slice thickness of 0.75 mm, and slice increment of 0.4 mm, for each tube-detector array. By merging 70 % of the high (140 kV) X-ray spectrum and 30 % of the low (80/100 kV) X-ray spectrum, a series of grayscale images is created that is similar to an image obtained using a single-energy CT at 120 kV. This series aims at optimizing the spatial and contrast resolution, and is used for clinical cardiac CT interpretation of coronary artery morphology and stenoses. For the analysis of myocardial perfusion, high-voltage and low-voltage data are reconstructed separately using a dedicated dual-energy convolution kernel (D26f or D30f) with a temporal resolution of 330 ms, slice thickness of 0.75 mm, and an increment of 0.4 mm (Ruzsics et al. 2008; Ko et al. 2011; Schwarz et al. 2008). Ruzsics et al. used a 1.5-mm slice thickness and a 0.5-mm increment to optimize the signal/noise ratio (Schwarz et al. 2008).

4.4 Post-Processing, Display, and Analysis

A single DECT data acquisition can be used to generate a virtual non-contrast image, two single-energy images based on high (140 kV) and low (80 or 100 kV) X-ray spectra, a dual-spectrum merged image, and an iodine distribution image; the iodine distribution can also be superimposed in color over the merged image (merged image with color-coded iodine distribution) (Fig. 4). The reconstructed high- and low-voltage data sets, obtained with DECT, are loaded into a dedicated algorithm, heart perfusion blood volume

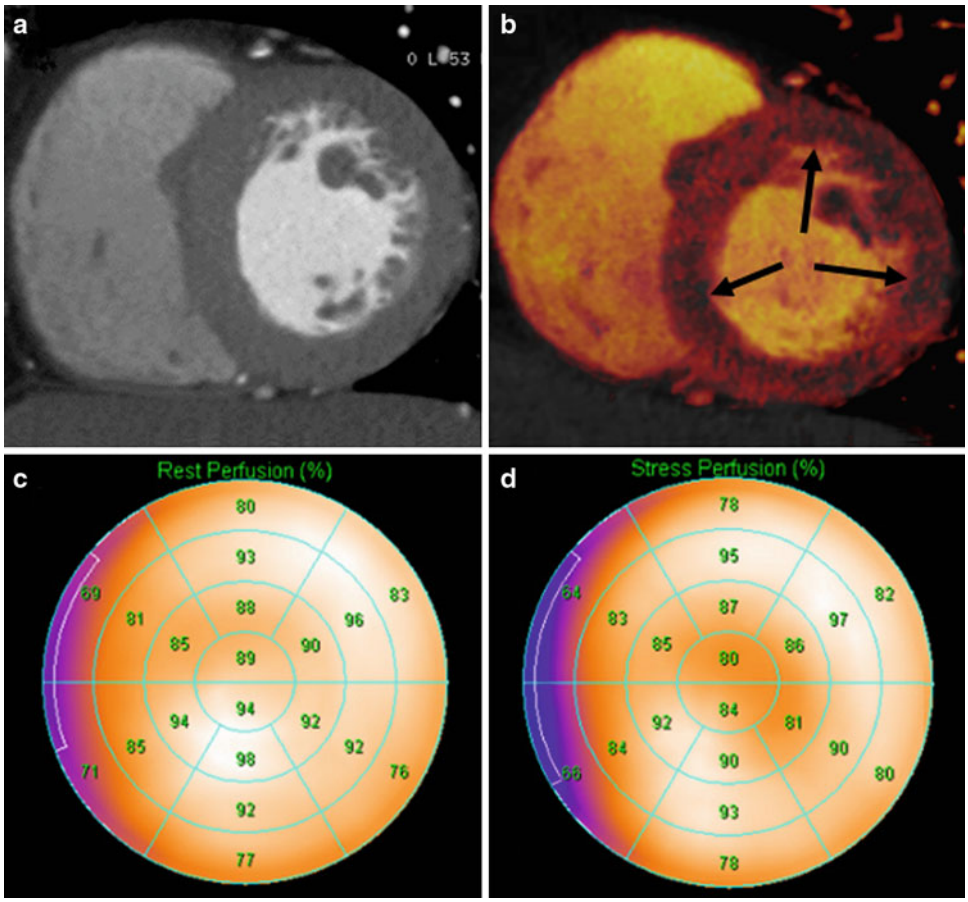

Fig. 6 Comparison of stress DECT perfusion and myocardial perfusion SPECT for balanced ischemia. The CT perfusion image at rest (**a**) does not show any perfusion defects in the left ventricular (LV) myocardium. DECT-based iodine distribution mapping during adenosine infusion (**b**) reveals concentric blood pool deficits (*arrows*) in mid LV myocardium. Findings are not correlated with myocardial perfusion SPECT acquired at rest (**c**) and stress (**d**), which reveal limitation of myocardial perfusion SPECT for balanced ischemia. Conventional coronary angiogram (not shown) reveals significant stenoses at the left main coronary artery and the 3 major epicardial coronary arteries

(heart PBV), for the evaluation of myocardial perfusion. The heart PBV algorithm is incorporated in the dual-energy-image post-processing software application of the Syngo-Multimodality Workplace (syngo Dual Energy, Siemens). Differences in the attenuation of iodine at the two different energies allow for the computation of the iodine distribution within the myocardium and the generation of virtual non-contrast images. The attenuation of epicardial fat on the merged reconstruction is measured for fat calibration of the heart PBV algorithm. In addition, the broad range of iodine concentrations that this study produces requires normalization of the iodine distribution map to the areas of normal myocardial perfusion (Schwarz et al. 2008). Areas with high iodine content, including the myocardium or any cardiac chamber, can be chosen for this process; we primarily normalize using the right ventricular lumen (Fig. 5). The color-coded iodine distribution maps are superimposed onto a grayscale multiplanar reformats of the myocardium. We employ a 70 % overlay of the iodine distribution map over the merged reconstruction with 5-mm thick multiplanar-reformatted short and long axis views for the evaluation of myocardial perfusion. Myocardial blood pool deficits on DECT-based iodine distribution maps are defined as contiguous, circumscribed areas of decreased or absent iodine content within the left ventricular (LV) myocardium, relative to the remote normal myocardium. Myocardial blood pool deficits are assessed quickly and accurately by visual analysis because DECT-based iodine distribution map highlights the areas of decreased iodine in the LV myocardium. Accordingly, visual analysis is mainly used over quantitative analysis for the detection of myocardial blood pool deficits. The AHA/ACC-segmental model (17 segment model) is used to report the findings at perfusion analysis (Schwarz et al. 2008).

5 Overview of Imaging Modalities for Coronary Artery Disease

Conventional coronary angiography (CCA) is considered as the established, anatomic gold standard for the diagnosis of CAD by direct visualization and grading of coronary stenosis. However, CCA is invasive, costly, and not without risk. In addition, anatomical assessment of the hemodynamic significance of coronary stenosis, determined by CCA, correlates poorly with functional assessment of the fractional flow reserve (FFR) (Chandrasekar et al. 2001; Meijboom et al. 2008). SPECT myocardial perfusion

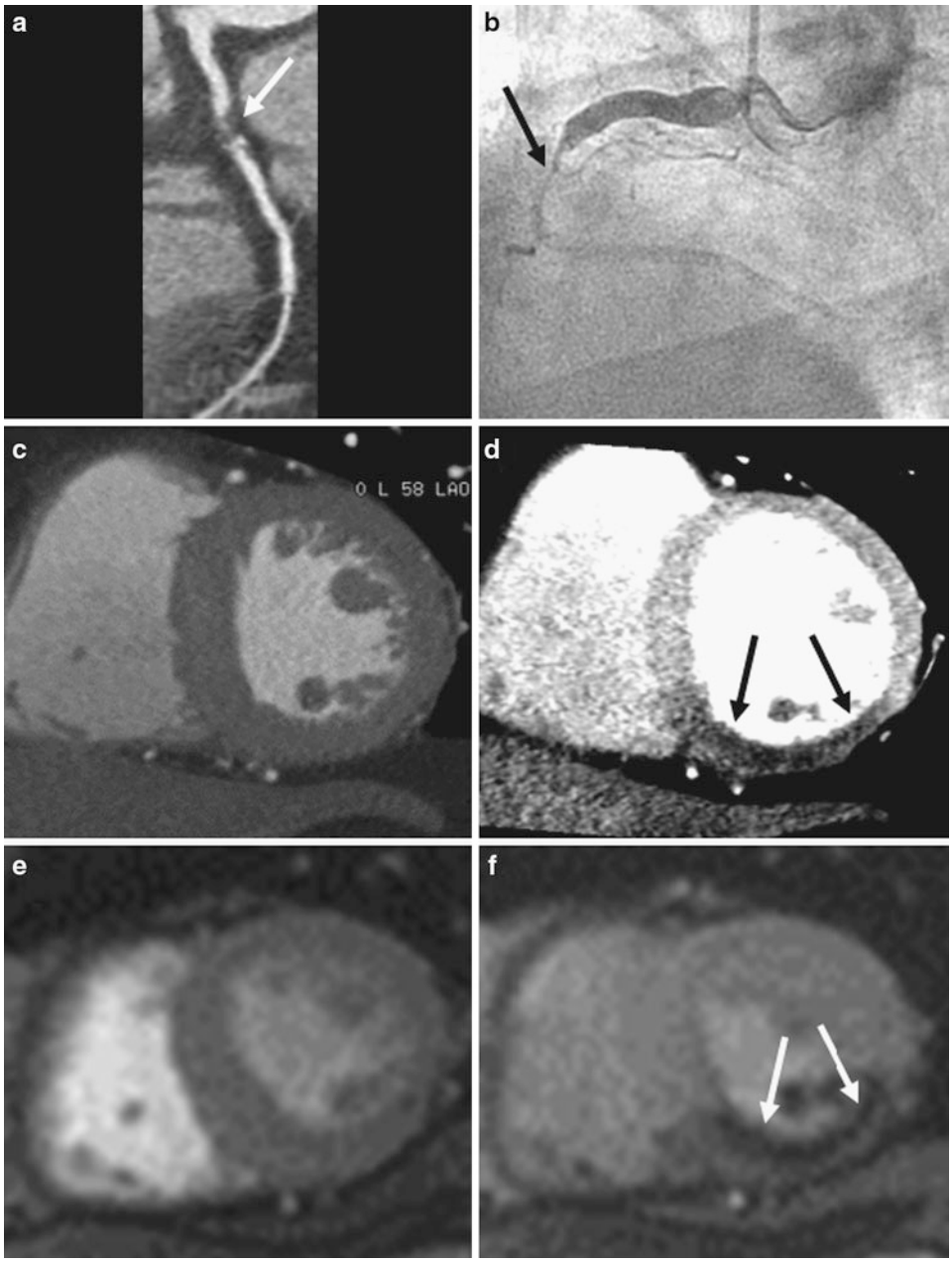

Fig. 7 Representative example of single-energy CT perfusion identifying single-vessel disease. Curved multiplanar reformatted coronary CT angiographic image (**a**) shows total occlusion with non-calcified plaque (*arrow*) in the middle segment of the right coronary artery (RCA). Conventional coronary angiogram (**b**) confirms the subtotal occlusion (*arrows*) in the middle RCA. Rest (**c**) and stress (**d**) single-energy CT perfusion images reveal reversible transmural perfusion defects (*arrows*) in the mid inferoseptal and the inferior left ventricular myocardium. Findings are in good correlation with cardiac MR acquired at rest (**e**) and stress (**f**), which reveal reversible subendocardial perfusion defect (*arrows*) in the same myocardial areas

imaging (MPI) is an accepted clinical standard for the detection and quantification of myocardial ischemia. However, SPECT has the disadvantages of poor spatial resolution, radiation exposure, and attenuation artifacts. In addition, SPECT does not detect subclinical, non-obstructive coronary atherosclerosis and consistently underestimates the true extent of multivessel CAD (balanced ischemia) (Hachamovitch et al. 1996; Heller et al. 2009) (Fig. 6). Recent technical advances and improvements in cardiac CT have allowed for the non-invasive detection of significant coronary stenosis with high diagnostic accuracy. In addition, CCTA visualizes the coronary vessel wall, thereby, providing plaque composition and size, and vascular remodeling (Mühlenbruch et al. 2007; Vanhoenacker et al. 2007). However, CCTA has a tendency to overestimate the severity of CAD in patients with high pretest probability of CAD. Furthermore, in its current form, CCTA does not provide information regarding the hemodynamic significance of coronary stenosis. Determining the hemodynamic significance of a morphologically intermediate stenosis (50–70 % lumen reduction) remains crucial before a referral for the revascularization treatment (Meijboom et al. 2008; Gaemperli et al. 2008). Consequently, there is great interest in combining non-invasive CCTA with SPECT-MPI. However, the hybrid imaging system requires the cost associated with combining two

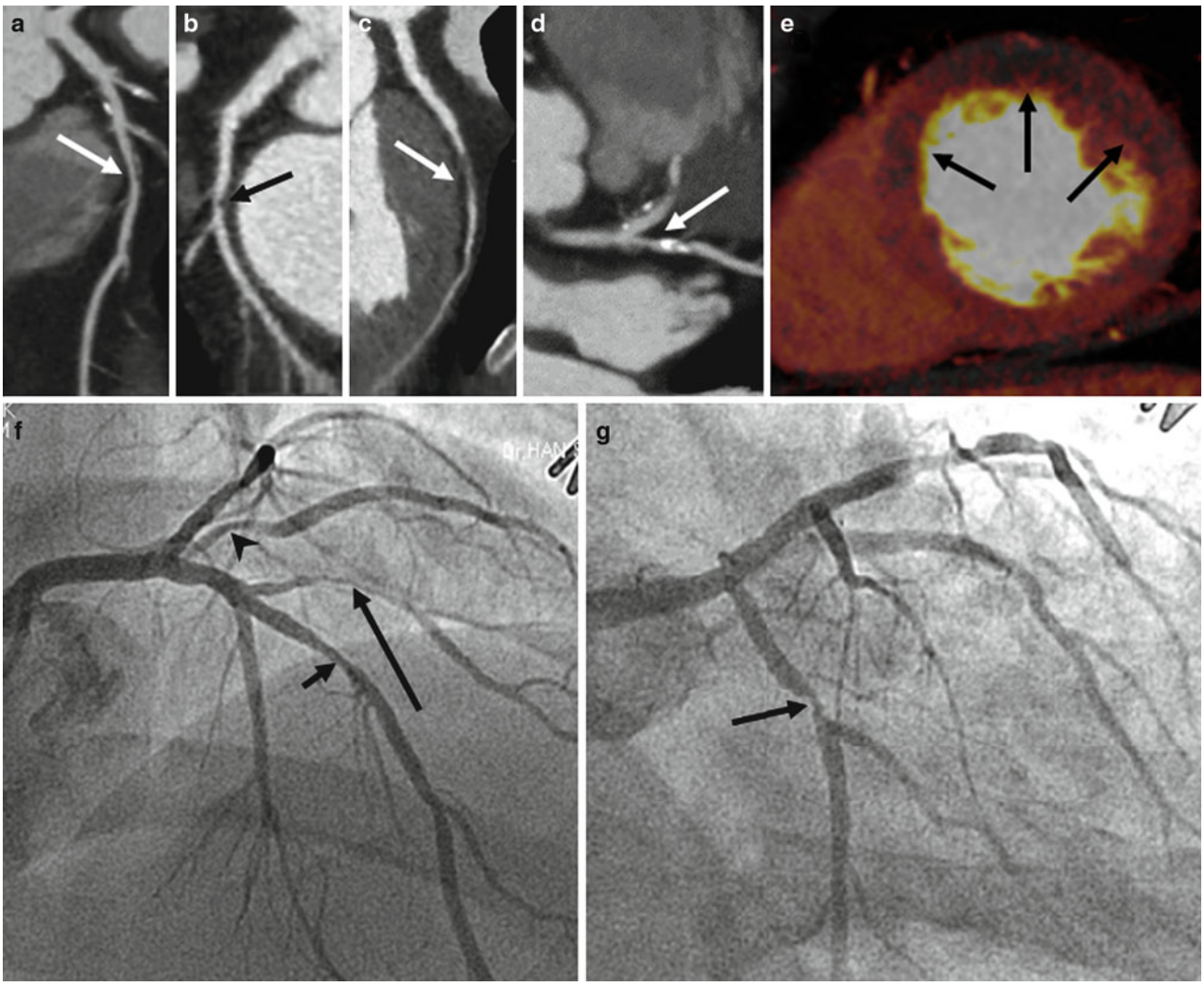

Fig. 8 Representative example of rest DECT perfusion identifying multivessel disease. Coronary CT angiograms (**a**–**d**) show significant stenoses with mixed calcified and non-calcified plaques (**a**, *arrow*) in the middle segment of the left anterior descending coronary artery (LAD), non-calcified plaque (**b**, *arrow*) in the proximal segment of the left circumflex artery (LCx) and the first diagonal branch (D1, *arrow* in **c**) and calcified plaque (**d**, *arrow*) in the ramus intermedius (RI). DECT-based iodine distribution mapping at rest (**e**) reveals blood pool deficits (*arrows*) in the mid anteroseptum, anterior and anterolateral left ventricular myocardium. Conventional coronary angiograms (**f**, **g**) confirm the presence of significant stenoses in LAD (*short arrow*), D1 (*long arrow*), RI (*arrowhead*), and LCx (*middle arrow*)

imaging modalities and increases the radiation burden to the patient (Santana et al. 2009; Gaemperli et al. 2007). Recently, cardiac magnetic resonance (MR) with adenosine stress has been established as a non-invasive diagnostic modality with a high diagnostic accuracy for inducible perfusion defect, without radiation exposure or attenuation artifacts. In particular, cardiac MR has superior spatial resolution over SPECT, and thereby allows for a depiction of subendocardial perfusion defects in patients with microvascular disease. However, adenosine stress cardiac MR perfusion can be limited by availability, claustrophobia, obesity, poor gating, motion artifacts, and contraindications, such as pacemaker or defibrillators (Nandalur et al. 2007; Watkins et al. 2009).

6 Overview of Single-Energy CT Perfusion Imaging

Myocardial perfusion is strictly defined as the flow of blood to the myocardium and is often used as a relative myocardial blood volume or regional level of myocardial iodine enhancement. CT myocardial perfusion images are obtained using a static (single-phase first-pass myocardial enhancement imaging) or dynamic acquisition (quantitative time resolved myocardial perfusion imaging). Several CT-based MPI studies in animal models have demonstrated that the concentration of iodinated contrast agent in myocardium is directly proportional to the measured CT attenuation

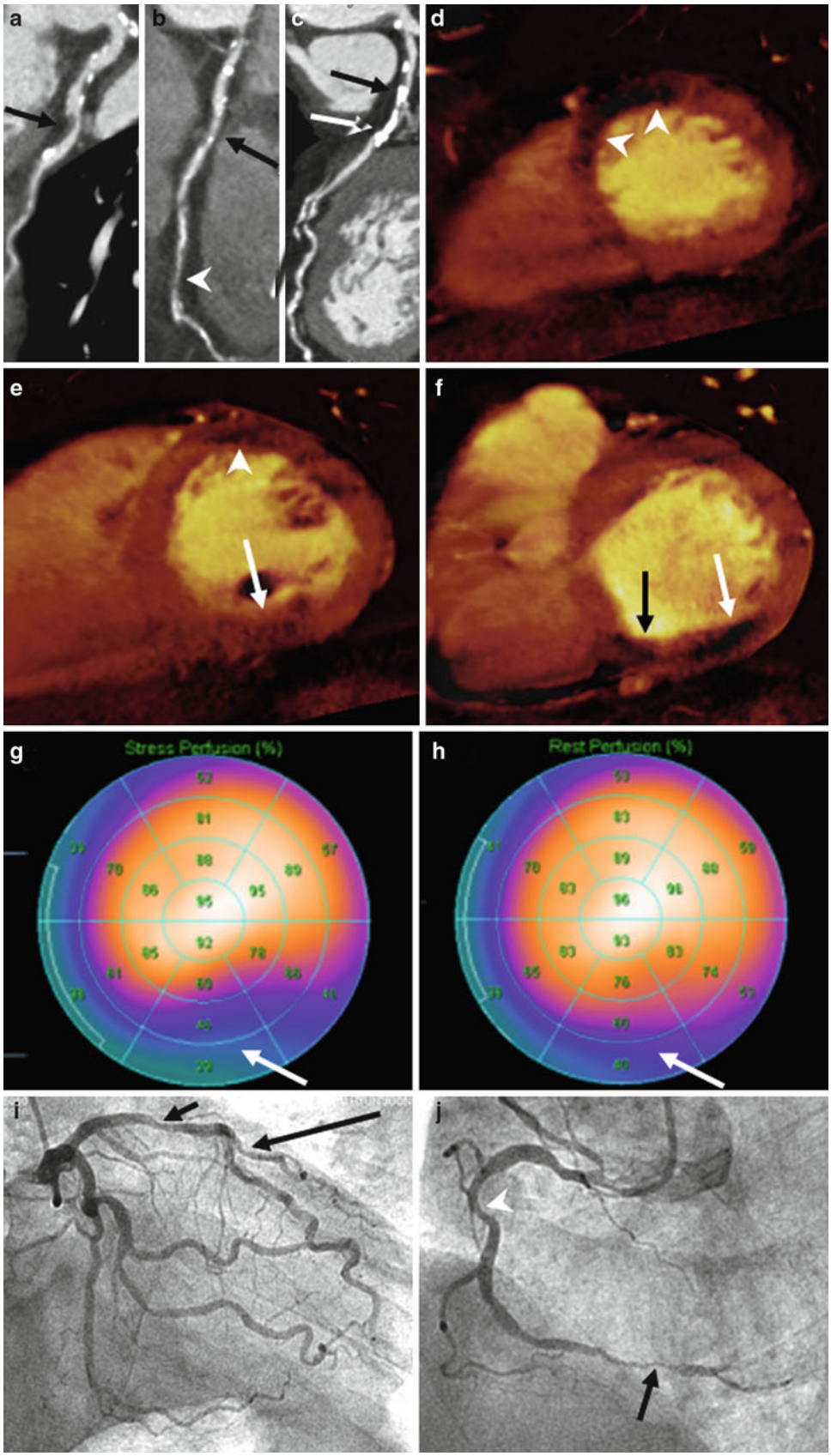

Fig. 9 Comparison of coronary CT angiography, rest DECT perfusion, myocardial perfusion SPECT, and conventional coronary angiography. Coronary CT angiograms (**a–c**) show significant stenoses with non-calcified plaque (*arrow*) in the proximal segment of the left circumflex artery (**a)** and mixed calcified and non-calcified plaques (*arrow*) in the middle segment of the right coronary artery (RCA) and subtotal occlusion with non-calcified plaque (*arrowhead*) in the distal segment of RCA (**b**). Severe calcification (*arrows*) can render the proximal left anterior descending coronary artery (LAD) uninterpretable regarding the presence of significant stenosis (**c**). DECT-based iodine distribution mapping at rest (**d–f**) reveals blood pool deficits in the apical to mid anterior and apical septum (*arrowheads*) and mid to basal inferior (*arrows*) left ventricular (LV) myocardium. Myocardial perfusion SPECT at stress (**g**) and rest (**h**) show partially reversible perfusion defects (*arrows*) in inferior and inferolateral LV myocardium, corresponding to old myocardial infarction in RCA territory. However, SPECT images do not detect ischemic perfusion defects in LAD territory which is shown on rest DECT perfusion images. Conventional coronary angiograms (**i**, **j**) confirm the presence of significant stenoses in the proximal LAD (**i**, *short arrow*), D1 (**i**, *long arrow*), middle RCA (**j**, *arrowhead*), and distal RCA (**j**, *middle arrow*)

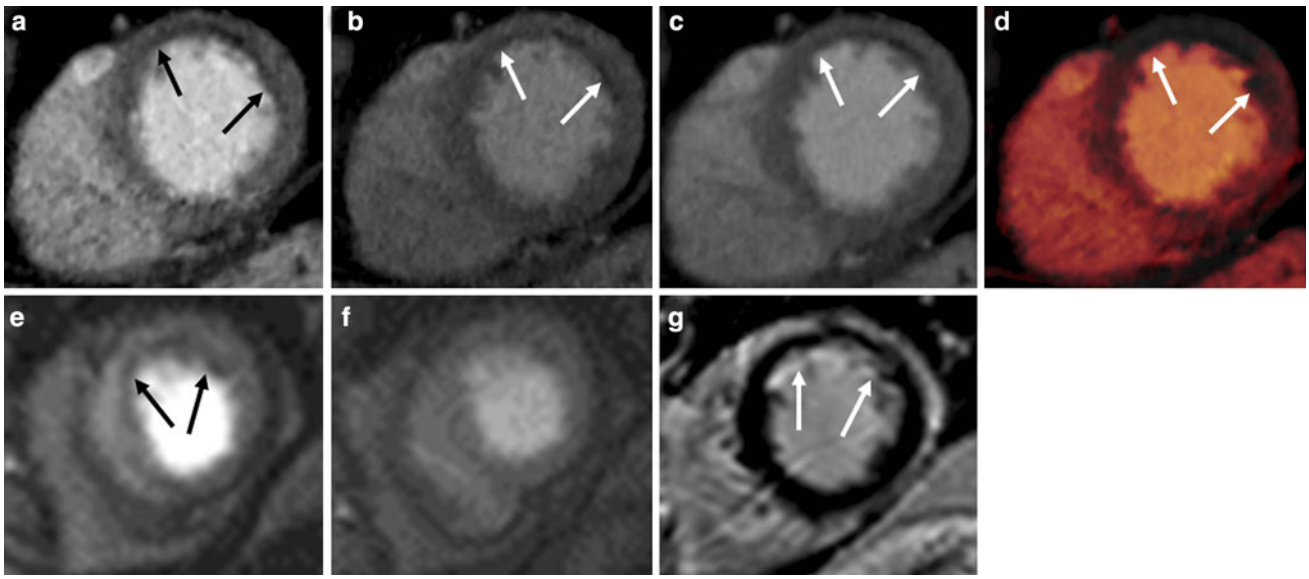

Fig. 10 Rest DECT-based iodine distribution map compared with single-energy CT spectra. Better visualizes blood pool deficits (*arrows*) in the apical anterior and lateral left ventricular (LV) myocardium compared to reconstruction images using 80-kV CT spectra (**a**), 140-kV CT spectra (**b**), and merged data (**c**). DECT-based iodine distribution map at rest (**d**). Stress (**e**) and rest (**f**) perfusion and delayed contrast-enhanced (**g**) cardiac MR images confirm subendocardial myocardial infarction with peri-infarct ischemia (*arrows*) in the apical anterior and lateral LV wall

number; that iodinated contrast agent has similar pharmacokinetics to gadolinium-based contrast agents used for stress cardiac MR perfusion; that adenosine stress CT perfusion imaging correlates well with microsphere-derived myocardial blood flow; and, that ischemic myocardial perfusion defect can be diagnosed by an adenosine-induced stress CT perfusion imaging (George et al. 2006, 2007). Studies using adenosine-induced stress CT perfusion imaging have shown good diagnostic accuracy for the detection of ischemic myocardium caused by hemodynamically significant coronary artery stenosis, and increasing the value of CCTA through the detection of hemodynamically significant CAD (Blankstein et al. 2009; Rocha-Filho et al. 2010; Ko et al. 2012b) (Fig. 7). More recently, dynamic CT perfusion has provided results comparable to cardiac MR perfusion for the differentiation between normal and ischemic myocardium. Dynamic CT perfusion has also provided an incremental diagnostic value for the detection of hemodynamically significant coronary stenosis by quantifying myocardial blood flow (Bamberg et al. 2011). With the technical advances of multidetector computed tomography (MDCT), including dual-source CT and wide-area detector CT, CT has grown increasingly capable. By combining direct visualization and grading of coronary stenosis and plaque visualization obtained by CCTA with myocardial perfusion imaging provided by CT perfusion, CT is a single technological modality advantageously poised to provide a potential one-stop shop for the coronary risk assessment and possibly the approach to coronary intervention.

7 Dual-Energy CT Perfusion Imaging

7.1 Dual-Energy CT at Rest for Myocardial Perfusion

Rest DECT perfusion is acquired using retrospective ECG-gating with tube current modulation and a single-phase first-pass contrast enhancement protocol. With two synchronous CT acquisitions at different tube voltages, DECT allows for the assessment of myocardial perfusion status (or myocardial blood volume) by analyzing the iodine distribution within the myocardium (Fig. 8). The clinical evidence supporting the accuracy and feasibility of rest DECT for the assessment of myocardial perfusion deficits comes from three published single-center studies. Ruzsics et al. (2008) performed the first systematic investigation into the usefulness of cardiac DECT for diagnosing CAD and myocardial ischemia; they demonstrated that DECT had 91 % sensitivity and 91 % specificity with 91 % accuracy, in comparison with SPECT, for detecting any type of myocardial ischemia on a segmental basis; compared to CCA, DECT was found to have 92 % sensitivity, 79 % specificity, and 90 % accuracy for detecting the myocardial blood pool deficits on a segmental basis. In a recent study by Ruzsics et al. (2009), 36 patients with equivocal or incongruous SPECT results underwent single-phase, contrast-enhanced DECT at rest. DECT correctly identified 85 of 89 (96 %) fixed perfusion defects, and 60 of 68 (88 %) reversible myocardial perfusion defects. Overall,

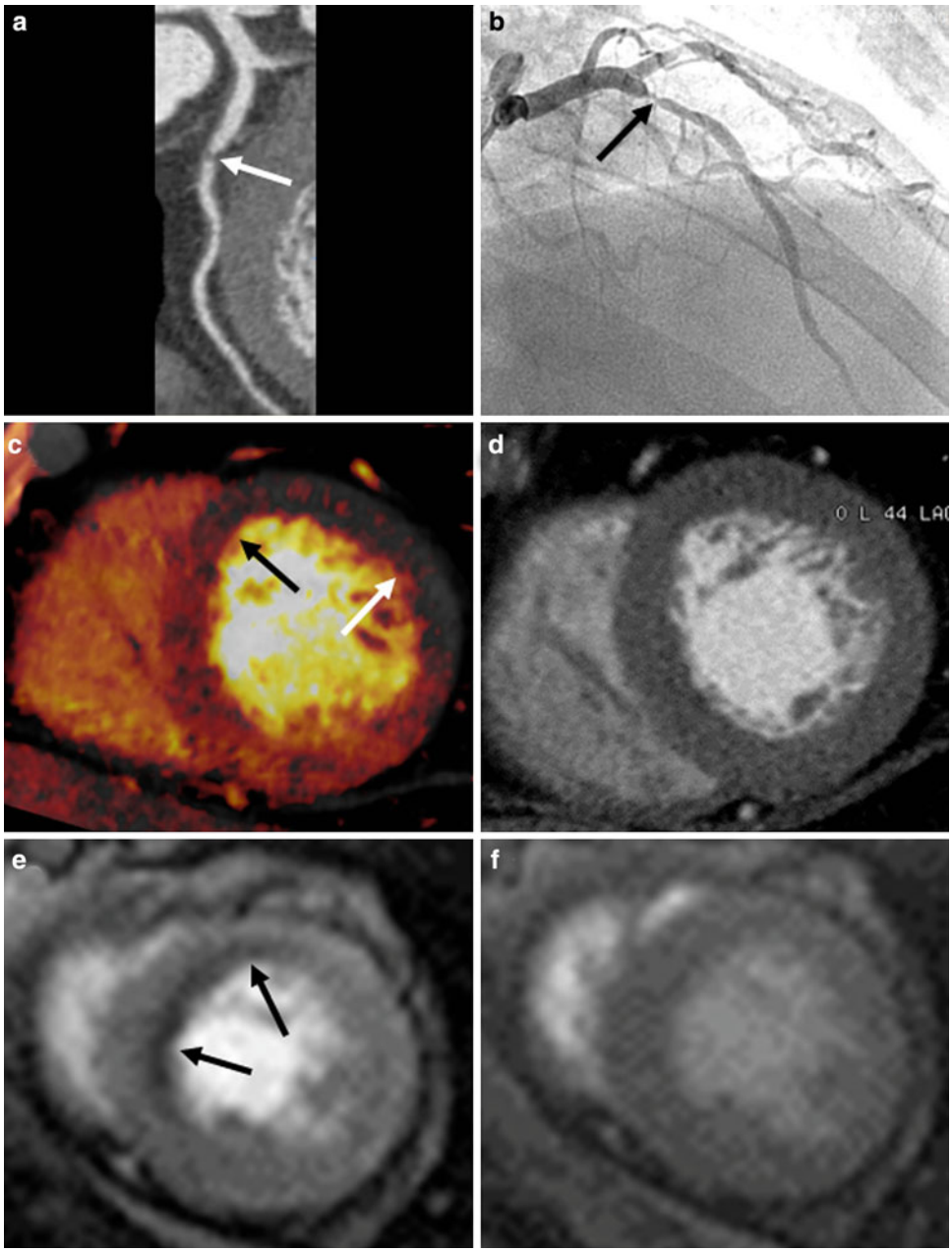

Fig. 11 Representative example of stress DECT perfusion. Curved multiplanar reformatted coronary CT angiographic image (**a**) shows severe stenosis with non-calcified plaque (*arrow*) in the proximal segment of the left anterior descending coronary artery (LAD). Conventional coronary angiogram (**b**) confirms the presence of severe stenosis (*arrow*) in the proximal LAD. DECT-based iodine map during adenosine infusion (**c**) reveals transmural blood pool deficits (*arrows*) in the apical septum, anterior and lateral left ventricular (LV) myocardium. The rest CT perfusion image (**d**) does not show any perfusion defects in the LV myocardium. Cardiac MR images acquired at stress (**e**) and rest (**f**) show reversible subendocardial perfusion defects (*arrows*) in the apical septal and anterior LV myocardium. The extent of stress-induced myocardial perfusion defect is larger on stress DECT than on stress cardiac MR

DECT had a sensitivity of 92 % and a specificity of 93 % with an accuracy of 93 % for type-independent detection of myocardial perfusion defects seen on SPECT. Interestingly, rest DECT is able to depict reversible perfusion defects only seen on stress SPECT images (Fig. 9). Although DECT iodine distribution maps at rest had a sensitivity of 88 %, a specificity of 89 %, and accuracy of 89 % for the detection of reversible perfusion defect, performance of rest DECT was substantially lower for the detection of reversible perfusion defects than that of mixed and fixed perfusion defects (Ruzsics et al. 2009). The physiological mechanism behind such a concordance remains controversial as DECT was not performed under stress. Possible explanations for DECT detection of reversible perfusion defects, as hypothesized by Ruzsics et al. (2008, 2009), include the superior spatial resolution of CT for smaller areas of ischemia compared with SPECT, an intrinsic vasodilatory effect of the iodinated contrast agent, and different myocardial distribution kinetics of the iodinated contrast agent compared with the radiopharmaceutical tracers of SPECT.

Most recently, Wang et al. (2011) demonstrated on a per-vessel basis that sensitivity, specificity, and accuracy of DECT coronary angiography without DECT perfusion were 82, 91, and 86 %, respectively; with the addition of DECT perfusion, an overall improvement to 90, 86, and 88 %, respectively, was observed. This study demonstrated an

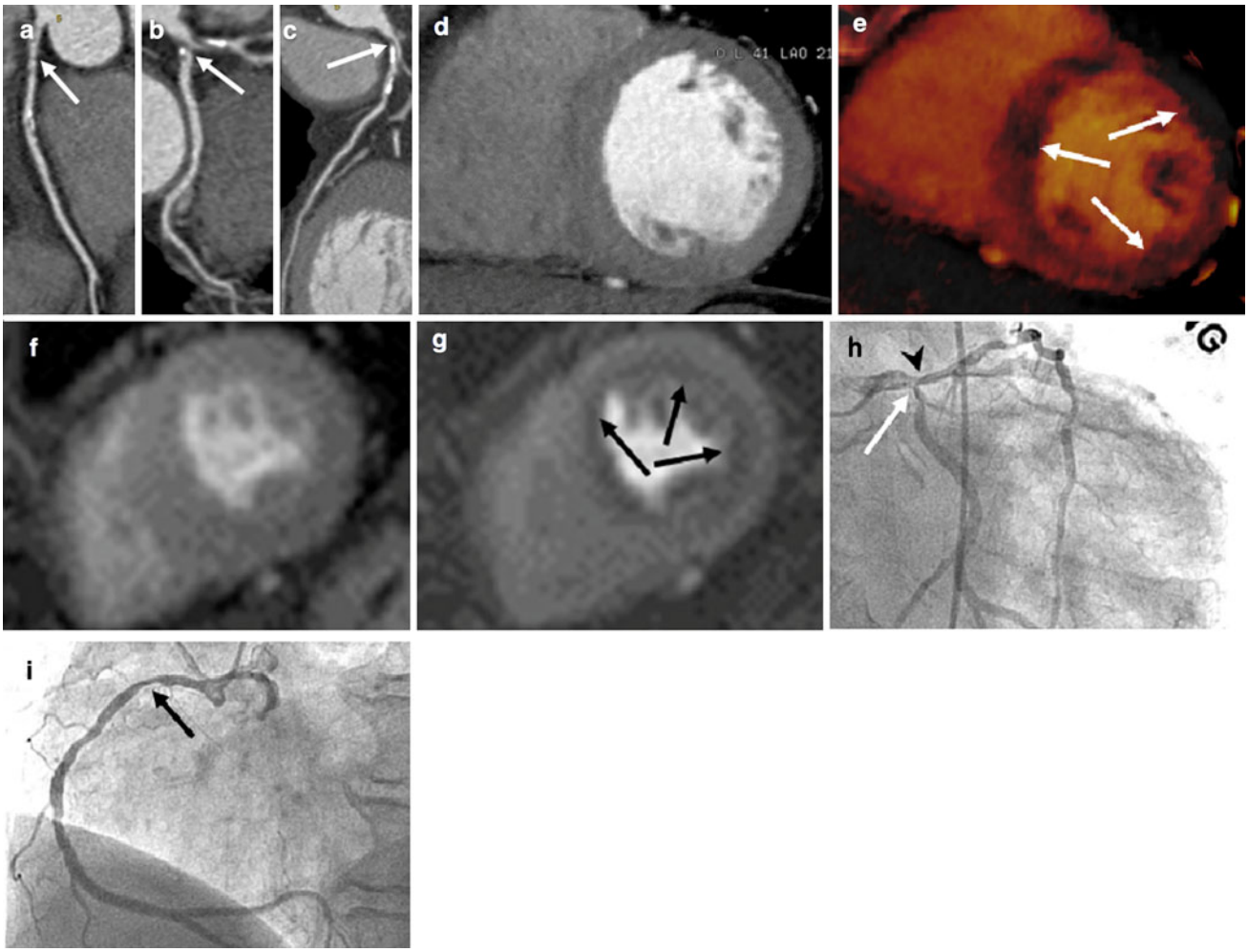

Fig. 12 Example of stress DECT perfusion for multivessel coronary artery disease. Curved multiplanar reformatted coronary CT angiographic images (**a**–**c**) show significant stenoses with non-calcified plaque (**a**, *arrow*) in the proximal segment of right coronary artery (RCA) and mixed calcified and non-calcified plaque (**b**, *arrow*) in the ostia of the left circumflex artery (LCX) and the left anterior coronary artery (LAD) (**c**, *arrow*). The CT perfusion image at rest (**d**) does not show any perfusion defects in the left ventricular (LV) myocardium. DECT-based iodine distribution map during adenosine infusion (**e**) reveals concentric blood pool deficits (*arrows*) in mid LV myocardium. Findings are in good correlation with cardiac MR acquired at rest (**f**) and stress (**g**), which reveal a reversible subendocardial perfusion defect (*arrows*) in the same myocardial areas. Conventional coronary angiogram findings (**h**, **i**) confirm the presence of significant stenoses in LAD ostium (**h**, *arrowhead*), LCx ostium (**h**, *arrow*), and proximal RCA (**i**, *arrow*)

incremental value of DECT on the detection of CAD (Fig. 9).

DECT-based color-coded iodine distribution map might be more sensitive to the detection of hypoperfused myocardium than single-energy CT-based gray scale image (Fig. 10). Arnoldi et al. (2011) compared the performance of cardiac CT on the basis of single-energy image reconstructions, merged image reconstructions, and DECT iodine distribution maps for the detection of reversible and fixed myocardial perfusion deficits seen on SPECT. They demonstrated that the four image reconstruction strategies had relatively similar, high specificity for the detection of perfusion deficits on SPECT. However, sensitivity, negative predictive value, and accuracy for mixed perfusion deficits were highest with DECT iodine maps and were 91, 97, and 93 %, respectively. In addition, DECT iodine distribution maps had highest area under the curve values (0.84–0.93) for both observers in the detection of purely fixed and mixed perfusion defects seen on SPECT. These results might be explained by the distribution map of iodinated contrast material, based on DECT-based material decomposition, is better suited than visual analysis in the differences in CT attenuation values between ischemic and non-ischemic myocardium. DECT may be helpful to improve the specificity of myocardial single-phase first-pass enhancement CT imaging.

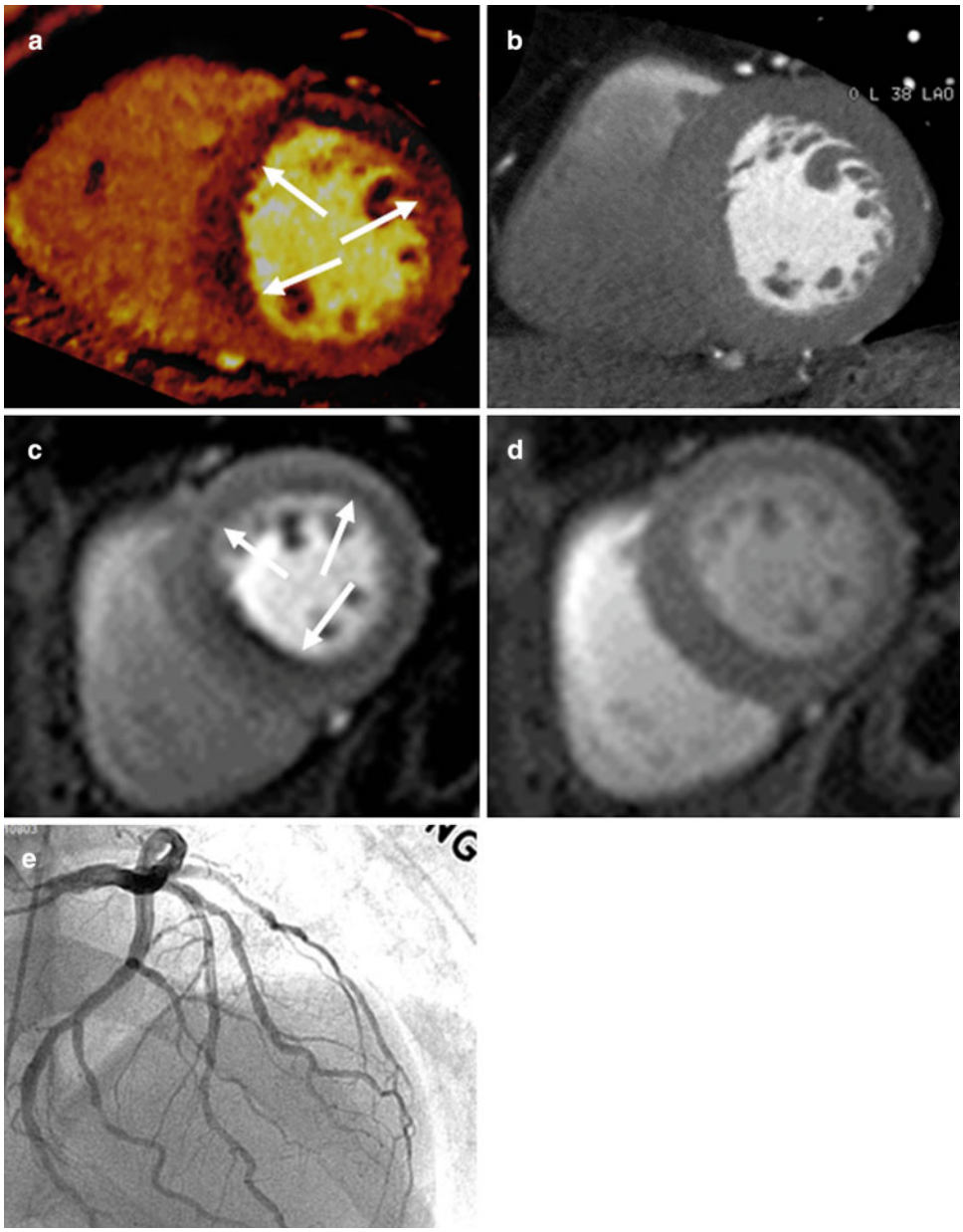

Fig. 13 Example of stress DECT perfusion for microvascular angina. DECT-based iodine distribution mapping during adenosine infusion (**a**) reveals subendocardial blood pool deficits (*arrows*) in the mid anterior, septal, and lateral left ventricular (LV) myocardium. The rest CT perfusion (**b**) does not show any perfusion defects in the LV myocardium. Cardiac MR images acquired at stress (**c**) and rest (**d**) reveal a reversible subendocardial perfusion defect (*arrows*) in the entire mid LV myocardium. Extent of stress-induced myocardial perfusion defect is larger on stress cardiac MR than on stress DECT. Conventional coronary angiogram finding (**e**) shows the left coronary dominance without any significant stenoses. These findings are consistent with microvascular angina

These studies can be summarized as follows: (1) DECT allows analysis of the iodine distribution within the myocardium by exploiting the absorption characteristics of iodine at different X-ray energies, (2) DECT allows the reproducible differentiation of iodine distribution within the myocardium to detect myocardial blood pool deficits in a good correlation with a clinical reference standard, such as SPECT, (3) DECT acquired at rest is able to detect areas of reversible, stress induced perfusion deficits as seen on SPECT, (4) DECT iodine distribution maps have good diagnostic performance for the detection of fixed and mixed myocardial blood pool deficits compared with single-energy CT spectra, and (5) rest DECT perfusion may improve the diagnostic performance of the detection of CAD (synergistic clinical value). Accordingly, DECT imaging of the heart enable the integrative assessment of the coronary artery morphology and the myocardial blood supply in patients with known or suspected CAD.

7.2 Dual-Energy CT Under Stress for Myocardial Perfusion

Rest DECT perfusion had a much lower positive predictive value (26 %) for the detection of purely reversible perfusion defects than that of the mixed (85 %) and fixed (59 %) perfusion defects on per-myocardial segmental analysis (Arnoldi et al. 2011). The result suggests that DECT

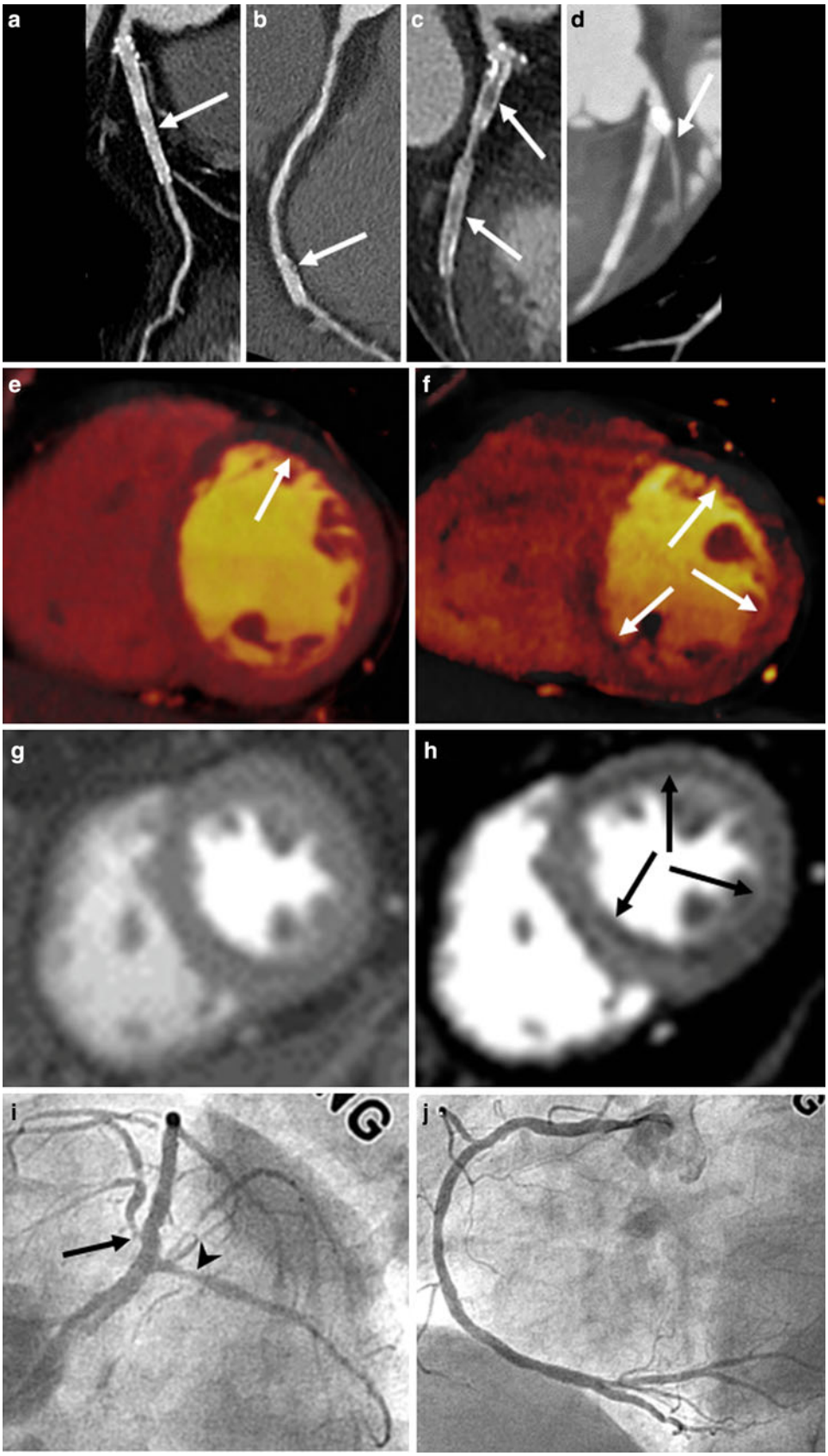

Fig. 14 Example of rest and stress DECT perfusion for stent evaluation. Curved multiplanar reformatted coronary CT angiographic images (**a**–**d**) show a patent stent (*arrow*) in the big first diagonal branch (D1, **a**) and the distal segment of the right coronary artery (RCA, **b**) but significant in-stent restenosis (*arrows*) in the proximal and distal segments of the left circumflex artery (LCx, **c**). In addition, significant stenosis (*arrow*) is noted at the ostium of the first obtuse marginal branch (OM1, **d**). DECT-based iodine distribution map at rest (**e**) reveals blood pool deficits (*arrows*) in the mid anterior LV myocardium. Stress DECT-based iodine distribution map (**f**) shows blood pool deficits (*arrows*) in the mid anterior, inferoseptal, inferior, and lateral LV myocardium. Findings are in good correlation with cardiac MR acquired at rest (**g**) and stress (**h**), which reveal reversible subendocardial perfusion defect (*arrows*) in the same myocardial areas. Conventional coronary angiograms (**i**, **j**) show significant stenosis (*arrow*) in the ostium of the left anterior descending coronary artery (**i**) and also significant intent restenosis (*arrowhead*) in the proximal LCx stent (**i**). There are no in-stent restenosis in the big D1 stent (**i**) and distal RCA stent (**j**)

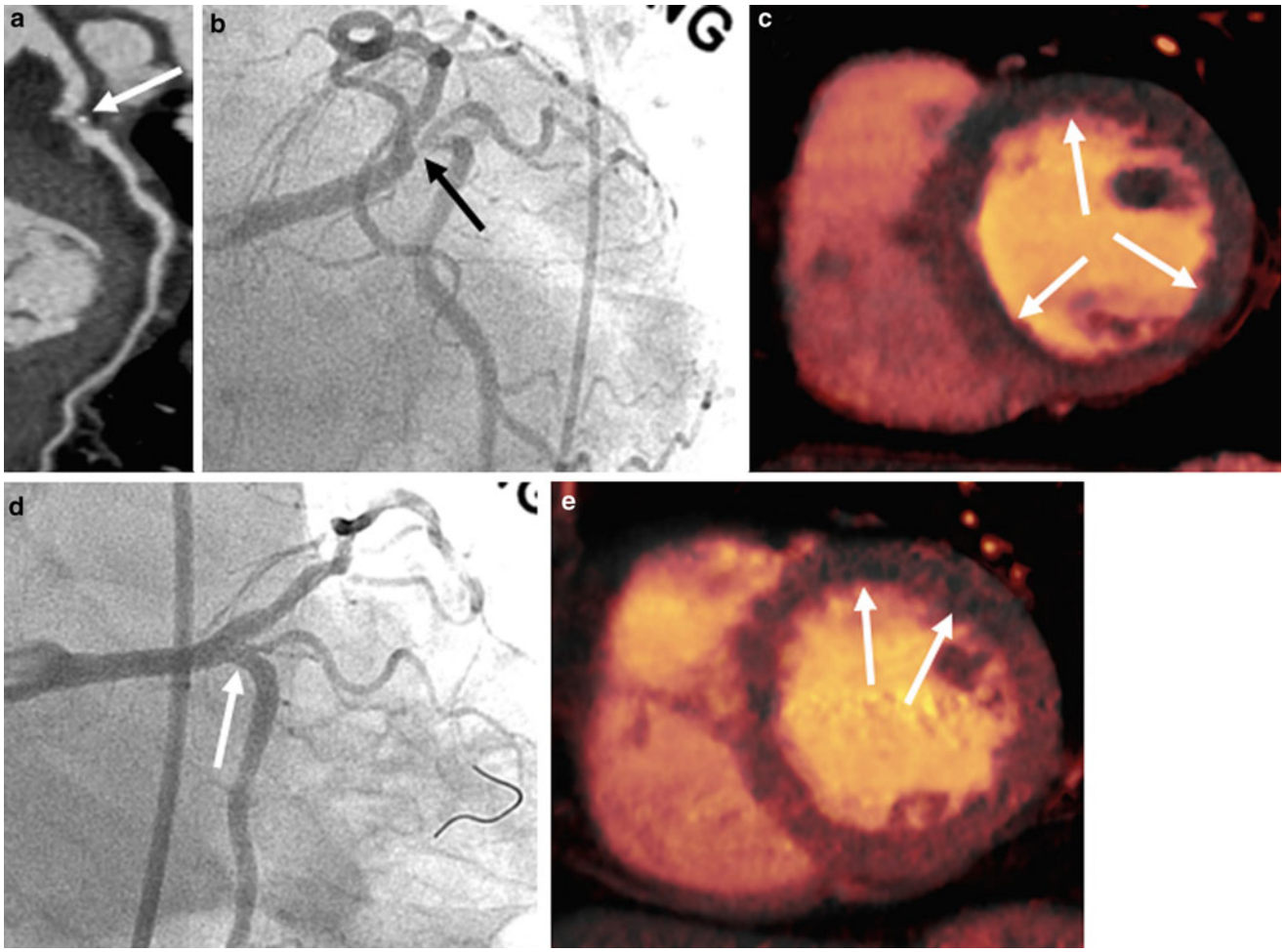

Fig. 15 Example of stress DECT perfusion for stent evaluation. Curved multiplanar reformatted coronary CT angiographic image (**a**) shows significant stenosis with mixed calcified and non-calcified plaques (*arrow*) in the ostium of the left circumflex artery (LCx). Conventional coronary angiogram finding (**b**) confirms the presence of significant stenosis (*arrow*) in LCx ostium. DECT-based iodine distribution mapping during adenosine infusion (**c**) reveals concentric blood pool deficits (*arrows*) in the mid LV myocardium. The patient underwent percutaneous coronary intervention with stent implantation in the LCx ostium. Conventional coronary angiogram (**d**) shows restoration of the expected normal lumen diameter of LCx ostium (*arrow*). DECT-based iodine distribution map during adenosine infusion (**e**) reveals disappearance of previously noted blood pool deficits in the mid lateral, inferior, and inferoseptal LV myocardium but shows persistent blood pool deficits (*arrows*) in the mid anterior LV myocardium

perfusion with administration of pharmacologic stressors is more physiologically acceptable and feasible than DECT at rest in detecting reversible myocardial ischemia because adenosine increases the difference in myocardial perfusion between the ischemic and normally perfused myocardium. The rationale that an adenosine stress DECT-based iodine distribution map might be sensitive for the detection of hemodynamically significant stenosis causing a reversible myocardial perfusion deficit is supported by the advantages of the combined application of DECT and adenosine-induced stress CT perfusion imaging (Figs. 11, 12, 13, 14, 15). The clinical evidence supporting the accuracy and feasibility of stress DECT for the assessment of myocardial perfusion deficits comes from two published single-center studies. Adenosine stress DECT perfusion was first evaluated in 41 patients with known CAD identified on CCTA, which were scheduled to undergo CCA. We demonstrated that stress DECT perfusion had a sensitivity, specificity, and accuracy of 89, 78, and 82 %, respectively, for the detection of myocardial segments with reversible perfusion deficits; adenosine stress cardiac MR perfusion, performed in 28 patients, was the gold standard for comparison. Compared with CCA, stress DECT perfusion had a sensitivity, specificity, and accuracy of 89, 78, and 82 %, respectively, for the detection of vascular territories with ischemic perfusion defects that were supplied by a vessel with ≥50 % stenosis on CCA (Ko et al. 2011). Most recently, we evaluated the incremental value of stress DECT perfusion in 45 patients

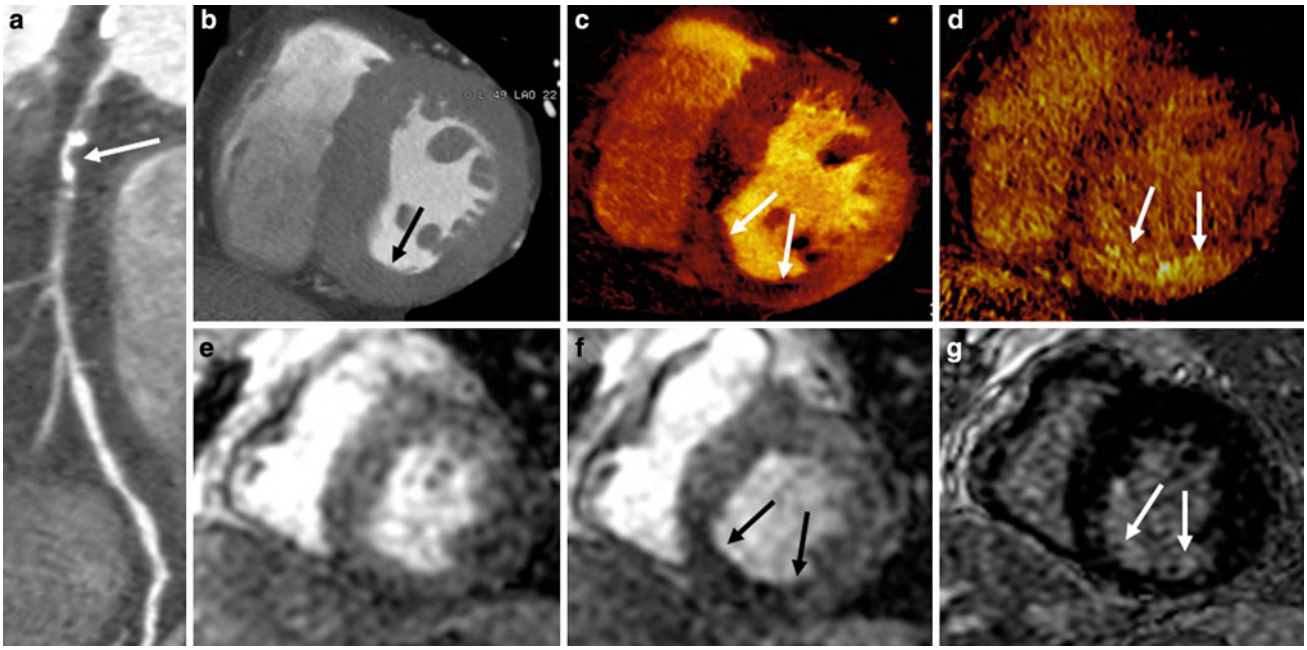

Fig. 16 Example of stress DECT perfusion identifying peri-infarct ischemia. Curved multiplanar reformatted coronary CT angiographic image (**a**) shows total occlusion with mixed calcified and non-calcified plaques (*arrow*) in the proximal segment of right coronary artery (RCA). The rest CT perfusion image (**b**) reveals thinned mid inferior left ventricular (LV) myocardium without perfusion deficit (*arrow*). DECT-based iodine distribution mapping during adenosine infusion (**c**) reveals subendocardial blood pool deficits (*arrows*) in the mid inferior and inferoseptal LV myocardium. Delayed iodine uptake (*arrows*) representing myocardial infarction is noted on delayed-phase DECT (**d**). These findings (*arrows*) are in good correlation with rest (**e**) and stress (**f**) perfusion and delayed contrast-enhanced (**g**) cardiac MR images, corresponding to old subendocardial myocardial infarction with peri-infarct ischemia at RCA territory

with known CAD, confirmed on CCTA, who were scheduled for CCA (Ko et al. 2012a). We illustrated that the stress DECT perfusion, compared with CCA, had a sensitivity of 89 %, specificity of 74 %, PPV of 80 %, and NPV of 85 % for the detection of vascular territories with myocardial perfusion defects, supplied by significant coronary stenosis. Sensitivity, specificity, positive predictive value, and negative predictive value of the CCTA on a per-vessel basis, before stress DECT perfusion, were 92, 68, 74, and 88 %, respectively, and after stress DECT perfusion were 93, 86, 88, and 91 %, respectively, for the detection of significant coronary stenoses. We demonstrated that the combination of CCTA and stress DECT perfusion had incremental diagnostic value over CCTA alone for the detection of CAD (Ko et al. 2012a). These two studies can be summarized as follows: (1) stress DECT perfusion allows good diagnostic accuracy in detecting stress-induced myocardial perfusion deficits, as seen on stress cardiac MR perfusion, (2) that stress DECT perfusion plays a complementary role to enhance the diagnostic accuracy of CCTA for detecting CAD and (3) the clinical impact and the incremental value of DECT perfusion need to be evaluated in larger cohorts and multicenter studies.

7.3 Comparison Between Rest Dual-Energy CT and Stress Dual-Energy CT Perfusion Imaging

Both rest and stress DECT perfusion use a single acquisition of volume data during the first-pass enhancement phase for the assessment of myocardial blood volume distribution. Rest DECT is focused on the morphological and functional assessment of coronary stenoses during a single cardiac examination. However, stress DECT perfusion is primarily aimed to detect myocardial perfusion abnormalities (Fig. 16). Accordingly, contrast agent injection protocol needs to be modified for stress DECT perfusion imaging, while rest DECT uses the same protocol as routine CCTA.

The clinical evidence on utilizing iodine distribution maps for the assessment of myocardial blood-pool deficits has generally demonstrated good agreement between rest DECT perfusion and SPECT findings. More importantly, rest DECT perfusion has the potential to identify myocardial segments with stress induced ischemia, seen on SPECT. Accordingly, rest DECT has been considered to be a revolutionary tool for myocardial perfusion imaging, particularly in light of its utility for the detection of myocardial

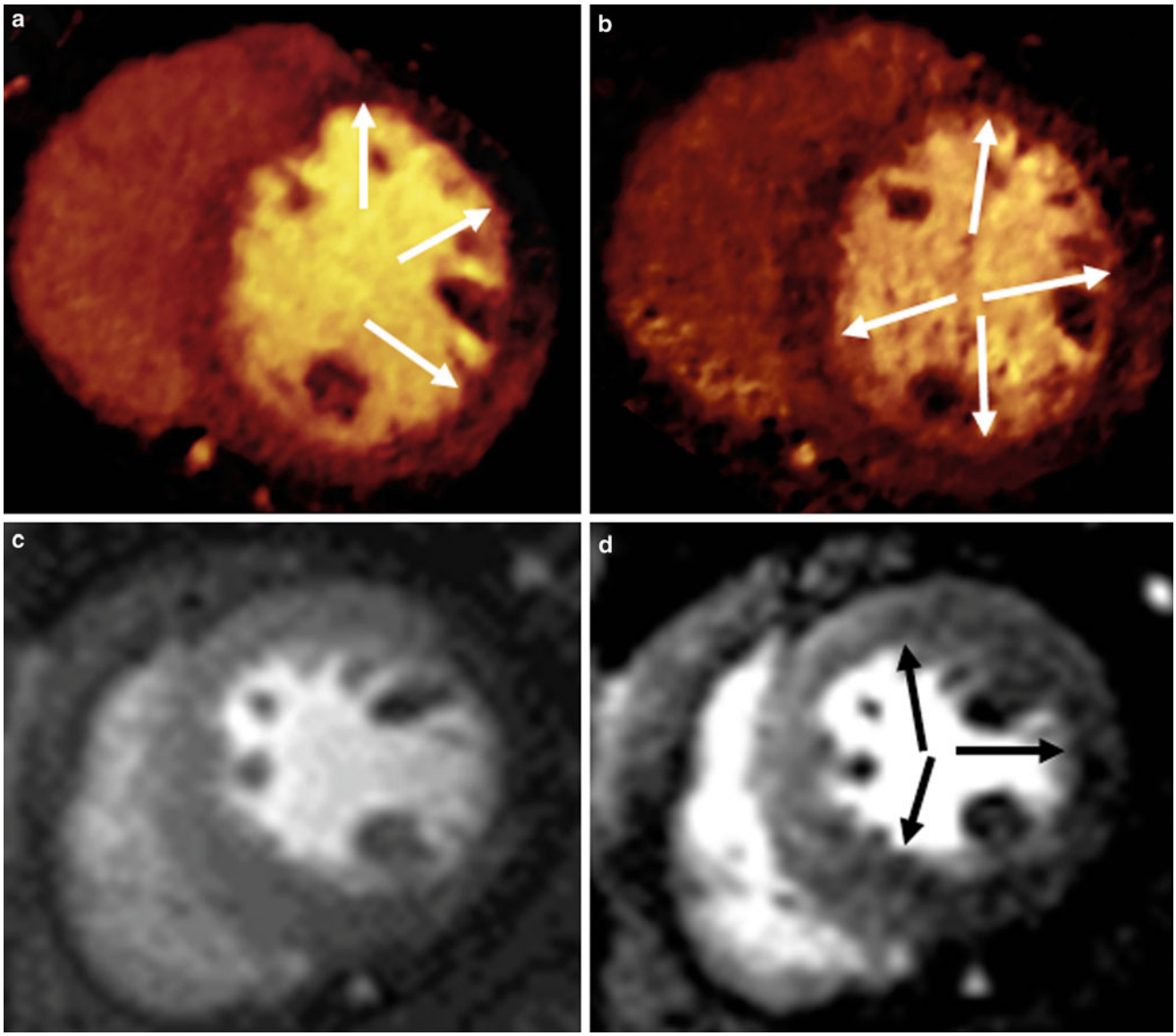

Fig. 17 Example of the superiority of stress DECT perfusion imaging when compared to rest DECT perfusion imaging identifying reversible perfusion defects. DECT-based iodine distribution maps at rest (**a**) shows blood pool deficits (*arrows*) in the mid anteroseptal, anterior, and lateral left ventricular (LV) myocardium. Stress DECT iodine distribution map (**b**) shows blood pool deficits (*arrows*) in the mid anterior, lateral, inferoseptal, and inferior LV myocardium. Rest (**c**) and stress (**d**) cardiac MR perfusion images reveal reversible perfusion defects (*arrows*) in the mid anterior, lateral, inferoseptal, and inferior LV myocardium. Conventional coronary angiogram (not shown) reveals significant stenoses in the ostium of the left anterior descending coronary artery, first diagonal branch, first obtuse marginal branch, posterior descending coronary artery, and the posterolateral branch. Stress DECT perfusion is more sensitive for the detection of reversible myocardial blood pool deficits, than rest DECT perfusion

ischemia without the need for pharmacologic vasodilator agents. The combination of morphologic imaging of coronary arteries and functional imaging of myocardial perfusion may be a powerful non-invasive imaging method that provides comprehensive information, for CAD diagnosis and treatment planning. However, only a few studies are available to date and these have typically included too few patients. In addition, there has been a tendency for selection bias due to the specific recruitment of patients with abnormal SPECT results, which leads to the overoptimistic assessment and false positives of rest DECT perfusion results. In addition, the mechanism of rest DECT perfusion for the detection of subtle differences in myocardial perfusion without the administration of a pharmacologic stressor needs to be more systematically investigated for clinical applications. Stress DECT perfusion might be more sensitive for the detection of myocardial blood pool deficits, especially reversible perfusion deficits, than rest DECT

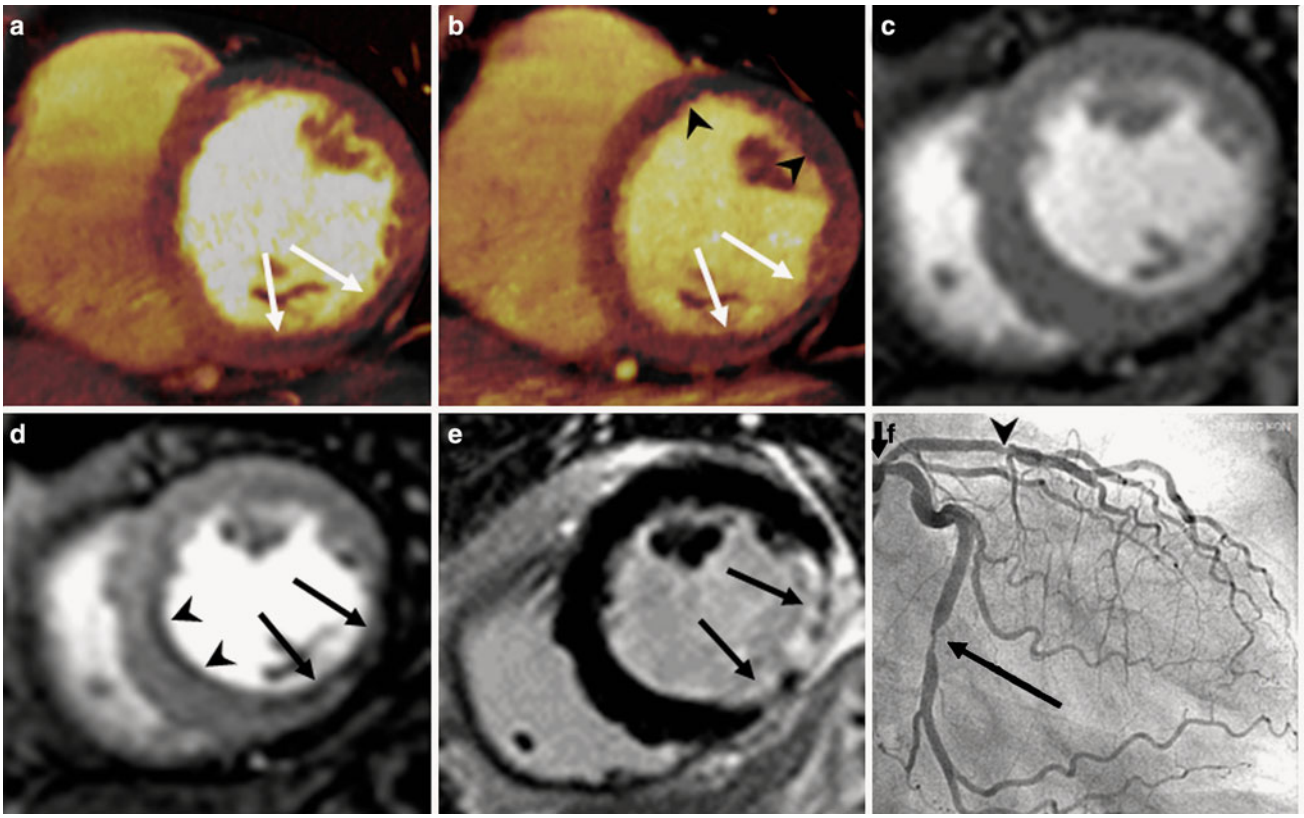

Fig. 18 Example of correlation among rest and stress DECT perfusion and cardiac MR. DECT-based iodine distribution maps at rest (**a**) and stress (**b**) show blood pool deficits (*arrows*) in the thinned mid inferolateral and inferior left ventricular (LV) myocardium. Rest (**c**) and stress (**d**) cardiac MR perfusion images reveal partially reversible subendocardial perfusion defects (*arrows*) at the corresponding left circumflex artery (LCx) territory. Delayed-phase cardiac MR image (**e**) shows delayed transmural hyperenhancement (*arrows*) in the corresponding myocardium. Stress DECT iodine distribution map (**b**) reveals stress-induced blood pool deficits (*arrowheads*) in the mid anterior and anteroseptal LV myocardium. Reversible perfusion defect (*arrowhead*) is only noted in the mid anteroseptum of LV myocardium on rest (**c**) and stress (**d**) cardiac MR perfusion images. Conventional coronary angiogram (**f**) shows significant stenoses in the ostium (*short arrow*) and proximal segment (*arrowhead*) of the left anterior descending coronary artery and distal LCx (*long arrow*)

perfusion. Furthermore, stress DECT perfusion may be better at detecting small areas of myocardial ischemia and balanced myocardial ischemia in multivessel disease or microvascular disease, compared to rest DECT perfusion and SPECT (Figs. 14, 17). Although the results of clinical trials using stress DECT perfusion are promising, the published studies come from a single center and have included a limited number of patients. In addition, stress DECT perfusion is rather susceptible to cardiac motion artifacts, which degrade image quality and affect diagnostic accuracy for the detection of myocardial ischemia. Given the temporal resolution of 280 or 330 ms associated with the dual-source DECT, it is not feasible to accurately identify coronary stenoses with stress DECT. Thus, prospective studies with a direct comparison of rest DECT and stress DECT in the same patient are needed to systematically determine the exact performance of rest DECT and stress DECT, compared with the clinical reference standards, such as adenosine stress cardiac MR perfusion, SPECT or FFR. (Fig. 18)

8 Challenges, Pitfalls, and Limitations of Dual-Energy CT Perfusion

8.1 Radiation Dose

Patient's exposure to ionizing radiation is a major concern in DECT perfusion. Recent studies have demonstrated that rest DECT can be performed with radiation doses similar to the single-energy CCTA (mean of 12 mSv), using the conversion coefficient of 0.014 $mSv \bullet mGy^{-1}\ cm^{-1}$ (Ruzsics et al. 2008, 2009; Wang et al. 2011; Hausleiter et al. 2009). DECT scans routinely rely on ECG-dependent tube current modulation, but cannot use prospective ECG-triggering or high-pitch factor ECG-synchronized spiral mode like single-energy CCTA or stress CT perfusion due to limitations of the contemporary dual-source CT in dual-voltage mode. However, rest DECT has significantly lower radiation dose compared with the combination of CCTA or CCA and SPECT. The average stress DECT perfusion effective

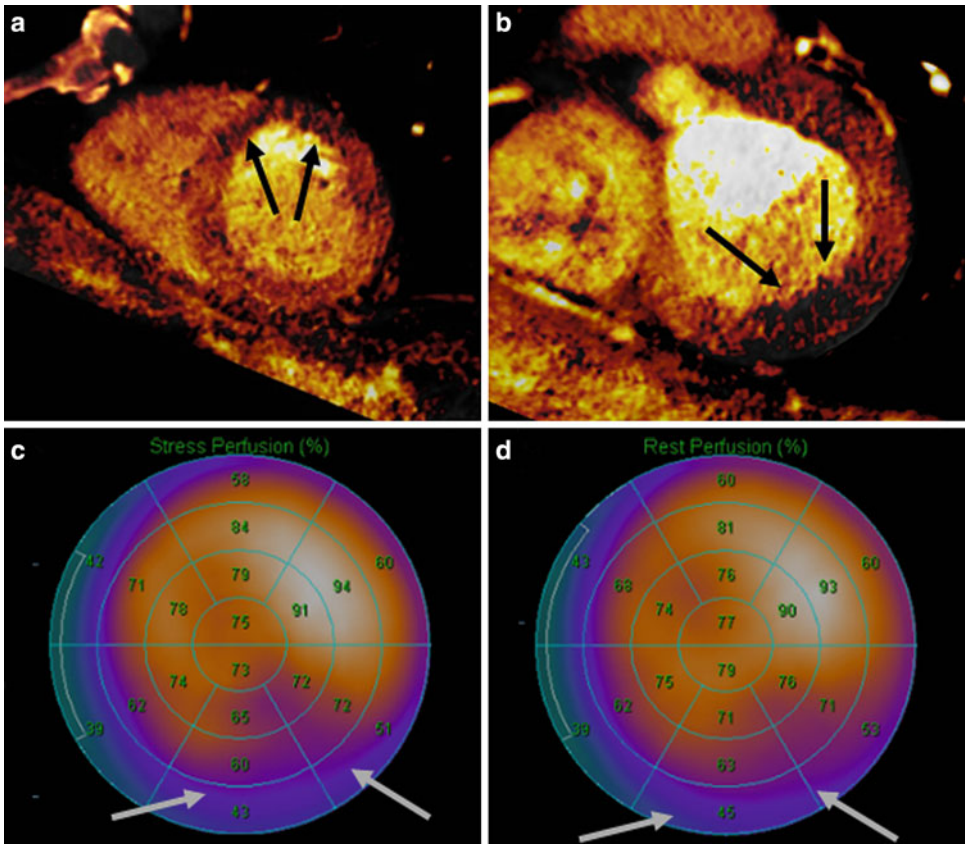

Fig. 19 Beam-hardening artifacts. Rest DECT iodine distribution maps (**a**, **b**) show blood pool deficits (*arrows*) in the apical anterior and septal (**a**) and basal inferolateral left ventricular (LV) myocardium (**b**). These lesions are not seen in the myocardial perfusion SPECT at stress (**c**) and rest (**d**). Fixed perfusion defects (*arrows*) seen on SPECT (**c**, **d**) are probably associated with attenuation artifacts in the basal inferior and inferolateral LV myocardium

radiation dose using 80/140 kV (5.8 mSv) was lower than that of single-energy CT perfusion (9.5 mSv) and SPECT under stress (9.2 mSv) in the recent study (Blankstein et al. 2009). The average effective radiation exposure for combined protocol of retrospective CCTA and stress DECT perfusion (14.5 mSv) was comparable with or even higher than combined single-energy prospective CCTA rest/stress CT protocol (12 mSv) and rest/stress SPECT (13 mSv) (Ko et al. 2011, 2012a; Blankstein et al. 2009). However, prospective ECG-gating permits radiation dose reductions for routine CCTA, allowing combined prospective CCTA/stress DECT perfusion to be performed with radiation doses comparable to or lower than rest/stress SPECT and combined single-energy CCTA/stress CT perfusion. Accordingly, stress DECT perfusion has the potential to become an attractive alternative to standard SPECT for the detection of myocardial ischemia, considering its relatively low radiation exposure, simple study protocol, short examination time, and high spatial resolution.

8.2 Artifacts

The recognition of differences in iodine concentration between ischemic myocardium and normally perfused myocardium is crucial in DECT perfusion. An iodine distribution map contains a very broad range of iodine concentrations within the myocardium (normal variation in CT attenuation in different myocardial areas) and may be compromised by artifacts, such as beam hardening, cardiac motion, reconstruction, and misalignment. Normal LV myocardial enhancement, using a 320-slice MDCT coronary angiography, demonstrated that the lateral wall had significantly lower HU values when compared with the anterior, septal, and inferior walls in healthy patients without identified CAD (Crossett et al. 2011). Therefore, normal non-uniform attenuation values within the LV myocardium may be misinterpreted as perfusion defects on CT perfusion. Beam-hardening artifacts are commonly noted in CT perfusion and create focal areas of hypoattenuation in the myocardium, mainly seen in the LV basal inferior, apical anterior, and apical inferior walls (Figs. 19, 20). Beam hardening is caused by the selective absorption of low-energy photons by bony structures (spine, sternum, ribs), the contrast filled LV cavity, or the descending thoracic aorta (Rodriguez-Granillo et al. 2010; Mehra et al. 2011). DECT perfusion is prone to cardiac motion artifacts, particularly with the elevated heart rates required for the stress phase acquisition. In dual-energy mode, temporal resolution of dual-source CT is reduced, preventing freezing of cardiac motion as would be possible in single-energy mode, and thereby causing heart motion artifacts in DECT-

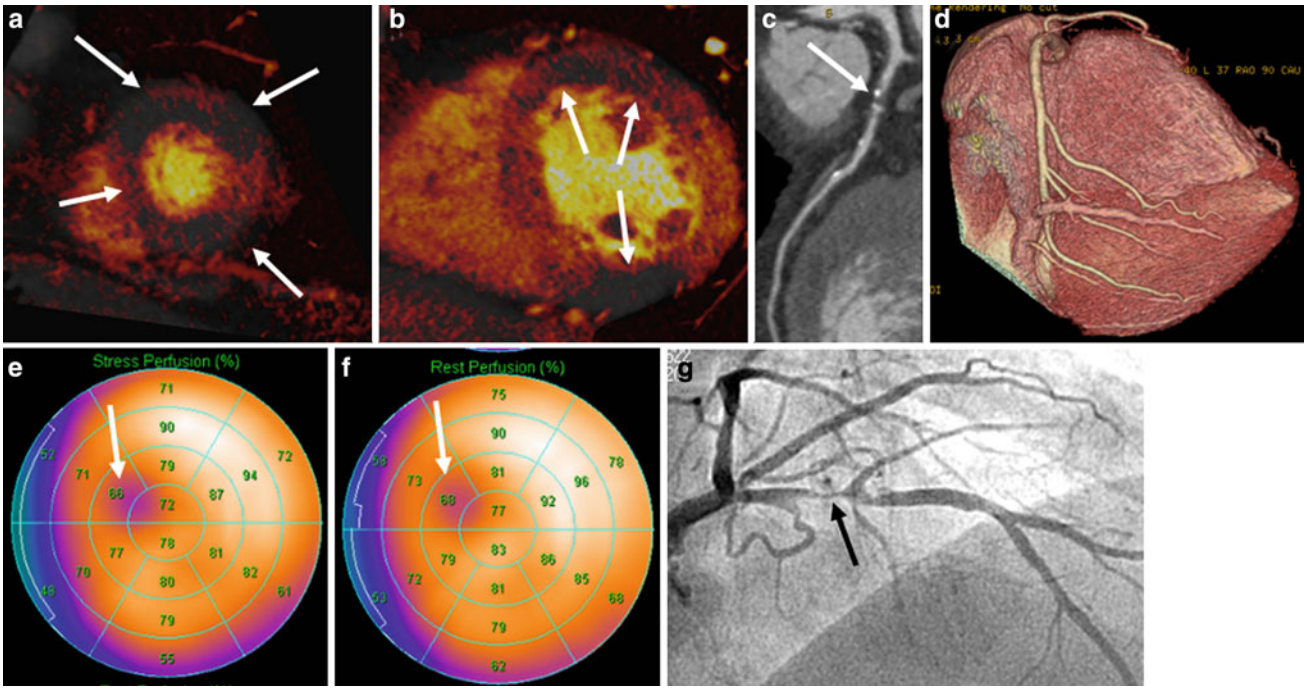

Fig. 20 Example of true and false positive rest DECT perfusion. DECT-based iodine distribution maps at rest (**a**, **b**) reveal blood pool deficits (*arrows*) in the apical to mid anterior and inferior and apical septum of left ventricular (LV) myocardium, corresponding to significant stenoses in the left anterior descending coronary artery (LAD) and the right coronary artery (RCA). Curved multiplanar reformatted coronary CT angiographic image (**c**) shows severe stenosis with mixed calcified and non-calcified plaques (*arrow*) in the proximal segment of LAD. Three-dimensional volume-rendered reconstruction image (**d**) reveals right coronary dominance without stenoses in RCA branches. Myocardial perfusion SPECT at stress (**e**) and rest (**f**) show fixed perfusion defect (*arrows*) in the apical anteroseptum of LV myocardium. Conventional coronary angiogram (**g**) confirms the presence of severe stenosis in the proximal LAD (*arrow*). The false positive finding of DECT in the apical to mid inferior LV wall is related to the beam-hardening artifact

based myocardial iodine distribution maps (Ko et al. 2011, 2012a). Cardiac motion artifacts cause hypoenhanced or hyperenhanced areas that can mimic or mask perfusion defects (Fig. 21). Accordingly, stress DECT perfusion is not preferred in patients with high or irregular heart rates.

Multiphase evaluation helps to differentiate a true perfusion defect, an area of hypoattenuation that persists through all cardiac phases, from a cardiac motion artifact, which often disappears or changes location. Cone-beam artifact is the most common reconstruction artifact and presents as hypo- and hyperattenuation bands that most often affect the LV inferior wall. These artificial bands continue outside the cardiac silhouette across the entire field of view and can be differentiated from true perfusion defects, which are confined to the cardiac silhouette. Misalignment artifacts are based on the limited scan coverage of the dual-source DECT scanner, requiring the heart to be imaged over several heart beats. The temporal difference or non-uniformity in the cardiac position in any given heart beat gives rise to relative attenuation differences between the LV anterior and inferior walls (Mehra et al. 2011).

9 Summary and Conclusion

Contrast-enhanced rest DECT perfusion enables the evaluation of changes in the status of the myocardial blood supply. The rest DECT iodine distribution map makes hypoperfused myocardial areas more conspicuous and permits the identification of areas of reversible myocardial ischemia when compared with stress DECT results. Therefore, rest DECT has expanded the clinical application of MDCT as a "one-stop shop" imaging modality to identify both CAD and myocardial blood pool deficits in a single examination. Stress DECT perfusion has the potential to become a robust clinical tool for the detection of myocardial ischemia. The combined approach of CCTA and stress DECT perfusion allows identification of hemodynamically significant coronary lesions in high-risk patients with a large calcified plaque burden or stents, and thereby, provides useful information in assessing the need for CCA and revascularization procedures (Fig. 22). The radiation exposure for stress DECT perfusion is lower than stress

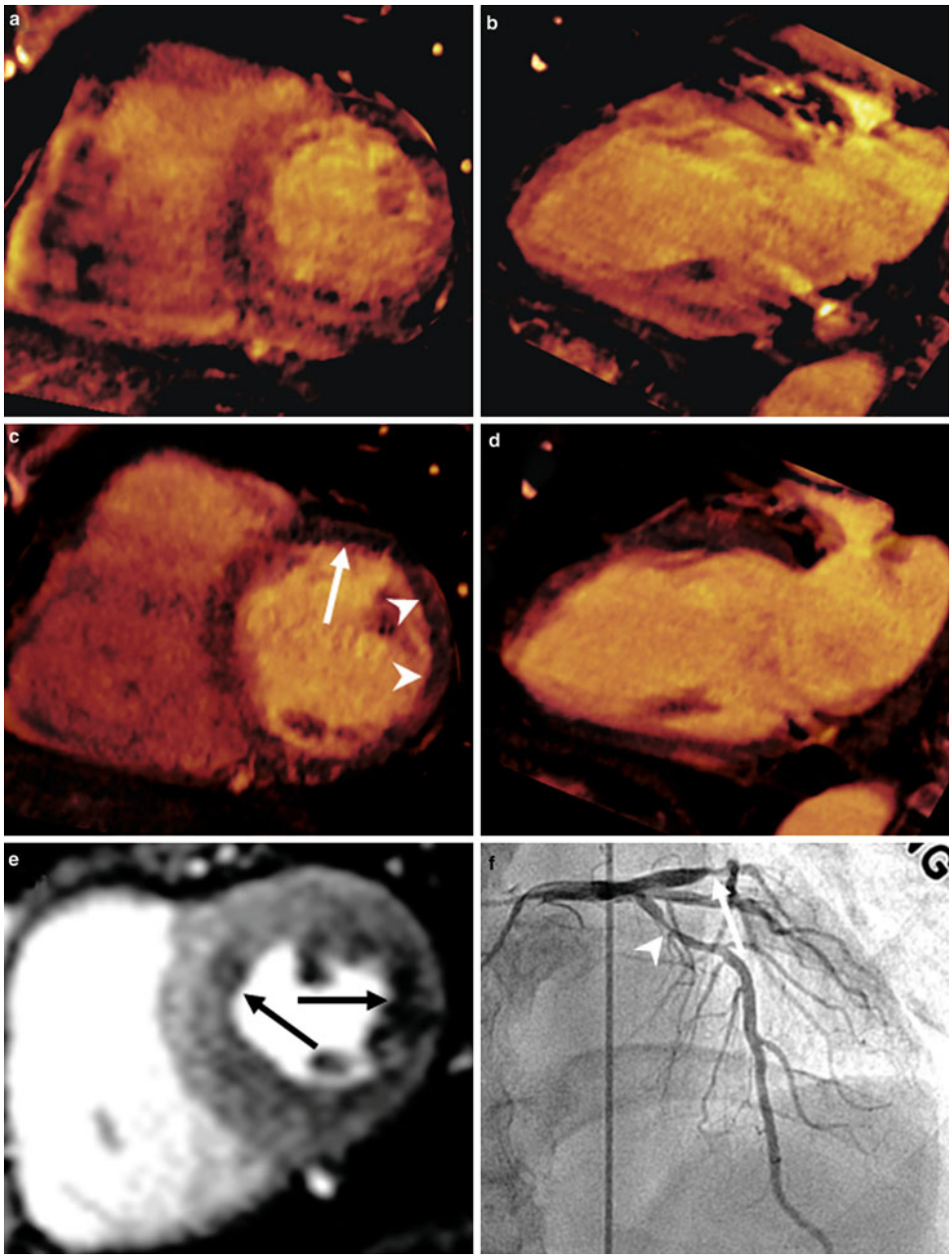

Fig. 21 Cardiac motion artifacts. Cardiac motion during image acquisition distorts the image and creates bands that appear to have reduced iodine uptake, possibly mimicking or masking myocardial blood pool deficits. Short axis (**a**) and two-chamber (**b**) views of stress DECT iodine distribution maps reveal severe cardiac motion artifacts due to a high heart rate (mean heart rate of 88 beats per minute), leading to inability to assess perfusion abnormalities. Short axis (**c**) and two-chamber (**d**) views of rest DECT iodine distribution maps show band-like blood pool deficits (*arrow*) in the mid anterior left ventricular (LV) myocardium, corresponding to cardiac motion artifact due to a heart rate of 78 beats per minute. Subendocardial blood pool deficit (*arrowheads*) is noted in the mid anterolateral LV myocardium on rest DECT iodine distribution map (**c**). Stress cardiac MR perfusion image (**e**) reveals stress-induced perfusion defects (*arrows*) in the mid-anteroseptal and mid-lateral LV myocardium. Conventional coronary angiogram (**f**) shows significant stenoses in the proximal segment of the left anterior descending coronary artery (*arrow*) and the left circumflex artery (*arrowhead*)

SPECT. Despite these promising results, however, stress DECT perfusion imaging is relatively less well known and less performed than a single-energy stress CT perfusion imaging. At present, most clinical data on DECT perfusion imaging are based on small diagnostic, single-center studies. Cardiac motion artifacts and beam hardening artifacts are major causes of false positive results when evaluating DECT-based myocardial iodine distribution maps for the detection of perfusion abnormalities. Diagnostic performance of rest DECT perfusion imaging needs to be validated with a direct comparison between the rest DECT and stress DECT perfusion by using adequate gold standards, such as stress cardiac MR perfusion. Stress DECT perfusion requires technological advances and optimized acquisition and reconstruction protocols to enhance the diagnostic accuracy of CT perfusion with reduced radiation exposure to patients. In addition, the clinical impact and the incremental value of DECT perfusion need to be further evaluated in larger cohorts and multicenter studies. These efforts can promote the use of DECT perfusion in clinical practice. In conclusion, DECT of the heart is the promising complementary perfusion imaging technique in the diagnosis of CAD and has the potential to provide a new paradigm to the non-invasive assessment of CAD (Fig. 22).

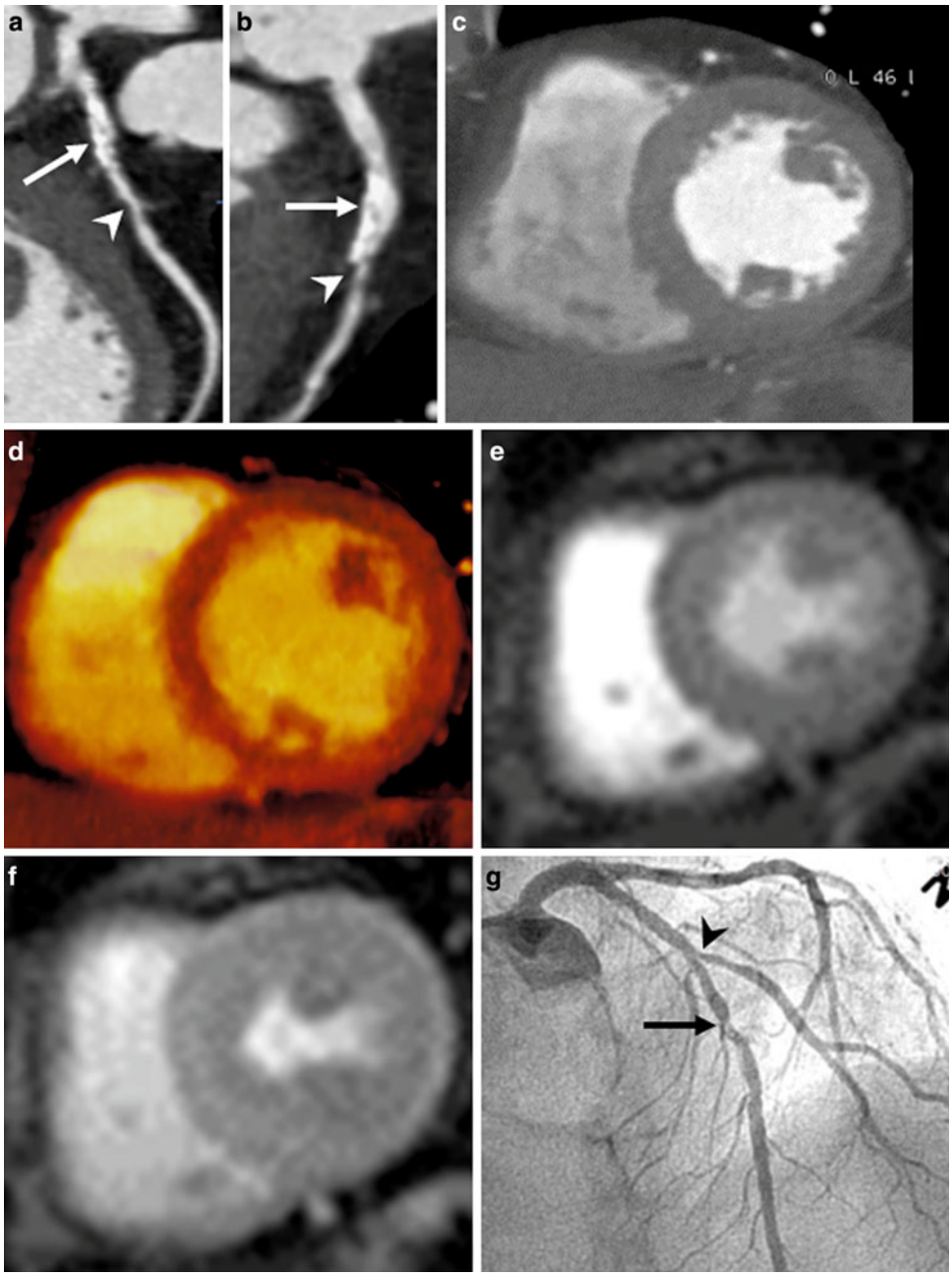

Fig. 22 Combined approach of coronary CT angiography and stress DECT perfusion. Curved multiplanar reformatted coronary CT angiographic images (**a**, **b**) show heavily calcified plaque (*arrows*) in the proximal segment of the left anterior descending coronary artery (LAD) and significant stenoses (*arrowheads*) with non-calcified plaque in the middle LAD (**a**) and first diagonal branch (D1, **b**). Rest CT perfusion image (**c**) and stress dual-energy CT-based iodine distribution map (**d**) does not show blood pool deficits in the left ventricular (LV) myocardium. Rest (**e**) and stress (**f**) cardiac MR perfusion images confirm no stress inducible perfusion defects in the LV myocardium. Conventional coronary angiogram finding (**g**) confirms the presence of significant (75 % lumen reduction) stenosis in the ostium of D1 (*arrowhead*) and insignificant stenoses in proximal and middle LAD (*arrow*). The patient did not undergo percutaneous coronary intervention treatment for D1 stenosis because of the results of the DECT and cardiac MR perfusion studies

Acknowledgments The author sincerely thanks Dr. Meong Gun Song, Department of Thoracic Surgery at Konkuk University Medical Center, Dr. Tae-Hwan Lim, Department of Radiology at Asan Medical Center, Dr. Bernhard Krauss, Jungmin Hwang, and the CT technologists and the Radiology Department nursing staff at Konkuk University Medical Center.

References

Arnoldi E, Lee YS, Ruzsics B et al (2011) CT detection of myocardial blood volume deficits: dual-energy CT compared with single-energy CT spectra. J Cardiovasc Comput Tomogr 5:421–429

Bamberg F, Becker A, Schwarz F et al (2011) Detection of hemodynamically significant coronary artery stenosis: incremental diagnostic value of dynamic CT-based myocardial perfusion imaging. Radiology 260:689–698

Blankstein R, Shturman LD, Rogers IS et al (2009) Adenosine-induced stress myocardial perfusion imaging using dual-source cardiac computed tomography. J Am Coll Cardiol 54:1072–1084

Chandrasekar B, Doucet S, Bilodeau L et al (2001) Complications of cardiac catheterization in the current era: a single-center experience. Catheter Cardiovasc Interv 52:289–295

Chiro GD, Brooks RA, Kessler RM et al (1979) Tissue signatures with dual-energy computed tomography. Radiology 131:521–523

Crossett MP, Schneider-Kolsky M, Troupis J (2011) Normal perfusion of the left ventricular myocardium using 320 MDCT. J Cardiovasc Comput Tomogr 5:406–411

Flohr TG, McCollough C, Bruder H et al (2006) First performance evaluation of a dual source CT (DSCT) system. Eur Radiol 16:256–268

Gaemperli O, Schepis T, Valenta I et al (2007) Cardiac image fusion from stand-alone SPECT and CT: clinical experience. J Nucl Med 48:696–703

Gaemperli O, Schepis T, Valenta I et al (2008) Functionally relevant coronary artery disease: comparison of 64-section CT angiography with myocardial perfusion SPECT. Radiology 248:414–423

George RT, Silva C, Cordeiro MA et al (2006) Multidetector computed tomography myocardial perfusion imaging during adenosine stress. J Am Coll Cardiol 48:153–160

George RT, Jerosch-Herold M, Silva C et al (2007) Quantification of myocardial perfusion using dynamic 64-detector computed tomography. Invest Radiol 42:815–822

Hachamovitch R, Berman DS, Kiat H et al (1996) Exercise myocardial perfusion SPECT in patients without known coronary artery disease: incremental prognostic value and use in risk stratification. Circulation 93:905–914

Hausleiter J, Meyer T, Hermann F et al (2009) Estimated radiation dose associated with cardiac CT angiography. JAMA 301:500–507

Heller GV, Calnon D, Dorbala S (2009) Recent advances in cardiac PET and PET/CT myocardial perfusion imaging. J Nucl Cardiol 16:962–969

Johnson TR, Krauss B, Sedlmair M et al (2007) Material differentiation by dual energy CT: initial experience. Eur Radiol 17:1510–1517

Kang DK, Schoepf UJ, Bastarrika G, Nance JW, Abro JA, Ruzsics B (2010) Dual-energy computed tomography for integrative imaging of coronary artery disease: principles and clinical applications. Semin Ultrasound CT MRI 31:276–291

Ko SM, Choi JW, Song MG et al (2011) Myocardial perfusion imaging using adenosine-induced stress dual-energy computed tomography of the heart: comparison with cardiac magnetic resonance imaging and conventional coronary angiography. Eur Radiol 21:26–35

Ko SM, Choi JW, Hwang HK et al (2012a) Diagnostic performance of combined noninvasive anatomic and functional assessment with dual-source CT and adenosine-induced stress dual-energy CT for detection of significant coronary stenosis. Am J Roentgenol 98:512–520

Ko BS, Cameron JD, Meredith IT et al (2012b) Computed tomography stress myocardial perfusion imaging in patients considered for revascularization: a comparison with fractional flow reserve. Eur Heart J 33:67–77

Mehra V, Valdiviezo C, Arbab-zadeh A et al (2011) A stepwise approach to the visual interpretation of CT-based myocardial perfusion. J Cardiovasc Comput Tomogr 5:357–369

Meijboom WB, van Mieghem CA, van Pelt N et al (2008) Comprehensive assessment of coronary artery stenoses. Computed tomography coronary angiography versus conventional coronary angiography and correlation with fractional flow reserve in patients with stable angina. J Am Coll Cardiol 52:636–643

Millner MR, McDavid WD, Waggener RG, Dennis MJ, Payne WH, Sank VJ (1979) Extraction of information from CT scans at different energies. Med Phys 6:70–71

Mühlenbruch G, Seyfarth T, Soo CS, Pregalathan N, Mahnken AH (2007) Diagnostic value of 64-slice multi-detector row cardiac CTA in symptomatic patients. Eur Radiol 17:603–609

Nandalur KR, Dwamena BA, Choudhri AF, Nandalur MR, Carlos RC (2007) Diagnostic performance of stress cardiac magnetic resonance imaging in the detection of coronary artery disease: a meta-analysis. J Am Coll Cardiol 50:1343–1353

Petersilka M, Bruder H, Krauss B, Stierstorfer K, Flohr TG (2008) Technical principles of dual source CT. Eur J Radiol 68:362–368

Rocha-Filho JA, Blankstein R, Shturman LD et al (2010) Incremental value of adenosine-induced stress myocardial perfusion imaging with dual-source CT at cardiac CT angiography. Radiology 254:410–419

Rodriguez-Granillo GA, Rosales MA, Degrossi E, Rodriguez AE (2010) Signal density of left ventricular myocardial segments and impact of beam hardening artifact: implications for myocardial perfusion assessment by multidetector CT coronary angiography. Int J Cardiovasc Imaging 26:345–354

Ruzsics B, Lee H, Zwerner PL, Gebregziabher M, Costello P, Schoepf UJ (2008) Dual-energy CT of the heart for diagnosing coronary artery stenosis and myocardial ischemia-initial experience. Eur Radiol 18:2414–2424

Ruzsics B, Schwarz F, Schoepf UJ et al (2009) Comparison of dual-energy computed tomography of the heart with single photon emission computed tomography for assessment of coronary artery stenosis and of the myocardial blood supply. Am J Cardiol 104:318–326

Santana CA, Garcia EV, Faber TL et al (2009) Diagnostic performance of fusion of myocardial perfusion imaging (MPI) and computed tomography coronary angiography. J Nucl Cardiol 16:201–211

Schwarz F, Ruzsics B, Schoepf UJ et al (2008) Dual-energy CT of the heart-principles and protocols. Eur J Radiol 68:423–433

Vanhoenacker PK, Heijenbrok-Kal MH, Van Heste R et al (2007) Diagnostic performance of multidetector CT angiography for assessment of coronary artery disease: meta-analysis. Radiology 244:419–428

Vlahos I, Godoy MC, Naidich DP (2010) Dual-energy computed tomography imaging of the aorta. J Thorac Imaging 25:289–300

Wang R, Yu W, Wang Y et al (2011) Incremental value of dual-energy CT to coronary CT angiography for the detection of significant coronary stenosis: comparison with quantitative coronary angiography and single photon emission computed tomography. Int J Cardiovasc Imaging 27:647–656

Watkins S, McGeoch R, Lyne J et al (2009) Validation of magnetic resonance myocardial perfusion imaging with fractional flow reserve for the detection of significant coronary heart disease. Circulation 120:2207–2213

CT Evaluation of the Myocardial Supply-Fast kV-Switching Dual-Energy CT

Donya A. Al-Hassan, Amr M. Ajlan, and Jonathon Leipsic

Contents

Abstract

Cardiovascular computed tomography (CT) has undergone significant technical developments over the past decade. The introduction of multi-detector row computed tomography (MDCT) with wider detector coverage, faster gantry rotation speed, multiple X-ray sources, electrocardiographic (ECG)-based tube current modulation, and integration of new iterative reconstruction algorithms has allowed for tangible improvements in diagnostic accuracy. Utilizing these technical advancements, recent attempts have been made to develop CT myocardial perfusion (CTP) imaging strategies. Moreover, the evaluation of myocardial perfusion defects on routine coronary CT angiography (cCTA) has been shown to be of additional value above that of assessing coronary anatomy alone, particularly in the acute chest pain setting. Unfortunately, there are many limitations that currently hinder CT perfusion with single-energy CT imaging, including artifacts. This chapter provides an overview of the role of single-source dual-energy CT in the evaluation of the myocardial perfusion and the current state of Rapid-kVp switching dual-energy CT.

1 Introduction

Coronary CT angiography (cCTA) is an established noninvasive modality that has shown a high diagnostic accuracy for the detection or exclusion of coronary artery disease (CAD) (Meijboom et al. 2008b). Although highly accurate in estimating the degree of luminal stenosis, cCTA has a limited role in determining the hemodynamic significance of detected CAD. This limitation is not surprising, as invasive coronary angiography (ICA) shares similar limitations, largely to the same degree. This unreliable relationship between anatomical stenosis and both global and lesion specific ischemia has raised concerns that the use of cCTA may

D. A. Al-Hassan (✉) · J. Leipsic
Department of Radiology, St Paul's Hospital, Vancouver, BC, Canada
e-mail: donya.alhassan@gmail.com

A. M. Ajlan
Department of Radiology, King Abdulaziz University Hospital, Jeddah, Saudi Arabia

J. Leipsic
The Division of Nuclear Medicine, Department of Radiology, Providence Health Care, University of British, Vancouver, Canada

U. J. Schoepf et al. (eds.), *CT Imaging of Myocardial Perfusion and Viability*, Medical Radiology. Diagnostic Imaging,
DOI: 10.1007/174_2012_791, © Springer-Verlag Berlin Heidelberg 2013
Published Online: 9 January 2013

encourage unnecessary ICA and coronary revascularization. Prior multicenter randomized trials have delineated the clinical and economic effectiveness of an integrated anatomic-physiologic approach to CAD by invasive methods, as compared to an anatomic approach alone. Incremental to stenosis assessment by ICA, the addition of fractional flow reserve (FFR) for physiologic determination of lesion-specific ischemia improves identification of patients who benefit from coronary revascularization by restricting revascularization to individuals with severe stenosis that specifically cause ischemia. In the Fractional Flow Reserve versus Angiography for Multicenter Evaluation (FAME) trial of patients with anatomically obstructive CAD, a combined diagnostic approach of stenosis- and ischemia-guided revascularization by ICA and FFR, respectively, was superior to stenosis-guided revascularization alone for enhancing event-free survival (Harvey and Hecht 2009; Meijboom et al. 2008a; Schuijf et al. 2011).

In addition, the FFR-guided group had shorter length of hospitalization, thereby leading to lower healthcare costs and similar or improved post-procedural quality of life (Pijls et al. 2010). On the basis of this date the ability to combine both anatomical and functional evaluation of CAD utilizing a single noninvasive modality is highly desired in clinical practice. Such noninvasive testing offers the potential to improve the selection of patients with CAD who may benefit from invasive testing and revascularization (Shaw et al. 2008; Brian et al. 2011; Pijls et al. 2010; Tonino et al. 2010).

2 Clinical Background

Cardiovascular computed tomography (CT) has undergone tremendous technical developments over the past decade. The introduction of multi-detector row computed tomography (MDCT), wider detector coverage, faster gantry rotation speed, multiple X-ray sources, electrocardiographic (ECG)-based tube current modulation, and integration of new iterative reconstruction algorithms have allowed improvements in diagnostic accuracy and have enabled progressive radiation dose reduction (Hsiao et al. 2010; Entrikin et al. 2011; Beckmann 2006; Goldman 2008). Utilizing these technical advancements, recent attempts have been made to develop CT myocardial perfusion (CTP) imaging strategies. Several single center studies have shown that CTP imaging has good diagnostic accuracy as compared to single-photon emission computed tomography (SPECT), cardiac magnetic resonance (CMR), and FFR. (Gaemperli et al. 2008; Melikian et al. 2010).

Moreover, the evaluation of myocardial perfusion defects on routine coronary CTA has been shown to be of additional value above that of assessing coronary anatomy alone, particularly in the acute chest pain setting. (Tops et al. 2008; Weininger et al. 2010). While these early results are promising, significant improvements still need to be made to overcome associated technological limitations.

3 Limitations of CTP with Single-Energy CT

Myocardial hypoperfusion manifests as an area of hypoattenuation (i.e., myocardial perfusion defect) on intravenous (IV) contrast-enhanced CT studies. Different qualitative and quantitative strategies have been used to detect areas of myocardial perfusion defects during the first-pass diffusion of contrast material into the left ventricular myocardial segments (Brian et al. 2011). Unfortunately, there are many limitations that currently hinder CT perfusion with single-energy CT imaging, including artifacts, radiation exposure, and contrast load. The most commonly encountered artifact is that of beam-hardening (Kitagawa et al. 2010). Beam hardening is inherent in single-energy CT acquisitions that produce an X-ray beam composed of photons with a wide range of energy levels (i.e., polychromatic beam). As the X-ray beam is transmitted through a high-density object, preferential absorption of lower-energy photons occurs, creating a filtered beam containing high-energy photons. This can distort myocardial Hounsfield units (HU, i.e., attenuation units), with both artificial reduction and elevation of these values being possible, depending on the path of the X-ray beam. This artifactual distortion of myocardial attenuation can act to confound CT assessment of myocardial perfusion (Kitagawa et al. 2010; Zatz and Alvarez 1977).

The issue of beam-hardening is particularly problematic in CTP imaging, as the high iodine concentration in the aorta and cardiac chambers contributes a high burden of artifact. These artifacts are most commonly identified in the apical and inferobasal left ventricular myocardial segments, where HU measurements are typically reduced Fig. 1. In addition, paradoxically increased HU measurements in the ventricular septum are commonly encountered as a result of the same phenomenon having an opposite result. These artifacts not only reduce reader confidence, but can also result in erroneous iodine quantification in dynamic CTP imaging using dual-source single-energy technology (Rodríguez-Granillo et al. 2010a; So et al. 2009).

In a recent study evaluating asymptomatic patients without history of or CT findings for obstructive CAD, beam-hardening related differences between the inferobasal myocardial segment and the reminder of the myocardium were identified in 72 % of patients, mimicking a perfusion defect (Rodríguez-Granillo et al. 2010a, b).

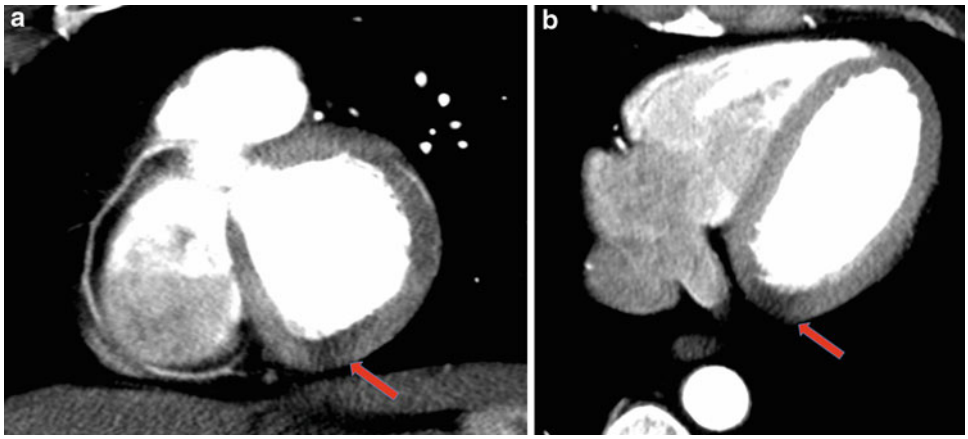

Fig. 1 A 58-year-old female patient with no prior cardiac history. Single-energy CCTA reconstructed in **a** basal two-chambers short-axis, and **b** basal four-chambers transverse axial plane. The images demonstrate transmural hypo-attenuation in the inferobasal left ventricular myocardial segment (*arrow*) consistent with beam-hardening artifact in this region in the absence of significant coronary artery disease. Normal attenuation is identified in the remaining of the myocardium

4 Technical Background of Dual-Energy technique in Myocardial perfusion

Dual-energy CT has been recently introduced into clinical practice offering the potential to help reduce these artifacts and their impact on image quality and diagnostic accuracy of CTP imaging. Currently, dual-energy CT has been commercially introduced with two separate mechanisms. One method implements a dual-source system, in which two X-ray tube-detector pairs are mounted onto the same rotating gantry at an angular offset of 90° (or 94° for the 2nd generation scanner), with one tube operating at a peak kilovoltage (kVp) of 80 or 100 kVp, and the other operating at 140 kVp (So et al. 2011; Karcaaltincaba and Aykut 2010).

A second approach has been more recently introduced, which generates single-source dual-energy X-rays based on ultrafast, submillisecond kVp switching (Ko et al. 2012; Silva et al. 2011). The fundamental basis of rapid kVp switching is the acquisition of two different tube voltages alternating on a view-by-view basis with a minimal delay between low (e.g., 80 kVp) and high (e.g., 140 kVp) projections during a single x-ray gantry rotation. This offers the potential for precise temporal registration of views, thereby minimizing the misalignment error from cardiac motion. This technique also relies on new detector and scintillator materials that have ultrafast decay times, enabling the reduction of image noise between projection views. The reduction in noise allows both high- and low-energy data sets to be acquired simultaneously for axial and helical acquisitions at the full 50 cm field of view (Chandra 2011; Wu et al. 2009).

5 Material Decomposition

In diagnostic imaging, X-ray photons interact with different tissues by two distinct mechanisms: the photoelectric effect and Compton scatter. The total attenuation of photons through a specific material is dependent on the contributions of these two effects. Depending on the tissue attenuation coefficient and the energy of the photons delivered, the relative contribution of these interactions to image generation will vary. Compton scatter predominates as the photon energy increases. On the other hand, the photoelectric interaction predominates when lower-energy photons interact with large atomic number materials such as iodine based IV contrast material. Thus, CT numbers (i.e., attenuation values, HU) will vary dramatically with high atomic number materials, whereas with soft tissues, blood and collagen, the CT numbers tend to be less variable and therefore display similar behavior at different photon energies. Recognizing different tissue atomic numbers, attenuation coefficients, and their behavior with variable photon energies, material differentiation can be achieved through spectral monochromatic photon energy (Johnson et al. 2007; Ko et al. 2012).

Owing to the tightly synchronized acquisition, dual-energy single-source/detector CT offers the potential of projection-based monochromatic imaging. To do this, the alternating 80 and 140 kVp raw data (i.e., projection views) are transformed into density (or amount) of the two selected basis materials: water and iodine (So et al. 2011), which can then be reconstructed into corresponding water and iodine images. These two materials are selected owing to their abundance in the typical imaged field of view and due to the significant differences in the way they interact with variable X-ray energy levels. From these material density images, projection-based monochromatic energy images can be generated from their linear combination (Matsumoto et al. 2011).

This process of converting the measured attenuations into density projections, reconstructing the density images, and further processing to obtain a monochromatic attenuation coefficient at any desired photon energy is known as "material decomposition", which offers the potential for material quantification and characterization and may allow for dynamic quantified myocardial perfusion Fig. 2a, b (So et al. 2012).

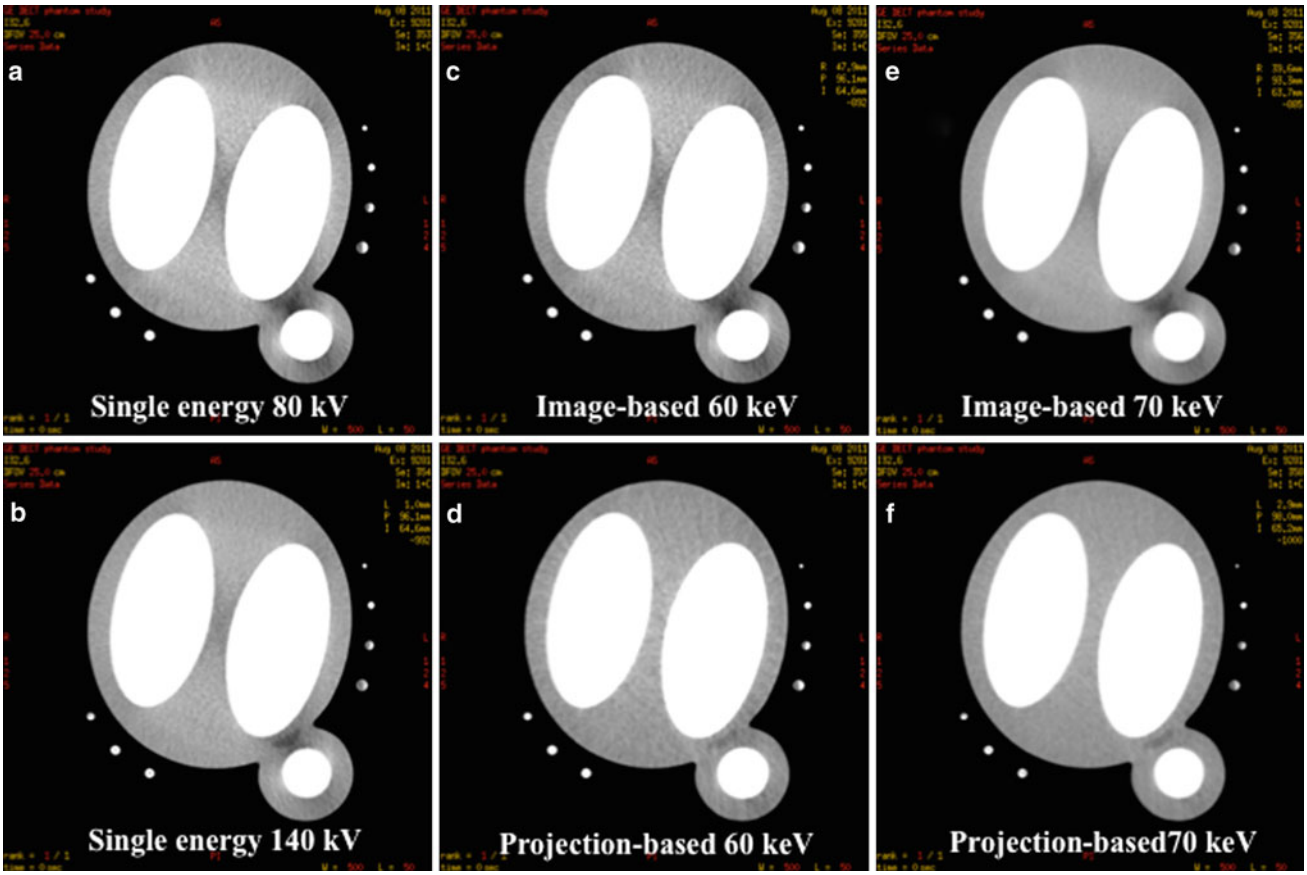

Fig. 2 Transverse axial images of a myocardial phantom consisting of two inner chambers filled with contrast representing the ventricular chambers and a contrast-filled cylinder for the aorta. **a, b** Beam-hardening artifact became evident within the myocardial area when the images of the phantom were obtained with 80 kVp single-energy CT and 140 kVp single-energy CT. **c, e** The same artifact was constant with image-based reconstructing mono energies at 60 and 70 keV. **d, f** However, the hypo-attenuation area became less evident at projection-based reconstructing mono energies of 60 and 70 keV, which show homogenous enhancement of the myocardial phantom

Importantly, these monochromatic images are reconstructed from raw projection data, which is unique to the single-source dual-energy platform. In addition, the projection-based technique applied in single-source dual-energy CT requires the 80 kVp and 140 kVp projection sets to be obtained from the same angle, which is only possible for single-source dual-energy systems (So et al. 2012).

Essentially, each monochromatic dataset is a representation of how the imaged object would appear if the X-ray source produced only monochromatic X-ray photons.

6 Iodine Mapping and Quantitative Measurement of Myocardial perfusion with Rapid kVp Switching Dual-Energy CT

Initial experiments in both phantom and animal models have shown great promise for the reduction of beam-hardening artifacts utilizing single-source rapid-kVp-switching dual-energy scanning. Additionally, there is the capacity for material density imaging from dual-energy data to quantify iodine as a surrogate for myocardial blood, facilitating quantification of myocardial perfusion. Ting Lee and colleagues recently used a myocardial phantom consisting of two inner chambers filled with contrast, representing the ventricular chambers, and a contrast-filled cylinder for the aorta to evaluate the efficacy of single-source dual-energy scanning to reduce beam-hardening artifacts Fig. 3 (So et al. 2011). Using the phantom, a region of simulated ischemic defect was placed in the basal lateral wall of the left ventricle. Both chambers and the aortic cylinder were placed in water-filled or diluted contrast-filled rings. The images were acquired with two single-energy techniques at 80 and 140 kVp using the dual-energy scan protocol with rapid kVp switching, allowing projection-based reconstruction monochromatic energy imaging.

Projection-based dual-energy CT showed significantly greater uniformity of the mean attenuation throughout the myocardium suggesting a significant reduction of

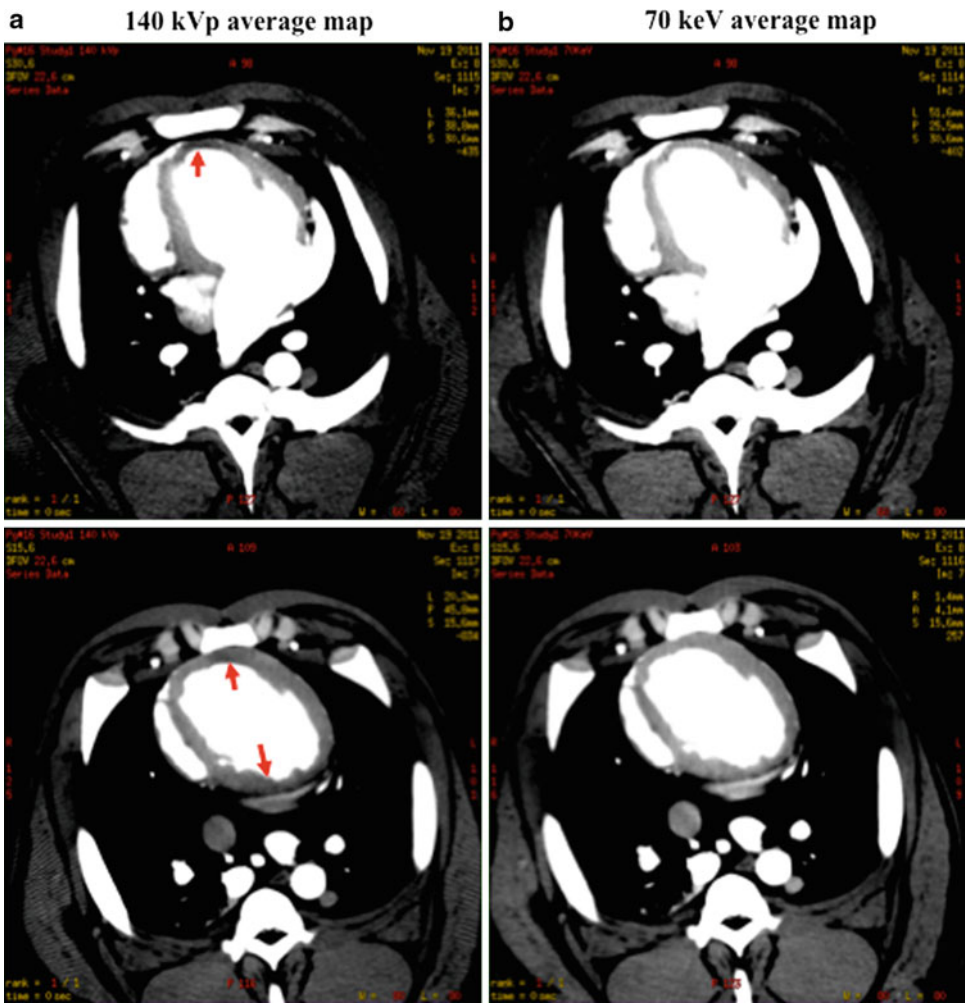

Fig. 3 Myocardial perfusion map in a nonatherosclerotic swine **a** using 140 kVp single-energy CT and **b** perfusion map of projection-based single-source dual-energy 70 keV. Note the significant reduction in beam hardening (*arrows*) at 70 keV as compared to the other reconstructions

beam-hardening. Subsequently, this same group performed similar experiments using a Gammex tissue characterization phantom then followed this experiment to determine optimal imaging parameters for iodine sensitivity detection or contrast-to-noise ratio. Rather than using a single iodine concentration, this phantom model consisted of multiple iodine-filled chambers of variable concentrations of iodine solutions. Using the same imaging techniques that were applied to the myocardial phantom, projection-based monochromatic energy imaging (i.e., 70 kilo electron volt 'keV') showed the highest sensitivity for iodine detection and also achieved the highest contrast-to-noise ratio compared to imaged-based single-energy or dual-energy techniques (So et al. 2011).

Building on this, additional studies have been performed with a porcine model, in which normal (non-ischemic) pigs were scanned and evaluated with rapid kVp switching dual-energy CT with the use of a Discovery CT750 HD scanner (GE Health care, Waukasha, WI). Two scans were performed, using 140 and 80 kVp alternating at 0.2-ms intervals, 630 mA, and 0.5-s gantry rotation period initiated at 3–4 s after IV contrast injection Fig. 4. The projection-based dual-energy 70 keV images and the corresponding 140 kVp single-energy imaging sets were then analyzed using CTP software. Myocardial average attenuation maps and corresponding aortic and myocardial time-density curve perfusion maps and values were derived and calculated across the maximal cross section of the left ventricular lateral, apical, and septal walls, as well as the aorta. Beam-hardening artifacts were greatly reduced, with the projection-based dual-energy 70 keV images resulting in uniform enhancement throughout the myocardium; this allowed more robust and accurate time-attenuation curve derivation and ultimately accurate quantification of myocardial perfusion defects.

These initial experiences suggest that projection-based monochromatic energy imaging is superior to polychromatic imaging and image-based monochromatic imaging in reducing beam-hardening and in iodine quantification.

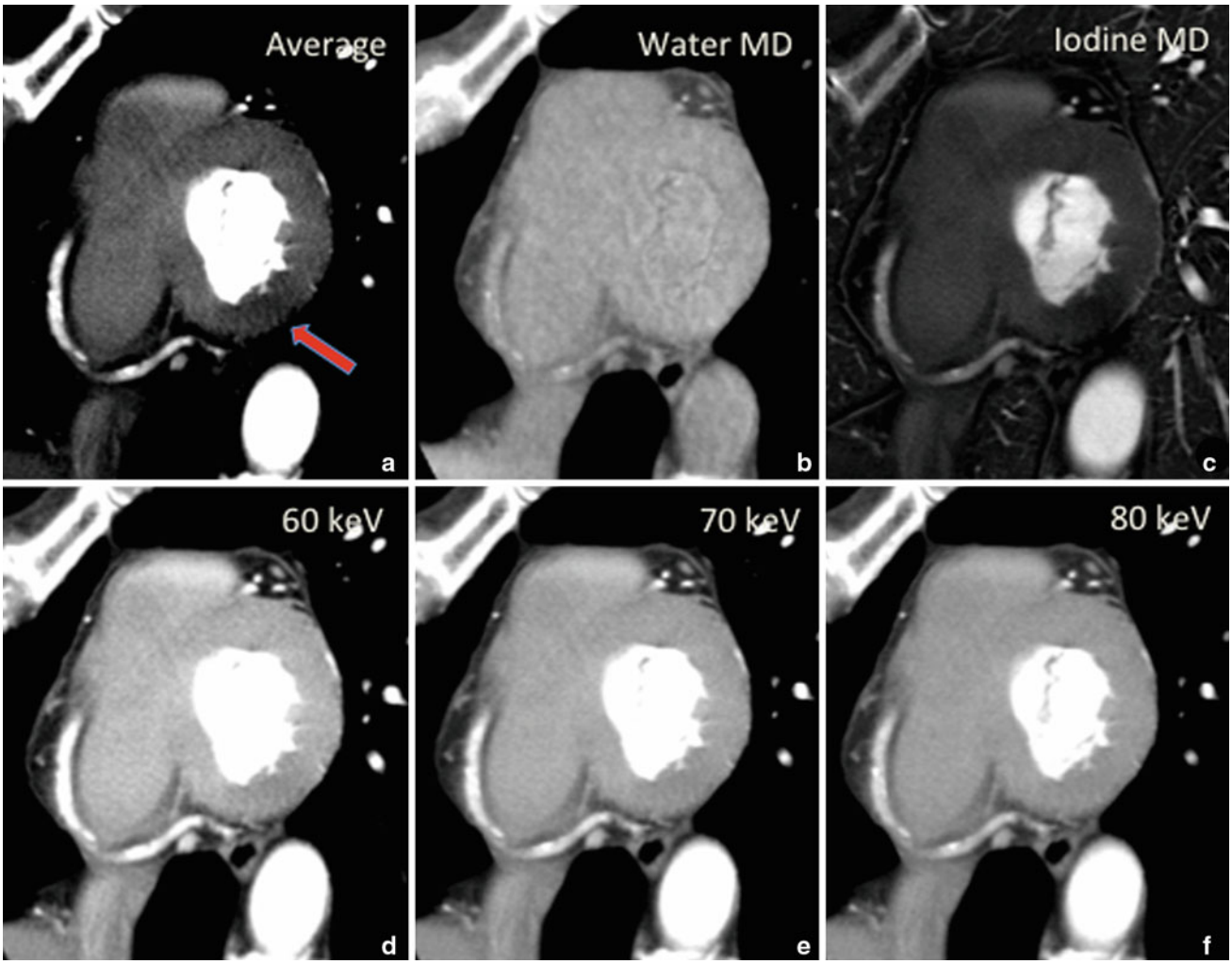

Fig. 4 A 62-year-old patient known to have hypertension, dyslipidemia, and diabetes mellitus came with atypical chest pain. Reconstructed short-axis views of the basal left ventricle, *top* row, and the corresponding images in transverse axial plane, *bottom* row **a** average map, **b** material decomposition of water, and **c** material decomposition of iodine equivalent density images. Reconstructed images obtained with **d** 60 keV, **e** 70 keV, and **f** 80 keV. The beam-hardening effect was significantly reduced in the 70 keV map

7 Early Human Experiences

Early human experiences with rapid kVp switching dual-energy CT have shown promising results. While the degree of beam-hardening reduction is not as profound as noted in the in vitro studies, there was a significant reduction observed, particularly in the basal inferior wall and the mid septum. In a matched cohort of 30 patients without obstructive CAD who underwent both a clinical single-energy coronary CTA and an experimental rapid kVp switching CT, there was 50 % reduction in beam-hardening artifact in the basal inferior wall and mid septum at 80 keV Fig. 2c, d, and e. In a larger cohort of 49 patients undergoing dual-energy CT alone, contrast-to-noise and signal-to-noise ratios were found to be optimized at 70–80 keV for the myocardium and 65 keV for coronary analysis (Leipsic et al. unpublished data). At the time of the submission of this chapter, experiences with the use of rapid kVp switching CT in the assessment of pathological perfusion cases were extremely limited, precluding any comment on the potential impact on the diagnostic accuracy of CTP imaging using such a technique.

8 Future Outlook: the Potential for Clinical Application

Single-source dual-energy CTP imaging has only recently moved beyond the phantom and animal experiment sphere and is now being utilized in patients. As stated above, initial human experiences have supported the prior data from both phantom and animal experiments, showing a reduction in beam-hardening and consistent ability to routinely quantify

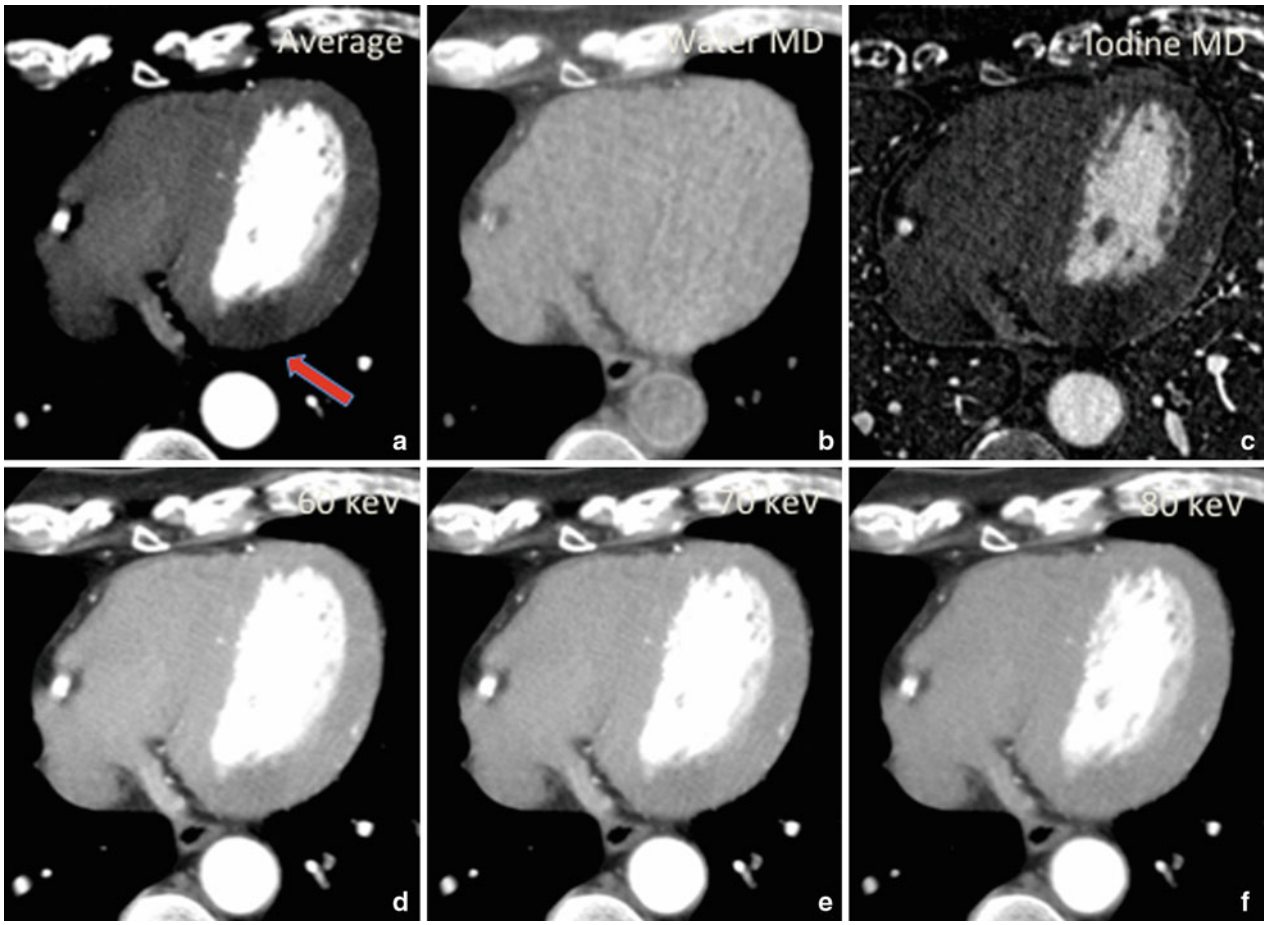

Fig. 4 continued

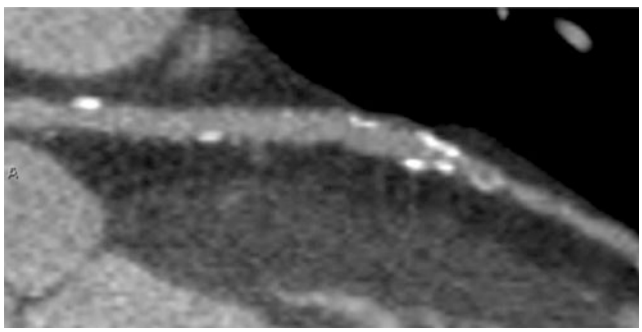

Fig. 5 Example of the application of DECT monochromatic imaging in a 63-year-old asymptomatic patient with risk factors. Separation of calcium from iodine has been demonstrated in the left main coronary artery allowing more accurate luminal assessment

iodine in the myocardium. Continued study is needed to evaluate the impact, if any, of this beam-hardening reduction on the diagnostic accuracy of CTP. Additionally, future trials are needed to investigate the potential of material decomposition to characterize and more robustly segment coronary artery plaques Fig. 5. Initial experiences suggest that projection-based monochromatic imaging might reduce partial volume averaging of calcified plaque, allowing more accurate luminal assessment in the setting of calcified plaques. However, this experience remains limited and further studies involving larger multicenter cohorts with invasive angiographic, and likely, intravascular ultrasound correlation is needed to confirm these findings.

References

Beckmann EC (2006) CT scanning the early days. Br J Radiol 79(937):5–8

Brian SK et al (2011) CT stress myocardial perfusion imaging using multidetector CT—a review. J Cardiovasc Comput Tomogr 5(6):345–356

Chandra N, Langan DA (2011) Gemstone Detector: dual energy imaging via fast kVp switching. In: Johnson T, Fink C, Schönberg SO, Reiser MF (eds) Dual energy CT in clinical practice, Medical Radiology, Springer, Heidelberg, pp 35–41, ISBN 978-3-642-01739-1. doi: 10.1007/174_2010_35, url:http://dx.doi.org/10.1007/174_2010_35

Entrikin DW, Leipsic JA, Carr JJ (2011) Optimization of radiation dose reduction in cardiac computed tomographic angiography. Cardiol Rev 19(4):163–176

Gaemperli O et al (2008) Functionally relevant coronary artery disease: comparison of 64-section CT angiography with myocardial perfusion SPECT. Radiology 248(2):414–423

Goldman LW (2008) Principles of CT: multislice CT. J Nucl Med Technol 36(2):57–68 quiz 75–76

Harvey SH (2009) Is coronary computed tomographic angiography the "gold standard" for coronary artery disease? J Cardiovasc Comput Tomogr 3(5):334–339

Hsiao EM, Rybicki FJ, Steigner M (2010) CT coronary angiography: 256-slice and 320-detector row scanners. Curr Cardiol Rep 12(1):68–75

Johnson TRC et al (2007) Material differentiation by dual energy CT: initial experience. Eur Radiol 17(6):1510–1517

Karcaaltincaba M, Aykut A (2010) Dual-energy CT revisited by multidetector CT: review of principles and clinical applications. Diagn Interv Radiol 17(3):181–194. doi:10.4261/1305-3825.DIR.3860-10.0

Kitagawa K et al (2010) Characterization and correction of beam-hardening artifacts during dynamic volume CT assessment of myocardial perfusion. Radiology 256(1):111–118

Ko JP et al (2012) Dual-energy computed tomography: concepts, performance, and thoracic applications. J Thorac Imaging 27(1):7–22

Matsumoto K et al (2011) Virtual monochromatic spectral imaging with fast kilovoltage switching: improved image quality as compared with that obtained with conventional 120-kVp CT. Radiology 259(1):257–262

Meijboom WB, Van Mieghem CAG et al (2008a) Comprehensive assessment of coronary artery stenoses. J Am Coll Cardiol 52(8):636–643

Meijboom WB, Meijs MFL et al (2008b) Diagnostic accuracy of 64-slice computed tomography coronary angiography. J Antimicrob Chemother 52(25):2135–2144

Melikian N et al (2010) Fractional flow reserve and myocardial perfusion imaging in patients with angiographic multivessel coronary artery disease. JCIN 3(3):307–314

Pijls NH, Fearon WF, Tonino PA, Siebert U, Ikeno F, Bornschein B, van't Veer M, Klauss V, Manoharan G, EngstrØm T, Oldroyd KG, Ver Lee PN, MacCarthy PA, De Bruyne B (2010) Fractional flow reserve versus angiography for guiding percutaneous coronary intervention in patients with multivessel coronary artery disease: 2-year follow-up of the FAME (Fractional Flow Reserve Versus Angiography for Multivessel Evaluation) study investigators. J Am Coll Cardiol 56(3):177–84. doi:10.1016/j.jacc.2010.04.012

Rodríguez-Granillo GA, Rosales MA, Degrossi E, Rodriguez AE (2010a) Signal density of left ventricular myocardial segments and impact of beam hardening artifact: implications for myocardial perfusion assessment by multidetector CT coronary angiography. Int J Cardiovasc Imaging 26(3):345–354

Rodríguez-Granillo GA, Ingino CA, Lylyk P (2010b) Myocardial perfusion imaging and infarct characterization using multidetector cardiac computed tomography. World J Cardiol 2(7):198–204

Schuijf JD et al (2011) Current applications and limitations of coronary computed tomography angiography in stable coronary artery disease. Heart 97(4):330–337

Shaw LJ et al (2008) Optimal medical therapy with or without percutaneous coronary intervention to reduce ischemic burden: results from the clinical outcomes utilizing revascularization and aggressive drug evaluation (COURAGE) trial nuclear substudy. Circulation 117(10):1283–1291

Silva AC et al (2011) Dual-energy (spectral) CT: applications in abdominal imaging. Radiographics 31(4):1031–1046 discussion 1047–1050

So A, Lee T-Y (2011) Quantitative myocardial CT perfusion: a pictorial review and the current state of technology development. J Cardiovasc Comput Tomogr 5(6):467–481

So A et al (2009) Beam hardening correction in CT myocardial perfusion measurement. Phys Med Biol 54(10):3031–3050

So A et al (2011) Quantitative myocardial perfusion imaging using rapid kVp switching dual energy CT: preliminary experience. J Cardiovasc Comput Tomogr 5(6):430–442

So A et al (2012) Prospectively ECG triggered rapid kV-switching dual energy CT for quantitative imaging of myocardial perfusion. JACC Cardiovasc Imaging 5(8):829–836. doi:10.1016/j.jcmg.2011.12.026

Tonino PAL et al (2010) Angiographic versus functional severity of coronary artery stenoses in the FAME study. JAC 55(25):2816–2821

Tops LF et al (2008) Noncoronary applications of cardiac multidetector row computed tomography. JACC Cardiovasc Imaging 1(1):94–106

Weininger M et al (2010) Adenosine-stress dynamic real-time myocardial perfusion CT and adenosine-stress first-pass dual-energy myocardial perfusion CT for the assessment of acute chest pain: initial results. Eur J Radiol 81(12):3703-3710. doi:10.1016/j.ejrad.2010.11.022

Wu X, Langan DA, Xu D et al (2009) Monochromatic CT image representation via fast switching dual kVp. Proc SPIE 7258:725845

Zatz LM, Alvarez RE (1977) An inaccuracy incomputed tomography: the energy dependence dependence of CT values. Radiology 124(1):91–97

Dynamic, Time-Resolved CT Imaging of Myocardial Perfusion: Dual-Source CT

Gorka Bastarrika, Lucas L. Geyer, and U. Joseph Schoepf

Contents

Abstract

A comprehensive approach to coronary artery disease (CAD) requires the assessment of the anatomy and morphology of the coronary vessels as well as collection of information regarding myocardial perfusion and vascularization. To date, despite its excellent diagnostic accuracy for detection of CAD, cardiac CT remains a purely morphological test that does not enable one to obtain reliable data on the hemodynamic significance of any given coronary artery stenosis. In regular clinical practice, hemodynamic significance is derived via nuclear medicine or cardiac magnetic resonance (CMR)-based myocardial perfusion imaging techniques or by means of the invasive estimation of the fractional flow reserve (FFR) during conventional coronary angiography. Due to technical advances, however, we may be at the beginning of a new era in cardiac CT imaging. As shown by some preliminary animal and clinical studies, second-generation DSCT-based dynamic myocardial perfusion imaging may be useful to establish the physiological significance of CAD. In this chapter, the rationale behind dynamic, time-resolved myocardial DSCT perfusion imaging is introduced, first-pass myocardial DSCT perfusion imaging protocols are proposed, and initial preclinical and clinical evidence on myocardial DSCT perfusion imaging is described. Finally, most relevant limitations of this new imaging technology are discussed.

1 Introduction

Coronary artery disease (CAD) remains the most common cause of morbidity and mortality in western countries. In the United States, the current prevalence of coronary artery

G. Bastarrika (✉)
Cardiothoracic Imaging, Department of Medical Imaging, Sunnybrook Health Sciences Centre, Toronto, ON, Canada
e-mail: gorka.bastarrika@sunnybrook.ca

L. L. Geyer
Department of Clinical Radiology, University Hospitals LMU Munich, Munich, Germany

U. J. Schoepf
Department of Radiology and Radiological Science, Medical University of South Carolina, Charleston, SC, USA

U. J. Schoepf
Division of Cardiology, Department of Medicine, Medical University of South Carolina, Charleston, SC, USA

U. J. Schoepf et al. (eds.), *CT Imaging of Myocardial Perfusion and Viability*, Medical Radiology. Diagnostic Imaging,
DOI: 10.1007/174_2012_772, © Springer-Verlag Berlin Heidelberg 2012
Published Online: 16 December 2012

disease (CAD) is estimated at 16,300,000 (7.0 %) individuals, about 7 % adults above the age of 20 (8.3 % for men and 6.1 % for women). In 2008, in the United States alone, CAD mortality was 405,309 (216,248 males and 189,061 females), of whom 133,958 adults (72,447 males and 61,511 females) died of myocardial infarction (Roger et al. 2012). Current observations point toward significant decay in cardiovascular disease mortality mainly due to substantial improvements in prevention and medical management (Rosamond et al. 2008). Undoubtedly, advances in noninvasive imaging strategies are playing a significant role in this field.

To date, conventional invasive coronary angiography remains the standard of reference for establishing coronary artery atherosclerosis and to assess the degree of CAD. In 2009, an estimated 1,072,000 cardiac catheterizations were performed for inpatients in the United States. Even if this procedure is generally safe, it was predicted that in-hospital death rate was approximately of 0.9 % (Roger et al. 2012).

In an effort to avoid unnecessary complications related to procedures performed for diagnostic purposes of CAD only, the last decade has seen exponential growth in noninvasive diagnostic imaging modalities. Among those, multidetector computed tomography (MDCT), in particular, has shown to be an attractive alternative for accurately detecting CAD. This technology has emerged as a powerful diagnostic tool that enables robust anatomical imaging of the heart and coronary vasculature. With latest scanner generations, there is increasing evidence that MDCT can replace conventional coronary angiography in various clinical settings (Taylor et al. 2010). Coronary CT angiography (cCTA) is widely used to aid in the diagnosis of CAD, particularly when other tests reveal equivocal results (Miller et al. 2008; Vanhoenacker et al. 2007; von Ballmoos et al. 2011). Moreover, the results of a number of studies have shown that coronary MDCT angiography bears independent prognostic information over conventional clinical risk factors in patients known or suspected to have CAD, particularly when no disease is detected (Min et al. 2007, 2011; Bamberg et al. 2011a). Thus, cCTA-derived information is very useful for the initial diagnosis of CAD (i.e. visualization and quantification of coronary artery plaques and stenosis) and successful planning for revascularization. The cCTA-based approach, however, may be insufficient if CAD requires complete assessment. As said, cCTA provides a restricted perspective of CAD. Proper assessment of the disease requires not only knowledge of the coronary anatomy and morphology, but also information about the status of myocardial vascularization (King et al. 2008). In fact, the latter becomes critical as myocardial perfusion itself defines the actual functional relevance of a certain coronary stenosis, represents a strong determinant for choosing the appropriate therapy, and determines a patient's prognosis (Shaw et al. 2008; Tonino et al. 2010). In regular clinical practice, the physiological significance of coronary artery stenosis is established by means of myocardial perfusion imaging (MPI) modalities during exercise-induced or pharmacologically-induced hyperemia/stress, or by estimating the fractional flow reserve (FFR) during conventional coronary angiography. Vasodilator stress can be induced with adenosine, dipyridamole, or novel selective adenosine A2A receptor agonists (regadenoson) (Buhr et al. 2008). Even if such pharmacological "stress" is not physiologically equivalent to the stress produced by physical exercise itself, it appears to have similar diagnostic and prognostic effects, as shown by nuclear MPI modalities. Single photon emission computed tomography (SPECT) is the most widely available and most extensively validated MPI modality (Hendel et al. 2009); although, due to a higher spatial resolution, cardiac magnetic resonance (CMR) imaging (Hendel et al. 2006) has demonstrated its superiority over the latter for detecting nontransmural perfusion defects (Schwitter et al. 2008). Other MPI modalities include positron emission computed tomography (PET) (Dorbala et al. 2009) and contrast-enhanced echocardiography (Arnold et al. 2010). A recent meta-analysis has shown that CMR seems to be superior for the diagnosis of obstructive CAD compared with echocardiography and SPECT, while echocardiography and SPECT demonstrate similar diagnostic performance (de Jong et al. 2012). In another meta-analysis, SPECT, CMR, and PET all yielded a high sensitivity, with the PET technique achieving the highest diagnostic performance (pooled sensitivity of 84 % and pooled specificity of 81 %). According to this study, CMR may provide an alternative to PET with similar diagnostic accuracy yet without ionizing radiation (Jaarsma et al. 2012). Finally, estimation of the FFR during conventional coronary angiography has been shown to allow depiction of ischemia-producing coronary artery lesions. Routine measurement of this parameter in patients with multivessel CAD who are undergoing percutaneous coronary intervention with drug-eluting stents has shown to significantly reduce the rate of the composite end point of death, nonfatal myocardial infarction, and repeat revascularization at 1 year (Tonino et al. 2009).

The added clinical value of CT in the context of coronary artery stenosis and MPI is undergoing vigorous investigation. Besides the context of hybrid imaging modalities (Flotats et al. 2011), CT-based approaches are gaining increasing relevance. Just from a morphological perspective, the comparison between CAD as shown by cCTA and as shown by SPECT has revealed information that is complementary. One study demonstrated that only 45 % of patients with an abnormal cCTA had abnormal MPI; in this contribution, even in patients with obstructive CAD on cCTA, 50 % still had a normal MPI, revealing that normal myocardial perfusion did not exclude the presence of coronary atherosclerosis (Schuijf et al. 2006). Moreover, the

combined noninvasive approach of cCTA and MPI has been shown to have excellent accuracy for the detection of flow-limiting coronary stenosis and may be used as a gatekeeper for conventional coronary angiography, avoiding redundant revascularization procedures (Gaemperli et al. 2009). Besides morphological imaging, the value of CT itself as standalone modality for MPI has been investigated using single-energy (George et al. 2006, 2007, 2009; Blankstein et al. 2009) and dual-energy CT techniques based on dual-source CT (DSCT) technology (Ruzsics et al. 2008, Ruzsics 2009), with promising results.

Consequently, given the fact that DSCT shall provide both morphological and anatomical information of the heart, most recent research has focused on evaluating its ability to provide a comprehensive assessment of cardiac anatomy, function, perfusion, and viability within the same examination (Bastarrika et al. 2009). The recently introduced second-generation DSCT enables real-time dynamic perfusion imaging by means of a dedicated "shuttle" mode that captures the passage of a contrast medium bolus through the myocardium. The system is equipped with two 128-section detectors that provide greater detector coverage compared with first generation DSCT (Lell et al. 2009; Leschka et al. 2009) and allow fast prospectively ECG-triggered image acquisition at two alternating table positions during contrast medium infusion (Bastarrika et al. 2010a; Bamberg et al. 2010). Animal models (Mahnken et al. 2010; Bamberg et al. 2012) and preliminary human studies (Bamberg et al. 2011b; Bastarrika et al. 2010b; Wang et al. 2012; Ho et al. 2010) have shown that first-pass myocardial perfusion with DSCT is feasible and may be a suitable tool for myocardial perfusion imaging.

2 Rationale Behind Dynamic, Time-Resolved Myocardial DSCT Perfusion Imaging

Recent developments in cardiac CT imaging have focused on the integrative assessment of CAD, including detection of coronary artery stenosis and the appraisal of its hemodynamic significance for cardiac function, perfusion, and viability (Bastarrika et al. 2009; Vliegenthart et al. 2012).

The idea of CT evaluation of myocardial perfusion with characterization of microvessel responses to vasoactive substances was originated in the era of electron beam CT (Wolfkiel et al. 1987; Bell et al. 1999; Gould et al. 1988; Lerman et al. 1999). Later, with newer generation MDCT systems, preclinical studies investigating CT image acquisition under adenosine-induced stress demonstrated the feasibility of detecting reversible ischemia and accurately measuring myocardial blood flow during first-pass contrast-enhanced CT comparable to stress nuclear MPI examinations (George et al. 2006, 2007). George et al. (2009) evaluated the transmural extent of perfusion abnormalities to predict atherosclerosis causing myocardial ischemia by adenosine stress with 64- and 256-row MDCT in patients with a history of abnormal myocardial perfusion SPECT. For the purpose of their study, they compared the combination of cCTA and myocardial CT perfusion imaging with the combination of SPECT and quantitative coronary angiography as the reference standard in the detection of obstructive atherosclerosis causing perfusion abnormalities. Authors reported sensitivity, specificity, positive and negative predictive values in the per-patient analysis as 86, 92, 92, and 85 %, respectively, and 79, 91, 75, and 92 % in the per-vessel/territory analysis. According to the authors, this study demonstrated that the combination of cCTA and CT perfusion imaging can detect atherosclerosis causing perfusion abnormalities when compared with the combination of quantitative coronary angiography and SPECT (George et al. 2009). In another study, Blankstein et al. (2009) sought to determine the feasibility of performing a comprehensive cardiac CT examination incorporating stress and rest myocardial perfusion imaging together with cCTA in 34 patients, with respect to nuclear stress test and conventional coronary angiography (Blankstein et al. 2009). In this study, on a per-vessel basis, CT perfusion alone had a sensitivity of 79 % and a specificity of 80 % for the detection of stenosis greater than 50 %, whereas SPECT MPI had a sensitivity of 67 % and a specificity of 83 %. For the detection of vessels with 50 % or greater stenosis and a corresponding SPECT perfusion abnormality, CT perfusion had a sensitivity of 93 % and a specificity of 74 %. According to these authors, adenosine stress CT can identify stress-induced myocardial perfusion defects with diagnostic accuracy comparable to SPECT and with the advantage of providing information on coronary stenosis (Blankstein et al. 2009).

One potential disadvantage of the single spiral acquisition mode for demonstrating the true hemodynamic significance of coronary artery stenosis via myocardial perfusion is that this acquisition mode simply provides a one-time static snapshot of the state of the myocardial blood supply during the time the respective portion of the myocardium is scanned. Consequently, more cranial portions of the heart may eventually be imaged during a different perfusion phase than the most caudal portions. Further, this approach cannot capture all phases of myocardial contrast kinetics and thus may provide only limited information regarding the extent of microvascular disease (Bastarrika et al. 2010b).

Recently introduced dynamic, time-resolved myocardial DSCT perfusion fulfills the principle of real-time perfusion imaging, as it demonstrates the actual wash-in and wash-out dynamics of iodinated contrast material in normal and diseased myocardium. This approach relies on dynamic time-resolved image acquisition at multiple time points during

contrast medium passage through the myocardium. A few years ago, animal experiments demonstrated the feasibility of this concept with MDCT and showed the potential for visual and semiquantitative assessment of first-pass myocardial perfusion (Mahnken et al. 2006). Nevertheless, with the limited coverage provided by the detectors of those early MDCT systems, the acquisition had to be restricted to a single transaxial image. More advanced volume-CT systems, such as 256-MDCT (George et al. 2009), 320-MDCT (George et al. 2012), and second-generation DSCT, enable dynamic time-resolved perfusion imaging with greater volume coverage along the z-axis of the heart (Bastarrika et al. 2010a; Bamberg et al. 2010). The second-generation DSCT has 73 mm volume coverage and can acquire perfusion data at two alternating table positions in ECG-triggered mode during end systole with rapid back-and-forth CT scanner table movements ("*shuttle mode*"), thus being a suitable tool to establish real-time passage of contrast through the myocardium. It could be said that dynamic, time-resolved myocardial DSCT perfusion imaging resembles the CMR imaging model. The tissue kinetics of iodine contrast agents and gadolinium chelates are similar (Gerber et al. 2006). Therefore, myocardial ischemia or infarction will appear as an area of hypoattenuation in first-pass imaging and myocardial infarction will be shown as a subendocardial hyperattenuating area in delayed-enhancement images (Lardo et al. 2006). Moreover, CT dynamic first-pass perfusion imaging combines high spatial and temporal resolution in a similar fashion as CMR and allows comparable results in terms of estimation of transmurality of myocardial perfusion defects (Nagel et al. 2009). Contrary to CMR perfusion using gadolinium-based contrast agents, in CT there is a linear relationship between myocardial contrast medium enhancement by the myocardium and iodine concentration, a feature that enables proper direct quantification of myocardial blood flow (Mahnken et al. 2006).

As said, the main advantage of volumetric myocardial DSCT perfusion is that it offers unprecedented ability to obtain quantitative measurements of tissue blood flow in healthy and diseased myocardium, far beyond mere assessment of two-dimensional region of interest-based density measurements or single slice-based time-attenuation curves. Further, combined with coronary DSCT angiography, the protocol appears as an appealing approach to the integrative assessment of CAD.

3 Imaging Study Protocol

3.1 Patient Preparation

Appropriate selection of patients suitable for myocardial DSCT perfusion is the cornerstone for diagnostic, high-quality examinations. Inadequate inclusion of obese individuals or patients with severe arrhythmia will lead to nondiagnostic tests. The study should not be performed in patients with hemodynamically and clinically unstable conditions, known contrast media allergy, severe arrhythmia, impaired renal function (creatinine > 1.5 mg/dl), inability to perform a 30-second breath hold, and pregnant or breastfeeding women. Individuals with contraindications for adenosine including 2nd or 3rd degree atrioventricular block, sick sinus syndrome, long QT syndrome, severe hypotension, and severe asthma should be excluded. Patients need to be in supine, feet-first position. Any treatment with beta-adrenergic blocking agents and/or nitrates should be discontinued prior to the scanning. Two antecubital 18-gauge size intravenous lines are required, one for intravenous contrast administration and the other for adenosine infusion. After placement of ECG electrodes and clear identification of QRS complex, detailed explanation of the imaging procedure has to be given to patients so as to obtain their maximum cooperation.

3.2 Acquisition Protocol

Exams are acquired in cranio-caudal direction with simultaneous recording of the ECG signal (Fig. 1). As a general rule, the acquisition should be planned over a previously acquired cCTA reconstructed during systole at 250 ms after the R-peak, in order to ensure appropriate coverage of the whole heart during the first-pass myocardial perfusion acquisition. Studies are obtained in end-inspiration with a standardized acquisition time of 30 s. If patients cannot hold their breath for 30 s, they shall be instructed to slowly release their breath and continue breathing shallowly.

The stress dynamic acquisition mode is started 3–4 min after the beginning of the infusion of intravenous adenosine (dose of 140 μg/kg/min). Myocardial perfusion CT data are acquired every other R–R′ interval at two alternating table positions in ECG-triggered mode at end systole (250 ms after the R-peak), with the table shuttling back-and-forth between the two positions during image acquisition (table acceleration: 300 mm/s^2). A complete dataset of the whole cardiac volume is acquired every $\sim$2.8 s. Given a detector width of 38 mm and a 10 % overlap between the two acquisition ranges, the anatomic coverage of this imaging technique is 73 mm. Recommended image acquisition parameters are 100 kV tube voltage and 300 mAs. The image acquisition sequence should be initiated 4 s prior to the arrival of the contrast medium bolus front as determined by the initial test bolus injection in order to ensure baseline acquisition of noncontrast images prior to the onset of first-pass perfusion. The myocardial DSCT perfusion examination requires 50 ml of contrast agent followed by 50 ml of

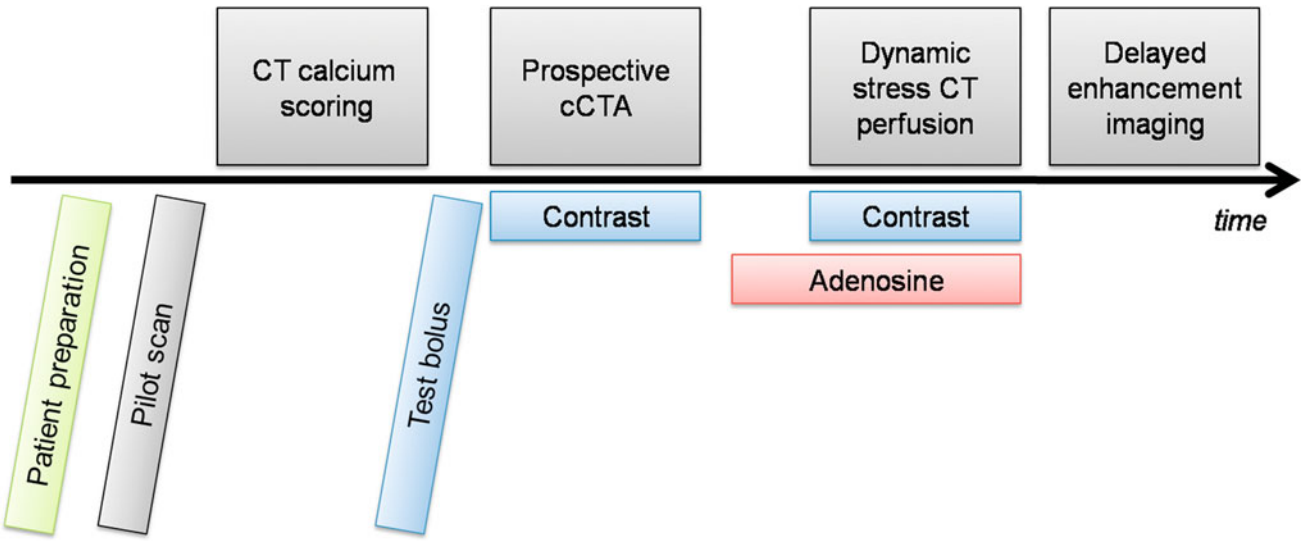

Fig. 1 Comprehensive cardiac DSCT protocol for the assessment of coronary artery disease (CAD) using a second-generation DSCT system. The protocol comprises coronary artery calcium scoring, morphological coronary CT angiography (cCTA), and functional assessment by time-resolved myocardial DSCT perfusion and delayed-enhancement imaging. If the proposed entire cardiac DSCT study is considered, including all four scans, the estimated radiation dose is approximately 18 mSv (Bastarrika et al. 2010b). A detailed description of scan parameters, medication, and contrast medium administration is shown in Table 1

saline, injected at 6 ml/s. The estimated radiation dose provided to patients with this dynamic stress-DSCT perfusion acquisition mode is approximately 10 mSv.

3.3 Data Reconstruction, Postprocessing, and Evaluation

To maintain CT value stability and high temporal resolution of the images, myocardial perfusion datasets are reconstructed using an approach that combines the results of two reconstructions into one final image stack. The high frequency components that predominantly contain the anatomical information (e.g. edges) are taken from a dual-source cardiac partial reconstruction providing 75-ms temporal resolution, whereas the low frequency components that predominantly contain the contrast information are taken from a 360° reconstruction providing 0.28-s temporal resolution (Bruder et al 2009).

For image analysis, myocardial perfusion datasets are reconstructed with 3 mm slice thickness every 2 mm with a medium sharpness convolution algorithm. Studies are processed using a dedicated software tool (Volume Perfusion software, syngo VA31, Siemens). Dynamic stress CT perfusion may be evaluated using qualitative, semiquantitative, or quantitative approaches. For qualitative analysis, it is recommended that dynamic stress-DSCT perfusion images are interpreted visually in conjunction with delayed-enhancement CT images. This approach may help to differentiate fixed from reversible myocardial perfusion defects (Bastarrika et al. 2010b).

For the semiquantitative perfusion analysis, dynamic stress CT perfusion image datasets need to be reformatted into 10 mm slice thickness, short-axis multiplanar reformats representative of basal, mid, and apical portions of the left ventricular myocardium so as to reproduce the 16-segment American Heart Association model (Cerqueira et al. 2002). Semiquantitative perfusion analysis is based on computing the upslope of the signal intensity over time curve from unenhanced myocardium to maximum signal intensity during the myocardial first-pass of the contrast agent, according to the "myocardial-to-left ventricular upslope index" method (Christian et al. 2004). In order to obtain the respective curves, epicardial and endocardial borders of the myocardium have to be defined with the aid of software. All perfusion parameters are usually normalized to blood pool signal intensity curves (Christian et al. 2004; Nagel et al. 2003).

For absolute myocardial perfusion quantification, a dedicated parametric deconvolution technique based on a two compartment model of intra- and extravascular space is used to fit the time-attenuation curves (Mahnken et al. 2010). In order to increase the precision of the fit, double sampling of the arterial input function (AIF) is performed. The input function is sampled in the descending aorta at every table position and combined into one AIF that possesses twice the sampling rate of the tissue time-attenuation curve (TAC). The algorithm then determines the maximum slope from the fit model curve for every voxel and calculates myocardial blood flow (MBF) according to the following relationship: MBF = Max Slope (TissueTAC)/Maximum (AIF), where the maximum slope reflects the

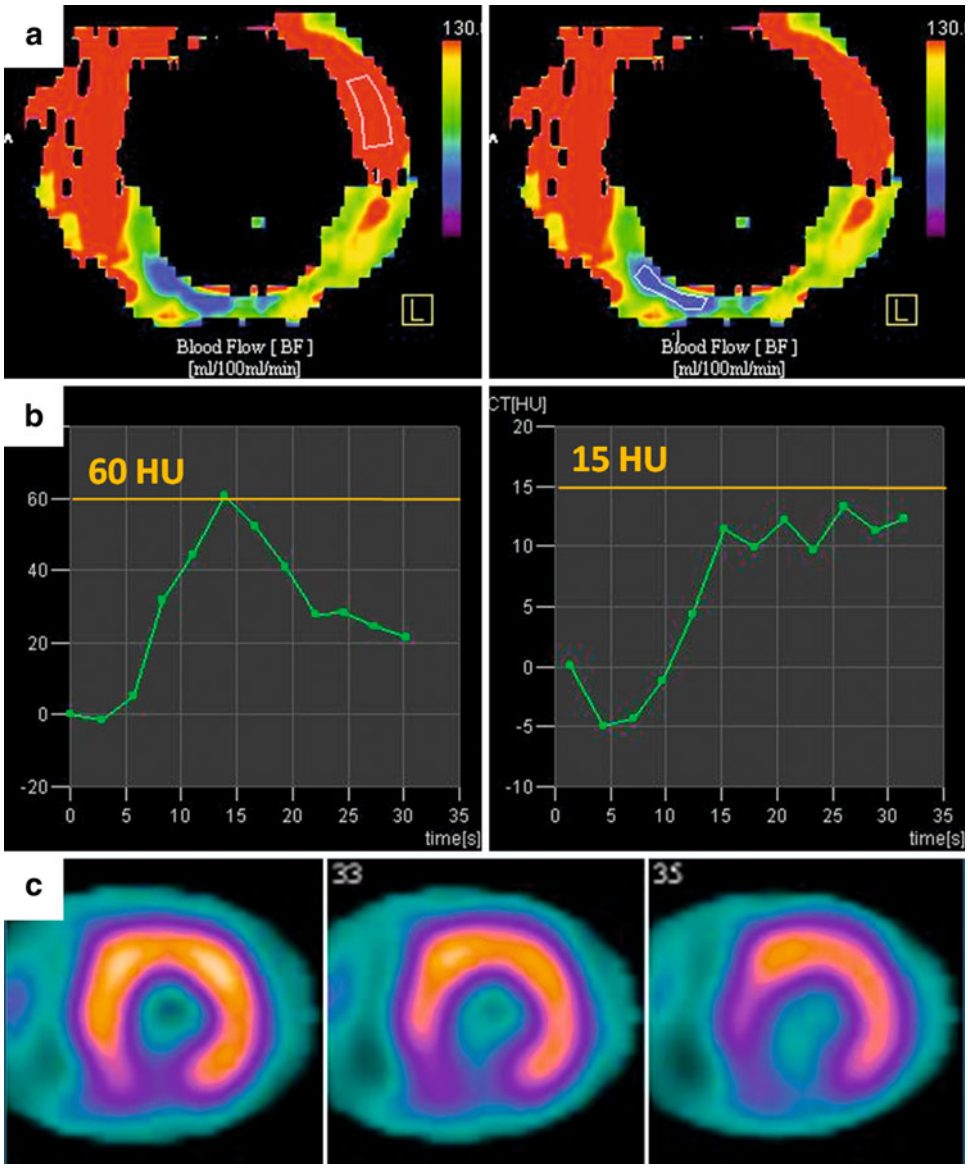

Fig. 2 Quantitative and semiquantitative assessment of myocardial perfusion using dynamic, time-resolved DSCT perfusion imaging in a 53-year-old male with abnormal ECG. **a** Short-axis, color-coded perfusion maps (blood flow, BF) for quantitative assessment. The *blue* and *green* colored sections in the inferior wall reveal an area of hypoperfusion during the first-pass myocardial DSCT perfusion imaging. In contrast, the predominantly *red* colored wall segments represent normally perfused areas. **b** Semiquantitative assessment of myocardial perfusion. As shown, graphs demonstrate changes in HU values over time measured by ROI analysis in the myocardial segment of interest (each corresponding image is depicted above). The normally perfused segment (*left*) shows a higher maximum HU value (60 HU vs. 15 HU) and there is delayed wash-in and wash-out of contrast in the hypoperfused segment (*right*). **c** Short-axis stress perfusion SPECT imaging. The perfusion defect in the inferior wall on SPECT closely matches the CT perfusion map

tissue TAC and the maximum (AIF) indicates the maximum AIF value (Bamberg et al. 2010) (Fig. 2).

4 Integrative Cardiac DSCT Protocol for the Assessment of Coronary Artery Disease

A suggested study protocol for comprehensive assessment of CAD using a second-generation DSCT system, including coronary artery calcium quantification, coronary DSCT angiography, first-pass myocardial perfusion, and delayed-enhancement imaging should be performed as follows (Table 1) (Bastarrika et al. 2010c).

4.1 Single Heart-beat, High-pitch CT Calcium Scoring

2 × 64 × 0.6 mm detector collimation (2 × 128 × 0.6 mm sections) by means of the z-flying focal spot technique, 280 ms gantry rotation time, 120 kV tube potential, and 73 mAs per rotation tube current time product.

4.2 Prospectively ECG-triggered Coronary CT Angiography

With 2 × 64 × 0.6 mm detector collimation (2 × 128 × 0.6 mm sections), 280 ms gantry rotation time, and

Table 1 Comprehensive cardiac DSCT protocol for the assessment of coronary artery disease

		Coronary Calcium[a]	Coronary CT angiography[b]	Dynamic DSCT perfusion	Delayed enhancement[c]
Current	Voltage (kVp)	120	120	100	80
	Current (mAs)	73	320	300	320
	Modulation (R–R′ int.)	70 % R–R′	Max. 70 %; min. 30–90 % R–R′	250 ms post R	70 % R–R′
Acquisition	Collimation (mm)	2 × 64 × 0.6	2 × 64 × 0.6	2 × 64 × 1.2	2 × 64 × 0.6
	Sections	2 × 128 × 0.6 mm	2 × 128 × 0.6 mm	2 × 128 × 1.2 mm	2 × 128 × 0.6 mm
	Rotation time (ms)	280	280	280	280
Reconstruction	Thickness/ Incr. (mm)	3/1.5	0.75/0.3	3/2	0.75/0.3
	Algorithm	B35	B26f (B46f if calcification or stent)	B23f	B26f
Medication	Adenosine	–	–	140 µg/kg/min	–
Test	Region of interest	–	Ascending aorta	–	–
	Test bolus (CM/S/F)	–	15/50 ml at 6 ml/s	–	–
Delay	Test bolus	–	Peak time + 4 s	4 s prior to the arrival of the CM bolus front	–
Contrast	Concentration (mg I/ml)	–	High iodine concentration (370–400 mg I/ml)		–
	Protocol (ml)	–	70 ml CM + 50 ml mixture (30 % CM/70 % S) + 30 ml S at 6 ml/s	50 ml CM + 50 ml S at 6 ml/s	–

Modified from Bastarrika et al. (2010c)

Note: *kVp* kilovolt peak, *mAs* milliampere per second, *R–R′int* R–R′ interval, *mm* millimeters, *ms* milliseconds, *CM* contrast medium, *S* saline, *F* flow, *mg I/ml* milligrams if iodine per milliliter, *ml* milliliter, *max* maximum, *min* minimum, *s* seconds, *µg/kg/min* microgram per kilogram per minute

[a] Acquired with single heart-beat/high-pitch (3.4)

[b] Acquired with prospective ECG-triggering

[c] Acquired with prospective ECG-triggering or with single heart-beat/high-pitch (3.4)

320 mAs per rotation tube current time product, 120 or 100 kV tube potential should be used for patients with body mass index greater than 25 kg/m^2 or less than 25 kg/m^2, respectively. Full radiation dose window should be set at 70 % of the R–R′ interval in patients with heart rates at or below 70 beats/min (bpm), and at 40 % of the R–R′ interval in patients with a heart rate above 70 bpm. If functional information is desired, adaptive prospective ECG-triggering may be used with the reduced dose (20 % of the nominal tube current) applied between 30 and 90 % of the R–R′ interval. Intravenous contrast is administered using a triphasic injection protocol with injection of 70 ml of pure, undiluted, high iodine concentration contrast material followed by a constant volume of 50 ml of a 70:30 % saline-to-contrast medium mixture, and finally 30 ml of pure saline, all injected at 6 ml/s. The study acquisition delay time may be estimated using the bolus tracking technique or the test bolus technique. For the latter, injection of 15 ml contrast medium at 6 ml/s, followed by 50 ml of saline is recommended. The actual delay time is calculated as the time of peak contrast medium attenuation in a region of interest in the ascending aorta plus 4 s. For coronary artery evaluation, datasets are reconstructed using 0.75 mm section thickness and 0.3 mm reconstruction increment at 40 or 70 % R–R′ depending on the heart rate (described above). An additional reconstruction during systole at 250 ms after the R-peak is recommended to plan the coverage range of the dynamic, time-resolved stress-DSCT perfusion acquisition.

4.3 Dynamic, Time-Resolved First-Pass Myocardial DSCT Perfusion

(Described Above)

4.4 Delayed-Enhancement Imaging

This last acquisition is performed 6 min after the first-pass myocardial DSCT perfusion study using a regular prospectively ECG-triggered mode with image acquisition at 70 % of the R–R′ interval, 2 × 64 × 0.6 mm detector collimation (2 × 128 × 0.6 mm sections), 280 ms gantry rotation time, 80 kV tube voltage, and 320 mAs per rotation tube current time product. Single heart-beat high-pitch DSCT acquisition may also be used for delayed-enhancement imaging in order to save radiation dose.

5 First-Pass Myocardial DSCT Perfusion Imaging: Preclinical Studies

Early studies performed to address feasibility of first-pass myocardial perfusion imaging using MDCT were performed in animal models. The major restriction of these initial studies was that they were limited by the width of the CT detector, so they could only aim at obtaining images corresponding to a specific section of the heart (George et al. 2007; Mahnken et al. 2006; Daghini et al. 2007). In the first study, evaluating the feasibility of myocardial first-pass perfusion imaging with MDCT, Mahnken et al. (Mahnken et al. 2006) included five pigs with acute myocardial infarction and compared dynamic contrast-enhanced MDCT results with the extension of the myocardial infarction after sacrifice. The authors concluded that MDCT allowed for the differentiation of infarcted myocardium (shown as hypoperfused area) and normal myocardium, and that MDCT had the potential for visual and semiquantitative assessment of first-pass myocardial perfusion (Mahnken et al. 2006). George et al. (2007) conducted another study on the ability of dynamic 64-row MDCT to provide an accurate measurement of myocardial blood flow during first-pass MDCT, using semiquantitative and quantitative analysis methods. In their study, myocardial perfusion was analyzed using a model-based deconvolution approach and two upslope methods. Results were compared with the microsphere-derived myocardial blood flow measurements. The authors concluded that measurement of myocardial blood flow provided by MDCT using upslope and model-based deconvolution methods correlated well with microsphere myocardial blood flow (George et al. 2007). Finally, in a different study, Daghini et al. (2007) assessed the ability of electron beam computed tomography and 64-row MDCT to evaluate indices of endothelial function and microvascular perfusion as determined by the myocardial microvascular permeability-surface area product and the fractional vascular volume. Obtained time-attenuation curves were analyzed using indicator-dilution and Patlak models. The authors concluded that the assessments obtained by 64-row MDCT were not reliable when using indicator-dilution analysis, likely due to the method's sensitivity to scan duration, but the quantifications obtained using the Patlak model were feasible (Daghini et al. 2007).

With the advent of second-generation DSCT technology with higher temporal resolution, broader detectors, extended coverage, and implementation of a new scan mode that allows for dynamic scanning with a z-coverage of twice the detector width so as to include the whole heart in the acquisition, research on myocardial CT perfusion imaging has been invigorated (Haberland et al. 2010). In the first investigation of feasibility, preliminary animal experience study Mahnken et al. (2010) quantified differences in regional myocardial perfusion by assessing volumetrically myocardial blood flow, first-pass distribution volume, and intravascular blood volume in pigs with 80 % stenosis of the left anterior descending coronary artery. They observed that the amount of myocardial blood flow in the post-stenotic myocardium was significantly lower than the quantity of myocardial blood flow in the remaining normal myocardium, thus concluding that myocardial perfusion with DSCT is able to demonstrate the hemodynamic effect of high-grade coronary artery stenosis (Mahnken et al. 2010). In a more recent study, Bamberg et al. (2012) determined the accuracy of DSCT dynamic stress myocardial perfusion imaging to estimate myocardial blood flow in a porcine animal model with variable degrees of induced coronary artery stenosis in comparison with microsphere-derived myocardial blood flow. In this study, 50 and 75 % diameter luminal narrowing of the left anterior descending coronary artery were achieved after stent placement and balloon catheter inflation. Animals underwent adenosine-stress and rest myocardial DSCT perfusion with the described "shuttle mode" acquisition technique. Authors concluded that myocardial blood flow estimated by DSCT at rest and stress showed a valid difference with varying degrees of coronary stenosis. However, they noted that DSCT overestimated the amount of myocardial blood flow compared with microsphere-derived myocardial blood flow quantification (Bamberg et al. 2012).

6 First-Pass Myocardial DSCT Perfusion Imaging: Clinical Studies

In the clinical setting, the first technical note on dynamic first-pass myocardial DSCT perfusion published by Bamberg et al. (2010) detailed the principles of using

model-based determination of regional myocardial blood flow by DSCT and demonstrated its in vivo applicability. After this proof of concept, the same group conducted a study in 33 patients who were suspected of having or were known to have CAD so as to determine the feasibility of dynamic, first-pass myocardial DSCT perfusion imaging to detect hemodynamically significant coronary artery stenosis (Bamberg et al. 2011b). In this study, the FFR was considered as the standard of reference. Authors observed that the diagnostic accuracy of DSCT for the detection of anatomically significant coronary artery stenosis was high, but had a low positive predictive value for the detection of hemodynamically significant stenosis. With the use of DSCT-derived myocardial blood flow quantification, almost 50 % of the coronary lesions were graded as not hemodynamically significant, a fact that significantly increased the positive predictive value of the test from 49 to 78 %. According to these authors, the presence of a coronary artery stenosis with a corresponding myocardial blood flow less than 75 ml/100 ml/min had a high risk for hemodynamic significance (Bamberg et al. 2011b).

Using a similar cardiac DSCT perfusion imaging protocol, Bastarrika et al. (2010b) provided the first clinical evidence revealing that dynamic first-pass DSCT perfusion imaging under adenosine stress may enable the evaluation of qualitative and semiquantitative perfusion parameters in a comparable fashion as CMR. In this study, sensitivity, specificity, and positive and negative predictive values for detection of myocardial perfusion defects at DSCT compared with MRI were 86.1, 98.2, 93.9, and 95.7 %, respectively. Semiquantitative analysis of DSCT data showed significant differences between ischemic and nonischemic myocardium with a signal intensity upslope that was comparable to MRI-derived values. Authors found moderate correlation, however, between absolute DSCT-derived quantification of myocardial blood flow and semiquantitative DSCT measurements (Bastarrika et al. 2010b). The same group expanded their observation to 30 consecutive patients who underwent dynamic myocardial CT perfusion imaging under regadenoson stress and compared myocardial perfusion defects on DSCT with respect to CMR and SPECT, leading to similar conclusions (Weininger et al. 2011) (Fig. 3).

Wang et al. (2012) evaluated the feasibility of adenosine-stress dynamic myocardial perfusion imaging with second-generation DSCT for detecting myocardial ischemia in comparison with conventional catheter coronary angiography and SPECT in 30 patients. Authors quantified DSCT-derived myocardial blood flow and compared this value with the ones obtained for stress and rest SPECT. Sensitivity, specificity, and positive and negative predictive values for myocardial DSCT perfusion for the identification of segments with perfusion defects with respect to SPECT were 85, 92, 55, and 98 %, respectively. On a per-vessel basis, sensitivity, specificity, and positive and negative predictive values for detecting flow-obstructing stenosis were, respectively, 100, 76, 54, and 100 % for DSCT perfusion; 90, 51, 35, and 95 % for cCTA; and 90, 81, 58, and 97 % for DSCT perfusion combined with cCTA. According to the authors, myocardial DSCT perfusion combined with cCTA improves diagnostic accuracy for identifying flow-obstructing stenosis compared with cCTA alone (Wang et al. 2012).

In another study, Ho et al. (2010) assessed the ability of DSCT myocardial perfusion imaging to detect abnormal flow reserve and infarction in comparison with SPECT in 35 patients who underwent myocardial DSCT perfusion under dipyridamole stress. Authors correlated perfusion defects detected on DSCT to coronary stenosis visualized on cCTA and conventional coronary angiography. Sensitivity, specificity, and positive and negative predictive values of dynamic DSCT perfusion for identifying segments with perfusion defects were 83, 78, 79, and 82 %, respectively. Compared with conventional coronary angiography, sensitivity, specificity, and positive and negative predictive values of dynamic DSCT were 95, 65, 78, and 79 %, respectively. The authors concluded that vasodilator-stress myocardial DSCT perfusion imaging may be feasible at a radiation dose similar to SPECT (~9 mSv). Dynamic DSCT perfusion identified areas of abnormal flow reserve and infarction with a high degree of correlation to SPECT, as well as to stenosis detected in cCTA and conventional coronary angiography (Ho et al. 2010).

Finally, there is not much clinical evidence about the use of dynamic, time-resolved myocardial DSCT perfusion imaging in the setting of patients with acute chest pain. Weininger et al. (2012) detailed their initial experience performing myocardial stress perfusion DSCT in 20 consecutive patients who presented with acute chest pain and were clinically referred for stress/rest SPECT and CMR. Individuals were randomly assigned to adenosine-stress dynamic, real-time myocardial perfusion DSCT or adenosine-stress first-pass dual-energy myocardial perfusion CT. According to their results, real-time perfusion DSCT (versus SPECT) had 86 % (84 %) sensitivity, 98 % (92 %) specificity, 94 % (88 %) positive predictive value, and 96 % (92 %) negative predictive value in comparison with perfusion CMR for the detection of myocardial perfusion defects. Authors concluded that compared to both CMR and SPECT, dynamic, real-time perfusion CT and first-pass dual-energy perfusion CT showed good agreement for the detection of myocardial perfusion defects in patients with acute chest pain (Weininger et al. 2012).

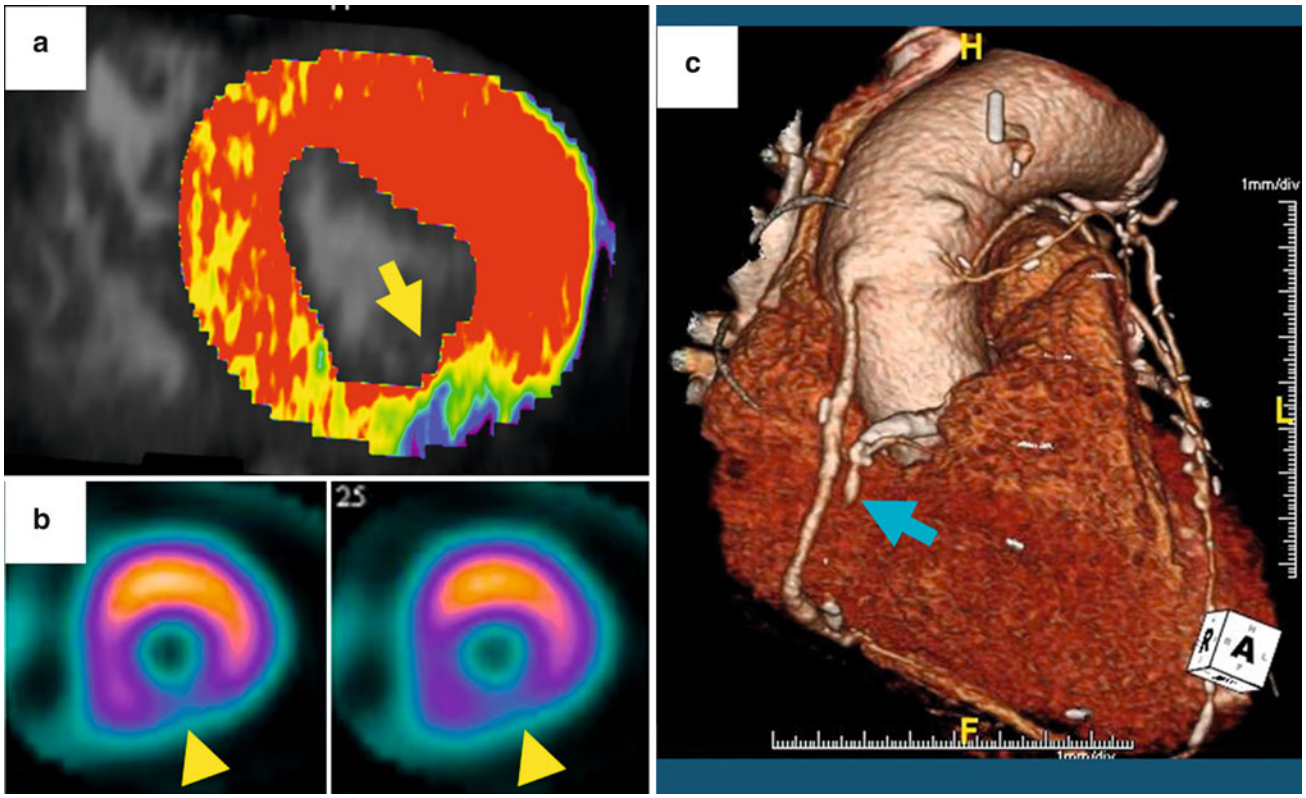

Fig. 3 Assessment of myocardial perfusion using a dynamic, time-resolved DSCT protocol in a 69-year-old male with history of prior myocardial infarction in 1970s, status post coronary artery bypass graft (CABG) in 1999, and percutaneous coronary intervention in 2001. **a** Short-axis overlay image of a color perfusion map on a morphological grayscale image. The *blue* and *green* colored section in the inferolateral wall (*yellow arrow*) indicates an area of hypoperfusion during first-pass myocardial DSCT perfusion imaging. In contrast, the predominantly *red* colored wall segments represent normally perfused areas. **b** Short-axis stress perfusion SPECT imaging. The perfusion deficit in the inferolateral wall (*yellow arrow head*) correlates with CT findings. Rest perfusion SPECT images (not shown) also demonstrated a corresponding perfusion deficit in that area, indicating nonreversible perfusion defect/infarction. **c** 3D-volume rendered image showing complete occlusion of the right coronary artery (*blue arrow*), which is the cause of the perfusion defect and patency of the adjacent CABG

7 Limitations of Dynamic, Time-Resolved Myocardial DSCT Perfusion Imaging

There are a number of limitations inherent to the technique itself that need to be addressed before dynamic, time-resolved myocardial DSCT perfusion imaging is fully established in clinical practice. Dynamic adenosine-stress acquisitions are long and complex examinations that require exhaustive medical supervision and considerable patient collaboration. Besides a relatively low temporal resolution, the acquisition coverage is of 73 mm along the z-axis of the patient, which may be insufficient for encompassing the entire heart, particularly in patients with dilated cardiomyopathy (Bamberg et al. 2011b). Therefore, end-systolic triggering is recommended for myocardial DSCT perfusion with the second-generation DSCT system. The advantages of this approach include a smaller left ventricular coverage requirement, fewer beam-hardening artifacts due to a reduced amount of intraventricular contrast, a thicker myocardial wall so as to provide a more robust basis for assessing perfusion deficits, and a reduced susceptibility to extrasystolia (Bamberg et al. 2010). Further improvements in CT technology should aim at providing greater coverage along the z-axis to approach that of latest generation single-source 320-row CT systems (George et al. 2012).

The generalized clinical use of first-pass myocardial DSCT perfusion will require further decreasing radiation exposure. The dynamic CT perfusion acquisition mode per se aims at quantifying myocardial perfusion and does not allow proper evaluation of the coronary tree, for which a regular prospectively ECG-triggered cCTA is required. Further, radiation dose also increases if coronary artery calcium quantification and delayed-enhancement acquisition protocols are added. According to recently available data, the total amount of radiation a patient receives with the perfusion protocol described here is within the range of values depicted for routine retrospectively ECG-gated cCTA (Stolzmann et al. 2008), and is similar to the radiation dose from SPECT examinations (Ho et al. 2010;

Gerber et al. 2009)—around 10 mSv. If the proposed entire cardiac CT protocol is considered, including coronary artery calcium quantification, prospectively ECG-triggered cCTA, dynamic CT perfusion imaging, and delayed-enhancement acquisition, the radiation dose reaches approximately 18 mSv (Bastarrika et al. 2010b). Similarly, radiation dose will raise if rest perfusion imaging is acquired in addition to the stress perfusion scan (George et al. 2009). Current trends in nuclear (Chang et al. 2010) and MRI myocardial perfusion imaging (Krittayaphong et al. 2009) dictate, however, that the stress perfusion only provides sufficient information regarding myocardial ischemia. A potential approach to avoid rest perfusion imaging may be to use the cCTA obtained prior to stress perfusion as a substitute for a dedicated rest perfusion acquisition. Hence, considering the high amount of radiation given in those studies, development of strategies to reduce radiation exposure becomes necessary. In this sense, the recently introduced iterative reconstruction algorithms may play an important role.

Another limitation that should be mentioned relates to the presence of artifacts that may hamper quantitative assessment of myocardial perfusion defects. Beam-hardening artifacts, caused by an adjacent bone or by large concentrations of iodine in the ventricle and the descending aorta, may be the reason for apparent reduction in attenuation in the myocardium. This can lead to incorrectly estimate myocardial perfusion parameters (Kitagawa et al. 2010). As conventional segmentation algorithms fail to clearly distinguish between iodine and bone, sophisticated algorithms based on the calculation of the time-dependent iodine distribution by analyzing the voxel changes of a cardiac perfusion examination are being developed (i.e. dynamic iterative beam-hardening correction algorithm). As a result of the latter, there is a reduction in the beam-hardening artifacts induced by the contrast agent dynamics, as well as those due to bone, thus allowing for an improved assessment of contrast agent uptake in the myocardium (Stenner et al. 2010). Moreover, perfusion imaging depends on stable CT values, which are best achieved using data in 360° symmetry. The conventional partial scan reconstructions used to achieve high temporal resolution do not fulfill this criterion and are prone to artifacts. Angular position of data acquisition depends on the correlation between rotation time and heart rate, which conducts to random image artifacts when partial scan reconstructions are employed (McCollough et al. 2008). Therefore, sophisticated image reconstruction techniques need to be applied so as to avoid these artifacts (Bruder et al 2009).

Finally, myocardial DSCT perfusion protocols should be tailored to patient requirements, and guidelines for the appropriate use of the technique should be stated. Further, there is lack of large validation studies proving the clinical usefulness of dynamic, time-resolved myocardial DSCT perfusion imaging. Few studies have shown its potential by obtaining comparable results to those offered by CMR or SPECT. Further research is warranted to fully determine the diagnostic accuracy of myocardial DSCT perfusion imaging. In the mean time, cardiac DSCT perfusion may become an option for patients with CMR contraindications and for patients in whom simultaneous assessment for coronary artery stenosis is desired.

8 Conclusion

An integrative cardiac CT acquisition protocol including dynamic, time-resolved myocardial DSCT perfusion imaging seems to be promising for overall assessment of CAD. Myocardial perfusion imaging together with cCTA and delayed-enhancement CT acquisition may respond to the major clinical questions in any given individual with suspicion of CAD. However, myocardial first-pass DSCT perfusion is still at its early stages and further investigation and development is required, first, to establish the accuracy DSCT-derived myocardial perfusion parameters, and second, to overcome limitations inherent to this innovative myocardial perfusion imaging mode. Reduction of the total acquisition time, increased heart coverage, development of new radiation dose saving strategies, correction of artifacts, and appropriate selection of patients are strongly encouraged. Dynamic, time-resolved first-pass myocardial DSCT perfusion imaging is an attractive approach to CAD, but it still remains to be seen whether myocardial perfusion imaging by this technology will be beneficial compared with already established imaging modalities and clinical standards.

References

Arnold JR, Karamitsos TD, Pegg TJ, Francis JM, Olszewski R, Searle N et al (2010) Adenosine stress myocardial contrast echocardiography for the detection of coronary artery disease: a comparison with coronary angiography and cardiac magnetic resonance. JACC Cardiovasc Imaging 3(9):934–943

Bamberg F, Klotz E, Flohr T, Becker A, Becker CR, Schmidt B et al (2010) Dynamic myocardial stress perfusion imaging using fast dual-source CT with alternating table positions: initial experience. Eur Radiol 20(5):1168–1173

Bamberg F, Sommer WH, Hoffmann V, Achenbach S, Nikolaou K, Conen D et al (2011a) Meta-analysis and systematic review of the long-term predictive value of assessment of coronary atherosclerosis by contrast-enhanced coronary computed tomography angiography. J Am Coll Cardiol 57(24):2426–2436

Bamberg F, Becker A, Schwarz F, Marcus RP, Greif M, von Ziegler F et al (2011b) Detection of hemodynamically significant coronary artery stenosis: incremental diagnostic value of dynamic CT-based myocardial perfusion imaging. Radiology 260(3):689–698

Bamberg F, Hinkel R, Schwarz F, Sandner TA, Baloch E, Marcus R et al (2012) Accuracy of dynamic computed tomography adenosine

stress myocardial perfusion imaging in estimating myocardial blood flow at various degrees of coronary artery stenosis using a porcine animal model. Invest Radiol 47(1):71–77

Bastarrika G, Lee YS, Huda W, Ruzsics B, Costello P, Schoepf UJ (2009) CT of coronary artery disease. Radiology 253(2):317–338

Bastarrika G, Ramos-Duran L, Schoepf UJ, Rosenblum MA, Abro JA, Brothers RL et al (2010a) Adenosine-stress dynamic myocardial volume perfusion imaging with second generation dual-source computed tomography: concepts and first experiences. J Cardiovasc Comput Tomogr 4(2):127–35

Bastarrika G, Ramos-Duran L, Rosenblum MA, Kang DK, Rowe GW, Schoepf UJ (2010b) Adenosine-stress dynamic myocardial CT perfusion imaging: initial clinical experience. Invest Radiol 45(6):306–313

Bastarrika G, Kang DK, Abro JA, Schoepf UJ (2010c) Comprehensive assessment of coronary disease using perfusion CT with pharmacologically induced stress. Radiologia 52(5):469–472

Bell MR, Lerman LO, Rumberger JA (1999) Validation of minimally invasive measurement of myocardial perfusion using electron beam computed tomography and application in human volunteers. Heart 81(6):628–635

Blankstein R, Shturman LD, Rogers IS, Rocha-Filho JA, Okada DR, Sarwar A et al (2009) Adenosine-induced stress myocardial perfusion imaging using dual-source cardiac computed tomography. J Am Coll Cardiol 54(12):1072–1084

Bruder H, Raupach R, Klotz E. Spatio-temporal filtration of dynamic CT data using diffusion filters. In: Samei E, Hsieh J (eds) Medical imaging 2009: physics of medical imaging, 1. Proceeding of SPIE, vol 7258. Society of Photo Optical, Bellingham, WA, pp 725857–725810

Buhr C, Gossl M, Erbel R, Eggebrecht H (2008) Regadenoson in the detection of coronary artery disease. Vasc Health Risk Manag 4(2):337–340

Cerqueira MD, Weissman NJ, Dilsizian V, Jacobs AK, Kaul S, Laskey WK et al (2002) Standardized myocardial segmentation and nomenclature for tomographic imaging of the heart: a statement for healthcare professionals from the Cardiac Imaging Committee of the Council on Clinical Cardiology of the American Heart Association. Circulation 105(4):539–542

Chang SM, Nabi F, Xu J, Raza U, Mahmarian JJ (2010) Normal stress-only versus standard stress/rest myocardial perfusion imaging similar patient mortality with reduced radiation exposure. J Am Coll Cardiol 55(3):221–230

Christian TF, Rettmann DW, Aletras AH, Liao SL, Taylor JL, Balaban RS et al (2004) Absolute myocardial perfusion in canines measured by using dual-bolus first-pass MR imaging. Radiology 232(3):677–684

Daghini E, Primak AN, Chade AR, Zhu X, Ritman EL, McCollough CH et al (2007) Evaluation of porcine myocardial microvascular permeability and fractional vascular volume using 64-slice helical computed tomography (CT). Invest Radiol 42(5):274–282

de Jong MC, Genders TS, van Geuns RJ, Moelker A, Hunink MG (2012) Diagnostic performance of stress myocardial perfusion imaging for coronary artery disease: a systematic review and meta-analysis. Eur Radiol 22(9):1881–1895

Dorbala S, Hachamovitch R, Curillova Z, Thomas D, Vangala D, Kwong RY et al (2009) Incremental prognostic value of gated Rb-82 positron emission tomography myocardial perfusion imaging over clinical variables and rest LVEF. JACC Cardiovasc Imaging 2(7):846–854

Flotats A, Knuuti J, Gutberlet M, Marcassa C, Bengel FM, Kaufmann PA et al (2011) Hybrid cardiac imaging: SPECT/CT and PET/CT. A joint position statement by the European Association of Nuclear Medicine (EANM), the European Society of Cardiac Radiology (ESCR) and the European Council of Nuclear Cardiology (ECNC). Eur J Nucl Med Mol Imaging 38(1): 201–212

Gaemperli O, Husmann L, Schepis T, Koepfli P, Valenta I, Jenni W et al (2009) Coronary CT angiography and myocardial perfusion imaging to detect flow-limiting stenoses: a potential gatekeeper for coronary revascularization? Eur Heart J 30(23):2921–2929

George RT, Silva C, Cordeiro MA, DiPaula A, Thompson DR, McCarthy WF et al (2006) Multidetector computed tomography myocardial perfusion imaging during adenosine stress. J Am Coll Cardiol 48(1):153–160

George RT, Jerosch-Herold M, Silva C, Kitagawa K, Bluemke DA, Lima JA et al (2007) Quantification of myocardial perfusion using dynamic 64-detector computed tomography. Invest Radiol 42(12):815–822

George RT, Arbab-Zadeh A, Miller JM, Kitagawa K, Chang HJ, Bluemke DA et al (2009) Adenosine stress 64- and 256-row detector computed tomography angiography and perfusion imaging: a pilot study evaluating the transmural extent of perfusion abnormalities to predict atherosclerosis causing myocardial ischemia. Circ Cardiovasc Imaging 2:174–182

George RT, Arbab-Zadeh A, Miller JM, Vavere AL, Bengel FM, Lardo AC et al (2012) Computed tomography myocardial perfusion imaging with 320-row detector computed tomography accurately detects myocardial ischemia in patients with obstructive coronary artery disease. Circ Cardiovasc Imaging 5(3):333–340

Gerber BL, Belge B, Legros GJ, Lim P, Poncelet A, Pasquet A et al (2006) Characterization of acute and chronic myocardial infarcts by multidetector computed tomography: comparison with contrast-enhanced magnetic resonance. Circulation 113(6):823–833

Gerber TC, Carr JJ, Arai AE, Dixon RL, Ferrari VA, Gomes AS et al (2009) Ionizing radiation in cardiac imaging: a science advisory from the American Heart Association Committee on Cardiac Imaging of the Council on Clinical Cardiology and Committee on Cardiovascular Imaging and Intervention of the Council on Cardiovascular Radiology and Intervention. Circulation 119(7): 1056–1065

Gould RG, Lipton MJ, McNamara MT, Sievers RE, Koshold S, Higgins CB (1988) Measurement of regional myocardial blood flow in dogs by ultrafast CT. Invest Radiol 23(5):348–353

Haberland U, Klotz E, Abolmaali N (2010) Performance assessment of dynamic spiral scan modes with variable pitch for quantitative perfusion computed tomography. Invest Radiol 45(7):378–386

Hendel RC, Patel MR, Kramer CM, Poon M, Carr JC, Gerstad NA et al (2006) ACCF/ACR/SCCT/SCMR/ASNC/NASCI/SCAI/SIR 2006 appropriateness criteria for cardiac computed tomography and cardiac magnetic resonance imaging: a report of the American College of Cardiology Foundation Quality Strategic Directions Committee Appropriateness Criteria Working Group, American College of Radiology, Society of Cardiovascular Computed Tomography, Society for Cardiovascular Magnetic Resonance, American Society of Nuclear Cardiology, North American Society for Cardiac Imaging, Society for Cardiovascular Angiography and Interventions, and Society of Interventional Radiology. J Am Coll Cardiol 48(7):1475–1497

Hendel RC, Berman DS, Di Carli MF, Heidenreich PA, Henkin RE, Pellikka PA et al (2009) ACCF/ASNC/ACR/AHA/ASE/SCCT/SCMR/SNM 2009 appropriate use criteria for cardiac radionuclide imaging: a report of the American College of Cardiology Foundation Appropriate Use Criteria Task Force, the American Society of Nuclear Cardiology, the American College of Radiology, the American Heart Association, the American Society of Echocardiography, the Society of Cardiovascular Computed Tomography, the Society for Cardiovascular Magnetic Resonance, and the Society of Nuclear Medicine: endorsed by the American College of Emergency Physicians. Circulation 119(22):e561–e587

Ho KT, Chua KC, Klotz E, Panknin C (2010) Stress and rest dynamic myocardial perfusion imaging by evaluation of complete time-attenuation curves with dual-source CT. JACC Cardiovasc Imaging 3(8):811–820

Jaarsma C, Leiner T, Bekkers SC, Crijns HJ, Wildberger JE, Nagel E et al (2012) Diagnostic performance of noninvasive myocardial perfusion imaging using single-photon emission computed tomography, cardiac magnetic resonance, and positron emission tomography imaging for the detection of obstructive coronary artery disease: a meta-analysis. J Am Coll Cardiol 59(19):1719–1728

King SB 3rd, Smith SC Jr, Hirshfeld JW Jr, Jacobs AK, Morrison DA, Williams DO et al (2008) 2007 Focused Update of the ACC/AHA/SCAI 2005 Guideline Update for Percutaneous Coronary Intervention: a report of the American College of Cardiology/American Heart Association Task Force on Practice Guidelines: 2007 Writing Group to Review New Evidence and Update the ACC/AHA/SCAI 2005 Guideline Update for Percutaneous Coronary Intervention, Writing on Behalf of the 2005 Writing Committee. Circulation 117(2):261–295

Kitagawa K, George RT, Arbab-Zadeh A, Lima JA, Lardo AC (2010) Characterization and correction of beam-hardening artifacts during dynamic volume CT assessment of myocardial perfusion. Radiology 256(1):111–118

Krittayaphong R, Boonyasirinant T, Saiviroonporn P, Nakyen S, Thanapiboonpol P, Yindeengam A et al (2009) Myocardial perfusion cardiac magnetic resonance for the diagnosis of coronary artery disease: do we need rest images? Int J Cardiovasc Imaging 25(Suppl 1):139–148

Lardo AC, Cordeiro MA, Silva C, Amado LC, George RT, Saliaris AP et al (2006) Contrast-enhanced multidetector computed tomography viability imaging after myocardial infarction: characterization of myocyte death, microvascular obstruction, and chronic scar. Circulation 113(3):394–404

Lell M, Marwan M, Schepis T, Pflederer T, Anders K, Flohr T et al (2009) Prospectively ECG-triggered high-pitch spiral acquisition for coronary CT angiography using dual source CT: technique and initial experience. Eur Radiol 19(11):2576–2583

Lerman LO, Siripornpitak S, Maffei NL, 2nd Sheedy PF Ritman EL (1999) Measurement of in vivo myocardial microcirculatory function with electron beam CT. J Comput Assist Tomogr 23(3):390–398

Leschka S, Stolzmann P, Desbiolles L, Baumueller S, Goetti R, Schertler T et al (2009) Diagnostic accuracy of high-pitch dual-source CT for the assessment of coronary stenoses: first experience. Eur Radiol 19(12):2896–2903

Mahnken AH, Bruners P, Katoh M, Wildberger JE, Gunther RW, Buecker A (2006) Dynamic multi-section CT imaging in acute myocardial infarction: preliminary animal experience. Eur Radiol 16(3):746–752

Mahnken AH, Klotz E, Pietsch H, Schmidt B, Allmendinger T, Haberland U et al (2010) Quantitative whole heart stress perfusion CT imaging as noninvasive assessment of hemodynamics in coronary artery stenosis: preliminary animal experience. Invest Radiol 45(6):298–305

McCollough CH, Schmidt B, Yu L, Primak A, Ulzheimer S, Bruder H et al (2008) Measurement of temporal resolution in dual source CT. Med Phys 35(2):764–768

Miller JM, Rochitte CE, Dewey M, Arbab-Zadeh A, Niinuma H, Gottlieb I et al (2008) Diagnostic performance of coronary angiography by 64-row CT. N Engl J Med 359(22):2324–2336

Min JK, Shaw LJ, Devereux RB, Okin PM, Weinsaft JW, Russo DJ et al (2007) Prognostic value of multidetector coronary computed tomographic angiography for prediction of all-cause mortality. J Am Coll Cardiol 50(12):1161–1170

Min JK, Dunning A, Lin FY, Achenbach S, Al-Mallah M, Budoff MJ et al (2011) Age- and sex-related differences in all-cause mortality risk based on coronary computed tomography angiography findings results from the International Multicenter CONFIRM (Coronary CT Angiography Evaluation for Clinical Outcomes: An International Multicenter Registry) of 23,854 patients without known coronary artery disease. J Am Coll Cardiol 58(8):849–860

Nagel E, Klein C, Paetsch I, Hettwer S, Schnackenburg B, Wegscheider K et al (2003) Magnetic resonance perfusion measurements for the noninvasive detection of coronary artery disease. Circulation 108(4):432–437

Nagel E, Lima JA, George RT, Kramer CM (2009) Newer methods for noninvasive assessment of myocardial perfusion: cardiac magnetic resonance or cardiac computed tomography? JACC Cardiovasc Imaging 2(5):656–660

Roger VL, Go AS, Lloyd-Jones DM, Benjamin EJ, Berry JD, Borden WB et al (2012) Heart disease and stroke statistics—2012 update: a report from the American Heart Association. Circulation 125(1):e2–e220

Rosamond W, Flegal K, Furie K, Go A, Greenlund K, Haase N et al (2008) Heart disease and stroke statistics—2008 update: a report from the American Heart Association Statistics Committee and Stroke Statistics Subcommittee. Circulation 117(4):e25–e146

Ruzsics B, Lee H, Zwerner PL, Gebregziabher M, Costello P (2008) Schoepf UJ. Dual-energy CT of the heart for diagnosing coronary artery stenosis and myocardial ischemia-initial experience, Eur Radiol

Ruzsics B, Schwarz F, Schoepf UJ, Lee YS, Bastarrika G, Chiaramida SA et al (2009) Comparison of dual-energy computed tomography of the heart with single photon emission computed tomography for assessment of coronary artery stenosis and of the myocardial blood supply. Am J Cardiol 104(3):318–326

Schuijf JD, Wijns W, Jukema JW, Atsma DE, de Roos A, Lamb HJ et al (2006) Relationship between noninvasive coronary angiography with multi-slice computed tomography and myocardial perfusion imaging. J Am Coll Cardiol 48(12):2508–2514

Schwitter J, Wacker CM, van Rossum AC, Lombardi M, Al-Saadi N, Ahlstrom H et al (2008) MR-IMPACT: comparison of perfusion-cardiac magnetic resonance with single-photon emission computed tomography for the detection of coronary artery disease in a multicentre, multivendor, randomized trial. Eur Heart J 29(4):480–489

Shaw LJ, Berman DS, Maron DJ, Mancini GB, Hayes SW, Hartigan PM et al (2008) Optimal medical therapy with or without percutaneous coronary intervention to reduce ischemic burden: results from the clinical outcomes utilizing revascularization and aggressive drug evaluation (COURAGE) trial nuclear substudy. Circulation 117(10):1283–1291

Stenner P, Schmidt B, Allmendinger T, Flohr T, Kachelrie M (2010) Dynamic iterative beam hardening correction (DIBHC) in myocardial perfusion imaging using contrast-enhanced computed tomography. Invest Radiol 45(6):314–323

Stolzmann P, Scheffel H, Schertler T, Frauenfelder T, Leschka S, Husmann L et al (2008) Radiation dose estimates in dual-source computed tomography coronary angiography. Eur Radiol 18(3):592–599

Taylor AJ, Cerqueira M, Hodgson JM, Mark D, Min J, O'Gara P et al (2010) ACCF/SCCT/ACR/AHA/ASE/ASNC/NASCI/SCAI/SCMR 2010 appropriate use criteria for cardiac computed tomography. A report of the American College of Cardiology Foundation Appropriate Use Criteria Task Force, the Society of Cardiovascular Computed Tomography, the American College of Radiology, the American Heart Association, the American Society of Echocardiography, the American Society of Nuclear Cardiology, the North American Society for Cardiovascular Imaging, the Society for Cardiovascular Angiography and Interventions, and the Society for

Cardiovascular Magnetic Resonance. J Am Coll Cardiol 56(22): 1864–1894

Tonino PA, De Bruyne B, Pijls NH, Siebert U, Ikeno F, van' t Veer M et al (2009) Fractional flow reserve versus angiography for guiding percutaneous coronary intervention. N Engl J Med 360(3):213–224

Tonino PA, Fearon WF, De Bruyne B, Oldroyd KG, Leesar MA, Ver Lee PN et al (2010) Angiographic versus functional severity of coronary artery stenoses in the FAME study fractional flow reserve versus angiography in multivessel evaluation. J Am Coll Cardiol 55(25):2816–2821

Vanhoenacker PK, Heijenbrok-Kal MH, Van Heste R, Decramer I, Van Hoe LR, Wijns W et al (2007) Diagnostic performance of multidetector CT angiography for assessment of coronary artery disease: meta-analysis. Radiology 244(2):419–428

Vliegenthart R, Henzler T, Moscariello A, Ruzsics B, Bastarrika G, Oudkerk M et al (2012) CT of coronary heart disease: Part 1 CT of myocardial infarction, ischemia, and viability. AJR Am J Roentgenol 198(3):531–547

von Ballmoos MW, Haring B, Juillerat P, Alkadhi H (2011) Meta-analysis: diagnostic performance of low-radiation-dose coronary computed tomography angiography. Ann Intern Med 154(6): 413–420

Wang Y, Qin L, Shi X, Zeng Y, Jing H, Schoepf UJ et al (2012) Adenosine-stress dynamic myocardial perfusion imaging with second-generation dual-source CT: comparison with conventional catheter coronary angiography and SPECT nuclear myocardial perfusion imaging. AJR Am J Roentgenol 198(3):521–529

Weininger M, Schoepf UJ, Ramachandra A, Fink C, Rowe GW, Costello P et al (2012) Adenosine-stress dynamic real-time myocardial perfusion CT and adenosine-stress first-pass dual-energy myocardial perfusion CT for the assessment of acute chest pain: initial results. Eur J Radiol 81(12):3703–3710

Weininger M, Spears J, Rowe G, Costello P, Bastarrika G, Schoepf UJ (2011) First-pass myocardial stress perfusion imaging using 2nd generation dual-source CT. Presented at the 97th scientific assembly and annual meeting. Radiological Society of North America, 27 November–2 December, Chicago, IL

Wolfkiel CJ, Ferguson JL, Chomka EV, Law WR, Labin IN, Tenzer ML et al (1987) Measurement of myocardial blood flow by ultrafast computed tomography. Circulation 76(6):1262–1273

Dynamic, Time-Resolved Imaging of Myocardial Perfusion Using 256-Slice Computed Tomography

Teruhito Mochizuki, Akira Kurata, and Teruhito Kido

Contents

Abstract

Historically, myocardial perfusion scintigraphy (MPS) has been used to assess myocardial perfusion. Magnetic resonance imaging (MRI) has been used to assess both myocardial perfusion and delayed enhancement (viability). However, computed tomography (CT) has advantages over MPS and MRI in terms of spatial resolution, availability, simplicity, and shorter test time. CT can assess myocardial perfusion as increased myocardial contrast density. Adenosine triphosphate (ATP) or adenosine stress perfusion CT is comparable to MPS and MRI for the assessment of myocardial perfusion reserve (ischemia). When dynamic (first-pass) data are acquired, absolute myocardial blood flow (MBF, ml $g^{-1}min^{-1}$) can be measured by analyzing the time–density curve of myocardium and blood pool. Using wide-range multislice CT (256- to 320-slice CT) for dynamic acquisition, whole-heart regional MBF can be measured. In this chapter, the potential of 256-slice CT in the assessment of myocardial perfusion and viability is illustrated.

Abbreviations

ATP	Adenosine triphosphate
MDCT	Multidetector-row CT
MPS	Myocardial perfusion scintigraphy
MRI	Magnetic resonance imaging
CABG	Coronary artery bypass grafting
CT	Computed tomography
LDA	Low-density area
MBF	Myocardial blood flow
ED	End-systole
ES	End-systole

T. Mochizuki (✉) · A. Kurata · T. Kido
Department of Radiology, Ehime University School of Medicine, Shitsukawa Toon Ehime, Japan
e-mail: tmochi@m.ehime-u.ac.jp

U. J. Schoepf et al. (eds.), *CT Imaging of Myocardial Perfusion and Viability*, Medical Radiology. Diagnostic Imaging,
DOI: 10.1007/174_2013_912, © Springer-Verlag Berlin Heidelberg 2013
Published Online: 15 September 2013

1 Introduction

We proposed the potential of single-helical computed tomography (CT) for coronary imaging in 1999 (Mochizuki et al. 1999). Presently, the coronary arteries and plaque are evaluated using noninvasive multidetector-row CT (MDCT). An assessment of coronary artery stenosis and myocardial perfusion is essential for determining a treatment strategy for patients with coronary artery disease. Myocardial perfusion has usually been assessed with myocardial perfusion scintigraphy (MPS). Nuclear medicine has also been useful for the detection of myocardial ischemia and for the determination of viability and prognosis for patients with coronary artery disease (Hachamovitch et al. 2003, 2005). Recent reports have shown advantages of myocardial perfusion MRI over MPS (Sakuma et al. 2005). MRI is also reported to assess myocardial perfusion and delayed enhancement (i.e., assessment of myocardial ischemia and viability) better than CT (Nieman et al. 2008). However, CT has advantages over MRI in terms of spatial resolution, availability, simplicity, and shorter test time. We proposed the potential of single-helical CT for the assessment of myocardial perfusion (Mochizuki et al. 1999). With the use of wide-range multislice CT (256- to 320-slice CT), the whole heart can be scanned in 1 rotation, enabling whole-heart dynamic acquisition. In this chapter, the potential of CT (mainly 256-CT) for the assessment of myocardial perfusion and viability will be illustrated.

Ischemia, here, means "the reduction of myocardial perfusion reserve," which can be depicted as a low-density area (LDA) on an adenosine triphosphate (ATP) or adenosine-loaded scan.

2 Protocols

The protocol for performing full cardiac CT, including perfusion CT, is shown in Fig. 1. Myocardial perfusion CT can be performed alone (Kurata et al. 2005); however, coronary CT angiography is supplemented in most cases, with an added option for the delayed scan to assess myocardial viability. Because the time when myocardial ischemia is visible as an LDA is short, timing is very important to ensure that the scan shows the myocardial ischemia. To achieve the best timing, we use a test injection of 20 % diluted contrast medium (i.e., 10 ml of contrast medium is diluted to 50 ml), which is the same volume as the real scan. This test injection protocol provides a similar time–density curve, although the peak is low. Using this protocol, the timing can be adjusted easily to obtain the best result. Perfusion CT can be acquired at 1 point or dynamically. The best timing for myocardial enhancement is about 5 s later than that for coronary CT angiography. A standard ATP-stress protocol for myocardial perfusion scintigraphy (Miyagawa et al. 1995) can be applied to the ATP-stress perfusion CT.

The use of dynamic (first-pass) acquisition allows the best timing to depict ATP-induced ischemia as LDA. For the dynamic data acquisition, the use of low kilovolts and milliampere setting and iterative reconstruction are recommended to reduce radiation dose. The dynamic data acquisition allows quantification of myocardial blood flow (MBF), which is discussed later.

Perfusion CT should be done first to avoid polluting the dynamic data by the prior injection of contrast medium. Coronary CT angiography is performed later. Although the best scan timing for myocardial enhancement is about 5 s later, the acquisition for CT angiography can be used for the rest perfusion data. This method is considered not to increase the patient's radiation dose.

Finally, as an option when the patient may have had a myocardial infarction, a delayed enhancement scan should be performed to assess myocardial damage (i.e., to assess viability).

3 Patterns (Normal, Ischemia, Infarction)

Enhancement patterns of stress/rest (or delayed scan) are illustrated in Fig. 2. The normal pattern is normal/normal (no delayed enhancement), the ischemic pattern is LDA/normal (no delayed enhancement), and the myocardial infarction pattern is LDA/LDA (delayed enhancement). In patients with myocardial infarction history, myocardial thinning is often seen, demonstrating scar formation.

Angina pectoris in a patient with triple-vessel disease before and after coronary artery bypass grafting (CABG) is shown in Fig. 3. In this case, ATP-induced ischemia is seen as subendocardial LDA in the septum, the inferior wall, and in the lateral wall before CABG. CABG was performed in which the left internal mammary artery was used to bypass the proximal left anterior descending artery, a saphenous vein graft was placed in the left circumflex artery, and no grafting was done to the right coronary artery. Ischemia (LDA on ATP-stress) in the septum and lateral wall was diminished following CABG, but ischemia remained in the untreated inferior wall. The ischemia can be seen clearly with high spatial resolution.

A patient with old myocardial infarction is shown in Fig. 4. In this case, subendocardial to transmural LDA is seen on both ATP-stress and rest scans with delayed enhancement. Myocardial wall thinning is also seen in the old myocardial infarction.

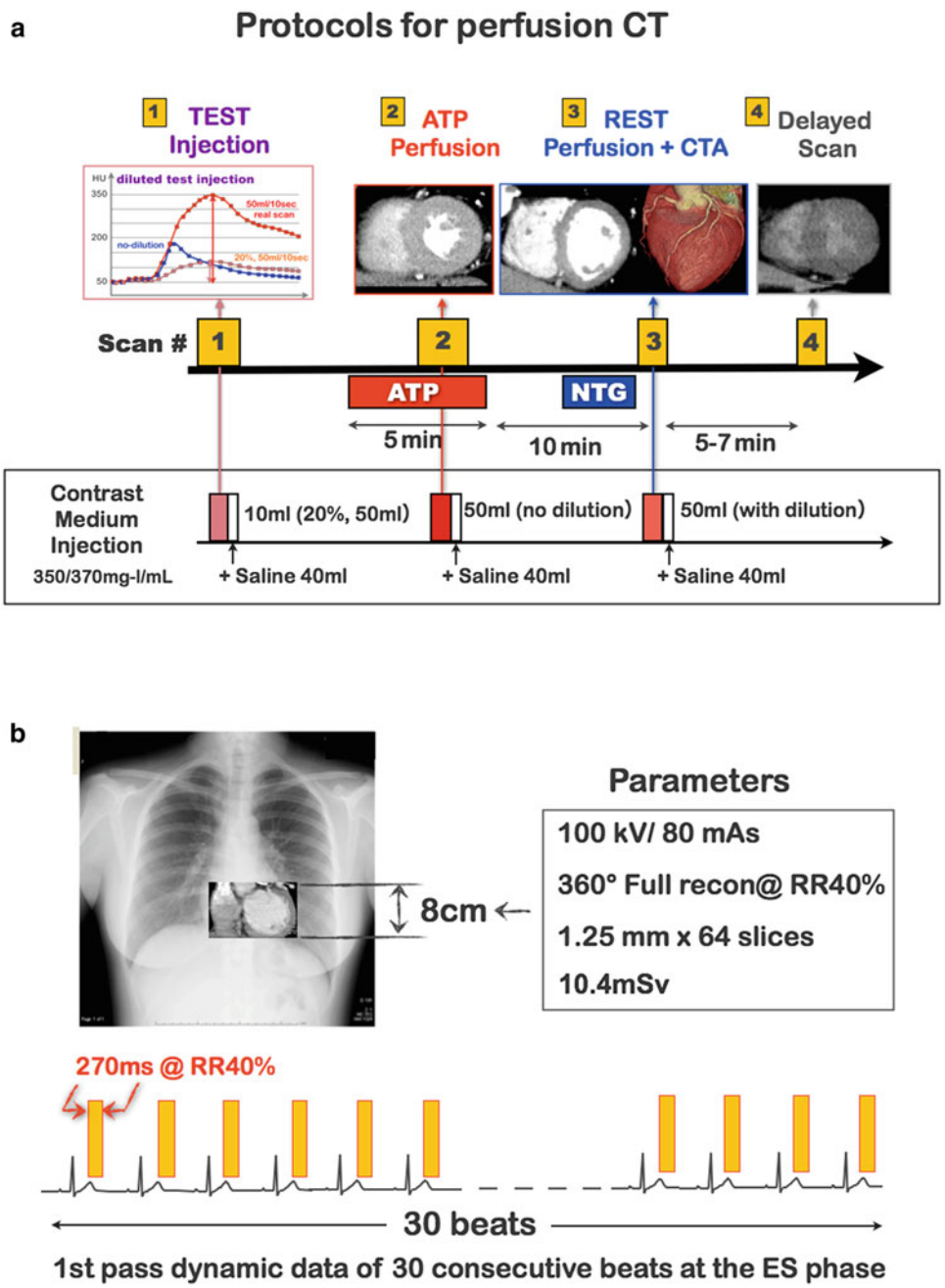

Fig. 1 **a** Study protocol for a full cardiac computed tomography (CT) scan, including perfusion CT scan, is illustrated. Scan #1 is a test injection, scan #2 is an adenosine triphosphate (ATP)-stress dynamic (first-pass) perfusion CT, scan #3 is a rest (non-ATP) perfusion CT (coronary CT angiography), and scan #4 is a delayed scan. **b** Dynamic (first-pass) acquisition protocol for 256-slice computed tomography. Because the z-axis coverage is 8 cm, the end-systolic (ES) phase is targeted to cover whole heart in 1 rotation. For accurate quantification of myocardial blood flow (ml g^{-1} min^{-1}), 1 rotation image (270 ms) is used to reduce artifacts. Scan parameters are optimized for 256-slice CT

4 Dynamic (First-Pass) Data Acquisition

Dynamic data acquisition during injection of the contrast medium enables visualization of the myocardial perfusion as an increase of density (Hounsfield units), although this requires an increase in radiation dose. Myocardial infarction is depicted as subendocardial or transmural low-density arc. Ischemic lesions can be depicted as low-density arcs on ATP-stress or adenosine stress acquisition. The advantage of dynamic acquisition over one-point acquisition is that it increases the detectability of a LDA, which appears only for a short period. Motion artifacts are distinguished from true findings by observing the cine (paging) of the dynamic images. Moreover, dynamic acquisition provides a time-density curve of myocardium and the aorta or left ventricle, enabling quantification of MBF.

5 Quantification of MBF

Absolute MBF (ml $g^{-1}min^{-1}$) has been quantified by ^{15}O–H_2O or ^{13}N–NH_3 dynamic (first-pass) positron emission tomography (PET) (Iida et al. 2000; Herzog et al. 2009). If similar dynamic data are obtained with CT, then MBF can

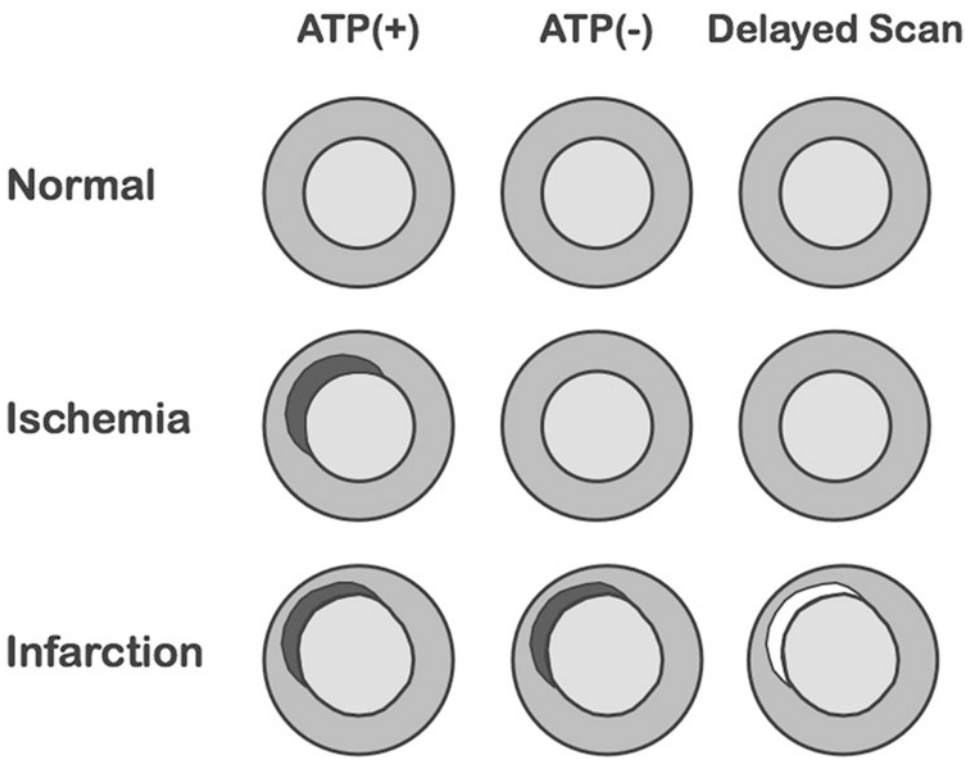

Fig. 2 Enhancement patterns of stress/rest and delayed scans are illustrated. In patients with ischemia, the low-density arc is seen only on adenosine triphosphate (ATP)-stress. In patients with myocardial infarction, the low-density arc is seen on both the ATP-stress and the rest scan, and the high-density arc is seen on the delayed scan

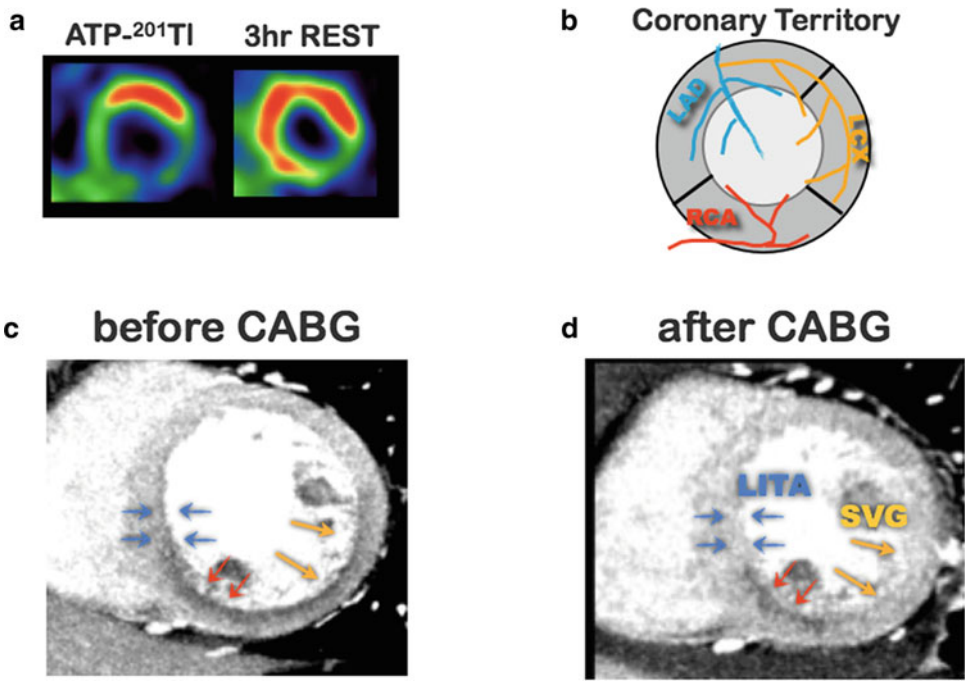

Fig. 3 A case of angina pectoris with triple-vessel disease before and after coronary artery bypass grafting (*CABG*). This patient had 50 % stenosis in the left main trunk (*LMT*), 90 % stenosis in the right coronary artery (*RCA*), and 90 % stenosis in the left circumflex (*LCX*) artery. Adenosine triphosphate (*ATP*)-induced ischemia is seen as a subendocardial low-density area (*LDA*) in the septum, the inferior wall, and the lateral wall before CABG. After CABG, in which the left internal mammary artery (*LITA*) was used to bypass the left anterior descending (*LAD*) artery, a saphenous vein graft (*SVG*) was placed to the LCX, and no grafting was done to the RCA, ischemia (LDA on ATP-stress) in the septum and lateral wall diminished, whereas ischemia remained in the untreated RCA territory

be generated (Kido et al. 2008; Bamberg et al. 2011). Assessing MBF before and after CABG allows better evaluation of the outcome of CABG (Shikata et al. 2010). Figure 5 demonstrates a patient with angina pectoris with chronic total obstruction of the left anterior ascending artery with collaterals. In this case, in addition to the improvement of MBF reserve on ATP-stress scan, the motion of the anterior wall improved from akinesis to normokinesis. In

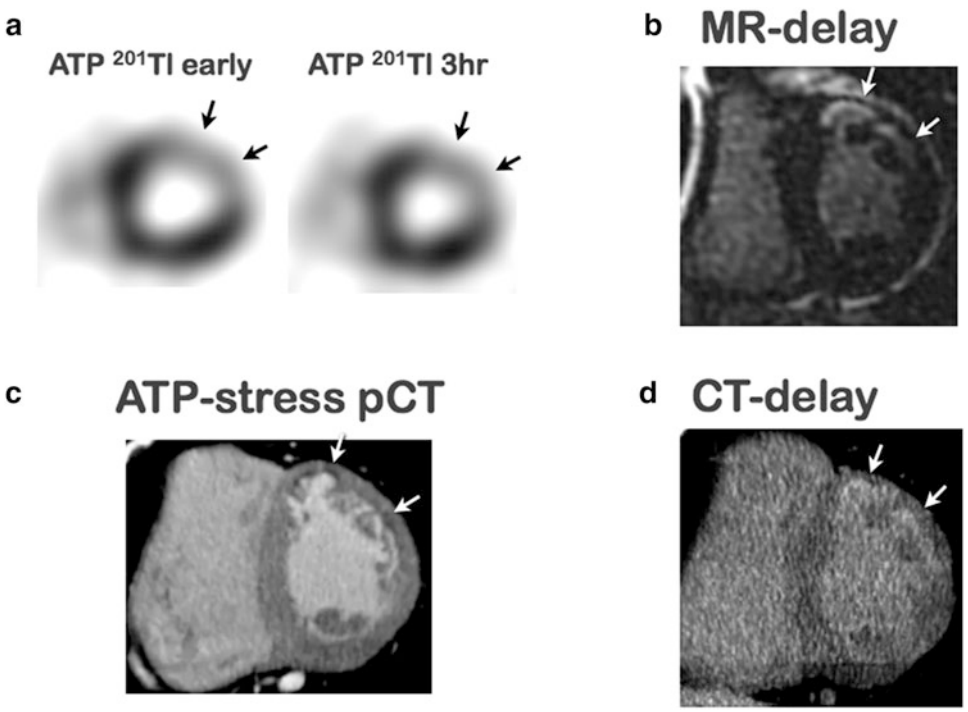

Fig. 4 A patient with old myocardial infarction. Comparable adenosine triphosphate (ATP)-stress/3 h rest ^{201}Tl scan shows fixed defect (fixed severe hypoperfusion) in the anterolateral wall (**a**). Magnetic resonance (*MR*)-delayed enhancement is seen in the infarction (**b**). In the ATP-stress dynamic computed tomography (*CT*), perfusion defect is seen in same anterolateral wall (**c**) and the old myocardial enhancement is seen in the delayed scan (**d**)

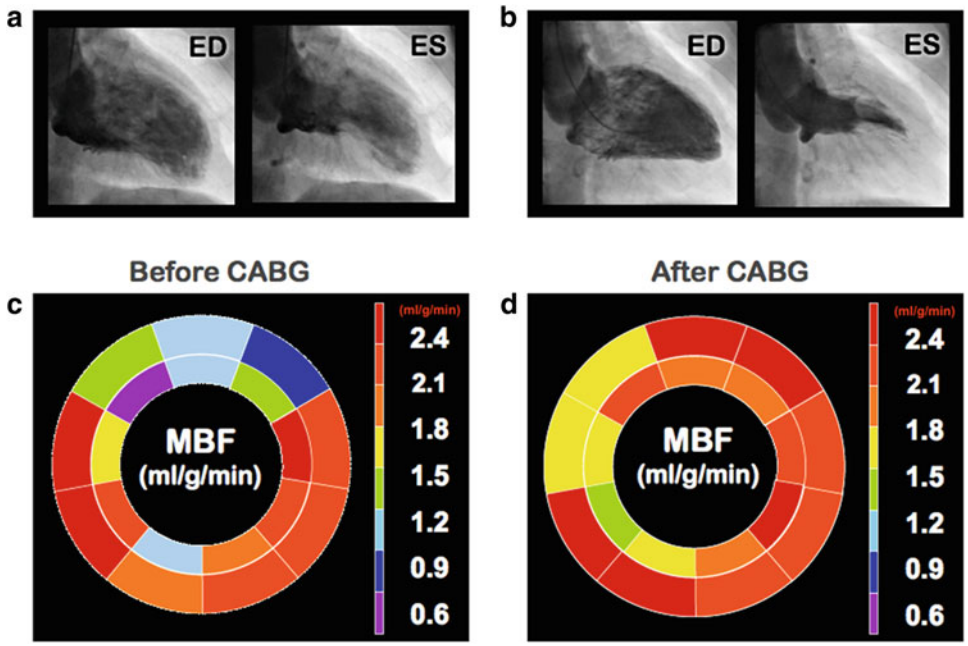

Fig. 5 A patient with angina pectoris showing chronic total obstruction of the left anterior ascending artery (*LAD*) with collaterals on the computed tomography image. Before coronary artery bypass grafting (*CABG*), ischemia is seen as low myocardial blood flow (*MBF*) in the akinetic anterior wall on adenosine triphosphate (*ATP*)-stress. After CABG, the MBF on ATP-stress is improved. Accordingly, MBF improved and wall motion also improved from akinesis to normokinesis (Revised from Fig. 3 in the reference: Shikata et al. Am Heart J 2010;160: 528–534)

most cases, after successful CABG surgery, an increase of MBF was observed on the ATP-stress scan (Fig. 6). There several methods to generate MBF from the dynamic data (Patlak et al. 1985; Lee et al. 2009; Slomka et al. 2012; Pack et al. 2008).

A wide-range detector such as 256-slice CT or 320-slice CT can cover the whole heart in one rotation, enabling dynamic acquisition of the whole heart (Fig. 7) and allowing regional MBF of the whole heart to be generated. However, our 256-slice CT has actually 128 detector rows,

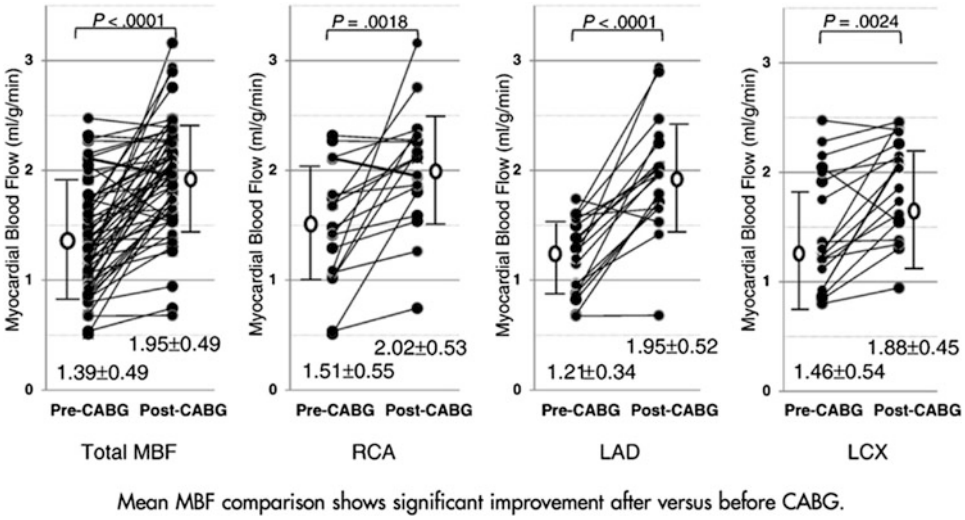

Fig. 6 MBF assessment before and after coronary artery bypass grafting (*CABG*). In most cases, after successful CABG, myocardial blood flow (*MBF*) increased on adenosine triphosphate-stress (Shikata et al. Am Heart J 2010;160: 528–534)

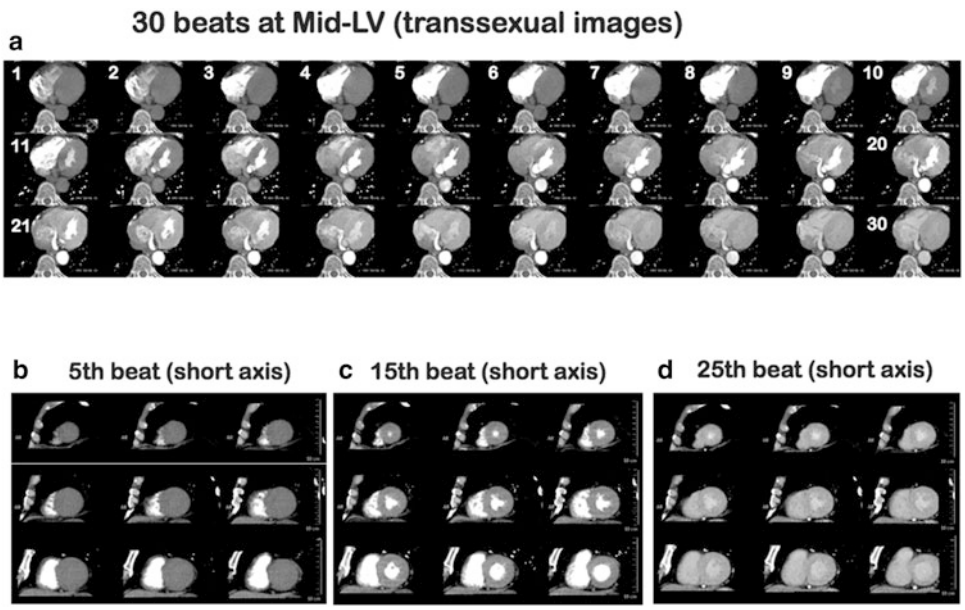

Fig. 7 Whole-heart dynamic (first-pass) perfusion 256-slice computed tomography scan. Blood flow is observed as contrast enhancement at the mid-left ventricular (*LV*) level in the transaxial image (**a**) From these images, gapless whole-heart short axial images can be generated throughout the 30 beats (**b**–**d**)

covering 8 cm in the z-axis. To cover the whole heart, we target the systolic phase when the left ventricle is small and the respiratory phase when the heart is in a more horizontal position than a vertical position, which can reduce scan range.

In our protocol, 30 consecutive systolic phases (beats) were acquired to obtain detailed input, which provides more accurate quantification. To reduce the radiation dose, thinning out the acquisition betas with interpolation is an option that may result in enough input being retained to measure MBF. Figure 8a, b show anterolateral ischemia on ATP-stress with both dynamic perfusion CT and MRI. As shown in this figure, ischemia is observed as LDA in a short period. The MBF generated by the 256-slice CT is comparable to that generated by MRI. The MBF of the whole heart can be expressed by concentric circles (Fig. 8c, d).

6 Delayed Enhancement

Viability assessment and delayed enhancement are described in detail in another chapter. Here, the delayed scan is described as an additional option for the perfusion CT protocol. Gadolinium-enhanced delayed MRI highlights myocardial infarction with higher contrast than CT (Nieman et al. 2008). However, CT has advantages over MRI in terms of spatial resolution and easy availability. Figure 9

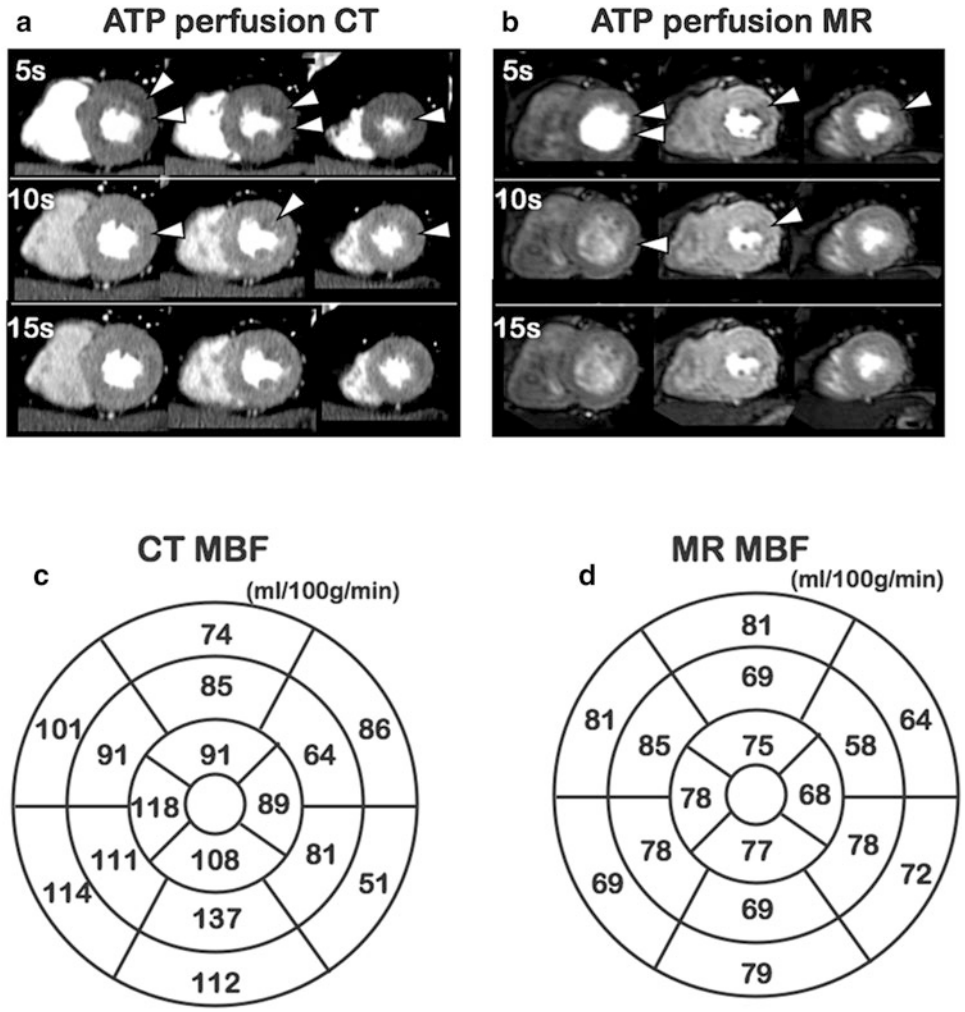

Fig. 8 An adenosine triphosphate (*ATP*)-stress computed tomography (*CT*) scan of a patient with anterolateral ischemia. Flow dynamics demonstrates transient ischemia as a low-density area (**a**). Comparable ATP-stress dynamic magnetic resonance imaging (*MRI*) shows the matched transient hypointense area in the same region (**b**). From the time-density curve of the whole-heart dynamic data, regional myocardial blood flow (ml/100 g/min) can be generated. This data can be graphically depicted using a Bull's Eye map (**c**). Comparable MRI values are illustrated in **d**

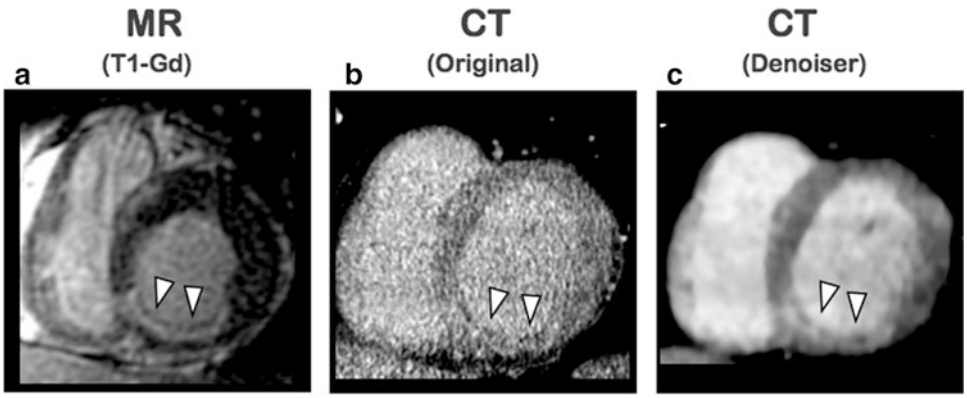

Fig. 9 Delayed enhancement images in a patient with inferior myocardial infarction. **a** Gadolinium (*Gd*)-enhanced T1, **b** original computed tomography (*CT*) using delayed enhancement, **c** CT using delayed enhancement with denoiser filter. By using the sophisticated denoiser filter, delayed enhancement can be highlighted as clearly with CT as with magnetic resonance imaging (*MRI*)

demonstrates delayed enhancement in a patient with old myocardial infarction and compares CT with MRI. When a sophisticated denoiser filter is used, faint delayed enhancement can clearly be highlighted. This enables more accurate assessment of the infarct area, or high-density area.

References

Bamberg F et al (2011) Detection of hemodynamically significant coronary artery stenosis: incremental diagnostic value of dynamic CT-bases myocardial perfusion imaging. Radiology 260:528–534

Hachamovitch R et al (2003) Comparison of the short-term survival benefit associated with revascularization compared with medical therapy in patients with no prior coronary artery disease undergoing stress myocardial perfusion single photon emission computed tomography. Circulation 107:2900–2906

Hachamovitch R et al (2005) Prognostic score for prediction of cardiac mortality risk after adenosine stress myocardial perfusion scintigraphy. J Am Coll Cardiol 45:722–729

Herzog BA et al (2009) Long-term prognostic value of 13 N-ammonia myocardial perfusion emission tomography added value of coronary flow reserve. J Am Coll Cardiol 52:150–156

Iida H et al (2000) Quantitative assessment of regional myocardial blood flow using oxygen-15-labelled water and positron emission tomography: a multicentre evaluation in Japan. Eur J Nucl Med 27:748–749

Kido T et al (2008) Quantification of regional myocardial blood flow using first-pass multidetector-row computed tomography and adenosine triphosphate in coronary artery disease. Circ J 72:1086–1091

Kurata A et al (2005) Myocardial perfusion imaging using adenosine triphosphate stress multi-slice computed tomography: alternative to stress myocardial perfusion scintigraphy. Circ J 69:550–557

Lee DC et al (2009) Quantification of absolute myocardial blood flow by magnetic resonance perfusion imaging. JACC Cardiovasc Imaging 2:761–770

Miyagawa M et al (1995) Thallium-201 myocardial tomography with intravenous infusion of adenosine triphosphate in diagnosis of coronary artery disease. J Am Coll Cardiol 26:1196–1201

Mochizuki T et al (1999b) Demonstration of acute myocardial infarction by subsecond spiral computed tomography: early defect and delayed enhancement. Circulation 99:2058–2059

Mochizuki T et al (1999a) LAD stenosis detected by subsecond spiral CT. Circulation 99:1523

Nieman K et al (2008) Reperfused myocardial infarction: contrast-enhanced 64-section CT in comparison to MR imaging. Radiology 247:49–56

Pack NA et al (2008) Estimating myocardial perfusion from dynamic contrast-enhanced CMR with a model-independent deconvolution method. J Cardiovasc Magn Reson 10:12

Patlak CS et al (1985) Graphical evaluation of blood-to-brain transfer constants from multiple-time uptake data. Generalizations J Cereb Blood Flow Metab 5:584–590

Sakuma H et al (2005) Diagnostic accuracy of stress first-pass contrast-enhanced myocardial perfusion MRI compared with stress myocardial perfusion scintigraphy. AJR Am J Roentgenol 185:95–102

Shikata F et al (2010) Regional myocardial blood flow measured by stress multidetector computed tomography as a predictor of left ventricular function after coronary artery bypass grafting. Am Heart J 160:528–534

Slomka PJ et al (2012) Comparison of clinical tools for measurement of regional stress and rest myocardial blood flow with 13 N-ammonia PET/CT. J Nucl Med 53:171–181

Dynamic, Time-Resolved CT Imaging of Myocardial Perfusion: 320-Slice CT

Narinder S. Paul

Contents

Abstract

Cardiac Computed Tomography has progressed beyond providing a purely detailed anatomical description of coronary disease, to a comprehensive demonstration of anatomic-physiological disturbance that forms the basis of a "one stop shop" for assessment of coronary disease. The 320MDCT wide area detector provides a unique capability to assess the whole heart during a single gantry rotation. This chapter outlines the scientific advances made using the 320MDCT: in animal models of cardiac ischemia followed by translational work in human subjects; initially with discussion of single centre trials followed by introduction of the Core 320 multi-centre trial.

1 Introduction

Computed tomography coronary angiography (CTCA) provides an accurate and non-invasive imaging tool for exclusion of significant coronary artery disease (CAD). However, the presence of arterial disease on CTCA correlates poorly with perfusion abnormalities noted on myocardial perfusion imaging (MPI) (Hacker et al. 2005; Schuijf et al. 2006; Klocke et al. 2003). Myocardial perfusion imaging (MPI) lacks the anatomical resolution of CTCA for coronary disease but is established as a useful tool in the diagnosis and prognosis of patients with CAD (Klocke et al. 2003). Therefore there has been considerable interest in providing a "one stop" comprehensive cardiac assessment with computed tomography (CT) by combining the high spatial resolution images of coronary artery anatomy provided by CTCA with myocardial perfusion indices from CT perfusion (CTP). As dipyridamole or adenosine induced coronary vasodilatation has been demonstrated to provide equivalent cardiac stress as compared to exercise stress testing with single-photon emission tomography

N. S. Paul (✉)
Joint Department of Medical Imaging
and the Peter Munk Cardiac Centre,
Toronto General Hospital, University of Toronto,
Toronto, Canada
e-mail: narinder.paul@uhn.on.ca

U. J. Schoepf et al. (eds.), *CT Imaging of Myocardial Perfusion and Viability*, Medical Radiology. Diagnostic Imaging,
DOI: 10.1007/174_2012_792, © Springer-Verlag Berlin Heidelberg 2013
Published Online: 17 January 2013

(SPECT) in diagnosing CAD (Nguyen et al. 1990; Parodi et al. 1991; Coyne et al. 1991; Nishimura et al. 1992; Gupta et al. 1992), these agents have been incorporated into CTP protocols.

The purpose of this chapter is to highlight advances in myocardial perfusion and viability imaging using the Aquilion CT series (Toshiba Medical Systems, Otawara, Japan) culminating in the Aquilion ONE, 320 multi detector row computed tomography (320MDCT) scan unit.

CT perfusion image acquisition is performed during first pass myocardial perfusion of iodinated contrast medium (CM) through the blood pool and the left ventricular (LV) myocardium. Regions of interest (ROIs) are prescribed in the blood pool and LV myocardium to create time attenuation curves (TACs) from which the myocardial blood flow (MBF) can be calculated. Accurate data analysis relies on the validity of several assumptions including: (1) there is complete mixing of the iodinated contrast with the blood before it arrives in the heart, (2) there is minimal recirculation of the iodinated contrast, (3) the measured CT attenuation number (in Hounsfield Unit, HU) accurately corresponds to the concentration of the iodinated contrast, (4) the volume of iodinated contrast is negligible compared to the blood volume, (5) the iodinated contrast does not induce physiologic or hemodynamic changes during cardiac transit, and (6) the iodinated contrast remains within the intravascular compartment during first pass perfusion (Rumberger and Bell 1992; Rumberger et al. 1987).

An initial investigation into myocardial viability assessment by computer tomography was performed using 32MDCT in canine and porcine models (Lardo et al. 2006). Ten anesthetised and mechanically ventilated canines had induced occlusion of the proximal left anterior descending (LAD) coronary artery by inflating a 3-mm angioplasty balloon for 90 min. Quantification of MBF was performed by measurement of injected neutron activated microspheres into the LV cavity before, during, and after LAD occlusion. Cardiac CT was administered, the animals were sacrificed, and post mortem analysis was performed. Similarly, LAD occlusion was performed in seven anesthetised and mechanically ventilated pigs that had inflation of a 3-mm balloon in the mid LAD for 60 min. The animals recovered for 8 weeks and then had cardiac CT performed under sedation. The pigs were subsequently sacrificed and post mortem analysis was performed. Cardiac CT was performed using a detector collimation of 32 × 0.5 mm, tube potential of 135 kV, tube current of 420 mA, gantry rotation of 400 ms, and a pitch of 7.2. The heart rate was controlled to less than 100 bpm by using 2–5 mg of intravenous propranolol, and post infarct arrhythmias were suppressed by using intravenous lidocaine. A 150 mL bolus of intravenous CM containing 320 $mg{\cdot}mL^{-1}$ iodine was injected and image acquisition was triggered at a density threshold of 150 HU in the ascending aorta. Retrospectively gated cardiac imaging was performed at first pass and every 5 min for 40 min. Axial 0.5-mm images were reconstructed at 75 % of the R–R interval with additional image reconstructions for functional analysis. Image analysis was performed with proprietary cardiac software (Toshiba Medical Systems) that performed automated border detection with delineation of endocardial and epicardial borders. Qualitative and quantitative analysis revealed peak myocardial attenuation at 5 min following injection of CM with decrease in attenuation over 40 min. Areas of hyper- and hypo-attenuation were manually traced and represented infarcted myocardium and areas of microvascular obstruction respectively. The MDCT assessment of infarct size and depth correlated well with post mortem assessment. This study demonstrated that 32MDCT can accurately determine myocardial viability by delineating and characterising acute and chronic myocardial infarction.

Early validation of first-pass, contrast-enhanced helical 64MDCT imaging was used to detect a myocardial flow deficit due to an induced stenosis in the left anterior descending (LAD) coronary artery during adenosine stress imaging (George et al. 2006). The research was performed using a canine model in which a 50 % LAD artery stenosis was induced. Baseline and post-stress MBF were measured using neutron-activated microspheres that were injected into the left atrium and sampled in the descending thoracic aorta. Intravenous propranolol (5–20 mg) was used to maintain a heart rate below 100 bpm. Intravenous adenosine was infused for 5 min at 140–210 $mcg{\cdot}kg^{-1}{\cdot}min^{-1}$. Intravenous CM containing 320 mg $iodine{\cdot}mL^{-1}$ was injected at 2.5 $mL{\cdot}s^{-1}$ for 40 s. Automated threshold-triggered image acquisition was initiated at a density threshold of 180 HU in the descending thoracic aorta using retrospective ECG gating, detector collimation of 32 × 0.5 mm, tube potential of 120 kV, tube current of 400 mA, a gantry rotation of 400 ms, and a helical pitch 6.4–8.8. Segmented image reconstruction was performed at 10 % phase intervals of the acquired R–R cycle. The 80 % phase was chosen for image reconstruction and 4-mm LV short axis images were reconstructed. ROIs were located through LV wall segments in the LAD territory and remote myocardium. Measurement values from the remote myocardium were used to define the mean and standard deviation (SD) of attenuation (in HU) for normal-perfused myocardium. Therefore, under-perfused myocardium was defined as one SD below this threshold. The results in seven canine models demonstrated significant differences in qualitative assessment and semi-quantitative assessment of perfused (180.4 ± 41.9 HU) and under-perfused (92.3 ± 39.5 HU) myocardium. Calculations of flow reserve in perfused (7.3 ± 4.7) and under-perfused (0.17 ± 0.07) myocardium also showed significant differences. This study demonstrated that first-pass, contrast-enhanced helical

64MDCT imaging can detect significant LAD territory flow disturbance using adenosine stress; and that MDCT derived parameters of LV myocardial perfusion have good correlation with microsphere-derived absolute MBF.

Subsequent research prompted evaluation of myocardial perfusion with dynamic CTP in six canines with induced 50 % LAD stenosis (George et al. 2007). Image acquisition relied on a stationary table during gantry rotation and injection of iodinated contrast material (CM) in order to record changes in tissue attenuation over time. This allowed TAC to be plotted and enabled quantification of absolute MBF.

Each canine was positioned such that the mid to distal LV was in the scan plane. Intravenous adenosine (140 mcg·kg^{-1}·min^{-1}) was infused for 5 min followed by 30 mL of intravenous CM containing 320 mg iodine·mL^{-1} injected at 10 mL·s^{-1}. Image acquisition occurred using a detector collimation of 8 mm × 4 mm, tube potential of 120 kV, tube current of 150 mA, a gantry rotation time of 400 ms, and a scan time of 70 s. Intravenous metoprolol (5–20 mg) was used to maintain a heart rate below 100 bpm; respiratory motion was suppressed using pancuronium (0.1 mg·kg^{-1}). The MBF was measured during adenosine infusion, by injecting neutron-activated microspheres into the left atrium and performing quantitative measurements in the proximal descending aorta. Short-axis images through the LV were reconstructed using 8 mm slice thickness and ROIs were located through the target anterior LV wall and the remote inferior and lateral walls to create TAC. The TAC was normalised for the arterial input function (AIF) by using the ratio of the LV blood pool upslope to the LV blood pool peak enhancement. A dual compartment deconvolution method was applied to the myocardial upslope-to-LV-upslope and myocardial upslope-to-LV-max ratio to evaluate dynamic MDCT myocardial perfusion. This analysis demonstrated a strong correlation between the semi-quantitative CT imaging results and the microsphere MBF measurements. This study confirmed the accuracy of 64MDCT perfusion using the myocardial upslope normalized to the LV blood pool upslope or the maximum LV attenuation density, and also the application of model-based deconvolution analysis to dynamic MDCT TAC.

Although dynamic CTP analysis was shown to be accurate for myocardial perfusion, the limited scan coverage with 64MDCT required adaptation of the technique with helical acquisition for whole-LV assessment. The next stage in evolution of CTP utilized a combination of dynamic image acquisition; incorporating images acquired during bolus tracking to acquire the AIF curve together with ECG-gated helical acquisition of the entire LV myocardium (George et al. 2010). The technique was initially validated in four healthy canines scanned on 64MDCT using bolus tracking and a helical scan mode during injection of iodinated (320 mg iodine·mL^{-1}) CM at 4 mL·s^{-1} using a triphasic protocol: an initial 16 mL of 100 % CM followed by 40 mL of 30 % CM–70 % normal saline mixture, and a final 50 cc of 100 % normal saline. A retrospective ECG-gated acquisition was used with 64 × 0.5 mm detector collimation, 120 kV tube potential, 400 mA tube current, 400 ms gantry rotation time, and a helical pitch of 14.4–16.2. The bolus tracking data were reconstructed at 400 ms intervals using a 2 mm slice thickness, ROIs were prescribed in the aortic root to create the TAC for the early part of the AIF. Helical images were then reconstructed at 80 % of the R–R interval using a 4 mm slice thickness and a ROI prescribed in the intravascular blood pool from the aortic root through the LV outflow tract to the LV apex. The signal intensity of the blood pool was correlated with the time of image acquisition for the axial slices and the data used to construct the latter part of the TAC of the AIF. The TAC was adjusted for baseline attenuation. After a washout period of 10 min, the canine hearts were re-scanned during injection of iodinated intravenous CM; a dynamic MDCT scan was performed for 60 s through the aortic root using the same X-ray tube exposure parameters as for the helical scan with and a detector collimation of 4 × 8 mm. Images were reconstructed at 8 mm slice thickness and 400 ms intervals. A ROI was prescribed in the aortic root and plotted against time for a TAC. Data values were corrected for baseline attenuation. The bolus tracking and helical acquisitions were repeated in seven canines that had induced LAD stenosis. Neutron activated microspheres were injected following the helical acquisition and sampled in the descending thoracic aorta in order to measure the myocardial blood flow. The AIF was calculated from the bolus tracking and helical acquisitions and myocardial perfusion was measured in the left ventricle. This study demonstrated that the early and late phases of the TAC of the AIV could be calculated using available data from the automated bolus tracking threshold trigger in cardiac CT and that the helically acquired MDCT images had good correlation with microsphere generated indices of MBF ($R2 = 0.86$, $P < 0.001$).

Increased appreciation of LV myocardial blood flow, specifically the differential blood supply to the LV wall with increased perfusion to the subendocardium compared with the subepicardial segments, created interest in evaluation of a transmural perfusion ratio (TPR) (George et al. 2009). In this study, 40 patients with documented abnormal SPECT MPI had CTCA and CTP within 60 days. Patients were randomized to stress/perfusion cardiac CT with either 64MDCT or with 256MDCT. All patients received similar preparation with oral/intravenous metoprolol to maintain a heart rate below 65 bpm and intravenous hydration with 250–500 mL normal saline. All patients had an infusion of

intravenous adenosine (140 mcg·kg^{-1}·min^{-1}) for 5 min prior to injection of 90–95 mL of CM containing 370 mg·mL^{-1} iodine injected at 5 mL·s^{-1} followed by 30 mL of normal saline. Patients scanned with 64MDCT had image acquisition triggered automatically at a threshold of 150 HU in the LV blood pool. The retrospectively ECG-gated acquisition was performed using 64 × 0.5 mm detector collimation, tube potential of 120 kVp, tube current of 400 mA, gantry rotation of 400 ms, and a pitch that varied with heart rate. Images were obtained for a combined stress CTCA-CTP study. Patients scanned with 256MDCT had an initial test bolus injection of 20 mL CM (370 mg iodine mL^{-1}) at 5 mL·s^{-1} to determine peak arterial enhancement. For CTP imaging, a triphasic intravenous protocol was used at 5 mL·s^{-1}: 50 mL of 100 % contrast (370 mg iodine mL^{-1}), 20 mL of 50 % contrast and saline, and 30 mL normal saline. The detector collimation was 128 × 1.0 mm, tube potential was 120 kV, tube current was 200 mA, gantry rotation was 500 ms, and scan time was 1.5 s. A 10-min rest/wash-out period was required after acquisition of the stress CTP images prior to a second injection of 60 mL iodinated CM at 5 mL·s^{-1} to obtain a diagnostic CTCA and rest perfusion images using a detector collimation of 256 × 0.5 mm, a tube potential of 120 kV, a tube current of 350 mA, a gantry rotation of 500 ms, and a scan time 1.5 s. Cardiac perfusion analysis was performed for all patients using contiguous 3-mm images orientated in the short axis of the left ventricle from end diastolic phases (80–100 % R–R) by using an automated border detection algorithm to define the subendocardial, mid-myocardial, and subepicardial borders in a 16-segment LV anatomical perfusion model. The TPR was defined as the attenuation ratio of the subendocardium to the subepicardium and was calculated separately for each segment. Invasive catheter coronary angiography and quantitative coronary analysis were performed in 27 patients. In patients without CAD, the mean TPR was 1.12 ± 0.13 with good interobserver variability for rest ($\kappa = 0.72$, 95 % CI, 0.63–0.802) and stress ($\kappa = 0.63$, 95 % CI, 0.56–0.70) images. The TPR decreased with increasing luminal stenosis and measured 1.09 ± 0.11 for 30–49 % stenosis, 1.06 ± 0.14 for a 50–69 % stenosis, and 10.91 ± 0.10 for a high grade stenosis (≥70 %). This study demonstrated a significant inverse relationship between the TPR and the severity of luminal stenosis.

Increased experience of CTP analysis reinforced the importance of standardising image assessment in order to understand the range of normal appearances and to minimise misinterpretation of artifacts. For qualitative image analysis, a narrow window (W200–300) and level setting (L100–150) is recommended for stress, rest, and delayed enhancement images (Ko et al. 2011). Typical values of attenuation for non-enhanced myocardium ranges from 40

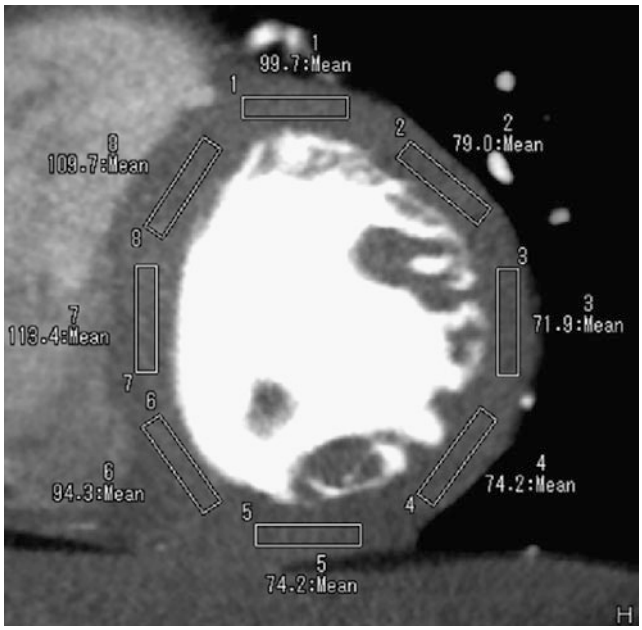

Fig. 1 Short-axis reconstruction through the left ventricle illustrating locations of ROI and corresponding LV myocardium attenuation values (in HU)

to 60 HU, and normal myocardium enhances from 100 to 120 HU (Valdiviezo 2010). The regional distribution of LV wall enhancement was evaluated in consecutive patients who had cardiac CT performed using 320MDCT without vasodilator stress (Crossett et al. 2011). Image acquisition was performed using a detector collimation of 240–320 × 0.5 mm, a tube potential of 100–135 kV, a tube current of 400–580 mA, a gantry rotation of 350 ms, and a temporal exposure window of 70–80 % of the R–R interval. Oral metoprolol (50–100 mg) with supplementary intravenous metoprolol (5–30 mg) was administered to maintain a heart rate below 65 bpm. Sublingual nitrates (40 mcg) were given followed by a dual phase injection of iodinated CM containing 350 mg·mL^{-1} iodine with an initial bolus of 75 mL at 6 mL·s^{-1} followed by 50 mL of normal saline at the same rate. Image acquisition was triggered at a threshold of 300 HU in the descending thoracic aorta. Twenty-one patients had normal epicardial arteries. In these patients, 5-mm thick short axis images were reconstructed through the left ventricle at basal, mid, and apical regions. Eight identical rectangular ROIs were placed in the mid myocardium, covering all segments but not restricted to the American Heart Association 17-segment model (Fig. 1).

Analysis of the LV myocardium enhancement demonstrated that the lateral myocardial LV wall has a mean attenuation of 79.4 HU (42.3–162.7 HU) in the mid ventricle compared with the inferior, septal, and anterior LV wall segments at this level, which demonstrate a mean attenuation of 103.9 HU (11.4–159.6 HU). This study suggested that there is differential enhancement of the left

ventricle myocardium at rest in patients with normal epicardial coronary arteries as demonstrated on 320MDCT.

Assessment of CTP using 320MDCT and vasodilator stress was performed in a cohort of patients without documented CAD (Kühl et al. 2012). This prospective study recruited healthy subjects to one of three groups, each with 14 subjects as follows: group 1a had MPI at rest using ^{13}NH3–PET, group 1b had rest CTCA–CTP, and group 2 had rest CTCA–CTP and stress CTP using adenosine infusion at 140 mcg·mL^{-1}·min^{-1}. LV analysis was performed using a 16-segment AHA model (apex excluded). The myocardium was divided into three layers: the sub-endocardium, the mid-myocardium, and the sub-epicardium; the relative TPR was calculated for each segment. The results confirmed the differential segmental perfusion of the LV myocardium that had been previously demonstrated on CTP; the highest values were measured in anteroseptal segments, 1, 2, 3, 7, 8, 9, while the lowest values were observed in the lateral wall in segments, 5, 6, 11, 12, and 16. This pattern of perfusion was mirrored by ^{13}NH3–PET. At rest, sub-endocardial perfusion was higher than for the mid-myocardium and the sub-epicardium. With vasodilator stress, there was a 21 and 23 % increase in perfusion to the mid-myocardium and the sub-epicardium, respectively, which eliminated any significant density gradient between these layers. Similarly, the overall increase in myocardial perfusion due to vasodilator stress also led to a significant reduction in segmental variation of relative perfusion values. This study demonstrated that segmental differences in LV myocardium perfusion seen with 320MDCT in healthy subjects are mirrored using ^{13}NH3–PET imaging and that this may be a true physiological phenomenon rather than artifact. In addition, vasodilator stress significantly increases overall myocardial perfusion and decreases the segmental and transmural variation in LV perfusion.

However, motion and beam hardening artifacts can influence the relationship between the measured CT attenuation number and concentration of iodinated contrast (Mehra et al. 2011a, b). Motion artifact are minimized through the use of beta blockers during combined CTCA and CTP protocols. Beam hardening artifacts occur when there is preferential absorption of low-kV photons as the X-ray beam passes through the iodinated CM. The resulting higher energy emergent X-ray beam produces beam-hardening artifacts which simulate perfusion defects in the LV myocardium (Brooks and Di Chiro 1976; Zatz and Alvarez 1977).

The characteristics of beam hardening artifacts were evaluated in a phantom study using the 320MDCT (Kitagawa et al. 2010). An anthropomorphic LV urethane phantom was constructed with and without lesions that simulated perfusion defects that measured 50 % of the LV wall thickness in depth and 90 ° in circumference. An 18-mm syringe simulated the thoracic aorta and both were placed in an anthropomorphic chest phantom, which had water bags placed within the thoracic cavity and around the chest phantom. The phantom was scanned with a 320MDCT unit using the following imaging protocol: collimation of 320 × 0.5 mm, tube voltage of 120 kV, tube current of 500 mA, and gantry rotation time of 350 ms. Half-reconstruction 3-mm thick images orientated along the LV short axis were reconstructed using a standard body kernel, FC13, without beam hardening correction (BHC); another set of images were reconstructed using the standard body kernel, FC03, but with BHC. The LV cavity and syringe were filled with water, scanned, and then filled with iodinated CM and re-scanned. The BHC correction algorithm compared the degree of beam hardening from areas of high contrast (iodinated contrast) to those from areas of water density in order to produce a corrected image (Olson et al. 1981). The attenuation of the "normal" perfused myocardium was measured without BHC. Beam hardening was defined if the measured attenuation was less than 2 SD of this value. The algorithm was then tested in a canine model with an induced 50 % reduction in hyperaemic flow either in the LAD or left circumflex (Cx) coronary arteries. The animal was placed in a 256MDCT such that the scan range covered the entire heart. Intravenous metoprolol (5–30 mg) was given to achieve a heart rate below 100 bpm and pancuronium (0.1 mg·kg^{-1}) to minimise respiratory motion artifacts. An infusion of intravenous adenosine (0.14 mg·kg^{-1}·min^{-1}) was given over 5 min during which time intravenous CM containing 370 mg iodine·mL^{-1} was injected at 4 cc·s^{-1} for 6 s. Image acquisition was performed using a dynamic volume CT scan mode with a detector collimation of 256 × 0.5 mm, a gantry rotation time of 500 ms, tube potential of 120 kV, tube current of 100 mA, and a scan time of 60 s. Short axis 0.5 mm images were created through the mid ventricle using a mid-diastolic phase and multi-segmented reconstruction, with and without BHC. ROIs were drawn in the LV wall and in the left and right ventricular cavities; TACs were calculated for each ROI. Upslope analysis was performed by comparing the TAC for the LV blood pool to the peak enhancement in myocardium, normalized by the peak LV blood pool enhancement. Assessment of MBF was compared with injected microspheres. The phantom data confirmed that beam hardening artifacts interfered with the demonstration of perfusion defects. However, the BHC algorithm effectively improved the demonstration of the true defects and accounted for the presence of iodinated CM in the LV cavity and descending thoracic aorta. The BHC had a variable influence on improving the upslope perfusion analysis in the canine model with an unpredictable performance in the interventricular septum. This study demonstrated that beam hardening artifact is an important confounder in CT assessment of myocardial perfusion and that it can be partially corrected in vivo using a BHC algorithm.

Table 1 Per vessel territory diagnostic accuracy of computed tomography coronary angiography, computed tomography myocardial perfusion imaging, and quantitative coronary angiography compared with fractional flow reserve (n = 86)

	CTA DS≥50%	Perfusion defect on CTP	CTA DS ≥50 % and perfusion defect on CTP	CTA DS ≥50 % or perfusiondefect on CTP	QCA DS≥50 %	QCA DS≥70%
True positive (n)	38	31	28	41	29	11
False positive (n)	18	7	1	24	17	1
True negative (n)	27	38	44	21	28	44
False negative (n)	3	10	13	0	12	30
Sensitivity (%)	93 (84–100)	76 (62–89)	68 (54–83)	100 (89–00)	71 (55–87)	27 (12–41)
Specificity (%)	60 (43–77)	84 (73–96)	98 (93–100)	47 (31–63)	62 (47–78)	98 (93–100)
PPV (%)	68 (53–82)	82 (67–96)	97 (89–100)	63 (49–77)	63 (46–80)	92 (72–100)
NPV (%)	90 (79–100)	79 (65–93)	77 (64–90)	100 (81–100)	70 (54–86)	59 (48–71)
Kappa statistic	0.52 (0.35–0.69)	0.60 (0.43–0.77)	0.67 (0.52–0.82)	0.52 (0.37–0.68)	0.33 (0.13–0.53)	0.25 (0.10–0.40)
Accuracy (%)	76	80	84	73	66	64

Intracoronary pressure-derived fractional flow reserve (FFR) is the clinical gold standard for assessing the need for revascularization of a discovered coronary artery stenosis (Pijls et al. 1996). The utility of CTP and combination CTCA/CTP with 320MDCT for evaluating patients under consideration for revascularization was compared with FFR in 42 patients who presented with chest pain and had greater than 50 % luminal stenosis on coronary angiography (Ko et al. 2012). All patients had FFR, CTA, CTP, and delayed contrast enhanced cardiac CT within 14 days of the catheter coronary angiography. Of this study cohort, 31 out of 42 (74 %) patients had perfusion abnormalities on CTP, 22 patients (52 %) had a single-vessel territory perfusion defect and 9 (21 %) had two-vessel territory perfusion defects. The majority (60 %) of perfusion defects were located in the LAD territory. All perfusion defects on CTP were reversible. FFR was performed in 68 % of all vessels and when compared with CTA, CTA had a sensitivity, specificity, PPV, and NPV of 93, 60, 68, and 90 % for significant coronary artery disease. In comparison with FFR, CTP had the following performance; sensitivity 76 %, specificity 84 %, PPV 82 %, and NPV 79 %. The combination of a stenosis ≥50 % on CTA and a perfusion defect on CTP had a sensitivity of 68 %, NPV 77 %, specificity 98 %, and PPV of 97 %. These results are illustrated in Table 1.

Interestingly, the combination of stenosis greater than 50 % on CTCA and a corresponding perfusion defect on CTP had 84 % accuracy for predicting ischemia, whereas a stenosis of greater than 50 % on CTA without a perfusion defect had 100 % accuracy for excluding a significant stenosis. The combination of CTCA and CTP was superior to QCA in predicting the need for coronary revascularization. However, discordant findings remained problematic as 37 % of vessels with a normal CTP and greater than 50 % stenosis on CTCA were above the ischemic threshold on FFR, and 67 % of vessels with greater than 50 % stenosis on CTCA and a perfusion defect had normal FFR. The likely explanation for the false positive CTP results was beam hardening or motion artifacts; false negative findings were likely due to a small perfusion defect or motion artifact.

As the majority of patients referred for assessment of CAD will initially have non-invasive cardiac imaging under physiological stress, and in most cases this will be single photon emission computed tomography (SPECT MPI), there is increased interest in comparing the performance of CTCA and CTP against SPECT–MPI. A prospective study of 50 patients (36 males) with intermediate-to-high pre-test probability for CAD and a clinically indicated SPECT–MPI had a research 320MDCT scan performed within 60 days (George et al. 2012). Patients with a heart rate above 65 bpm were given oral or intravenous metoprolol. All patients were given

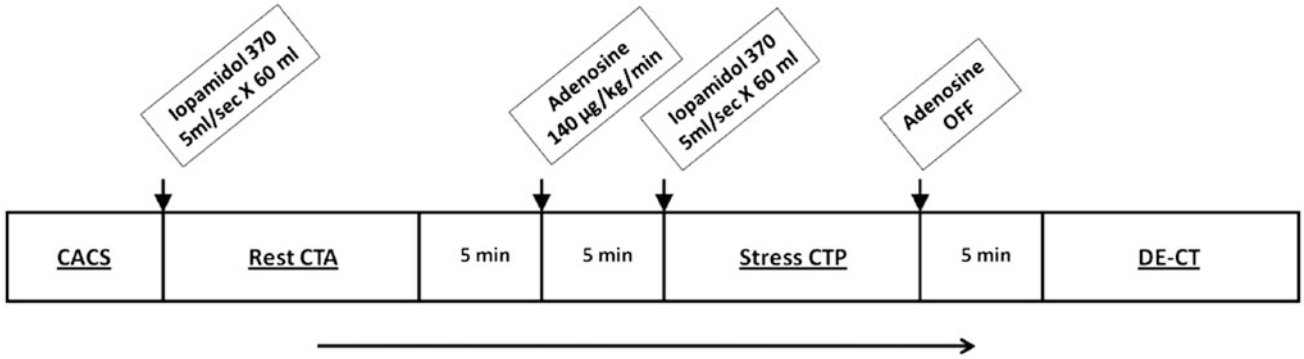

Fig. 2 Outline of a comprehensive cardiac computed tomography (CT) protocol for coronary artery calcium scoring (CACS), rest CT angiography and perfusion (CTA), stress CT perfusion (CTP), and delayed enhanced CT (DECT)

Table 2 Diagnostic accuracy of myocardial computed tomography perfusion and coronary computed tomography angiography (using >50 and >70 % diameter stenosis thresholds) to diagnose reversible ischemia compared with the reference standard single photon emission computed tomography myocardial perfusion imaging

	CTP versus SPECT	CTA Stenosis ≥50 % versus SPECT	CTA Stenosis ≥70 % versus SPECT
Per patient analysis versus SPECT			
Sensitivity	72 (46–89) 13/18	56 (31–78) 10/18	39 (18–64) 7/18
Specificity	91 (74–98) 29/32	75 (56–88) 24/32	91 (74–98) 29/32
PPV	81 (54–95) 13/16	56 (31–78) 10/18	70 (35–92) 7/10
NPV	85 (68–94) 29/34	75 (56–88) 24/32	73 (56–85) 29/40
AUC	0.81 (0.68–0.91) $P < 0.001$	0.65 (0.51–0.78) $P = 0.07$	0.65 (0.50–0.78) $P = 0.08$
Per vessel analysis vs SPECT			
Sensitivity	50 (32–68) 16/32,	25 (12–44) 8/32	22 (10–40) 7/32
Specificity	89 (82–94) 105/118	85 (77–90) 100/118	96 (90–98) 113/118
PPV	55 (35–73) 16/29	31 (15–52) 8/26	58 (29–84) 7/12
NPV	87 (79–92) 105/121	81 (72–87) 100/124	82 (74–88) 113/138
AUC	0.70 (0.62–0.77) $P < 0.001$	0.55 (0.47–0.63) $P = 0.40$	59 (0.51–0.67) $P = 0.13$

SPECT indicates single photon emission computed tomography
CTP computed tomography myocardial perfusion imaging
CTA computed tomography coronary angiography
PPV positive predictive value
NPV negative predictive value
AUC area under the receiver operator characteristic curve

intravenous hydration with 250–500 mL normal saline. The protocol is shown in Fig. 2.

Analysis of rest and stress CTP were performed on a dedicated workstation (Myoperfusion, Toshiba Medical Systems, Otawara, Japan). 3 mm short axis images through the LV were analyzed using a 16-segment model (apex excluded) and by dividing the LV wall into the subendocardium, mid-myocardium, and subepicardium. The mean attenuation of each myocardial layer for each segment was calculated. The ratio of the subendocardial attenuation to the subepicardial attenuation for each segment was calculated to represent the transmural perfusion ratio (TPR). A ratio of less than 0.99 was recorded as abnormal. Coronary CTA analysis was performed using a 19-segment model for vessels larger than 1.5 mm in diameter; uninterpretable segments were excluded from analysis. A luminal stenosis over 50 % was taken as abnormal with a secondary analysis based on luminal stenosis greater than 70 %. 19 patients had coronary angiography. The mean Agatston score was 170 ± 281 (0–1148), CTCA

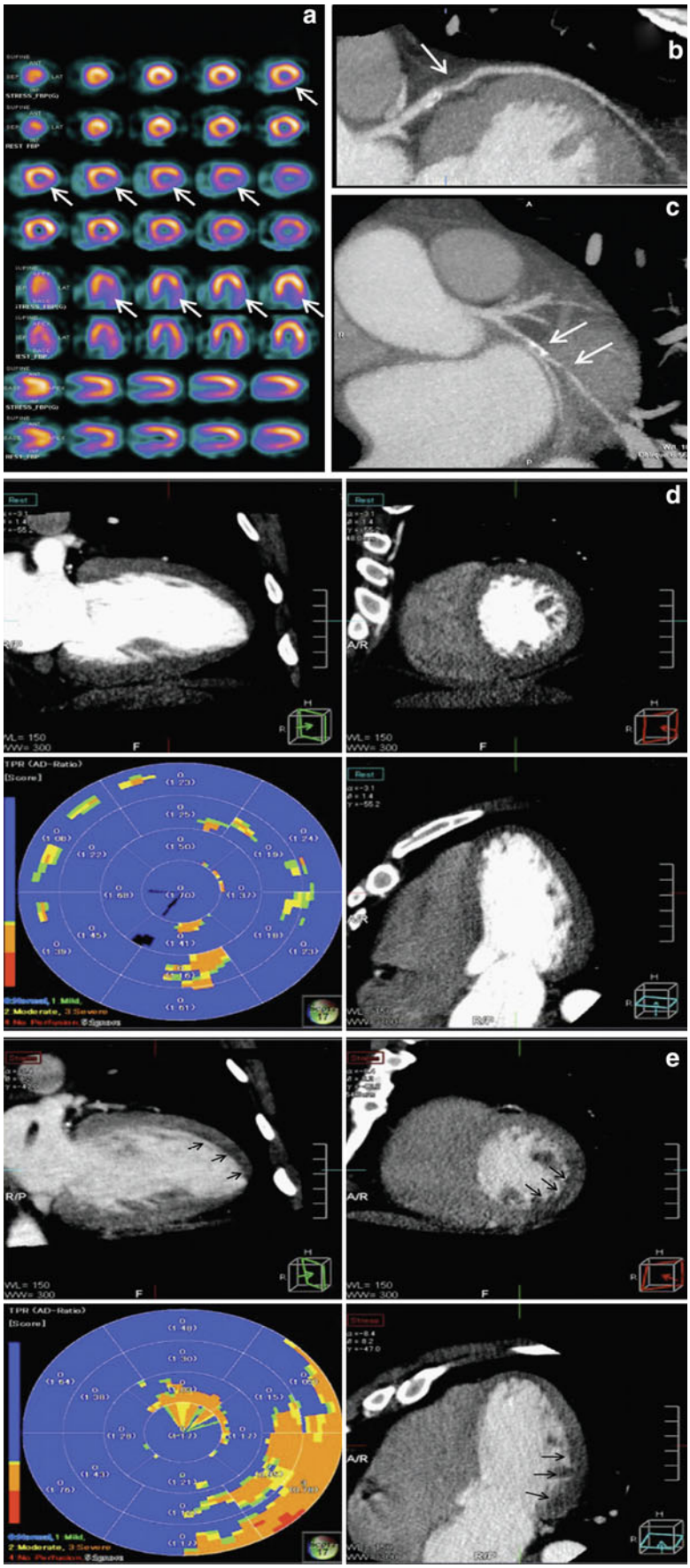

Fig. 3 55-year-old with exertional chest pressure. **a** Short axis, horizontal, and vertical long axis myocardial perfusion images from single photon emission computed tomography demonstrating a reversible perfusion deficit in the basal to midinferolateral wall consistent with myocardial ischemia (*white arrows*). **b** and **c** An intermediate severity stenosis (50–69%) in the mid LAD artery and a severe stenoses in the left circumflex (70–99%) and obtuse marginal branch (70–99%; *white arrows*). **d** The quantitative analysis of rest computed tomography perfusion (CTP) using a 16-segment polar plot, with *blue* representing normal perfusion (transmural perfusion ratio [TPR]_0.99). **e** Adenosine stress CTP. The 16-segment polar plot and images demonstrate abnormal perfusion in the inferolateral and distal anterior wall (*white arrow*). Abnormal TPR (_0.99) is displayed in *yellow*, *orange*, and *red*

Table 3 Diagnostic accuracy of myocardial computed tomography perfusion to diagnose reversible ischemia in the presence of obstructive atherosclerosis (using >50 % and >70 %) diameter stenosis thresholds

	CTP versus CTA Stenosis ≥50 % + SPECT	CTP versus CTA Stenosis ≥70 % + SPECT
Per patient analysis versus CTA/SPECT		
Sensitivity	100 (60–100) 8/8	100 (56–100) 7/7
Specificity	81 (65–91) 34/42	79 (64–89) 34/43
PPV	50 (26–74) 8/16	44 (21–69) 7/16
NPV	100 (87–100) 34/34	100 (87–100) 34/34
AUC	0.91 (0.79–0.97) $P < 0.001$	0.90 (0.78–0.96) $P < 0.001$
Per vessel analysis versus CTA/SPECT		
	Sensitivity 100 (60–100) 8/8	100 (56–100) 7/7
Specificity	85 (78–90) 121/142	85 (77–90) 120/142
PPV	28 (13–47) 8/29	25 (11–44) 7/28
NPV	100 (96–100) 121/121	100 (96–100) 121/121
AUC	0.93 (0.87–0.96) $P < 0.001$	0.92 (0.87–0.96) $P < 0.001$

CTA indicates computed tomography coronary angiography
SPECT single photon emission computed tomography
CTP computed tomography myocardial perfusion imaging
PPV positive predictive value
NPV negative predictive value
AUC area under the receiver operator characteristic curve

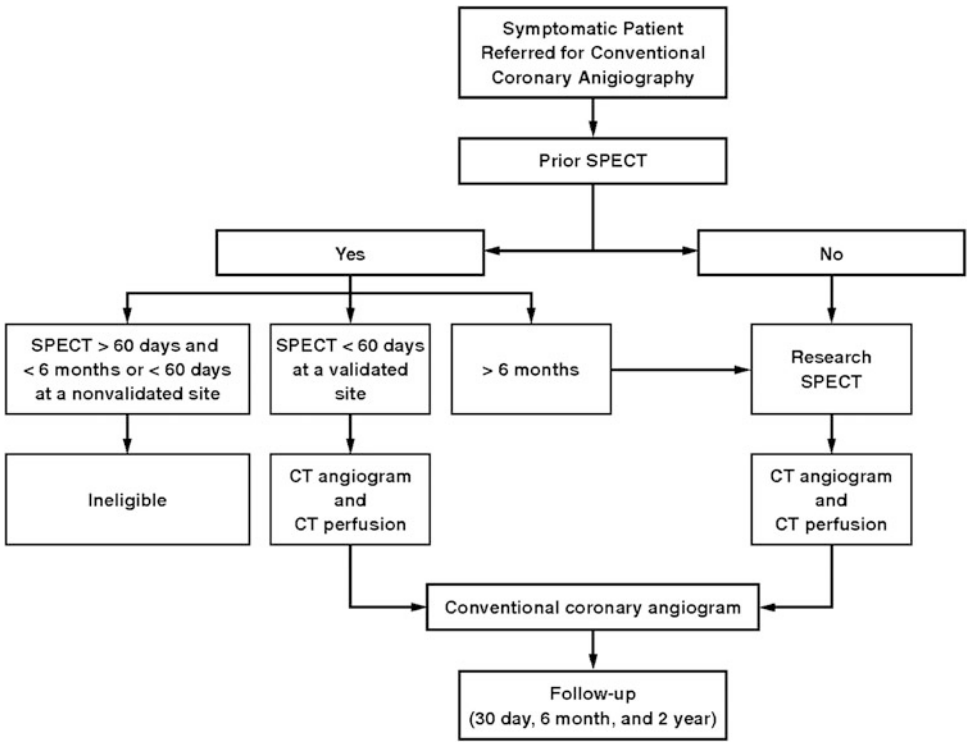

Fig. 4 Overall enrollment strategy of CORE320 Multicenter study. All patients enrolled with clinical indication for invasive coronary angiography will undergo either clinical or research SPECT study at validated site, MDCT angiography and perfusion study, and invasive coronary angiography within 60 days of each other

demonstrated luminal stenosis greater than 50 % in 18 out of 50 (36 %) patients and greater than 70 % stenosis in 10 out of 50 (20 %) patients. CT perfusion (CTP) demonstrated perfusion abnormalities in 36 % (18 out of 50) patients and 21 % (32 out of 150) vascular territories, 75 % (24 out of 32) of which were reversible defects and 22 % (7 out of 32) were partially reversible. Figure 3 illustrates a case example of perfusion defects seen on 320MDCT.

The sensitivity, specificity, PPV, NPV, and AUC for 50 %-lesions on CTCA to predict a perfusion deficit on SPECT–MPI was 56, 75, 56, 75, and 0.65 %, respectively. The corresponding values for lesions constituting greater than 70 % luminal stenosis on CTCA were 39, 91, 70, 73, and 0.65 % (Table 2).

Using CTP in isolation, the sensitivity, specificity, PPV, NPV, and AUC improved to 72, 91, 81, 85, and 0.81 %, respectively; when CTP was compared to a combination of CTCA and SPECT, there was a significant improvement in performance characteristics (Table 3).

The study was limited with a suboptimal per-vessel sensitivity of CTP compared with SPECT, it was theorized that this could be due to false-positive SPECT studies or inaccuracies in TPR analysis due to motion, beam hardening, and reconstruction artifacts, all of which could result in underestimating the presence of ischemia. The total radiation dose from the calcium score (CACS), rest, stress, and delayed cardiac CT was 13.8 ± 2.9 mSv, comparable to that for a rest-stress MPI 13.1 ± 1.7 mSv. This study demonstrated the utility of 320MDCT to perform combined CT angiography and perfusion imaging in intermediate to high risk CAD patients, and to provide accurate data of myocardial ischemia at a radiation dose comparable to SPECT MPI.

The encouraging results from this single center study using the 320MDCT are being evaluated in an international, multicenter study with 16 participating hospitals located in eight countries, the CORE320 trial (George et al. 2011; Vavere et al. 2011). This collaborative effort aims to test the accuracy of CTCA in demonstrating ≥50 % coronary artery stenosis and a corresponding perfusion defect on CTP in comparison with (a) QCA-determined ≥50 % stenosis and a corresponding perfusion defect on SPECT MPI, and with (b) QCA-determined ≥50 % stenosis. The study outline is illustrated in Fig. 4.

The study will enroll 400 patients with suspected CAD, who have been referred for coronary catheterization, and who have a research or clinical SPECT MPI performed within 60 days of the coronary catheterization. A research CTCA and CTP will be performed using the protocol outlined in Fig. 2 without the delayed enhanced CT acquisition. The anticipation is that this study will provide sufficient clinical data to evaluate the utility of combined 320MDCT coronary angiography and myocardial perfusion for comprehensive assessment of myocardial viability and ischemia in comparison to established clinical standards which in turn could lead to a change in clinical practice towards the use of 320MDCT as a first line assessment in appropriate patients.

The use of 320MDCT facilitates through-plane temporal homogeneity of image acquisition with a significant reduction in radiation dose and significant improvement in image quality for cardiac CT compared to 64MDCT acquisitions (Torres et al. 2010; Abadi et al. 2011). The utility of performing both anatomical assessment of CAD and functional evaluation of myocardial perfusion is a powerful combination for non-invasive imaging assessment of myocardial viability (Williams et al. 2011; Nasis et al. 2010). It is conceivable that stable patients with a clinical suspicion of CAD and no contraindications to cardiac CT would have an initial CTCA performed at rest. Patients with evaluable coronary artery segments larger than 1.5 mm in diameter and coronary artery stenosis greater than 50 % would require no further imaging, whereas other patients could proceed to have CT myocardial perfusion assessment using vasodilator stress. This combination of imaging with 320MDCT could potentially effectively triage the majority of patients with suspected CAD.

References

Abadi S, Mehrez H, Ursani A, Parker M, Paul N (2011) Direct quantification of breast dose during coronary CT angiography and evaluation of dose reduction strategies AJR 196(2):152–158

Brooks RA, Di Chiro G (1976) Beam hardening in X-ray reconstructive tomography. Phys Med Biol 21(3):390–398

Coyne EP, Belvedere DA, van de Streek PR, Weiland FL, Evans RB, Spaccavento LJ (1991) Thallium-201 scintigraphy after intravenous infusion of adenosine compared with exercise thallium testing in the diagnosis of coronary artery disease. J Am Coll Cardiol 17:1289–1294

Crossett MP, Schneider-Kolsky M, Troupis J (2011) Normal perfusion of the left ventricular myocardium using 320MDCT. JCCT 5:406–411

George RT, Arbab-Zadeh A, Cerci RJ, Vavere AL, Kitagawa K, Dewey M, Rochitte CE, Arai AE, Paul N, Rybicki FJ, Lardo AC, Clouse ME, Lima JA (2011) Diagnostic performance of combined noninvasive coronary angiography and myocardial perfusion imaging using 320-MDCT: the CT angiography and perfusion methods of the CORE320 multicenter multinational diagnostic study. AJR Am J Roentgenol 197(4):829–837

George RT, Arbab-Zadeh A, Miller JM, Kitagawa K, Chang HJ, Bluemke DA et al (2009) Adenosine stress 64- and 256-row detector computed tomography angiography and perfusion imaging: a pilot study evaluating the transmural extent of perfusion abnormalities to predict atherosclerosis causing myocardial ischemia. Circ Cardiovasc Imaging 2:174–182

George RT, Arbab-Zadeh A, Miller JM, Vavere AL, Bengel FM, Lardo AC, Lima JA (2012) Computed tomography myocardial perfusion imaging with 320-row detector CT accurately detects myocardial ischemia in patients with obstructive coronary artery disease. Circ Cardiovasc Imaging 5: 333–340

George RT, Ichihara T, Lima JAC, Lardo AC (2010) A method for reconstructing the arterial input function during helical CT: implications for myocardial perfusion distribution imaging. Radiology 255(2):396–404

George RT, Jerosch-Herold M, Silva C, Kitagawa K, Bluemke DA, Lima JA et al (2007) Quantification of myocardial perfusion using dynamic 64-detector computed tomography. Invest Radiol 42:815–822

George RT, Silva C, Cordeiro MA, di Paula A, Thompson DR, McCarthy WF et al (2006) Multidetector computed tomography

myocardial perfusion imaging during adenosine stress. J Am Coll Cardiol 48:153–160

Gupta NC, Esterbrooks DJ, Hilleman DE, Mohiuddin SM (1992) Comparison of adenosine and exercise thallium-201 single-photon emission computed tomography (SPECT) myocardial perfusion imaging. The GE SPECT Multicenter Adenosine Study Group. J Am Coll Cardiol 19:248–257

Hacker M, Jakobs T, Matthiesen F et al (2005) Comparison of spiral multidetector CT angiography and myocardial perfusion imaging in the noninvasive detection of functionally relevant coronary artery lesions: first clinical experiences. J Nucl Med 46:1294–1300

Kitagawa K, George RT, Arbab-Zadeh A, Lima JAC, Lardo AC (2010) Characterization and correction of beam-hardening artifacts during dynamic volume CT assessment of myocardial perfusion. Radiology 256(1):111–118

Klocke FJ, Baird MG, Lorell BH et al (2003) ACC/AHA/ASNC guidelines for the clinical use of cardiac radionuclide imaging—executive summary: a report of the American College of Cardiology/American Heart Association Task Force on practice guidelines (ACC/AHA/ASNC Committee to revise the 1995 guidelines for the clinical use of cardiac radionuclide imaging). J Am Coll Cardiol 42:1318–1333

Ko B, Cameron J, Defrance T, Seneviratne S (2011) CT stress myocardial perfusion imaging using Multidetector CT—a review. JCCT 5(6):345–356

Ko B, Cameron J, Meredith I, Leung M, Antonis P, Nasis A, Crossett M, Hope S, Lehman S, Troupis J, DeFrance T, Seneviratne S (2012) Computed tomography stress myocardial perfusion imaging in patients considered for revascularization: a comparison with fractional flow reserve. Eur Heart J 33:67–77

Kühl T, Linde J, Fuchs A, Kristensen T, Kelbæk H, George R, Hove J, Kofoed KF (2012) Patterns of myocardial perfusion in humans evaluated with contrast-enhanced 320 multi detector computed tomography. Int J Cardiovasc Imaging 28(7):1739–1747

Lardo AC, Cordeiro MA, Silva C, Amado LC, George RT, Saliaris AP, Schuleri KH, Fernandes VR, Zviman M, Nazarian S, Halperin HR, Wu KC, Hare JH, Lima JAC (2006) Contrast enhanced multidetector computed tomography viability imaging following myocardial infarction: characterization of myocyte death, microvascular obstruction and chronic scar. Circulation 113:394–404

Mehra V, Ambrose M, Valdiviezo-Schlomp C, Schuleri K, Lardo AC, Lima JA, George RT (2011a) CT-based myocardial perfusion imaging-practical considerations: acquisition, image analysis, interpretation, and challenges. J Cardiovasc Transl Res 4(4): 437–448

Mehra V, Valdiviezo C, Arbab-Zadeh A, Ko B, Seneviratne S, Cerci R, Lima J, George R (2011b) A stepwise approach to the visual interpretation of CT-based myocardial perfusion. JCCT 5(6): 357–369

Nasis A, Seneviratne S, DeFrance T (2010) Advances in contrast-enhanced cardiovascular CT for the evaluation of myocardial perfusion. Curr Cardiovasc Imaging Rep 3:372–381

Nguyen T, Heo J, Ogilby JD, Iskandrian AS (1990) Single photon emission computed tomography with thallium-201 during adenosine-induced coronary hyperemia: correlation with coronary arteriography, exercise thallium imaging and two-dimensional echocardiography. J Am Coll Cardiol 16:1375–1383

Nishimura S, Mahmarian JJ, Boyce TM, Verani MS (1992) Equivalence between adenosine and exercise thallium-201 myocardial tomography: a multicenter, prospective, crossover trial. J Am Coll Cardiol 20:265–275

Olson EA, Han KS, Pisano DJ (1981) CT reprojection polychromaticity correction for three attenuators. IEEE Trans Nucl Sci 28(4): 3628–3640

Parodi O, Marcassa C, Casucci R et al (1991) Accuracy and safety of technetium-99 m hexakis 2-methoxy-2-isobutyl isonitrile (sestamibi) myocardial scintigraphy with high dose dipyridamole test in patients with effort angina pectoris: a multicenter study. Italian Group of Nuclear Cardiology. J Am Coll Cardiol 18:1439–1444

Pijls NH, de Bruyne B, Peels K, van der Voort PH, Bonnier HJ, Bartunek JKJJ, Koolen JJ (1996) Measurement of fractional flow reserve to assess the functional severity of coronary-artery stenoses. N Engl J Med 334:1703–1708

Rumberger JA, Bell MR (1992) Measurement of myocardial perfusion and cardiac output using intravenous injection methods by ultrafast (cine) computed tomography. Invest Radiol 27:S40–S46

Rumberger JA, Feiring AJ, Lipton MJ, Higgins CB, Ell SR, Marcus ML (1987) Use of ultrafast computed tomography to quantitate regional myocardial perfusion: A preliminary report. J Am Coll Cardiol 9:59–69

Schuijf JD, Wijns W, Jukema JW, Atsma DE, de Roos A, Lamb HJ, Stokkel MPM, Dibbets-Schneider P, Decramer I, De Bondt P, van der Wall EE, Vanhoenacker PK, Bax JJ (2006) Relationship between noninvasive coronary angiography with multi-slice computed tomography and myocardial perfusion imaging. J Am Coll Cardiol 48(12):2508–2514

Torres F, Crean A, Nguyen ET, Doyle D, Menezes R, Ayyappan AP, Abadi S, Paul N (2010) Abolition of respiratory motion artifact in CT coronary angiography with ultrafast examinations: a comparison between 64-row and 320-row multidetector scanners. Can Assoc Radiol J 61:5–12

Valdiviezo C, Ambrose M, Mehra V, Lardo AC, Lima JAC, George RT (2010) Quantitative and qualitative analysis and interpretation of CT perfusion imaging. J Nucl Cardiol 17:1091–1100

Vavere AL, Simon GG, Lima JAC (2011) Diagnostic performance of combined noninvasive coronary angiography and myocardial perfusion imaging using 320 row detector computed tomography: design and implementation of the CORE320 multicenter, multinational diagnostic study. JCCT 5:370–381

Williams M, Reid J, McKillop G, Weir N, van Beek E, Uren N, Newby D (2011) Cardiac and coronary CT. Comprehensive imaging approach in the assessment of coronary heart disease. Heart 97:1198–1205

Zatz LM, Alvarez RE (1977) An inaccuracy in computed tomography: the energy dependence of CT values. Radiology 124(1):91–97

CT Assessment of the Myocardial Blood Supply: Quantitative Imaging

Ullrich Ebersberger, Justin R. Silverman, Young Jun Cho, and Lucas L. Geyer

Contents

Abstract

Myocardial perfusion computed tomography (CTP) is a promising imaging technique on the verge of expanding the capabilities of CT. Especially, the capability of CTP to enable quantitative evaluations may provide a more accurate assessment of the hemodynamic significance of CAD. Two different approaches currently used are discussed in this chapter: 1. Dual energy CT 2. Dynamic, time-resolved quantitative imaging.

Abbreviations

CAD	Coronary artery disease
cCTA	Coronary CT angiography
CTP	Myocardial perfusion computed tomography
DECT	Dual-energy computer tomography
FFR	Coronary fractional flow reserve
ICA	Invasive coronary angiography
MBF	Myocardial blood flow
MRPI	Magnetic resonance myocardial perfusion imaging
SPECT	Single photon emission computed tomography

U. Ebersberger (✉) · J. R. Silverman · Y. J. Cho · L. L. Geyer
Department of Radiology and Radiological Science,
Medical University of South Carolina, Charleston, SC, USA
e-mail: ebersberger@gmx.net

U. Ebersberger
Department of Cardiology and Intensive Care Medicine, Heart Center Munich-Bogenhausen, Munich, Germany

Y. J. Cho
Department of Radiology, Konyang University College of Medicine, Daejeon, Korea

L. L. Geyer
Department of Clinical Radiology,
University Hospitals LMU Munich, Munich, Germany

1 Introduction

To date, non-invasive coronary CT angiography (cCTA) has been shown to be a safe and accurate alternative to invasive coronary angiography (ICA) in patients with a low-to-intermediate pretest likelihood for coronary artery disease (CAD), thus justifying its inclusion in current CT guidelines (Leber et al. 2007; Taylor et al. 2010). In such patient cohorts, cCTA is a strong method for ruling out CAD but is restricted to anatomic informations. In patients with coronary lesions, especially when calcified plaques are

U. J. Schoepf et al. (eds.), *CT Imaging of Myocardial Perfusion and Viability*, Medical Radiology. Diagnostic Imaging,
DOI: 10.1007/174_2012_773, © Springer-Verlag Berlin Heidelberg 2013
Published Online: 17 April 2013

present, the diagnostic accuracy of this approach is severely hampered; this is largely due to beam hardening artifacts. Therefore, a pure anatomic perspective of such patients often has limited utility in the absence of additional assessments.

In the last decade, strong evidence has been generated underlining the importance of functional assessments such as magnetic resonance myocardial perfusion imaging (MRPI) at 1.5 and 3.0 T, and the invasive measurement of coronary fractional flow reserve (FFR) for the evaluation of hemodynamic relevance of coronary lesions (Hamon et al. 2010; Tonino et al. 2009; De Bruyne et al. 2012). The FAME-study was able to demonstrate that coronary intervention guided by FFR functional assessment results in a superior outcome with significantly lower mortality after one and two years (Tonino et al. 2009). The observed effect was mainly due to a systematic overestimation of the hemodynamic severity of intermediate lesions when relying on anatomic information of angiography alone; this resulted in a subsequent higher number of index PCIs in the non-FFR group. Other studies have focused on the promising diagnostic performance of MRI first-pass perfusion imaging using FFR as the gold standard (Hamon et al. 2010).

In light of technical developments, myocardial perfusion computed tomography (CTP) is a promising imaging technique on the verge of expanding the capabilities of CT. Initial studies demonstrated a good correlation with single photon emission computed tomography (SPECT) and ICA in the diagnosis of myocardial perfusion defects (Bamberg et al. 2011; Wang et al. 2012; Ruzsics et al. 2009). Given the possibility of myocardial blood flow (MBF)/myocardial blood volume quantification in the context of existing anatomic information, CTP is highly attractive and may lead to a further improvement of diagnostic accuracy and an expansion of the indications for appropriate use of cardiac CT.

2 Pathophysiological Background

Previous chapters have extensively described the feasibility of CTP provided by the enormous technical developments in this sector. In contrast with other imaging modalities, CT offers the opportunity to assess both morphology and function within a single session. Therefore, hemodynamically relevant stenoses can be identified by matching visible coronary plaques with perfusion defects in the corresponding myocardial segments. In general, a perfusion deficit is defined as an imbalance between myocardial oxygen supply and demand. According to the so-called ischemic cascade, it is considered an early, often persistent, measurable sign of ischemia, even before metabolic disorders, ventricular dysfunction, or infarction occur (Nesto and Kowalchuk 1987). Whereas an even inflow of blood in healthy myocardium homogeneously distributes iodinated contrast medium resulting in a uniform pattern of attenuation, a perfusion deficit results in myocardial hypoenhancement caused by decreased or absent iodine content within the affected myocardial area (Nikolaou et al. 2005). It has to be mentioned that myocardial hypoenhancement is not specific for ischemia but can also be found in infarction or other cardiac diseases that cause inhomogeneous myocardial perfusion, such as cardiomyopathy. As the evaluation of viability is described in later chapters, let us leave infarction aside as we focus on the assessment of myocardial perfusion deficits caused by ischemia.

3 Definition of Quantitative Assessment of Myocardial Perfusion

The preceding chapters have discussed different approaches to a qualitative assessment of CTP in great detail. However, a quantitative evaluation may provide a more accurate assessment of the hemodynamic significance of CAD. In contrast with other non-invasive imaging modalities, such as MRI or PET, CT has the advantage of a linear relation between contrast enhancement and contrast media (iodine) concentration. This permits the direct quantification of MBF without the need for correction methods.

In literature, the term “quantitative” is not uniformly used in the context of myocardial perfusion imaging, even with respect to CTP. In particular, when non-dynamic—usually arterial-phase—CT protocols are used, a quantitative assessment of perfusion deficits refers to HU measurements in hypoenhanced (hypoperfused) versus healthy myocardium (Cury et al. 2008; Nagao et al. 2008). These studies have demonstrated that myocardial perfusion deficits show significantly lower HU values. However, there is a substantial variance of measured HU because myocardial contrast enhancement depends on a number of independent variables, e.g., contrast injection protocol or cardiac output. In addition, the timing of the scan is a crucial influencing factor, particularly in single-phase first pass CTP (Bischoff et al. 2012). Therefore, this hampers the establishment of a cut-off (an absolute HU value) to differentiate between normal and hypoperfused tissue.

In addition, first experiences have shown that electron beam CT (Rumberger et al. 1987; Wolfkiel et al. 1987) as well as multi-detector CT (George et al. 2007; Mahnken et al. 2006) can provide quantitative time-resolved information on myocardial perfusion, mostly defined by MBF.

However, this technique is more sophisticated, requiring an understanding of contrast material kinetics. Whereas healthy myocardium demonstrates a rapid wash-in and wash-out of iodinated contrast material, ischemic myocardium is characterized by a relatively depressed wash-in and noticeably slower wash-out (George et al. 2006, 2007; Mahnken et al. 2006). The associated CT protocols and initial experiences are discussed in a later section of this chapter. First, the use of dual-energy CT (DECT) for quantitative assessment of myocardial perfusion is introduced.

4 Dual-Energy CT Technique

The basic principle of DECT is extensively described by Ko (CT evaluation of the myocardial blood supply - Dual-source dual-energy CT). In short, iodine shows specific absorption characteristics for X-rays of different energy levels. Exploiting this property, DECT allows for the computation of iodine distribution within the myocardium as a visualization of the myocardial blood volume (Kang et al. 2010).

The actual, clinically feasible CT protocols consist of a contrast enhanced, single- or triple-phase dual-energy acquisition during the arterial phase post contrast media injection. Technical details can be found in various chapters. In brief, DECT raw data are typically reconstructed as four different image sets: (1) high energy CT spectrum (140 kV), (2) low energy CT spectrum (80, 100 kV), (3) merging data (30 % of the low and 70 % of high energy CT spectrum), and 4. DECT-based overlay of iodine distribution on "virtual non-contrast" images.

5 Dual-Energy CT in Quantitative Assessment of Myocardial Perfusion

At the time of this chapter's submission, quantitative CTP using dual-energy techniques is still in an experimental stage. Besides characterization of iodine distribution, DECT offers the ability to reduce beam-hardening artifacts by monochromatic image calculation. Beam hardening is caused by the polychromatic nature of the X-rays used in CT imaging and by energy-dependent attenuation, presenting quite a challenge to quantitative perfusion imaging (Brooks and Di Chiro 1976). The mean energy level of the polychromatic CT spectrum is altered due to the absorbance of lower-energy X-rays as they pass through the contrast media-filled heart chambers (So and Lee 2011). Initial results of animal studies are promising, with a reduction of beam hardening artifacts providing more accurate measurements in dynamic CTP protocols (So et al. 2011, 2012). Moreover, new algorithms have been published to improve the temporal resolution of dual-source CT in dual-energy mode (Nance et al. 2011). In light of this background, we can expect further developments in dynamic quantitative CTP using DECT (Fig. 1).

6 Dynamic, Time-Resolved Quantitative Imaging

As the basis of dynamic, time-resolved CT imaging and its acquisition protocols are discussed at length in previous chapters, this section will lay its focus on the clinical implications of the semi-quantitative data generated.

Due to technical advances, including higher temporal resolution, broader detectors, and acquisition techniques that allowed for whole heart coverage, dynamic perfusion imaging has become feasible and the focus of ongoing investigations (Fig. 2). Preliminary animal studies in pigs were able to quantify MBF during rest and adenosine induced hyperemia using the "shuttle mode" at 2 alternating table positions. MBF was shown to be significantly reduced in pigs with an induced 80 % coronary stenosis underlining the potential of CT to assess functional parameters as well (Mahnken et al. 2010). In an initial clinical experience, Bamberg et al. (2010) demonstrated the feasibility of a model-based semi-quantitative determination of MBF using dynamic myocardial stress CTP imaging in a female patient with myocardial ischemia. These results were further strengthened by Bastarrika's working group, who were able to recruit 10 patients and showed comparable results (Bastarrika et al. 2010). Larger, single-center cohorts followed and confirmed the prospect of using dynamic CTP to expand existing CT capabilities (Fig. 3). Dynamic CTP has been evaluated against FFR, and an MBF cut of point of 75 mL × 100 mL^{-1} min^{-1} has been supported as the best discriminatory value to detect a significant coronary lesion (Bamberg et al. 2011). A recent study by Wang et al. showed dynamic CTP in good correlation to SPECT and catheter angiography; this study also documented an improvement in diagnostic accuracy for identifying flow-obstructive coronary stenosis when compared to CTA alone (Wang et al. 2012). However, in this study, an MBF cut-off value of 90 mL × 100 mL^{-1} min^{-1} was introduced, underlining that caution is in order when solely relying on quantitative values. Larger clinical trials are warranted to observe the influence of factors such as gender, race, BMI, and severity of coronary disease. If scientifically supported properly, quantitative values hold a certain attractiveness. Given the ever-growing emphasis on evidence-based medicine, the clinical arena would surely appreciate quantitative values for guiding decision-making and therapy.

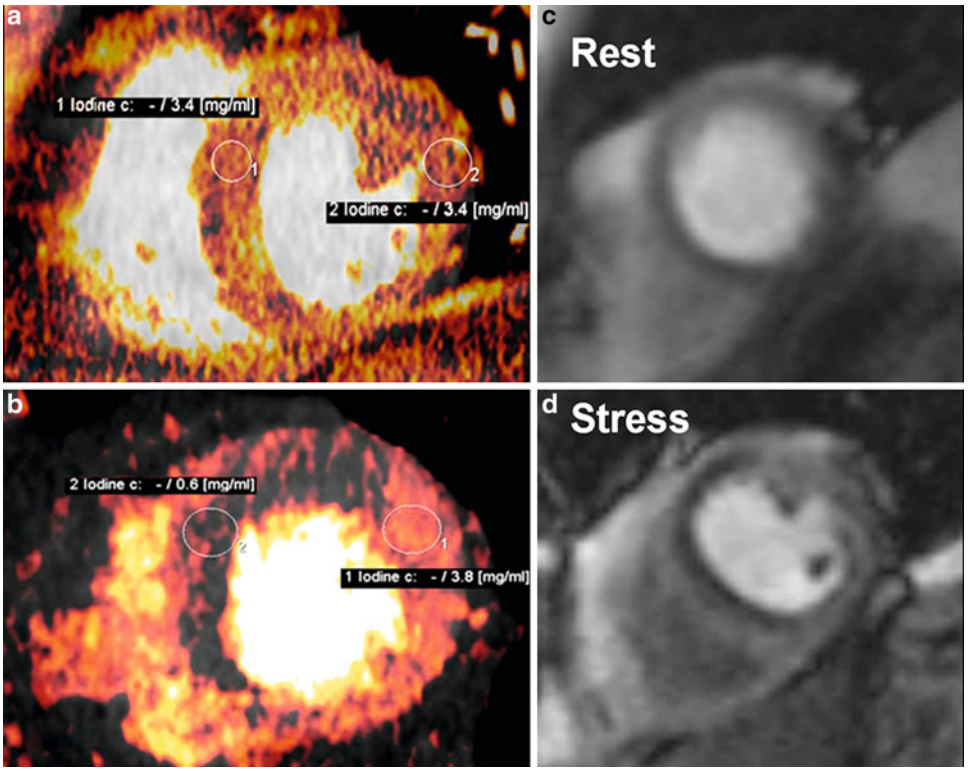

Fig. 1 Detection of myocardial perfusion defects by dual energy CT. 45-year-old man with LAD stenosis. Images a and c were acquired at rest, whereas images b and d were obtained during pharmacological stress. DECT (**a**, **b**) showed normal iodine concentrations of 3.4 mg/ml during rest. During stress imaging, quantitative iodine concentration decreased within the antero-septal myocardium (0.6 mg/ml) compared to healthy myocardium within the lateral wall (3.4 mg/ml–3.8 mg/ml). MRPI (**c**, **d**) confirms reversible ischemia in the mid-ventricular anteroseptal myocardium

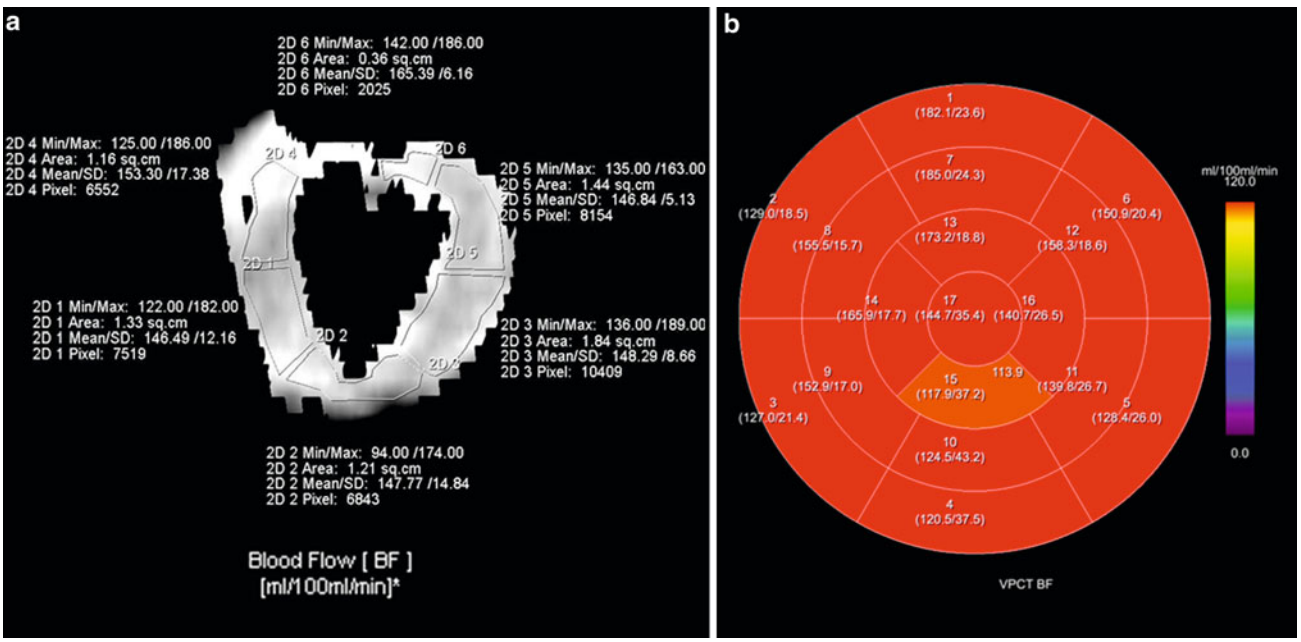

Fig. 2 Standard cardiac perfusion maps. Visualization of MBF on a short axis reformation at the mid-ventricular level (**a**) and 3D-visualization on 17- segment polar map using the prototype software (**b**). Note: incomplete volume coverage in segments 1 and 2 is seen on the manual 2D visualization (**a**)

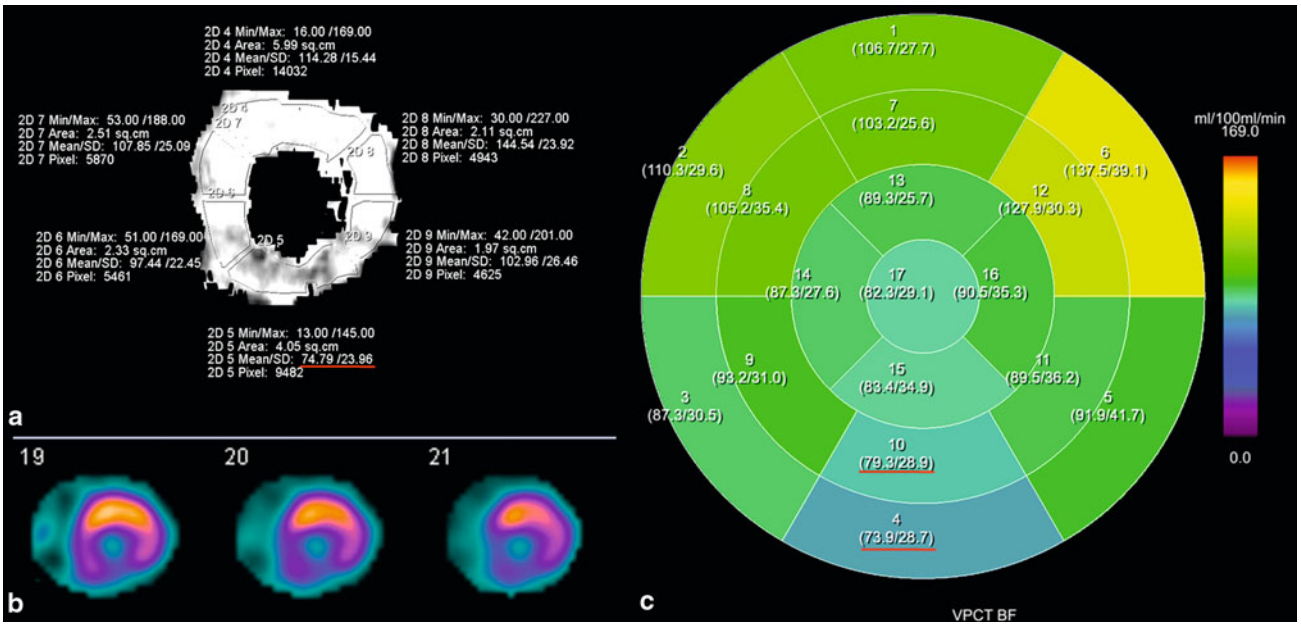

Fig. 3 Detection of myocardial perfusion defects by myocardial blood flow (MBF). Quantitative assessment of perfusion defects on 2D-perfusion map with decreased MBF (mean 74.79 mg/ml) at the low-to-mid cavity level (**a**) confirmed by SPECT imaging at stress (**b**); 3DVisualization: the 17-segmented polar map of MBF (**c**) shows correlating positive perfusion defects mainly in the inferior wall (segment 4: mean 79.3 mg/ml; and segment 10: mean 73.9 mg/ml)

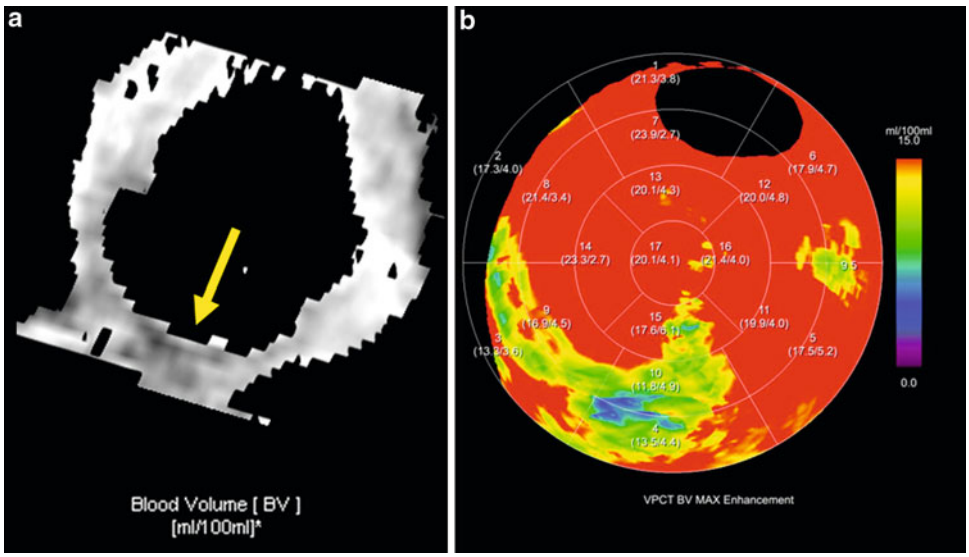

Fig. 4 Detection of myocardial perfusion defects by myocardial blood volume (MBV). Qualitative assessment of perfusion defects on 2D-perfusion map with hypoenhancement in the inferoseptal myocardium (**a**). 3D-Visualization: the 17-segmented polar map of MBV (**b**) shows correlating positive perfusion defects with 11.8 ml/ 100 ml–13.5 ml/ 100 ml. Note: insufficient volume coverage of anterobasal segments

A current draw-back of quantitative assessments is the time consuming post processing of myocardial perfusion data sets, which relies on two-dimensional region-of-interest measurements. This laborious evaluation regimen is hardly compatible with clinical work-flow. However, recently introduced semi-automated evaluation software

shows a significant time saving potential when compared to manual assessments and could integrate quantitative measurements into clinical practice (Fig. 4).

References

Bamberg F, Klotz E, Flohr T, Becker A, Becker CR, Schmidt B, Wintersperger BJ, Reiser MF, Nikolaou K (2010) Dynamic myocardial stress perfusion imaging using fast dual-source CT with alternating table positions: initial experience. Eur Radiol 20(5):1168–1173. doi:10.1007/s00330-010-1715-9

Bamberg F, Becker A, Schwarz F, Marcus RP, Greif M, von Ziegler F, Blankstein R, Hoffmann U, Sommer WH, Hoffmann VS, Johnson TRC, Becker H-CR, Wintersperger BJ, Reiser MF, Nikolaou K (2011) Detection of hemodynamically significant coronary artery stenosis: incremental diagnostic value of dynamic CT-based myocardial perfusion imaging. Radiology 260(3):689–698. doi:10.1148/radiol.11110638

Bastarrika G, Ramos-Duran L, Rosenblum MA, Kang DK, Rowe GW, Schoepf UJ (2010) Adenosine-stress dynamic myocardial CT perfusion imaging: initial clinical experience. Invest Radiol 45(6):306–313. doi:10.1097/RLI.0b013e3181dfa2f2

Bischoff B, Bamberg F, Marcus R, Schwarz F, Becker HC, Becker A, Reiser M, Nikolaou K (2012) Optimal timing for first-pass stress CT myocardial perfusion imaging. Int J Cardiovasc Imaging. doi:10.1007/s10554-012-0080-y

Brooks RA, Di Chiro G (1976) Beam hardening in X-ray reconstructive tomography. Phys Med Biol 21(3):390–398

Cury RC, Nieman K, Shapiro MD, Butler J, Nomura CH, Ferencik M, Hoffmann U, Abbara S, Jassal DS, Yasuda T, Gold HK, Jang IK, Brady TJ (2008) Comprehensive assessment of myocardial perfusion defects, regional wall motion, and left ventricular function by using 64-section multidetector CT. Radiology 248(2):466–475. doi:10.1148/radiol.2482071478

De Bruyne B, Pijls NHJ, Kalesan B, Barbato E, Tonino PAL, Piroth Z, Jagic N, Mobius-Winckler S, Rioufol G, Witt N, Kala P, MacCarthy P, Engstrøm T, Oldroyd KG, Mavromatis K, Manoharan G, Verlee P, Frobert O, Curzen N, Johnson JB, Jüni P, Fearon WF (2012) Fractional flow reserve–guided PCI versus medical therapy in stable coronary disease. New Engl J Med: 120827230013003. doi:10.1056/NEJMoa1205361

George RT, Silva C, Cordeiro MA, DiPaula A, Thompson DR, McCarthy WF, Ichihara T, Lima JA, Lardo AC (2006) Multidetector computed tomography myocardial perfusion imaging during adenosine stress. J Am Coll Cardiol 48(1):153–160. doi:10.1016/j.jacc.2006.04.014

George RT, Jerosch-Herold M, Silva C, Kitagawa K, Bluemke DA, Lima JA, Lardo AC (2007) Quantification of myocardial perfusion using dynamic 64-detector computed tomography. Invest Radiol 42(12):815–822. doi:10.1097/RLI.0b013e318124a884

Hamon M, Fau G, Née G, Ehtisham J, Morello R, Hamon M (2010) Meta-analysis of the diagnostic performance of stress perfusion cardiovascular magnetic resonance for detection of coronary artery disease. J Cardiovasc Magn Reson 12(1):29. doi:10.1186/1532-429X-12-29

Kang DK, Schoepf UJ, Bastarrika G, Nance JW Jr, Abro JA, Ruzsics B (2010) Dual-energy computed tomography for integrative imaging of coronary artery disease: principles and clinical applications. Semin Ultrasound CT MR 31(4):276–291. doi:10.1053/j.sult.2010.05.004

Leber AW, Johnson T, Becker A, von Ziegler F, Tittus J, Nikolaou K, Reiser M, Steinbeck G, Becker CR, Knez A (2007) Diagnostic accuracy of dual-source multi-slice CT-coronary angiography in patients with an intermediate pretest likelihood for coronary artery disease. Eur Heart J 28(19):2354–2360. doi:10.1093/eurheartj/ehm294

Mahnken AH, Bruners P, Katoh M, Wildberger JE, Gunther RW, Buecker A (2006) Dynamic multi-section CT imaging in acute myocardial infarction: preliminary animal experience. Eur Radiol 16(3):746–752. doi:10.1007/s00330-005-0057-5

Mahnken AH, Klotz E, Pietsch H, Schmidt B, Allmendinger T, Haberland U, Kalender WA, Flohr T (2010) Quantitative whole heart stress perfusion CT imaging as noninvasive assessment of hemodynamics in coronary artery stenosis: preliminary animal experience. Invest Radiol 45(6):298–305. doi:10.1097/RLI.0b013e3181dfa3cf

Nagao M, Matsuoka H, Kawakami H, Higashino H, Mochizuki T, Murase K, Uemura M (2008) Quantification of myocardial perfusion by contrast-enhanced 64-MDCT: characterization of ischemic myocardium. Am J Roentgenol 191(1):19–25. doi:10.2214/AJR.07.2929

Nance JW Jr, Bastarrika G, Kang DK, Ruzsics B, Vogt S, Schmidt B, Raupach R, Flohr TG, Schoepf UJ (2011) High-temporal resolution dual-energy computed tomography of the heart using a novel hybrid image reconstruction algorithm: initial experience. J Comput Assist Tomogr 35(1):119–125. doi:10.1097/RCT0b013e3181f87475

Nesto RW, Kowalchuk GJ (1987) The ischemic cascade: temporal sequence of hemodynamic, electrocardiographic and symptomatic expressions of ischemia. Am J Cardiol 59(7):23C–30C

Nikolaou K, Sanz J, Poon M, Wintersperger BJ, Ohnesorge B, Rius T, Fayad ZA, Reiser MF, Becker CR (2005) Assessment of myocardial perfusion and viability from routine contrast-enhanced 16-detector-row computed tomography of the heart: preliminary results. Eur Radiol 15(5):864–871. doi:10.1007/s00330-005-2672-6

Rumberger JA, Feiring AJ, Lipton MJ, Higgins CB, Ell SR, Marcus ML (1987) Use of ultrafast computed tomography to quantitate regional myocardial perfusion: a preliminary report. J Am Coll Cardiol 9(1):59–69

Ruzsics B, Schwarz F, Schoepf UJ, Lee YS, Bastarrika G, Chiaramida SA, Costello P, Zwerner PL (2009) Comparison of dual-energy computed tomography of the heart with single photon emission computed tomography for assessment of coronary artery stenosis and of the myocardial blood supply. Am J Cardiol 104(3):318–326. doi:10.1016/j.amjcard.2009.03.051

So A, Lee TY (2011) Quantitative myocardial CT perfusion: a pictorial review and the current state of technology development. J Cardiovasc Comput Tomogr 5(6):467–481. doi:10.1016/j.jcct.2011.11.002

So A, Lee TY, Imai Y, Narayanan S, Hsieh J, Kramer J, Procknow K, Leipsic J, Labounty T, Min J (2011) Quantitative myocardial perfusion imaging using rapid kVp switch dual-energy CT: preliminary experience. J Cardiovasc Comput Tomogr 5(6):430–442. doi:10.1016/j.jcct.2011.10.008

So A, Hsieh J, Imai Y, Narayanan S, Kramer J, Procknow K, Dutta S, Leipsic J, Min JK, Labounty T, Lee TY (2012) Prospectively ECG-triggered rapid kV-switching dual-energy CT for quantitative imaging of myocardial perfusion. JACC Cardiovasc Imaging 5(8):829–836. doi:10.1016/j.jcmg.2011.12.026

Taylor AJ, Cerqueira M, Hodgson JMB, Mark D, Min J, O'gara P, Rubin GD (2010) ACCF/SCCT/ACR/AHA/ASE/ASNC/NASCI/SCAI/SCMR 2010 appropriate use criteria for cardiac computed tomography. JAC 56(22):1864–1894. doi:10.1016/j.jacc.2010.07.005

Tonino PAL, De Bruyne B, Pijls NHJ, Siebert U, Ikeno F, Van t Veer M, Klauss V, Manoharan G, Engstrøm T, Oldroyd KG, Ver Lee

PN, MacCarthy PA, Fearon WF, Investigators FS (2009) Fractional flow reserve versus angiography for guiding percutaneous coronary intervention. New Engl J Med 360(3):213–224. doi: 10.1056/NEJMoa0807611

Wang Y, Qin L, Shi X, Zeng Y, Jing H, Schoepf UJ, Jin Z (2012) Adenosine-stress dynamic myocardial perfusion imaging with second-generation dual-source CT: comparison with conventional catheter coronary angiography and SPECT nuclear myocardial perfusion imaging. Am J Roentgenol 198(3):521–529. doi: 10.2214/AJR.11.7830

Wolfkiel CJ, Ferguson JL, Chomka EV, Law WR, Labin IN, Tenzer ML, Booker M, Brundage BH (1987) Measurement of myocardial blood flow by ultrafast computed tomography. Circulation 76(6):1262–1273

Part IV
Viability

Why are We Interested in Viability?

Rozemarijn Vliegenthart and Daniel Lubbers

Contents

Abstract

The number of patients with left ventricular (LV) dysfunction due to coronary artery disease is increasing, as more patients now survive with acute myocardial infarction (MI) through primary reperfusion therapy. Severe LV dysfunction after MI, especially in combination with heart failure, is associated with a poor prognosis. Differentiation between reversible and irreversible LV dysfunction is important, as in the first situation, surgical revascularization improves prognosis. In case of reversible LV dysfunction, the myocardium can be stunned or hibernating. These principles are described. Myocardial viability assessment by noninvasive imaging techniques are indicated for this purpose. The different established imaging modalities for myocardial viability assessment are discussed in this chapter.

Abbreviations

ACS	Acute coronary syndrome
ABG	Coronary artery bypass grafting
CAD	Coronary artery disease
CHF	Congestive heart failure
DSE	Dobutamine stress echocardiography
FDG	Fluorine-18-labeled deoxyglucose
LGE	Late Gadolinium enhancement
LV	Left ventricular
MI	Myocardial infarction
MVO	Microvascular obstruction
NPV	Negative predictive value
PET	Positron emission tomography
PCI	Percutaneous coronary intervention
PPV	Positive predictive value
SPECT	Single photon emission computed tomography
Tc	Technetium

R. Vliegenthart (✉) · D. Lubbers
Center for Medical Imaging—North East Netherlands, University of Groningen, University Medical Center Groningen, Groningen, The Netherlands
e-mail: r.vliegenthart@umcg.nl

R. Vliegenthart
Department of Radiology, University of Groningen, University Medical Center Groningen, Groningen, The Netherlands

D. Lubbers
Department of Radiology, Nij Smellinghe Hospital, Drachten, The Netherlands

U. J. Schoepf et al. (eds.), *CT Imaging of Myocardial Perfusion and Viability*, Medical Radiology. Diagnostic Imaging,
DOI: 10.1007/174_2012_774, © Springer-Verlag Berlin Heidelberg 2012
Published Online: 24 December 2012

1 Background

The number of patients with congestive heart failure (CHF) related to left ventricular (LV) dysfunction is rising. Also, the incidence of CHF-related mortality has increased considerably in the last decades (Deedwania 2003). An important cause of the rising prevalence of LV dysfunction is the improved ability to treat acute coronary syndrome (ACS), decreasing the initial mortality from ACS. In the developed world, about two-thirds of LV dysfunction cases result from coronary artery disease (CAD) and (chronic) ischemic heart disease (Gheorgiade and Bonow 1998). Following myocardial infarction (MI), a process of infarct expansion and subsequent increase in LV volume can be observed. LV remodeling occurs due to a progressive increase in end-diastolic and end-systolic volumes at an initially maintained ejection fraction. An increase in LV end-diastolic volume of at least 20 % compared to baseline is often used to define infarct remodeling (Bolognese et al. 2002; Savoy et al. 2006). This remodeling can affect the LV systolic function and the patient's prognosis. The occurrence of severe LV dysfunction after MI, especially if combined with clinical CHF, is associated with a poor prognosis. These patients are at high risk of cardiac death and have high probability of recurrent hospitalizations due to CHF. In addition, they frequently have severe impairment of exercise capacity and daily activities. The estimated annual treatment cost for CHF in the United States is over 10 billion dollars (Abraham and Bristow 1997). In recent years, there have been considerable advances in medical therapy for LV dysfunction and the resulting symptoms of CHF (SOLVD investigators 1991; Pitt et al. 2000; Cohn et al. 1986; Pitt et al. 1999; Colucci et al. 2000; Abraham and Hayes 2003). However, the prognosis for CHF patients remains poor. For example, the Framingham Heart Study showed a 5-year mortality rate of 45 % in women and 59 % in men (Levy et al. 2002). Although medical therapy can be very beneficial, the best therapy in an appropriately selected patient is revascularization. Already by the 1970s, myocardial regions with abnormal wall motion by echocardiography were found to frequently recover function after coronary artery bypass grafting (CABG) (Chatterjee et al. 1973; Rees et al. 1971). Clinical trials have shown improved survival in patients with multivessel CAD and LV dysfunction after revascularization (Rahimtoola 1985).

LV dysfunction is not always the result of irreversible myocardial necrosis and scarring. After an initial ischemic injury, various processes can occur that lead to LV dysfunction, apart from myocyte death. These processes are to a certain extent reversible and include LV remodeling, impairment of energy metabolism, and myocyte dysfunction (Dilsizian 2003). In case of dysfunction due to myocardial necrosis and fibrotic replacement of myocardium, no recovery is to be expected after revascularization. However, if the LV dysfunction is due to myocardium that is jeopardized by ischemic injury but still viable, recovery may be possible. In these patients revascularization can result in better long-term survival, symptomatic improvement, and improved LV function (Baker et al. 1994; Bounous et al. 1988). Patients with LV dysfunction caused by CAD have, however, higher peri-operative risk compared to patients with normal ejection fraction. Therefore, appropriate selection of candidates for surgical revascularization is key: patients with dysfunctional but viable myocardium who are expected to show functional recovery (Blitz and Laks 1996). It is crucial to determine the risk-versus-benefit ratio for the individual patient with LV dysfunction due to CAD (Buckley and Di Carli 2011). Also, apart from viability, clinicians are often interested in whether there is presence of ischemia. If complete revascularization is not an option, detection of ischemia may assist in targeting the coronary artery that is likely to provide the most benefit. Noninvasive imaging of the myocardium provides essential information to derive the best clinical decision.

2 Concepts in Myocardial Viability

Prolonged ischemia of the myocardium triggers a cascade of events including edema and myocardial cell death (mainly necrosis). Infarcted myocytes lose cellular integrity by rupture of cell membranes. Infarcted myocardium does not benefit from revascularization. During the first days after acute coronary occlusion, the infarct volume can almost double in size, even without additional cell death. This is caused by an increase in edema and cellular elements (Reimer and Jennings 1979). Conversely, during the next 4–6 weeks after MI, infarct volume can diminish to about 25 % of its size in the acute phase as necrotic myocytes are replaced by scar tissue. In the months after acute MI, wall thinning of the infarct area and adjacent myocardium can be observed (Ganame et al. 2011). Even after restoring coronary flow in the acute phase, an area of residual myocardial perfusion abnormality may remain, called microvascular obstruction (MVO). The presence of MVO results in a more extensive final infarct size, LV remodeling, and lack of functional recovery (Bogaert et al. 2007), and is related to a worse prognosis (Ito et al. 1996; Wu et al. 1998; Lepper et al. 2000). In chronically infarcted myocardium, the necrotic and apoptotic myocytes have been replaced by collagenous scar tissue. This scar tissue has a small intracellular space and a large effective extracellular volume. Just like necrotic myocardium, scarred myocardium does not regain functionality after

revascularization. The size of the final infarct is related to the extent of LV remodeling and LV dysfunction (Lund et al. 2007; Orn et al. 2007).

The outcome of ischemic injury in the typical clinical setting is not clear-cut. Not always does ischemic injury result in infarct and irreversible LV dysfunction. Sometimes the result is partly or completely reversible LV dysfunction. In those cases, revascularization can lead to improved contractile function. In such cases of reversible LV dysfunction, two states of the myocardium are important, myocardial stunning and hibernation.

2.1 Myocardial Stunning

Myocardial stunning refers to reversible contractile dysfunction that can occur in the setting of restored coronary blood supply, after a brief period of impaired coronary perfusion (Heyndrickx et al. 1978; Braunwald and Kloner 1982). In myocardial stunning after reperfused ACS, coronary blood flow has been restored but contractility has not returned to baseline, which means that there is a mismatch in perfusion and contractility. Stunning can also develop after a period of unstable angina or exercise-induced ischemia. Episodes leading to stunning can be single or multiple, brief or prolonged, but by definition are not severe enough to cause myocardial necrosis. Stunned myocardium shows prolonged but transient dysfunction, that can last for hours to weeks (Kloner et al. 1998). In case of myocardial stunning, the myocardium is dysfunctional and viable. In the 1980s, small studies were already investigating myocardial functional recovery after thrombolytic treatment of ACS (plus coronary angioplasty in some cases) (Topol et al. 1985). After revascularization there was no immediate improvement in contractility. However, 10 days after the myocardial infarction, 85 % of reperfused infarct zone segments demonstrated improved wall motion versus 30 % of non-reperfused segments. The exact pathogenesis of myocardial stunning is still unclear. A variety of factors can be involved, including the presence of oxygen-free radicals (Schwaiger and Schricke 2000). In imaging, stunning is visible as a normally perfused, hypokinetic region that shows improvement under dobutamine.

2.2 Myocardial Hibernation

Myocardial hibernation is described as a condition of chronic contractile dysfunction due to severe CAD and chronically reduced rest perfusion (Rahimtoola 1989). The LV dysfunction associated with hibernation may be a protective response of the myocardium to meet the reduced supply of oxygen and substrates. Myocytes affected by this chronic low flow are thought to down-regulate their metabolic needs, and thus their energy demand. This limits cell death by preserving cell membrane integrity and glucose metabolism, but comes at the expense of contractile function (Rahimtoola 1982; Kloner et al. 1998; Baker et al. 1991; Gewirtz et al. 1994; Ragosta et al. 1993; Shavalkar et al. 1996; Dispersyn et al. 1999; Wilson 1999). A new balance in perfusion and contractility is reached (Braunwald and Rutherford 1986). Myocyte function can be restored to normal—partially or completely—if the myocardial oxygen supply–demand relationship is improved, either by increasing blood flow and/or by reducing demand (Rahimtoola 1989). The time course of functional recovery of hibernating myocardium may vary considerably and depends on several factors, such as the severity and duration of myocardial ischemia, the timing and completeness of myocardial revascularization, and the extent of microstructural changes in the dysfunctional myocardium (Vanoverschelde et al. 2000).

Recently, the concept that chronically reduced perfusion of the myocardium results in hibernation has been questioned. Studies have shown that resting blood flow in hibernating myocardium is not decreased to the extent that would account for the degree of contractile dysfunction. Rather, the myocardial perfusion reserve is significantly decreased (Conversano et al. 1996; Vanoverschelde et al. 1993; Marinho et al. 1996). The idea has arisen that stunning and hibernation may not be discrete entities but instead may exist on a continuum. Hibernation is likely a manifestation of chronic stunning due to repetitive, intermittent ischemic episodes (Braunwald and Kloner 1982; Marinho et al. 1996). Observations suggest that hibernation could develop during a time of repetitive stunning, with initial (near-) normal flow but reduced flow reserve, and with decreased resting flow in a later phase (Bax et al. 2003). Over time, microstructural changes in the myocardium can also occur, including changes in structural proteins, metabolism changes to a more fetal form, and apoptosis (Balliga et al. 2000; Vanoverschelde et al. 2000). In imaging, hibernating myocardium is diagnosed by an area of reduced contractility with improvement under low-dose dobutamine, normal or increased metabolism, and decreased perfusion.

3 Clinical Importance of Assessing Myocardial Viability

LV function is a well-established and strong prognostic factor after ACS (Burns et al. 2002). The development of LV systolic dysfunction after MI, especially if associated with clinical CHF, is associated with poor survival. For example, in the Coronary Artery Surgery Study, medically treated patients with an LV ejection fraction below 35 %

had a 10-year survival of only 30 %, compared to a survival of 60 % for patients with an ejection fraction of 35–49 %, and a survival of approximately 90 % for those with an ejection fraction of at least 50 % (Emond et al. 1994). The surgical treatment for ischemic heart failure (STICH) trial studied 1,212 patients with an ejection fraction of 35 % or less and CAD amenable to CABG, who were randomized to optimal medical treatment alone or with CABG. The trial showed that CABG resulted in 19 % lower risk of cardiovascular death, although overall mortality was not lower compared to medical treatment alone (Velazquez et al. 2011).

As described above, LV dysfunction can be due to an irreversible process, such as infarction, necrosis, or scarring, but also due to myocardial hibernation or stunning, in which case the LV dysfunction is partly or completely reversible. Differentiation between reversible and irreversible causes of LV dysfunction has important implications. Revascularization can result in survival benefit, symptomatic improvement, and improved contractile function in patients with reversible causes of LV dysfunction, i.e., hibernating myocardium (Baker et al. 1994). The main goal of myocardial viability assessment is to identify patients whose symptoms and prognosis may improve after revascularization. Among patients with reduced LV function, those with hibernating myocardium have the worst prognosis if not referred for revascularization. In contrast, patients with LV dysfunction predominantly due to scarring do not seem to benefit from a revascularization procedure, but fare better with medical treatment. In a meta-analysis of more than 3,000 patients with reduced ejection fraction who underwent myocardial viability assessment, the annual mortality rate for patients with viable myocardium who were treated medically was 16 %, compared to 3 % for those undergoing revascularization (Allman et al. 2002). Revascularization improved survival of patients with viable myocardium by approximately 80 %. In contrast, there was a trend towards increased mortality in patients without viable myocardium who underwent revascularization, 7.7 % versus 6.2 %. No significant difference in predictive power was found between nuclear techniques and dobutamine echocardiography. In a nonrandomized subgroup of the STICH trial, myocardial viability was assessed by single-photon emission computed tomography (SPECT) and/or dobutamine stress echocardiography (DSE). In this selected cohort, a survival benefit of CABG on top of medical treatment in the case of viable myocardium could not be demonstrated (Bonow et al. 2011). Due to issues with the study design, conclusions need to be drawn with caution. The findings suggest that viability assessment on its own may not be the only determinant of outcome in patients with LV dysfunction.

In selecting patients for revascularization, the identification of potentially reversible LV dysfunction should not be the only consideration. Many factors influence the clinical outcome, such as comorbidity, patient frailty, prior revascularization, and extent of LV remodeling (Buckley and Di Carli 2011). The clinical decision to revascularize is generally easy in cases of severe LV dysfunction, debilitating anginal symptoms, mild LV remodeling, adequate target vessels for revascularization, and minimal comorbidity (Baker et al. 1994). Survival benefit in these patients likely results from revascularization of myocardial territories at risk, including areas of ischemia. However, in patients with estimated high-risk revascularization, clinical decision making can be more difficult, involving careful weighing of the risks and benefits of a revascularization procedure. In both settings, myocardial viability assessment is crucial to determine the optimal clinical management for the individual patient.

4 Noninvasive Imaging Approaches to Evaluate Myocardial Viability

According to current guidelines and appropriateness criteria documents, there is a choice in noninvasive imaging techniques that can be applied to assess myocardial viability (Klocke et al. 2003; Hendel et al. 2006, 2009; Beanlands et al. 2007a; Sicari et al. 2008; Douglas et al. 2011). Options include single photon emission computed tomography (SPECT), fluorine-18-labeled deoxyglucose (FDG)-positron emission tomography (PET), dobutamine echocardiography, and MRI. Different principles underlie the assessment of viability by these modalities. Nuclear imaging techniques rely on intact cellular membranes for uptake and retention of radiotracers (thallium-201, technetium-99m), as well as intact glucose uptake (FDG). Dobutamine echocardiography/MRI investigates contractile reserve of dysfunctional myocardium based on the inotropic effect of low-dose dobutamine. Delayed contrast enhancement MRI can assess the presence and extent of myocardial infarction in the acute and late phase after MI (dependent on rupture of cell membranes in necrosis and increased interstitial space in scar tissue, respectively). While all techniques above are accepted modalities for myocardial viability assessment, dobutamine echocardiography is the first choice technique for evaluating wall motion abnormalities in most patients. On the other hand, MRI provides optimal tissue characterization for assessment of infarct and scar composition. Computed tomography has only recently entered the stage of myocardial viability assessment. Computed tomography for this indication is the focus of the chapters by Kerl and by Ruszics.

Table 1 Overview of established noninvasive imaging techniques for viability assessment, with test characteristics for prediction of improvement in regional contractility after revascularization

Imaging technique	Criteria for viability	Sens	Spec	PPV	NPV	Advantages	Disadvantages
SPECT Thallium-201 Technetium-99m	 Perfusion/redistribution, >50 % peak levels Perfusion, >50 % peak levels	 87 83	 54 65	 67 74	 79 76	Available Reproducible Extensive experience	Radiation Spatial resolution Long acquisition protocols
FDG-PET	(Perfusion/) Metabolism, >50 % peak activity	92	63	74	87	High accuracy Quantitative measures	Not widely available Expensive
Echocardiography LV wall thickness Dobutamine	 ED wall thickness >6 mm contractile reserve[a]	 94 80	 48 78	 53 75	 93 83	Available Cheap	Operator dependent Suboptimal image quality in 20 %
MRI LV wall thickness LGE Dobutamine	 ED wall thickness >5.5 mm <50 % transmural LGE contractile reserve	 96 95 81	 38 51 91	 71 69 93	 85 90 75	Spatial resolution Tissue characterization infarct size	Not possible in case of intracardiac devices and claustrophobia

Sens is sensitivity; Spec is specificity; PPV is positive predictive value; NPV is negative predictive value; SPECT is single-photon emission computed tomography; FDG is fluorine-18-labeled deoxyglucose; PET is positron emission tomography; LV is left ventricle; ED is end-diastolic; MRI is magnetic resonance imaging; LGE is late gadolinium enhancement.

[a] Preferable biphasic response.

Test characteristics for echocardiography LV wall thickness based on Cwajg et al. (2000), for MRI based on meta-analysis by Romero et al. (2012), for other imaging techniques based on meta-analysis by Schinkel et al. (2007).

It is important to consider the mechanism being targeted for viability assessment in order to understand advantages and limitations of each modality. In response to myocardial hypoperfusion, metabolic changes occur first, while subsequent steps lead to changes in myocardial contractility (Taegtmeyer 2010). Thus, modalities that make use of intact cell membrane function, a process that is affected early in the cascade, show a low probability of recovery post-revascularization if viability is absent (high sensitivity), while modalities that assess contractile function, a process that is affected only later, show a high probability of functional recovery if viability is present (high specificity). Apart from differences in diagnostic accuracy, modalities differ with regard to spatial resolution, availability, cost, radiation dose, and versatility. An overview of characteristics of the noninvasive modalities is provided in the included Table 1.

4.1 Nuclear Techniques

4.1.1 Single-photon Emission Computed Tomography

SPECT imaging uses single photon emitting radioisotopes to study the viability of the myocardium. The uptake of the radionuclide perfusion tracers depends on myocardial blood flow and the integrity of the cell membrane. Myocardial segments with maintained radiotracer uptake at rest are viable. However, segments with reduced radiotracer uptake may or may not be viable. In the latter cases, myocardial viability can be assessed by imaging myocardial metabolism or contractile reserve. A strong point of SPECT is the extensive clinical experience as well as the multitude of studies showing the ability of SPECT to predict viability. Also, SPECT imaging is widely available, easy to perform, and highly reproducible. However, due to the limited spatial resolution of SPECT, detection of small non-transmural infarcts is difficult. Additionally, both thallium-201 and technetium-99m studies are subject to attenuation artifacts from the diaphragm and breasts, although this can generally be solved by attenuation corrected SPECT. Finally, a disadvantage compared to MRI and DSE is the associated radiation burden.

4.1.1.1 Thallium-201

Thallium-201, one of the earliest radionuclide tracers, is actively extracted from the blood across the myocyte cell membrane via the sodium potassium-adenosine triphosphate pump. This transport system is unaffected by hypoxia unless irreversible injury is present. Images obtained early after radiotracer injection represent blood flow, whereas retention and redistribution of thallium over a 4–24 h period reflect intact cell membrane function, and thus, viability. Areas of LV dysfunction with thallium-201 activity >50 % of peak levels early after radiotracer injection are considered to be viable. Patients who have segments with < 50 % of peak levels undergo redistribution imaging after 4 or 24 h. Thallium-201 redistributes over time into viable cells

independent of the extent of first-pass perfusion. It has been shown that imaging 4 h after stress injection can underestimate the presence of viable myocardium as compared to imaging results at 24 h (Perrone Filardi et al. 1996) and compared to metabolic imaging with FDG-PET (Brunken et al. 1992). Modified protocols that involve reinjection of radiotracer (Bonow et al. 1991; Dilsizian et al. 1990) were found to improve the detection of viable myocardium. Zimmerman et al. (1995) showed that regional thallium-201 activity in redistribution and reinjection images is proportional to the mass of preserved viable myocytes in jeopardized myocardium. Images are often interpreted visually, but relative quantification of regional radiotracer uptake may provide more objective and accurate results (Qureshi et al. 1997). The most common protocols used for viability detection with thallium-201 are: (1) stress-redistribution-reinjection imaging, which provides information about inducible ischemia and cellular viability (Dilsizian et al. 1990); and (2) rest-redistribution imaging, which provides information about myocardial blood flow at rest and cellular integrity (Ragosta et al. 1993). The probability of functional recovery post-revascularization decreases as regional thallium-201 uptake declines. Areas with little or no thallium-201 uptake are unlikely to recover function after revascularization (Perrone Filardi et al. 1996). In a meta-analysis of 40 studies, the weighted mean sensitivity of thallium-201 imaging was 87 %, specificity 54 %, positive predictive value (PPV) 67 %, and negative predictive value (NPV) 79 % (Schinkel et al. 2007). Thallium-201 was found to provide important long-term prognostic information in patients with severe LV dysfunction who underwent CABG (Gurserer et al. 2002). Disadvantages of thallium-201 include a long half-life (73 h) which leads to a relatively high radiation dose, and suboptimal image quality in the cases of obesity and large breasts, which can result in false-positives.

4.1.1.2 Technetium

In recent times, Technetium (Tc)-99m has become the preferred SPECT radiotracer. 99mTc-labeled agents emit higher energy photons than thallium-201, yielding better image quality. Also, the shorter half-life time of 99mTc allows the administration of a higher dose. Flow tracers such as 99mTc-sestamibi and 99mTc-tetrofosmin are lipophilic and positively charged. Unlike thallium-201, Tc-99m-sestamibi and Tc-99m-tetrofosmin are passively transported via the sarcolemmal membrane and bind to the inner membrane of mitochondria (Piwnicka-Worms et al. 1994). Uptake and retention of 99mTc-sestamibi and 99mTc-tetrofosmin is dependent on cell membrane integrity and mitochondrial function (Travin et al. 2005). Regional 99mTc-sestamibi and 99mTc-tetrofosmin activity is closely correlated with the results obtained in thallium-201 imaging (Udelson et al. 1994; Matsunari et al. 1997). The use of nitrates prior to the injection of Tc-99m-labeled tracers enhances collateral flow and thus myocardial uptake in areas of resting hypoperfusion (Aoki et al. 1991). This improves the evaluation of myocardial viability. Another method to enhance the detection of viability is simultaneous assessment of LV function using gated SPECT imaging, which allows assessment of contractility. An example patient is shown in Fig. 1. In combination with low dose dobutamine infusion, gated SPECT imaging can be used to evaluate contractile reserve (Iskandrian et al. 1998). Like in thallium-201 imaging, apart from visual analysis, quantification of tracer uptake can be performed in Tc-99m SPECT imaging. Dysfunctional myocardial segments with >50 % of peak levels are considered viable and have a good probability of functional recovery after revascularization. In contrast, segments showing <50 % tracer uptake at rest have poor viability and a much lower probability of improved function after revascularization. In addition to viability imaging, rest SPECT images can be used for assessment of infarct size (Gibbons et al. 2005). In the previously mentioned meta-analysis, the reported weighted mean sensitivity for technetium-99m SPECT was 83 %, specificity 65 %, PPV 74 %, and NPV 76 % for predicting regional functional improvement after revascularization (Schinkel et al. 2007). Most of the 26 studies in the meta-analysis applied Tc-99m-sestamibi as tracer. Tc-99m SPECT imaging with use of nitrates resulted in better specificity and NPV than without nitrates, with comparable sensitivity and PPV.

4.1.2 Positron Emission Tomography

In PET imaging, radiotracers are used that emit positrons. Upon encountering an electron, the positron annihilates together with the electron, resulting in the production of a pair of 511 keV photons that travel at 180° from each other (Slart et al. 2006). PET imaging consists of detection of these photons when they hit the detectors within a pre-specified time interval (coincidence detection). The radiotracer is then assumed to be positioned directly between the two detectors. A low-resolution CT or a radionuclide transmission image is performed together with PET to correct for attenuation of photons. PET imaging can be applied to assess viability by the measurement of myocardial perfusion and/or metabolism (Fig. 2). Myocardial perfusion is assessed using rubidium-82 or N-13 ammonia. Commonly, myocardial metabolism is assessed by FDG, a glucose analog. The high temporal and spatial resolution of PET (Bacharach et al. 2003) combined with the attenuation correction allows quantification of small amounts of radiotracer uptake and estimation of myocardial blood flow (Al Mallah et al. 2010). Due to the very short half-life of most radiotracers (a few minutes), PET protocols are fast and

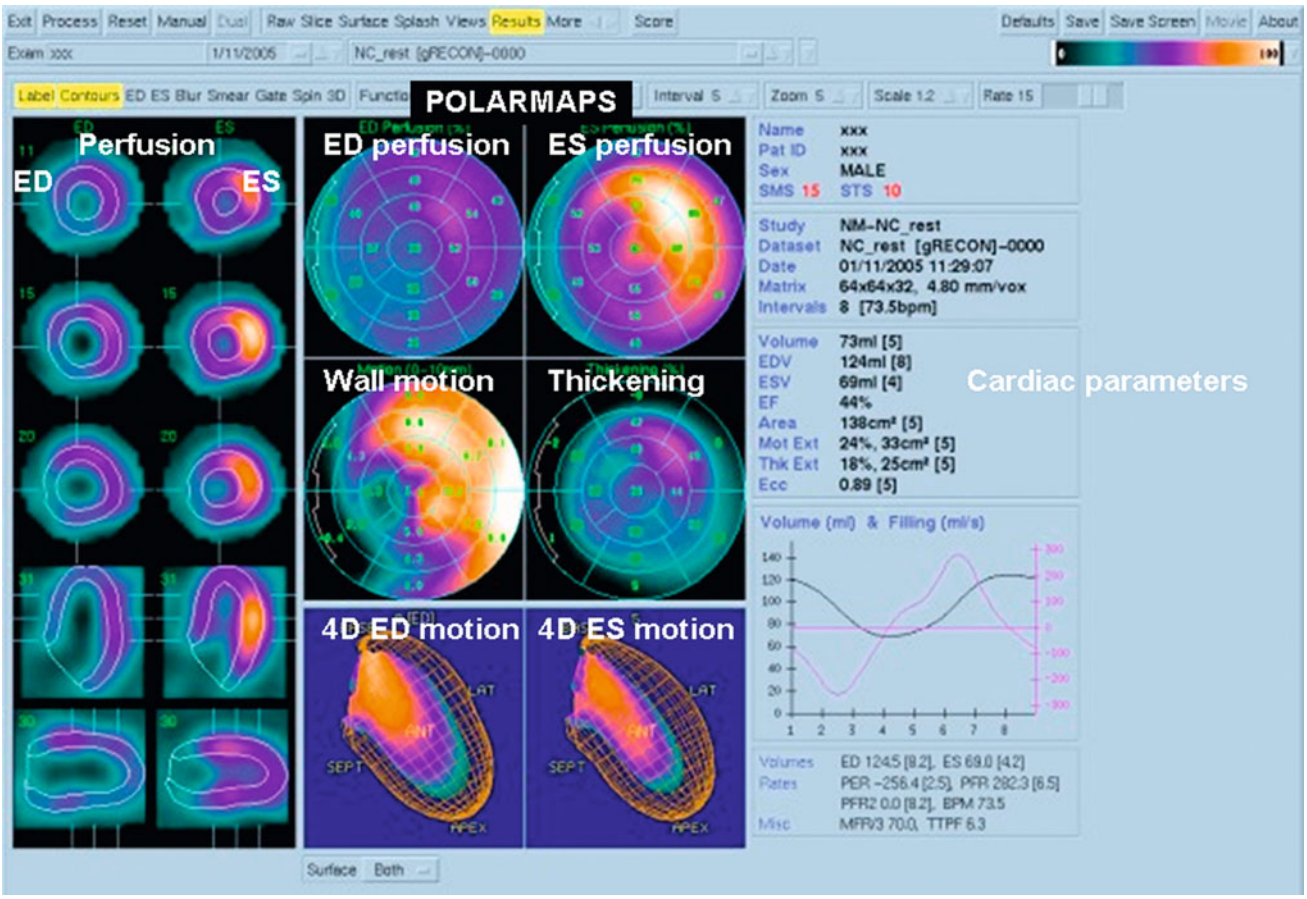

Fig. 1 Gated single-photon emission computed tomography myocardial perfusion scintigram in a patient with a history of inferoseptal infarct. *Left* perfusion and endo-/epicardial contours, cross-sections of the left ventricle in end-diastole (ED) and end-systole (ES). Middle, above: bull's eye views of the left ventricle of perfusion in ED and ES, wall motion and thickening. Middle, below: four-dimensional view of wall-motion in ED and ES. Color scale ranges from light yellow (normal perfusion/function) to green (no perfusion/function). On the right side the calculated cardiac parameters, including ED and ES volume and ejection fraction. Courtesy of Dr RHJA Slart, University Medical Center Groningen

radiation exposure is lower than for SPECT. FDG has a 2-h half-life that allows transport to sites without an on-site cyclotron. Disadvantages of PET include the high costs of the technology and the limited availability of PET scanners and radiotracers.

The typical FDG PET viability study consists of FDG PET images paired with resting myocardial perfusion images, which can be obtained using SPECT or PET. In viable but dysfunctional myocardium, FDG uptake increases due to a shift to anaerobic metabolism and a preference for glucose rather fatty acid metabolism (Dilsizian et al. 2008). The specific pattern of regional perfusion and metabolism allows classification of myocardium as normal, hibernating, or scar. A myocardial area with a severe perfusion and metabolism defect (termed a flow-metabolism "match"), indicates a transmural or nearly transmural infarct. A territory with a less severe, matched perfusion and metabolism defect represents a non-transmural infarct without viability. Segments with reduced perfusion and normal or increased glucose metabolism (mismatch) indicate jeopardized, viable myocardium. In myocardial areas with repetitive stunning, myocardial perfusion is normal or nearly normal, FDG uptake is normal or reduced, but stress perfusion, if performed, is typically reduced. FDG imaging can theoretically miss viable tissue in regions of thinned myocardium due to partial volume effects (Kuhl et al. 2006).

PET has a high accuracy for the prediction of functional recovery after revascularization (Tillisch et al. 1986; vom Dahl et al. 1994). The accuracy of PET remains high even in patients with the most severe left ventricular dysfunction (LVEF < 25 %) (Marin-Neto et al. 1998). In a meta-analysis of 24 studies (Schinkel et al. 2007), PET had a weighted mean sensitivity of 92 %, specificity of 63 %, PPV of 74 %, and NPV of 87 %. FDG-PET has been considered the reference standard for viability imaging given the extensive clinical experience, the considerable

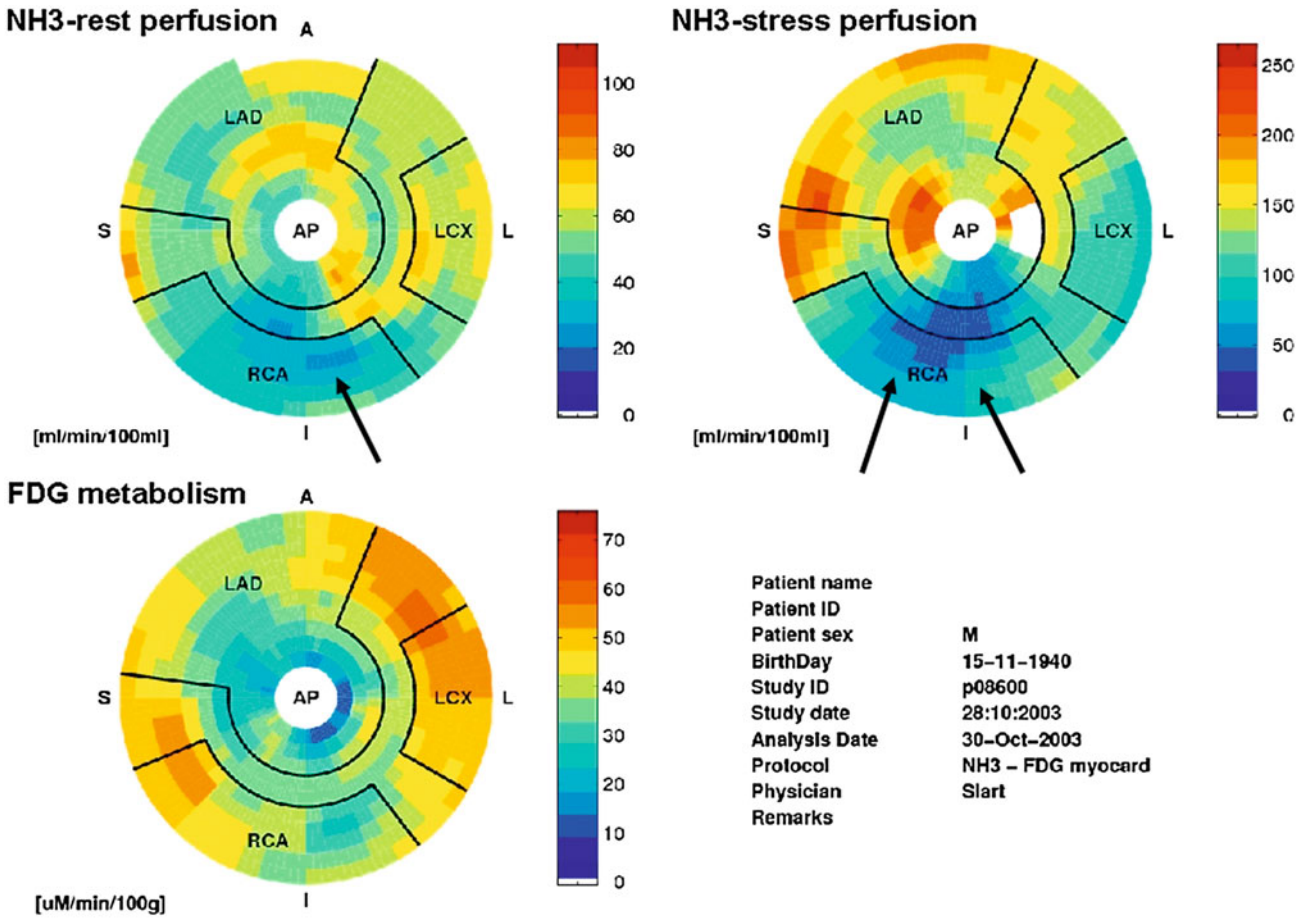

Fig. 2 Positron emission tomography examination. Polarmaps of the left ventricle showing absolute quantification of myocardial perfusion and FDG metabolism. The upper-left polarmap shows rest ^{13}N-ammonia perfusion, the *upper right* polarmap depicts dipyridamole stress ^{13}N-ammonia perfusion, the *lower* polarmap shows FDG metabolism. The color scale of the polarmaps ranges from *red* (good perfusion/viability) to *blue* (no perfusion/viability). The stress ^{13}N-ammonia polarmap shows a considerable perfusion defect of the inferior left ventricular wall, extending to the basolateral wall (*arrows*). This defect is largely reversible as shown on the rest ^{13}N-ammonia polarmap (ischemia), with a small persistent perfusion defect (*arrow*). The persistent perfusion defect shows glucose metabolism on the FDG polarmap, indicating myocardial viability. Courtesy of Dr RHJA Slart, University Medical Center Groningen

research data, and its relatively high accuracy for predicting functional recovery following revascularization. Exercise and functional capacity have been found to improve to a greater extent in patients with multiple areas of intact viability by FDG-PET, compared to patients with less viable myocardium (Di Carli et al. 1995; Marwick et al. 1992). The extent of perfusion-metabolism PET mismatch, in particular, identifies patients who will have the largest improvement in heart failure symptoms (Di Carli et al. 1995). PET viability imaging can identify patients with LV dysfunction who will derive the most prognostic benefit from revascularization in terms of reduction of cardiovascular events and mortality (Eitzman et al. 1992; Rohatgi et al. 2001). The value of PET was recently assessed in a randomized trial, the PET and Recovery Following Revascularization (PPAR-2) trial. PET-guided management was compared to routine management of patients with ischemic cardiomyopathy (Beanlands et al. 2007b). In the PET arm, recommendations regarding revascularization were based on the amount of viable myocardium. The study found that the composite endpoint of cardiac events/hospitalizations did not occur significantly less in patients randomized into the PET-based approach compared to the routine care arm (30 vs. 36 %). However, in patients who underwent the treatment that was guided by PET results, there was a significant reduction in mortality rate compared with the routine care arm. In a sub-study, the number of viable, ischemic segments (with perfusion-metabolism mismatch) was strongly related to the prognostic benefit of revascularization (D'Egidio et al. 2009). The capability to perform quantitative assessment of perfusion and metabolism is a particular strength of PET.

4.2 Echocardiography

4.2.1 Morphological Assessment

With echocardiography, myocardial viability can be evaluated through measures of LV wall thickness or myocardial contractile reserve (response to dobutamine infusion). The simplest type of viability assessment by echocardiography concerns LV morphology. Patients with a severely dilated LV are unlikely to show functional recovery after revascularization. The higher the LV end-systolic volume, the less likely the LV is to show improvement of contractile function (Bax et al. 2004). For LV volume measurement, three-dimensional echocardiography is more accurate than two-dimensional echocardiography (Lang et al. 2006). Thinned myocardial segments in patients with chronic CAD typically represent non-viable scar. An LV end-diastolic wall thickness >6 mm has been used as a marker to predict functional recovery post-revascularization (Cwajg et al. 2000). Sensitivity was 94 %, specificity—48 %, indicating that patients who will not benefit from revascularization can be identified, but that end-diastolic wall thickness does not predict patients who will recover LV function. In a study by La Canna et al. (2000), patients with referral for CABG underwent echocardiography (morphological and dobutamine stress evaluation) and thallium-201 studies. LV end-diastolic wall thickness >5 mm had higher sensitivity but lower specificity than viability by dobutamine echocardiography or thallium-201 studies. Myocardial segments with LV end-diastolic wall thickness <6 mm very rarely have contractile reserve on dobutamine echocardiography (Schinkel et al. 2002). Thus, an LV end-diastolic wall thickness below 5–6 mm makes contractile recovery after revascularization very unlikely.

4.2.2 Dobutamine Stress Echocardiography

DSE has long been used to assess jeopardized myocardium for viability. Stress echocardiography relies on dynamic assessment of myocardial wall thickening and wall motion during administration of an inotropic agent. The most extensive experience is available with low-dose dobutamine (Pierard et al. 1990; Smart et al. 1993; Watada et al. 1994; Cigarroa et al. 1993; Perrone Filardi et al. 1995; Sicari et al. 2003; Pagano et al. 1998). Dobutamine is a synthetic catecholamine leading to a considerable increase in systolic blood pressure and heart rate, and an increase in myocardial oxygen demand. It has both a positive inotropic and a chronotropic action. The inotropic effect occurs before the chronotropic effect. This positive inotropic effect, which occurs at low doses of dobutamine, is applicable in myocardial viability assessment (Kuijpers et al. 2004; Nagel et al. 1999). DSE is a widely available technique and is relatively easy to implement. However, DSE involves subjective assessment of regional wall motion, which makes the accuracy of the technique operator dependent. Also, suboptimal echo windows limit its use in approximately 20 % of patients.

To assess myocardial contractile reserve, images are obtained at baseline and under increasing doses of dobutamine. Dobutamine infusion typically starts at 5 μg kg body weight^{-1} min^{-1} for 3 min, increasing every 3 min to 10, 20, and in some cases, 30, and 40 μcg kg body weight^{-1} min^{-1}. In case of a low-dose dobutamine stress protocol, 20 μcg kg body weight^{-1} min^{-1} is the highest dose used. If ischemia is tested in the same examination, doses up to 40 μcg kg body weight^{-1} min^{-1} (high-dose) are infused. At each stage, echocardiographic images are reviewed to identify new wall motion abnormalities and worsening or improvement of pre-existing wall motion abnormalities.

Dysfunctional myocardial segments can present four different responses to dobutamine infusion (Nagueh et al. 1997): (1) progressive worsening of function. This likely represents hibernating myocardium, served by a critically stenosed coronary artery, or a significant scar. In this case there is no contractile reserve, and any increase in energy demand leads to ischemia. (2) No change in LV dysfunction, indicating scar. (3) Sustained improvement in contractility with increasing dobutamine doses; there is likely enough coronary flow even at high oxygen demands, for example in stunned myocardium. (4) A biphasic response in which a segment shows improvement in contractile function at low dose (5–10 μg kg^{-1} min^{-1}) with worsening at a higher dose (at least 20 μg kg^{-1} min^{-1}). Hibernating segments showing a biphasic response have contractile reserve, but this reserve is restricted usually due to concurrent coronary stenosis, resulting in ischemia at higher doses. The benefit of proceeding to higher doses of dobutamine, even if contractile reserve is demonstrated at lower doses, is to observe such a biphasic response.

The biphasic response has the best predictive value of the four possible responses to dobutamine in determining improvement in LV function after revascularization. Two studies in this field demonstrated that 72–75 % of dysfunctional segments with a biphasic response showed functional recovery following revascularization (Afridi et al. 1995; Cornell et al. 1998). Functional improvement post-revascularization is less likely in cases of worsening function (9–35 %) or sustained improvement (15–22 %), while recovery is not to be expected in case of no response to dobutamine (4–13 %). High-dose dobutamine protocols have a significantly higher sensitivity and a similar specificity to low-dose dobutamine protocols (Schinkel et al. 2007), and thus, are recommended if there are no contraindications to high-dose dobutamine. In a meta-analysis of 41 studies using DSE to predict improved ventricular function after revascularization (Schinkel et al. 2007), the sensitivity and specificity were 80 % and 78 %, respectively, and the PPV and NPV were

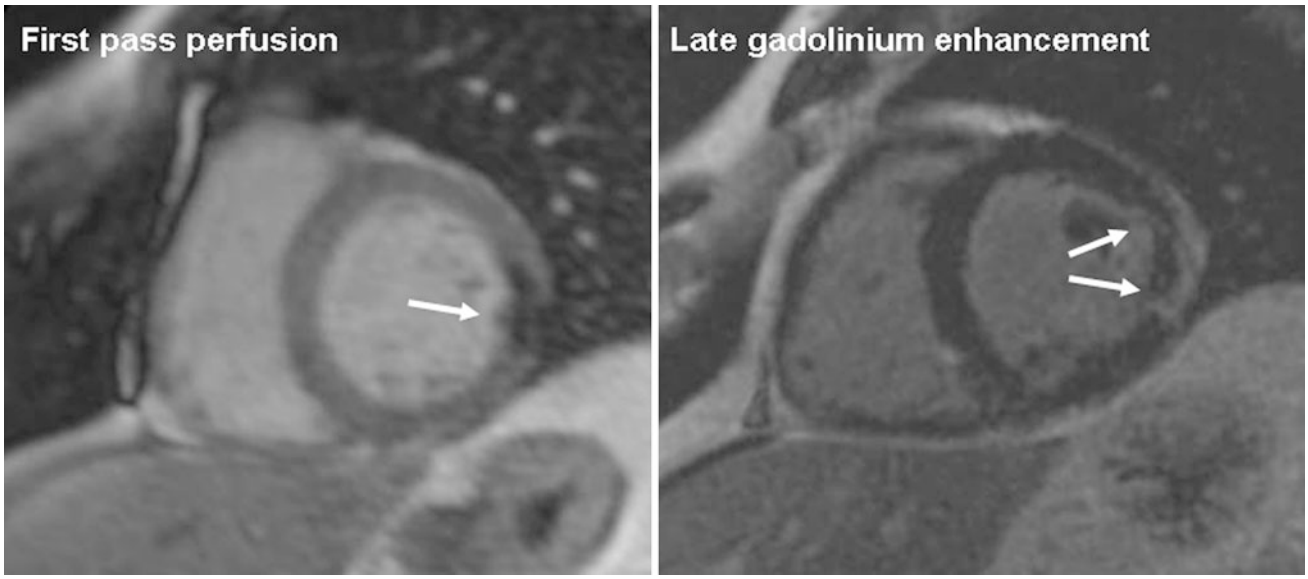

Fig. 3 Magnetic resonance imaging examination in a patient with a partly reperfused infarction, 1 day after the acute coronary syndrome. Midventricular short-axis images. The *left image* shows a focal perfusion defect during first pass of contrast in the lateral wall, indicative of impaired perfusion and microvascular obstruction. The *right image* shows late gadolinium enhancement of this area, reflective of necrosis and edema, with a central hypointense area that represents microvascular obstruction. On invasive coronary angiography (not shown), patient had an occluded obtuse marginal branch of the left circumflex coronary artery that could not be reperfused

75 % and 83 %, respectively. Only eight of these studies used a high-dose protocol. The high-dose protocols yielded slightly higher sensitivity (83 versus 79 %) and NPV (85 versus 82 %) than the low-dose studies. In the comparison of DSE and nuclear techniques (Schinkel et al. 2007), nuclear imaging modalities had a higher sensitivity for prediction of regional LV functional recovery, while DSE had higher specificity. Nuclear techniques also had higher sensitivity of global contractile function compared to DSE, at similar specificity. In general, DSE has a tendency to underestimate viability while nuclear imaging modalities tend toward the overestimation of viability. A substantial number of non-viable segments by DSE will be interpreted as viable by nuclear imaging (Panza et al. 1995; Cornel et al. 1999). In the presence of significant myocardial viability on DSE, patients who undergo revascularization were found to have a much more favorable prognosis than those treated medically (Afridi et al. 1998; Chaudhry et al. 1999). Conversely, patients with mostly non-viable myocardium on DSE did not derive prognostic benefit from revascularization.

4.3 Magnetic Resonance Imaging

4.3.1 Imaging Findings in Acute and Chronic Situations

Viability imaging with MRI revolves around two approaches: morphology and function. In acute situations, early after primary percutaneous coronary intervention (PCI), function loss and edema are more pronounced; while in the chronic situation, more structural changes occur, ultimately also leading to function loss. Different indices play a role in the assessment of prognosis after myocardial infarction, such as infarct size, right ventricular involvement, papillary muscle involvement, pericarditis, and microvascular obstruction.

T2-weighted imaging (short-tau inversion recovery—STIR-imaging) can be used to assess the amount of edema, visible as high signal intensity. Edema is a sign of acute injury that becomes less pronounced in time. T2-weighted imaging, especially so-called $T2^*$ imaging, can also be used to detect hemorrhage in an area of high signal intensity due to edema. Intramyocardial hemorrhage is associated with more severe infarct-related injury (Kumar et al. 2011).

Another helpful technique is first-pass perfusion imaging. In acute or chronic MI, perfusion images can be normal. This implies that perfusion status has recovered, which is a favorable prognostic sign. Prognosis is worse when perfusion imaging is abnormal, specifically with an area of reduced myocardial enhancement after the injection of an intravenous contrast agent (see Fig. 3). This can imply that there is microvascular obstruction (MVO), also called the no-reflow phenomenon. Multiple factors have been suggested that play a role in the no-reflow phenomenon, including microvascular spasm, endothelial dysfunction, inflammation, edema, embolization of thrombus, and plaque (Krug et al. 1996; Kloner et al. 1974). To a certain extent, MVO can also be PCI-procedure related. Taylor et al. (2006) described that elective PCI immediately impaired resting function as assessed with cardiac MRI. Because

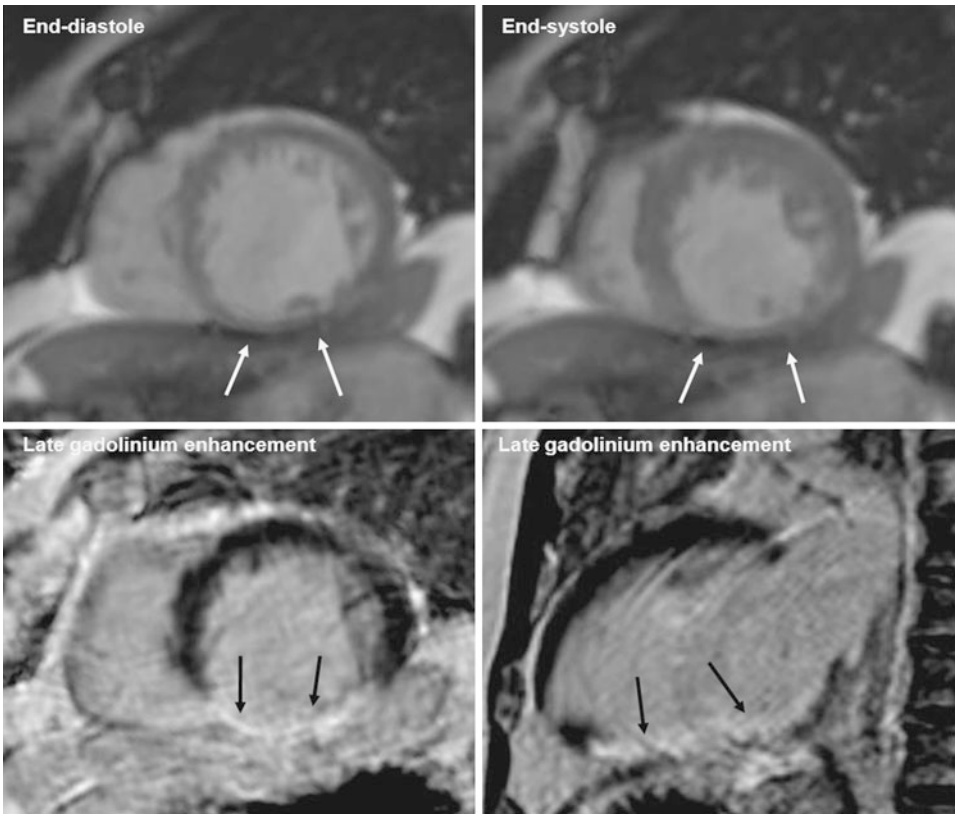

Fig. 4 Magnetic resonance imaging examination. Patient with history of myocardial infarction in right coronary artery territory. *Upper row* shows midventricular short axis cine slice images in end-diastole (*left*) and end-systole (*right*). Left ventricle dysfunction. Thinning of the inferior wall (<5.5 mm), without thickening/contractility in systole. Vertical long axis (*left*) and short axis (*right*) lower images show transmural late gadolinium enhancement in the inferior wall. Conclusion: Transmural infarction of the inferior wall without viable myocardium

first-pass perfusion imaging is a dynamic technique involving single-shot acquisition frames, the technique has relatively low signal- and contrast-to-noise ratios. A recent study showed that MVO is actually best detectable on delayed contrast enhancement MRI due to better contrast-to-noise ratio (see Fig. 3) (Nijveldt et al. 2009). However, the absence of a non-enhancing core on late enhancement images does not exclude the presence of MVO, as there is gradual filling-in of the MVO area with contrast in the minutes following contrast injection.

Functional cine imaging can be used to assess areas of hypokinesia, akinesia, or even dyskinesia as an expression of ischemic damage. In the setting of chronic MI, wall thinning can occur (Fig. 4). In the literature, an end-diastolic wall thickness of more than 5.5 or 6 mm is mentioned as the cut-off for myocardium that recovers function after revascularization (Romero et al. 2012). In a study by Stork et al. (2007), edema on T2-weighted images and wall thinning were accurate measures for differentiating acute from chronic MI, respectively. Delayed contrast enhancement and MVO did not play a role. On the other hand, T2-weighted imaging can substantially underestimate the extent of infarct in the presence of MVO.

4.3.2 Late Gadolinium Enhancement

One way to assess myocardial viability by cardiac MRI is the evaluation of late gadolinium enhancement (LGE). In the LGE technique, a T1-weighted imaging sequence is performed 8–10 min after the administration of the contrast agent, Gadolinium. Static imaging is performed, with more signal averaging and thus a higher signal-to-noise ratio than first-pass perfusion imaging. The signal from the myocardium is "nulled", using an inversion recovery pulse. This results in normal myocardium appearing dark; areas with LGE will then appear relatively bright. The nulling ensures optimal visual contrast between normal and abnormal myocardium. The optimal inversion time for nulling of the normal myocardium differs per patient and sometimes has to be optimized during the acquisition of multiple slices.

The LGE technique aims to detect regions with delayed Gadolinium uptake. It is important to note that in ischemic cardiomyopathy, delayed enhancement can reflect different pathologies. In the acute phase of MI, hyperenhancing myocardium indicates the area of necrosis and edema (see Fig. 3). Similar to the decrease in infarct size during the first weeks after MI, the extent of LGE volume in MRI decreases during the weeks after acute MI in canine models and in

patients (Rochitte et al. 1998; Fieno et al. 2004; Ibrahim et al. 2010). In the chronic situation, LGE identifies scarred myocardium—more factually, increased interstitial space. Thus, the statement, "bright is dead," does not accurately reflect the meaning of LGE. LGE hardly ever only reflects cell death. In a landmark study by Kim et al. (2000), the pattern of LGE in ischemic cardiomyopathy was found to correspond to the myocardial perfusion territory of the specific coronary artery. It was also shown that recovery of myocardial function after revascularization depends on the transmural extent of infarction. Contractile function is very likely to recover if there is no late enhancement and unlikely to recover in the case of more than 50 % transmural late enhancement (Fig. 4). However, in cases with 1–25 % transmural late enhancement, the probability of functional recovery is approximately 65 %; the probability of functional recovery is 43 % if transmurality is 26–50 % (Kim et al. 2000; Dilsizian 2007). Recovery of function after revascularization appears to be related to the ratio of viable-to-scarred myocardium within dysfunctional myocardial segments. Different cut-off values for transmural extent of hyperenhancement have been applied to determine whether or not functional recovery post-revascularization can be expected, ranging from >0 to >75 % (Romero et al. 2012). Due to its superior spatial resolution, LGE by MRI is better than SPECT and PET at identifying regions of subendocardial scar (Klein et al. 2002).

Due to the fact that at least an 8 min waiting time is mandatory after contrast injection, the DCE technique is always combined with dynamic perfusion imaging (which also requires a contrast agent). After contrast administration and perfusion imaging, typically a stack of short-axis cine images of the LV are acquired for LV functional parameter assessment. Cine MRI is considered the reference standard for measurements of global LV function (Task Force European Society of Cardiology 1998).

4.3.3 Dobutamine MRI

Wall motion imaging by cardiac MRI provides important information about global and regional myocardial function. For adequate wall motion analysis, the entire cardiac cycle needs to be captured. Additionally, good contrast between the myocardial wall and the blood pool is needed. Fast imaging with steady-state free precession sequences results in improved image quality compared with gradient echo acquisition techniques (Barkhausen et al. 2001; Plein et al. 2001). The capture of the entire cardiac cycle can be obtained with retrospective electrocardiographic gating, allowing for cine-loops to be acquired. Parallel imaging allows for either reduced acquisition time or improvement of temporal resolution. The consistently high level of spatial and temporal resolution with which cine MRI images can be acquired enables the detection of small alterations of systolic wall motion up to heart rates of 200 beats per minute. This allows for analysis of regional function with dobutamine MRI in multiple slice positions. The rationale for the use and dosage of dobutamine for evaluation of myocardial viability is similar in MRI as in echocardiography (see Sect. 4.2). Often, improvement in systolic wall thickening of more than 2 mm is used as cut-off to predict functional recovery (Romero et al. 2012).

Visual evaluation of changes in myocardial contractility during infusion of dobutamine can be challenging. Myocardial tagging, a technique using non-selective radiofrequency pulses separated by spatial modulation of magnetization encoding gradients, can be helpful in regional LV functional analysis. The absence of inward movement of these grid lines can be used to diagnose absence of viability. Generally, improvement of a rest wall motion abnormality during low-dose dobutamine is a sign that there is still functional recovery possible, and can be used as a sign of viability. Use of myocardial tagging was shown to facilitate detection of wall motion abnormalities compared to non-tagged MRI images (Kuijpers et al. 2003).

4.3.4 Diagnostic and Prognostic Accuracy of MRI

While the validation for the DCE-MRI technique has been particularly extensive, the number of patient studies on diagnostic accuracy is smaller. A recent meta-analysis compared the diagnostic accuracy of the three described MRI methods for assessing viability (Romero et al. 2012). In total, 24 studies met the inclusion criteria, comprising 698 patients. End-diastolic wall thickness of more than 5.5 or 6 mm (in total four studies) had weighted sensitivity of 96 %, specificity of 38 %, PPV of 71 %, NPV of 85 %, and overall accuracy of 68 %. For late enhancement (more than 50 % transmurality, 11 studies), these parameters were 95, 51, 69, 90 and 70 %, respectively. For improved systolic wall thickening on low-dose dobutamine MRI (>2 mm increase, 9 studies), test characteristics were 81, 91, 93, 75, and 84 %, respectively. Thus, wall thickness and DCE showed the highest sensitivity, and low-dose dobutamine MRI had the highest specificity. Prediction of improvement of contractile function can be difficult when based solely on morphological information. Wellnhofer et al. (2004) showed that DCE and dobutamine MRI can provide complementary information in predicting functional recovery after revascularization.

So far, only a few studies have been published on the prognostic value of viability assessment by MRI. In studies comprising more than 300 patients each, extent and transmurality of scar on MRI was found to predict major cardiac adverse events beyond clinical and functional parameters (Kwong et al. 2006; Kwon et al. 2009). Gerber et al. (2012) recently showed that patient survival was considerably worse when dysfunctional but viable myocardium on DCE-

MRI was treated medically instead of interventionally. Medically treated patients with dysfunctional but viable myocardium on DCE-MRI had a higher mortality than patients with non-viable myocardium. This is in line with meta-analysis results by Allman et al. (2002) for echocardiography and nuclear techniques. The worse prognosis in medically treated patients with viable versus non-viable myocardium is possibly related to increased arrhythmogenic vulnerability in still-viable myocardium, which can lead to cardiac death (Fallavollita et al. 2005). Lastly, in medically treated, chronic MI patients who underwent both DCE-MRI and dobutamine echocardiography, infarct size on MRI was a stronger prognostic factor than contractile reserve on echocardiography (Kelle et al. 2009). However, in the case of a large myocardial scar, contractile reserve was found to be more important as predictor of cardiac events.

5 Conclusion

Ischemic cardiomyopathy with LV dysfunction is a major burden in westernized societies, associated with high morbidity and mortality, and substantial costs. LV dysfunction can be reversible or irreversible, depending on whether underlying myocardium is viable or non-viable. Dysfunctional but viable myocardial segments with the potential for functional recovery are considered to be stunned or hibernating. In the case of reversible LV dysfunction, surgical revascularization can lead to improved prognosis in appropriately selected patients. Noninvasive imaging methods can be used to assess myocardial viability, to assist patient management optimization. The identification of viable myocardium differs for the discussed imaging modalities, and is generally based on morphology (mainly MRI) and/or function (nuclear techniques, dobutamine echocardiography, and MRI).

References

Abraham WT, Bristow MR (1997) Specialized centers for heart failure management. Circulation 96:2755–2757

Abraham WT, Hayes DL (2003) Cardiac resynchronization therapy for heart failure. Circulation 108:2596–2603

Afridi I, Kleiman NS, Raizner AE et al (1995) Dobutamine echocardiography in myocardial hibernation. Optimal dose and accuracy in predicting recovery of ventricular function after coronary angioplasty. Circulation 91:663–670

Afridi I, Grayburn PA, Panza JA, Oh JK, Zoghbi WA, Marwick TH (1998) Myocardial viability during dobutamine echocardiography predicts survival in patients with coronary artery disease and severe left ventricular systolic dysfunction. J Am Coll Cardiol 32:921–926

Allman KC, Shaw LJ, Hachamovitch R et al (2002) Myocardial viability testing and impact of revascularization on prognosis in patients with coronary artery disease and left ventricular dysfunction: a meta-analysis. J Am Coll Cardiol 39:1151–1158

Al-Mallah MH, Sitek A, Moore SC, Di Carli M, Dorbala S (2010) Assessment of myocardial perfusion and function with PET and PET/CT. J Nucl Cardiol 17:498–513

Aoki M, Sakai K, Koyanagi S, Takeshita A, Nakamura M (1991) Effect of nitroglycerin on coronary collateral function during exercise evaluated by quantitative analysis of thallium-201 single photon emission computed tomography. Am Heart J 121: 1361–1366

Bacharach SL, Bax JJ, Case J et al (2003) PET myocardial glucose metabolism and perfusion imaging: Part 1—Guidelines for data acquisition and patient preparation. J Nucl Cardiol 10:543–556

Baker WB, Klein MS, Reardon MJ et al (1991) Reversible cardiac dysfunction (hibernation) from ischemia due to compression of the coronary arteries by a pseudoaneurysm. N Engl J Med 325: 1858–1861

Baker DW, Jones R, Hodges J, Massie BM, Konstam MA, Rose EA (1994) Management of heart failure III. The role of revascularization in the treatment of patients with moderate or severe left ventricular systolic dysfunction. JAMA 272:1528–1534

Baliga RR, Schaper J, Narula JP (2000) Role of apoptosis in myocardial hibernation and myocardial stunning. In: Iskandrian AE, Van Der Wall EE (eds) Myocardial Viability, 2nd edn. Kluwer Academic Publishers, Dordrecht, pp 21–45

Barkhausen J, Ruehm SG, Goyen M, Buck T, Laub G, Debatin JF (2001) MR evaluation of ventricular function: true fast imaging with steady-state precession versus fast low-angle shot cine MR imaging: feasibility study. Radiology 219:264–269

Bax JJ, Wahba FF, Van Der Waal EE (2003) Myocardial viability/ hibernation. In: Iskandrian AE, Verani MS (eds) Nuclear cardiac imaging. Oxford University Press, New York, pp 386–398

Bax JJ, Schinkel AFL, Boersma E et al (2004) Extensive left ventricular remodeling does not allow viable myocardium to improve in left ventricular ejection fraction after revascularization and is associated with worse long-term prognosis. Circulation 110(suppl 1):II18–II22

Beanlands RS, Chow BJ, Dick A et al (2007a) CCS/CAR/CANM/ CNCS/CanSCMR joint position statement on advanced noninvasive cardiac imaging using positron emission tomography, magnetic resonance imaging and multidetector computed tomographic angiography in the diagnosis and evaluation of ischemic heart disease—executive summary. Can J Cardiol 23:107–119

Beanlands RSB, Nichol G, Huszti E et al (2007b) F-18-fluorodeoxyglucose positron emission tomography imaging-assisted management of patients with severe left ventricular dysfunction and suspected coronary disease: a randomized, controlled trial (PARR-2) (see comment). J Am Coll Cardiol 50:2002–2012

Blitz A, Laks H (1996) The role of coronary revascularization in the management of heart failure: identification of candidates and review of results. Curr Opin Cardiol 11:276–290

Bogaert J, Kalantzi M, Rademakers FE, Dymarkowski S, Janssens S (2007) Determinants and impact of microvascular obstruction in successfully reperfused ST-segment elevation myocardial infarction. Assessment by magnetic resonance imaging. Eur Radiol 17:2572–2580

Bolognese L, Neskovic AN, Parodi G et al (2002) Left ventricular remodeling after primary coronary angioplasty: patterns of left ventricular dilation and long-term prognostic implications. Circulation 106:2351–2357

Bonow RO, Dilsizian V, Cuocolo A, Bacharach SL (1991) Identification of viable myocardium in patients with chronic coronary artery disease and left ventricular dysfunction. Comparison of

thallium scintigraphy with reinjection and PET imaging with 18F-fluorodeoxyglucose (see comment). Circulation 83:26–37

Bonow RO, Maurer G, Lee KL et al (2011) Myocardial viability and survival in ischemic left ventricular dysfunction. N Engl J Med 364:1617–1625

Bounous EP, Mark DB, Pollock BG et al (1988) Surgical survival benefits for coronary disease patients with left ventricular dysfunction. Circulation 78:I151–I157

Braunwald E, Kloner RA (1982) The stunned myocardium: prolonged, postischemic ventricular dysfunction. Circulation 66:1146–1149

Braunwald E, Rutherford JD (1986) Reversible ischemic left ventricular dysfunction: evidence for the ''hibernating myocardium''. J Am Coll Cardiol 8:1467–1470

Brunken RC, Mody FV, Hawkins RA, Nienaber C, Phelps ME, Schelbert HR (1992) Positron emission tomography detects metabolic viability in myocardium with persistent 24-hour single-photon emission computed tomography 201Tl defects. Circulation 86:1357–1369

Buckley O, Di Carli M (2011) Predicting benefit from revascularization in patients with ischemic heart failure: imaging f myocardial ischemia and viability. Circulation 123:444–450

Burns RJ, Gibbons RJ, Yi Q et al (2002) The relationships of left ventricular ejection fraction, end-systolic volume index and infarct size to six-month mortality after hospital discharge following myocardial infarction treated by thrombolysis. J Am Coll Cardiol 39:30–36

Chatterjee K, Swan HJ, Parmley WW et al (1973) Influence of direct myocardial revascularization on left ventricular asynergy and function in patients with coronary heart disease: with and without previous myocardial infarction. Circulation 47:276–286

Chaudhry FA, Tauke JT, Alessandrini RS, Vardi G, Parker MA, Bonow RO (1999) Prognostic implications of myocardial contractile reserve in patients with coronary artery disease and left ventricular dysfunction. J Am Coll Cardiol 34:730–738

Cigarroa CG, deFilippi CR, Brickner ME, Alvarez LG, Wait MA, Grayburn PA (1993) Dobutamine stress echocardiography identifies hibernating myocardium and predicts recovery of left ventricular function after coronary revascularization. Circulation 88: 433–436

Cohn JN, Archibald DG, Ziesche S et al (1986) Effect of vasodilator therapy on mortality in chronic congestive heart failure. Results of a Veterans Administration Cooperative Study. N Engl J Med 314:1547–1552

Colucci WS, Elkayam U, Horton DP et al for the Nesiritide Study Group (2000) Intravenous nesiritide, a natriuretic peptide, in the treatment of decompensated congestive heart failure. N Engl J Med 343:246–253

Conversano A, Walsh JF, Geltman EM et al (1996) Delineation of myocardial stunning an hibernation by positron emission tomography in advanced coronary artery disease. Am Heart J 131: 440–450

Cornel JH, Bax JJ, Elhendy A, Maat AP, Kimman GJ, Geleijnse ML, Rambaldi R, Boersma E, Fioretti PM (1998) Biphasic response to dobutamine predicts improvement of global left ventricular function after surgical revascularization in patients with stable coronary artery disease: implications of time course of recovery on diagnostic accuracy. J Am Coll Cardiol 31:1002–1010

Cornel JH, Bax JJ, Elhendy A et al (1999) Agreement and disagreement between "metabolic viability" and "contractile reserve" in akinetic myocardium. J Nucl Cardiol 6:383–388

Cwajg JM, Cwajg E, Nagueh SF, He ZX, Qureshi U, Olmos LI et al (2000) End-diastolic wall thickness as a predictor of recovery of function in myocardial hibernation: relation to restredistribution T1–201 tomography and dobutamine stress echocardiography. J Am Coll Cardiol 35:1152–1161

D'Egidio G, Nichol G, Williams KA et al (2009) Increasing benefit from revascularization is associated with increasing amounts of myocardial hibernation: a substudy of the PARR-2 trial. JACC: Cardiovasc Imaging 2:1060–1068

Deedwania PC (2003) The key to unraveling the mystery of mortality in heart failure. An integrated approach. Circulation 107: 1719–1721

Di Carli MF, Asgarzadie F, Schelbert HR, Brunken RC, Laks H, Phelps ME, Maddahi J (1995) Quantitative relation between myocardial viability and improvement in heart failure symptoms after revascularization in patients with ischemic cardiomyopathy. Circulation 92:3436–3444

Dilsizian V (2003) Myocardial viability: reversible left ventricular dysfunction. In: Dilsizian V, Narula J, Braunwald E (eds) Atlas of nuclear cardiology. Current Medicine, Philadelphia, pp 19–46

Dilsizian V (2007) Cardiac magnetic resonance versus SPECT: are all non-infarct myocardial regions created equal? J Nucl Card 14:9–14

Dilsizian V, Rocco TP, Freedman NM, Leon MB, Bonow RO (1990) Enhanced detection of ischemic but viable myocardium by the reinjection of thallium after stress-redistribution imaging. N Engl J Med 323:141–146

Dilsizian V, Bacharach SL, Beanlands RS, Bergmann SR, Delbeke D, Gropler RJ, Knuuti J, Schelbert HR, Travin M (2008) PET myocardial perfusion and metabolism clinical imaging. http://www.asnc.org/imageuploads/ImagingGuidelinesPETJuly2009.pdf

Dispersyn GD, Ausma J, Thone F et al (1999) Cardiomyocyte remodelling during myocardial hibernation and atrial fibrillation: prelude to apoptosis. Cardiovasc Res 43:947–957

Douglas PS, Garcia MJ, Haines DE et al (2011) ACCF/ASE/AHA/ASNC/HFSA/HRS/SCAI/SCCM/SCCT/SCMR 2011 Appropriate Use Criteria for Echocardiography. A Report of the American College of Cardiology Foundation Appropriate Use Criteria Task Force, American Society of Echocardiography, American Heart Association, American Society of Nuclear Cardiology, Heart Failure Society of America, Heart Rhythm Society, Society for Cardiovascular Angiography and Interventions, Society of Critical Care Medicine, Society of Cardiovascular Computed Tomography, Society for Cardiovascular Magnetic Resonance American College of Chest Physicians. J Am Soc Echocardiogr 24:229–267

Eitzman D, al-Aouar Z, Kanter HL et al (1992) Clinical outcome of patients with advanced coronary artery disease after viability studies with positron emission tomography (see comment). J Am Coll Cardiol 20:559–565

Emond M, Mock M, Davis K et al (1994) Long-term survival of medically treated patients in the Coronary Artery Surgery Study (CASS) registry. Circulation 90:2645–2657

Fallavollita JA, Riegel BJ, Suzuki G, Valeti U, Canty JM Jr (2005) Mechanism of sudden cardiac death in pigs with viable chronically dysfunctional myocardium and ischemic cardiomyopathy. Am J Physiol Heart Circ Physiol 289:H2688–H2696

Fieno DS, Hillenbrand HB, Rehwald WG et al (2004) Infarct resorption, compensatory hypertrophy, and differing patterns of ventricular remodeling following myocardial infarctions of varying size. J Am Coll Cardiol 43:2124–2131

Ganame J, Messalli G, Masci PG, Dymarkowski S, Abbasi K, Van de Werf F, Janssens S, Bogaert J (2011) Time course of infarct healing and left ventricular remodelling in patients with reperfused ST segment elevation myocardial infarction using comprehensive magnetic resonance imaging. Eur Radiol 21:693–701

Gerber BL, Rousseau MF, Ahn SA et al (2012) Prognostic value of myocardial viability by delayed-enhanced magnetic resonance in patients with coronary artery disease and low ejection fraction: impact of revascularization therapy. J Am Coll Cardiol 59:825–835

Gewirtz H, Fischman AJ, Abraham S et al (1994) Positron emission tomographic measurements of absolute regional myocardial blood

flow permits identification of nonviable myocardium in patients with chronic myocardial infarction. J Am Coll Cardiol 23:851–859
Gheorgiade M, Bonow RO (1998) Chronic heart failure in the United States. A manifestation of coronary artery disease. Circulation 97:282–289
Gibbons RJ, Miller TD (2005) Tc-99m sestamibi infarct size as a surrogate endpoint. J Nucl Cardiol 12:12–19
Gursurer M, Emre A, Gercekoglu H, Uslubas S, Aksoy M, Ersek B (2002) Long-term prognostic value of stress-redistribution-reinjection Tl-201 imaging in patients with severe left ventricular dysfunction and coronary artery bypass surgery. Int J Cardiovasc Imaging 18:125–133
Hendel RC, Patel MR, Kramer CM et al (2006) ACCF/ACR/SCCT/SCMR/ASNC/NASCI/SCAI/SIR 2006 appropriateness criteria for cardiac computed tomography and cardiac magnetic resonance imaging. A report of the American College of Cardiology Foundation Quality Strategic Directions Committee Appropriateness Criteria Working Group. J Am Coll Cardiol 48:1475–1497
Hendel RC, Berman DS, Di Carli MF et al (2009) ACCF/ASNC/ACR/AHA/ASE/SCCT/SCMR/SNM 2009 Appropriate Use Criteria for Cardiac Radionuclide Imaging: A Report of the American College of Cardiology Foundation Appropriate Use Criteria Task Force, the American Society of Nuclear Cardiology, the American College of Radiology, the American Heart Association, the American Society of Echocardiography, The Society of Cardiovascular Computed Tomography, The Society for Cardiovascular Magnetic Resonance, and The Society of Nuclear Medicine. J Am Coll Cardiol 53:2201–2229
Heyndrickx GR, Baig H, Nellens P et al (1978) Depression of regional blood flow and wall thickening after brief coronary occlusions. Am J Physiol 234:H653–H659
Ibrahim T, Hackl T, Nekolla SG et al (2010) Acute myocardial infarction: serial cardiac MR imaging shows a decrease in delayed enhancement of the myocardium during the 1st week after reperfusion. Radiology 254:88–97
Iskandrian AE, Acio E (1998) Methodology of a novel myocardial viability protocol. J Nucl Cardiol 5:206–209
Ito H, Maruyama A, Iwakura K et al (1996) Clinical implications of the "no reflow" phenomenon: a predictor of complications and left ventricular remodeling in reperfused anterior wall myocardial infarction. Circulation 93:223–228
Kelle S, Roes SD, Klein C et al (2009) Prognostic value of myocardial infarct size and contractile reserve using magnetic resonance imaging. J Am Coll Cardiol 54:1770–1777
Kim RJ, Wu E, Rafael A et al (2000) The use of contrast-enhanced magnetic resonance imaging to identify reversible myocardial dysfunction. New Engl J Med 343:1445–1453
Klein C, Nekolla SG, Bengel FM et al (2002) Assessment of myocardial viability with contrast enhanced magnetic resonance imaging: comparison with positron emission tomography. Circulation 105:162–167
Klocke FJ, Baird MG, Lorell BH et al (2003) ACC/AHA/ASNC guidelines for the clinical use of cardiac radionuclide imaging—executive summary: a report of the American College of Cardiology/American Heart Association Task Force on Practice Guidelines (ACC/AHA/ASNC Committee to Revise the 1995 Guidelines for the clinical use of Cardiac Radionuclide Imaging). Circulation 108:1404–1418
Kloner RA, Ganote CE, Jennings RB (1974) The "no-reflow" phenomenon after temporary coronary occlusion in the dog. Clin Investig 54:1496–1508
Kloner RA, Bolli R, Marban E et al (1998) Medical and cellular implications of stunning, hibernation, and preconditioning. An NHLBI workshop. Circulation 97:1848–1867
Krug A, de Rochemont WM, Korb G (1996) Blood supply of the myocardium after temporary coronary occlusion. Circ Res 19:57–62
Kuhl HP, Lipke CS, Krombach GA et al (2006) Assessment of reversible myocardial dysfunction in chronic ischaemic heart disease: comparison of contrast-enhanced cardiovascular magnetic resonance and a combined positron emission tomography-single photon emission computed tomography imaging protocol. Eur Heart J 27:846–853
Kuijpers D, Ho KY, van Dijkman PR, Vliegenthart R, Oudkerk M (2003) Dobutamine cardiovascular magnetic resonance for the detection of myocardial ischemia with the use of myocardial tagging. Circulation 107:1592–1597
Kuijpers D, van Dijkman PR, Janssen CH, Vliegenthart R, Zijlstra F, Oudkerk M (2004) Dobutamine stress MRI. Part II. Risk stratification with dobutamine cardiovascular magnetic resonance in patients suspected of myocardial ischemia. Eur Radiol 14:2046–2052
Kumar A, Green JD, Sykes JM, Ephrat P, Carson JJ, Mitchell AJ, Wisenberg G, Friedrich MG (2011) Detection and quantification of myocardial reperfusion hemorrhage using T2*-weighted CMR. JACC Cardiovasc Imaging 4:1274–1283
Kwon DH, Halley CM, Carrigan TP et al (2009) Extent of left ventricular scar predicts outcomes in ischemic cardiomyopathy patients with significantly reduced systolic function: a delayed hyperenhancement cardiac magnetic resonance study. J Am Coll Cardiol Imaging 2:34–44
Kwong RY, Chan AK, Brown KA, Chan CW, Reynolds HG, Tsang S, Davis RB (2006) Impact of unrecognized myocardial scar detected by cardiac magnetic resonance imaging on event-free survival in patients presenting with signs or symptoms of coronary artery disease. Circulation 113:2733–2743
La Canna G, Rahimtoola SH, Visioli O et al (2000) Sensitivity, specificity, and predictive accuracies of non-invasive tests, singly and in combination, for diagnosis of hibernating myocardium. Eur Heart J 21:1358–1367
Lang RM, Mor-Avi V, Sugeng L et al (2006) Three-dimensional echocardiography: the benefits of the added dimension. J Am Coll Cardiol 48:2053–2069
Lepper W, Hoffmann R, Kamp O et al (2000) Assessment of myocardial reperfusion by intravenous myocardial contrast echocardiography and coronary flow reserve after primary percutaneous transluminal coronary angioplasty in patients with acute myocardial infarction. Circulation 101:2368–2374
Levy D, Kenchaiah S, Larson MG et al (2002) Long-term trends in the incidence of and survival with heart failure. N Engl J Med 93:1397–1402
Lund GK, Stork A, Muellerleile K et al (2007) Prediction of left ventricular remodeling and analysis of infarct resorption in patients with reperfused myocardial infarcts by using contrast-enhanced MR imaging. Radiology 245:95–102
Marinho NV, Keogh BE, Costa DC et al (1996) Pathophysiology of chronic left ventricular dysfunction: new insights from the measurement of absolute myocardial blood flow and glucose utilization. Circulation 93:737–744
Marin-Neto JA, Dilsizian V, Arrighi JA, Perrone-Filardi P, Bacharach SL, Bonow RO (1998) Thallium scintigraphy compared with 18F-fluorodeoxyglucose positron emission tomography for assessing myocardial viability in patients with moderate versus severe left ventricular dysfunction. Am J Cardiol 82:1001–1007
Marwick TH, Nemec JJ, Lafont A, Salcedo EE, MacIntyre WJ (1992) Prediction by postexercise fluoro-18 deoxyglucose positron emission tomography of improvement in exercise capacity after revascularization. Am J Cardiol 69:854–859

Matsunari I, Fujino S, Taki J et al (1997) Quantitative rest technetium-99m tetrofosmin imaging in predicting functional recovery after revascularization: comparison with rest-redistribution thallium-201. J Am Coll Cardiol 29:1226–1233

Nagel E, Lehmkuhl HB, Bocksch W et al (1999) Noninvasive diagnosis of ischemia-induced wall motion abnormalities with the use of high-dose dobutamine stress MRI: comparison with dobutamine stress echocardiography. Circulation 99:763–770

Nagueh SF, Vaduganathan P, Ali N et al (1997) Identification of hibernating myocardium: comparative accuracy of myocardial contrast echocardiography, rest-redistribution thallium-201 tomography and dobutamine echocardiography. J Am Coll Cardiol 29:985–993

Nijveldt R, Hofman MB, Hirsch A, Beek AM, Umans VA, Algra PR, Piek JJ, van Rossum AC (2009) Assessment of microvascular obstruction and prediction of short-term remodeling after acute myocardial infarction: cardiac MR imaging study. Radiology 250:363–370

Orn S, Manhenke C, Anand IS, Squire I, Nagel E, Edvardsen T, Dickstein K (2007) Effect of left ventricular scar size, location, and transmurality on left ventricular remodeling with healed myocardial infarction. Am J Cardiol 99:1109–1114

Pagano D, Bonser RS, Townend JN, Ordoubadi F, Lorenzoni R, Camici PG (1998) Predictive value of dobutamine echocardiography and positron emission tomography in identifying hibernating myocardium in patients with postischaemic heart failure. Heart 79:281–288

Panza JA, Dilsizian V, Laurienzo JM et al (1995) Relation between thallium uptake and contractile response to dobutamine: implications regarding myocardial viability in patients with chronic coronary artery disease and left ventricular dysfunction. Circulation 91:990–998

Perrone Filardi P, Pace L, Prastaro M, Piscione F, Betocchi S, Squame F et al (1995) Dobutamine echocardiography predicts improvement of hypoperfused dysfunctional myocardium after revascularization in patients with coronary artery disease. Circulation 91:2556–2565

Perrone-Filardi P, Pace L, Prastaro M et al (1996) Assessment of myocardial viability in patients with chronic coronary artery disease. Rest-4-hour-24-hour 201T1 tomography versus dobutamine echocardiography. Circulation 94:2712–2719

Pierard LA, De Landsheere CM, Berthe C, Rigo P, Kulbertus HE (1990) Identification of viable myocardium by echocardiography during dobutamine infusion in patients with myocardial infarction after thrombolytic therapy: comparison with positron emission tomography. J Am Coll Cardiol 15:1021–1031

Pitt B, Zannad F, Remme WJ et al (1999) Randomized aldactone evaluation study investigators: the effect of spironolactone on morbidity and mortality in patients with severe heart failure. N Engl J Med 341:709–717

Pitt B, Poole-Wilson PA, Segal R et al (2000) Effect of losartan compared with captopril on mortality in patients with symptomatic heart failure: randomized trial—the losartan heart failure study ELITE II. Lancet 355:1582–1587

Piwnicka-Worms DP, Kronauge JF, LeFurgey A et al (1994) Mitochondrial localization and characterization of 99Tcsestamibi in heart cells by electron probe x-ray microanalysis and 99Tc-NMR spectroscopy. Magn Reson Imaging 12:641–652

Plein S, Bloomer TN, Ridgway JP, Jones TR, Bainbridge GJ, Sivananthan MU (2001) Steady-state free precession magnetic resonance imaging of the heart: comparison with segmented k-space gradient-echo imaging. J Magn Reson Imaging 14: 230–236

Qureshi U, Nagueh SF, Afridi I et al (1997) Dobutamine echocardiography and quantitative rest-redistribution 201Tl tomography in myocardial hibernation. Relation of contractile reserve to 201Tl uptake and comparative prediction of recovery of function. Circulation 95:626–635

Ragosta M, Beller GA, Watson DD et al (1993) Quantitative planar rest redistribution 201-Tl imaging in detection of myocardial viability and prediction of improvement in left ventricular function after coronary artery bypass surgery in patients with severely depressed left ventricular function. Circulation 87: 1630–1641

Rahimtoola SH (1982) Coronary bypass surgery for chronic angina—1981: a perspective. Circulation 65:225–241

Rahimtoola SH (1985) A perspective on the three large multicenter randomized clinical trials of coronary bypass surgery for chronic stable angina. Circulation 72(suppl V):V123–V135

Rahimtoola SH (1989) The hibernating myocardium. Am Heart J 117:211–221

Rees G, Bristow JD, Kremkau EL et al (1971) Influence of aortocoronary bypass surgery on left ventricular performance. N Engl J Med 284:1116–1120

Reimer KA, Jennings RB (1979) The "wavefront phenomenon" of myocardial ischemic cell death. II. Transmural progression of necrosis within the framework of ischemic bed size (myocardium at risk) and collateral flow. Lab Invest 40:633–644

Rochitte CE, Lima JA, Bluemke DA et al (1998) Magnitude and time course of microvascular obstruction and tissue injury after acute myocardial infarction. Circulation 98:1006–1014

Rohatgi R, Epstein S, Henriquez J et al (2001) Utility of positron emission tomography in predicting cardiac events and survival in patients with coronary artery disease and severe left ventricular dysfunction. Am J Cardiol 87:1096–1099

Romero J, Xue X, Gonzalez W, Garcia MJ (2012) CMR imaging assessing viability in patients with chronic ventricular dysfunction due to coronary artery disease: a meta-analysis of prospective trials. JACC Cardiovasc Imaging 5:494–508

Savoye C, Equine O, Tricot O et al (2006) Left ventricular remodeling after anterior wall acute myocardial infarction in modern clinical practice [from the REmodelage VEntriculaire (REVE) study group]. Am J Cardiol 98:1144–1149

Schinkel AFL, Bax JJ, Boersma E et al (2002) Assessment of residual myocardial viability in regions with chronic electrocardiographic Q-wave infarction. Am Heart J 144:865–869

Schinkel AF, Bax JJ, Poldermans D, Elhendy A, Ferrari R, Rahimtoola SH (2007) Hibernating myocardium: diagnosis and patient outcomes. Curr Probl Cardiol 32:375–410

Schwaiger M, Schricke U (2000) Hibernating and stunned myocardium. Pathophysiological considerations. In: Iskandrian AE, Van Der Wall EE (eds) Myocardial viability, 2nd edn. Kluwer Academic Publishers, Dordrecht, pp 1–20

Shivalkar B, Maes A, Borgers M et al (1996) Only hibernating myocardium invariably shows early recovery after coronary revascularization. Circulation 94:308–315

Sicari R, Picano E, Cortigiani L, Borges AC, Varga A, Palagi C et al (2003) VIDA (Viability Identification with Dobutamine Administration) Study Group. Prognostic value of myocardial viability recognized by low-dose dobutamine echocardiography in chronic ischaemic left ventricular dysfunction. Am J Cardio 92:1263–1266

Sicari R, Nihoyannopoulos P, Evangelista A et al (2008) Stress echocardiography expert consensus statement: European Association of Echocardiography (EAE) (a registered branch of the ESC). Eur J Echocardiogr 9:415–437

Slart RHJA, Bax JJ, van Veldhuisen DJ et al (2006) Imaging techniques in nuclear cardiology for the assessment of myocardial viability. Int J Cardiovasc Imaging 22:63–80

Smart SC, Sawada S, Ryan T, Segar D, Atherton L, Berkovitz K et al (1993) Low-dose dobutamine echocardiography detects reversible

dysfunction after thrombolytic therapy of acute myocardial infarction. Circulation 88:405–415

Stork A, Muellerleile K, Bansmann PM et al (2007) Value of T2-weighted, first-pass and delayed enhancement, and cine CMR to differentiate between acute and chronic myocardial infarction. Eur Radiol 17:610–617

Taegtmeyer H (2010) Tracing cardiac metabolism in vivo: one substrate at a time. J Nucl Med 51(Suppl 1):80S–87S

Task Force of the European Society of Cardiology, in collaboration with the Association of European Paediatric Cardiologists (1998) The clinical role of magnetic resonance in cardiovascular disease. Eur Heart J 19:19–39

Taylor AJ, Al-Saadi N, Abdel-Aty H et al (2006) Elective percutaneous coronary intervention immediately impairs resting microvascular perfusion assessed by cardiac magnetic resonance imaging. Am Heart J 151:891.e1–891.e7

The SOLVD investigators (1991) Effect of enalapril on survival in patients with reduced left ventricular ejection fractions and congestive heart failure. N Engl J Med 325:293–302

Tillisch J, Brunken R, Marshall R et al (1986) Reversibility of cardiac wall-motion abnormalities predicted by positron tomography. N Engl J Med 314:884–888

Topol EJ, Weiss JL, Brinker JA et al (1985) Regional wall motion improvement after coronary thrombolysis with recombinant tissue plasminogenactivator: importance of coronary angioplasty. J Am Coll Cardiol 6:426–433

Travin MI, Bergmann SR (2005) Assessment of myocardial viability. Semin Nucl Med 35:2–16

Udelson JE, Coleman PS, Metherall J et al (1994) Predicting recovery of severe regional ventricular dysfunction. Comparison of resting scintigraphy with 201Tl and 99mTc-sestamibi. Circulation 89:2552–2561

Vanoverschelde JLJ, Wijns W, Depre C et al (1993) Mechanisms of chronic regional postischemic dysfunction in humans. New insights from the study of noninfarcted collateral-dependent myocardium. Circulation 87:1513–1523

Vanoverschelde JL, Depre C, Gerber BL et al (2000) Time course of functional recovery after coronary artery bypass graft surgery in patients with chronic left ventricular ischemic dysfunction. Am J Cardiol 85:1432–1439

Velazquez EJ, Lee KL, Deja MA et al (2011) Coronary-artery bypass surgery in patients with left ventricular dysfunction. N Engl J Med 364:1607–1616

vom Dahl J, Eitzman DT, al-Aouar ZR et al (1994) Relation of regional function, perfusion, and metabolism in patients with advanced coronary artery disease undergoing surgical revascularization. Circulation 90:2356–2366

Watada H, Ito H, Oh H, Masuyama T, Aburaya M, Hori M et al (1994) Dobutamine stress echocardiography predicts reversible dysfunction and quantitates the extent of irreversibly damaged myocardium after reperfusion of anterior myocardial infarction. J Am Coll Cardiol 24:624–630

Wellnhofer E, Olariu A, Klein C et al (2004) Magnetic resonance low-dose dobutamine test is superior to scar quantification for the prediction of functional recovery. Circulation 109:2172–2174

Wilson JM (1999) Reversible congestive heart failure caused by myocardial hibernation. Tex Heart Inst J 26:19–27

Wu KC, Zerhouni EA, Judd RM, Lugo-Olivieri CH, Barouch LA, Schulman SP et al (1998) Prognostic significance of microvascular obstruction by magnetic resonance imaging in patients with acute myocardial infarction. Circulation 97:765–772

Zimmermann R, Mall G, Rauch B et al (1995) Residual 201Tl activity in irreversible defects as a marker of myocardial viability. Clinicopathological study. Circulation 91:1016–1021

CT Approaches for the Assessment of Myocardial Viability

Andreas H. Mahnken

Contents

Abstract

Coronary artery disease is one of the most common causes of death. Treatment of coronary artery disease and its sequelae is costly and may pose an unnecessary risk to the patient if performed needlessly. Imaging of myocardial viability became well established for optimizing indication an resource allocation in patients suffering from myocardial infarction. While myocardial viability imaging is routinely performed using ^{18}Fluorodeoxyglucose-positron emission tomography, single photon emission computed tomography or magnetic resonance imaging, multislice-spiral computed tomography (MSCT) techniques emerged as new tool for visualization of myocardial infarction. This chapter describes different concepts of MSCT viability imaging such as unenhanced CT for assessing calcifications and fatty infiltrations. The focus will be direct visualization of nonviable myocardium by depiction of delayed myocardial contrast enhancement. The clinical relevance of the different MSCT techniques is described. Basic concepts on how to perform late phase MSCT are introduced.

Despite advances in prevention and treatment, coronary artery disease (CAD) remains one of the most common causes of death. In 2012, about 935,000 US Americans are expected to suffer myocardial infarction (MI). In 2009, estimated 1,133,000 percutaneous coronary interventions (PCI) and an additional 416,000 coronary artery bypass graft (CABG) surgeries were performed in the US alone. Mean hospital charges per PCI were US$60,309 and US$124,404 per CABG. With a total expenditure of US$190.3 billion, CAD is the most important driver of direct health expenditure and of major socio-economic relevance (Roger et al. 2012). Even more important are the medical hazards associated with PCI and CABG surgery. With a mean in-hospital death rate of 0.95 % per PCI and 1.75 % per CABG surgery, these procedures introduce unnecessary risk to the patient when performed needlessly.

A. H. Mahnken (✉)
Department of Radiology,
Marburg University Hospital, Philipps University,
Marburg, Germany
e-mail: mahnken@med.uni-marburg.de

U. J. Schoepf et al. (eds.), *CT Imaging of Myocardial Perfusion and Viability*, Medical Radiology. Diagnostic Imaging,
DOI: 10.1007/174_2012_764, © Springer-Verlag Berlin Heidelberg 2012
Published Online: 16 November 2012

Consequently, strategies for optimizing indication and resource allocation are needed.

The idea of viability imaging goes back for more than four decades, when clinical observations in patients with ischemic heart failure showed recovery of ventricular function after CABG surgery (Rees et al. 1971). This condition of potentially reversible, chronic ischemic myocardial dysfunction has been described as hibernating myocardium (Diamond et al. 1978; Rahimtoola 1985). During the following decades, many experimental and clinical investigations showed that spatial extent and degree of ischemic injury could predict the individual patient's outcome and long-term survival (Gersh and Anderson 1993). The transmural extent of MI was identified as a particularly relevant determinant of functional recovery and long-term outcome. In patients with a transmural extent of MI of less than 25 %, left ventricular function usually improves after revascularization. Even with up to 50 % irreversibly damaged myocardium, an improvement of regional function can be achieved by revascularization therapy (Choi et al. 2001), whereas functional improvement is rare in MI with a transmural extent of 75 % or more (Kim et al. 2000). Areas of completely transmural MI will not recover function at all. As therapeutic decisions depend on the quality of diagnostic information, techniques for the direct assessment of myocardial injury were sought. Direct visualization of myocardial viability emerged as the most appealing concept as it permits prediction of the individual patient's prognosis as well as the effect of revascularization therapy. Consequently, assessment of myocardial viability is essential not only for risk assessment but also for treatment planning.

Over the past decades, several cross-sectional imaging techniques were established for assessing myocardial perfusion and viability. Well-established techniques for assessing myocardial viability are low-dose dobutamine stress echocardiography, single photon emission computed tomography (SPECT) with ^{201}thallium, or ^{99m}technetium-labeled tracers, ^{18}F-fluorodeoxyglucose (^{18}FDG) positron emission tomography (PET), and magnetic resonance (MR) imaging. Of these, contrast-enhanced MR imaging has emerged as the clinically accepted gold standard for the evaluation of myocardial viability (Wagner et al. 2003). Its high spatial and temporal resolution permits the detection of small myocardial scars and allows for differentiating of transmural and non-transmural infarction. Moreover, MR imaging provides reliable information on global and regional ventricular function. This is an essential advantage compared with SPECT or ^{18}FDG-PET, which both provide less spatial and temporal resolution.

Multi-detector row computed tomography (MDCT) is a more recent addition to viability imaging. While MDCT is widely being used now for the visualization of the coronary arteries, it also allows for the assessment of left ventricular function (Sarwar et al. 2009), myocardial perfusion (Ho et al. 2010), and myocardial viability (Mahnken et al. 2005). Computed tomography (CT) actually preceded MR imaging for assessing myocardial viability, with different CT approaches to the assessment of MI and viability being developed in the late 1970s (Adams et al. 1976; Higgins et al. 1978). Electron beam computed tomography (EBCT) (Hamada et al. 1992) and, as an anecdotal development, the "dynamic spatial reconstructor" (Scanlan et al. 1980) were successfully tested for imaging MI. For various reasons none of these CT techniques became a routine tool in clinical routine practice. With the introduction of cardiac MR imaging in clinical routine, radiologists and cardiologists lost sight of CT for imaging myocardial viability. It took more than two decades for CT imaging of myocardial viability to reemerge from oblivion. Nowadays robust technique of coronary CT angiography (cCTA) was the driver of cardiac CTs rapid development. Although, it is currently not considered appropriate for imaging of myocardial viability (Taylor et al. 2010), MDCT holds the unique potential to become a comprehensive cost-effective imaging strategy that can assess both myocardial viability and coronary arteries. Moreover, it offers an alternative to MR imaging for the ever increasing patient population with implants, such as cardiac pacemakers or deep brain stimulators.

1 Classification of Ischemic Injury of the Myocardium

Although a classification may appear somewhat artificial and some issues in separating the different stages of myocardial injury are still unresolved, it is important to understand that there are different types of reversibly and permanently damaged myocardium. Simplified, it comes down to four different conditions of ischemic myocardium: viable (reversible injury) and necrotic myocardium (irreversible injury), each with acute or chronic states. These different categories of myocardial injury present with more or less unique image characteristics, which can be accounted for by different pathophysiology. Thus, understanding the etiology of ischemic injury and the response of the myocardium to ischemia is essential for imaging the ischemically injured heart.

1.1 Reversible: Acute (Stunning)

Myocardial stunning covers a variety of pathologic stages where contractile dysfunction of viable myocardium persists though the coronary flow is restored (Bolli and Marban 1999). Contractile dysfunction is caused by single or repeated brief periods of myocardial ischemia followed by restoration of blood flow. Myocardial stunning has been

described in association with exercise-induced ischemia, heart transplantation, acute myocardial ischemia, and peri-infarction dysfunction (Braunwald and Kloner 1982). It is also thought to be the result of reperfusion injury (Braunwald and Kloner 1982). Stunning persists for a variable time, ranging from 1 h to several weeks, but contractile function eventually returns to normal after restoration of myocardial perfusion.

1.2 Reversible: Chronic (Hibernation)

Hibernation refers to chronically dysfunctional but viable myocardium with a reduced blood flow at rest (Shen and Vatner 1995). In reaction to a prolonged perfusion deficit, contractile function is diminished as result of subsequently reduced myocyte metabolism. Hibernation may in fact be the result of repetitive episodes of stunning, which have a cumulative effect, thereby causing prolonged postischemic dysfunction (Shivalkar et al. 1999). Multivessel disease with hemodynamically relevant coronary artery stenoses represents the most common reason for myocardial hibernation. Consequently, successful revascularization therapy is needed to improve myocardial function (Tillisch et al. 1986). In contrast to myocardial stunning, function does not recover spontaneously in hibernating myocardium. Moreover, functional recovery takes much longer (Bax et al. 2001). Hibernation has to be considered as an unstable situation. Hibernating myocardium is not completely adapted to chronic malperfusion and longer periods of dysfunction and more severely reduced myocardial perfusion are thought to cause more extensive damage to the myocardium. As a result, chronically hypoperfused myocardium may lose its potential for functional recovery over time (Schwarz et al. 1998), with an evidence that it will eventually become irreversibly damaged (Kloner et al. 1998). Despite these relevant differences, both stunning and hibernating myocardium are clinically covered by the term "viable myocardium", because both entities require revascularization.

1.3 Irreversible: Acute (Acute MI)

Acute MI is an irreversible myocardial damage where the loss of the cell membrane integrity marks the point of cell necrosis. At that point, the intracellular space becomes accessible for extracellular contrast media. Interstitial edema further increases the distribution volume for contrast material. As a result, wash-in and wash-out of contrast material is markedly delayed when compared with the intravascular space. These changes represent the pathophysiological basis for delayed myocardial contrast enhancement.

In acute MI, cell death does not occur simultaneously in the entire infarction zone. Most of the myocardial thickening and, therefore, the highest local energy demand occurs within the endocardial half of the myocardium (Myers et al. 1986). Consequently, cell death starts in the subendocardial layer of the myocardium and necrosis spreads like a wave front toward the subepicardial myocardium (Reimer et al. 1977). While the lateral boundaries of the infarct zone are defined by the occluded vessel territory, the transmural extent of necrosis is a function of the duration of ischemia. With acute MI starting endocardially, the development of transmural MI may be prevented by early coronary artery revascularization. The myocardium at risk in the mid-myocardial and subepicardial layer might be salvaged (Kim et al. 2000).

If myocardial ischemia persists for more than 2 h, restoration of blood flow in the epicardial coronary arteries does not necessarily result in restoration of microvascular flow. As a consequence, so-called microvascular obstruction ("no-reflow") occurs. This phenomenon may persist for more than 4 weeks while major steps of infarct healing take place. Clinically, it is correlated with an increased cardiac mortality and a reduced long-term prognosis (Wu et al. 1998).

1.4 Irreversible: Chronic (Chronic MI)

In the chronic stage of MI, starting approximately 72 h after acute MI, remodeling of the myocardium can be observed. Remodeling is a condition that results in changes in size, shape, and function of the heart after different types of cardiac injury. It is a maladaptive alteration in ventricular geometry and function and will affect both ischemically injured and uninjured myocardium. Remodeling may occur in several clinical conditions including MI, pressure, or volume overload (e.g., valvular disease), myocarditis, and idiopathic dilated cardiomyopathy. In MI remodeling usually starts only few hours after the event. First, thinning of the necrotic myocardium can be observed; within 6 weeks, the necrotic myocardium is replaced by scar tissue that is markedly thinner than healthy myocardium. The time course of this process is defined by the severity of the underlying disease and the occurrence of secondary events, such as recurrent MI (Cohn et al. 2000).

2 CT Techniques for Imaging of Myocardial Viability

A variety of CT approaches have been developed for assessing the presence or absence of viable myocardium. These include indirect approaches, such as unenhanced CT

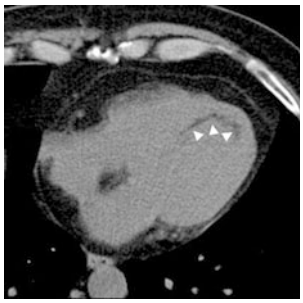

Fig. 1 67-year-old man with a history of MI. The unenhanced CT scan shows fatty metaplasia of the subendocardial myocardium of the septum and left ventricular apex (*arrowheads*). This finding is known to occur in up to 62 % of patients with a history of MI and may be used as an indicator for non-viable myocardium

for assessing fatty infiltrations or calcifications and arterial phase CT measurement of end-diastolic wall thickness, and the more important direct approach of late phase contrast-enhanced CT for depiction of delayed myocardial contrast enhancement.

3 Left Ventricular Myocardial Fatty Metaplasia

Histological evaluations suggest that myocardial fat is common in left ventricular scars with up to 84 % of MI scars containing mature fat (Su et al. 2004); thus, the presence of fatty scars may be used as a rough indicator of previous MI. As the fat is located inside scar tissue, which by definition represents irreversibly damaged myocardium, fatty metaplasia may even serve as a surrogate parameter for viability. On CT, myocardial fat can be detected from unenhanced as well as arterial phase CT images (Fig. 1). It has been reported to be present in 22–62 % of patients with a history of chronic MI (Ahn et al. 2009; Zafar et al. 2008; Ichikawa et al. 2009). In comparison with ^{99m}Tc-sestamibi SPECT, the detection of fatty metaplasia on unenhanced CT images showed an excellent sensitivity of 92 % with a positive predictive value of 77 % for detecting chronic MI (Gupta et al. 2011). However, it also occurs in about 3 % of patients without a history of MI (Ichikawa et al. 2009). In addition, the extent of fatty metaplasia is not related to infarct size.

Unlike fatty deposits in the right ventricle seen in arrhythmogenic right ventricular dysplasia (ARVD), the diagnostic value of fatty metaplasia of left ventricular myocardium has not yet been determined. In relation to viability imaging, however, one has to be aware of this entity as the presence of fat in areas of scarred myocardium may affect interpretation of late phase CT images. Since the attenuation values of fat are quite low, chronic MI may be visualized as a substantially lower attenuation area in comparison with ischemic myocardium as seen on cCTA or CT myocardial perfusion imaging (Nieman et al. 2006). Furthermore, fatty metaplasia of the left ventricular myocardium may indicate the benefit of an additional late phase CT scan in patients referred for coronary calcium scoring or cCTA.

4 End-Diastolic Wall Thickness

Parallel to resting MR imaging, CT measurement of end-diastolic wall thickness is a surrogate parameter of myocardial viability. Myocardial segments with an end-diastolic wall thickness less than 6 mm on CT are likely to represent scar tissue (Fig. 2a; Nieman et al. 2006). In these segments, regional function is unlikely to improve after revascularization. Extreme cases may evolve into ventricular aneurysms, which may also develop myocardial calcifications (Fig. 3).

While there are no studies on the predictive value of end-diastolic wall thickness as measured from cardiac CT for functional recovery after revascularization, it is reasonable to assume that data from resting MR imaging can be transferred for interpreting cardiac CT in this respect. Through MR imaging, it has been shown that a left ventricular wall thickness greater than 5.5 mm in the context of chronic MI predicts viability and subsequent functional recovery with a sensitivity of 92 % and a specificity of 56 % (Baer et al. 1995). In acute MI or subacute MI, before remodeling—wall thinning—is complete, the diagnostic value of end-diastolic wall thickness is limited. In these settings, the effects of edema and cellular infiltrates on wall thickness are thought to contribute to an almost normal wall thickness. Correspondingly, in subacute MI, no difference in end-diastolic wall thickness was seen between viable and non-viable myocardium at 3 weeks after the event (Sandstede et al. 1999).

5 Delayed Myocardial Contrast Enhancement

Unenhanced CT only indirectly indicates the presence of scar tissue, while arterial phase CT visualizes areas of reduced contrast enhancement, which may represent reduced perfusion, microvascular obstruction, myocardial necrosis, or a combination of these entities. To overcome this restriction, CT techniques specific to myocardial viability have been sought.

In the late 1970s, Carlsson et al. and Higgins et al. developed the concept of late phase CT for imaging scar tissue by delayed myocardial contrast enhancement (Higgins et al. 1978; Carlsson et al. 1977). Electron microscopy with energy dispersive X-ray analysis demonstrated a significant increase in the Na^+/K^+ ratio in regions with delayed contrast enhancement on late phase CT (Newell et al. 1982). This observation confirmed delayed contrast enhancement as a surrogate marker for myocardial necrosis as the increased Na^+/K^+ ratio indicates the loss of cellular membrane integrity, which is defined as the point of irreversible

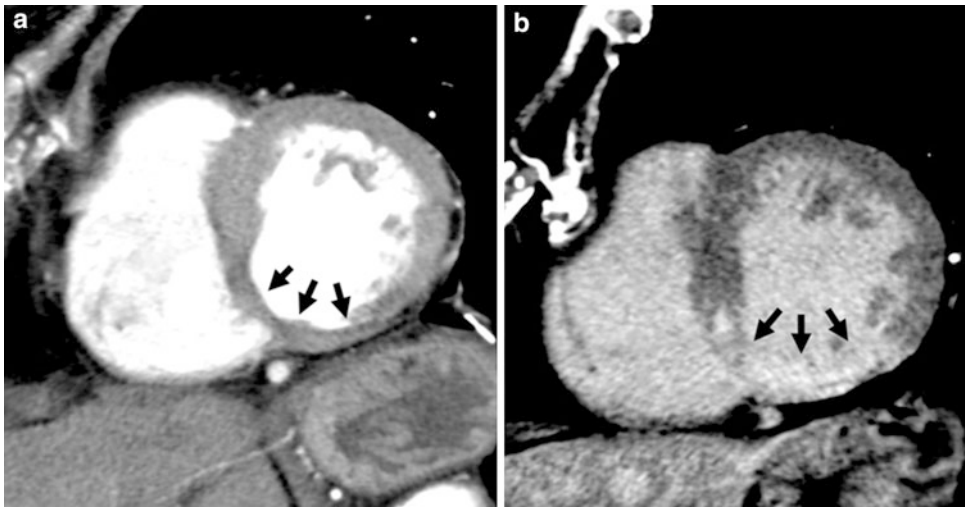

Fig. 2 72-year old female with chronic MI. Arterial phase CT shows wall thinning (<6 mm) of the infero-septal and inferior segments of the left ventricular myocardium (**a**, *arrows*). Corresponding to the distinct wall thinning, transmural delayed myocardial contrast enhancement is present, indicating the absence of viable myocardium (**b**, *arrows*)

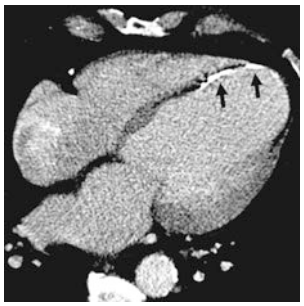

Fig. 3 61-year-old man with a history of chronic MI. The left myocardium underwent severe remodeling and the patient developed an anterior wall aneurysm. In addition, the necrotic myocardium presents some calcifications (*arrows*)

myocyte injury. These initial observations were followed by several studies on the use of delayed contrast-enhanced EBCT for the assessment of MI (Naito et al. 1990; Masuda et al. 1984). However, CT imaging of MI was superseded by MR imaging and became forgotten.

Over the past decade, a variety of animal and patient studies have shown the feasibility of scar imaging using late-phase CT (Fig. 2b; Buecker et al. 2005). These studies demonstrated delayed myocardial contrast enhancement in acute and chronic MI. In acute and subacute MI, delayed myocardial contrast enhancement is due to myocyte membrane dysfunction. Myocyte membrane, if damaged, becomes permeable to contrast material, resulting in a marked increase in distribution volume. In addition, there is a slower wash-in and wash-out infarcted myocardium, further reenforcing delayed myocardial contrast enhancement. In chronic MI, myocytes are replaced by scar tissue with an increased extracellular space between loosely distributed collagen fibers. Despite these different pathophysiological mechanisms, acute and chronic MI both show delayed myocardial contrast enhancement.

In the subendocardial center of MI, myocytes become necrotic due to the obstruction of the microvasculature, also known as "no-reflow phenomenon". This is a multifactorial process including vasoconstriction, distal embolization, and interstitial edema. On late phase CT imaging, this region remains hypoattenuated and is surrounded by a hyperenhanced rim of infarcted myocardium.

Delayed myocardial contrast enhancement is typically assessed from a second CT scan obtained 5–15 min after a routine cCTA (Gerber et al. 2006; Baks et al. 2006). The latter basically represents a first-pass arterial phase providing morphological information on perfusion. Myocardium showing reduced contrast enhancement during arterial phase may represent hypoperfusion due to coronary stenosis or occlusion, MI, microvascular obstruction, lipomatous metaplasia, or any combination thereof. While the use and diagnostic value of arterial phase imaging is discussed elsewhere (see CT imaging of myocardial viability: experimental and clinical evidence), one has to be aware that it has to be interpreted together with late phase images, if available, as different combinations of early hypoenhancement and delayed hyperenhancement have different meanings and vary in prognostic relevance (Koyama et al. 2005).

As contrast kinetics in iodinated- and gadolinium-based extracellular contrast materials are almost identical, CT suffers the same limitations as MR imaging. Thus, delayed myocardial contrast enhancement on CT is not specific for MI. Recent studies demonstrated delayed myocardial contrast enhancement in other pathologies, such as dilated cardiomyopathy, myocarditis, and sarcoidosis (Kaminaga et al. 1994; Smedema et al. 2006; Dambrin et al. 2007).

5.1 How to Do Late Phase CT Imaging

One of the keys for successful late phase CT imaging for the assessment of delayed myocardial contrast enhancement is the contrast injection protocol. Both the total amount of iodine as well as its administration are critical factors.

In order to achieve sufficient contrast enhancement, up to 1 g iodine/kg bodyweight has been administered in animal studies. In a 75 kg patient, this would equal 250 mL of contrast material with 300 mg iodine mL^{-1} (e.g., iopromide 300). In a 105 kg patient, 350 mL of the same contrast material would be needed. For several reasons, including the potential risk of acute kidney injury, less contrast material should be used. From our experience, approximately 0.5–0.6 mg iodine/kg bodyweight is sufficient to achieve adequate delayed myocardial contrast enhancement. This still results in a total volume of approximately 120–175 mL of contrast material. Considering scanner technology at the time of this writing, where coronary CT angiograms can be obtained with as little as 50 ml of contrast material, the acquisition of late phase CT images must be planned prior to contrast injection or different contrast injection strategies are needed to avoid unnecessary exposure of patients to contrast material.

Traditionally, the total amount of contrast material is administered in a single bolus injection after the proper delay time for coronary imaging has been determined by a test-bolus injection or by using the bolus tracking technique. A different approach is to administer a smaller bolus for coronary imaging, followed by low flow injection (0.1–0.3 mL s^{-1}) for several minutes with or without a subsequent wash-out phase (Fig. 4). A wash-out phase will help to improve the contrast between blood pool and hyperenhancing myocardium, as it allows the contrast material to become eliminated from the blood pool. Without a wash-out phase, the relatively high concentration of contrast material in the blood pool may obscure small areas of subendocardial hyperenhancement. The use of a multiphasic injection protocol also permits for more sophisticated approaches toward viability imaging by means of CT as it allows for reacting on the findings from the arterial phase scan. Thus, in patients scheduled for cCTA, it would be feasible to add a late phase CT in the presence of segments presenting with hypoattenuation and/or reduced wall thickness. With a single bolus technique, these patients would need a second appointment for a dedicated work-up of pathologic CT findings in the myocardium.

There are also some technical considerations regarding the late phase scan itself. While typical delays range from 5 to 15 min after contrast injection, there are some animal-research data indicating that approximately 6 min appears to be the optimal delay after a single bolus injection of a monomeric contrast agent (Mahnken et al. 2009). Dual phase injection techniques provide the best image quality about 5–10 min after start of contrast injection, with image quality depreciating at 15 min (Brodoefel et al. 2007). Given that iodine attenuation improves at lower tube voltage, the use of 80 or 100 kV scan protocols—depending on the

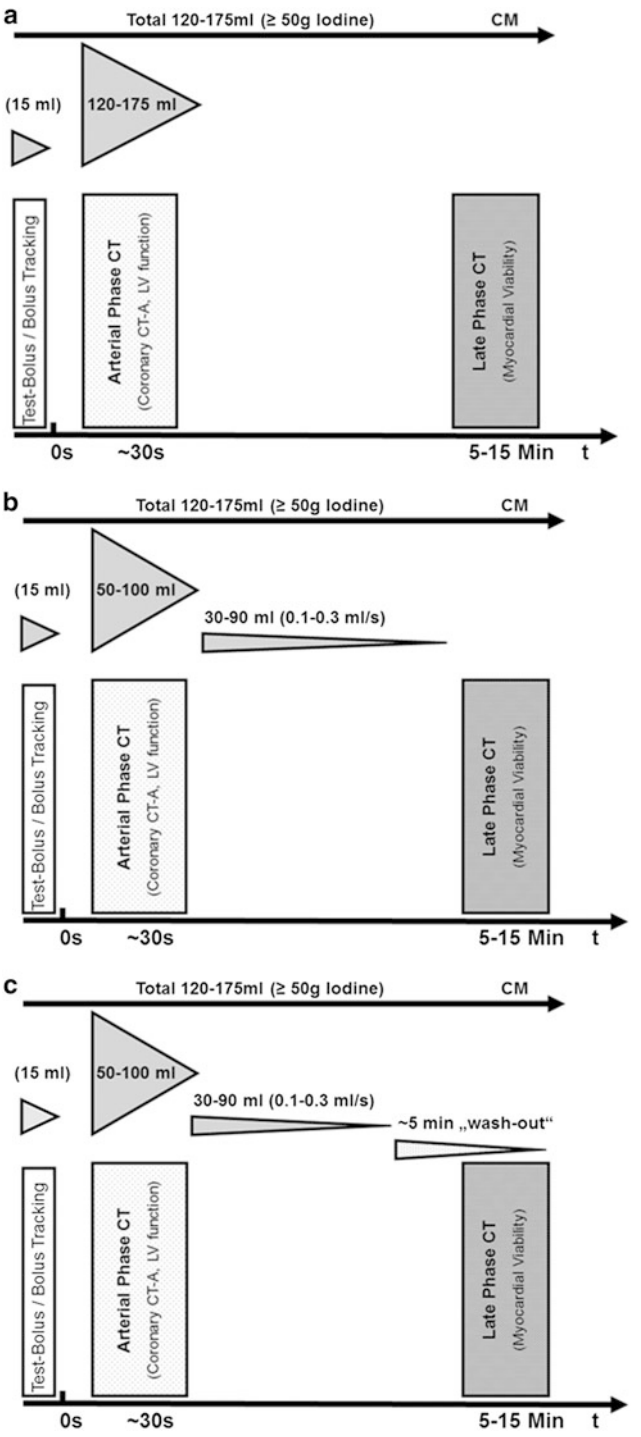

Fig. 4 Different contrast injection protocols are discussed for coronary CT angiography with subsequent late phase imaging for assessing myocardial viability. Traditionally, the total amount of contrast material is injected in a single bolus injection and late phase images are obtained at 5–15 min after contrast injection (**a**). A different approach is to administer a smaller contrast bolus for coronary imaging, followed by slow flow injection (0.1–0.3 mL s^{-1}) for several minutes (**b**). Adding an additional wash-out phase improves contrast between blood pool and areas of delayed myocardial contrast enhancement (**c**)

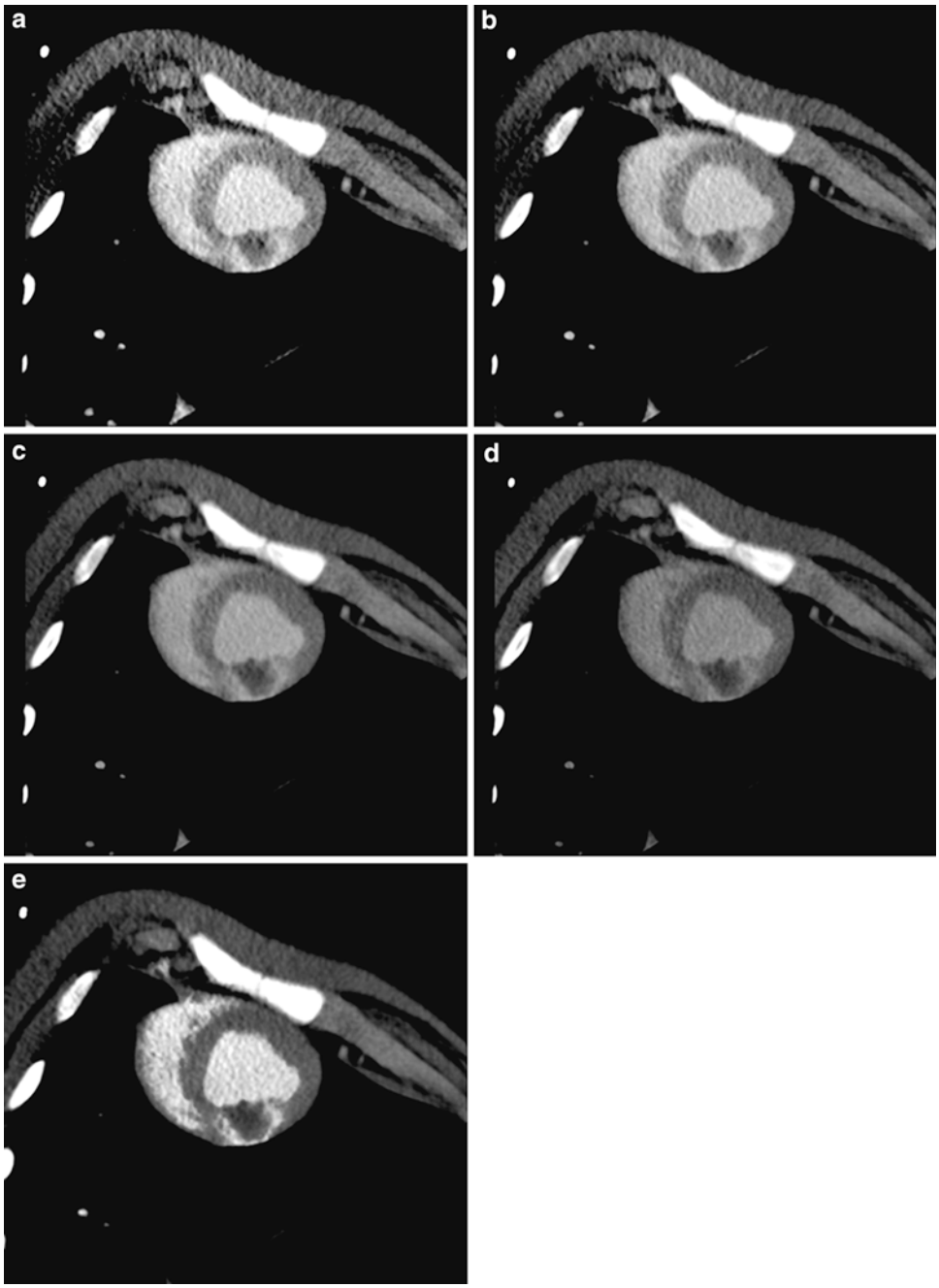

Fig. 5 Visualization of delayed myocardial contrast is strongly influenced by tube voltage with iodine attenuation improving at lower tube voltage. In this example of experimental myocardial infarction in pigs, the best contrast at single energy CT is seen at 80 kV (**a**) and 100 kV (**b**). Contrast-to-noise ratio decreases with 120 kV (**c**) and is poor at 140 kV (**d**). Contrast-to-noise ratio can be markedly improved using dual energy CT with nonlinear image blending (**e**). All images are shown with identical window settings (W250HU/C150HU). Of note, there is a large residual perfusion defect inside the area of myocardial hyperenhancement indicating microvascular obstruction

patient's body weight—is recommended; however, the tube current-time product should be increased accordingly to avoid photon starvation. In fact, 80 kV scans were shown to provide the best contrast-to-noise ratios with single energy CT (Fig. 5; Mahnken et al. 2007). Lowering tube voltage, even with adaptation of the tube current-time product, helps to reduce the radiation dose of the additional viability scan. A different approach is the use of dual energy CT for assessing delayed myocardial contrast enhancement. However, the potential of improved contrast visualization comes at the price of a higher radiation exposure when compared with single energy CT. Finally, prospective ECG-triggering should be used for all late phase CT scans in order to minimize radiation exposure (Wang et al. 2011). As motion artifacts affect the assessment of the myocardium markedly less than the coronaries, the use of prospective ECG-triggering appears to be justified even at higher heart rates.

As late phase CT images typically come with a relatively poor contrast-to-noise ratio of the hyperenhancing myocardium, the proper post-processing will help to improve visualization of the delayed contrast enhancing myocardium. For reducing image noise, thick multiplanar reformats (5–10 mm

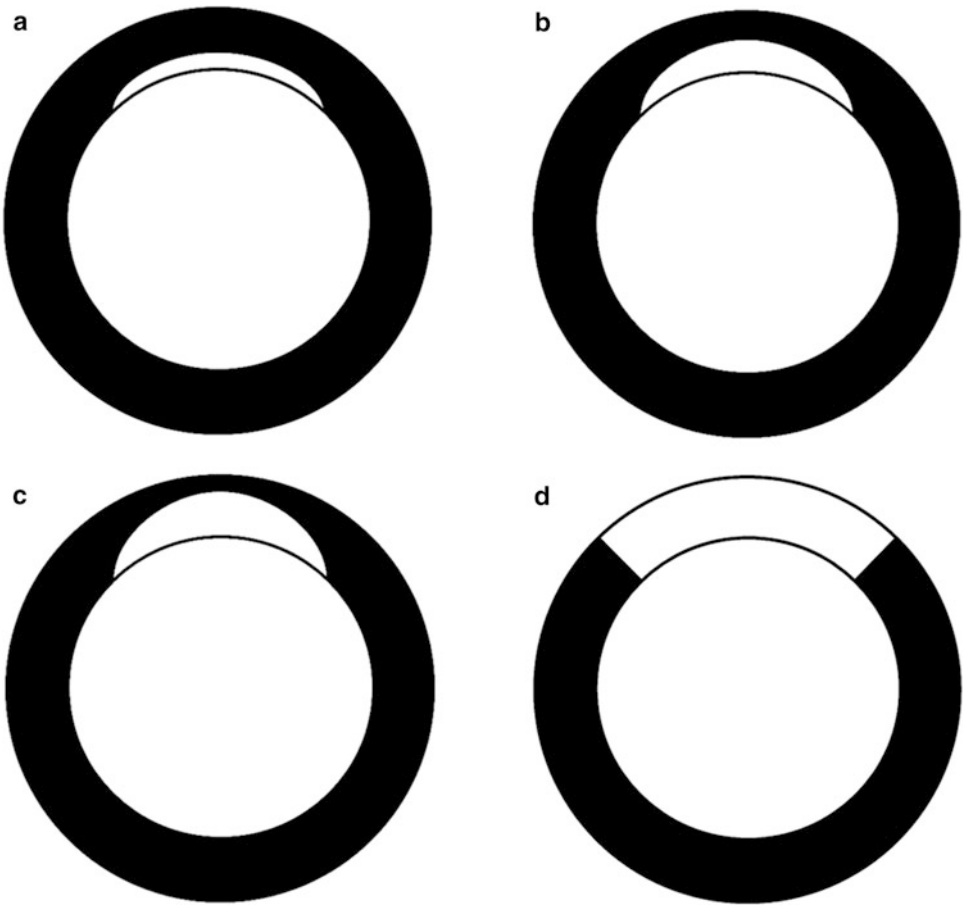

Fig. 6 Dysfunctional but viable myocardium may recover function after revascularization therapy. Recovery of global and regional function depends on the transmural extent of MI. In subendocardial MI with less than 25 % of the left ventricular wall thickness being necrotic, global improvement of left ventricular function can be expected (**a**). If delayed myocardial contrast enhancement comprises up to 50 % of the transmural extent, regional function is likely to improve (**b**). Segments with more than 75 % delayed myocardial contrast enhancement rarely show functional improvement (**c**). In segments with transmural hyperenhancement there will be no functional recovery after revascularization (**d**)

section thickness) should be reconstructed along the short and long axes of the left ventricle using a smooth convolution kernel. For image reading, the use of narrow window settings following the so-called 'half-contour principle' is recommended (Thompson and Stanford 1994), where the window center roughly equals the HU values in the area of infarction with a window width of twice the value of the window center. In case dual energy CT is used, a nonlinear mixing technique appears to favorably improve visualization of infarcted myocardium (Fig. 5).

5.2 Assessment of Late Phase CT Images

Late phase CT data are best assessed using reformats along the standard short and long axes of the left ventricle (Cerqueira et al. 2002). The presence and transmurality of delayed myocardial contrast enhancement is assessed from these data. For clinical purposes, it appears to be sufficient to semi-quantitatively (e.g., ≤25 %, ≤50 %, ≥75 %) assess the transmural extent of delayed myocardial contrast enhancement (Fig. 6). From personal experience, the transmural extent appears to be somewhat overestimated by CT, in comparison with MR imaging. Technique and relevance for exact quantification of MI size is discussed in chapter (see "CT Assessment of Myocardial Viability-Quantitative Imaging"). For a quick clinical workup, the presence of residual perfusion defects in the infarct core need to be noted. Like the transmural extent of delayed myocardial contrast enhancement, these residual perfusion defects correlate with functional recovery. In fact, they were shown to be the strongest predictor of persistent myocardial dysfunction (Kim et al. 2012). However, it needs to be stressed that arterial phase (early perfusion defects) and late phase CT (residual perfusion defects and delayed myocardial contrast enhancement) need to be assessed side by side, as different enhancement patterns have different prognostic implications (Fig. 7; Koyama et al. 2005; Ko et al. 2007). Moreover, arterial phase imaging provides information on the coronary arteries and areas of delayed myocardial contrast enhancement can be correlated to coronary pathology using dedicated software for image fusion (Mahnken et al. 2010).

The presence of transmural perfusion defects on arterial phase CT was shown to be a better predictor of persistent myocardial dysfunction than transmural delayed myocardial contrast enhancement (Kim et al. 2012). These findings are in accordance with Lessick et al., who reported that persistent myocardial dysfunction is clearly related to the

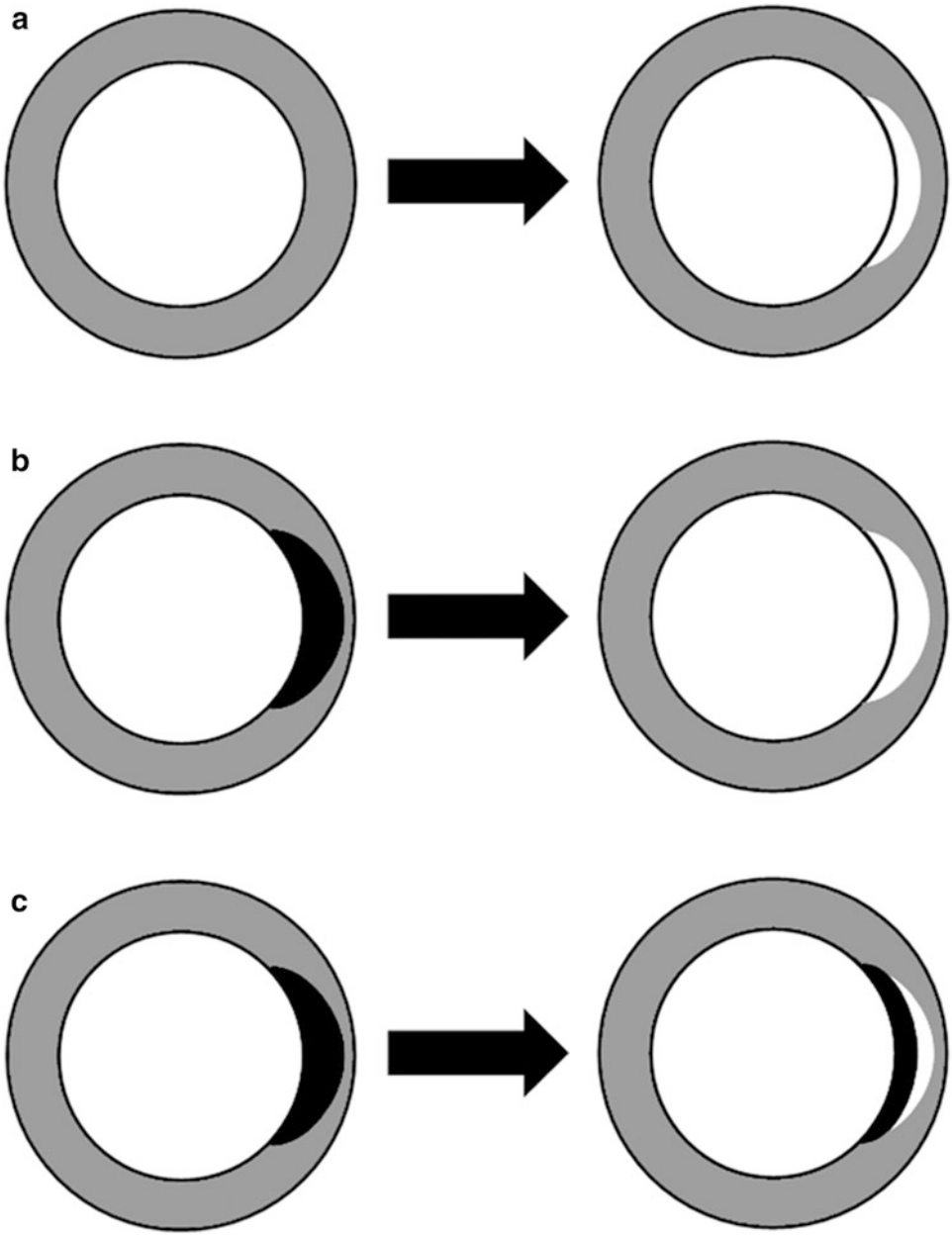

Fig. 7 Arterial (*left*) and late phase CT imaging (*right*) need to be assessed together, as ischemic injury presents with different contrast enhancement patterns. These patterns are related to functional recovery after myocardial infarction. Global left ventricular function and wall thickening is likely to improve if no early perfusion deficit, but delayed contrast enhancement (*white* region) is seen (**a**). Prognosis decreases if hypoattenuating areas (*black* regions) are seen during arterial phase with corresponding areas of delayed enhancement on late phase CT images (**b**). In patients with early and late phase perfusion deficits, corresponding to microvascular obstruction, poorest results are to be expected (**c**)

presence of both early perfusion defects and delayed myocardial contrast enhancement (Lessick et al. 2007). In an early study assessing the impact of different contrast patterns on functional recovery, Koyama et al. reported that global left ventricular function and wall thickness on follow-up examination in MI patients was best in a group with delayed myocardial contrast enhancement, but without early or residual perfusion defects (Koyama et al. 2005). In contrast, results were poorest in groups with early and residual perfusion defects and delayed myocardial contrast enhancement. Considering these findings, one may assume that normal arterial phase CT is a more promising predictor of a good prognosis, whereas pathologic late phase CT is a more powerful predictor of poor prognosis.

When interpreting the results of the different CT techniques for imaging of myocardial viability one has to be aware that there are distinct differences in the sensitivity and specificity for the prediction of functional recovery as well as for the estimated extent of the ischemic injury. The same is true when comparing different imaging techniques such as SPECT or dobutamine stress MR imaging with CT. These differences, however, do not indicate one method is better than another one, but simply indicate that each of these imaging techniques detects different aspects of viable

myocardium, e.g., SPECT assesses regions with a reduced number of viable cells, while delayed contrast enhancement in late phase CT or MR imaging refers to an increased extracellular space.

5.3 Late Phase CT After PCI

A completely different approach toward CT imaging of delayed myocardial contrast enhancement is its use after coronary angiography and PCI in MI. In this setting, the intra-arterially applied contrast material from coronary angiography is utilized for late phase contrast-enhanced CT without re-injection being needed. As a logistical challenge, CT imaging needs to be performed reasonably quickly—usually within 30 min—after the end of the angiographic procedure. Otherwise wash-out of the contrast material may limit image quality and subsequently the diagnostic value.

This idea has first been applied in 2006 using ungated chest CT with 5 mm sections obtained at the level of the mid-ventricle. At that time, the authors did not focus on the prognostic value of delayed myocardial contrast enhancement but did establish a correlation between delayed myocardial contrast enhancement and myocardial blood flow in the ischemically injured region as measured in the target vessel with a Doppler-tipped flow wire (Kato et al. 2006).

The concept was soon adopted for assessing myocardial viability in acute MI. Applying this technique, Habis et al. showed 97 % accuracy with 99 % positive and 79 % negative predictive values for detecting viable myocardial segments (Habis et al. 2007). Subsequent studies confirmed the validity of this approach, with transmural delayed contrast enhancement being associated with higher defect scores on ^{201}Thallium SPECT and markedly poorer recovery of global left ventricular function (Sato et al. 2008). This technique was also proven reliable in comparison with delayed contrast enhanced MR imaging (Habis et al. 2009). While post PCI CT can reliably distinguish transmural from subendocardial MI, its sensitivity is somewhat worse than MR imaging for limited acute MI. The latter they usually has a good prognosis and this drawback may not be of clinical relevance (Habis et al. 2009). Therefore, this approach provides an attractive option for assessing the individual patient's prognosis immediately after PCI for acute MI (Sato et al. 2012). Although, sufficient data has yet to be collected as of this writing, this approach may prove helpful for very early risk stratification in patients with reperfused acute MI.

The combination of myocardial viability imaging and non-invasive cCTA with analysis of end-diastolic wall thickness offers a comprehensive examination strategy for evaluation of patients with known or suspected ischemic heart disease.

References

Adams DF, Hessel SJ, Judy PF, Stein JA, Abrams HL (1976) Computed tomography of the normal and infarcted myocardium. AJR Am J Roentgenol 126:786–791

Ahn SS, Kim YJ, Hur J, Lee HJ, Kim TH, Choe KO, Choi BW (2009) CT detection of subendocardial fat in myocardial infarction. AJR Am J Roentgenol 192:532–537

Baer FM, Voth E, Schneider CA, Theissen P, Schicha H, Sechtem U (1995) Comparison of low-dose dobutamine-gradient-echo magnetic resonance imaging and positron emission tomography with 18F-fluorodeoxyglucose in patients with chronic coronary artery disease. A functional and morphological approach to the detection of residual myodardial viability. Circulation 91:1006–1015

Baks T, Cademartiri F, Moelker AD, Weustink AC, van Geuns RJ, Mollet NR, Krestin GP, Duncker DJ, de Feyter PJ (2006) Multislice computed tomography and magnetic resonance imaging for the assessment of reperfused acute myocardial infarction. J Am Coll Cardiol 48:144–152

Bax JJ, Visser FC, Poldermans D, Elhendy A, Cornel JH, Boersma E, van Lingen A, Fioretti PM, Visser CA (2001) Time course of functional recovery of stunned and hibernating segments after surgical revascularization. Circulation 104(12 Suppl 1):I314–I318

Bolli R, Marban E (1999) Molecular and cellular mechanisms of myocardial stunning. Physiol Rev 79:609–634

Braunwald E, Kloner RA (1982) The stunned myocardium: prolonged, postischemic ventricular dysfunction. Circulation 66:1146–1149

Brodoefel H, Reimann A, Klumpp B, Fenchel M, Ohmer M, Miller S, Schroeder S, Claussen C, Scheule A, Kopp AF (2007) Assessment of myocardial viability in a reperfused porcine model: evaluation of different MSCT contrast protocols in acute and subacute infarct stages in comparison with MRI. J Comput Assist Tomogr 31:290–298

Buecker A, Katoh M, Krombach GA, Spuentrup E, Bruners P, Gunther RW, Niendorf T, Mahnken AH (2005) A feasibility study of contrast enhancement of acute myocardial infarction in multislice computed tomography: comparison with magnetic resonance imaging and gross morphology in pigs. Invest Radiol 40:700–704

Carlsson E, Lipton MJ, Berninger WH, Doherty P, Redington RW (1977) Selective left coronary myocardiography by computed tomography in living dogs. Invest Radiol 12:559–562

Cerqueira MD, Weissman NJ, Dilsizian V, Jacobs AK, Kaul S, Laskey WK, Pennell DJ, Rumberger JA, Ryan T (2002) American Heart Association writing group on myocardial segmentation and registration for cardiac imaging. Standardized myocardial segmentation and nomenclature for tomographic imaging of the heart: a statement for healthcare professionals from the cardiac imaging committee of the council on clinical cardiology of the American Heart Association. Circulation 105:539–542

Choi KM, Kim RJ, Gubernikoff G, Vargas JD, Parker M, Judd RM (2001) Transmural extent of acute myocardial infarction predicts long-term improvement in contractile function. Circulation 104:1101–1107

Cohn JN, Ferrari R, Sharpe N (2000) Cardiac remodeling-concepts and clinical implications: a consensus paper from an international forum on cardiac remodeling. Behalf of an international forum on cardiac remodeling. J Am Coll Cardiol 35:569–582

Dambrin G, Laissy JP, Serfaty JM, Caussin C, Lancelin B, Paul JF (2007) Diagnostic value of ECG-gated multidetector computed tomography in the early phase of suspected acute myocarditis. A

preliminary comparative study with cardiac MRI. Eur Radiol 17:331–338

Diamond GA, Forrester JS, deLuz PL, Wyatt HL, Swan HJ (1978) Post-extrasystolic potentiation of ischemic myocardium by atrial stimulation. Am Heart J 95:204–209

Gerber BL, Belge B, Legros GJ, Lim P, Poncelet A, Pasquet A, Gisellu G, Coche E, Vanoverschelde JLJ (2006) Characterization of acute and chronic myocardial infarcts by multidetector computed tomography: comparison with contrast-enhanced magnetic resonance. Circulation 113:823–833

Gersh BJ, Anderson JL (1993) Thrombolysis and myocardial salvage. Results of clinical trials and the animal paradigm-paradoxic or predictable? Circulation 88:296–306

Gupta M, Kadakia J, Hacioglu Y, Ahmadi N, Patel A, Choi T, Yamada G, Budoff M (2011) Non-contrast cardiac computed tomography can accurately detect chronic myocardial infarction: validation study. J Nucl Cardiol 18:96–103

Habis M, Capderou A, Ghostine S, Daoud B, Caussin C, Riou JY, Brenot P, Angel CY, Lancelin B, Paul JF (2007) Acute myocardial infarction early viability assessment by 64-slice computed tomography immediately after coronary angiography: comparison with low-dose dobutamine echocardiography. J Am Coll Cardiol 49:1178–1185

Habis M, Capderou A, Sigal-Cinqualbre A, Ghostine S, Rahal S, Riou JY, Brenot P, Angel CY, Paul JF (2009) Comparison of delayed enhancement patterns on multislice computed tomography immediately after coronary angiography and cardiac magnetic resonance imaging in acute myocardial infarction. Heart 95:624–629

Hamada S, Naito H, Takamiya M (1992) Evaluation of myocardium in ischemic heart disease by ultrafast computed tomography. Jpn Circ J 56:627–631

Higgins CB, Sovak M, Schmidt W, Siemers PT (1978) Uptake of contrast materials by experimental acute myocardial infarctions: a preliminary report. Invest Radiol 13:337–339

Ho KT, Chua KC, Klotz E, Panknin C (2010) Stress and rest dynamic myocardial perfusion imaging by evaluation of complete time-attenuation curves with dual-source CT. JACC Cardiovasc Imaging 3:811–820

Ichikawa Y, Kitagawa K, Chino S, Ishida M, Matsuoka K, Tanigawa T, Nakamura T, Hirano T, Takeda K, Sakuma H (2009) Adipose tissue detected by multislice computed tomography in patients after myocardial infarction. JACC Cardiovasc Imaging 2:548–555

Kaminaga T, Naito H, Takamiya M, Hamada S, Nishimura T (1994) Myocardial damage in patients with dilated cardiomyopathy: CT evaluation. J Comput Assist Tomogr 18:393–397

Kato M, Dote K, Sasaki S, Ueda K, Goto K, Takemoto H, Habara S, Hasegawa D, Matsuda O, Nakano Y, Naganuma T (2006) Plain computed tomography for assessment of early coronary microcirculatory damage after revascularization therapy in acute myocardial infarction. Circ J 70:1475–1480

Kim RJ, Wu E, Rafael A, Chen EL, Parker MA, Simonetti O, Klocke FJ, Bonow RO, Judd RM (2000) The use of contrast-enhanced magnetic resonance imaging to identify reversible myocardial dysfunction. N Engl J Med 343:1445–1453

Kim T, Choi BJ, Kang DK, Sun JS (2012) Assessment of myocardial viability using multidetector computed tomography in patients with reperfused acute myocardial infarction. Clin Radiol 67:754–765

Kloner RA, Bolli R, Marban E, Reinlib L, Braunwald E (1998) Medical and cellular implications of stunning, hibernation, and preconditioning: an NHLBI workshop. Circulation 97:1848–1867

Ko SM, Kim YW, Han SW, Seo JB (2007) Early and delayed myocardial enhancement in myocardial infarction using two-phase contrast-enhanced multidetector-row CT. Korean J Radiol 8:94–102

Koyama Y, Matsuoka H, Mochizuki T, Higashino H, Kawakami H, Nakata S, Aono J, Ito T, Naka M, Ohashi Y, Higaki J (2005) Assessment of reperfused acute myocardial infarction with two-phase contrast-enhanced helical CT: prediction of left ventricular function and wall thickness. Radiology 235:804–811

Lessick J, Dragu R, Mutlak D, Rispler S, Beyar R, Litmanovich D, Engel A, Agmon Y, Kapeliovich M, Hammerman H, Ghersin E (2007) Is functional improvement after myocardial infarction predicted with myocardial enhancement patterns at multidetector CT? Radiology 244:736–744

Mahnken AH, Koos R, Katoh M, Wildberger JE, Spuentrup E, Buecker A, Günther RW, Kühl HP (2005) Assessment of myocardial viability in reperfused acute myocardial infarction using 16-slice computed tomography in comparison to magnetic resonance imaging. J Am Coll Cardiol 45:2042–2047

Mahnken AH, Bruners P, Mühlenbruch G, Emmerich M, Hohl C, Günther RW, Wildberger JE (2007) Low tube voltage improves computed tomography imaging of delayed myocardial contrast enhancement in an experimental acute myocardial infarction model. Invest Radiol 42:123–129

Mahnken AH, Jost G, Bruners P, Sieber M, Seidensticker PR, Günther RW, Pietsch H (2009) Multidetector computed tomography (MDCT) evaluation of myocardial viability: intraindividual comparison of monomeric vs. dimeric contrast media in a rabbit model. Eur Radiol 19:290–297

Mahnken AH, Bruners P, Friman O, Hennemuth A (2010) The culprit lesion and its consequences: combined visualization of the coronary arteries and delayed myocardial enhancement in dual-source CT: a pilot study. Eur Radiol 20:2834–2843

Masuda Y, Yoshida H, Morooka N, Watanabe S, Inagaki Y (1984) The usefulness of X-ray computed tomography for the diagnosis of myocardial infarction. Circulation 70:217–225

Myers JH, Stirling MC, Choy M, Buda AJ, Gallagher KP (1986) Direct measurement of inner and outer wall thickening dynamics with epicardial echocardiography. Circulation 74:164–172

Naito H, Saito H, Ohta M, Takamiya M (1990) Significance of ultrafast computed tomography in cardiac imaging: usefulness in assessment of myocardial characteristics and cardiac function. Jpn Circ J 54:322–327

Newell JD, Higgins CB, Abraham JL (1982) Uptake of iodinated contrast material by the ischemically damaged myocardial cell. Invest Radiol 17:61–65

Nieman K, Cury RC, Ferencik M, Nomura CH, Abbara S, Hoffmann U, Gold HK, Jang IK, Brady TJ (2006) Differentiation of recent and chronic myocardial infarction by cardiac computed tomography. Am J Cardiol 98:303–308

Rahimtoola SH (1985) A perspective on the three large multicenter randomized clinical trials of coronary bypass surgery for chronic stable angina. Circulation 72:V123–V135

Rees G, Bristow JD, Kremkau EL, Green GS, Herr RH, Griswold HE, Starr A (1971) Influence of aortocoronary bypass surgery on left ventricular performance. N Engl J Med 284:1116–1120

Reimer KA, Lowe JE, Rasmussen MM, Jennings RB (1977) The wavefront phenomenon of ischemic cell death. 1. Myocardial infarct size vs duration of coronary occlusion in dogs. Circulation 56:786–794

Roger VL, Go AS, Lloyd-Jones DM, Benjamin EJ, Berry JD, Borden WB, Bravata DM, Dai S, Ford ES, Fox CS, Fullerton HJ, Gillespie C, Hailpern SM, Heit JA, Howard VJ, Kissela BM, Kittner SJ, Lackland DT, Lichtman JH, Lisabeth LD, Makuc DM, Marcus GM, Marelli A, Matchar DB, Moy CS, Mozaffarian D, Mussolino ME, Nichol G, Paynter NP, Soliman EZ, Sorlie PD, Sotoodehnia N, Turan TN, Virani SS, Wong ND, Woo D (2012) American Heart Association Statistics Committee and Stroke Statistics Subcommittee. Heart disease and stroke statistics—2012 update: a report from the American Heart Association. Circulation 125:e2–e220

Sandstede J, Bertsch G, Beer M, Kenn W, Werner E, Pabst T, Lipke C, Kretschmer S, Neubauer S, Hahn D (1999) Detection of myocardial viability by low-dose dobutamine cine MR imaging. Magn Reson Imaging 17:1437–1443

Sarwar A, Shapiro MD, Nasir K, Nieman K, Nomura CH, Brady TJ, Cury RC (2009) Evaluating global and regional left ventricular function in patients with reperfused acute myocardial infarction by 64-slice multidetector CT: a comparison to magnetic resonance imaging. J Cardiovasc Comput Tomogr 3:170–177

Sato A, Hiroe M, Nozato T, Hikita H, Ito Y, Ohigashi H, Tamura M, Takahashi A, Isobe M, Aonuma K (2008) Early validation study of 64-slice multidetector computed tomography for the assessment of myocardial viability and the prediction of left ventricular remodeling after acute myocardial infarction. Eur Heart J 29:490–498

Sato A, Nozato T, Hikita H, Akiyama D, Nishina H, Hoshi T, Aihara H, Kakefuda Y, Watabe H, Hiroe M, Aonuma K (2012) Prognostic value of myocardial contrast delayed enhancement with 64-slice multidetector computed tomography after acute myocardial infarction. J Am Coll Cardiol 59:730–738

Scanlan JG, Gustafson DE, Chevalier PA, Robb RA, Ritman EL (1980) Evaluation of ischemic heart disease with a prototype volume imaging computed tomographic (CT) scanner: preliminary experiments. Am J Cardiol 46:1263–1268

Schwarz ER, Schoendube FA, Kostin S, Schmiedtke N, Schulz G, Buell U, Messmer BJ, Morrison J, Hanrath P, vom Dahl J (1998) Prolonged myocardial hibernation exacerbates cardiomyocyte degeneration and impairs recovery of function after revascularization. J Am Coll Cardiol 31:1018–1026

Shen YT, Vatner SF (1995) Mechanism of impaired myocardial function during progressive coronary stenosis in conscious pigs. Hibernation versus stunning? Circ Res 76:479–488

Shivalkar B, Flameng W, Szilard M, Pislaru S, Borgers M, Vanhaecke J (1999) Repeated stunning precedes myocardial hibernation in progressive multiple coronary artery obstruction. J Am Coll Cardiol 34:2126–2136

Smedema JP, Truter R, de Klerk PA, Zaaiman L, White L, Doubell AF (2006) Cardiac sarcoidosis evaluated with gadolinium-enhanced magnetic resonance and contrast-enhanced 64-slice computed tomography. Int J Cardiol 112:261–263

Su L, Siegel JE, Fishbein MC (2004) Adipose tissue in myocardial infarction. Cardiovasc Pathol 13:98–102

Taylor AJ, Cerqueira M, Hodgson JM, Mark D, Min J, O'Gara P (2010) American College of Cardiology Foundation Appropriate Use Criteria Task Force; Society of Cardiovascular Computed Tomography; American College of Radiology; American Heart Association; American Society of Echocardiography; American Society of Nuclear Cardiology; North American Society for Cardiovascular Imaging; Society for Cardiovascular Angiography and Interventions; Society for Cardiovascular Magnetic Resonance. ACCF/SCCT/ACR/AHA/ASE/ASNC/NASCI/SCAI/SCMR 2010 Appropriate Use Criteria for Cardiac Computed Tomography. A Report of the American College of Cardiology Foundation Appropriate Use Criteria Task Force, the Society of Cardiovascular Computed Tomography, the American College of Radiology, the American Heart Association, the American Society of Echocardiography, the American Society of Nuclear Cardiology, the North American Society for Cardiovascular Imaging, the Society for Cardiovascular Angiography and Interventions, and the Society for Cardiovascular Magnetic Resonance. Circulation 122:e525–e555

Thompson BH, Stanford W (1994) Evaluation of cardiac function with ultrafast computed tomography. Radiol Clin North Am 32:537–551

Tillisch J, Brunken R, Marshall R, Schwaiger M, Mandelkern M, Phelps M, Schelbert H (1986) Reversibility of cardiac wall motion abnormalities predicted by positron emission tomography. N Engl J Med 314:884–888

Wagner A, Mahrholdt H, Holly TA, Elliott MD, Regenfus M, Parker M, Klocke FJ, Bonow RO, Kim RJ, Judd RM (2003) Contrast-enhanced MRI and routine single photon emission computed tomography (SPECT) perfusion imaging for detection of subendocardial myocardial infarcts: an imaging study. Lancet 361:374–379

Wang R, Zhang Z, Xu L, Ma Q, He Y, Lu D, Yu W, Fan Z (2011) Low dose prospective ECG-gated delayed enhanced dual-source computed tomography in reperfused acute myocardial infarction comparison with cardiac magnetic resonance. Eur J Radiol 80:326–330

Wu KC, Zerhouni EA, Judd RM, Lugo-Olivieri CH, Barouch LA, Schulman SP, Blumenthal RS, Lima JA (1998) Prognostic significance of microvascular obstruction by magnetic resonance imaging in patients with acute myocardial infarction. Circulation 97:765–772

Zafar HM, Litt HI, Torigian DA (2008) CT imaging features and frequency of left ventricular myocardial fat in patients with CT findings of chronic left ventricular myocardial infarction. Clin Radiol 63:256–262

CT Imaging of Myocardial Viability: Experimental and Clinical Evidence

J. Matthias Kerl

Contents

Abstract

The visualization of myocardial viability is one of the most relevant applications of cardiovascular imaging. There are several novel techniques to assess myocardial viability using CT. This chapter will give an overview of these techniques and detail the supporting experimental and clinical evidence.

Coronary artery disease and myocardial infarction (MI) are among the most common causes of morbidity and mortality in Western societies (Mokdad et al. 2004). Currently, contrast-enhanced multidetector computed tomography (MDCT) is a promising method for efficient and noninvasive detection of coronary artery stenosis (Becker et al. 2002; Hoffmann et al. 2005). Major advances in MDCT technology are making way for a versatile cardiovascular imaging technique that could provide information on anatomy, function, tissue perfusion, and viability. The visualization of myocardial viability is one of the most relevant applications of cardiovascular imaging. It has been shown that the differentiation between viable and nonviable myocardium is crucial in the decision for further therapy in patients with acute coronary syndrome. Akinetic but still viable (hibernating) myocardial segments significantly benefit from interventional myocardial revascularization. Comparatively, revascularization does not improve the function of akinetic, nonviable myocardial segments and exposes the patient to unnecessary procedural risks (Beek et al. 2003; Kim et al. 1999). The presence and extent of MI are important predictors of functional recovery of myocardial contractility after surgical or interventional revascularization (Selvanayagam et al. 2004). Choi et al. reported that in patients presenting with a first MI involving less than 25 % of wall thickness, successful reperfusion led to improved global left ventricular function in 67 % of cases. On the other hand, when myocardial necrosis involved more than 75 % of wall thickness, functional recovery was

J. Matthias Kerl (✉)
Department of Diagnostic and Interventional Radiology,
Goethe-University Frankfurt am Main,
Frankfurt am Main, Germany
e-mail: matthias.kerl@gmail.com

U. J. Schoepf et al. (eds.), *CT Imaging of Myocardial Perfusion and Viability*, Medical Radiology. Diagnostic Imaging,
DOI: 10.1007/174_2012_771, © Springer-Verlag Berlin Heidelberg 2012
Published Online: 19 December 2012

unlikely (Choi et al. 2001). Similar findings were published by Kim et al. for patients with chronic, stable coronary artery disease and reduced left ventricular function after bypass surgery (Kim et al. 2000). Consequently, rapid time to reperfusion post-acute MI is vital to ensure maximal myocardial tissue salvage.

Current modalities used to identify hibernating myocardium include PET, SPECT, MRI, myocardial contrast echography, intracoronary ultrasound, and dobutamine stress testing (Brunken et al. 1986; Burt et al. 1995; Mahrholdt et al. 2002; McFalls et al. 2003; Sicari et al. 1997; Takeuchi et al. 2003). Over the last decade, the mainstay for differentiating viable from nonviable myocardium and acute from chronic MI has been late enhancement magnetic resonance imaging (LE-MRI) (Abdel-Aty et al. 2004).

With advancing technology, MDCT has been shown to be a promising alternative imaging technique for assessing myocardial viability and evaluating the transmural extent of myocardial necrosis after MI. This has important implications as CT is more widely available than MRI and could be performed in patients with contraindications to MRI, such as metallic implants and implantable cardioverter-defibrillators.

There are several novel techniques to assess myocardial viability using CT. This chapter will give an overview of these techniques and detail the supporting experimental and clinical evidence.

1 First-Pass Arterial Phase Imaging

In several animal studies, contrast-enhanced arterial phase CT imaging has been shown to be helpful for the detection of MI (Baks et al. 2006; Buecker et al. 2005; Mahnken et al. 2005; Writing Group et al. 2010). Studies concentrating on arterial phase imaging report a deficit of contrast in the area of MI, resulting in hypoenhancement of the corresponding myocardium (Fig. 1). This is a result of reduced contrast distribution due to impaired blood flow in the area of MI. Hoffmann et al. reported that MDCT permits the detection and further characterization of acute MI in a porcine model (Hoffmann et al. 2004). In this study, CT detected all areas of induced infarction; infarcted myocardium demonstrated a 76.1 % reduction in microsphere-determined blood flow accompanied by a significant reduction of myocardial CT attenuation in comparison with normal myocardium (Hoffmann et al. 2004). Yim et al. also reported on the evaluation of myocardial viability in a reperfused porcine model with chronic MI (Yim et al. 2009). In clinical routine, Nikolaou et al. investigated 106 patients of whom 27 patients had a proven MI (Nikolaou et al. 2004). MDCT detected 23 of 27 myocardial infarctions resulting in a sensitivity of 85 %, specificity of 91 %, and accuracy of 90 %. Nikolaou et al. additionally noted a significant difference concerning the Hounsfield units (HU) of infarcted versus noninfarcted myocardium with distinct hypoenhancement in the infarcted myocardium (Nikolaou et al. 2004). Another study, published by Cury et al., reported a sensitivity of 94 % (32 of 34) and specificity of 97 % (66 of 68) for the detection of acute MI by CT compared to transthoracic echocardiography and SPECT (Cury et al. 2008). Similar results were published by Cheng et al., who compared dual source coronary CT angiography (cCTA) to SPECT both at rest and during stress. At rest, cCTA was found to have a sensitivity of 100 % and a specificity of 78 %; during stress, sensitivity, and specificity were found to be 83.3 and 90.3 %, respectively (Cheng et al. 2010). Hence, imaging the myocardium for perfusion deficits during arterial phase cCTA is a promising tool for detection and documenting the extent of MI, without applying additional radiation dose. However, the main limitation of first-pass arterial phase imaging of MI is that hypoattenuation during arterial phase cCTA is also seen in other conditions that cause impaired myocardial perfusion. Therefore, it is not yet possible to differentiate nonviable acute MI from viable hypoperfused myocardium with a single arterial phase cCTA.

2 Dynamic Myocardial CT Perfusion Imaging

Assessment of myocardial perfusion CT requires time-resolved imaging of the myocardial wash-in and wash-out of iodinated contrast material. The utility of myocardial perfusion imaging with MDCT has been established in animal and human trials (Mahnken et al. 2006; George et al. 2006). However, previous CT generations were limited by restricted volume coverage for time-resolved volume image acquisition during the infusion of contrast medium. With the introduction of new generation scanners, including wide detector array CT and dual source CT (DSCT), research on dynamic myocardial CT perfusion imaging is once again in the limelight (George et al. 2009; Dewey et al. 2009; Lell et al. 2009; Leschka et al. 2009). Bamberg et al. investigated the accuracy of CT dynamic stress myocardial perfusion imaging to estimate myocardial blood flow (MBF) in a porcine animal model with variable degrees of induced coronary artery stenosis in comparison with microsphere-derived MBF. The study reported a valid difference but an underestimated correlation of the MBF in CT in comparison with microsphere-derived MBF. Bastarrika et al. investigated the use of adenosine-stress dynamic myocardial volume perfusion imaging with second generation DSCT. In their study, they evaluated the qualitative and quantitative assessment of myocardial blood flow using CT in

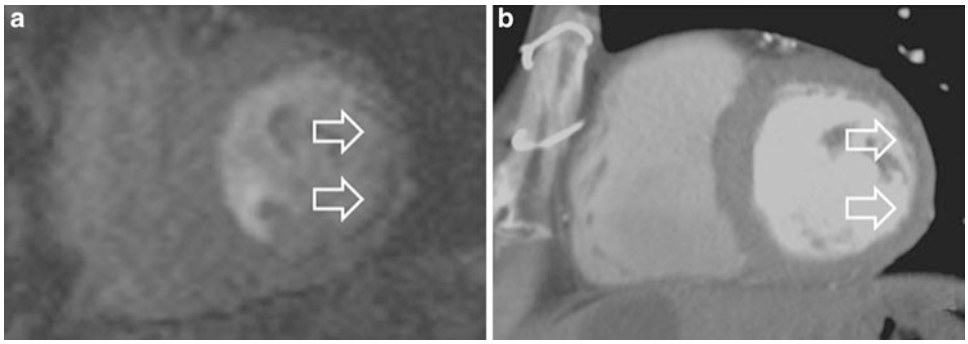

Fig. 1 48-year-old man with prior myocardial infarction in *right* coronary artery territory. First-pass perfusion MRI (**a**) and first-pass CT images (**b**) in short axis view show perfusion deficit consistent with chronic myocardial infarction of the inferior wall of the *left* ventricle with myocardial wall thinning

comparison with stress perfusion and viability MRI (Bastarrika et al. 2010). Their sensitivity, specificity, positive predictive value, and negative predictive value for the detection of myocardial perfusion defects using CT, compared with MRI, were 86.1, 98.2, 93.9, and 95.7 %, respectively, on a per-segment basis. Additionally, their semiquantitative analysis of CT data showed significant differences between ischemic and nonischemic myocardium with a signal intensity upslope that was comparable with MRI-derived values. A similar study by Bamberg et al. concluded that a combined assessment, including coronary artery anatomy evaluation by CT angiography and a dedicated dynamic CT-based stress perfusion imaging to estimate MBF, permits accurate identification of hemodynamically significant coronary artery stenosis (Bamberg et al. 2011). Comparable results were published by Ho et al., who reported a sensitivity, specificity, positive predictive value, and negative predictive value for identifying segments with perfusion defects of 83, 78, 79, and 82 % (Ho et al. 2010). Similar results in studies using DSCT were reported by George et al., using 256- and 320-MDCT (George et al. 2006, 2009).

Despite the promising findings for dynamic myocardial CT perfusion imaging, the modality is still limited by a comparatively high radiation dose. While latest cCTA techniques cut the radiation dose down to 1 mSv, the radiation exposure of a dynamic myocardial CT perfusion examination was reported around 12–13 mSv, which is equivalent to nuclear techniques, e. g., SPECT (Lell et al. 2009; Bamberg et al. 2011). Furthermore, the literature on dynamic myocardial CT perfusion is sparse and more clinical trials are needed before it can be adopted into mainstream clinical use.

3 Delayed Enhancement CT

The presence and transmural extent of an MI are important predictors of functional recovery after surgical and percutaneous revascularization (Selvanayagam et al. 2004). Nowadays, myocardial late enhancement MRI (LE-MRI) is considered the gold standard for the evaluation of the transmural extent of an MI (Kim et al. 1999). Moreover, the phenomenon of myocardial late enhancement (LE) is considered to be an evidence for the presence of nonviable myocardium and is associated with acute as well as chronic MI (Choi et al. 2001; Mahrholdt et al. 2002; Wu et al. 2001). LE-MRI has proven utility in clinical routine for differentiating viable from nonviable myocardium and acute from chronic MI (Abdel-Aty et al. 2004). Myocardial segments exhibiting greater than 50 % transmural extent of delayed enhancement can be defined as nonviable, as 90 % of such segments show no improvement in contractility after revascularization (Kim et al. 2000). With the introduction of MDCT, LE has also become a focus of CT research. On LE-CT examination, a segment affected by MI will show increased attenuation when compared with normal myocardium (Fig. 2). Several animal studies proved the reliability of LE-CT in acute and chronic MI in comparison with MRI, SPECT, and TTC staining (Baks et al. 2006; Buecker et al. 2005; Lardo et al. 2006). Results of these studies not only demonstrate the feasibility of LE-CT, but also a good correlation between the size of an MI in LE-CT and that observed through LE-MRI or TTC staining (Baks et al. 2006; Buecker et al. 2005; Lardo et al. 2006; Mahnken et al. 2007; Brodoefel et al. 2007a). An animal study by Mahnken et al. found that the reduction in infarct size over time is a process that can also be demonstrated using CT (Mahnken et al. 2007). Subsequent human studies published results with sensitivities between 78 and 97 % and specificities from 90 to 98 %, in comparison to SPECT and LE-MRI on a segmental basis (Mahnken et al. 2005; Gerber et al. 2006; Paul et al. 2005). Therefore, CT imaging may aid in predicting clinical outcomes, as the presence and size of both LE and perfusion defects on CT were found to be predictive of myocardial dysfunction after acute MI (Lessick et al. 2007; Sato et al. 2012). In addition to MI size, LE-CT has demonstrated the ability to differentiate between acute and chronic MI. In the acute phase MDCT, myocardial infarction showed higher attenuation values

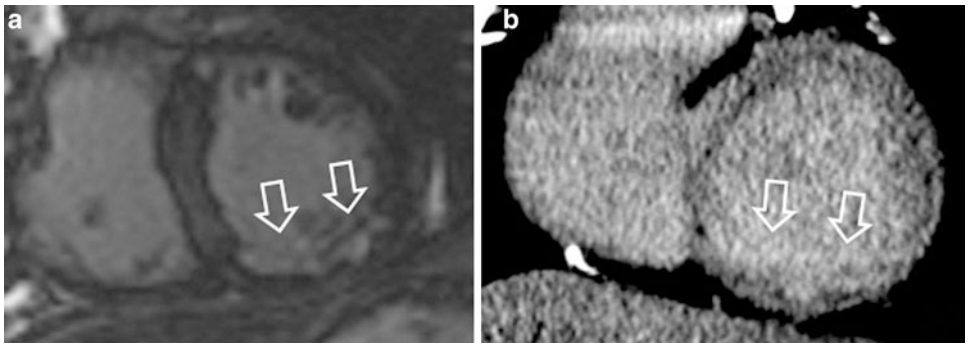

Fig. 2 53-year-old man with prior myocardial infarction in *right* coronary artery territory. MRI late enhancement (**a**) and CT late enhancement (**b**) findings in short axis view are consistent with chronic myocardial infarction of the inferior wall of the *left* ventricle with myocardial wall thinning

compared to normal myocardium, while "no-reflow" areas revealed hypodense regions surrounded by hyperenhanced myocardium (Buecker et al. 2005). These "no-reflow" areas represent the core of the MI, which can become necrotic as a consequence of intense and constant ischemia. Furthermore, the presence of "no-reflow" areas may be the finding that is most predictive of a residual perfusion defect after revascularization (Paul et al. 2005). In chronic MI, necrotic myocardial cells are replaced by scar tissue in reperfused and occlusive MI presenting with the typical LE. Due to the development of scar tissue with increased interstitial space, the increased distribution volume in the peri-infarction zone might be responsible for the small overestimation of infarct size seen with LE-CT (Wu et al. 2001; Allard et al. 1988).

With the introduction of the latest MDCT and DSCT generations, which employ more sophisticated scanning techniques, LE-CT has become a key focus in the area of cardiovascular imaging. The reduction in radiation dose applied during LE-CT must be particularly emphasized. As radiation dose associated with retrospectively ECG-gated CT was reported within the range of 4.5 mSv for an LE-scan, several methods have recently been described to lower the radiation dose (Nieman et al. 2008). An animal study by Broedefel et al. investigated the efficacy of low-dose CT imaging of late enhancement in acute MI. Starting with a standard protocol using 120 kV and 800 mAs for an LE-CT examination, the tube voltage was lowered to 80 kV and the tube current was reduced to 400 mAs; this resulted in higher contrast for late enhancement and good correlation with MRI. Additionally, the lower X-ray tube settings resulted in a radiation dose reduction from 15.6 to 2.8 mSv. (Brodoefel et al. 2007b). Reimann et al. investigated this approach in a feasibility study looking at the practicality of a low dose 80 kV protocol for detecting LE and found promising results (Reimann et al. 2008). In addition to lower tube voltages, the introduction of high-pitch DSCT has permitted further reductions in radiation dose with CT (Lell et al. 2009; Leschka et al. 2009). Using this method for LE-CT, Goetti et al. reported radiation doses of 0.7–1.02 mSv with good accuracy when compared to the gold standard, MRI (Goetti et al. 2011).

Although results from studies using LE-CT to assess myocardial viability have been promising, there are still some points of concern. First, as of this writing, there is no clear agreement on the most appropriate protocol for LE-CT. Two important protocol variables are the scan delay and the mode of contrast administration. The optimal scan delay must allow contrast material to accumulate in infarcted myocardium over several minutes, yet avoid the rapid vanishing of the contrast out of the myocardium. Selection of an ideal scan delay is essential for accurate LE-CT images. Some publications suggest that the best contrast between MI and normal myocardium is seen 5–10 min after injection (Brodoefel et al. 2007b; Deseive et al. 2011).

Although LE-CT does not have a clear place in current clinical practice, it may have a role in dedicated MI imaging in patients with contraindications to MRI. Further research is needed to determine the optimal scan delay and thus improve accuracy. However, current research has shown promising results for radiation dose reduction in LE-CT, which has previously been a major drawback of LE-CT.

4 Dual Energy CT

Dual energy CT (DECT) is one of the latest evolutions in CT technology. Introduced to the market in 2006, DECT is a dual source system equipped with two x-ray tubes and detector arrays mounted in the same gantry, perpendicular to each other (Flohr et al. 2006). The tubes can be operated simultaneously and independently, using different potentials at the same time, generating different X-ray spectra. This has made it possible to scan the same voxel simultaneously with two different energy levels. As described elsewhere, some materials show characteristic levels of CT attenuation (as measured in HUs), depending on the X-ray spectrum to which they are exposed; DECT allows material differentiation in clinical routine, notably the separation of iodine (Johnson et al. 2007). In dual source, single-energy mode, both X-ray tubes are operated with the same potential, usually 120 kV, to achieve a temporal resolution as low as 83 ms. When operated in dual energy mode for cCTA, the

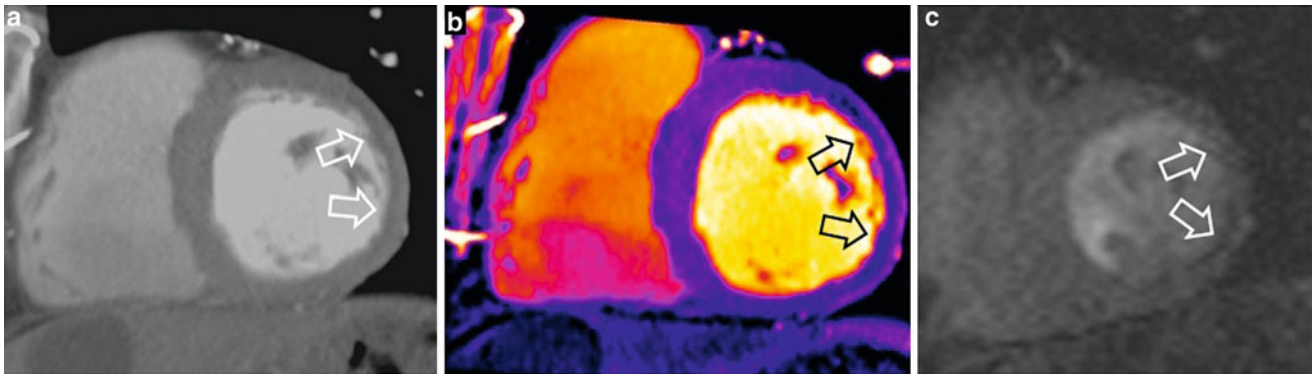

Fig. 3 54-year-old man with prior myocardial infarction in *left* anterior descending coronary artery territory. First-pass grayscale CT images (**a**) and DECT color coded perfusion map (**b**) show lateral hypoenhancement, indicating myocardial infarction, which is in good agreement with findings shown on first-pass perfusion MRI (**c**)

tube voltages are typically set to 140 kV on system A and 100 kV on system B (Schwarz et al. 2008). With these DECT settings, the best achievable temporal resolution is 165 ms, which equals that of a 64-slice scanner—a scanner generation that has shown consistently high diagnostic accuracy in the detection of significant coronary artery stenosis compared with cardiac catheterization (Herzog et al. 2007). However, this significant trade-off in temporal resolution comes with the potential benefit of material differentiation using DECT (Johnson et al. 2007). Iodine, which is used as a contrast material in CTA, has a very unique dual-energy characteristic (Zatz 1976). This enables the visualization of iodine distribution in different tissues of the body and the separation demarcation of various materials. For the evaluation of myocardial viability, DECT may be used as a first-pass arterial phase or LE-CT imaging technique (Fig. 3). Recently, Kerl et al. investigated the feasibility and performance of DECT during the arterial phase in cCTA for the detection of chronic infarction, compared with LE-MRI and histopathology, in a porcine model of reperfused myocardial infarction (Kerl et al. 2011a). In this feasibility study, they found a sensitivity and specificity for DECT of 72 and 88 %, respectively, compared to 78 and 92 %, respectively, for LE-MRI, and 60 and 93 %, respectively, for the 100 kV dataset of the DECT scan, all versus histopathology. This comparably low sensitivity of all methods might be explained by the higher heart rate of the piglets, and therefore a reduced image quality as well as motion artifacts. Another study by Zhang et al. found superior results for DECT in terms of sensitivity and specificity (92 and 80 %) for detecting acute myocardial infarction in dogs (Zhang et al. 2010). In the first systematic analysis of the potential usefulness of DECT for comprehensive CAD imaging in humans, rest- DECT correctly identified 26 of 29 (90 %) fixed myocardial perfusion defects observed on SPECT (Ruzsics et al. 2008). Another investigation comparing SPECT and DECT in first-pass arterial phase cCTA, Ruzsics et al. reported an overall sensitivity for DECT of 92 % and a specificity of 93 %, with 93 % accuracy for detecting any type of myocardial perfusion defect seen on SPECT. Contrast defects seen with DECT correctly identified 96 % of 89 fixed and 88 % of 68 reversible myocardial perfusion defects (Ruzsics et al. 2009).

In summary, there is emerging evidence for the application of DECT first-pass arterial phase imaging as a comprehensive CAD assessment tool. However, further research is required to confirm these results.

In addition to DECT first-pass arterial phase imaging, recent research investigated the use of LE-DECT for imaging MI and viability (Fig 4). Deseive et al. studied the performance of LE-DECT, in comparison with LE-MRI, for the detection of irreversibly damaged myocardium in a porcine model of reperfused chronic myocardial infarction using histopathology as the standard of reference (Deseive et al. 2011). They reported a sensitivity of 76 % and a specificity of 93 % for LE-DECT compared to a sensitivity of 62 % and sensitivity of 97 % in 100 kV imaging. These results are concordant with the results of Bauer et al. (2010), who investigated DECT-LE in humans matched with delayed LE-MRI. In this study, 36 patients with coronary artery bypass grafts were examined with LE-DECT and 3-T MRI, resulting in a sensitivity of 70 % for LE-DECT. However, only 22 of the patients (61 %) showed delayed enhancement on MRI. Again, in this patient population, the DECT studies suffered from artifacts arising from sternal wires and implanted metallic devices, affecting sensitivity. Apart from assessing MI extent and myocardial viability, DECT has an additional benefit concerning the reduction of radiation dose during cCTA (Kerl et al. 2011b).

In a nutshell, DECT shows promising results in arterial phase cCTA as well as in LE-CT. However, DECT imaging of the myocardium needs further refinement to reduce

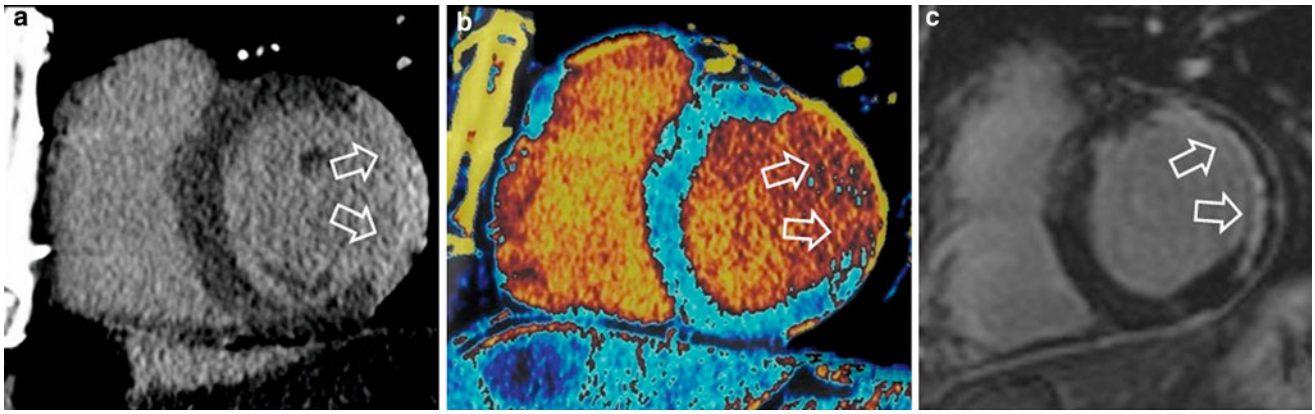

Fig. 4 54-year-old man with prior myocardial infarction in *left* anterior descending coronary artery territory. Late enhancement grayscale CT images (**a**) and late enhancement DECT color coded perfusion map (**b**) show lateral hyper enhancement, indicating myocardial infarction, which is in good agreement with findings shown on late enhancement MRI (**c**)

motion and metal artifacts before widespread use can be expected. If advanced artifact reduction can be achieved, DECT may become a multipurpose method for comprehensive CAD imaging and sophisticated myocardial viability examination.

5 Conclusion

MDCT is an effective and reliable imaging modality for evaluation of myocardial viability. It is of particular utility in patients who have contraindications to MRI yet require assessment post myocardial infarction. Rapidly advancing technology has increased the appeal of CT as a noninvasive imaging modality that can obtain accurate information on a diverse range of chronic heart diseases. Despite this potential, more studies are needed to refine and validate CT assessment of myocardial infarction and viability, and to define appropriate patient populations who may benefit from these CT applications in terms of diagnostic efficiency and improved outcome.

References

Abdel-Aty H, Zagrosek A, Schulz-Menger J, Taylor AJ, Messroghli D, Kumar A, Gross M, Dietz R, Friedrich MG (2004) Delayed enhancement and t2-weighted cardiovascular magnetic resonance imaging differentiate acute from chronic myocardial infarction. Circulation 109:2411–2416

Allard M, Doucet D, Kien P, Bonnemain B, Caille JM (1988) Experimental study of dota-gadolinium. Pharmacokinetics and pharmacologic properties. Investig Radiol 23(Suppl 1): S271–S274

Baks T, Cademartiri F, Moelker AD, Weustink AC, van Geuns RJ, Mollet NR, Krestin GP, Duncker DJ, de Feyter PJ (2006) Multislice computed tomography and magnetic resonance imaging for the assessment of reperfused acute myocardial infarction. J Am Coll Cardiol 48:144–152

Bamberg F, Becker A, Schwarz F, Marcus RP, Greif M, von Ziegler F, Blankstein R, Hoffmann U, Sommer WH, Hoffmann VS, Johnson TR, Becker HC, Wintersperger BJ, Reiser MF, Nikolaou K (2011) Detection of hemodynamically significant coronary artery stenosis: incremental diagnostic value of dynamic ct-based myocardial perfusion imaging. Radiology 260:689–698

Bastarrika G, Ramos-Duran L, Rosenblum MA, Kang DK, Rowe GW, Schoepf UJ (2010) Adenosine-stress dynamic myocardial ct perfusion imaging: initial clinical experience. Invest Radiol 45:306–313

Bauer RW, Kerl JM, Fischer N, Burkhard T, Larson MC, Ackermann H, Vogl TJ (2010) Dual-energy CT for the assessment of chronic myocardial infarction in patients with chronic coronary artery disease: comparison with 3-T MRI. AJR Am J Roentgenol 195:639–646

Becker CR, Knez A, Leber A, Treede H, Ohnesorge B, Schoepf UJ, Reiser MF (2002) Detection of coronary artery stenoses with multislice helical CT angiography. J Comput Assist Tomogr 26:750–755

Beek AM, Kuhl HP, Bondarenko O, Twisk JW, Hofman MB, van Dockum WG, Visser CA, van Rossum AC (2003) Delayed contrast-enhanced magnetic resonance imaging for the prediction of regional functional improvement after acute myocardial infarction. J Am Coll Cardiol 42:895–901

Brodoefel H, Klumpp B, Reimann A, Fenchel M, Heuschmid M, Miller S, Schroeder S, Claussen C, Scheule AM, Kopp AF (2007a) Sixty-four-MSCT in the characterization of porcine acute and subacute myocardial infarction: determination of transmurality in comparison to magnetic resonance imaging and histopathology. Eur J Radiol 62:235–246

Brodoefel H, Klumpp B, Reimann A, Ohmer M, Fenchel M, Schroeder S, Miller S, Claussen C, Kopp AF, Scheule AM (2007b) Late myocardial enhancement assessed by 64-MSCT in reperfused porcine myocardial infarction: diagnostic accuracy of low-dose ct protocols in comparison with magnetic resonance imaging. Eur Radiol 17:475–483

Brunken R, Tillisch J, Schwaiger M, Child JS, Marshall R, Mandelkern M, Phelps ME, Schelbert HR (1986) Regional perfusion, glucose metabolism, and wall motion in patients with chronic electrocardiographic q wave infarctions: evidence for persistence of viable tissue in some infarct regions by positron emission tomography. Circulation 73:951–963

Buecker A, Katoh M, Krombach GA, Spuentrup E, Bruners P, Gunther RW, Niendorf T, Mahnken AH (2005) A feasibility study of contrast enhancement of acute myocardial infarction in multislice computed tomography: comparison with magnetic resonance imaging and gross morphology in pigs. Invest Radiol 40:700–704

Burt RW, Perkins OW, Oppenheim BE, Schauwecker DS, Stein L, Wellman HN, Witt RM (1995) Direct comparison of fluorine-18-fdg spect, fluorine-18-fdg pet and rest thallium-201 spect for detection of myocardial viability. J Nucl Med Off Publ Soc Nucl Med 36:176–179

Cheng W, Zeng M, Arellano C, Mafori W, Goldin J, Krishnam M, Ruehm SG (2010) Detection of myocardial perfusion abnormalities: standard dual-source coronary computed tomography angiography versus rest/stress technetium-99 m single-photo emission CT. British J Radiol 83:652–660

Choi KM, Kim RJ, Gubernikoff G, Vargas JD, Parker M, Judd RM (2001) Transmural extent of acute myocardial infarction predicts long-term improvement in contractile function. Circulation 104:1101–1107

Cury RC, Nieman K, Shapiro MD, Butler J, Nomura CH, Ferencik M, Hoffmann U, Abbara S, Jassal DS, Yasuda T, Gold HK, Jang IK, Brady TJ (2008) Comprehensive assessment of myocardial perfusion defects, regional wall motion, and left ventricular function by using 64-section multidetector CT. Radiology 248:466–475

Deseive S, Bauer RW, Lehmann R, Kettner M, Kaiser C, Korkusuz H, Tandi C, Theisen A, Schachinger V, Schoepf UJ, Vogl TJ, Kerl JM (2011) Dual-energy computed tomography for the detection of late enhancement in reperfused chronic infarction: a comparison to magnetic resonance imaging and histopathology in a porcine model. Invest Radiol 46:450–456

Dewey M, Zimmermann E, Deissenrieder F, Laule M, Dubel HP, Schlattmann P, Knebel F, Rutsch W, Hamm B (2009) Noninvasive coronary angiography by 320-row computed tomography with lower radiation exposure and maintained diagnostic accuracy: comparison of results with cardiac catheterization in a head-to-head pilot investigation. Circulation 120:867–875

Flohr TG, McCollough CH, Bruder H, Petersilka M, Gruber K, Suss C, Grasruck M, Stierstorfer K, Krauss B, Raupach R, Primak AN, Kuttner A, Achenbach S, Becker C, Kopp A, Ohnesorge BM (2006) First performance evaluation of a dual-source CT (DSCT) system. Eur Radiol 16:256–268

George RT, Silva C, Cordeiro MA, DiPaula A, Thompson DR, McCarthy WF, Ichihara T, Lima JA, Lardo AC (2006) Multidetector computed tomography myocardial perfusion imaging during adenosine stress. J Am Coll Cardiol 48:153–160

George RT, Arbab-Zadeh A, Miller JM, Kitagawa K, Chang HJ, Bluemke DA, Becker L, Yousuf O, Texter J, Lardo AC, Lima JA (2009) Adenosine stress 64- and 256-row detector computed tomography angiography and perfusion imaging: A pilot study evaluating the transmural extent of perfusion abnormalities to predict atherosclerosis causing myocardial ischemia. Circ Cardiovasc Imag 2:174–182

Gerber BL, Belge B, Legros GJ, Lim P, Poncelet A, Pasquet A, Gisellu G, Coche E, Vanoverschelde JL (2006) Characterization of acute and chronic myocardial infarcts by multidetector computed tomography: comparison with contrast-enhanced magnetic resonance. Circulation 113:823–833

Goetti R, Feuchtner G, Stolzmann P, Donati OF, Wieser M, Plass A, Frauenfelder T, Leschka S, Alkadhi H (2011) Delayed enhancement imaging of myocardial viability: low-dose high-pitch CT versus MRI. Eur Radiol 21:2091–2099

Herzog C, Zwerner PL, Doll JR, Nielsen CD, Nguyen SA, Savino G, Vogl TJ, Costello P, Schoepf UJ (2007) Significant coronary artery stenosis: comparison on per-patient and per-vessel or per-segment basis at 64-section CT angiography. Radiology 244:112–120

Ho KT, Chua KC, Klotz E, Panknin C (2010) Stress and rest dynamic myocardial perfusion imaging by evaluation of complete time-attenuation curves with dual-source CT. JACC Cardiovasc Imaging 3:811–820

Hoffmann U, Millea R, Enzweiler C, Ferencik M, Gulick S, Titus J, Achenbach S, Kwait D, Sosnovik D, Brady TJ (2004) Acute myocardial infarction: contrast-enhanced multi-detector row CT in a porcine model. Radiology 231:697–701

Hoffmann MH, Schmid FT, Jeltsch M, Wunderlich A, Duerk JL, Schmitz B, Aschoff AJ (2005) Multislice mr first-pass myocardial perfusion imaging: impact of the receiver coil array. J Magn Reson Imaging 21:310–316

Johnson TR, Krauss B, Sedlmair M, Grasruck M, Bruder H, Morhard D, Fink C, Weckbach S, Lenhard M, Schmidt B, Flohr T, Reiser MF, Becker CR (2007) Material differentiation by dual energy CT: initial experience. Eur Radiol 17:1510–1517

Kerl JM, Deseive S, Tandi C, Kaiser C, Kettner M, Korkusuz H, Lehmann R, Herzog C, Schoepf UJ, Vogl TJ, Bauer RW (2011a) Dual energy CT for the assessment of reperfused chronic infarction—a feasibility study in a porcine model. Acta Radiol 52:834–839

Kerl JM, Bauer RW, Maurer TB, Aschenbach R, Korkusuz H, Lehnert T, Deseive S, Ackermann H, Vogl TJ (2011b) Dose levels at coronary CT angiography–a comparison of dual energy-, dual source- and 16-slice CT. Eur Radiol 21:530–537

Kim RJ, Fieno DS, Parrish TB, Harris K, Chen EL, Simonetti O, Bundy J, Finn JP, Klocke FJ, Judd RM (1999) Relationship of mri delayed contrast enhancement to irreversible injury, infarct age, and contractile function. Circulation 100:1992–2002

Kim RJ, Wu E, Rafael A, Chen EL, Parker MA, Simonetti O, Klocke FJ, Bonow RO, Judd RM (2000) The use of contrast-enhanced magnetic resonance imaging to identify reversible myocardial dysfunction. N Engl J Med 343:1445–1453

Lardo AC, Cordeiro MA, Silva C, Amado LC, George RT, Saliaris AP, Schuleri KH, Fernandes VR, Zviman M, Nazarian S, Halperin HR, Wu KC, Hare JM, Lima JA (2006) Contrast-enhanced multidetector computed tomography viability imaging after myocardial infarction: characterization of myocyte death, microvascular obstruction, and chronic scar. Circulation 113: 394–404

Lell M, Marwan M, Schepis T, Pflederer T, Anders K, Flohr T, Allmendinger T, Kalender W, Ertel D, Thierfelder C, Kuettner A, Ropers D, Daniel WG, Achenbach S (2009) Prospectively ecg-triggered high-pitch spiral acquisition for coronary ct angiography using dual source ct: technique and initial experience. Eur Radiol 19:2576–2583

Leschka S, Stolzmann P, Desbiolles L, Baumueller S, Goetti R, Schertler T, Scheffel H, Plass A, Falk V, Feuchtner G, Marincek B, Alkadhi H (2009) Diagnostic accuracy of high-pitch dual-source ct for the assessment of coronary stenoses: first experience. Eur Radiol 19:2896–2903

Lessick J, Dragu R, Mutlak D, Rispler S, Beyar R, Litmanovich D, Engel A, Agmon Y, Kapeliovich M, Hammerman H, Ghersin E (2007) Is functional improvement after myocardial infarction predicted with myocardial enhancement patterns at multidetector CT? Radiology 244:736–744

Mahnken AH, Koos R, Katoh M, Wildberger JE, Spuentrup E, Buecker A, Gunther RW, Kuhl HP (2005) Assessment of myocardial viability in reperfused acute myocardial infarction using 16-slice computed tomography in comparison to magnetic resonance imaging. J Am Coll Cardiol 45:2042–2047

Mahnken AH, Bruners P, Katoh M, Wildberger JE, Gunther RW, Buecker A (2006) Dynamic multi-section ct imaging in acute myocardial infarction: preliminary animal experience. Eur Radiol 16:746–752

Mahnken AH, Bruners P, Kinzel S, Katoh M, Muhlenbruch G, Gunther RW, Wildberger JE (2007) Late-phase MSCT in the different stages of myocardial infarction: animal experiments. Eur Radiol 17:2310–2317

Mahrholdt H, Wagner A, Judd RM, Sechtem U (2002) Assessment of myocardial viability by cardiovascular magnetic resonance imaging. Eur Heart J 23:602–619

McFalls EO, Murad B, Haspel HC, Marx D, Sikora J, Ward HB (2003) Myocardial glucose uptake after dobutamine stress in chronic hibernating swine myocardium. J Nucl Cardiol Off Publ Am Soc Nucl Cardiol 10:385–394

Mokdad AH, Marks JS, Stroup DF, Gerberding JL (2004) Actual causes of death in the united states, 2000. J Am Med Assoc 291:1238–1245

Nieman K, Shapiro MD, Ferencik M, Nomura CH, Abbara S, Hoffmann U, Gold HK, Jang IK, Brady TJ, Cury RC (2008) Reperfused myocardial infarction: contrast-enhanced 64-section CT in comparison to mr imaging. Radiology 247:49–56

Nikolaou K, Knez A, Sagmeister S, Wintersperger BJ, Boekstegers P, Steinbeck G, Reiser MF, Becker CR (2004) Assessment of myocardial infarctions using multidetector-row computed tomography. J Comput Assist Tomogr 28:286–292

Paul JF, Wartski M, Caussin C, Sigal-Cinqualbre A, Lancelin B, Angel C, Dambrin G (2005) Late defect on delayed contrast-enhanced multi-detector row CT scans in the prediction of spect infarct size after reperfused acute myocardial infarction: initial experience. Radiology 236:485–489

Reimann AJ, Kuettner A, Klumpp B, Heuschmid M, Schumacher F, Teufel M, Beck T, Burgstahler C, Schroder S, Claussen CD, Kopp AF (2008) Late enhancement using multidetector row computer tomography: a feasibility study with low dose 80 kv protocol. Eur J Radiol 66:127–133

Ruzsics B, Lee H, Zwerner PL, Gebregziabher M, Costello P, Schoepf UJ (2008) Dual-energy CT of the heart for diagnosing coronary artery stenosis and myocardial ischemia-initial experience. Eur Radiol 18:2414–2424

Ruzsics B, Schwarz F, Schoepf UJ, Lee YS, Bastarrika G, Chiaramida SA, Costello P, Zwerner PL (2009) Comparison of dual-energy computed tomography of the heart with single photon emission computed tomography for assessment of coronary artery stenosis and of the myocardial blood supply. Am J Cardiol 104:318–326

Sato A, Nozato T, Hikita H, Akiyama D, Nishina H, Hoshi T, Aihara H, Kakefuda Y, Watabe H, Hiroe M, Aonuma K (2012) Prognostic value of myocardial contrast delayed enhancement with 64-slice multidetector computed tomography after acute myocardial infarction. J Am Coll Cardiol 59:730–738

Schwarz F, Ruzsics B, Schoepf UJ, Bastarrika G, Chiaramida SA, Abro JA, Brothers RL, Vogt S, Schmidt B, Costello P, Zwerner PL (2008) Dual-energy ct of the heart–principles and protocols. Eur J Radiol 68:423–433

Selvanayagam JB, Kardos A, Francis JM, Wiesmann F, Petersen SE, Taggart DP, Neubauer S (2004) Value of delayed-enhancement cardiovascular magnetic resonance imaging in predicting myocardial viability after surgical revascularization. Circulation 110:1535–1541

Sicari R, Picano E, Landi P, Pingitore A, Bigi R, Coletta C, Heyman J, Casazza F, Previtali M, Mathias W Jr, Dodi C, Minardi G, Lowenstein J, Garyfallidis X, Cortigiani L, Morales MA, Raciti M (1997) Prognostic value of dobutamine-atropine stress echocardiography early after acute myocardial infarction. Echo dobutamine international cooperative (edic) study. J Am Coll Cardiol 29: 254–260

Takeuchi M, Yoshitani H, Miyazaki C, Haruki N, Otani S, Sakamoto K, Yoshikawa J (2003) Color kinesis during contrast-enhanced dobutamine stress echocardiography: feasibility and applicability. Circ J Off J Jpn Circ Soc 67:49–53

Writing Group M, Lloyd-Jones D, Adams RJ, Brown TM, Carnethon M, Dai S, De Simone G, Ferguson TB, Ford E, Furie K, Gillespie C, Go A, Greenlund K, Haase N, Hailpern S, Ho PM, Howard V, Kissela B, Kittner S, Lackland D, Lisabeth L, Marelli A, McDermott MM, Meigs J, Mozaffarian D, Mussolino M, Nichol G, Roger VL, Rosamond W, Sacco R, Sorlie P, Roger VL, Thom T, Wasserthiel-Smoller S, Wong ND, Wylie-Rosett J, American Heart Association Statistics C, Stroke Statistics S (2010) Heart disease and stroke statistics–2010 update: a report from the american heart association. Circulation 121:e46–e215

Wu E, Judd RM, Vargas JD, Klocke FJ, Bonow RO, Kim RJ (2001) Visualisation of presence, location, and transmural extent of healed q-wave and non-q-wave myocardial infarction. Lancet 357:21–28

Yim NY, Kim YH, Choi S, Seon HJ, Kim YC, Jeong GW, Min BI, Lee SR, Jeong MH, Kim JK, Park JG, Kang HK (2009) Multidetector-row computed tomographic evaluation of myocardial perfusion in reperfused chronic myocardial infarction: value of color-coded perfusion map in a porcine model. Int J Cardiovasc Imag 25(Suppl 1):65–74

Zatz LM (1976) The effect of the kvp level on emi values. selective imaging of various materials with different kvp settings. Radiology 119:683–688

Zhang LJ, Peng J, Wu SY, Yeh BM, Zhou CS, Lu GM (2010) Dual source dual-energy computed tomography of acute myocardial infarction: correlation with histopathologic findings in a canine model. Invest Radiol 45:290–297

CT Assessment of Myocardial Viability: Quantitive Imaging

Balazs Ruzsics

Contents

Abstract

Accurate quantification of myocardial-infarct size is critical for clinical decision making. Transmural extent of myocardial infarct predicts whether or not a patient will benefit substantially from revascularization therapy. To date, delayed-enhancement cardiac magnetic resonance (DE-CMR) imaging is the clinical standard for quantification of myocardial viability. Multidetector CT is reported by numerous authors to be a useful tool for characterizing and, more importantly, quantifying myocardial-infarct size. Thus, cardiac CT is a promising future tool for a complete coronary artery disease diagnostic workup. This chapter reviews the role of different CT-based imaging methods in precisely quantifying myocardial-infarct size.

1 Background

1.1 Myocardial Infarction: Imaging Perspective

Prolonged myocardial ischemic injury due to significant coronary artery disease leads to irreversible tissue damage and myocardial cell loss that manifest as myocardial infarction (MI). The infarcted-tissue "wave front" extends from the subendocardium toward the epicardial region. Visualization and, more importantly, accurate quantification of the MI extent facilitate clinical planning of therapeutic management by assessing the risk–benefit ratio of revascularization. Transmurality (i.e., transmural extent of MI) is dependent on the size and duration of ischemic insult. In the acute-phase, cell swelling (oncosis) appears with microangiopathy and edema in an injury response that ultimately causes myocardial dysfunction and irreversible injury. The process of resorption, the recovery of myocardial edema and condensation of necrosis, replaces the acutely injured/infarcted necrotic myocardium. Scar formation occurs with

B. Ruzsics (✉)
Royal Liverpool and Broadgreen University Hospital, UK
e-mail: Balazs.Ruzsics@rlbuht.nhs.uk

U. J. Schoepf et al. (eds.), *CT Imaging of Myocardial Perfusion and Viability*, Medical Radiology. Diagnostic Imaging,
DOI: 10.1007/174_2012_777, © Springer-Verlag Berlin Heidelberg 2012
Published Online: 19 December 2012

myocardial thinning as a chronic process of finalizing infarct remodeling.

The transmural extent of delayed contrast enhancement (DE) was found to be strongly related to the probability of improved contractility after revascularization: segments showing delayed enhancement of more than 75 % of myocardial thickness are unlikely to benefit from revascularization (Kim et al. 2000). DE-CMR is unsurpassed in its ability to differentiate viable from nonviable myocardial tissue, whether in the acute, subacute, or chronic phase of MI (Perazzolo Marra et al. 2011). Equally important, Sato et al. (2012) conducted a cardiac CT viability study involving 102 patients, reporting that myocardial DE size is a significant, independent predictor of cardiac events. Myocardial DE size on MDCT, obtained immediately after primary percutaneous coronary intervention (PCI), may provide promising information for predicting clinical outcome in patients with acute MI.

The core of infarct is often the most sensitive area to ischemic insult. Infarcted core may form an isolated histopathological entity within the infarction that has the highest edema content that eventually completely blocks microcirculation (i.e., microvascular obstruction) and limits iodinated and/or gadolinium-based contrast agent inflow to the center of infarct. Microvascular obstruction, so-called no-reflow phenomenon may occur in hemorrhagic infarcts and with reperfusion injury. A no-reflow zone has important prognostic implications for future functional recovery and morbidity. Presence of no-reflow zone predicts LV remodeling, late wall thinning, lack of functional recovery, and poor cardiovascular outcomes (Wu et al. 1998). Besides the well-supported usefulness of cardiac CT for delineating and/or excluding coronary artery disease, it is increasingly becoming a well-established imaging modality for myocardial function, perfusion, and viability. CT assessment of ischemic, infarcted myocardium (i.e., visualizing myocardial blood supply) uses a premise similar to myocardial perfusion DE-CMR. Contrast agents for CT and magnetic resonance imaging (MRI) have similar contrast kinetics that allows both the assessment of arterial blood supply and the evaluation of myocardial viability (Gerber et al. 2006).

Iodinated contrast enhancement within MI was first recognized on CT in the late 1970s (Adams et al. 1976; Higgins et al. 1978). Delayed-enhancement cardiac viability magnetic resonance imaging was established in the 1980s when initial reports confirmed the delayed gadolinium contrast enhancement on T1-weighted magnetic resonance images in 1984 (Wesbey et al. 1984; Ordovas and Higgins 2011). Cardiac MR (CMR) imaging, either by delayed contrast enhancement or by low-dose dobutamine challenge, is the noninvasive "gold-standard" for evaluating myocardial viability and infarct morphology (Judd et al. 1995; Kim et al. 1999; Fieno et al. 2000; Dendale et al. 1998; Sandstede et al. 1999; Wellnhofer et al. 2004).

The technological advantages of fast, multislice CT (MDCT) scanners provide information on myocardial viability and infarct size via accumulated iodine contrast in patients with MI (Lardo et al. 2006; Nieman et al. 2008). As of this writing, MDCT protocols for identification and quantification of infarcted myocardium use early arterial-phase acquisition and/or delayed MDCT acquisition (DE-MDCT) with either single or dual energy, utilizing iodinated or gadolinium-based contrast media with similar contrast agent myocardial tissue kinetics. DE-MDCT acquisition, similarly to DE-CMR, differentiates acute, subacute, and chronic MI. Investigators recently provided evidence for the use of DE-MDCT shortly after cardiac catheterization since both X-ray based imaging modalities use iodinated contrast agents. Without administering additional contrast material, patients are able to be scanned by MDCT for reperfusion assessment immediately after catheterization (Habis et al. 2009).

2 Technical Principles of Visualizing and Quantifying Infarcted Myocardium

Cardiac CT has a rather low signal-to-noise ratio (SNR) but better spatial resolution and, consequently, a less-pronounced partial volume effect compared with CMR. CMR, however, is well-known for excellent soft tissue contrast; further refinement of nulling the healthy myocardium helps to improve visualization of hyperenhancing, infarcted areas. CT generally lacks this capability, at least where single-energy techniques are concerned. Low-kilovoltage (kV) acquisition protocols have been described to improve the detection of areas of delayed contrast enhancement within the myocardium (Mahnken et al. 2007; Brodoefel et al. 2007a, b); however, image quality is diminished when imaging an obese patient due to high levels of image noise.

2.1 Contrast Administration

Regardless of whether a mono-, bi-, or triphasic contrast media injection protocol was used, an amount of approximately 120–140 mL iodine contrast medium is usually a prerequisite for the detection and quantification of myocardial hyperenhancement. Although contrast material is usually administered as a bolus during coronary CT angiography (cCTA) or a dedicated myocardial blood pool assessment, investigators (Brodoefel et al. 2007a, b) reported greater dynamic range in attenuation values between infarcted tissue and normal myocardium when the

Table 1 Animal experiment studies for quantification of MI

Study	Experimental model	Single-energy arterial-phase imaging	Single-energy delayed-enhancement MDCT	Dual-energy delayed-enhancement MDCT	Time of MI
Hoffmann et al. (2004)	Porcine model ($n = 7$)	+	−	−	Acute MI
Lardo et al. (2006)	Canine ($n = 10$) and porcine ($n = 7$) model	−	+	−	Actue (90 min) chronic (8 weeks)
Buecker et al. (2005)	Porcine model ($n = 14$)	−	+	−	Acute MI
Baks et al. (2006)	Porcine model ($n = 10$)	−	+	−	Acute MI (5–7) days
Mahnken et al. (2007)	Porcine model ($n = 7$)	−	+	−	Acute (day 7), subactute (day 28) and chronic (day 90) MI
Ruzsics et al. (2008)	Porcine model ($n = 5$)	−	+	−	Acute MI (6–7 days)
Varga-Szemes et al. (2012)	Porcine model ($n = 6$)	−	(ex vivo Gd DTPA)	−	Acute MI
Deseive et al. (2011)	Porcine model ($n = 8$)	−	−	+	Chronic (61 ± 4 days)

bolus is followed by a prolonged, low-flow injection (30 mL at 0.1 mL s^{-1}).

Latest technological advantage of high-pitch dual-source CT enables the use of two separate contrast administrations, a so-called "split-bolus technique," with two CT acquisitions in the same imaging session. It has been reported that a standard contrast-enhanced cCTA using a high-pitch protocol after the administration of an initial bolus of 70 mL iodinated contrast media can be successfully combined with a second dose of 70 mL of iodinated contrast media followed by a high-pitch, delayed CT acquisition for myocardium. In order to achieve an adequate dose and accumulation of iodine for the late phase acquisition, the second contrast bolus is administered 5 min after the first. After a total delay of approximately 15 min after the first injection, a second high-pitch delayed-enhancement scan can accurately delineate nonviable myocardium (Goetti et al. 2011).

2.2 Time of Image Acquisition

The optimal timing of the delayed acquisition is still subject to debate. The delayed acquisition should be triggered when the accumulation of iodine contrast is highest in infarcted myocardium, showing highest absolute attenuation values in the infarct and delineating differences of contrast between healthy and infarcted myocardium. A delay time of 5 to 15 min after contrast medium administration is frequently reported (Gerber et al. 2006; Choe et al. 2008; Jacquier et al. 2008) (Table 1, 2).

2.3 Reconstruction and Evaluation Parameters

According to a report by Blankstein et al. (2009), in general, delayed-enhancement CT studies are best viewed as thick (5 or 10 mm) multiplanar reformations with a narrow window width and level (e.g., a width of 200 HU and a level of 100 HU) or as maximum intensity projections.

2.4 Quantification Parameters

Percent-infarct per slice (PIS) is calculated for MDCT (PIS_{MDCT}) or MRI (PIS_{MRI}) as follows:

PIS_{MDCT} or $PIS_{MRI} = (\sum I_v)/n_{slice}$ (Kim et al. 2000) (summation of infarcted voxels over all myocardial voxels v in the slice)

where n_{slice} is the number of myocardial voxels in the slice.

Infarction fraction (IF) for MDCT (IF_{MDCT}) or MRI (IF_{MRI}) is calculated as follows:

$IF = (\sum I_v)/(\sum n_{slice})$ (Perazzolo Marra et al. 2011) (summation of infarcted voxels over all myocardial voxels v in the heart)

where $(\sum n_{slice})$ represents the total number of myocardial voxels obtained by summing the voxel counts from all slices.

Tissue mass is determined by taking into account the specific gravity of myocardium, 1.05 g/cm^3. In the same manner, from IF, the total volume of infarcted tissue is determined.

Table 2 Human experimental studies for quantification of MI

Study	Study Population	Single-energy Arterial-phase imaging	Single-energy Delayed-Enhancement MDCT	Dual-energy Delayed-Enhancement MDCT	Time of DE-MDCT acquisition
Gerbe et al. (2006)	Acute MI ($n = 16$)	+	+	–	10 min
	Chronic MI ($n = 21$)				
Nieman et al. (2008)	Acute MI ($n = 21$)	+	+	–	7 min
Jacquier et al. (2008)	Acute MI ($n = 19$)	+	+	–	5 and 10 min
Boussel et al. (2008)	Acute MI ($n = 19$)	–	+	–	10 min
Choe et al. (2008)	Acute MI ($n = 40$)	+	+	–	10 min
	Chronic MI ($n = 40$)				
Mahnken et al. (2005)	Acute MI ($n = 28$)	–	+	–	15 min
Kang et al. (2010)	Chronic MI ($n = 26$)	–	–	+	6 min

3 Cardiac CT: Evidence of Quantification of Myocardial Viability

Several comparative studies have been published to establish the role of MDCT for quantification of nonviable myocardium. MDCT viability studies compared their result to delayed-enhancement CMR (DE-CMR) as the clinical reference gold-standard imaging modality for viability assessment (Gerber et al. 2006; Nieman et al. 2008; Choe et al. 2008; Jacquier et al. 2008; Habis et al. 2009; Boussel et al. 2008; Nikolaou et al. 2005; Mahnken et al. 2005). Most of these studies have proven that DE-MDCT can identify and quantify infarct size from acute to chronic phases of infarct injury as a result of iodinated contrast accumulation induced hyperattenuation.

Histopathological evidence shows that areas of infarct shrink during the evolution of scarring due to myocardial remodeling. A significant difference in the area of delayed enhancement is prominent on DE-MDCT and DE-CMR images from acute to chronic phases of MI. DE-MDCT has the ability to accurately monitor microscopic evolution of scarring, myocardial-infarct remodeling, and reduction of infarct size (Mahnken et al. 2007). Interestingly, a recent study showed that peri-infarct edema in large acute MIs can be assessed on unenhanced CT (Mahnken et al. 2009).

No-reflow phenomenon can be well recognized as a central area of hypoattenuation within a hyperattenuated region in DE-MDCT images. In fact, a hypoattenuated core as seen on CT may be the finding that is most predictive of a residual perfusion defect 6 weeks after successful reperfusion of acute MI (Paul et al. 2005).

3.1 Single Energy for Quantifying MI

3.1.1 Arterial-Phase Imaging: Quantification of Area of Hypoattenuation

ECG-synchronized first-pass cCTA allows us to not just visualize the coronary artery tree and, consequently, grade coronary stenosis but also to characterize areas of decreased myocardial blood flow. Decreased perfusion, shown as hypoattenuated areas on CT images, may be secondary to a critical coronary artery stenosis or occlusion, microvascular obstruction, or myocardial scar. Thus, while a differential diagnosis is difficult to make, the diagnostic value of delineating the areas with deteriorated blood flow (hypoattenuation) is undeniable (Kramer et al. 1984; Gray et al. 1978; Doherty et al. 1981; Georgiou et al. 1992) Fig. 1.

With contrast-enhanced cCTA, chronic MI can ordinarily be recognized as a hypoattenuated region (>50 % HU decrease compared with surrounding myocardium) (Nikolaou et al. 2004) in a subendocardial or transmural distribution that persists in systole and diastole and is concordant with a coronary territory (Rubinshtein et al. 2009).

It is well established in CMR studies that the transmural extent of nonviable myocardium determines the success of functional recovery after revascularization. Thus, accurate and precise quantification of nonviable myocardium is critical for planning a revascularization strategy and for helping the physician assess the risks and benefits of the PCI procedure and/or coronary artery bypass graft surgery (Kim et al. 2000; Choi et al. 2001). In 2004, animal experiments provided evidence of not just delineation but also quantification of hypoattenuated area within acutely infarcted myocardium. Areas of low attenuation within porcine heart

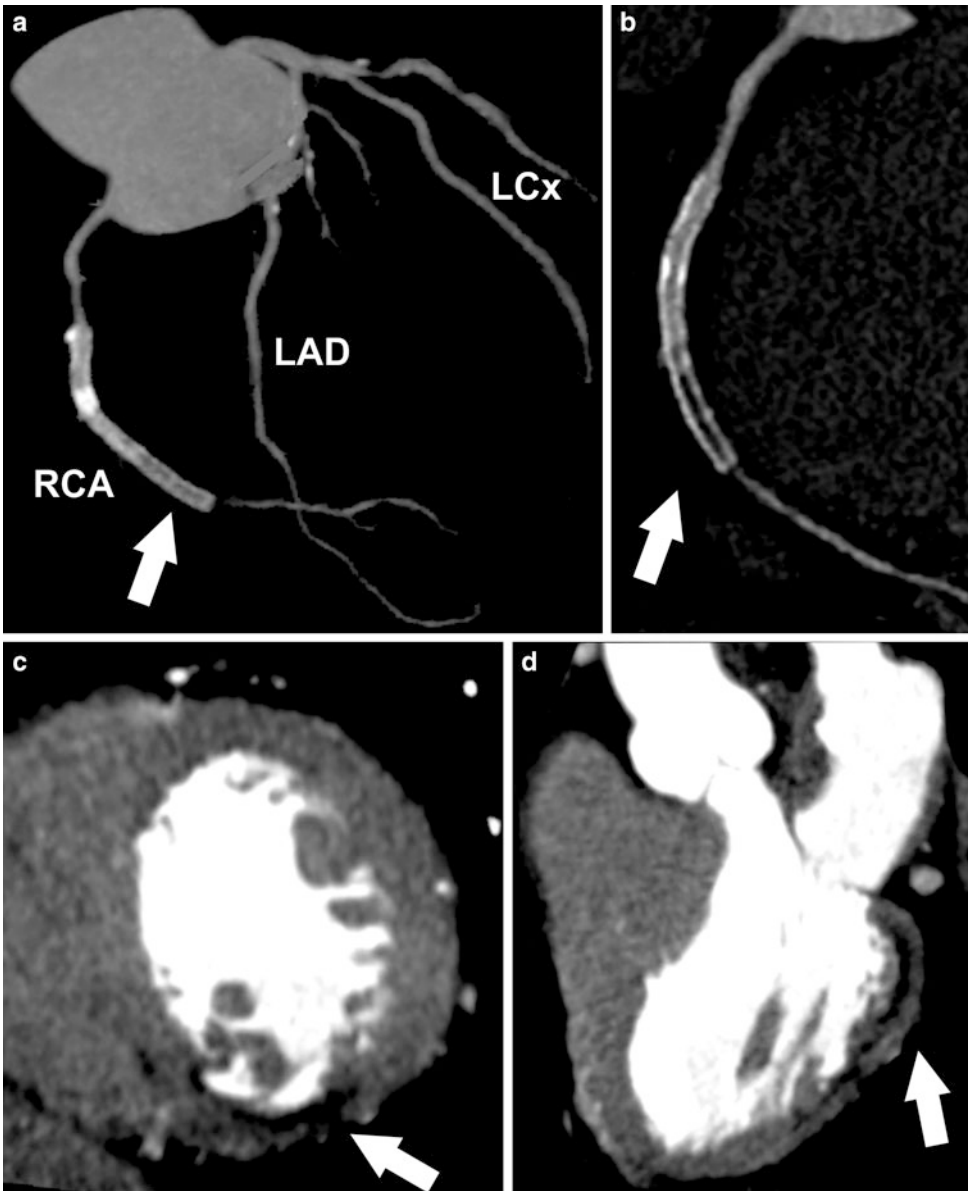

Fig. 1 Contrast enhanced, retrospectively ECG-gated dual-source CT study of a 61-year-old patient with prior history of acute coronary syndrome and myocardial infarct. (**a**) Coronary artery tree is shown with presence of RCA stent (*arrow*) (LAD: Left Anterior Descending, LCx: Left Circumflex, RCA: Right Coronary Artery). (**b**) Coronary artery disease of RCA is displayed revealing significant in-stent restenosis (*arrow*). **c** and **d** delineate MI as area of hypoattenuation (*arrow*) on early arterial-phase images with (**c**) dedicated short and (**d**) long axis view after first-pass contrast injection

showed good correlation with myocardial blood flow reduction and absolute MI size (Hoffmann et al. 2004).

Nikolaou et al. reported clinical correlation in 30 patients. First-pass CT angiography was able to detect all but one (10 out of 11) MI when compared to DE-CMR. Assuming MI size through blood flow defect quantification results in a significant underestimation (19 %) compared to true infarct size determined by DE-CMR.

Differentiation between ischemia and MI is not possible using first-pass cCTA acquisition alone (Nikolaou et al. 2005). Shapiro et al. (2010) investigated prognostic value of the extent of hypodense areas in patients with MI. It was found that the prognostic relevance of hypoperfused areas, as determined from arterial-phase CT, is unclear and remains such, because decreased myocardial attenuation on arterial-phase CT imaging is not necessarily indicative and, more importantly, not specific for MI. However, patients with MI often show hypoattenuation after first-pass iodinated contrast injection in the infarcted area.

Mahnken et al. (2005) showed the importance of arterial-phase detection but the area of hypoattenuation significantly underestimated the true infarct size compared with cardiac MRI. PIS_{MRI} versus PIS_{MDCT} were calculated and compared in each patient. Mean infarct size on MRI (PIS) was 31.2 ± 22.5 % per slice compared with 24.5 ± 18.3 % per slice for first-pass arterial-phase acquisition on MDCT. Actual MI on MDCT size was reportedly underestimated by 25 % compared with DE-CMR ($k = 0.635$). Reported underestimation and discrepancy in infarct size could be explained by the observation that parts of the reperfused

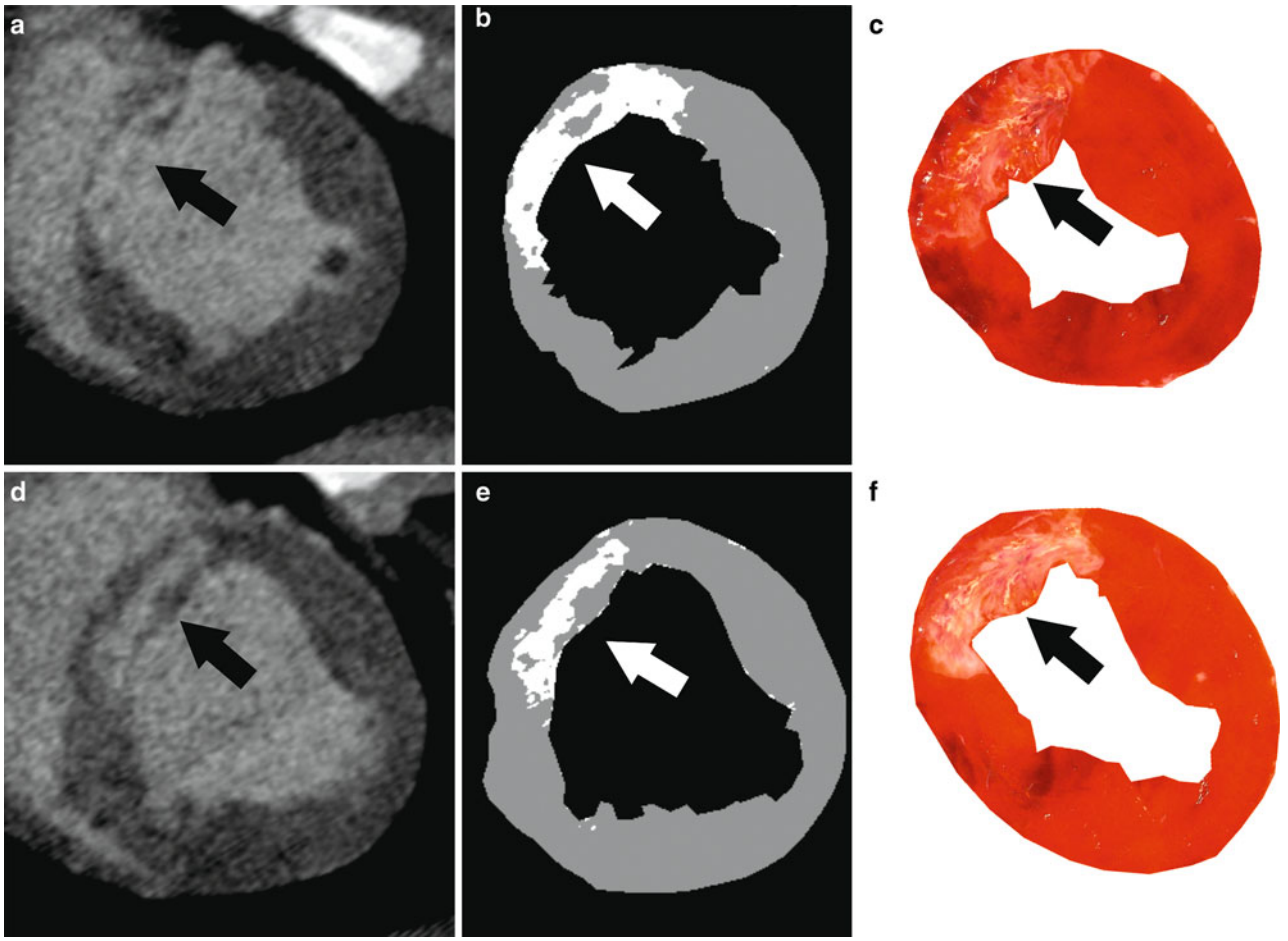

Fig. 2 Semiautomated method for visualizing and quantifying animal myocardial infarct. **a** and **d** display cardiac CT images in short axis after delayed MDCT acquisition. Accumulated iodine contrast in infarcted porcine heart is visible in LAD territory, i.e., anterior cardiac segments (*arrow*). **b** and **e** show corresponding threshold CT images with +2 S.D. threshold. Myocardial infarct is delineated as bright pixels on threshold images (arrow). Within the infarcted area, gray pixels represent microvascular obstruction (**b**). **e** and **f** show corresponding histopathological standard, post-mortem TTC images delineating in good agreement with myocardial-infarct location and size (*arrow*)

necrotic area display normal enhancement on first-pass perfusion but are hyperenhanced on delayed imaging. Thus, in patients with MI, early hypoattenuated regions represent only a fraction of MI.

In 42 subjects, Sanz et al. reported that quantified MI size in arterial-phase CT angiography imaging and DE-CMR were strongly correlated ($r = 0.87, p < 0.0001$). MI volume by MDCT was again proven to be underestimated in comparison with DE-CMR (2.7 ± 2.5 vs. 25.9 ± 19.9 mL, $p < 0.0001$) (Sanz et al. 2006).

In summary, first-pass iodinated contrast media MDCT hypoattenuation is not specific and, more importantly, not an accurate tool for securely diagnosing or quantifying myocardial infarct. Clinical correlation can help establishing the etiology (e.g., perfusion, MI, microvascular obstruction) of hypoattenuation on arterial-phase MDCT images. Quantification of areas with low attenuation significantly underestimates true MI size.

3.1.2 Delayed-Enhancement CT Imaging: Quantification of Area of Hyperattenuation

The delayed-hyperenhancement phenomenon of CMR is a well-established and widely-acceptable clinical tool for detecting and quantifying infarcted, nonviable myocardium. Contrast-enhanced CMR uses a GdDTPA contrast agent that has myocardial tissue kinetics that is similar to those of iodinated contrast agents. In acute MI, myocyte necrosis results in interstitial edema and membrane rupture, which allows iodinated contrast agents and gadolinium chelates to diffuse into the intracellular space (Jennings et al. 1985; 1990). Thus, just as GdDTPA of CMR, iodinated contrast material accumulates in the infarcted cardiac segments with a similar late-enhancement phenomenon visualized by delayed cardiac CT. Late DE-MDCT acquisition after iodinated contrast agent administration is capable of delineating MI as an area of hyperattenuation, i.e., myocardial region with high Hounsfield unit values. Usually,

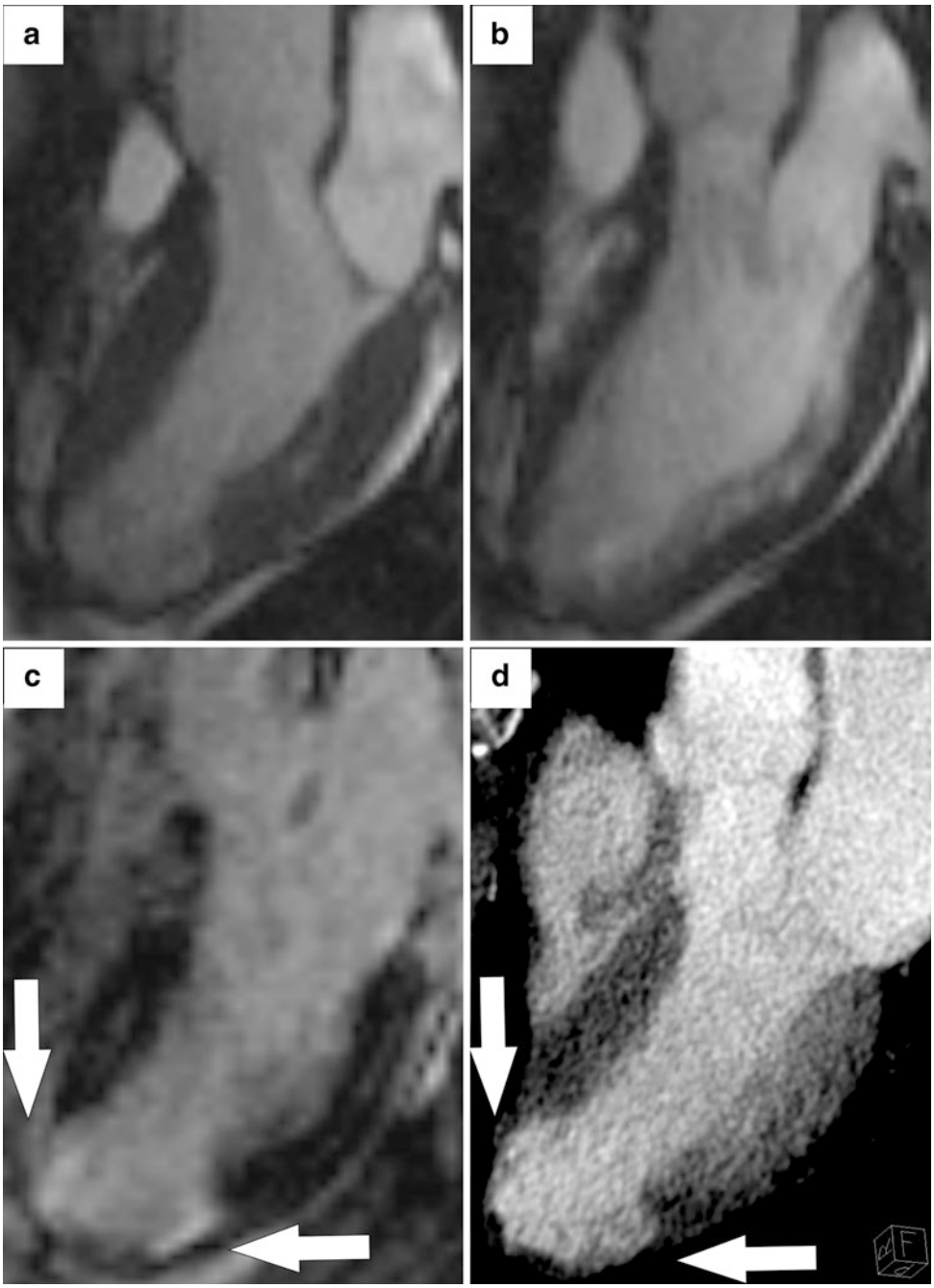

Fig. 3 Patient is a 49-year-old woman with known coronary artery disease and past medical history of myocardial infarct. End-systolic (**a**) and end-diastolic (**b**) cardiac MRI images allow visualization of akinetic apical segments. Delayed-enhancement MRI (**c**) and MDCT (**d**) images in long axis show good agreement in visualization of apical infarcted myocardium (*arrows*) in the corresponding akinetic territory. Iodine uptake on late-MDCT images shows good correlation with GdDTPA accumulation on late-MRI images

late-scan acquisition is considered to be 5–15 min after the administration of contrast agent.

GdDTPA and iodinated contrast agent accumulation is observed in both acute and chronic myocardial infarcts. In acute settings, necrosis is identified; in chronic infarcts, a dense collagen-rich scar is identified. Both histopathological entities show expanded extracellular space that delays washout of contrast media (Gerber et al. 2006).

Transmural extent of MI as detected and quantified with DE-MDCT predicts the recovery of regional systolic LV function after revascularization for acute STEMI (ST-elevation myocardial infarct, as observed on ECG) (Shapiro et al. 2010).

3.1.2.1 Animal Experiments

Several animal experiments have shown that the area of delayed enhancement could be not only just visualized but also quantified on late-MDCT images. Equally importantly, animal studies have the definite advantage over human studies through the use of a histological 2,3,5-

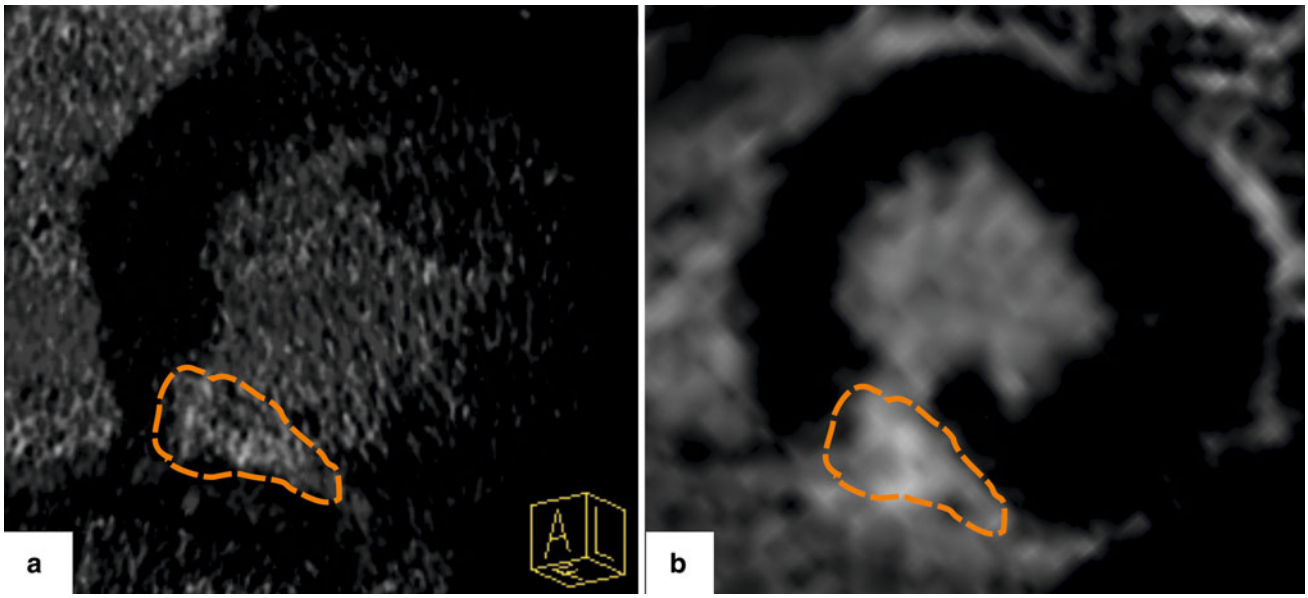

Fig. 4 Patient is a 46-year-old gentleman with past medical history of MI and inferior q wave on recent ECG. Delayed-enhancement MDCT image (**a**) shows the iodinated contrast accumulation as an area of hyperattenuation in short-axis reconstruction. The corresponding delayed-enhancement CMR image in short-axis view shows good agreement with CT findings and delineates inferior myocardial infarct as a bright area of hyperenhancement. The same volume and area of infarct are identified by both late-MDCT and -MRI with hand planimetry (*dashed line*)

Triphenyltetrazolium-Chloride (TTC) staining, the ultimate comparative ex vivo hystopathological reference standard (Gerber et al. 2006; Lardo et al. 2006) (Table 1, Fig. 2).

The role of MDCT in quantifying nonviable myocardium was reported in both acute and chronic animal MI. The transmural extent and volume of infarct by MDCT compared well with TTC staining (acute infarcts, PIS_{MDCT}: 21.1 ± 7.2 %, compared with PIS_{TTC}: 20.4 ± 7.4 %, mean difference of 0.7 %; chronic infarcts, 4.15 ± 1.93 % (PIS_{MDCT}) compared with 4.92 ± 2.06 % (PIS_{TTC}), mean difference of 20.76 %). Peak CT attenuation values were visualized 5 min after contrast agent administration. No-reflow zones at the center of MIs have also been identified accurately in acute studies and correlate well with reduced blood flow determined by microsphere distribution (Lardo et al. 2006).

Buecker et al. (2005) also quantified MI in porcine model (n = 14). Spatial extent of infarct was well correlated between TTC, DE-CMR, and DE-MDCT at 5 min post-contrast injection, with DE-MDCT slightly overestimating the infarct size.

Baks et al. (2006) have demonstrated an excellent correlation of both MRI and MDCT with TTC for quantification of subacute infarct in porcine model. Consequently, DE-CMR and DE-MDCT demonstrated a strong correlation in determining infarct size.

Mahnken et al. (2007) used a porcine model and performed sequential DE-CMR and DE-MDCT imaging in reperfused acute, subacute, and chronic MI (day 0, 7, 28 and 90). No significant differences were observed in infarct size between DE-MDCT and DE-CMR at all investigated timepoints. Bland–Altman plots showed good agreement (−3.4–1.9 %) for infarct size between DE-MDCT and TTC staining on day 90.

However, these animal studies employed user defined contour (hand planimetry), a method of semiautomated infarct detection. With the help of significant attenuation difference between nonviable myocardium and remote, healthy myocardium, automated algorithms with minimal user interface were developed to quantify infarct size; MI was defined as attenuation value two standard deviations (S.D.) above the mean healthy myocardium attenuation value (Ruzsics et al. 2008) (Fig. 2).

In a recently published ex vivo animal study, MI size was visualized and quantified in swines using GdDTPA contrast medium for both DE-CMR and DE- MDCT imaging. Authors have proven that accumulation of GdDTPA contrast medium was accurately visualized by MDCT in an ex vivo setting. Semiautomated quantification using a six-S.D. threshold limit (healthy myocardium + 6-S.D.) quantified infarct most precisely compared to TTC (Varga-Szemes et al. 2012).

Submillimeter resolution can be achieved with MDCT, markedly reducing the partial volume effects that are seen in MRI. However, this relative advantage of MDCT is to be taken in the context of certain limitations of the technique with respect to MRI. These include a relatively restricted dynamic range of attenuation (i.e., SI values between the normal and the nonviable myocardium) on MDCT.

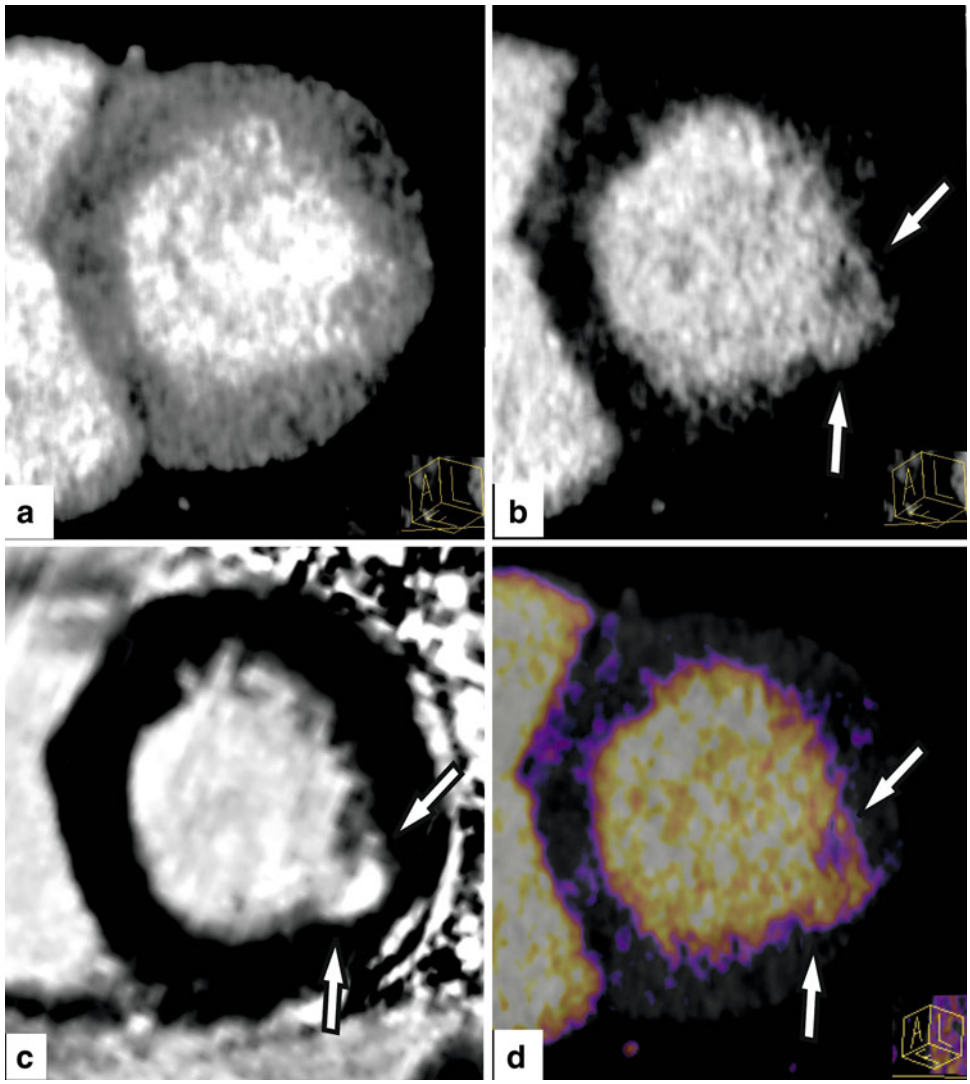

Fig. 5 Summary of dual-energy DE-MDCT image interpretation of a 65-year-old lady with recurrent chest pain. (**a**) Dual-energy DE-MDCT image generated by high tube voltage (140 kV) accurately delineates the endo- and epicardial borders of the myocardium. (**b**) Dual-energy DE-MDCT image generated by low tube voltage (80 kV) delineates iodine accumulation, i.e., myocardial infarct (*arrows*). Low tube voltage is more sensitive to iodine accumulation but less sensitive to myocardial borders than high tube voltage within the heart. (**c**) Clinical standard, contrast-enhanced CMR study shows hyperenhanced, nonviable myocardium in basal infero-lateral segment (*arrows*). (**d**) Corresponding dual-energy DE-MDCT merged (low and high voltage) image shows excellent agreement delineating infarcted myocardium in the same territory (*arrows*)

Therefore, the MDCT contrast-to-noise ratio is lower as compared to MRI (Nieman et al. 2008).

3.1.2.2 Human Studies

One of the first publications on the accurate quantification of human MI by cardiac MDCT dates back to early 2000 (Table 2).

Twenty-eight patients with reperfused acute MI underwent both first-pass and delayed MDTC examination on day 5 post MI (Mahnken et al. 2005). PIS_{MDCT} versus PIS_{MRI} showed good agreement ($k = 0.878$), with similar mean infarct size (33.3 ± 23.8 % per slice, compared with 31.2 ± 22.5 % per slice; $p = 0.398$). Bland Altmann analysis also confirmed good agreement between DE-MDCT and DE-CMR.

Gerber et al. (2006) investigated early and delayed imaging with both MDCT and CMR in 37 patients with acute or chronic MI. Assessment of absolute MI size on DE-MDCT and DE-CMR acquisitions (10 min after contrast agent administration) showed that infarct mass were highly correlated ($r = 089$, $p < 0.001$).

Similarly, Choe et al. (2008) studied 63 patients with reperfused acute or chronic MI, reporting a correlation coefficient of 0.81 ($p < 0.0001$) between the 5-min-delay MRI and the late-MDCT. It is also important to emphasize that DE-MDCT acquired with a 5-min-delay versus DE-CMR yielded comparable results but significant difference (25.9 ± 12.1 % vs. 22.8 ± 11.8 %, relatively) in calculated infarction fraction.

Excellent correlation between calculated infarction fraction on DE-MDCT versus DE-CMR ($IF_{MDCT} = 13$ % $\pm$ 9 vs. $IF_{MRI} = 15$ % $\pm$ 7) was also reported. DE-MDCT showed lower contrast-to-noise ratio compared with DE-CMR, but this finding had no significant influence on the quantification of MI size Nieman et al. 2008.

Optimizing the SNR and improving the contrast-to-noise ratio between nonviable and viable myocardium are key to a successful quantification of MI (Fig. 3). Delayed CT

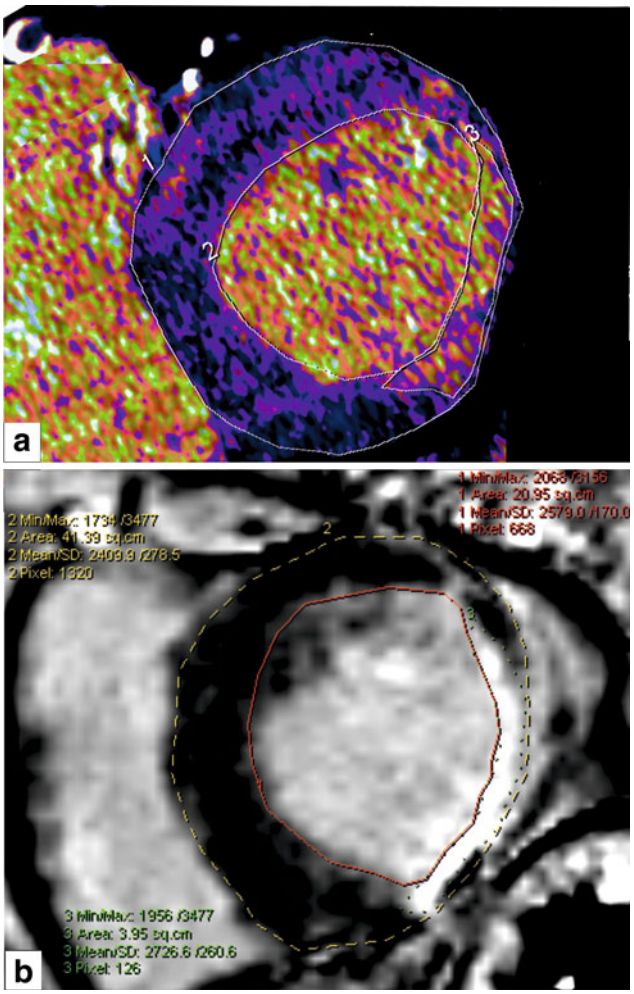

Fig. 6 Quantification of dual-energy DE-MDCT images of a 67-year-old patient with recurrent chest pain. Dual-energy DE-MDCT merged image (**a**) delineates infarcted area in lateral myocardial segment, combined low and high tube voltage information. (1) endocardial, (2) epicardial, and (3) myocardial-infarct contours are delineated with hand planimetry. Corresponding DE-CMR image delineates same lateral myocardial infarct as area of hyperenhancement. Corresponding hand planimetry of endocardiam, epicardium, and myocardial infarct also show good agreement

acquisitions 5 and 10 min after contrast injection were compared. It has been found in 19 patients that a 5-min-delay DE-MDCT yields a significantly higher SNR with overall better CT image quality than a 10-minute-delay DE-MDCT, but no significant difference was found in quantification of MI size between these two acquisition timings (Jacquier et al. 2008).

Similar to experimental animal settings, hand planimetry performed by multiple independent observers is the most frequently used tool for quantification of human MI size (Fig. 4). Significant agreement was found in acute infarct size using hand planimetry after percutaneous coronary intervention in 19 patients with acute MI. It has also been established that accurate visualization and quantification of MI is achievable with DE-MDCT without the requirement of an additional iodine contrast bolus injection (Habis et al. 2009; Boussel et al. 2008).

3.2 Dual Energy for Quantifying MI

Tissues in the human body show different absorption characteristics when penetrated with different X-ray spectra, which are typically generated by different kV settings of the X-ray tube. With the help of different energy levels, tissue differentiation by X-ray-based imaging modalities has been reported to be possible (Genant and Boyd 1977; Brody et al. 1981; Millner et al. 1979). It has also been recognized that iodine-based contrast media have unique X-ray absorption characteristics at different kV levels (Riederer and Mistretta 1977). Early experimental prototypes typically required the acquisition of two separate CT acquisitions at different kV levels with subsequent image coregistration, limiting clinical utility (Chiro et al. 1979; Kalender et al. 1986). Animal studies demonstrated that identifying and quantifying MI with dual-energy DE-MDCT is feasible (Zhang et al. 2010; Deseive et al. 2011).

Dual-energy acquisition for quantification of MI size in human infarcted myocardium helps to combine information of low-kV (80 or 100 kV) fine visualization of contrast accumulation differences within infarcted myocardium (Mahnken et al. 2005) and high-kV (140 kV) visualization of sharp endo- and epicardial borders (Fig. 5).

Kang et al. (2010) reported a close, linear correlation ($r = 0.9$) between DE-CMR and DE-MDCT for determining PIS in human infarcted heart ($n = 40$). The proposed method for determining infarct size is to evaluate the low- and high-voltage data separately. Images generated by the low tube voltage delineate absolute MI size (Fig. 5). Images generated by high tube voltage precisely visualize endo- and epicardial borders but lose sensitivity for depicting iodine accumulation in the infarcted area. Dual-energy DE-MDCT has also been shown to represent a good alternative for MI quantification; correlation statistics yield good agreement in quantification of infarct size between dual-energy DE-MDCT and DE-CMR (Fig. 6).

4 Radiation Protection

To date, accurate MI quantification is optimally achievable with an additional delayed acquisition and thus extra radiation. Radiation exposure varies between different equipment and protocols. Early animal experiments using 64-slice MDCT projected a radiation exposure of 15 mSv for men and 21 mSv for women (Baks et al. 2007).

Dual-source CT technology, the Care dose algorithm, the widely acknowledged prospective triggering, and FLASH methods were all developed for the purpose of significantly

reducing radiation exposure. Acquiring DE-MDCT with prospective ECG-triggering significantly limits radiation dose compared with retrospective ECG-gating (Chang et al. 2009). Thus, a delayed CT scan can be obtained at a low radiation dose of about 1 mSv.

Pushing this limit further, a recent study customized an ultra-low-dose high-pitch CT protocol (Goetti et al. 2011). Investigators reported an estimated mean radiation dose as low as 0.89 ± 0.07 mSv (range: 0.74–1.02 mSv, n = 24). With the help of latest dual-source CT equipment, this was achieved using a prospectively ECG-synchronized high-pitch (3.4 mm) 100 kV CT acquisition.

5 Future Perspective

Viability detection and, equally importantly, precise quantification are crucial for the management of MI. Evidence-based MDCT approaches for the determination of MI size are derived from the feasibility and initial accuracy studies highlighted earlier, most of which are limited by small, selective patient populations. Nevertheless, MDCT has been demonstrated as a promising clinical tool of the future for fully integrative cardiac assessment—not only coronary stenosis grading and myocardial ischemia/infarction detection, but also myocardial viability quantification. Clinical demand for MDCT only increases when a patient, needing a scan, has MRI-contraindicated pacemakers, defibrillators, or other metal implants.

Fast CT scanning is able to provide accurate information for patient viability in combination with acute PCI (Habis et al. 2009; Boussel et al. 2008). The prognostic value of quantifying nonviable myocardial area by DE-MDCT immediately after PCI strongly predicts the functional recovery and overall clinical outcome of patients with acute MI (Perazzolo Marra et al. 2011). High-pitch low radiation MDCT protocols are available and ready for widespread future clinical use with sub-mSv radiation. Prospective evidence-based trials with large patient populations are needed to assess the prognostic significance of these findings and their effect on diagnostic and therapeutic efficacy, and to establish the quantification of myocardial viability by MDCT as an integral component of routine, comprehensive coronary artery disease workup.

References

Adams DF, Hessel SJ, Judy PF, Stein JA, Abrams HL (1976) Differing attenuation coefficients of normal and infarcted myocardium. Science 192:467–469

Baks T, Cademartiri F, Moelker AD et al (2006) Multislice Computed Tomography and Magnetic Resonance Imaging for the Assessment of Reperfused Acute Myocardial Infarction. J Am Coll Cardiol 48:144–152

Baks T, Cademartiri F, Moelker AD, van der Giessen WJ, Krestin GP, Duncker DJ, de Feyter PJ (2007) Assessment of acute reperfused myocardial infarction with delayed enhancement 64-MDCT. Am J Roentgenol 188(2):135–137

Blankstein R, Rogers IS, Cury RC (2009) Practical tips and tricks in cardiovascular computed tomography: diagnosis of myocardial infarction. J Cardiovasc Comput Tomogr 3:104–111

Boussel L, Ribagnac M, Bonnefoy E et al (2008) Assessment of acute myocardial infarction using MDCT after percutaneous coronary intervention: comparison with MRI. AJR 191:441–447

Brodoefel H, Klumpp B, Reimann A et al (2007a) Late myocardial enhancement assessed by 64-MSCT in reperfused porcine myocardial infarction: diagnostic accuracy of low-dose CT protocols in comparison with magnetic resonance imaging. Eur Radiol 17:475–483

Brodoefel H, Reimann A, Klumpp B et al (2007b) Assessment of myocardial viability in a reperfused porcine model: evaluation of different MSCT contrast protocols in acute and subacute infarct stages in comparison with MRI. J Comput Assist Tomogr 31:290–298

Brody WR, Cassel DM, Sommer FG et al (1981) Dual-energy projection radiography: initial clinical experience. Am J Roentgenol 137:201–205

Buecker A, Katoh M, Krombach GA, Spuentrup E, Bruners P, Gunther RW, Niendorf T, Mahnken AH (2005) A feasibility study of contrast enhancement of acute myocardial infarction in multislice computed tomography: comparison with magnetic resonance imaging and gross morphology in pigs. Invest Radiol 40:700–704

Chang HJ, George RT, Schuleri KH et al (2009) Prospective electrocardiogram-gated delayed enhancement multidetector computed tomography accurately quantifies infarct size and reduces radiation exposure. JACC Cardiovasc Imaging 2:412–420

Chiro GD, Brooks RA, Kessler RM et al (1979) Tissue signatures with dual-energy computedtomography. Radiology 131:521–523

Choe YH, Choo KS, Jeon E-S, Gwon H-C, Choi J-H, Park J-E (2008) Comparison of MDCT and MRI in the detection and sizing of acute and chronic myocardial infarcts. Eur J Radiol 66:292–299

Choi KM, Kim RJ, Gubernikoff G, Vargas JD, Parker M, Judd RM (2001) Transmural extent of acute myocardial infarction predicts long-term improvement in contractile function. Circulation 104:1101–1107

Dendale P, Franken PR, Holman E, Avenarius J, van der Wall EE, de Roos A (1998) Validation of low-dose dobutamine magnetic resonance imaging for assessment of myocardial viability after infarction by serial imaging. Am J Cardiol 82:375–377

Deseive S, Bauer RW, Lehmann R, Kettner M, Kaiser C, Korkusuz H, Tandi C, Theisen A, Schächinger V, Schoepf UJ, Vogl TJ, Kerl JM (2011) Dual-energy computed tomography for the detection of late enhancement in reperfused chronic infarction: a comparison to magnetic resonance imaging and histopathology in a porcine model. Invest Radiol 46(7):450–456

Doherty PW, Lipton MJ, Berninger WH, Skioldebrand CG, Carlsson E, Redington RW (1981) Detection and quantitation of myocardial infarction in vivo using transmission computed tomography. Circulation 63:597–606

Fieno DS, Kim RJ, Chen EL, Lomasney JW, Klocke FJ, Judd RM (2000) Contrast-enhanced magnetic resonance imaging of myocardium at risk: distinction between reversible and irreversible injury throughout infarct healing. J Am Coll Cardiol 36:1985–1991

Genant HK, Boyd D (1977) Quantitative bone mineral analysis using dual energy computed tomography. Invest Radiol 12:545–551

Georgiou D, Bleiweis M, Brundage BH (1992) Conventional and ultrafast computed tomography in the detection of viable versus infarcted myocardium. Am J Card Imaging 6:228–236

Gerber BL, Belge B, Legros GJ et al (2006) Characterization of acute and chronic myocardial infarcts by multidetector computed

tomography: comparison with contrast-enhanced magnetic resonance. Circulation 113:823–833
Goetti R, Feuchtner G, Stolzmann P, Donati OF, Wieser M, Plass A, Frauenfelder T, Leschka S, Alkadhi H (2011) Delayed enhancement imaging of myocardial viability: low-dose high-pitch CT versus MRI. Eur Radiol 21(10):2091–2099
Gray WR, Buja LM, Hagler HK, Parkey RW, Willerson JT (1978) Computed tomography for localization and sizing of experimental acute myocardial infarcts. Circulation 58:497–504
Habis M, Capderou A, Sigal-Cinqualbre A et al (2009) Comparison of delayed enhancement patterns on multislice computed tomography immediately after coronary angiography and cardiac magnetic resonance imaging in acute myocardial infarction. Heart 95:624–629
Higgins CB, Sovak M, Schmidt W, Siemers PT (1978) Uptake of contrast materials by experimental acute myocardial infarctions: a preliminary report. Invest Radiol 23(Suppl):S271–S274
Hoffmann U, Millea R, Enzweiler C, Ferencik M, Gulick S, Titus J, Achenbach S, Kwait D, Sosnovik D, Brady TJ (2004) Acute myocardial infarction: contrast-enhanced multi-detector row CT in a porcine model. Radiology 231(3):697–701
Jacquier A, Boussel L, Amabile N et al (2008) Multidetector computed tomography in reperfused acute myocardial infarction: assessment of infarct size and noreflow in comparison with cardiac magnetic resonance imaging. Invest Radiol 43:773–781
Jennings RB, Schaper J, Hill ML, Steenbergen CJ, Reimer KA (1985) Effect of reperfusion late in the phase of reversible ischemic injury. Changes in cell volume, electrolytes, metabolites, and ultrastructure. Circ Res 56:262–278
Jennings RB, Murry CE, Steenbergen CJ, Reimer KA (1990) Development of cell injury in sustained acute ischemia. Circulation 82 (3 Suppl):II2–12
Judd RM, Lugo-Olivieri CH, Arai M, Kondo T, Croisille P, Lima JA, Mohan V, Becker LC, Zerhouni EA (1995) Physiological basis of myocardial contrast enhancement in fast magnetic resonance images of 2-day-old reperfused canine infarcts. Circulation 92:1902–1910
Kalender WA, Perman WH, Vetter JR, Klotz E (1986) Evaluation of a proto-type dual-energy computed tomographic apparatus. I. Phantom studies. Med Phys 13:334–339
Kang DK, Schoepf UJ, Bastarrika G, Nance JW Jr, Abro JA, Ruzsics B (2010) Dual-energy computed tomography for integrative imaging of coronary artery disease: principles and clinical applications. Semin Ultrasound CT MR 31(4):276–291
Kim RJ, Fieno DS, Parrish TB, Harris K, Chen EL, Simonetti O, Bundy J, Finn JP, Klocke FJ, Judd RM (1999) Relationship of MRI delayed contrast enhancement to irreversible injury, infarct age, and contractile function. Circulation 100:1992–2002
Kim RJ, Wu E, Rafael A et al (2000) The use of contrast enhanced magnetic resonance imaging to identify reversible myocardial dysfunction. N Engl J Med 343:1445–1453
Kramer PH, Goldstein JA, Herkens RJ, Lipton MJ, Brundage BH (1984) Imaging of acute myocardial infarction in man with contrast-enhanced computed transmission tomography. Am Heart J 108:1514–1523
Lardo AC, Cordeiro MA, Silva C et al (2006) Contrast-enhanced multidetector computed tomography viability imaging after myocardial infarction: Characterization of myocyte death, microvascular obstruction, and chronic scar. Circulation 113:394–404
Mahnken AH, Koos R, Katoh M et al (2005) Assessment of myocardial viability in reperfused acute myocardial infarction using 16-slice computed tomography in comparison to magnetic resonance imaging. J Am Coll Cardiol 45:2042–2047
Mahnken AH, Bruners P, Mühlenbruch G et al (2007a) Low tube voltage improves computed tomography imaging of delayed myocardial contrast enhancement in an experimental acute myocardial infarction model. Invest Radiol 42:123–129
Mahnken AH, Bruners P, Kinzel S et al (2007b) Latephase MSCT in the different stages of myocardial infarction: animal experiments. Eur Radiol 17:2310–2317
Mahnken AH, Bruners P, Bornikoel CM, Guenther RW, Krämer N (2009) Assessment of myocardial edema by computed tomography in myocardial infarction. JACC Cardiovasc Imaging 2:1167–1174
Millner MR, McDavid WD, Waggener RG, Dennis MJ, Payne WH, Sank VJ (1979) Extraction of information from CT scans at different energies. Med Phys 6:70–71
Nieman K, Shapiro MD, Ferencik M et al (2008) Reperfused myocardial infarction: contrast-enhanced sixty-four-section CT in comparison to MR imaging. Radiology 247:49–56
Nikolaou K, Knez A, Sagmeister S et al (2004) Assessment of myocardial infarctions using multidetector- row computed tomography. J Comput Assist Tomogr 28:286–292
Nikolaou K, Sanz J, Poon M et al (2005) Assessment of myocardial perfusion and viability from routine contrast-enhanced 16-detector-row computed tomography of the heart: preliminary results. Eur Radiol 15:864–871
Ordovas KG, Higgins CB (2011) Delayed contrast enhancement on MR images of myocardium: past, present, future. Radiology 261(2):358–374
Paul J-F, Wartski M, Caussin C et al (2005) Late defect on delayed contrast-enhanced multi-detector row CT scans in the prediction of SPECT infarct size after reperfused acute myocardial infarction: initial experience. Radiology 236:485–489
Perazzolo Marra M, Lima JAC, Illiceto S (2011) MRI in acute myocardial infarction. Eur Heart J 32:284–293
Riederer SJ, Mistretta CA (1977) Selective iodine imaging using K-edge energies in computerized x-ray tomography. Med Phys 4:474–481
Rubinshtein R, Miller TD, Williamson EE et al (2009) Detection of myocardial infarction by dual-source coronary computed tomography angiography using quantitated myocardial scintigraphy as the reference standard. Heart 95:1419–1422
Ruzsics B, Surányi P, Kiss P, Brott BC, Singh SS, Litovsky S, Aban I, Lloyd SG, Simor T, Elgavish GA, Gupta H (2008) Automated multidetector computed tomography evaluation of subacutely infarcted myocardium. J Cardiovasc Comput Tomogr 2(1):26–32
Sandstede JJW, Bertsch G, Beer M, Kenn W, Werner E, Pabst T, Lipke C, Kretschmer S, Neubauer S, Hahn D (1999) Detection of myocardial viability by low-dose dobutamine cine MR imaging. Magn Reson Imaging 17:1437–1443
Sanz J, Weeks D, Nikolaou K, Sirol M, Rius T, Rajagopalan S, Dellegrottaglie S, Strobeck J, Fuster V, Poon M (2006) Detection of healed myocardial infarction with multidetector-row computed tomography and comparison with cardiac magnetic resonance delayed hyperenhancement. Am J Cardiol 98:149–155
Sato A, Nozato T, Hikita H, Akiyama D, Nishina H, Hoshi T, Aihara H, Kakefuda Y, Watabe H, Hiroe M, Aonuma K (2012) Prognostic value of myocardial contrast delayed enhancement with 64-slice multidetector computed tomography after acute myocardial infarction. J Am Coll Cardiol 59(8):730–738
Shapiro MD, Sarwar A, Nieman K, Nasir K, Brady TJ, Cury RC (2010) Cardiac computed tomography for prediction of myocardial viability after reperfused acute myocardial infarction. J Cardiovasc Comput Tomogr 4:267–273
Varga-Szemes A, Ruzsics B, Kirschner R, Singh SP, Kiss P, Brott BC, Simor T, Elgavish A, Elgavish GA (2012) Determination of infarct size in ex vivo swine hearts by multidetector computed tomography using gadolinium as contrast medium. Invest Radiol 47(5):277–283

Wellnhofer E, Olariu A, Klein C, Grafe M, Wahl A, Fleck E, Nagel E (2004) Magnetic resonance low-dose dobutamine test is superior to scar quantification for the prediction of functional recovery. Circulation 109:2172–2174

Wesbey GE, Higgins CB, McNamara MT et al (1984) Effect of gadolinium-DTPA on the magnetic relaxation times of normal and infarcted myocardium. Radiology 153:165–169

Wu KC, Zerhouni EA, Judd RM, Lugo-Olivieri CH, Barouch LA, Schulman SP, Blumenthal RS, Lima JA (1998) Prognostic significance of microvascular obstruction by magnetic resonance imaging in patients with acute myocardial infarction. Circulation 97:765–772

Zhang LJ, Peng J, Wu SY, Yeh BM, Zhou CS, Lu GM (2010) Dual source dual-energy computed tomography of acute myocardial infarction: correlation with histopathologic findings in a canine model. Invest Radiol 45(6):290–297

Part V
Clinical Implementation

CT Myocardial Perfusion Imaging: Clinical Implementation

Yeon Hyeon Choe

Contents

Abstract

Despite advances, diagnosis of coronary artery diseases with coronary CT angiography (CCTA) is still hampered by artifacts from coronary artery calcium, stents, and cardiac motion. Recent CT techniques have enabled stress myocardial perfusion assessment in patients with ischemic heart diseases. Stress perfusion CT and CCTA can provide information on coronary artery anatomy and flow-limiting stenosis. CT perfusion information enhances the diagnostic accuracy of CCTA and may help to identify lesions appropriate for coronary intervention. CT perfusion is a potential economic alternative of other functional studies currently used in the evaluation of ischemic heart diseases.

Abbreviations

CAD	Coronary artery disease
CTP	CT stress myocardial perfusion
CCTA	Coronary CT angiography
FFR	Fractional flow reserve
ICA	Invasive coronary angiography
MBF	Myocardial blood flow
MDCT	Multidetector CT
MPS	Myocardial perfusion scintigraphy or SPECT
MRP	MRI stress myocardial perfusion
MDCT	Multidetector CT
MI	Myocardial infarction
NPV	Negative predictive value
PCI	Percutaneous coronary intervention
PPV	Positive predictive value

Y. H. Choe (✉)
Department of Radiology and Cardiovascular Imaging Center, Samsung Medical Center, Sungkyunkwan University School of Medicine, Seoul, Korea
e-mail: yhchoe@skku.edu

U. J. Schoepf et al. (eds.), *CT Imaging of Myocardial Perfusion and Viability*, Medical Radiology. Diagnostic Imaging,
DOI: 10.1007/174_2012_769, © Springer-Verlag Berlin Heidelberg 2012
Published Online: 17 November 2012

1 Introduction

Recently, there have been remarkable improvements in cardiac computed tomography (CT) technologies. The use of area-detector CT scanners (256-slice and 320-slice MDCT) and 128-slice dual-source scanners has decreased radiation dose to 0.5 mSv for coronary artery imaging. A meta-analysis of nine high quality trials has defined the diagnostic characteristics of coronary CT angiography using invasive coronary angiography as the gold standard. This study found that for the detection of coronary atherosclerotic plaques coronary CT angiography had a sensitivity of 96 % (95 % CI: 93–98 %) specificity of 86 % (95 % CI: 83–89 %), positive likelihood ratio of 6.38 (95 % CI: 5.18–7.87), and negative likelihood ratio of 0.06 (95 % CI: 0.03–0.10) (Gorenoi et al. 2012). However, the image quality in cardiac MDCT is degraded in patients with tachycardia or arrhythmia. Prior studies have shown that diagnostic image quality is typically obtained in 88–100 % of coronary artery segments (Hamon et al. 2007). The causes of image degradation include cardiac and respiratory motion artifacts, misregistration artifacts, blooming artifacts from heavy calcifications and stents, streak artifacts from contrast materials, and poor contrast enhancement. Although the spatial resolution of cardiac CT is improving with the adoption of new detectors, blooming artifacts still occurs. Therefore, the diagnostic capability of CCTA in the detection of significant coronary artery disease (CAD) is suboptimal in some clinical scenarios. Furthermore, the detection of CAD alone is not enough. The physiological significance of CT-detected intermediate-stenosis lesions may not be clear; clinicians favor the use of additional functional studies (e.g., exercise tests, stress nuclear studies, and stress perfusion MR imaging) in such cases. The detection of myocardial perfusion deficits using resting-state CCTA is rarely feasible in cases with severe coronary stenosis. Since knowledge of the extent and severity of inducible myocardial ischemia is critical for selecting an effective treatment strategy for patients with suspected ischemic heart disease, it would be ideal if an imaging modality could simultaneously visualize coronary anatomy and provide information on myocardial perfusion.

Coronary flow velocity reserve and fractional flow reserve (FFR) are indices of clinical decision-making with respect to percutaneous coronary interventions (PCIs). However, FFR is influenced by conditions that affect hyperemic microvascular resistance and additionally lacks the theoretical solid foundation to be a gold standard. Invasive stenosis assessment will most likely be replaced by methods that directly measure actual perfusion, such as MRI perfusion imaging (MRP) (van de Hoef et al. 2012).

2 Patient Selection for Coronary CT Angiography Based on Pretest Probability of Coronary Artery Disease

Cardiac CT is considered appropriate in patients with low-to-intermediate pretest probability of CAD (Taylor et al. 2010). In these patients, the role of CT is to exclude significant CAD. Due to the high specificity of CCTA, negative results for CAD are generally reliable; however, CCTA may not be accurate in ruling out significant CAD in patients with intermediate stenotic lesions by CCTA.

Percutaneous coronary intervention of a functionally insignificant stenotic lesion increases the chance of an adverse event, such as stent thrombosis and restenosis, as well as subsequent repeat revascularization, myocardial infarction (MI), or death. The increased risk of adverse events in such a situation clearly exceeds the low risk associated with a hemodynamically insignificant stenosis without stent placement (Lindstaedt and Mugge 2011).

Angiography is inaccurate in assessing the functional significance of a coronary stenosis when compared with the FFR, not only in lesions with 50–70 % stenosis, but also in lesions with 70–90 % angiographic stenosis (Tonino et al. 2010). According to the FFR versus angiography in multivessel evaluation (FAME) study, in 50–70 % stenosis category, 35 % of stenoses were functionally significant (FFR $\leq$ 0.80). In the 71–90 % stenosis category, 80 % were functionally significant. Therefore, the decision to revascularize a coronary artery stenosis should be guided by evidence of myocardial ischemia (Tonino et al. 2010). According to the FAME study's follow-up results (Pijls et al. 2010), in 1,005 patients with multivessel CAD, the FFR-guided group received fewer stents than the angiography-guided group (2.7 $\pm$ 1.2 vs. 1.9 $\pm$ 1.3; $P < 0.001$) and experienced lower 2-year mortality rates and lower rates of MI (12.9 vs. 8.4 %). For lesions deferred on the basis of FFR >0.80, the rate of MI was 0.2 % after 2 years, and the rate of revascularization was 3.2 %.

The DEFER study demonstrated excellent 5-year outcomes after deferral of PCI for intermediate coronary stenoses based on an FFR-guided treatment strategy (Pijls et al. 2007). In 325 patients with an intermediate stenosis, FFR was measured just before the planned intervention. If FFR was $\geq$0.75, patients were randomly assigned to deferral ($n = 91$) or performance ($n = 90$) of PCI. The composite rate of cardiac death and acute MI was 3.3 and 7.9 %, respectively ($P = 0.21$).

Although, noninvasive cardiac stress imaging may help to determine the significance of a coronary artery lesion when there is single-vessel disease, these techniques have limitations in identifying the hemodynamic significance of

individual stenoses in patients with multivessel CAD (Lindstaedt and Mugge 2011). Reported sensitivities and specificities of stress echocardiography are 53–93 % and 70–100 %, respectively, under study conditions (Fox et al. 2006). The reported sensitivity of myocardial perfusion scintigraphy (MPS) ranges 70–98 %, but specificity only reaches 40–90 % (Fox et al. 2006). Myocardial perfusion imaging with single-photon emission computed tomography (SPECT) has poor concordance with FFR and tends to underestimate or overestimate the functional importance of coronary stenosis seen with angiography in comparison with FFR in patients with multivessel disease. These findings have important consequences in using MPS to determine the optimal revascularization strategy in patients with multivessel coronary disease. Compared to FFR, MPS underestimates the number of ischemic territories in 36 % of patients with multivessel disease (Melikian et al. 2010).

Adenosine-stress MRP is an accepted noninvasive test for the detection of myocardial ischemia (Schwitter et al. 2012). However, MRP is sometimes unable to differentiate subtle ischemia from artifacts (Hamon et al. 2010). The number of slices is also limited in MRP.

Recently, computational flow analysis of coronary CT data has become available for clinical applications (Koo et al. 2011). The results were comparable to those of FFR with catheterization. However, this process takes a supercomputer many hours to obtain the results, which are thus not immediately available after each CT examination. On a per-vessel basis, the accuracy, sensitivity, specificity, positive predictive value (PPV), and negative predictive value (NPV) for FFRCT were 84.3, 87.9, 82.2, 73.9, and 92.2 %, respectively, and for CCTA were 58.5, 91.4, 39.6, 46.5, and 88.9 %, respectively. The area under the receiver operator characteristics curve was 0.90 for FFRCT and 0.75 for CCTA ($P = 0.001$). The FFRCT and FFR results correlated well ($r = 0.717$, $P < 0.001$) with a slight underestimation by FFRCT (0.022 ± 0.116, $P = 0.016$).

In patients with CT-detected CAD with an intermediate degree of stenosis, diagnostic imaging should be used to guide further treatment. In this regard, stress myocardial perfusion imaging may be useful. FFR is invasive and time-consuming, and sometimes elevated despite an apparent tight stenosis (Pijls and Sels 2012). Adenosine-stress myocardial perfusion CT (CTP) is a beneficial modality because information on myocardial perfusion status is provided in addition to coronary artery anatomical information (Figs. 1, 2, 3, 4, 5, 6, 7). Therefore, CTP may also be useful in patients with intermediate-to-high pretest probability of CAD. CTP further helps to determine hemodynamic significance of morphologically significant stenosis (Bamberg et al. 2011) (Fig. 5).

The targets of adenosine CTP can be heavily calcified lesions, coronary artery stents, or multiple lesions with moderate to severe stenosis. In patients with small branch stenosis or occlusion, it may be difficult to assess the degree of stenosis of the involved vessel segments by CCTA. However, CTP may perform better in identifying perfusion abnormalities than CCTA, providing better detection of small branch lesions (Fig. 3). Therefore, CTP provides incremental values to the diagnostic accuracy of CCTA, beyond exclusion of significant CAD; patient-specific stenosis can be assessed for lesion-specific ischemia (Koo et al. 2011). In this way, the CTP technique may expand the clinical indications for CCTA.

3 MRI Perfusion and Coronary CT Angiography: Insights from the Combined Approach

According to a meta-analysis (Hamon et al. 2010), the overall patient-based analysis of stress myocardial perfusion MRI demonstrated a sensitivity of 89 % (95 % CI: 88–91 %) and a specificity of 80 % (95 % CI: 78–83 %). Stress perfusion MRI is highly sensitive for detection of CAD, but its specificity remains moderate.

MR-IMPACT II study showed that the sensitivity of MRP to detect CAD was superior to SPECT, while its specificity was inferior to SPECT (Schwitter et al. 2012). For MRI and SPECT, the sensitivity scores were 67 and 59 %, respectively, while the specificity scores for MRI and SPECT were 61 and 72 %, respectively.

MRI can be used to detect flow-limiting CAD as defined by FFR, using both visual and quantitative analyses. The sensitivity and specificity of visual MRP analysis to detect stenoses at a threshold FFR of <0.75 were 82 and 94 % ($P < 0.0001$), respectively, with an area under the receiver-operator characteristic curve of 0.92 ($P < 0.0001$) (Lockie et al. 2011). In the vessels interrogated with FFR, CCTA had a sensitivity, specificity, PPV, and NPV of 93, 60, 68, and 90 %, respectively (Ko et al. 2012a). Quantitative cross-sectional parameters of the coronary lesions derived from 64-slice CCTA are significantly correlated with functional assessment by invasively determined FFR (Kristensen et al. 2010). According to a study of 42 patients, the optimal cut-off value to predict an abnormal FFR (<0.75) was 73 % for area stenosis of CCTA (sensitivity 90 %, specificity 80 %, PPV 50 %, and NPV 97 %) and 56 % for diameter stenosis of CCTA (sensitivity 80 %, specificity 67 %, PPV 35 %, and NPV 94 %), respectively (Kristensen et al. 2010). A CCTA minimal lumen diameter cut-off value of 1.2 mm had a sensitivity of 70 % and

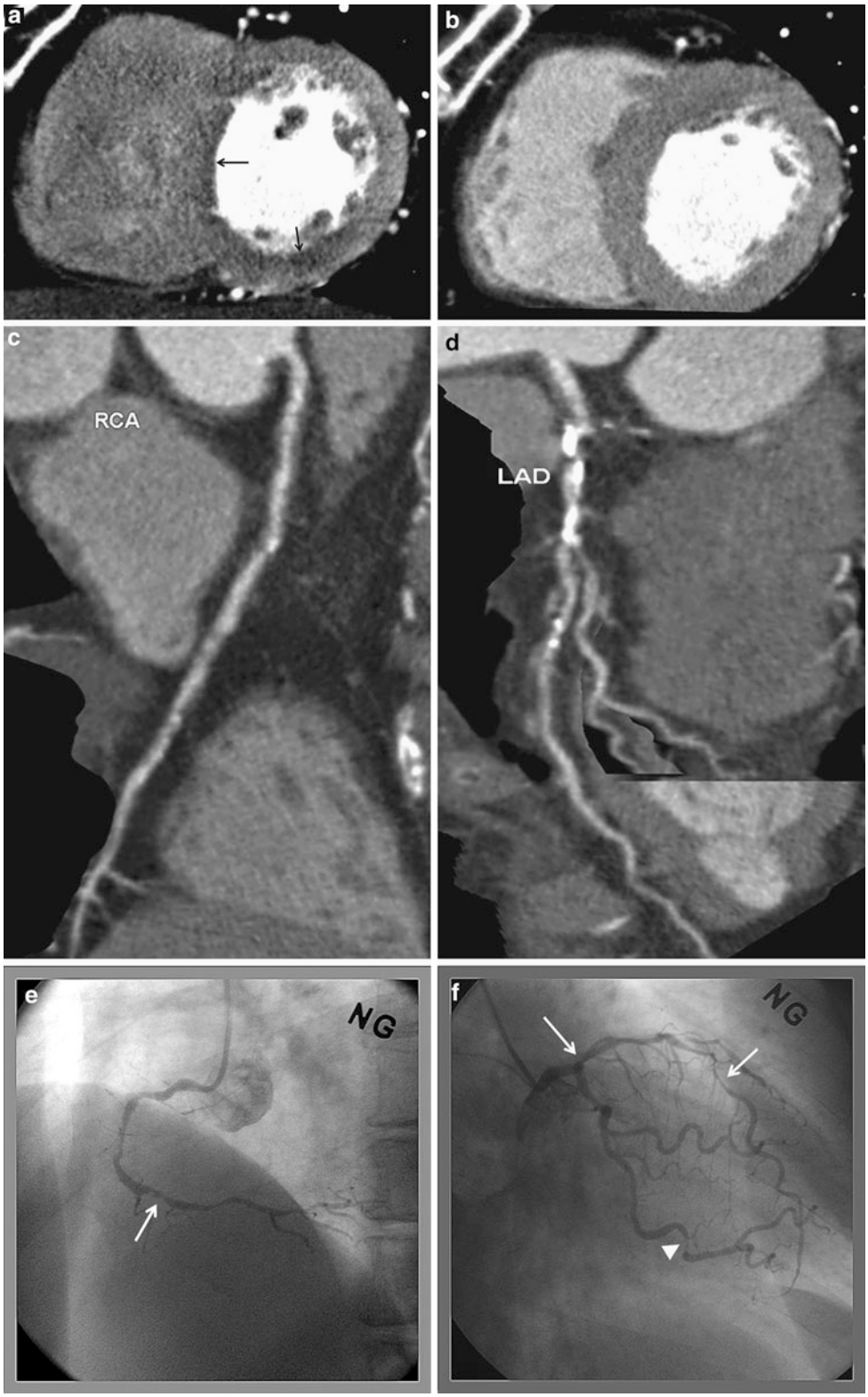

Fig. 1 A 72-year-old female with unstable angina. **a** Adenosine-stress 64-slice multidetector CT shows subendocardial perfusion defects in the septum and inferior wall (*arrows*). **b** Rest image shows no perfusion abnormalities. **c**, **d** Curved multiplanar reconstruction images show multiple stenoses in the right coronary artery (RCA) and calcifications in proximal-to-mid left anterior descending branch (LAD). **e**, **f** Catheter coronary angiography revealed focal tight stenosis in distal RCA (*arrow*), severe stenosis in proximal-to-mid LAD (*arrows*) and obtuse marginal branch (*arrowhead*)

specificity of 72 %, while a CCTA minimal lumen area cut-off value of 2 mm^2 had a sensitivity of 80 % and specificity of 78 %. According to a CCTA-FFR comparison study, 25.5 % (12/47) of lesions with 50–69 % stenosis severity by CCTA caused ischemia, as determined by an FFR $\leq$0.80 (Koo et al. 2011).

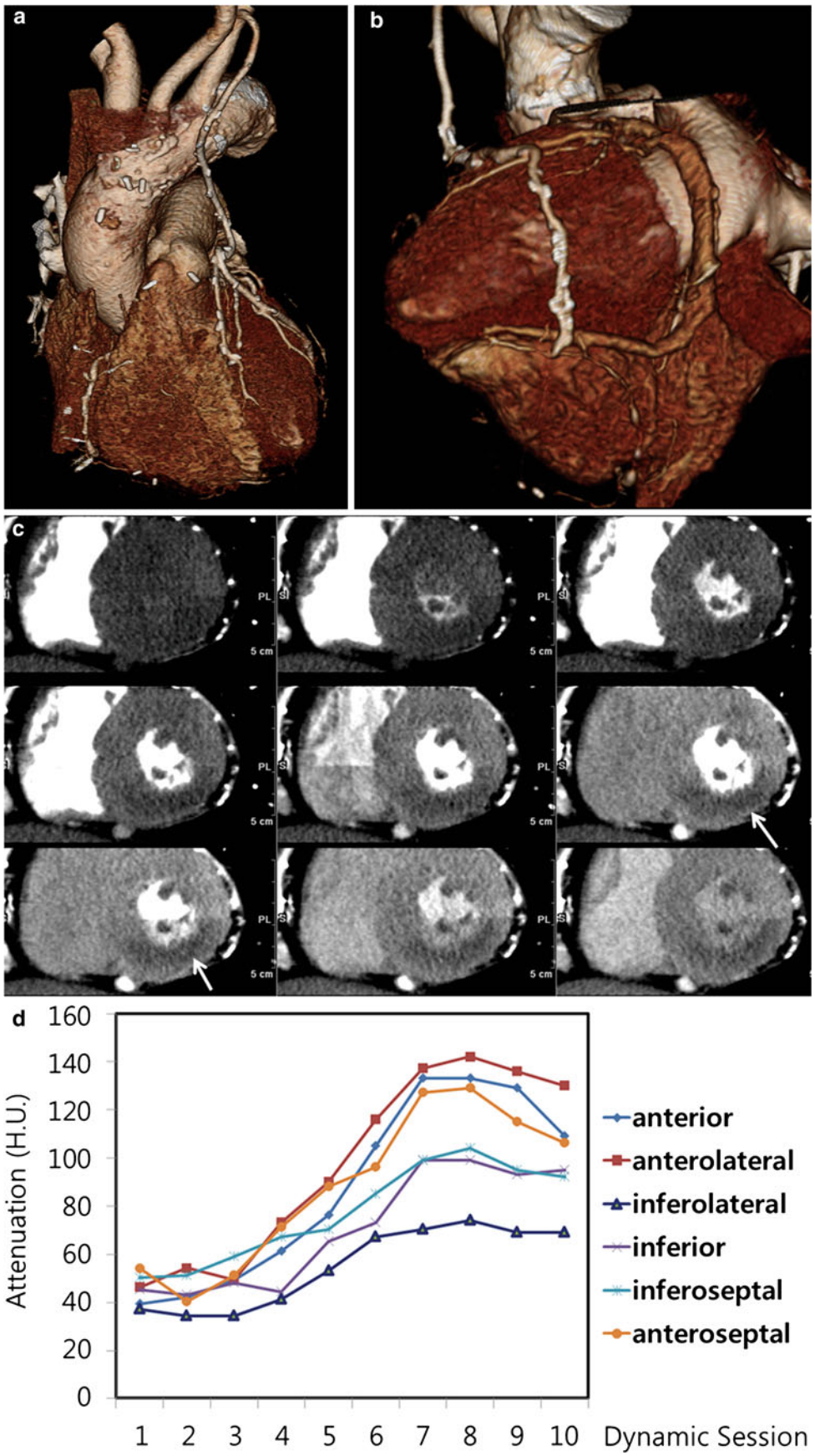

Fig. 2 Silent ischemia in 67-year-old male with coronary bypass grafts. **a**, **b** Coronary bypass grafts are seen patent with good anastomosis. **c** However, stress dynamic perfusion CT shows perfusion defects (*arrows*) in inferior wall without myocardium thinning. **d** Time-attenuation curve shows significant attenuation difference between anterior and inferolateral walls of the left ventricle

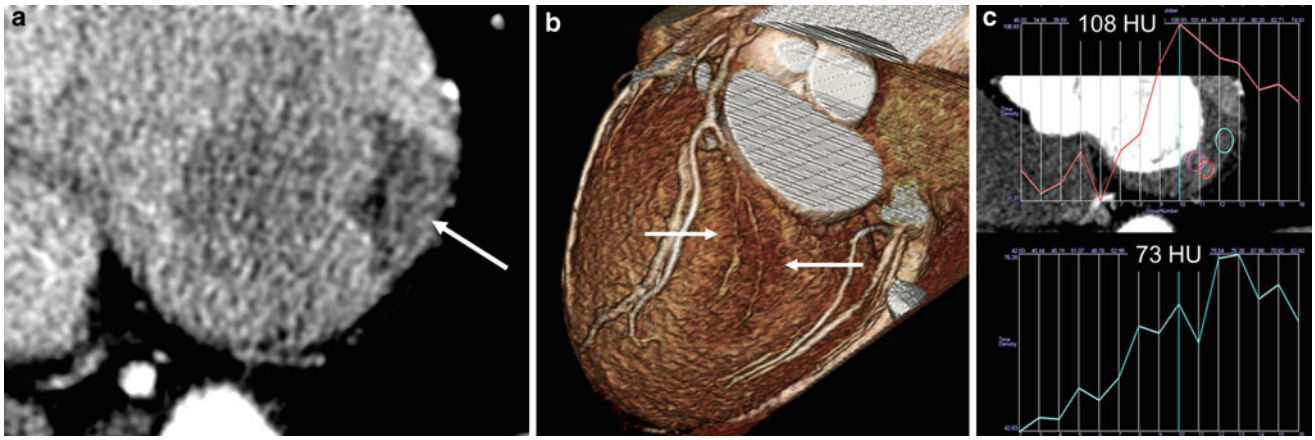

Fig. 3 Dynamic scan helps to diagnose a small branch lesion (silent ischemia in a 74-year-old male). **a** In this asymptomatic male with vascular occlusive disease, there was clearly visible myocardial ischemia in the basal inferolateral wall (*arrow*) due to occlusion of distal circumflex and obtuse marginal branches. **b** The small branch occlusion was overlooked on CT analysis, initially. In retrospect, volume-rendered image also showed evidence of ischemia with a *darker color* (*arrows*). **c** The peak attenuation number in the perfusion defect was 73 HU and that of normal area was 108 HU

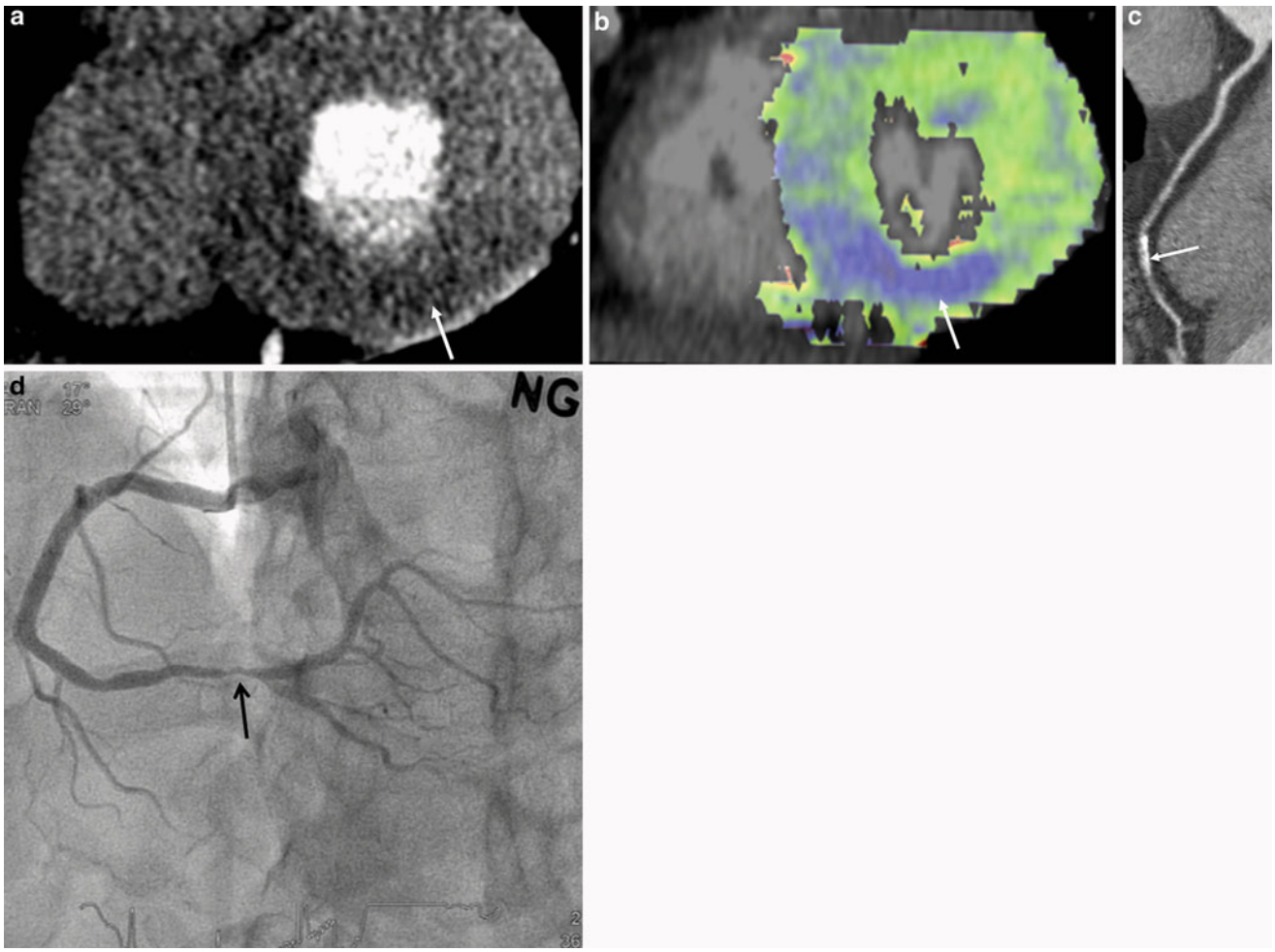

Fig. 4 A 55-year-old male with chest pain. **a**, **b** Short-axis reformatted stress perfusion CT (**a**) and flow map image (**b**) show decreased perfusion (*arrow*) in inferior wall. Myocardial blood flow measured 40–47 mL · 100 mg^{-1} min^{-1} in inferior wall and 86 mL · 100 mg^{-1} min^{-1} in normal myocardium. **c** Curved planar reformatted image shows calcifications in the distal right coronary artery. The degree of stenosis was uncertain. **d** Catheter angiogram shows severe stenosis (*arrow*) in distal right coronary artery

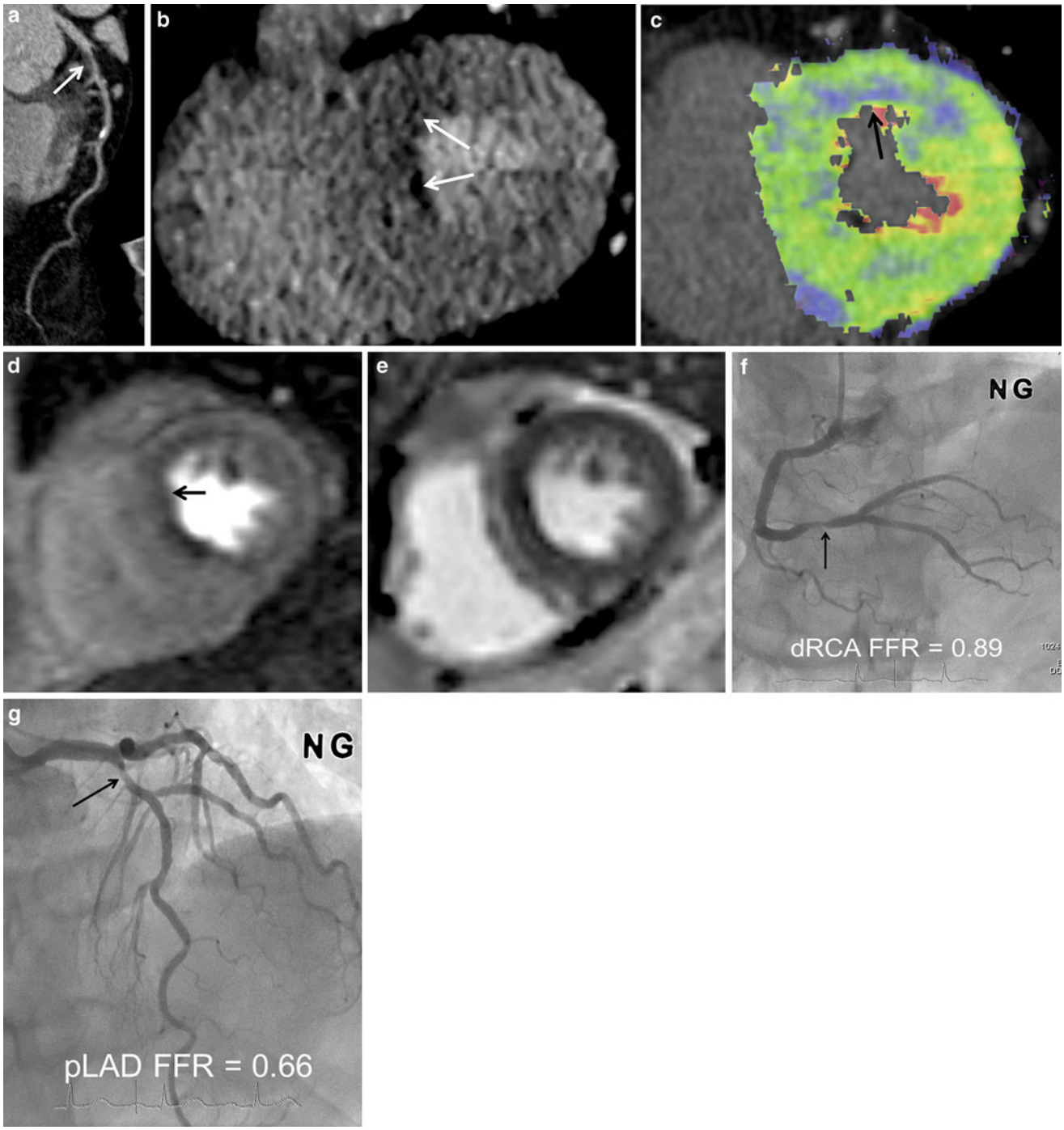

Fig. 5 A 74-year-old male with angina. **a** CT angiography shows intermediate degree stenosis (*arrow*) in the proximal left anterior descending branch (LAD) due to soft plaques. **b–e** CT perfusion reformatted images (**b**) and flow map images (**c**) show subendocardial perfusion defects (*arrows*) in anteroseptal wall. Myocardial blood flow measured 42 mL · 100 mg^{-1} min^{-1} in anteroseptal wall and 113 mL · 100 mg^{-1} min^{-1} in normal area. Stress MR perfusion image (**d**) shows perfusion defects (*arrow*) in the same region. There was no evidence of old myocardial infarction on late gadolinium-enhanced MR images (**e**). **f**, **g** Adenosine fractional flow reserve was 0.89 in distal right coronary artery (**f**) and 0.66 in proximal LAD (**g**). Percutaneous coronary intervention was performed in LAD only

According to Kirschbaum et al. (2011), MRP contributes significantly to the detection of functional significant lesions in patients with a positive CCTA. MRP and coronary flow reserve (CFR) were performed in 50 patients with significant CAD by CCTA. MRP showed reduced perfusion in 32 patients (64 %), and this finding was confirmed by CFR in

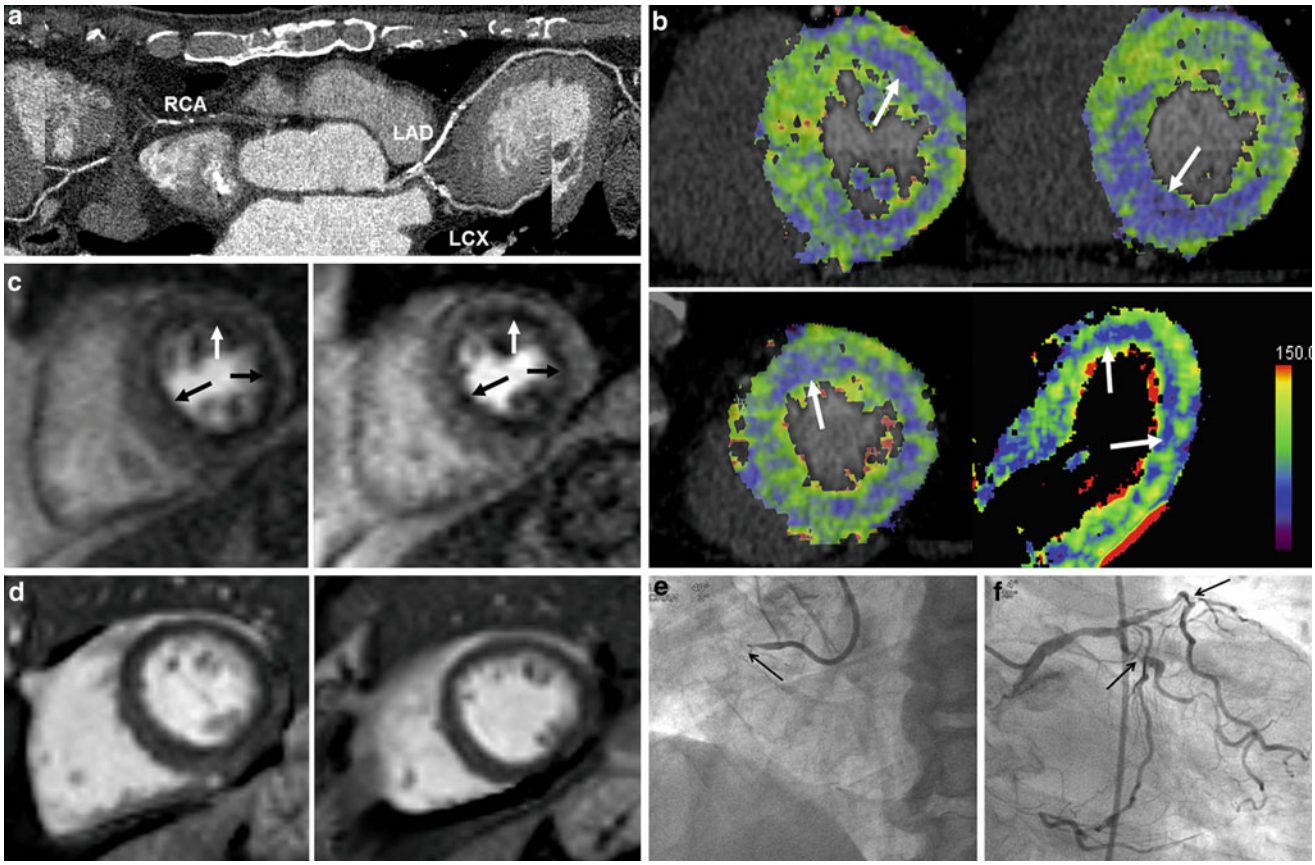

Fig. 6 Three-vessel disease with multisegment perfusion defects (70-year-old male with chest pain). **a** CT angiography shows dense calcifications in left main coronary artery, left anterior descending branch (LAD), circumflex artery (LCX), and occlusion in right coronary artery (RCA). **b** CT perfusion flow maps show decreased perfusion (*arrows*) in three-vessel territories. Myocardial blood flow measured 43–68 mL · 100 mg^{-1} min^{-1} in the areas with decreased perfusion. **c** Stress MRI perfusion shows subendocardial perfusion defects (*arrows*) in three-vessel territories. **d** Late gadolinium-enhanced MR images show no evidence of myocardial infarction. **e**, **f** Catheter angiography shows occlusion of proximal right coronary artery (*arrow*) (**e**) and severe stenosis in proximal segments of left anterior descending branch and circumflex artery (*arrows*) (**f**)

27 (84 %). All 18 cases of normal MRP (36 %) were confirmed by CFR. Of the 50 patients, 20 (40 %) had multivessel disease, with MRP showing a reduced perfusion index (MPRI < 2.0) in multiple perfusion territories in 15 patients. In the remaining five patients, multivessel disease was ruled out, which was confirmed by CFR. Pretest probability of a reduced CFR in patients with a positive CCTA was 54 % (27/50). The posttest probability after MRP was 84 %. The investigators of this study proposed an algorithm with CCTA as a first-line diagnostic test followed by MRP in patients with a positive CCTA.

In a study by van Werkhoven et al. (2010), normal perfusion on MRI was observed in 33 % (5/15) of patients with significant obstructive CAD on CCTA. The majority of patients (83 %) were presented with an intermediate pretest likelihood of CAD. In all patients without significant stenosis on CCTA and normal perfusion on MRI ($n = 29$), significant stenosis was absent on invasive coronary angiography (ICA). All patients with abnormalities on both CCTA and MRI ($n = 10$) had significant stenoses on ICA. The anatomical and functional data obtained with CCTA and MRI is complementary for the assessment of CAD. These findings support the sequential or combined assessment of anatomy and function (van Werkhoven et al. 2010).

According to Groothuis et al. (2010), the combination of both techniques enabled the clinician to evaluate both the morphology and functional relevance of CAD—comprehensively and noninvasively. Of patients without CAD on CCTA, 90.5 % (57 of 63; 95 % CI: 82.6–95.0 %) had normal myocardial perfusion on MRP. Myocardial ischemia was detected by MRP in 42.3 % (22 of 52; 95 % CI: 29.5–56 %) of patients with obstructive CAD on CCTA. Thus, CCTA can reliably rule out CAD, but detection of hemodynamically significant CAD is limited. In patients with known CAD, myocardial perfusion imaging may be more appropriate than CCTA as a first-line technique. SPECT is the modality most commonly used to assess myocardial perfusion; however, due to the increased

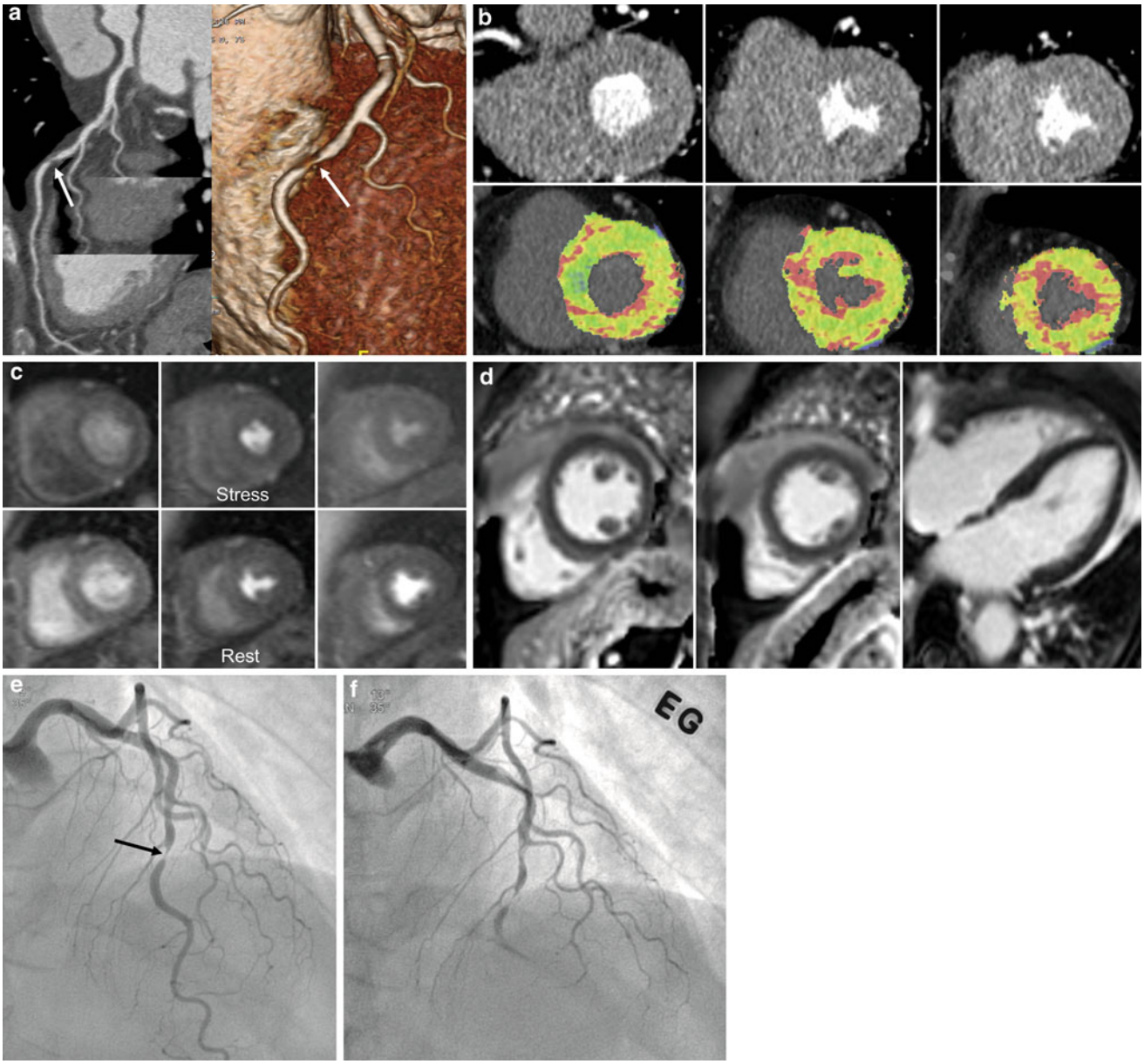

Fig. 7 A case with anatomy-physiology discrepancy (55-year-old female with chest pain). **a** CT angiography shows focal significant stenosis (*arrows*) in mid-left anterior descending branch (LAD). **b** CT perfusion reformatted and flow map images show no evidence of myocardial ischemia during stress. Myocardial blood flow measured 128 mL · 100 mg^{-1} min^{-1} overall. **c** There was no evidence of significant perfusion defects on stress and rest perfusion MR images. **d** Late gadolinium-enhanced images show no myocardial infarcts. **e**, **f** Catheter angiograms show a tight stenosis (*arrow*) in mid LAD (**e**) and spasm was induced in the LAD on intraarterial ergonovine injection (**f**)

radiation burden, SPECT might not be the ideal additional functional modality used along with CCTA to evaluate patients suspected of having CAD. According to a SPECT–CCTA comparison study by Schuijf et al. (2006), of 40 patients and 62 vessels with obstructive CAD at CCTA, SPECT findings were normal in 20 patients (50 %) and 38 vessel territories (61 %).

However, according to Scheffel et al. (2010), all tested combinations of low-dose CCTA and MRP, with or without late gadolinium enhancement, were unable to improve the diagnostic performance over that of low-dose CCTA alone. Using ICA as the gold standard, low-dose CCTA outperforms MRI with regard to sensitivity and NPV, whereas MRI is more specific and has a higher PPV than low-dose CCTA.

4 Clinical Results for Adenosine-Stress Myocardial Perfusion CT

Recent literature has shown the potential advantage of MDCT for CCTA during adenosine-stress (Bamberg et al. 2012; Bastarrika et al. 2010; Bettencourt et al. 2011; Cury et al. 2011; Feuchtner et al. 2011; George et al. 2009; Ho et al. 2010; Ko et al. 2011, 2012a, b; Nagao et al. 2011; Rocha-Filho et al. 2010; Ruzsics et al. 2009; Tamarappoo et al. 2010; Wang et al. 2012; Weininger et al. 2010) (Table 1). The feasibility of adenosine-stress CT has been documented by George et al. (2006) in an experimental animal model. According to Rocha-Filho et al. (2010), adenosine-stress perfusion imaging (single static scan) in addition to 64-slice dual-source CCTA demonstrated improved sensitivity, specificity, PPV, and NPV of CCTA for CAD diagnosis (83–91, 71–91, 66–86, and 87–93 %, respectively).

Feuchtner et al. (2011) used high-pitch stress perfusion CT (single scan) in 39 patients, yielding a per-vessel sensitivity of 96 % with 88 % specificity, 93 % PPV, and 94 % NPV in the detection of perfusion defects in comparison with cardiac MRI; the per segment sensitivity was 78 % with 87 % specificity, 83 % PPV, and 84 % NPV. In 25 patients with CAD, confirmed by ICA, the addition of CTP to CCTA improved accuracy from 84 to 95 % for the detection of stenosis >70 %.

Coronary CT angiography during adenosine infusion is possible with the use of an area-detector CT (256- or 320-slice CT). Ko et al. (2012a) compared CTP with FFR in 42 patients using a 320-detector row CT scanner and prospective electrocardiography (ECG)-gating for the detection of stenosis >50 %. FFR $\leq$ 0.8 was considered as an indication of significant ischemia. CTP imaging correctly identified 31 of 41 (76 %) ischemic territories and 38 of 45 (84 %) non-ischemic territories. Per-vessel territory sensitivity, specificity, PPV, and NPV of CTP were 76, 84, 82, and 79 %, respectively. The combination of $\geq$50 % stenosis on CTA and a perfusion defect on CTP was 98 % specific for ischemia, while the presence of <50 % stenosis on CTA and normal perfusion on CTP was 100 % specific for exclusion of ischemia. Mean radiation for CTP and combined CT was 5.3 and 11.3 mSv, respectively.

Contemporary MDCT techniques enable dynamic acquisition of image data during adenosine-stress administration. According to Bamberg et al. (2010), data are acquired, alternating between two table positions, covering 73 mm during systolic phases for 30 s using 100 kVp. Radiation dose was 2.3 mSv for CCTA and 9.6 mSv for dynamic scanning. Ho et al. (2010) used this technique for myocardial perfusion imaging in 35 patients. There was a 1.5-fold difference between stress and rest myocardial blood flow (MBF) in normal tissue. In reversible defects, MBF was 0.65 $\pm$ 0.21 mL/mL/min and 0.63 $\pm$ 0.18 mL/mL/min at stress and rest, respectively. In comparison with nuclear myocardial perfusion imaging, the sensitivity, specificity, PPV, and NPV of CTP for identifying segments with perfusion defects was 83, 78, 79, and 82 %, respectively. The sensitivity, specificity, PPV, and NPV of CTP compared with ICA were 95, 65, 78, and 79 %, respectively.

According to Bamberg et al. (2011), the diagnostic accuracy of CCTA was low for the detection of hemodynamically significant stenosis (PPV per coronary segment, 49 %; 95 % CI: 36–60 %). With the use of estimated MBF to reclassify lesions depicted with CT angiography, 30 of 70 (43 %) coronary lesions were graded as hemodynamically insignificant, which significantly increased PPV to 78 % (95 % CI: 61–89 %; $P = 0.02$). The presence of a coronary artery stenosis with a corresponding MBF less than 75 mL/100 mL/min had a high risk for hemodynamic significance (odds ratio, 86.9; 95 % CI:17.6–430.4). In a pig model, in the ischemia group, MBF under stress was 74.0 $\pm$ 21.9 mL/100 mL/min in the post-stenotic myocardium and 117.4 $\pm$ 18.6 mL/100 mL/min in the remaining normal myocardium ($P = 0.0024$) (Mahnken et al. 2010). CTP is moderately accurate in identifying ischemia as assessed by FFR in patients considered for revascularization, while CCTA/CTP is highly accurate in the detection and exclusion of ischemia in territories where CCTA and CTP are concordant.

The results of Weininger et al. (2010) suggested the clinical feasibility of CTP in patients with acute chest pain. Compared to MRI and SPECT, dynamic real-time perfusion CT and first-pass dual-energy perfusion CT showed good agreement for the detection of myocardial perfusion defects.

Myocardial blood flow measured by CTP may predict functional recovery of the left ventricle after coronary bypass graft surgery (CABG) (Shikata et al. 2010). In a study on 19 patients who underwent CABG, MBF in revascularized areas increased significantly (pre-CABG 1.18 $\pm$ 0.45 mL $\cdot$ g^{-1} $\cdot$ min^{-1}, post-CABG 1.99 $\pm$ 0.66 mL $\cdot$ g^{-1} $\cdot$ min^{-1}, $P < 0.001$), whereas nonischemic areas showed no significant difference (1.79 $\pm$ 0.70 and 1.97 $\pm$ 0.46 mL $\cdot$ g^{-1} $\cdot$ min^{-1}, $P = 0.14$).

CTP may provide information on MI (Nakauchi et al. 2012) with better sensitivity than rest imaging. However, CTP has limitations in the detection of nonviable myocardial segments. Late or delayed CT at 7–10 min after injection of 100–120 mL of contrast material may help to detect nonviable hyperenhancing lesions of MI on the addition of radiation (Choe et al. 2008). Fat infiltration in the infarct may suggest the diagnosis of old MI without providing information on the depth of myocardial fibrosis. A profoundly low MBF value of dynamic CTP suggests the diagnosis of nonviable myocardium. The cutoff value may be around

Table 1 Diagnostic accuracy and radiation dose of combined coronary CT angiography and CT perfusion according to each scan protocol in the diagnosis of significant coronary artery stenosis with myocardial ischemia

Authors/year	Number of patients	Scanner type	Reference standard	Protocol	Diagnostic parameters (added value with CTP)				Radiation dose (mSV)		
					Sensitivity (%)	Specificity (%)	PPV (%)	NPV (%)	CTP	CCTA	Total
Bamberg et al. 2011	33	128 ds	ICA (≥50 %)	P-CCTA, D-CTP	91	69	79	85	10.0	3.1	13.1
			FFR (≤0.75)		93 (−7)	87 (36)	75 (28)	96.7 (−3.3)			
Wang et al. 2012	30	128 ds	ICA (≥50 %)	P-CCTA, D-CTP	90 (0)	81 (30)	58 (23)	97 (2)	11.5	4.0	15.5
			SPECT		85	92	55	98			
Feuchtner et al. 2011	39	128 ds	ICA (≥70 %) ($n = 25$)	H-CTP, H- or P-CCTA	100 (2)	74 (47)	97 (13)	100 (20)	1.1	1.9	3.0
			MRI (1.5T) ($n = 30$)		78	88	83	84			
Ko et al. 2012a	42	320 ss	FFR (≤0.8)	P-CTP, delay P-CCTA, rest P-CCTA	68 (−25)	98 (38)	97 (29)	77 (−23)	6.4	5.8	13.7
Blankstein et al. 2009	34	64 ds	ICA (≥50 %), SPECT	R-CTP, P-CCTA, delay P-CCTA	79	80	73	84	9.5	2.0	12.7
			ICA (≥70 %), SPECT		86	68	42	95			
Rocha-Filho et al. 2010	35	64 ds	ICA (≥50 %)	R-CTP, P-CCTA	91 (8)	91 (20)	86 (20)	93 (6)	9.8	2.0	11.8
			ICA (≥70 %)		91 (9)	78 (14)	53 (15)	97 (4)			
Bettencourt et al. 2011	90	64 ss	ICA (≥50 %)	R-CTP, P-CCTA	61 (−30)	97 (17)	87 (27)	88 (−8)	4.1	1.0	6.8
			ICA (≥70 %)		69 (−28)	96 (15)	78 (26)	94 (−5)			
Ko et al. 2011	41	64 ds	ICA (≥50 %) (n = 41)	R-CCTA, R-E	89	76	81	86	5.8	8.6	14.4
			MRI (1.5T) (n = 28)		89	78	74	91			
Ko et al. 2012b	45	64 ds	ICA (≥50 %)	R-CCTA, R-E	93.2 (1.4)	85.5 (17.8)	88.3 (14.7)	91.4 (3.9)	5.7	10.8	16.5

Note CCTA = coronary CT angiography, CTP = stress CT perfusion, D = dynamic scan, ds = dual-source, E = dual energy, FFR = fractional flow reserve, H = high-pitch, ICA = invasive coronary angiography, NPV = negative predictive value, P = prospective, PPV = positive predictive value, R = retrospective helical, S = static or single scan, SPECT = single-photon emission tomography, ss = single source

Diagnostic accuracy was based on per segment (comparison with MRI or SPECT) or per-vessel territory (comparison with ICA or FFR)

Radiation dose was described or corrected with conversion factor of 0.017 for the calculation of effective radiation dose in all studies

Total dose refers to the sum of the radiation doses of all CT scans including calcium score and late CT scan according to the protocol in each study

50 mL · 100 mg^{-1} min^{-1}. Fixed perfusion defects on stress and rest images are highly suggestive of MI.

Recent technology enables dual-energy application in cardiac imaging, although cardiac motion artifacts are still barriers in obtaining appropriate information on iodine distribution in ischemic myocardium. Dual-energy CT has demonstrated effective visualization of resting ischemia (Ruzsics et al. 2009). However, further research is necessary to validate the usefulness of dual-energy CT for the assessment of myocardial ischemia at rest and under stress.

5 Stress CT Myocardial Perfusion Protocol

A typical example of stress CT myocardial perfusion protocol is as follows (Fig. 8):

- Precontrast calcium scoring.
- Test bolus technique or bolus-tracking technique for timing of stress CT, unless using a fixed delay time of 4–6 s before the start of image acquisition after commencement of contrast injection.
- Adenosine infusion.
- Stress CT (single-phase or dynamic multiphase).
- Coronary CT angiography.
- Late CT (optional, 6–10 min delay).

The whole examination requires 25–30 min in our institution, if operated by skillful and experienced technologists. Adoption of a dynamic rest perfusion CT may not be recommended because of additional radiation.

6 Patient Preparation and Contraindications of CT Myocardial Perfusion

Stressors such as dipyridamole and adenosine have been used in the field of nuclear cardiac imaging. Dipyridamole blocks adenosine reuptake. Adenosine dilates coronary arteries by interaction with adenosine-A_2 receptor. The direct infusion of adenosine at the dose of 140 · μg · kg^{-1} min^{-1} using an infusion pump increases coronary flow velocity 4.4-fold (Verani 2000). Image acquisition begins 3–6 min after initiation of adenosine infusion. The plasma half-life of adenosine is 2–10 s. Regadenoson is an adenosine A (2A) receptor agonist approved for use as a pharmacologic stress agent for radionuclide myocardial perfusion imaging in patients unable to undergo adequate exercise stress. Regadenoson is easy to dose in a 10 s bolus and appears to be generally well tolerated, with most adverse events beginning soon after administration and resolving within approximately 15 min. No unexpected treatment-emergent ECG changes occurred with regadenoson in phase III trials (Garnock-Jones and Curran 2010).

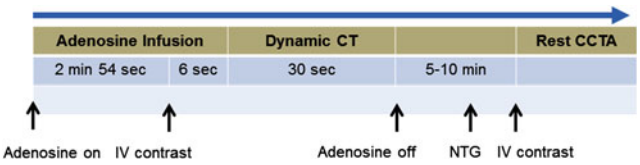

Fig. 8 A diagram of the CT perfusion protocol using a dynamic stress CT technique. *CCTA* coronary CT angiography, *IV* intravenous, *NTG* nitroglycerin

Patients must refrain from coffee, tea, chocolate, or any other source of caffeine for at least 24 h before the examination. Dipyridamole is discontinued for 24 h before CTP.

Contraindications of adenosine include:

- Asthma or active bronchospasm.
- Severe chronic obstructive pulmonary disease with rest hypoxia.
- Recent use of theophylline/caffeine.
- Advanced atrioventricular block.
- Severe hypotension.
- Sick sinus syndrome.
- Very early (within 2 days) after acute MI or unstable angina.

Adenosine is remarkably safe; while side effects occur in 80 % of patients with atrioventricular block in 8 % and ST-T change in 6 % (Verani 2000). Side effects resolve within 1–2 min after test completion. In case of severe reaction, 100 mg theophylline (aminophylline), an antagonist, is slowly injected intravenously and repeated for 2–3 min with a maximum dose of 300 mg.

It is advisable to monitor blood pressure, arterial oxygen level (pulse oxymeter), and ECG for myocardial ischemia and atrioventricular block during adenosine infusion. Three extremities are used. Intravenous routes are secured for adenosine infusion and contrast injection in each arm, respectively, and blood pressure is monitored in a lower extremity (calf). In the case of severe bradycardia associated with excessive adenosine infusion, aborting the dynamic CT scan should be considered.

7 Image Processing and Interpretation

The MMWP workstation (Siemens Medical Solutions, Erlangen, Germany) with Syngo VPCT body-myocardium (software) is one example of a commercial solution for image processing of dynamic perfusion data. Motion correction is performed after selecting a baseline image among those of the dynamic series; the more motion artifacts there are, the more myocardium that is lost. Then, myocardial segmentation is performed. The whole volume of the myocardium is included in the region-of-interest (ROI) for the segmentation process. Aortic attenuation is measured

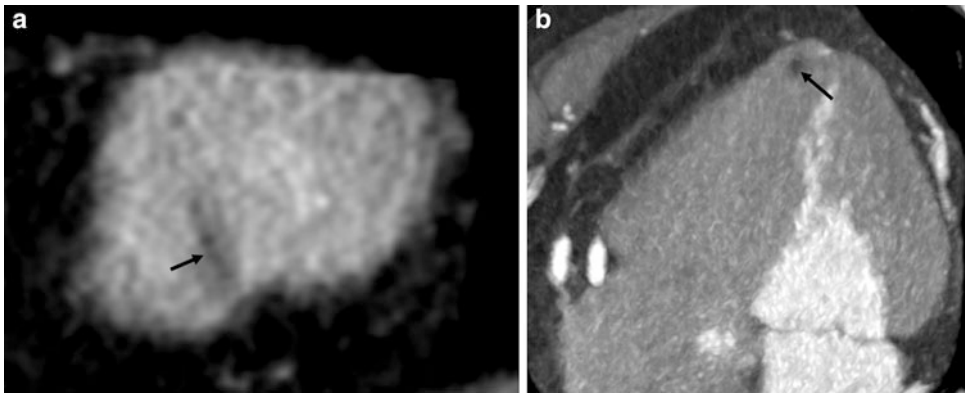

Fig. 9 A pitfall in image interpretation. **a** A focal area of nonspecific fat in apical myocardium mimics a perfusion defect on dynamic CT perfusion (*arrow*). **b** CT angiography image shows an area of fat (*arrow*) in the cardiac apex

for the calculation of the arterial input function. ROIs should be placed in the regions of normal and abnormal myocardium for the flow map analysis.

One should be careful when interpreting CTP in patients with significant motion artifacts, beam-hardening artifacts, anatomic variation, and nonspecific fat infiltration in the myocardium (Figs. 9, 10). Keep in mind that the basal interventricular septum and the mid-to-basal posterolateral wall show variable degrees of low attenuation or low MBF in normal subjects. Minimum intensity projection (MinIP) images with 3 mm thickness and diastolic images are better for depicting perfusion defects on reconstructed CT images (Ghoshhajra et al. 2011).

8 Radiation Dose

Recent CT techniques enable low-dose dynamic or static CTP. Adoption of automated dose modulation of X-ray tube current (and more recently, voltage) reduces the radiation dose received by patients during CT examination. In addition, iterative reconstruction methods permit further reductions of radiation dose. Currently, CTP delivers 1 mSv with low-dose high-pitch scanning, 10 mSv with dynamic scanning using a 128-slice dual-source CT scanner, and 5 mSv with a 320-slice area-detector CT, in addition to the dose associated with CCTA (Bamberg et al. 2010; Feuchtner et al. 2011; Ko et al. 2012a). Generally, static techniques for CTP deliver radiation doses to patients similar to those of CCTA.

Our results of dynamic CT perfusion from 330 consecutive patients showed maximum attenuation difference between normal and abnormal myocardium occurred at 12.0–24.3 s after initiation of contrast injection. The mean radiation dose of a dynamic stress scan was 12.1 ± 1.6 mSv (range, 9.2–16.4 mSv) with fixed tube current at 100 kVp, 7.7 ± 2.5 mSv (range, 3.3–16.1 mSv) with automatic tube current modulation, and 3.8 ± 1.3 mSv (range, 2.0–7.6 mSv) with automatic tube current modulation and half-duration (14 s) scan.

9 Cost Effectiveness of CT Perfusion

Between 20 and 25 % of patients can avoid invasive testing by undergoing functional testing as a gateway to angiography without substantial effects on outcomes (Sharples et al. 2007). Positive functional tests were confirmed by positive angiography in 83 % of SPECT patients, 89 % of MRI patients, and 84 % of stress echocardiography patients. In a randomized trial of 898 patients, negative functional tests were followed by positive angiograms in 31 % of SPECT patients, 52 % of MRI patients, and 48 % of stress echocardiography patients tested (Sharples et al. 2007).

Sixty-four-slice CT appears to be as good as, but cheaper than MPS for the diagnosis of CAD. Consequently, 64-slice CT is likely to be a cost-effective replacement for MPS in diagnosing CAD (Mowatt et al. 2008). Diagnostic strategies involving 64-slice CT seem to still require ICA for CT false-positives in terms of quantifying the degree of stenosis. Due to non-diagnostic CT images, approximately 3.6 % of the examined patients required a subsequent ICA (Gorenoi et al. 2012). The high specificity of 64-slice CT avoids the costs of unnecessary ICA in those who do not have CAD. The health-economics model using ICA as the reference standard showed that at a pretest probability for CAD of 50 % or lower, CCTA resulted in lower cost per patient with true positive diagnosis. At a pretest probability of CAD of 70 % or higher, ICA was associated with lower cost per patient with true positive diagnosis (Gorenoi et al. 2012). There is a trend of declining diagnostic cardiac catheterization, while the ratio of PCI over catheterization is increasing (Jones et al. 2011).

Using intracoronary pressure measurement as the reference standard, CCTA compared with ICA had a sensitivity of 80 % (95 % CI: 61–92 %) versus 67 % (95 % CI: 51–78 %), a specificity of 67 % (95 % CI: 47–83 %) versus 75 % (95 % CI: 60–86 %), an average positive likelihood ratio of 2.3 versus 2.6, and an average negative likelihood ratio of 0.3 versus 0.4, respectively (Gorenoi et al. 2012). From both a medical and a health-economics perspective,

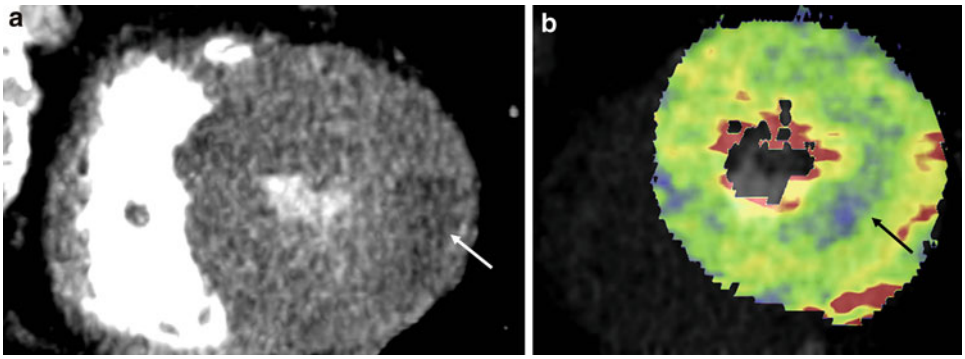

Fig. 10 Beam-hardening artifact. A band-like dark area (*arrow*) is due to beam-hardening artifacts from the highly attenuated descending thoracic aorta on a dynamic CT reformatted image (**a**) and color map image (**b**). Window width and level of the reformatted images were 229 and 77, respectively

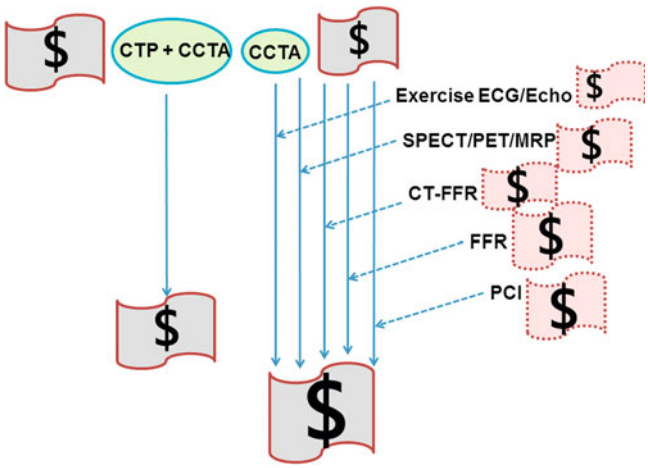

Fig. 11 A chart showing economic consideration using CT perfusion (CTP) and coronary CT angiography (CCTA) together. Expenses of an additional examination or examinations including exercise electrocardiography (ECG), exercise echocardiography (Echo), single-photon emission tomography (SPECT), positron emission tomography (PET), MRI perfusion (MRP), CT-fractional flow reserve (CT-FFR), FFR, and percutaneous coronary intervention (PCI) can be saved, if CTP and CCTA are performed together as a one-stop examination and provide relevant information on coronary artery disease

neither CCTA nor ICA may be recommended as the single diagnostic test for identifying or ruling out functionally relevant coronary stenoses (Gorenoi et al. 2012).

CTP (A) takes longer time than CCTA. It requires more personnel and it delivers a greater radiation and contrast material burden. However, its value may be equivalent to that of a combination of CCTA (B) with SPECT/PET or adenosine-stress perfusion MR imaging (C). Savings will be defined as the cost difference (B + A − C) (Fig. 11). Suppose that we have a patient with chest pain due to intermediate degree stenotic lesions in three vessels. If we can omit FFR (D) during catheterization because of having obtained information on coronary flow physiology, additional money can be saved. If we can differentiate hemodynamically significant lesions and not perform PCI on all intermediate lesions, we can achieve further savings (E). If CTP replaces diagnostic ICA (F), we can save money (F − A). If CTP replaces CT FFR (G), again, we can save money (G + B − A). An economic evaluation of CTP versus CCTA for health outcomes and costs should be performed in the future.

10 Limitations and Pitfalls

Current dynamic CT technology has limitations in anatomic coverage (7 cm) with a second generation dual-source CT. Beam-hardening artifacts are problematic for the interpretation of CT images. However, an algorithmic approach may solve this problem (Kitagawa et al. 2010). Relative low tissue contrast of CT may decrease the sensitivity of CTP. However, a MBF map obtained from CT data provides important information on myocardial perfusion.

Another limitation of the dual-source dynamic CTP protocol is the limited temporal resolution, as datasets are only acquired every two or four heartbeats. This limitation could result in an underestimation of blood flow, particularly during stress as temporal resolution requirements for MBF quantification become more critical with increasing MBF.

On the other hand, higher spatial resolution of CT compared with MRI may eliminate errors associated with dark-rim artifacts on MRP. The availability of CTP is still limited, because it is a new technique. Widespread use of CTP should be preceded by the results of basic and clinical research, with further education of radiologists, technologists, and clinicians.

Randomized trials will be needed to compare the clinical effectiveness of the CCTA/CTP examination with other modalities (Blankstein and Jerosch-Herold 2010). The prognostic value of CTP is not known and should be evaluated in the future.

11 Conclusions

Stress perfusion CTP and CCTA can provide information on coronary artery anatomy and physiology simultaneously. Wide-coverage (dual-source) CT scanners with prospective

ECG-gated scanning techniques permit low-radiation, dynamic imaging of the myocardium after contrast injection. CTP is expected to play some role in the evaluation of ischemic heart disease with coronary arteries that display an intermediate-to-high degree of stenosis for patients with intermediate-to-high pretest probability of CAD.

References

Bamberg F, Klotz E, Flohr T, Becker A, Becker CR, Schmidt B, Wintersperger BJ, Reiser MF, Nikolaou K (2010) Dynamic myocardial stress perfusion imaging using fast dual-source CT with alternating table positions: initial experience. Eur Radiol 20:1168–1173. doi:10.1007/s00330-010-1715-9

Bamberg F, Becker A, Schwarz F, Marcus RP, Greif M, von Ziegler F, Blankstein R, Hoffmann U, Sommer WH, Hoffmann VS, Johnson TR, Becker HC, Wintersperger BJ, Reiser MF, Nikolaou K (2011) Detection of hemodynamically significant coronary artery stenosis: incremental diagnostic value of dynamic CT-based myocardial perfusion imaging. Radiology 260:689–698. doi:10.1148/radiol.11110638

Bamberg F, Hinkel R, Schwarz F, Sandner TA, Baloch E, Marcus R, Becker A, Kupatt C, Wintersperger BJ, Johnson TR, Theisen D, Klotz E, Reiser MF, Nikolaou K (2012) Accuracy of dynamic computed tomography adenosine stress myocardial perfusion imaging in estimating myocardial blood flow at various degrees of coronary artery stenosis using a porcine animal model. Invest Radiol 47:71–77. doi:10.1097/RLI.0b013e31823fd42b

Bastarrika G, Ramos-Duran L, Rosenblum MA, Kang DK, Rowe GW, Schoepf UJ (2010) Adenosine-stress dynamic myocardial CT perfusion imaging: initial clinical experience. Invest Radiol 45:306–313. doi:10.1097/RLI.0b013e3181dfa2f2

Bettencourt N, Rocha J, Ferreira N, Pires-Morais G, Carvalho M, Leite D, Melica B, Santos L, Rodrigues A, Braga P, Teixeira M, Simoes L, Leite-Moreira A, Cardoso S, Nagel E, Gama V (2011) Incremental value of an integrated adenosine stress-rest MDCT perfusion protocol for detection of obstructive coronary artery disease. J Cardiovasc Comput Tomogr 5:392–405. doi:10.1016/j.jcct.2011.10.002

Blankstein R, Shturman LD, Rogers IS, Rocha-Filho JA, Okada DR, Sarwar A, Soni AV, Bezerra H, Ghoshhajra BB, Petranovic M, Loureiro R, Feuchtner G, Gewirtz H, Hoffmann U, Mamuya WS, Brady TJ, Cury RC (2009) Adenosine-induced stress myocardial perfusion imaging using dual-source cardiac computed tomography. J Am Coll Cardiol 54:1072–1084. doi:10.1016/j.jacc.2009.06.014

Blankstein R, Jerosch-Herold M (2010) Stress myocardial perfusion imaging by computed tomography a dynamic road is ahead. JACC Cardiovasc Imaging 3:821–823. doi:10.1016/j.jcmg.2010.06.008

Choe YH, Choo KS, Jeon ES, Gwon HC, Choi JH, Park JE (2008) Comparison of MDCT and MRI in the detection and sizing of acute and chronic myocardial infarcts. Eur J Radiol 66:292–299. doi:10.1016/j.ejrad.2007.06.010

Cury RC, Magalhaes TA, Paladino AT, Shiozaki AA, Perini M, Senra T, Lemos PA, Rochitte CE (2011) Dipyridamole stress and rest transmural myocardial perfusion ratio evaluation by 64 detector-row computed tomography. J Cardiovasc Comput Tomogr 5:443–448. doi:10.1016/j.jcct.2011.10.012

Feuchtner G, Goetti R, Plass A, Wieser M, Scheffel H, Wyss C, Stolzmann P, Donati O, Schnabl J, Falk V, Alkadhi H, Leschka S, Cury RC (2011) Adenosine stress high-pitch 128-slice dual-source myocardial computed tomography perfusion for imaging of reversible myocardial ischemia: comparison with magnetic resonance imaging. Circ Cardiovasc Imaging 4:540–549. doi:10.1161/circimaging.110.961250

Fox K, Garcia MA, Ardissino D, Buszman P, Camici PG, Crea F, Daly C, De Backer G, Hjemdahl P, Lopez-Sendon J, Marco J, Morais J, Pepper J, Sechtem U, Simoons M, Thygesen K, Priori SG, Blanc JJ, Budaj A, Camm J, Dean V, Deckers J, Dickstein K, Lekakis J, McGregor K, Metra M, Osterspey A, Tamargo J, Zamorano JL (2006) Guidelines on the management of stable angina pectoris: executive summary: the task force on the management of stable angina pectoris of the European society of cardiology. Eur Heart J 27:1341–1381. doi:10.1093/eurheartj/ehl001

Garnock-Jones KP, Curran MP (2010) Regadenoson. Am J Cardiovasc Drugs 10:65–71. doi:10.2165/10489040-000000000-00000

George RT, Silva C, Cordeiro MA, DiPaula A, Thompson DR, McCarthy WF, Ichihara T, Lima JA, Lardo AC (2006) Multidetector computed tomography myocardial perfusion imaging during adenosine stress. J Am Coll Cardiol 48:153–160. doi:10.1016/j.jacc.2006.04.014

George RT, Arbab-Zadeh A, Miller JM, Kitagawa K, Chang HJ, Bluemke DA, Becker L, Yousuf O, Texter J, Lardo AC, Lima JA (2009) Adenosine stress 64- and 256-row detector computed tomography angiography and perfusion imaging: a pilot study evaluating the transmural extent of perfusion abnormalities to predict atherosclerosis causing myocardial ischemia. Circ Cardiovasc Imaging 2:174–182. doi:10.1161/CIRCIMAGING.108.813766

Ghoshhajra BB, Rogers IS, Maurovich-Horvat P, Techasith T, Verdini D, Sidhu MS, Drzezga NK, Medina HM, Blankstein R, Brady TJ, Cury RC (2011) A comparison of reconstruction and viewing parameters on image quality and accuracy of stress myocardial CT perfusion. J Cardiovasc Comput Tomogr 5:459–466. doi:10.1016/j.jcct.2011.10.011

Gorenoi V, Schonermark MP, Hagen A (2012) CT coronary angiography vs. invasive coronary angiography in CHD. GMS Health Technol Assess 8:Doc02. doi:10.3205/hta000100

Groothuis JG, Beek AM, Brinckman SL, Meijerink MR, Koestner SC, Nijveldt R, Gotte MJ, Hofman MB, van Kuijk C, van Rossum AC (2010) Low to intermediate probability of coronary artery disease: comparison of coronary CT angiography with first-pass MR myocardial perfusion imaging. Radiology 254:384–392. doi:10.1148/radiol.09090802

Hamon M, Fau G, Nee G, Ehtisham J, Morello R (2010) Meta-analysis of the diagnostic performance of stress perfusion cardiovascular magnetic resonance for detection of coronary artery disease. J Cardiovasc Magn Reson 12:29. doi:10.1186/1532-429x-12-29

Hamon MMR, Riddell JW, Hamon M (2007) Coronary arteries: diagnostic performance of 16- versus 64-section spiral CT compared with invasive coronary angiography—meta-analysis. Radiology 245(3):720–731

Ho KT, Chua KC, Klotz E, Panknin C (2010) Stress and rest dynamic myocardial perfusion imaging by evaluation of complete time-attenuation curves with dual-source CT. JACC Cardiovasc Imaging 3:811–820. doi:10.1016/j.jcmg.2010.05.009

Jones WS, Patel MR, Holleran SA, Harrison JK, O'Connor CM, Phillips HR 3rd (2011) Trends in the use of diagnostic coronary angiography, percutaneous coronary intervention, and coronary artery bypass graft surgery across North Carolina. Am Heart J 162:932–937. doi:10.1016/j.ahj.2011.08.015

Kirschbaum SW, Nieman K, Springeling T, Weustink AC, Ramcharitar S, Mieghem C, Rossi A, Duckers E, Serruys PW, Boersma E, de Feyter PJ, van Geuns RJ (2011) Non-invasive diagnostic workup of patients with suspected stable angina by combined computed tomography coronary angiography and magnetic resonance perfusion imaging. Circ J 75:1678–1684

Kitagawa K, George RT, Arbab-Zadeh A, Lima JA, Lardo AC (2010) Characterization and correction of beam-hardening artifacts during

dynamic volume CT assessment of myocardial perfusion. Radiology 256:111–118. doi:10.1148/radiol.10091399

Ko BS, Cameron JD, Meredith IT, Leung M, Antonis PR, Nasis A, Crossett M, Hope SA, Lehman SJ, Troupis J, DeFrance T, Seneviratne SK (2012a) Computed tomography stress myocardial perfusion imaging in patients considered for revascularization: a comparison with fractional flow reserve. Eur Heart J 33:67–77. doi:10.1093/eurheartj/ehr268

Ko SM, Choi JW, Song MG, Shin JK, Chee HK, Chung HW, Kim DH (2011) Myocardial perfusion imaging using adenosine-induced stress dual-energy computed tomography of the heart: comparison with cardiac magnetic resonance imaging and conventional coronary angiography. Eur Radiol 21:26–35. doi:10.1007/s00330-010-1897-1

Ko SM, Choi JW, Hwang HK, Song MG, Shin JK, Chee HK (2012b) Diagnostic performance of combined noninvasive anatomic and functional assessment with dual-source CT and adenosine-induced stress dual-energy CT for detection of significant coronary stenosis. AJR Am J Roentgenol 198:512–520. doi:10.2214/ajr.11.7029

Koo BK, Erglis A, Doh JH, Daniels DV, Jegere S, Kim HS, Dunning A, DeFrance T, Lansky A, Leipsic J, Min JK (2011) Diagnosis of ischemia-causing coronary stenoses by noninvasive fractional flow reserve computed from coronary computed tomographic angiograms. Results from the prospective multicenter DISCOVER-FLOW (Diagnosis of Ischemia-Causing Stenoses Obtained Via Noninvasive Fractional Flow Reserve) study. J Am Coll Cardiol 58:1989–1997. doi:10.1016/j.jacc.2011.06.066

Kristensen TS, Engstrom T, Kelbaek H, von der Recke P, Nielsen MB, Kofoed KF (2010) Correlation between coronary computed tomographic angiography and fractional flow reserve. Int J Cardiol 144:200–205. doi:10.1016/j.ijcard.2009.04.024

Lindstaedt M, Mugge A (2011) Myocardial fractional flow reserve. Its role in guiding PCI in stable coronary artery disease. Herz 36:410–416. doi:10.1007/s00059-011-3486-8

Lockie T, Ishida M, Perera D, Chiribiri A, De Silva K, Kozerke S, Marber M, Nagel E, Rezavi R, Redwood S, Plein S (2011) High-resolution magnetic resonance myocardial perfusion imaging at 3.0-Tesla to detect hemodynamically significant coronary stenoses as determined by fractional flow reserve. J Am Coll Cardiol 57:70–75. doi:10.1016/j.jacc.2010.09.019

Mahnken AH, Klotz E, Pietsch H, Schmidt B, Allmendinger T, Haberland U, Kalender WA, Flohr T (2010) Quantitative whole heart stress perfusion CT imaging as noninvasive assessment of hemodynamics in coronary artery stenosis: preliminary animal experience. Invest Radiol 45:298–305. doi:10.1097/RLI.0b013e3181dfa3cf

Melikian N, De Bondt P, Tonino P, De Winter O, Wyffels E, Bartunek J, Heyndrickx GR, Fearon WF, Pijls NH, Wijns W, De Bruyne B (2010) Fractional flow reserve and myocardial perfusion imaging in patients with angiographic multivessel coronary artery disease. JACC Cardiovasc Interv 3:307–314. doi:10.1016/j.jcin.2009.12.010

Mowatt G, Cummins E, Waugh N, Walker S, Cook J, Jia X, Hillis GS, Fraser C (2008) Systematic review of the clinical effectiveness and cost-effectiveness of 64-slice or higher computed tomography angiography as an alternative to invasive coronary angiography in the investigation of coronary artery disease. Health Technol Assess 12:iii–iv, ix–143

Nagao M, Kido T, Watanabe K, Saeki H, Okayama H, Kurata A, Hosokawa K, Higashino H, Mochizuki T (2011) Functional assessment of coronary artery flow using adenosine stress dual-energy CT: a preliminary study. Int J Cardiovasc Imaging 27:471–481. doi:10.1007/s10554-010-9676-2

Nakauchi Y, Iwanaga Y, Ikuta S, Kudo M, Kobuke K, Murakami T, Miyazaki S (2012) Quantitative myocardial perfusion analysis using multi-row detector CT in acute myocardial infarction. Heart 98:566–572. doi:10.1136/heartjnl-2011-300915

Pijls NH, van Schaardenburgh P, Manoharan G, Boersma E, Bech JW, van't Veer M, Bar F, Hoorntje J, Koolen J, WijnsW J, de Bruyne B (2007) Percutaneous coronary intervention of functionally nonsignificant stenosis: 5-year follow-up of the DEFER Study. J Am Coll Cardiol 49:2105–2111. doi:10.1016/j.jacc.2007.01.087

Pijls NH, Fearon WF, Tonino PA, Siebert U, Ikeno F, Bornschein B, van't Veer M, Klauss V, Manoharan G, Engstrom T, Oldroyd KG, Ver Lee PN, MacCarthy PA, De Bruyne B (2010) Fractional flow reserve versus angiography for guiding percutaneous coronary intervention in patients with multivessel coronary artery disease: 2-year follow-up of the FAME (Fractional Flow Reserve Versus Angiography for Multivessel Evaluation) study. J Am Coll Cardiol 56:177–184. doi:10.1016/j.jacc.2010.04.012

Pijls NH, Sels JW (2012) Functional measurement of coronary stenosis. J Am Coll Cardiol 59:1045–1057. doi:10.1016/j.jacc.2011.09.077

Rocha-Filho JA, Blankstein R, Shturman LD, Bezerra HG, Okada DR, Rogers IS, Ghoshhajra B, Hoffmann U, Feuchtner G, Mamuya WS, Brady TJ, Cury RC (2010) Incremental value of adenosine-induced stress myocardial perfusion imaging with dual-source CT at cardiac CT angiography. Radiology 254:410–419. doi:10.1148/radiol.09091014

Ruzsics B, Schwarz F, Schoepf UJ, Lee YS, Bastarrika G, Chiaramida SA, Costello P, Zwerner PL (2009) Comparison of dual-energy computed tomography of the heart with single photon emission computed tomography for assessment of coronary artery stenosis and of the myocardial blood supply. Am J Cardiol 104:318–326. doi:10.1016/j.amjcard.2009.03.051

Scheffel H, Stolzmann P, Alkadhi H, Azemaj N, Plass A, Baumueller S, Desbiolles L, Leschka S, Kozerke S, Falk V, Boesiger P, Wyss C, Marincek B, Donati OF (2010) Low-dose CT and cardiac MR for the diagnosis of coronary artery disease: accuracy of single and combined approaches. Int J Cardiovasc Imaging 26:579–590. doi:10.1007/s10554-010-9595-2

Schuijf JD, Wijns W, Jukema JW, Atsma DE, de Roos A, Lamb HJ, Stokkel MP, Dibbets-Schneider P, Decramer I, De Bondt P, van der Wall EE, Vanhoenacker PK, Bax JJ (2006) Relationship between noninvasive coronary angiography with multi-slice computed tomography and myocardial perfusion imaging. J Am Coll Cardiol 48:2508–2514. doi:10.1016/j.jacc.2006.05.080

Schwitter J, Wacker CM, Wilke N, Al-Saadi N, Sauer E, Huettle K, Schonberg SO, Luchner A, Strohm O, Ahlstrom H, Dill T, Hoebel N, Simor T (2012) MR-IMPACT II: magnetic resonance imaging for myocardial perfusion assessment in coronary artery disease trial: perfusion-cardiac magnetic resonance vs. single-photon emission computed tomography for the detection of coronary artery disease: a comparative multicentre, multivendor trial. Eur Heart J. doi:10.1093/eurheartj/ehs022

Sharples L, Hughes V, Crean A, Dyer M, Buxton M, Goldsmith K, Stone D (2007) Cost-effectiveness of functional cardiac testing in the diagnosis and management of coronary artery disease: a randomised controlled trial. The CECaT trial. Health Technol Assess 11:iii–iv, ix–115

Shikata F, Imagawa H, Kawachi K, Kido T, Kurata A, Inoue Y, Hosokawa K, Nagao M, Higashino H, Mochizuki T, Ryugo M, Nagashima M (2010) Regional myocardial blood flow measured by stress multidetector computed tomography as a predictor of recovery of left ventricular function after coronary artery bypass grafting. Am Heart J 160:528–534. doi:10.1016/j.ahj.2010.06.026

Tamarappoo BK, Dey D, Nakazato R, Shmilovich H, Smith T, Cheng VY, Thomson LE, Hayes SW, Friedman JD, Germano G, Slomka PJ, Berman DS (2010) Comparison of the extent and

severity of myocardial perfusion defects measured by CT coronary angiography and SPECT myocardial perfusion imaging. JACC Cardiovasc Imaging 3:1010–1019. doi:10.1016/j.jcmg.2010.07.011

Taylor AJ, Cerqueira M, Hodgson JM, Mark D, Min J, O'Gara P, Rubin GD (2010) ACCF/SCCT/ACR/AHA/ASE/ASNC/NASCI/SCAI/SCMR 2010 Appropriate use criteria for cardiac computed tomography. A report of the American College of Cardiology Foundation Appropriate Use Criteria Task Force, the Society of Cardiovascular Computed Tomography, the American College of Radiology, the American Heart Association, the American Society of Echocardiography, the American Society of Nuclear Cardiology, the North American Society for Cardiovascular Imaging, the Society for Cardiovascular Angiography and Interventions, and the Society for Cardiovascular Magnetic Resonance. J Cardiovasc Comput Tomogr 4(407):e401–e433. doi:10.1016/j.jcct.2010.11.001

Tonino PA, Fearon WF, De Bruyne B, Oldroyd KG, Leesar MA, Ver Lee PN, Maccarthy PA, Van't Veer M, Pijls NH (2010) Angiographic versus functional severity of coronary artery stenoses in the FAME study fractional flow reserve versus angiography in multivessel evaluation. J Am Coll Cardiol 55:2816–2821. doi:10.1016/j.jacc.2009.11.096

van de Hoef TP, Nolte F, Rolandi MC, Piek JJ, van den Wijngaard JP, Spaan JA, Siebes M (2012) Coronary pressure-flow relations as basis for the understanding of coronary physiology. J Mol Cell Cardiol 52:786–793. doi:10.1016/j.yjmcc.2011.07.025

van Werkhoven JM, Heijenbrok MW, Schuijf JD, Jukema JW, van der Wall EE, Schreur JH, Bax JJ (2010) Combined non-invasive anatomical and functional assessment with MSCT and MRI for the detection of significant coronary artery disease in patients with an intermediate pre-test likelihood. Heart 96:425–431. doi:10.1136/hrt.2009.179531

Verani M (2000) Stress approaches: techniques. In: Pohost G, O'Rourke R, Berman D, Shah P (eds) Imaging in cardiovascular disease, 1st edn. Lippincott Williams & Wilkins, Philadelphia, pp 151–158

Wang Y, Qin L, Shi X, Zeng Y, Jing H, Schoepf UJ, Jin Z (2012) Adenosine-stress dynamic myocardial perfusion imaging with second-generation dual-source CT: comparison with conventional catheter coronary angiography and SPECT nuclear myocardial perfusion imaging. AJR Am J Roentgenol 198:521–529. doi:10.2214/ajr.11.7830

Weininger M, Schoepf UJ, Ramachandra A, Fink C, Rowe GW, Costello P, Henzler T (2010) Adenosine-stress dynamic real-time myocardial perfusion CT and adenosine-stress first-pass dual-energy myocardial perfusion CT for the assessment of acute chest pain: initial results. Eur J Radiol. doi:10.1016/j.ejrad.2010.11.022<

CT Imaging of Myocardial Perfusion and Viability: Future Perspectives

Felix G. Meinel and Justin R. Silverman

Contents

Abstract

The notion of evidence-based medicine (EBM) has transformed the science and practice of medicine substantially over the past decades. EBM has been defined as "the conscientious, explicit and judicious use of current best evidence in making decisions about the care of individual patients" (Sackett et al. 1996). EBM thus demands that medical procedures be justified by objective measures of performance. This general trend in healthcare has long been ignored by the radiological field, with the formal concept of evidence-based radiology (EBR), only recently established (Evidence-Based Radiology Working Group 2001; Sheehan et al. 2007; Collins 2007; Malone 2007; Dodd et al. 2004). At least in part, this may be explained by the conceptual framework of EBM, which is primarily designed to assess the efficacy of therapeutic procedures, such as pharmacological, surgical, or other interventions. Many criteria used to assess the quality of studies and levels of evidence in EBM are not directly applicable to diagnostic imaging.

1 Imaging in the Era of Evidence-based Radiology

The notion of evidence-based medicine (EBM) has transformed the science and practice of medicine substantially over the past decades. EBM has been defined as "the conscientious, explicit and judicious use of current best evidence in making decisions about the care of individual patients" (Sackett et al. 1996). EBM thus demands that medical procedures be justified by objective measures of performance. This general trend in healthcare has long been ignored by the radiological field, with the formal concept of evidence-based radiology (EBR), only recently established (Evidence-Based Radiology Working Group 2001; Sheehan

F. G. Meinel (✉) · J. R. Silverman
Division of Cardiovascular Imaging, Department of Radiology and Radiological Sciences, Medical University of South Carolina, Charleston, SC, USA
e-mail: meinel@musc.edu

U. J. Schoepf et al. (eds.), *CT Imaging of Myocardial Perfusion and Viability*, Medical Radiology. Diagnostic Imaging,
DOI: 10.1007/174_2013_931, © Springer-Verlag Berlin Heidelberg 2013
Published Online: 19 October 2013

et al. 2007; Collins 2007; Malone 2007; Dodd et al. 2004). At least in part, this may be explained by the conceptual framework of EBM, which is primarily designed to assess the efficacy of therapeutic procedures, such as pharmacological, surgical, or other interventions. Many criteria used to assess the quality of studies and levels of evidence in EBM are not directly applicable to diagnostic imaging.

In an effort to ease the application of EBM theory for diagnostic imaging, a hierarchical 6-step model has been developed specifically for radiology that can be used to classify measures of efficacy in studies investigating diagnostic rather than therapeutic procedures (Evidence-Based Radiology Working Group 2001). In this model, for a diagnostic test to reach the first level of efficacy (technical efficacy) requires a demonstration of technical feasibility and interpretability. At the second level (diagnostic accuracy efficacy), a diagnostic test is evaluated for diagnostic accuracy. The third level (diagnostic thinking efficacy) describes how helpful a test is for advancing the diagnostic process of confirming or excluding a diagnosis or narrowing the spectrum of differential diagnoses. At the fourth level (therapeutic efficacy), the impact of a diagnostic test on patient management must be demonstrated. The fifth level describes the impact of the test on the patient's outcome (patient outcome efficacy). Last, the sixth and highest level of efficacy consists of an overall benefit-cost analysis from a societal viewpoint (societal efficacy).

The level of efficacy evidence that can be derived from a diagnostic study further depends on the scientific rigor with which the study was designed and conducted. On one hand, many studies in diagnostic imaging have been derived from case reports, have failed to include a reference standard, or have investigated a very narrow spectrum of nonconsecutive patients. The more reliable (and therefore more valuable) studies were designed with adequate controls in an appropriate spectrum of consecutive patients using a suitable reference standard (Evidence-Based Radiology Working Group 2001).

2 Current Level of Evidence on CT Imaging of Myocardial Perfusion and Viability

The current evidence available for CT imaging of myocardial perfusion and viability is largely limited to studies operating at the lowest two levels of efficacy. As described throughout this book, the technical feasibility of the various CT myocardial perfusion imaging techniques is well established—likewise for delayed enhancement CT imaging for myocardial viability assessment. There is also a wealth of level 2 evidence that tests the accuracy of CT myocardial perfusion and viability imaging techniques against the established imaging reference standards of catheter angiography with or without FFR measurement, SPECT, and MRI. To date, these studies have been small, single center trials with the exception of the CORE320 trial. The CORE320 trial is a single vendor, multicenter study of the diagnostic accuracy of combined noninvasive CT angiography and single shot myocardial blood pool imaging using a 320-slice CT system, in comparison with invasive angiography (ICA) and single photon computed tomography-myocardial perfusion imaging (SPECT-MPI) (Vavere et al. 2011). Preliminary results of this trial suggest that the addition of CT blood pool imaging to coronary CT angiography may improve the accuracy for the detection of coronary artery disease and may predict revascularization within 30 days (Lima and Maurer 2012).

To date, explicit investigations of the impact of CT myocardial perfusion and viability imaging on diagnostic and therapeutic management (levels 3 and 4 efficacy) are lacking. With the exception of one, cost-effectiveness analysis on dual-energy CT in a limited number of patients (Meyer et al. 2012), no evidence is available on the higher level efficacies of CT myocardial perfusion and viability imaging, i.e., the impact on clinical outcomes and the associated overall cost-benefit ratio. This is not surprising given the novelty of the techniques. Development of higher level efficacy studies for imaging tests are complicated by the indirect influence of diagnostic tests on patient management and outcome. It is a therapeutic decision based on the results of an imaging test that change management and thus influence outcome. It is difficult to establish the higher level efficacy of a novel diagnostic test, as this largely depends upon the extent to which clinicians will accept the test's results and factor them into their therapeutic strategy.

3 What Needs to be Done?

Meeting this challenge will require radiologists to look beyond the realm of imaging to collaborate even more closely with clinicians. It is imperative that radiologists take the initiative to educate and update clinicians on novel technical developments in the field of CT myocardial perfusion imaging and the advantages they offer. Similarly, radiologists will need to depend on clinicians to guide the development of cardiac perfusion and viability imaging toward providing clinically valuable information that will improve patient management. Such an alliance will be essential for future studies that evaluate the higher level efficacy of CT techniques for cardiac perfusion and viability imaging.

As mentioned, the overwhelming majority of published literature on CT myocardial perfusion and viability imaging consists of single center studies evaluating a specific

technique in a small number of patients. In order for a technique to become clinically viable, the experience gained in these initial studies must be applied to larger, multicenter trials. As a first step in this direction, a large multicenter, multi-vendor CT perfusion registry (PRECEPT) has been initiated, which will pool the existing CT perfusion studies from participating sites. Patient demographic information and baseline clinical risk factors as well as follow-up data and comparative modalities such as SPECT, cardiac MRI and invasive catheter angiography will also be collected when available.

It can be anticipated that PRECEPT will significantly advance our current understanding of CT myocardial perfusion imaging on multiple fronts. First, there exist a number of technical implementations of CT myocardial perfusion imaging, the investigations of which have been presented in detail in chapter III of this book. However, it is largely unknown whether these many similar techniques are comparable in their technical success rate, interpretability, and diagnostic accuracy. It is hoped that PRECEPT will assist the technical optimization of CT myocardial perfusion imaging.

Second, with CT myocardial perfusion and viability imaging being relatively novel techniques, the optimal method for image interpretation is yet unclear. This is true for both quantitative and qualitative methods of evaluation. Qualitatively, a large registry may better identify typical perfusion patterns and lead to methods for differentiating these patterns from artifacts and other potential pitfalls. Quantitative analysis of dynamic CT myocardial perfusion imaging will almost certainly benefit from a large scale analysis. The normal ranges of myocardial perfusion parameters and the optimal myocardial blood flow diagnostic threshold have only been investigated in very small patient populations. Through a large registry, reliable, well-defined normal limits should be obtainable. Third, a large registry will be of great value in better defining the diagnostic accuracy of CT myocardial perfusion imaging compared to external reference standards. In particular, comparison can be made to invasive catheter angiography with fractional flow reserve measurements and cardiac MRI, the gold standards for the assessment of hemodynamically significant coronary artery disease, myocardial perfusion, and viability. Last, if sufficient follow-up data are available, the pooled data will be very useful in assessing the prognostic value of CT myocardial perfusion imaging for predicting future adverse cardiac events.

Registries with retrospectively pooled data, albeit very useful, have significant limitations. Particularly, with regards to the potential impact of CT perfusion and viability imaging on diagnostic differentiation, therapeutic strategy, patient outcome, and cost-effectiveness, results from a retrospectively pooled registry can only be regarded as hypothesis-generating and cannot replace evaluation in prospective, multicenter trials. Prospective trials in which therapeutic decisions are truly based on the result of CT myocardial perfusion imaging will be required to define the role that CT myocardial perfusion imaging may play in tomorrow's patient care.

From today's perspective, CT myocardial perfusion and viability imaging as a clinical staple may seem a long ways off, and many questions remain to be answered regarding patient selection, technique, and interpretation. However, the experience gained from coronary CTA can serve as a model and as an encouragement alike. Within just over a decade, coronary CTA has moved from an experimental laboratory procedure to a robust technique of clinical routine, with its role in acute and chronic chest pain clinical decision making having passed the gauntlet of large, prospective multicenter trials. The next few years will show whether CT imaging of myocardial perfusion and viability will be able to make a similar contribution to improving the diagnosis and management of patients with known or suspected heart disease.

References

Collins J (2007) Evidence-based medicine. J Am Coll Radiol 4:551–554

Dodd JD, MacEneaney PM, Malone DE (2004) Evidence-based radiology: how to quickly assess the validity and strength of publications in the diagnostic radiology literature. Eur Radiol 14:915–922

Evidence-Based Radiology Working Group (2001) Evidence-based radiology: a new approach to the practice of radiology. Radiology 220:566–575

Lima J, Maurer G (2012) Diagnostic performance of combined noninvasive coronary angiography and myocardial perfusion imaging using 320-row detector computer tomography: The CORE320 Multicenter, Multinational Study. ESC 2012 (Abstract 3936)

Malone DE (2007) Evidence-based practice in radiology: an introduction to the series. Radiology 242:12–14

Meyer M, Nance JW Jr, Schoepf UJ, Moscariello A, Weininger M, Rowe GW, Ruzsics B, Kang DK, Chiaramida SA, Schoenberg SO, Fink C, Henzler T (2012) Cost-effectiveness of substituting dual-energy CT for SPECT in the assessment of myocardial perfusion for the workup of coronary artery disease. Eur J Radiol 81:3719–3725

Sackett DL, Rosenberg WM, Gray JA, Haynes RB, Richardson WS (1996) Evidence based medicine: what it is and what it isn't. BMJ 312:71–72

Sheehan JJ, Ridge CA, Ward EV, Duffy GJ, Collins CD, Skehan SJ, Malone DE (2007) The process of evidence-based practice in radiology: an introduction. Acad Radiol 14:385–388

Vavere AL, Simon GG, George RT, Rochitte CE, Arai AE, Miller JM, Di Carli M, Arbab-Zadeh A, Dewey M, Niinuma H, Laham R, Rybicki FJ, Schuijf JD, Paul N, Hoe J, Kuribyashi S, Sakuma H, Nomura C, Yaw TS, Kofoed KF, Yoshioka K, Clouse ME, Brinker J, Cox C, Lima JA (2011) Diagnostic performance of combined noninvasive coronary angiography and myocardial perfusion imaging using 320 row detector computed tomography: design and implementation of the CORE320 multicenter, multinational diagnostic study. J Cardiovasc Comput Tomogr 5:370–381

Index

U. J. Schoepf et al. (eds.), *CT Imaging of Myocardial Perfusion and Viability*, Medical Radiology. Diagnostic Imaging,
DOI: 10.1007/978-3-642-33879-3, © Springer-Verlag Berlin Heidelberg 2014